Print ISSN : 2395-1990
Online ISSN : 2394-4099
www.ijsrset.com

Techno Science Academy
The International Open Access Publisher

IJSRSET

National Conference Emerging Trends in RF and Engineering Sciences (ETRES'18)

Organised by
Department of Electronics & Communication Engineering
Annamalai University, Chidambaram, Tamil Nadu, India

VOLUME 5, ISSUE 3, MARCH-APRIL-2018

INTERNATIONAL JOURNAL OF SCIENTIFIC RESEARCH IN SCIENCE, ENGINEERING AND TECHNOLOGY

UGC Approved Journal [Journal No : 47147]

Email : editor@ijsrset.com Website : http://ijsrset.com

National Conference Emerging Trends in RF and Engineering Sciences (ETRES'18)

On

(April 26-27, 2018)

Annamalai University

(Accredited with 'A' Grade by NAAC)

Organized by

Department of Electronics & Communication Engineering

Annamalai University, Chidambaram, Tamil Nadu, India

Website: annamalaiuniversity.ac.in

International Journal of Scientific Research in Science, Engineering and Technology

[Print ISSN: 2395-1990 | Online ISSN: 2394-4099]

Volume 5, Issue 3, March-April-2018

UGC Approved Journal [Journal No : 47147]

Published By

Technoscience Academy

(The International Open Access Publisher)

Website: www.technoscienceacademy.com

ORGANIZING COMMITTEE

Chief Patron

Prof.Dr.S.Manian,Ph.D
Vice-Chancellor
Annamalai University

Patron

Prof.Dr.K.Arumugam
Registrar
Annamalai University

Vice-Patron

Dr.C.Anthony Jeyasehar
Dean
Faculty of Engg. &Tech.
Annamalai University

Chairman

Dr.P.Kailasapathi
Prof & Head
Dept of ECE
Annamalai University

Vice Chairperson

Dr. G Yamuna
Prof of ECE
Annamalai University

Coordinator

Mr.T.Ravichandran
Associate Prof of ECE
Annamalai University

Directors

Dr.R.Gayathri
Asst.Prof of ECE
Dept of ECE
Annamalai University

Mrs.R.Kanimozhi
Asst.Prof of ECE
Dept of ECE
Annamalai University

Technical Reviewing Board (National)

1. Mr. Rajeev Jyoti , Deputy Director, Space Applications Centre, Indian Space Research Organisation, Ahmedabad
2. Dr.S.Ragavan(Microwaves, NIT, Trichy)
3. Dr.D.SriramKumar (Photonics, NIT, Trichy)
4. Dr.Vipul Sharma (RF & Antennas , Haridwar University)
5. Dr.T Theivasanthi (Nano Tech, Kalasalingam University)
6. Dr.G.Nagarajan (Networks, Pondicherry Engineering College)
7. Dr.Kumar (Nano Tech, Periyar Maniammai University)
8. Dr. T.Shanmuganantham (Antennas, Pondicherry University)
9. Dr. K.Ayyapppan (Networks, Rajiv Gandhi College of Engineering)
10. Dr. Gulam Nabi Alsath (Antennas, SSN College of Engineering)

Technical Reviewing Board (Annamalai University)

1. Dr.P.Kailasapathi (Wireless Communication)
2. Dr.G.Yamuna (Imaging)
3. Mr.T.Ravichandran (Signal Processing)
4. Dr.R.Gayathri (Antennas)
5. Dr.Malathi (Bio Medical)
6. Dr.J.Krishnan (Bio Medical)
7. Dr.J.Daniel (MEMS)
8. Dr.S.Jothilakshmi (Imaging, AI)

About the University

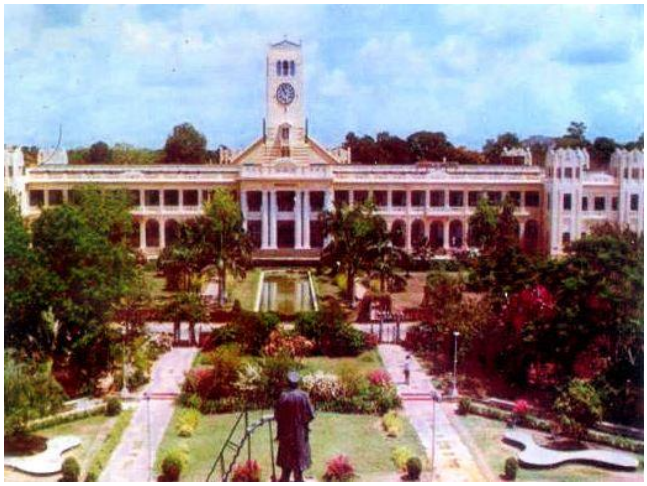

Annamalai University, established in 1929, by The Annamalai University Act, 1929, is the only unitary, residential, multi-faculty University in the State of Tamil Nadu with 10 Faculties and 49 Departments of Study. Recently, the Government of Tamil Nadu enacted The Annamalai University Act -2013, to bring the University under its direct ambit. The University, for the past 87 years, has crossed noteworthy milestones in the process of contributing to the cause of promoting higher education among the people for whom it would have remained a distant dream. The NAAC has accredited the University with „A" Grade in 2014, which is a recent feather added to its cap. At Annamalai, the curriculum is designed in line with the educational policies of the State and Cen-tral Government in order to addresses the global needs and at the same time striking a balance to serve the cause of national development and regional requirements. The syllabus is dynamic and constantly revamped to keep pace with the rapid developments. A central library, besides faculty and departmental libraries caters to the quest for knowledge of thousands of students of varied disciplines. Medical Facilities for Students Teaching & Non-teaching Staff and facilities for Sports and Cultural Activity makes campus life secure, interesting and meaningful. The University enjoys unstinted support from its alumni. Registered alumni associations exists and contribute generously to the growth of their Alma-Mater. Internal Quality Assurance Cell (IQAC) plays a proactive role in reviewing the current status and evolve a system for conscious, consistent and catalytic improvement in the performance of the institution.

Department of Electronics & Communication Engineering

The Department of Electronics and Communication Engineering, established under the Faculty of Engineering and Technology of the University in the year 2003, (started functioning as a separate department from Aug 2016) is well known for providing quality technical education to the students across the country and abroad through on and off campus modes. It offers Under-graduate, Post-graduate, and Doctoral programs. The Department conducts short-term programs, workshops, National and International Conferences regularly with a view to provide a platform for displaying the contributions made by researchers. The Department organizes students' level technical symposium, intradepartmental sports meet and extra- curricular activities every year for bringing out their academic excellence in the emerging areas, promoting the technical skills besides patronizing their interest in sports and cultural arenas. It arranges personality development and counseling classes to the students every week to mould their character.

MESSAGE

Dr. C. Antony Jeyasehar, B.E.(Hons.),M.E., Ph.D.,
Dean

I am very glad to hear that the Department of ECE is organizing a Two Day National Conference on Emerging Trends in RF & Engineering Sciences (ETRES'18) from 26th April 2018 to 27th April 2018. Conferences open up avenues for further research, as it is the cradle of ideas. Besides, candidates get an opportunity to showcase their respective fields. Development in any area requires empirical studies and research. When students are made aware of events taking place around them in the world, they too look forward to further research and inventions. Conferences of this sort must be organized frequently. I hope that this conference would certainly induce innovative ideas among the participants paving way for new inventions and new technologies in the field of RF and Engineering Sciences. My heartiest congratulations to the Conference Directors and wish them all success in this Endeavour.

C. Antony Jeyasehar

Dr. P. Kailasapathi, Prof & HEAD
Department of ECE

It is a great pleasure for me that our Department is conducting a Two Day National Conference on Emerging Trends in RF & Engineering Sciences (ETRES'18) on 26th and 27th April 2018. The Mission of this Conference is to provide value education and motivate young professionals in building cognitive characteristics, evoke creative expression and cultivate the budding Engineers with recent trends in technology, prepare emerging engineers with concept oriented subject knowledge supplemented with practical orientation to face challenges of modern world. Research and academics should go hand in hand in the making of better future technocrats and Engineers. The Conference has bench marked invited lecture sessions in which eminent professors from various fields of Engineering & Technology for imparting knowledge and experience to young aspirants. On the occasion of this event, I heartily welcome all the participants to this campus and wish them all success.

P. Kailasapathi

CONTENTS

Themed Section : Engineering and Technology
© 2018 IJSRSET | Volume 5 | Issue 3 | Print ISSN: 2395-1990 | Online ISSN: 2394-4099

Analysis and Implementation of Q-Leach Protocol Based On Genetic Algorithm for WSN

G.R. AnnushaKumar[1], V. Padmathilagam[2]

[1]Assistant professor in Electronics and Communication Engineering, Annamalai University, Chidambaram, Tamil Nadu, India

[2]Assistant Professor in Electrical and Electronics Engineering, Annamalai University, Chidambaram, Tamil Nadu, India

ABSTRACT

Wireless sensor networks have gained widespread significance in recent times due to their immense potentials that could be tapped for a wide range of applications. The evolution of wireless network protocols like 4G, 5G etc. has further accelerated the research prospects of wireless sensor networks. Among the many features of WSNs, one of the most important factors is that they could be deployed in remote locations where human intervention or presence is not possible or undesirable. Nodes in remote locations are powered by batteries which cannot be often replaced and hence appropriate energy management strategies form an integral part of an effective WSN deployment. Routing plays an essential role and forms the backbone of any WSN implementation. A well-known routing technique known as LEACH protocol and its variants have been extensively investigated and experimented in this research paper and a comprehensive comparative performance analysis has been inferred from this research article. A modified hybrid fusion routing algorithm Q LEACH has been proposed in this paper and maximum lifetime of the first and half the nodes is optimized using Genetic algorithm, with help of this methods lifetime is increased.

Keywords : Wireless Sensor Networks, Routing, LEACH Protocol, Genetic Algorithm, Energy Management, Lifetime Of WSNs

I. INTRODUCTION

Wireless sensor networks have in recent times have seen an increased usage over a wide range of applications ranging from a simple and effective home monitoring system [1] [2] from a remote location, hospital management, military applications, monitoring of remote locations for possible disaster prediction and management [3]. A simple wireless sensor network scheme is depicted in figure 1.

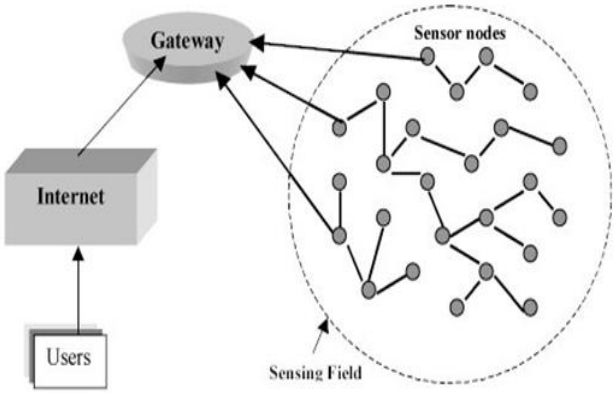

Figure 1. Illustration of Simple Scheme of WSN Deployment

As seen from the above figure, WSN are comprised of a number of nodes deployed in the field under study and information from these sensors being sensed and transmitted in the form of packets of information continuously to the source through a gateway through the wireless transfer protocol. The information from these nodes could also be transmitted to cloud to enable the users to access required information as and when required from any point of the globe. A wireless sensor network system includes sensor mode, sink node and management node. A large number of sensor nodes are established in the monitoring area, constituting a network through the way of self-organizing. The data monitored [4] by sensor nodes is transmitted along other nodes, one by one, that will reach the sink node after a multi-hop routing and then reach the management node through the wired and wireless Internet. Routing forms the backbone behind any WSN implementation as the efficiency of any WSN network is determined by how effectively the information from the sensor nodes is being transmitted from source to destination. It is further defined by several attributes such as packet loss which defines the number of packets that have been effectively transferred to destination to the total number of packets in the initial stage ready for transmission. Selection of shortest path for routing the information from source to destination plays a major role in the working of a routing algorithm. The routing algorithm should also be able to ensure smooth transfer of information even in cases of unpredictable eventual failure of links, channels or nodes due to low levels of energy levels in the battery or battery failures. In such circumstances, the routing algorithm should be able to discover an alternate path in the shortest time possible so as to ensure a smooth transition and thereby prevent traffic congestion in the failed path.

Another essential criterion with respect to routing efficiency is the network lifetime [5], which is governed by the battery efficiency and their efficient use. WSN nodes operate in an unattended environment and thus have irreplaceable batteries. Hence, an effective routing mechanism has been well investigated in this research paper in the form of the LEACH protocol, which is self-organizing and is characterized as an adaptive clustering protocol. It distributes energy among the nodes in a random manner and works on the principle of clustering.

II. LITERATURE SURVEY

Routing in WSNs is quite a challenging task due to the inherent incapability of using conventional IP based protocols [1] due to increasing maintenance of IDs in global addressing schemes. This also causes avoidable overheads with respect to IDs since knowledge about the data from source node is quite critical and more important rather than knowing about the location from where the data has been sent [6]. Routing is quite complex with extended implementations of wireless sensor networks like MANETs where the nodes are characterized by random mobility in a continuous manner which require continuous monitoring and dynamic management of routing to ensure uninterrupted flow of data from source to destination irrespective of change in topology of network [7]. An essential phenomenon in routing is continuous monitoring the location of the nodes in the network, which becomes critical in cases of MANETs as discussed above. For every hop from source to destination or between member nodes the location of every node [8] [9] at that particular point of time determines the selection of next nearest node for transmission of packets of data. Bandwidth utilization [10] has to be optimal given a specific application, which can be assured by ensuring that the routing protocol takes into consideration the redundancy among sensor data collected from different nodes. This redundancy appears as any type of data collected from all sensor nodes adopts a similar methodology. Every routing algorithm is constrained by many bounds and limitations with respect to optimality in energy consumption of every node [11], the total energy consumed from source to destination [12], packet

drop ratio [4], and node lifetime issues [13], the storage and processing capabilities [14], of each node in the routing path, etc.

An energy aware routing algorithm has been implemented [3] by assuming that nodes in a network are equipped with global positioning system (GPS). Initially the nodes are deployed randomly, and after deployment all the sensor nodes inform the location information to the base station before the set -up phase and steady state phase. After the location information is collected in the base station, the network coverage area A is divided into groups A1, A2, A3, etc. The groups are created based on the location of the node and cluster head election probability p .The group's creation is done with the BS and does not guzzle too much energy. In each group a CH is selected randomly for each round, therefore the elected cluster heads are distributed uniformly in the network. Then each CH sends identity message to the group member nodes before starting the steady state phase. In steady state phase, all the CHs receive and aggregate the data from group member nodes as in LEACH but instead of directly sending the data to the base station. Therefore, CH reduces the radio communication distance. In the proposed LEACH the residual energy remains up to 460 rounds when compared to LEACH which remains only for 193 rounds because the modified LEACH distributes the energy equally among all nodes compared to LEACH. In the modified LEACH first node dies in 240th round and in LEACH the first node dead at 102 rounds.

By using cluster heads and data aggregation [4] excessive energy consumption is avoided. Wireless sensor networks are often placed in an open environment and are susceptible to various attacks. Traditional cryptography methods are not effective in WSNs. More the initial energy more will be the net lifetime of the network, as the number of live nodes will be more. Simulation and analytical results reveal that the Modified LEACH protocol [10] outperforms the traditional LEACH in every aspect. Major issues here are, cluster head (CH) selection, forming clusters scheme and a routing algorithm for the data transmission between cluster heads and the base station. The cluster formation is carried out by exchanging messages between member nodes and the cluster head. The key function of the cluster head is rotated at predefined interval to assure even distribution of energy among the sensor nodes. The routing is based on the flawless hauling range data transmission between base station and cluster heads using multi-hop. Its performance is figured out by comparing with LEACH routing protocol using MATLAB. The advantage of LEACH is that each node has the same probability to be a cluster head, which makes the energy dissipation of each node be relatively balanced. Assisted LEACH (A-LEACH) achieves lessened and uniform distribution of dissipated energy by separating the tasks of Routing and Data Aggregation. It tells the concept of Helper Nodes which contain Cluster Heads for Multi-hop Routing. The designs of Q-LEACH for homogeneous networks, which establish stability period, network lifetime by optimization. In this paper, we have given a brief review of these techniques.

Clustering in WSN is the process of dividing the nodes of WSN into groups, where each group agrees on a central node, called the Cluster Head (CH)[15], which is responsible for storing the sensory data of all group members, and sending to the Base Station (BS). Cluster based routing is an effective research area in wireless sensor networks. The classical LEACH protocol [13],[15] has many advantages in energy efficiency, data aggregation and so on. Assisted-Leach Protocol abbreviated as LEACH. In most of the clustering protocols, the whole load of data aggregation and data routing is done by cluster heads. LEACH protocol directly transmits aggregated data from cluster heads to the base station. This reduces the lifetime of a network. We the concept of Helper Nodes where a node closer to the base station in every cluster is assigned the routing job whereas cluster heads take care of data aggregation. We give a new idea for the route formulation for the helper nodes to

reach the base station. Every helper node chooses as the next hop, the node nearest to the base station from all its neighboring helper nodes. The good clustering algorithm cannot only reduce the energy consumption of the sensor nodes can also reduce communication interference, improve the efficiency of the MAC and routing protocols. Therefore, it is proposed that a highly efficient and stable rational algorithm has become an urgent need to solve the problem. In this paper, considering the residual energy for each node, a more efficient. After receipt this information, the base station calculates the average energy value of all nodes, the nodes with residual energy higher than average are considered as the candidate, then the base station will choose a group of cluster heads from the candidate using the simulated annealing to minimize the objective function. According to this Q leach sensor, nodes are implied in the territory. In order to acquire better clustering, we partition the network into four parts.

III. Q-LEACH PROTOCOL

In Q-LEACH, network is partitioned into sub-sectors and hence, clusters formed within these sub-sectors are more deterministic in nature. Therefore, nodes are well distributed within a specific cluster and results in efficient energy drainage. Concept of randomized clustering as is given for optimized energy drainage is applied in each sector. Assigning CH probability P = 0.05 we start clustering process. Q-LEACH is a routing protocol, which chains the advantage of both locations based routing protocol and hierarchical based routing protocol. The restricted flooding concepts are exploited in which nodes that are located closer to the destination or in a promoting zone broadcasts the packet. Distance and forwarding zone information are calculated at the individual nodes to decide their advancement towards the destination. These nodes will show the packets and the process is repeated at each midway node until it reaches the destination and also uses clustering procedures in which nodes are convened into the cluster and cluster head is dispensed to each cluster to execute the data combination and blending in order to diminish the energy consumed by nodes within the cluster.

The hierarchical based routing protocol which is a cluster based protocol is the best protocol to reduce the useful energy consumption. Clustering is the task of grouping a set of objects in such a way that objects in the same group are more similar to each other than to those in other groups. In WSN, nodes are grouped into clusters and each cluster has a cluster head. The nodes in a cluster do not directly communicate with base station instead they send their data to the cluster head and then the cluster head send the aggregated data to the base station. The Fig 4 shows a clustered WSN in which three clusters are formed and each cluster is having a cluster head

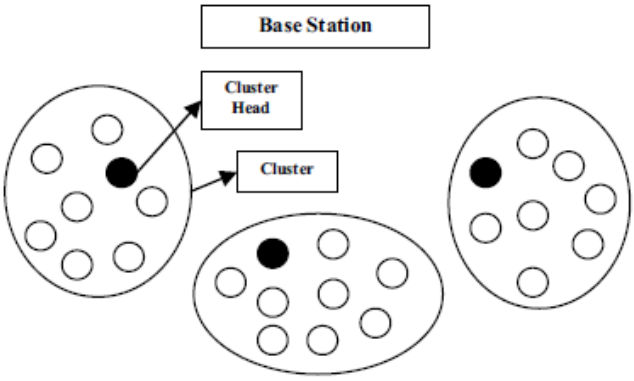

Figure 2. Cluster formations in LEACH

Sensor node form clusters and the cluster heads act as routers to the sink. This will save energy since the transmissions will only be done by Cluster Heads (CHs) rather than all sensor nodes. Optimal number of CHs is estimated to be 5% of the total number of nodes. In the LEACH protocol selection of cluster head is done in two phases.

A. Setup Phase

During the setup phase, each node generates a random number between 0 and 1. If the random number is smaller than the threshold value then that node becomes CH. The threshold value is calculated based on the following equation that is given below:

$$T(n) = \left\{ \frac{p}{1-p(r \bmod 1/p)} \right\}, if\ n \in G \quad (1)$$

Here p is the desired percentage of cluster heads and r is the current round, G is the group of nodes that has not been the CHs in the last rounds. The sensor node that is selected as a CH in previous round is not selected in the next rounds until all other nodes in the network become cluster heads.

B. Steady Phase

In the study phase, nodes send their data to the cluster head using a TDMA schedule. TDMA schedule allots time slots to every node. The CH aggregates the data and sends it to the base station (BS). In the Fig 4, sensor nodes are grouped to form clusters and each cluster is having a Cluster Head. The GA operators still can't stratify the optimization condition by desiring the optimal threshold value. The cluster head collects data from the nodes of its cluster is optimized, then it send the aggregated data to the base station. The nodes in the cluster do not directly communicate with the base station

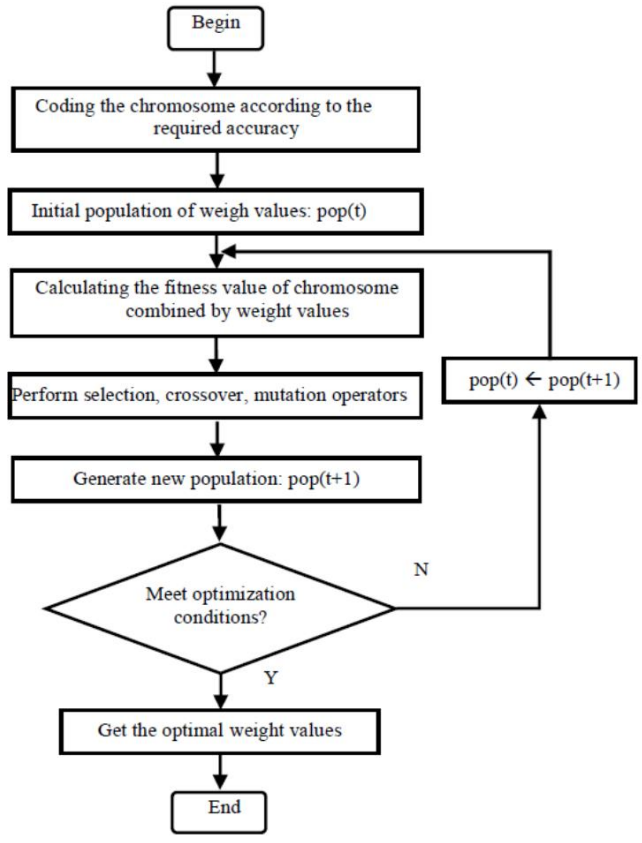

Figure 3. Flow chart of genetic algorithm for solving *wi*

Using genetic algorithm to determine the optimal solution of each weight value. In genetic algorithm [17], four parameters are presented. The size of the population pop_size = 50, cross probability pcro = 0.8, mutation probability pmut = 0.1 and weight accuracy of influence factors e = 0.001. The use of genetic algorithm for solving the wi process as shown in Fig.6, the specific operations as follows.

1) Coding the chromosome according to the required accuracy In the paper, set influence factor of the weight value accuracy e = 0.001 .Using binary encoding, solutions of weight value will be divided into (1 -- 0)* (1e + 3) equal portions .The length of gene string of weight value is calculated by the formula.

$$2^{m_i-1} < (1-0) * (1e+3) \le 2^{m_i} - 1 \quad (2)$$

The total length of a binary string combined by weight value is the length of an individual. And the total length of weight value chromosome is 30 in this paper.

2) Initial population of weight values By the size of the population and the length of the individual obtained in 1), the initial population of weights can be obtained.

3) Calculating the fitness value of chromosome combined by weight values. Before getting the fitness value of the individual, the encoding of the individual is needed to decode and the data is normalized. Fitness function determines the evolutionary process of genetic algorithm. In this paper, the performance of the network is evaluated jointly by the survival time of the first and half of nodes. Through repeated simulations and constantly modifying the fitness function, fitness function is eventually identified as formula

$$fitness = 0.7 * (FND - 50) + 0.3 * HND \quad (3)$$

Where FND is the lifetime of the first node, HND is the lifetime of the half of the nodes, represented by the number of rounds.

4) Perform selection, crossover and mutation operators

a) Selection Combine roulette wheel selection method and optimal individual preservation method in Q-LEACH. In roulette wheel selection method, chromosomes of high fitness values operate selection as a parent. The individual of the smallest fitness value is taken place by the historical best individual in the current population that can make the best individual into the next generation population.

b) Crossover Single potion cross is used in Q-LEACH, crossing the two neighboring individuals to generate more new individuals. If a cluster head node is crossed into an ordinary node, original cluster member nodes need to search a new cluster head.

c) Mutation Digit mutation is used in Q-LEACH, that is 0 to 1 or 1 to 0. 5) If the new weight value generated by GA operators still can't satisfy the optimization condition, then go to 3). Else draw the optimal weight values. After optimized by Genetic Algorithm, the individual with high fitness value corresponds to the first and half of the nodes.

IV. RESULTS AND DISCUSSION

In the proposed system, a fusion of LEACH is optimized by GA with first and half of the nodes and QDIR has been proposed in the form of Q-LEACH algorithm. It is a modification of the original LEACH algorithm where the behavior of the sensor nodes has been taken as an additional parameter and an evaluation formula modified accordingly. The degree of a node is computed based on its distance from others. A node x is considered to be a neighbor of another node y if x lies within the transmission range of y. Transmission range is the average distance of the all the nodes from the base-station.

Description of parameters used in the proposed algorithm

p	Probability of node to be a cluster head
$node\_distance\ (i)$	Distance of the ith node from base station
$S(i).xd, S(i)yd$	Location of the ith node
$sink.x, sink.y$	Location of the base station
$S(i).E$	Energy of the ith node
ETX	Transmit Energy
EDA	Data aggregation energy
$Efs, Eamp$	Transmit amplifier energy
$rmax$	Maximum number of rounds
$Eavg$	Average energy of the nodes
N	Number of nodes

The proposed algorithm is implemented in three steps, namely creation of network mode, assignment of initial energy and using the bubble sort algorithm based on distance metric of node to BS defined as

$$\text{node}_{\text{distance(i)}} = \sqrt{\text{S(i).xd} - (\text{sink.x}))\text{^} + (\text{S(i).yd} - (\text{sink.y}))\text{^}2} \quad (4)$$

Energy level in each cluster head is monitored using the pseudo code given below.

```
If (node_distance (i)>do)
S(i).E=S(i).E- ( (ETX+EDA)*(4000) +
        Emp*4000*(node_distance(i)*node_distance(i)*
        node_distance(i)*node_distance(i) ));
      Else
        S(i).E=S(i).E-  (  (ETX+EDA)*(4000)  +
        Efs*4000*( node_distance (i)* node_distance(i)
        ));
   For the next round r =1:1: rmax
     If (S(i).E >=Eavg) then
 i = nominee_clusterhead //nominated for cluster-
head selection
  Calculate node-degree of the chosen nominee for
cluster heads
      If (node_degree>=avg_degree)
                  If the neighborhood of the nominee
            cluster head is not a cluster head then
            i=cluster head  //cluster-head selected
         Dead node: if (S(i).E = 0) then
       Dead=i //ith node dies
     n=n-dead //n: decrease no of alive nodes
          Goto step-5
End
```

The following assumptions are taken into consideration.

- There exists only one base station and it is fixed at a far distance from the sensor nodes.
- The sensor nodes are homogeneous and energy constrained with uniform energy.
- Sensor nodes are immobile and all nodes are able to reach BS.
- The RAM size of each node must be sufficient enough to store the distance of the node from BS.
- The base station is situated at the center of the area space.

Parameters	Values
No. of nodes	100
Sink (base station)	50,50
Electric Energy	70nJ
Transmit amplifier energy	120pJ
Node distribution	Random
Data aggregation energy	5nJ
Initial energy	0.5
No. of rounds	1000

Table 1. The Numerical Parameter Settings for Experimentation Are Listed

According to this approach sensor, nodes are deployed in the territory and partitioned into four quadrants to improve the clustering process and thereby increase the network coverage. Additionally, the exact distribution of nodes in field is also well defined. Figure 5 describes the optimal approach of load distribution among sensor nodes.

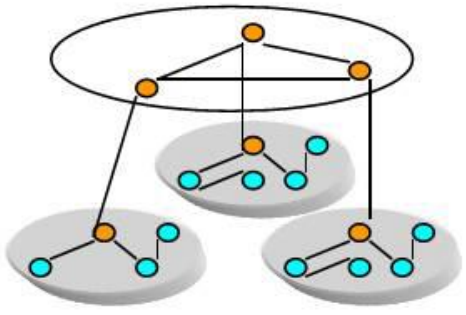

Figure 4. Structure of Clustered Wireless Sensor Network

Moreover, it also presents an idea of efficient clustering mechanism which yields significantly better coverage of whole network. We deployed random nodes in a 100m×100m filed. Based on location information, network is divided into four equal parts, i.e, (a1, a2, a3, a4). Defining overall network area as below:

$$A = a1 + a2 + a3 + a4 \quad (5)$$

$$a_n = A(x_m, y_m) \quad (6)$$

Where, n = 4, and m = 100. Hence, overall field is distributed as follows:

$$\lim^{ym=0:50}{}_{xm=0:50}\, a_n + \lim^{ym=0:50}{}_{xm=51:100}\, a_n + \lim^{ym=51:100}{}_{xm=0:50}\, a_n + \lim^{ym=51:100}{}_{xm=51:100}\, a_n \quad (7)$$

The partitioning of network into quadrants yields in efficient energy utilization of sensor nodes. Through this division optimum positions of CHs are defined. Moreover, transmission load of other sending nodes is also reduced. In conventional LEACH cluster are arbitrary in size and some of the cluster members are located far away. Due to this dynamic cluster formation, a farther node suffers through high energy drainage and thus, network performance degrades. Whereas, in Q-LEACH network is partitioned into sub-sectors and hence, clusters formed within these sub-sectors are more deterministic in nature. Therefore, nodes are well distributed within a specific cluster and results in efficient energy drainage. Concept of randomized clustering as is given for optimized energy drainage is applied in each sector. Assigning CH probability P = 0.05 we start clustering process. In every individual round nodes decides to become CH based upon and threshold T(n) given as:

Algorithm 1 Setup Phase

1: begin
2: **if** node εG −→ G =nodes which did not become CHs in current EPOCH **then**
3: **if** (NODE BELONGS TO ==_ areaA_) **then**

4: **if** (NUMBEROFCHs <= N/K_) **then**
5: TEMP=random number (0-1)
6: **if** (temp <= P
1–P(r,mod1/P)) **then**
7: node=CH A
8: NUMBER OF CHs = NUMBER OF CHs+1
9: **end if**
10: **else if** (NODE BELONGS TO ==_ areaB_) **then**
11: REPEAT STEP 4 : 8
12: **else if** (NODE BELONGS TO ==_ areaC_) **then**
13: REPEAT STEP 4 : 8
14: **else if** (NODE BELONGS TO ==_ areaD_) **then**
15: REPEAT STEP 4 : 8
16: **end if**
17: **end if**
18: **end if**

Algorithm 1 defines CHs selection mechanism. Overall network is divided into four areas as: Area A, B, C and D. Initially, each node decides whether or not to become a CH. The node chooses a random number between 0 and 1. If this number is less than certain threshold T(n), and condition for desired number of CHs in a specific area is not met, then the node becomes a CH. Similarly the same process continues for the rest of the sectors and optimum number of clusters is formed. Selection of clusters will depend upon receiving Signal Strength Indicator (RSSI) of advertisement.

The working principle is depicted in figure 6. After the decision of clusters, nodes must tell CHs about their association. On the basis of gathered information's from attached nodes, guaranteed time slots are allocated to nodes using Time Division Multiple Access (TDMA) approach. Moreover, this information is again broadcasted to sensor nodes in the cluster.

BS performs logical partitioning of network on the basis of gathered information's. The network is divided into four quadrants and broadcasts information to nodes. On the basis of threshold some nodes are elected as CH in each division. Normal nodes choose their CHs within their own quadrant based on RSSI. For association nodes send their requests to CHs. TDMA slots are assigned to every node for appropriate communication without congestion. Every node communicates in its allocated slot with its defined CH.

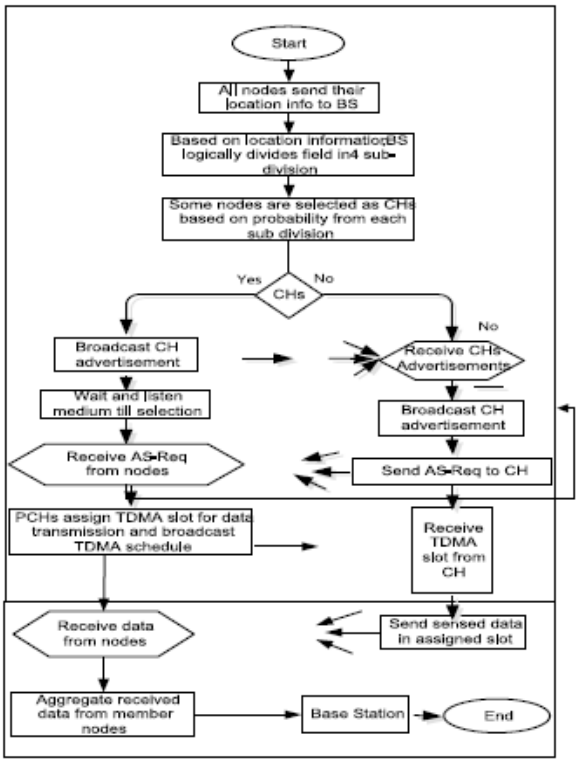

Figure 5. Working Principle of Q-LEACH

Algorithm 2 Node Association in Q-LEACH
1: N = Group of normal nodes
2: GC = Group of CHs
3: **if** N = (A, a1) **then**
4: Where
5: A = a1,a2,a3,a4
6: Check all possible ACHs
7: Check RSSI of CHs
8: Associate with ACHs
9: then
10: transfer of data occurs
11: **end if**
12: **if** N = (A, a2) **then**
13: Repeat step from 5 : 8 for BCHs
14: **end if**
15: **if** N = (A, a3) **then**
16: Repeat step from 5 : 8 for CCHs

17: **end if**
18: **if** N = (A, a4) **then**
19: Repeat step from 5 : 8 for DCHs
20: **end if**

Algorithm 2 defines the association of nodes with their appropriate CHs. Non-CHs nodes will locate themselves in specified area they belong to. Then they will search for all possible CHs, and on the basis of RSSI they will start an association. This process will continue until association phase comes to an end. Once a cluster setup phase is complete and nodes are assigned to TDMA slots every node communicates at its allocated time interval. A reset of the time radio of each non-cluster head node will remain off in order to optimize energy utilization. When all nodes data are received at the CHs then, the data is compressed and is sent to BS. The round completes and new selection of CHs will be initiated for the next round. In proposing idea, we implement above mentioned concept of localized coordination in each sector area. We used the same radio model as discussed for transmission and reception of information from sensor nodes to CHs and then to BS. Packet length K of 2000 bits is used in our simulations.

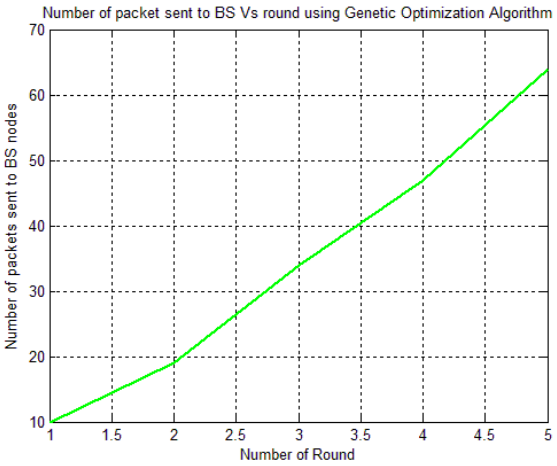

Figure 6. No of rounds vs no of packets send to the base station in LEACH protocol

A comparison of the number of packets sent to the BS in different rounds using different protocols using a genetic optimization algorithm is shown in figure 6. The life time of WSN depends upon the live nodes with respect to rounding. The number of those nodes is alive in each round during the simulation. The nodes are randomly deployed creating n number of groups named as clusters using genetic optimization with membership function. First of all, it is needed to choose a cluster head for each cluster of membership functions. From the sender node, the data are transmitted to the cluster head of different regions of genetic rule.

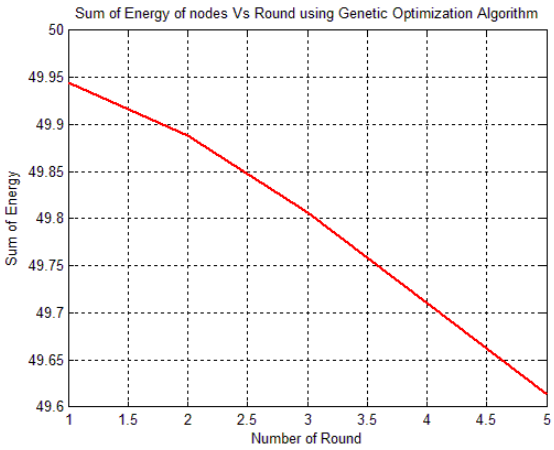

Figure 7. Sum of energy of nodes vs Round

The figure 7 shows that the sum of the energy of the nodes and rounds of LEACH protocol using a genetic optimization algorithm. In LEACH protocol, the sensor nodes in the WSN are randomly placed in the sensing area which can be regulated by base station using genetic algorithm. A sink node is present in the network that is placed near the base station. The entire sensor node has some and equal initial energy, each can transmit and receive data. Each node has storage capacity, but although we can harvest energy at the sensor node through ambient sources we ignore that part. In addition, the battery power at each node in the network can be regulated depending on its distance from the base station.

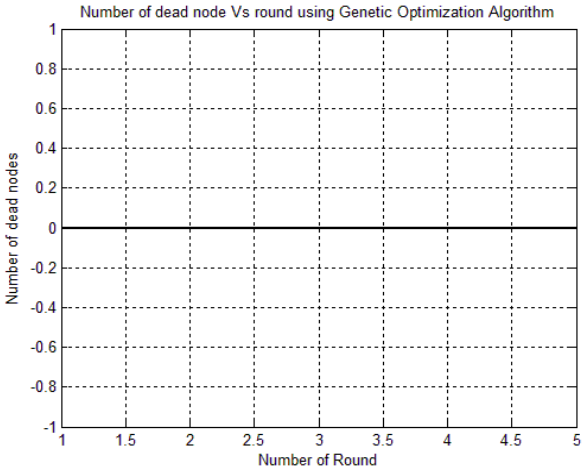

Figure 8. Dead Node Detection In LEACH Protocol

The genetic optimization algorithm is used to make the dead node as zero as shown in figure 9. The main concerns in WSNs are energy and network lifetime and there are many protocols introduce to overcome these concerns. LEACH with genetic optimization is an energy efficient protocol, which also prolong the network lifetime. But there is a drawback of this protocol that if the threshold is not reached, then there will be no communication and user will not come to know about dead nodes of network or all the nodes are dead in network. The genetic optimization rule is used to make the dead node zero.

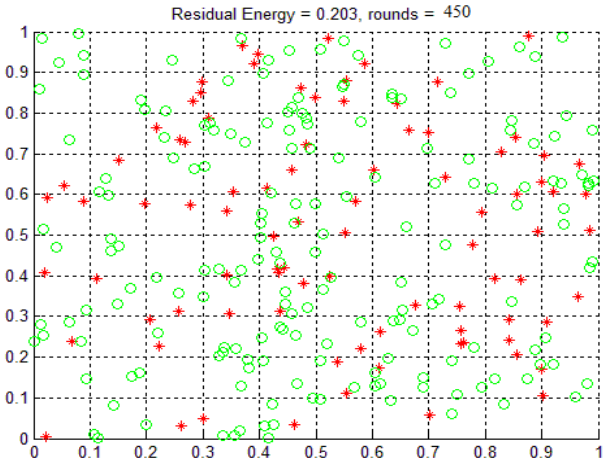

Figure 9. Residual Energy after Optimization

Figure 9. Shows the residual energy absorbed by the nodes and the nodes energy is optimized at the round of 450. The Cluster head's receive and aggregate the data from group member nodes as in Cluster but instead of directly sending the data to the base station that the remaining nodes be optimized and they get saturated by transferring the data to the cluster head. Therefore, CH reduces the radio communication distance. In the proposed LEACH the residual energy remains up to 460 rounds when compared to LEACH which remains only for 193 rounds because the modified LEACH distributes the energy equally among all nodes compared to LEACH.

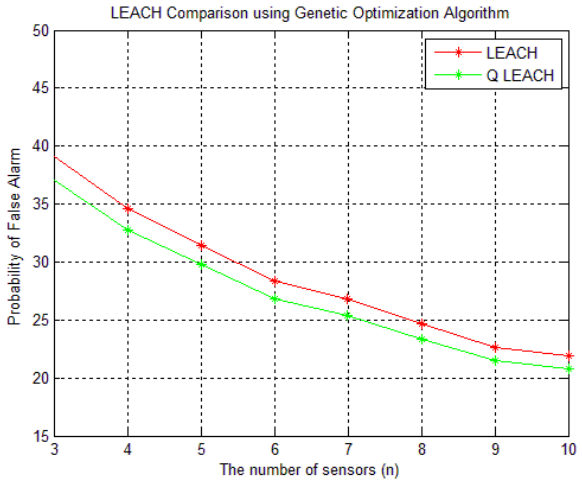

Figure 10. Comparison between the Present Method and the Proposed Method

The Figure 10. Shows the comparison between the present method and the proposed method of LEACH by using GA. In that the Proposed method Q-Leach the false alarm get reduced even though previous method also negligible, if using genetic algorithm but in Q-leach the number round increases the lifetime of the sensors and the false alarm of the node get reduced even more number of sensors node increases. The life time of the sensors node is increases compare with the LEACH by using GA in Q-leach due to energy optimized.

V. CONCLUSION

An efficient fusion routing protocol Q LEACH has been proposed and experimented in this research paper. The routing protocol works on a finite cluster based approach where any given WSN network under investigation is segmented into four quadrants with clusters being formulated in each quadrant. Clusters are formed within each of these quadrants and cluster

head is allotted to each cluster. The cluster heads in each quadrant play a centralized role of coordinating the route discovery and route maintenance to ensure smooth packet forwarding to the next nearest cluster from source to destination. A localized broadcasting strategy is employed within the nodes of the cluster by RREQ prior to determination of shortest path. Thy hybrid routing algorithm is achieved by fusion of conventional LEACH and Q – DIR to form QLEACH and experimental results justify the superior performance of proposed Genetic algorithm in terms of energy consumption and network lifetime. The main aim of this work is to enhance existing protocol such that more robust and optimized results can be achieved. Q-LEACH significantly improves network parameters and seems to be an attractive choice for WSNs by extending and enhancing overall network quality parameters.

VI. REFERENCES

[1] Jihye Kim, Gene Tsudik (2009), "SRDP: Secure route discovery for dynamic source routing in MANET's", Ad Hoc Networks, 7(6): 1097-1109.

[2] Jin R, T. Gao, J. Song, J. Zou and L. Wang (2013), "Passive cluster-based multipath routing protocol for wireless sensor networks", Wireless Networks, 19(8):1851-1866.

[3] Mohanty P and M Kabat M (2016), "Energy Efficient Reliable Multi-path Data Transmission in WSN for Healthcare Application", International Journal of Wireless Information Networks, 23(2):162-172.

[4] Chao C, I. Li, C. Yang and J. Li (2011), "An efficient diversity-driven selective forwarding approach for replicated data queries in wireless sensor networks", Journal of Systems Architecture, 57(9):830-839.

[5] Liu A, Z. Zheng, C. Zhang, Z. Chen and X. Shen (2012), "Secure and Energy-Efficient Disjoint Multipath Routing for WSNs", IEEE Transactions on Vehicular Technology, 61(7): 3255 - 3265.

[6] Kadri B, Moussaoui D, Feham M (2012), "An efficient key management scheme for hierarchical wireless sensor networks", Wireless Sensor Network, 4(6):155 – 161.

[7] Zhao L and Hong Z (2011), "Improved DV-Hop Localization Algorithm Based on Wireless Sensor Networks", Journal of Computer Applications, 31(5): 1189-1192.

[8] Jubin Sebastian E, Sreeraj V.R and Tauheed U Islam (2012), " Location Based Opportunistic Routing Protocol for Mobile Ad Hoc Networks", American Journal of Engineering Research, 1(1):16 - 21.

[9] Ahn, C.W., Ramakrishna, R.S. (2002), "A genetic algorithm for shortest path routing problem and the sizing of populations", IEEE Transactions on Evolutionary Computing, 6(6): 566–579.

[10] Ravneet Kaur, Deepika Sharma, Navdeep Kaur (2013), "Comparative analysis of LEACH and its descendants protocols in wireless sensor network", International journal of P2P network trends and technology, 3(1):22- 27.

[11] Shalli Rani, Jyoteesh Malhotra, Rajneesh Talwar (2013), " EEICCP—Energy Efficient Protocol for Wireless Sensor Networks", Wireless Sensor Network, 5:127-136.

[12] Doshi S, S. Bhandare, and T.X. Brown (2002), "An On-Demand Minimum Energy Routing Protocol for a Wireless Ad Hoc Network", ACM Mobile Computing and Comm. Reviews, 6(3):50 - 66.

[13] Zhao Y, Wu L, Li F, Lu S (2012), "On maximizing the lifetime of wireless sensor networks using virtual backbone scheduling", Transactions on parallel and distributed processing, 23:1528 – 1535.

[14] Ren J, Y. Zhang, K. Zhang and X. Shen (2016), "Adaptive and Channel-Aware Detection of Selective Forwarding Attacks in Wireless Sensor Networks", IEEE Transactions on Wireless Communications, 15(5): 3718-3731.

[15] Dehghani, Shahrzad, Mohammad Pourzaferani, and BehrangBarekatain (2015), "Comparison on Energy-efficient Cluster Based Routing Algorithms in Wireless Sensor Network", Procedia Computer Science, 72:535-542.

[16] Jin R, T. Gao, J. Song, J. Zou and L. Wang (2013), "Passive cluster-based multipath routing protocol for wireless sensor networks", Wireless Networks, 19(8):1851-1866.

[17] Yu Z, Bo J, Zhou Y. An Improved LEACH Routing Protocol Based on Genetic Algorithms for Wireless Sensor Network[J]. Journal of Computer Research and Development, 2010: S2.

Themed Section : Engineering and Technology
© 2018 IJSRSET | Volume 5 | Issue 3 | Print ISSN: 2395-1990 | Online ISSN : 2394-4099

Performance of Rectangular Microstrip Patch Antenna in Two Different Design Tools - A Comparative Study

E. Aravindraj[1], A. Kannan[2], Dr. K. Ayyappan[3],
[123]Department of ECE, Rajiv Gandhi College of Engg & Tech, Puducherry, India
aravindrtaj1794@gmail.com[1], kannanalagu@gmail.com[2], ayyapppan_ece@rgcetpdy.ac.in[3]

ABSTRACT

In this comparative study, Two antenna designing tools where compared each other to get appropriate output for the calculated design parameters. Here, there are four different rectangular microstrip patch antennas (RMPA) has been designed for four different frequencies like 2.4 GHz, 3.5 GHz, 5.2 GHz and 5.8 GHz separately using two different antenna design tools like Advanced design software (ADS) and High Frequency simulator software (HFSS). Flame Retardant (FR4) is used as the dielectric material with microstrip feed to the rectangular patch. The comparison is based on the variations obtained in the design parameters like length, width and height and their respective simulation parameters. Hence, by comparing the design parameters and simulation parameters obtained for the operating frequencies with both the tool, it has been concluded that which tools can work efficiently with accuracy. Thus, this paper provides t a clear opinion about which tool is suitable for getting appropriate simulation results for the corresponding calculated design values.

Keywords— Rectangular Microstrip patch antenna (RMPA), FR-4 substrate, Ground Plane, Microstrip feed, ADS and HFSS.

I. INTRODUCTION

Rectangular Microstrip Patch Antenna is a smaller in size, less in cost, lighter in weight. It can be integrated with many types of feeds. But, it has major limitations like low gain, less efficient, narrow bandwidth, etc [1]. MPA has become very widespread in mobile applications. It is increasingly more useful because it can be printed in the circuit board itself. It is also used in several wireless applications [2]. Permittivity of dielectric and its thickness will regulate the MPA. Thick substrates with less dielectric constant are used to increase the bandwidth and antenna efficiency, but the element size will be larger which difficult during portability. FR-4 is a composite material with low cost, high mechanical strength, reliability and convenient availability [3] [4]. It provides an actual value for high frequency.

Here, there are four different ISM band frequencies such as 2.4 GHz, 3.5 GHz, 5.2 GHz and 5.8 GHz are taken under account. The design parameters are calculated using pre-defined antenna design formulae and with the same design parameters antennas have been designed by two popular design software. Hence, from the calculated design values the RMPA are designed with slight changes made in the dimensions to get appropriate output for the corresponding frequency have obtained for the antenna design [5]. There are many different antenna designing software have been evolved such as Zeland's IE3D, Ansoft HFSS, Microwave studio CST, ADS, FEKO and Antenna Magus. From this list, there are two different tools like High Frequency

simulator software and Advanced Design System have been taken for comparison. Advanced Design System (ADS) is used in designing RF electronic, microwave Simulations and in digital applications with high speed.

MPA are used widely because of its robustness and compact to environment. This antenna design will provide a preferable impedance matching through microstrip feeding technique between the patch and the transmission line. It provides an extensive set of projects to demonstrate in designing various projects. It also provides platform for design the circuit and the antenna design. ADS has a affordable features such as maintaining a single source of design and reducing disk space by sharing designs [6]. High frequency simulator software (HFSS) has more advancement in 3D EM software used in designing antenna and complex RF electronic circuits. This level of analysis can give design sensitivity, performance and market with confidence in results [7]. It provides good designing properties in three-dimensional structure. Some key features for HFSS are designing and analysing the element, integrated on design with automated process with a linear circuits design.

II. ANTENNA DESIGN PARAMETERS

The operational antenna is made using the measurements obtained using the pre-defined antenna design formulae equations for calculating the by the patch, substrate and ground plane. The optimized design consists of a 0.04mm thicker microstrip patch and ground plane with substrate element placed in centre of the ground plane and the patch which has a thickness of 1.6mm denotes the geometric size of the antennas. Thus, these all combined together to make an efficient antenna design [8] [9]. The calculated size of the antenna varies while applying it into a structural design. Since, there will be an optimal value for the structural design which provides good output parameters for the design. Hereby, the design and geometry of the system has been explained below

A. Rectangular Microstrip Patch

The proposed design is a RMPA designed using ADS and HFSS tools as shown in Fig. 1 and Fig. 2. These rectangular patches have different dimensions according to the radiating frequency to which it is designed for. The mathematical value of 2.4 GHz operating frequency is 30x38x0.04mm for 2.4 GHz. In ADS tool, it is optimized as 33x45x0.04mm. In HFSS tool, it is 30x38x0.04mm.

The simulations are made for the designed antennas using ADS and HFSS software. Thus, the difference in the antenna design parameters and the output parameters are compared.

B. Substrate and Ground Plane

FR-4 is an electrical insulator with dielectric constant ($\varepsilon_r = 4.4$). Compared to other type of substrates FR-4 provides good parametric outputs. The characteristics of the FR-4 substrate provide a good mechanical strength and reliability [11]. FR-4 is used in the PCB boards, relays and switches. The height of the FR-4 substrate is considered as 1.6 mm. The height and the dielectric constant desire the geometric size of the antenna. The calculation of antenna design for the operating frequency (f_r =2.4 GHz, 3.5 GHz, 5.2 GHz and 5.8 GHz) is explained as follows [10] [11].

Patch Width (W): $$W = \frac{C}{2f_r}\sqrt{\frac{2}{\varepsilon_r}} \quad (1)$$

Where, c - Velocity of light
Effective Dielectric Constant (ε_{reff}):

$$\varepsilon_{reff} = \frac{\varepsilon_r+1}{2} + \frac{\varepsilon_r-1}{2}\left(1+\frac{12h}{W}\right)^{-1/2} \quad (2)$$

Patch Length Extension (ΔL):

$$\Delta L = 0.412h\left(\frac{\varepsilon_{reff}+0.3}{\varepsilon_{reff}-0.258}\right)\left(\frac{\frac{W}{h}+0.264}{\frac{W}{h}+0.8}\right) \quad (3)$$

Effective Patch Length (L_{eff}):

$$L_{eff} = \frac{c}{2f_r\sqrt{\varepsilon_{reff}}} \quad (4)$$

Patch Length (L):

$$L = L_{eff} - 2\Delta L \quad (5)$$

Substrate Width(W_s), Ground plane width(W_g):

$$W_s = W_g = 6h + W \quad (6)$$

Ground Plane length (L_g), Substrate length (L_s):

$$L_s = L_g = 6h + L \quad (7)$$

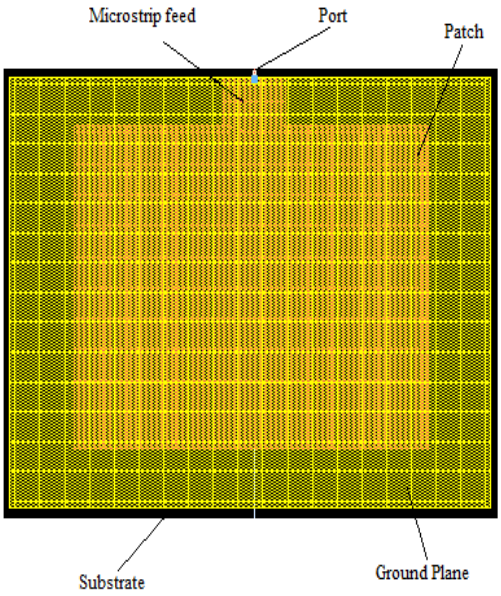

Figure 1. Design of Rectangular Microstrip Patch Antenna Using ADS Software

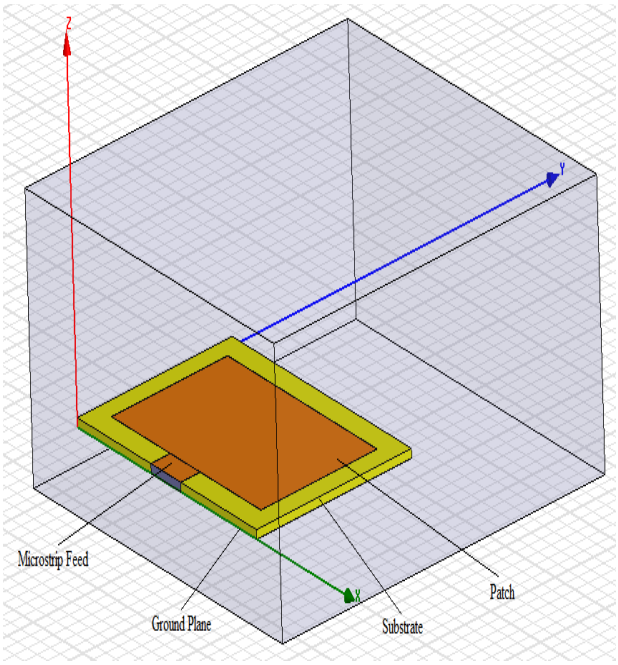

Figure 2. Design of Rectangular microstrip patch antenna using HFSS software

III. SIMULATION PARAMETERS AND RESULTS

The optimization antenna designs are simulated using ADS and HFSS software which provides a good platform for presenting the work effectively. The simulated antenna parameter shows that the antenna perfectly radiates at the ISM band of frequencies such as 2.4 GHz, 3.5 GHz, 5.2 GHz and 5.8 GHz [12]. But, the calculated values and optimization value slightly vary for the software design.

A. Simulation Parameters

The Table I shows the calculated value and the optimized values of the antenna design for the four different frequencies such as 2.4 GHz, 3.5 GHz, 5.2 GHz and 5.8 GHz. The HFSS software provides good simulation parameters with an optimized value which is almost equal to the optimized value. Compared to HFSS software, ADS provides design

Design Parameters	Calculated value in mm				Optimized value of ADS in mm				Optimized value of HFSS in mm			
	2.4 GHz	3.5 GHz	5.2 GHz	5.8 GHz	2.4 GHz	3.5 GHz	5.2 GHz	5.8 GHz	2.4 GHz	3.5 GHz	5.2 GHz	5.8 GHz
Patch Length(L)	30	20	12	11	33	24	15	12	30	20	13	11.6
Patch Width (W)	38	26	17	15	45	32	20	17	38	26	17	15.7
Patch Thick (t)	0.04	0.04	0.04	0.04	0.04	0.04	0.04	0.04	0.04	0.04	0.04	0.04
Substrate Length (L_s)	39	29	21	20	44	36.2	26	23	40	30	23	21.4
Substrate Width (W_s)	47	35	26	24	59	45	29	27	48	36	27	25.3
Substrate Height (h)	1.6	1.6	1.6	1.6	1.6	1.6	1.6	1.6	1.6	1.6	1.6	1.6
Ground Length (L_g)	39	29	21	20	44	36.2	26	23	40	30	23	21.4
Ground Width (W_g)	47	35	26	24	59	45	29	27	48	36	27	25.3
Ground Thick (t)	0.04	0.04	0.04	0.04	0.04	0.04	0.04	0.04	0.04	0.04	0.04	0.04

Table .1 Calculated and Optimized values of design parameters for ADS and HFSS software

parameters which slightly vary from the calculated value. The simulation parameters like Return loss and Bandwidth obtained from the proposed design is explained as:

1) **Return Loss**

The return loss is the loss of power due to the reflection of radiated signal from the obstacle which also affects the other signals radiated by the antenna. The Fig. 3a, 4a, 5a and 6a denotes the return loss value achieved by the ADS software. The Fig. 3b, 4b, 5b and 6b represents the return loss value of the designed antennas obtained the simulation made in HFSS software.

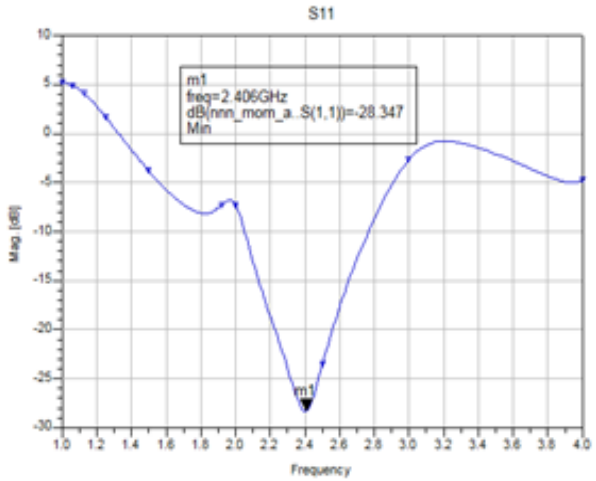

Figure 3(a). Return loss for 2.4 GHz using ADS

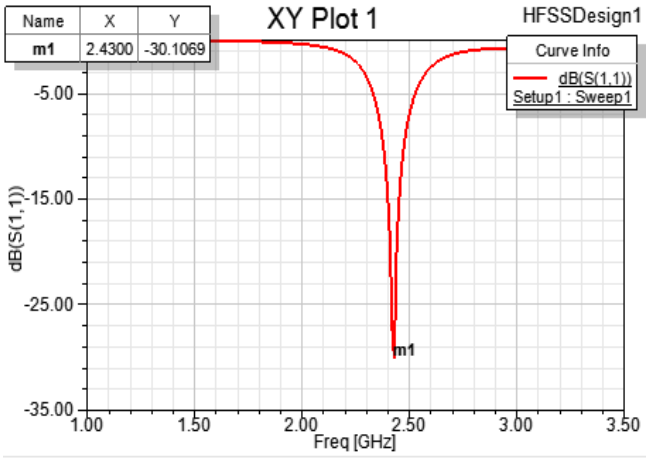

Figure 3(b). Return loss for 2.4 GHz using HFSS

The value of return loss in the antenna design for 2.4 GHz using ADS software is -28.347 dB as in fig. 3a. The return loss value obtained for 2.4 GHz operating frequency using HFSS Software is -30.16 as in fig. 3b.

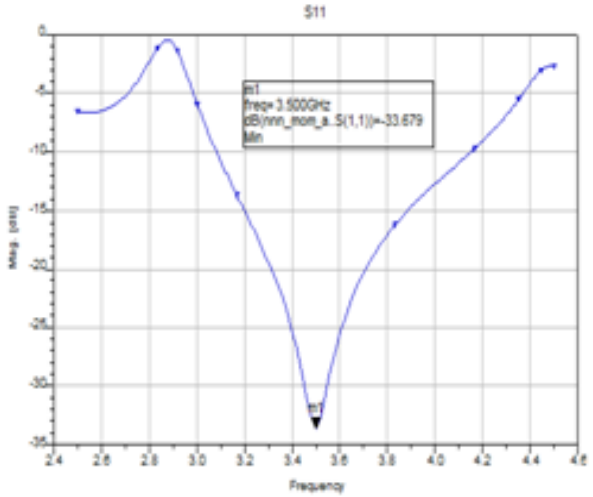

Figure 4(a). Return loss for 3.5 GHz using ADS

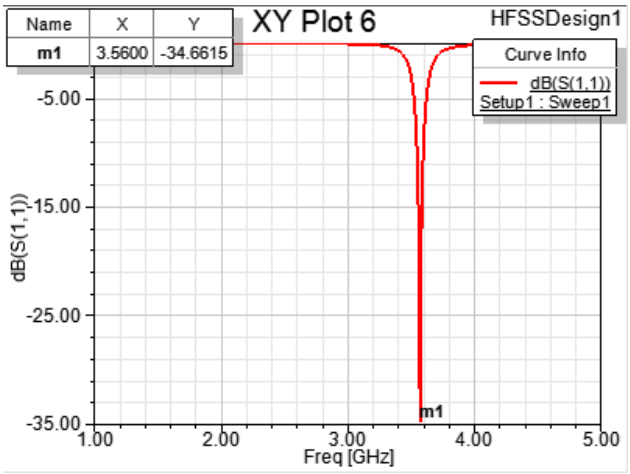

Figure 4(b). Return loss for 3.5 GHz using HFSS

The return loss for the operating frequency 3.5 GHz in ADS and HFSS software are shown in the Fig.4a and b respectively. Since, the return loss value in ADS and HFSS tool is -33.679dB and -34.66dB.

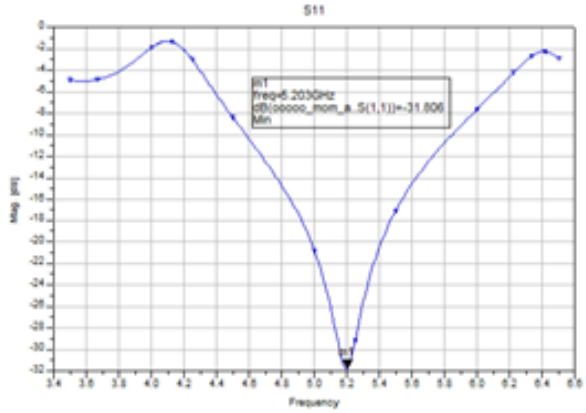

Figure 5(a). Return loss for 5.2 GHz using ADS

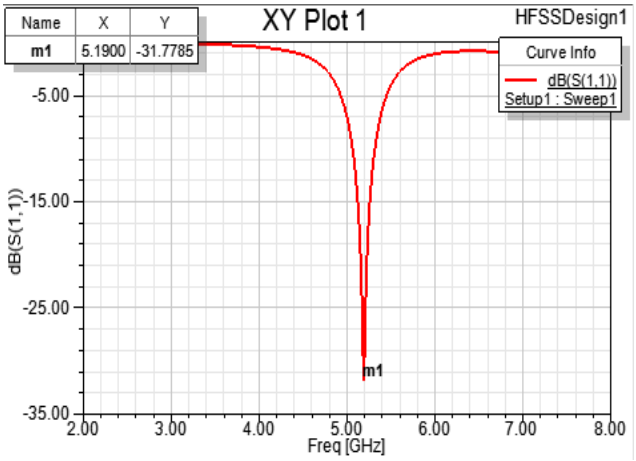

Figure 5(b). Return loss for 5.2 GHz using HFSS

As shown in Fig 5a and 5b, the return loss value for 5.2 GHz operating frequency in ADS and HFSS tool is -31.806dB and -31.776dB respectively

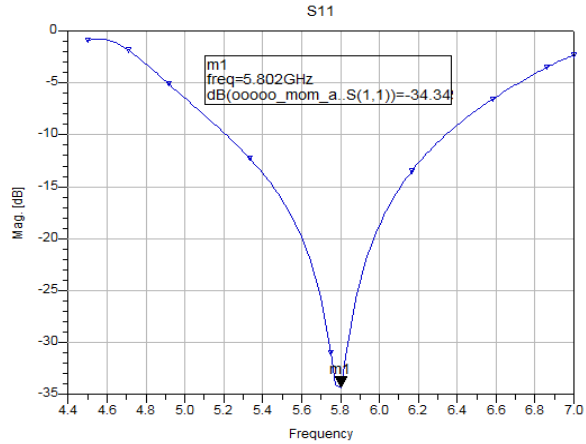

Figure 6(a). Return loss for 5.8 GHz using ADS

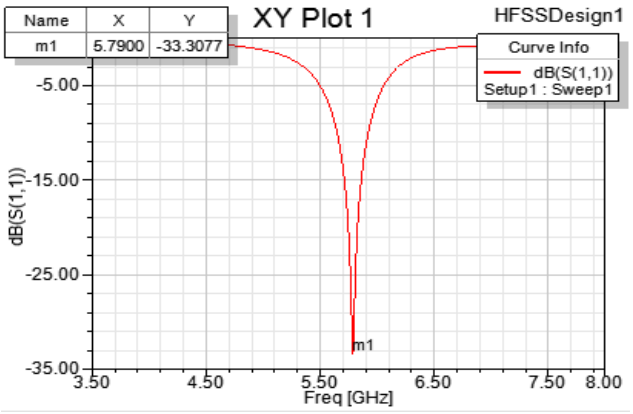

Figure 6(b). Return loss for 5.8 GHz using HFSS

The return loss value of the RMPA design using HFSS software is -33.30dB for 5.8 GHz and -34.34 dB using ADS.

2) **Bandwidth**

Bandwidth is the frequency range where the designed antenna radiates properly. The fig. 7a, 8a, 9a, 10a, 11a and fig. 7b, 8b, 9b, 10b, 11b shows the bandwidth range of the antenna design made by ADS and HFSS software respectively.

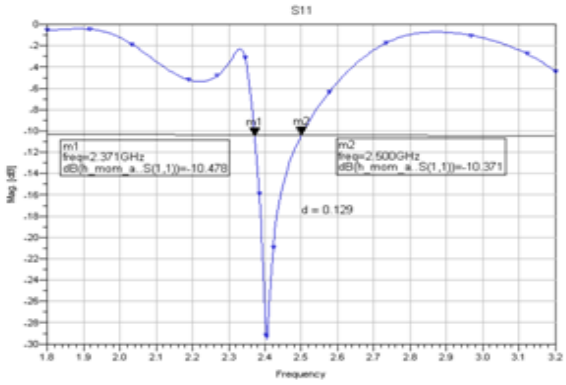

Figure 7 (a). Bandwidth for 2.4 GHz using ADS

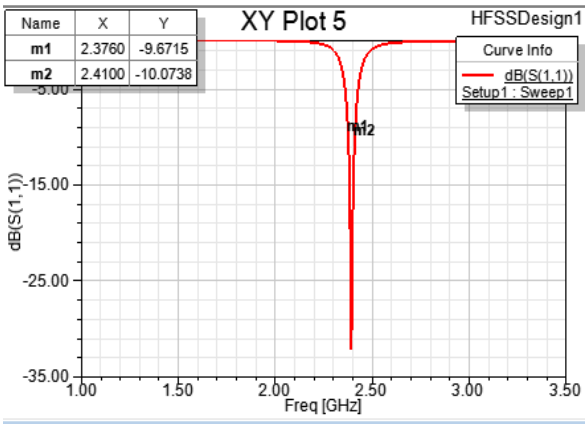

Figure 7(b). Bandwidth for 2.4 GHz using HFSS

The Bandwidth value obtained for 2.4 GHz operating frequency using HFSS Software is 90 MHz as in fig. 7b. The Bandwidth value of the antenna design for 2.4 GHz using ADS software is 130 MHz as in fig 7a.

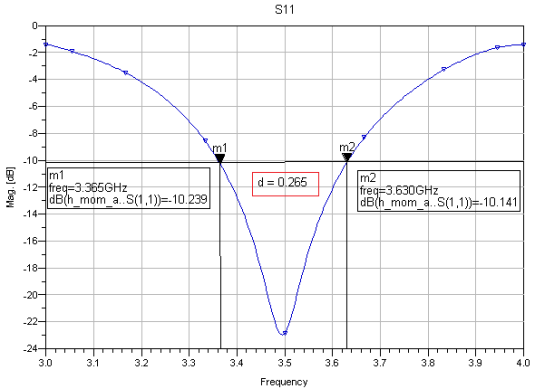

Figure 8(a). Bandwidth for 3.5 GHz using ADS

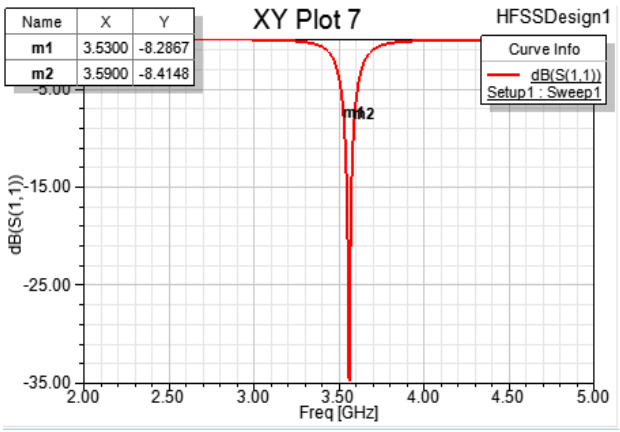

Figure 8(b). Bandwidth for 3.5 GHz using HFSS

The Bandwidth of the operating frequency 3.5 GHz in ADS and HFSS software are shown in the Fig.8a and b respectively. Since, the return loss value in ADS and HFSS tool is 265 MHz and 120 MHz.

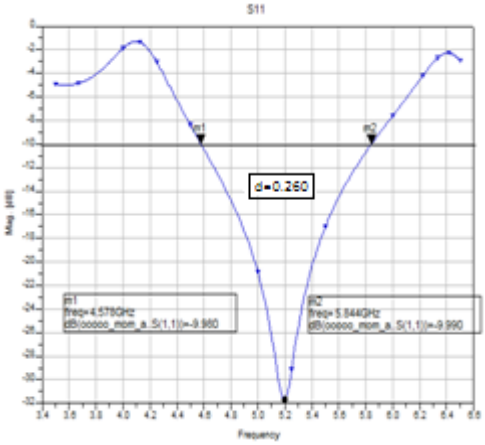

Figure 9(a). Bandwidth for 5.2 GHz using ADS

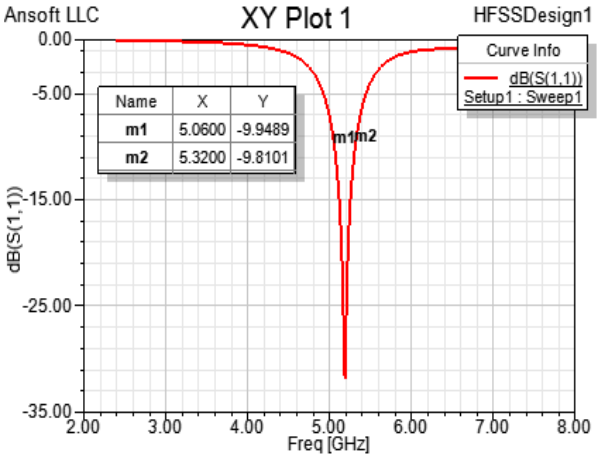

Figure 9(b). Bandwidth for 5.2 GHz using HFSS

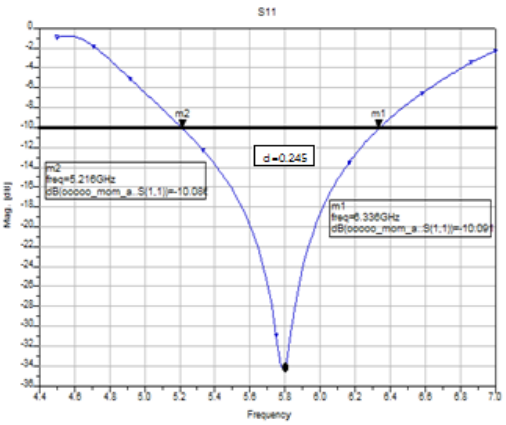

Figure 10(a). Bandwidth for 5.8 GHz using ADS

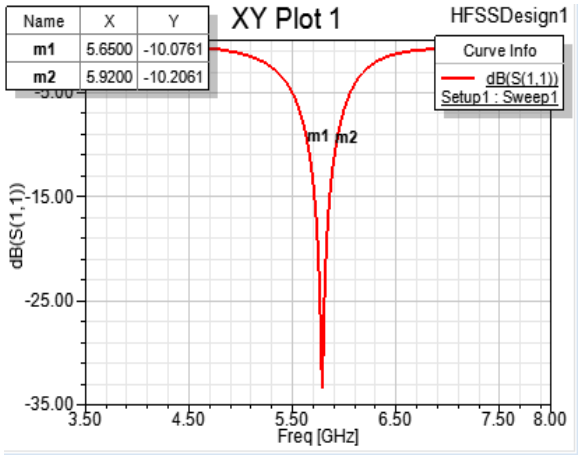

Figure 10(b). Bandwidth for 5.8 GHz using HFSS

As shown in Fig. 9a and b, Bandwidth value for 5.2 GHz operating frequency in ADS and HFSS tool is 260 MHz and 120 MHz respectively. The Bandwidth value of the RMPA design using ADS and HFSS software is 245 MHz and 170 MHz for 5.8 GHz as in fig. 10a and 10b.

B. Simulation Results

The antenna simulation parameters explained above are tabulated in Table II. The simulation results are obtained by using the ADS and HFSS software which provides the platform for preparing the RMPA. The proposed antenna provides good antenna parameters for all four operating frequencies.

Frequency (GHz)	Return loss (dB)		Bandwidth (MHz)	
	ADS	HFSS	ADS	HFSS
2.4 GHz	-28.34	-30.10	130	90
3.5 GHz	-33.67	-34.66	265	120
5.2 GHz	-31.80	-31.77	260	150
5.8 GHz	-34.34	-33.30	245	170

Table II. Simulation output obtained by ADS and HFSS software

IV. CONCLUSION

A RMPA designed for the given operation frequencies provides a good simulation parameter in both the software. The Advanced design software (ADS) and High frequency simulator software (HFSS) gives a good platform to design an antenna structure. Here, HFSS provides the output with the design parameters which are obtained from the design formula. Since, the calculated and the optimized value of the antenna design is nearly the same. But the ADS tool needs some changes in the design parameters of the antenna which varies from the calculated values. Thus, this paper concludes that the both the tools provides an efficient simulation parameters but taking design parameter under account HFSS tool provides accurate design for an operating frequency.

V. REFERENCES

[1] A. S. U. Constantine and A. Balanis, "Antenna Theory: Analysis and Design", *3rd ed: John Wiley& Sons, Inc*, pp. 811-882.

[2] T. Jayachitra, V.K Pandey and Anshuman Singh, "Design of Microstrip Patch Antenna for WLAN Applications," *International Journal of Advanced Research in Electrical, Electronics and Instrumentation Engineering*, Vol. 3, Special Issue 3, April 2014.

[3] A. A. Qureshi, M. U. Afzal, T. Taqueer and M. A. Tarar, "Performance Analysis of FR-4 Substrate for High Frequency Microstrip Antennas", *China-Japan Joint Microwave Conference*, Vol. 5, May 2011.

[4] Kiran Jain and Keshav Gupta, "Different Substrates Use in Microstrip Patch Antenna-A Survey", *International Journal of Science and Research*, ISSN 2319-7064, May 2014.

[5] Pradeep Kumar, Neha Thakur and Aman Sanghi, "Micro strip Patch Antenna for 2.4 GHz Wireless Applications", *International Journal of Engineering Trends and Technology,* Vol. 4, Issue 8, August 2013.

[6] E. Aravindraj and Dr. K. Ayyappan, "Design of slotted H-shaped patch antenna with dumbbell shaped DGS for 3.5 GHz WiMAX applications", *Indian Journal of Innovations and Developments*, Vol .5, no.2, February 2016.

[7] Ogunlade Michael Adegoke, Ismael Saad Eltoum, "Analysis and Design of Rectangular Microstrip Patch Antenna AT 2.4Ghz WLAN Applications", *International Journal of Engineering Research & Technology (IJERT*), Vol. 3 Issue 8, August – 2014.

[8] Muhammad Aamir Afridi, "Microstrip Patch Antenna − Designing at 2.4 GHz Frequency", *Biological and Chemical Research*, March 2015.

[9] Pradeep Kumar Sharma, Ritesh Saraswat and Jitendra Jangir, "Performance Analysis of Square Shaped Microstrip Patch Antenna For S Band Application", *International Journal of Modern Trends in Engineering and Research,* Vol. 03, Issue 10, October 2016.

[10] Ramesh Garg and Prakash Bhartia, Inder Bahl, "Microstrip Antenna Design Handbook", *Second Edition*, 1998.

[11] Vikram Thakur and Sanjeev Kashyap, "A Review Paper on Techniques and Design for Microstrip Patch Antenna", *International Journal of Advanced Research in Electrical, Electronics and Instrumentation Engineering*, Vol. 4, Issue 2, February 2015.

[12] E. Aravindraj and Dr. K. Ayyappan, " Survey on slotted H-shaped MPA design for different ISM band radio frequencies," *Indian Journal of Innovations and Developments*, Vol. 5, no.3, March, 2016.

[13] Hashibul Alam, "Design of rectangular microstrip patch antenna for IEEE 802.1503a (WPAN) with MB_OFDM ultra wide band communication system", *International Journal of Scientific and Research Publications*, Vol. 4, Issue 2, February 2014.

[14] Gyanender Kumar, Charanjeet Singh and Deepender Dabas, "Design and Simulation of Microstrip Patch Antenna for Wireless Communication", *International Journal of Engineering and Computer Science*, Vol. 3 Issue 5, May 2014.

Themed Section : Engineering and Technology
© 2018 IJSRSET | Volume 5 | Issue 3 | Print ISSN: 2395-1990 | Online ISSN: 2394-4099

Circuits for Digital Modulation Applications

Atul Kumar Varshney[1], Vipul Sharma[2]

[12]ECE Department, Faculty of Engineering and Technology, Gurukula Kangri Viswavidhyalyaya, Haridwar (U.K.), India

260984atul@gmail.com[1],vipul.s@rediffmail.com[2]

ABSTRACT

In this paper, some circuits for digital modulation applications circuits are performed using an IC and few components on project board. For generation of these circuits for digital communication modulation application experiments, various costly, heavy-weighted and tedious circuits and devices have been discovered and are available. This paper presents a very economic, light-weighted and simple circuits, those uses one or two LF 398 IC, LM 741 IC and a single resistor and/ or capacitor for generation of PAM, natural sampling, flat-top sampling, sample and hold, PAM-TDM, PWM, ASK, FSK & PSK modulation against conventional transistor based methods. Tested hardware circuits and their resultant observed waveforms have been included that justify behavior of the hardware circuitry. Laboratory implementation of digital modulation applications have been presented in this work.

Keywords: LF 398 IC, PAM, PWM, Natural Sampling, Flat-Top Sampling, Sample and Hold, PAM-TDM, ASK, FSK & PSK

I. INTRODUCTION

Analog signals, such as music, are often converted to, and stored in, digital form. To do this, the analog signal is periodically *sampled* (its instantaneous value is acquired by a circuit), and that constant value then hold and is converted to a digital word. For example, music signals are often sampled at 44 kHz, which means there are just a bit more than 20 microseconds available to sample, hold, and then convert the sampled value to a digital word. Then, the whole process of sample/hold/convert happens again. So, any type of analog-to-digital converter must contain, or be preceded by, a circuit which holds the voltage at the input to the ADC converter constant during the entire conversion time. Conversion times varied widely from nanoseconds (for flash ADCs) to microseconds (for successive approximation ADCs) to hundreds of milliseconds (for dual-slope integrator ADCs). In sample and hold experiment we will use a sample and hold integrated circuit, controlled by an external clock (square wave) signal, and observe its output for a variety of input signals. In addition, the *droop rate* of the sample and hold IC will be measured with different values of hold capacitor.

In natural sampling and flat top sampling experiments, the properties and limitations of the sampling theorem were investigated. Specific sampling circuits have been constructed and tested using a variety of input signals and sampling signals.

Modulation is the process by which some characteristics of the high frequency carrier is varied in accordance with a low frequency modulating message signal [1].

In Pulse amplitude modulation (PAM) experiment amplitude of square wave pulse is varied in accordance with sinusoidal message signal. A specific PAM circuit has been constructed and tested using a variety of input message signals and square wave carrier frequencies [1, 7, 8, 9, 10, 15].

In Pulse width modulation (PWM) experiment width or duration of square wave pulse is varied in accordance with sinusoidal message signal. A specific PAM circuit has been constructed and tested using a variety of input message signals and square wave pulse frequencies [1, 7, 8, 9, 10, 15].

In pulse amplitude modulation time division multiplexing (PAM-TDM) experiment variety of input signal combinations has been chosen and tested on hardware [7, 8].

In digital communications, the modulating wave consists of stream of binary digits or an M-ary encoded version of it. High frequency sinusoidal is best choice for carrier [9]. The modulation process involves switches or keying the amplitude, frequency, or phase in accordance with the incoming binary data. The result of this modulation process is amplitude shift keying (ASK), frequency shift keying (FSK), or phase shift keying (PSK), respectively [1, 7, 9]. PSK and FSK signals are much more widely used than ASK signals in microwave radio links and satellite channels because PSK and FSK modulations have constant envelope and do not have any amplitude nonlinearity [4, 10]. Numerous costly, heavy-weighted and tedious kit based circuits and devices have been discovered and are available for generation of these digital shifts keying techniques. This paper demonstrates a very economic, portable and simplest tested circuits using a single LF 398 IC [5] and a single 39 KΩ resistor for generation of ASK and FSK modulation whereas PSK modulation also consists a LM 741 op-amp inverter [2, 3]. Tested hardware circuits and their resultant observed waveforms have been included that justify behavior of the hardware circuitry. In addition, the added advantages of this paper are lower value of dc supply voltage and lower value of resistor that helps in lowering the cost of needed hardware circuitry.

The remaining sections of this paper describes literature review, circuit diagrams for generation of digital communication experiments, modulation techniques and their output waveforms followed by results and concluding remarks.

II. LITERATURE REVIEW

A. Sample And Hold LF 398 IC

LF 398 IC is an 8-Pin IC as shown in fig.1. LF 398 is very important IC for analog and digital communication modulation generation. Its functional diagram includes a precision half wave rectifier, a comparator that compares digital data (basically a square wave) with a logic reference voltage, an n-channel FET (MPF 102) that work as a switch and a voltage follower circuit as illustrated in fig. 2. Detailed connection diagram of LF 398 IC has been shown in fig.3 [17].

B. General Description

The LF198/LF298/LF398 is a monolithic sample-and-hold circuits which utilize BI-FET technology to obtain ultra-high dc accuracy with fast acquisition of signal and low drop rate. Operating as a unity gain follower, dc gain accuracy is 0.002% typical acquisition time is as low as 6 μs to 0.01%. A bipolar input stage is used to achieve low offset voltage and wide bandwidth. Input offset adjust is accomplished with a single pin, and does not degrade input offset drift. The wide bandwidth allows the LF198 to be included inside the feedback loop of 1 MHz op-amps without having stability problems. Input impedance of 10^{10} Ω allows high source impedances to be used without degrading accuracy.

P-channel junction FET's are combined with bipolar devices in the output amplifier to give drop rates as low as 5 mV/min by use of 1 μF hold capacitor. The JFET's have much lower noise than MOS devices used in previous designs and do not exhibit high

temperature instabilities. The overall design guarantees no feed-through from input to output in the hold mode, even for input signals equal to the supply voltages [12].

C. Features

Some important specifications of LF 398 IC [12]:

- Operates from ±5V to ±18V supplies
- Acquisition time < 10 μs
- TTL, PMOS, CMOS compatible logic input
- 0.5 mV typical hold step at C_h = 0.01 μF
- Gain accuracy 0.002%
- Low output noise in hold mode
- Input characteristics do not change during hold mode
- High supply rejection ratio in sample or hold
- Wide bandwidth
- Input offset voltage 7to 10mV.
- Input bias current 50 to 100nA.
- Input impedance very high (10^{10} Ω) of the order of few GΩ.
- Output impedance very low 4Ω. Logic and logic reference input current 10μA.
- Leakage current into hold capacitor 200nA.

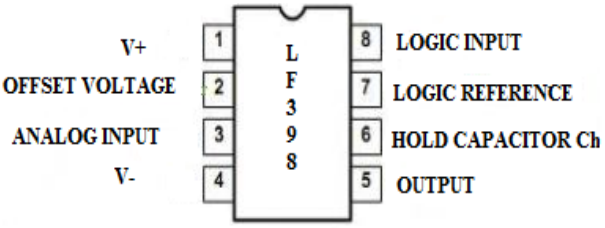

Figure1. Sample and Hold LF 398 IC

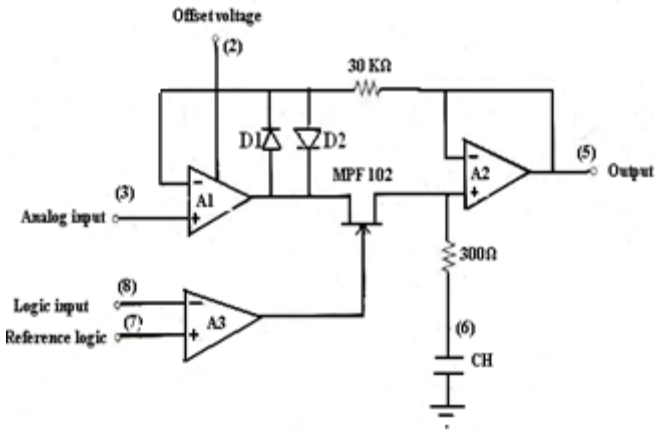

Figure 2. Functional diagram of LF 398 IC

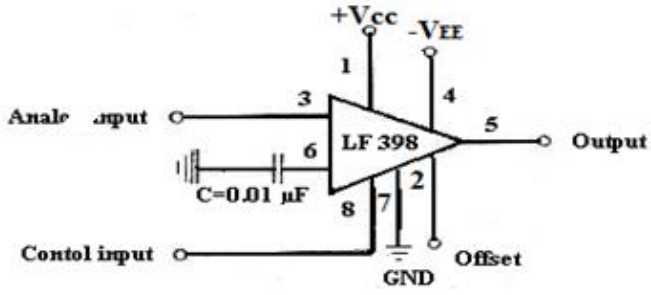

Figure 3. Connection diagram of LF 398 IC

D. Digital Modulation Techniques

Digital modulation can easily detect and correct the noise. Information security is more in digital modulation. Digital modulated signal can travel a long distance. Because of the following advantages digital modulation schemes are most widely used in all over the world for various modes of communications [2, 3, 17]. A verity of simulated results and waveforms for digital communication laboratory have been shown using PROTES software [18].

III. GENERATION METHODOLOGY AND OBTAINED RESULTS

Very cost-effective, simplest compact circuits those utilizes one or two LF 398 IC, LM 741 IC and a single resistor and/ or capacitor methodologies for generation of PAM, natural sampling, flat-top sampling, sample and hold, PAM-TDM circuits and methodologies of generation ASK, FSK and PSK digital modulation techniques. It uses LF 398 IC, few other circuit components have been illustrated and implemented on laboratory project board in fig. 4 to fig.12, and their results obtained on CRO screen have been shown.

A. Generation of Sample and Hold Waveform

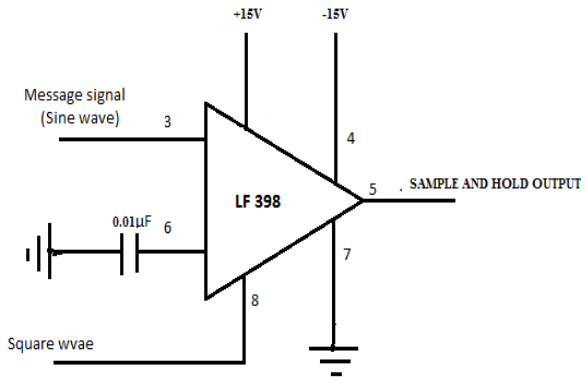

(a) Sample and hold circuit

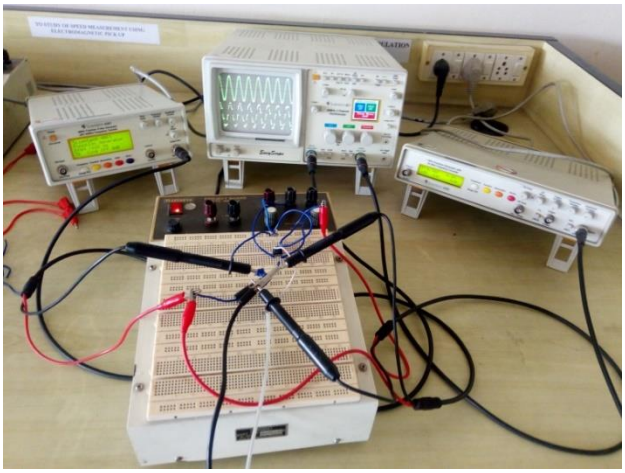

(b) Implementation of Sample and Hold Circuit

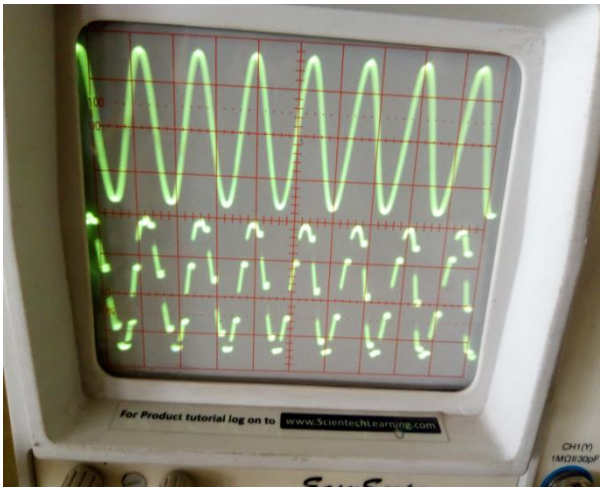

(c) Message signal and Sample and hold output waveform

Figure 4. Generation of Sample and Hold Output Waveform

B. Generation of Pulse Amplitude Modulation (Pam) Waveform

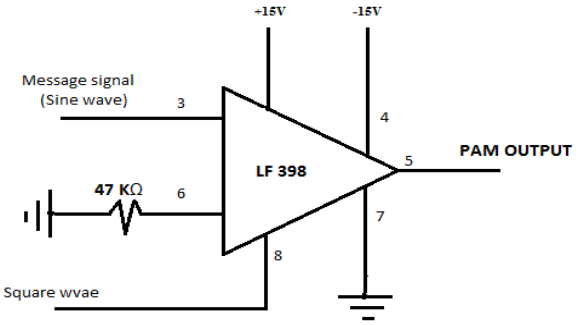

(a) PAM Circuit

(b) Implementation of PAM

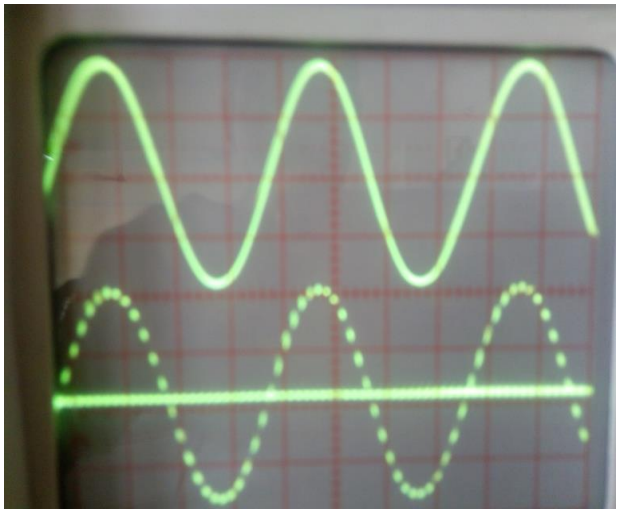

(c) Message Signal and PAM Output Waveform

Figure 5. Generation of PAM Output Waveform

C. Generation of Natural Sampling Waveform

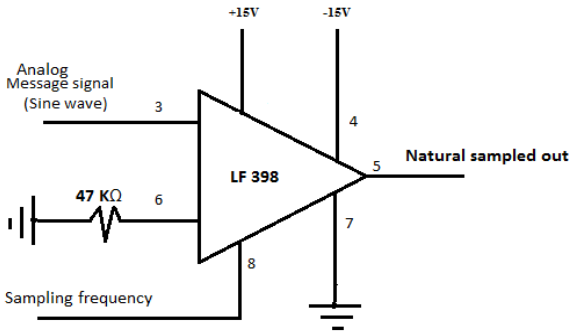

(a) Natural Sampling Circuit

(b) Implementation of Natural Sampling

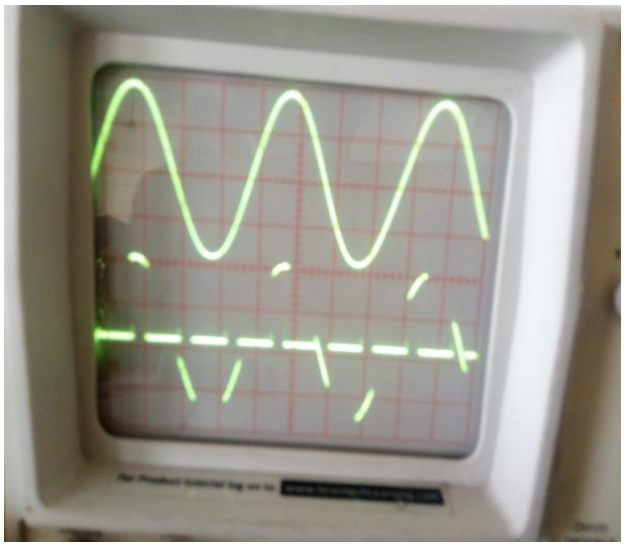

(c) Message Signal and Natural Sampling Output Waveforms

Figure 6. Generation of Natural Sampling Output Waveform

D. Generation of Flat Top Sampling Waveform

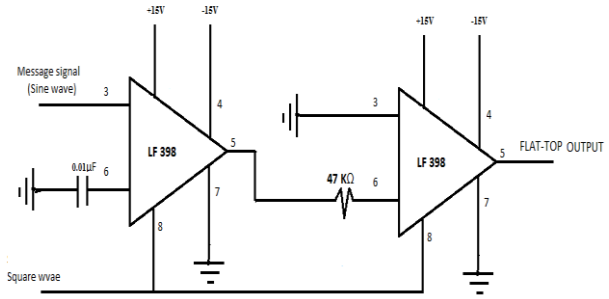

(a) Flat Top Sampling Circuit

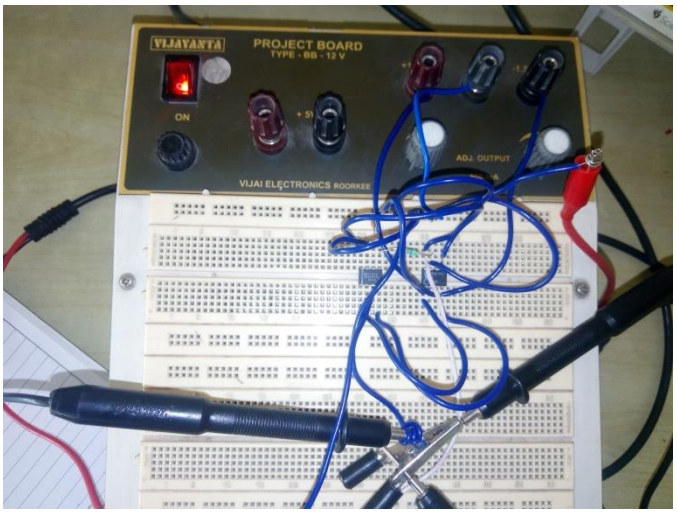

(b) Flat top sampling implementation

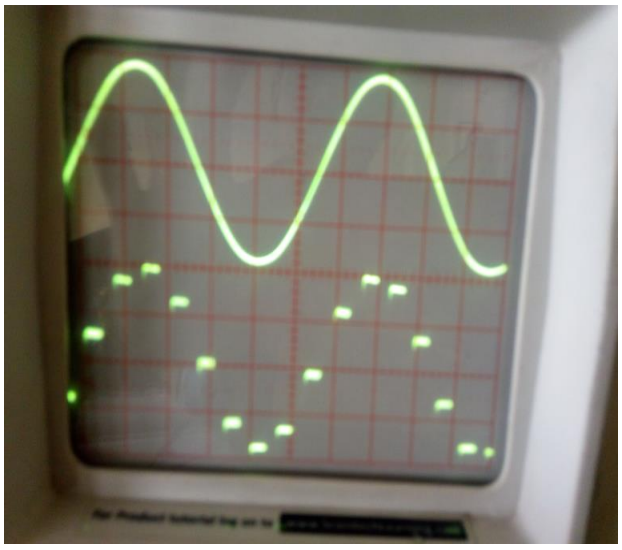

(c) Message signal and Flat top sampling output waveforms

Fig.7. Generation of flat top sampling waveform

E. Generation of Pulse Amplitude Modulation Time Division Multiplexing (PAM-TDM) Waveform

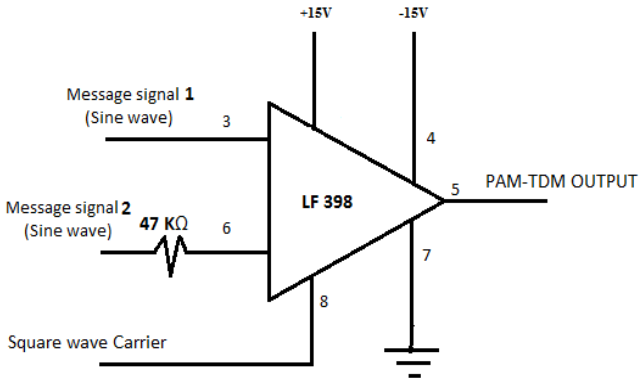

(a) PAM-TDM circuit

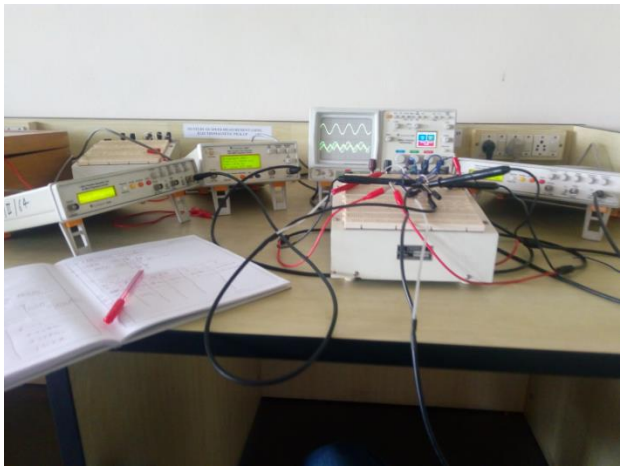

(b) Implementation of PAM-TDM circuit

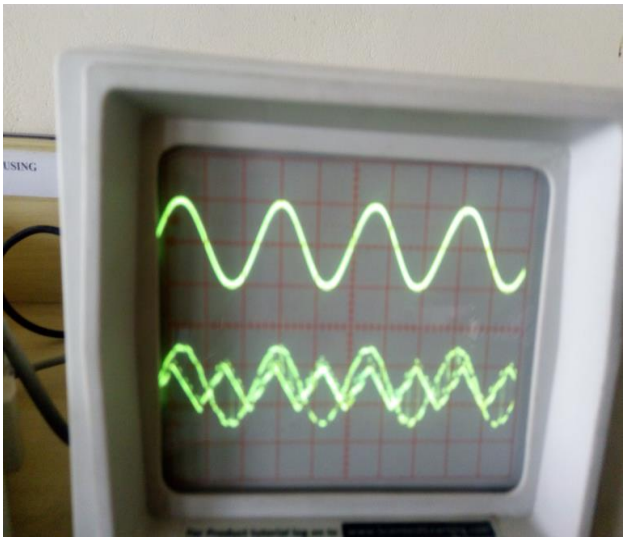

(c) Message Signal and PAM-TDM output

Figure 8. Generation of PAM-TDM

F. Generation of Amplitude Shift Keying (Ask) Waveform

ASK modulation realized using a LF 398 IC and a 39 KΩ resistor.

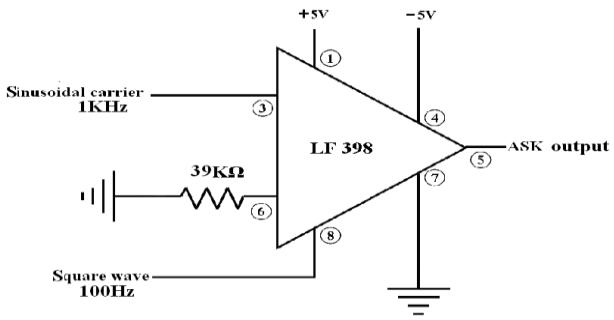

(a) ASK Generation Circuit

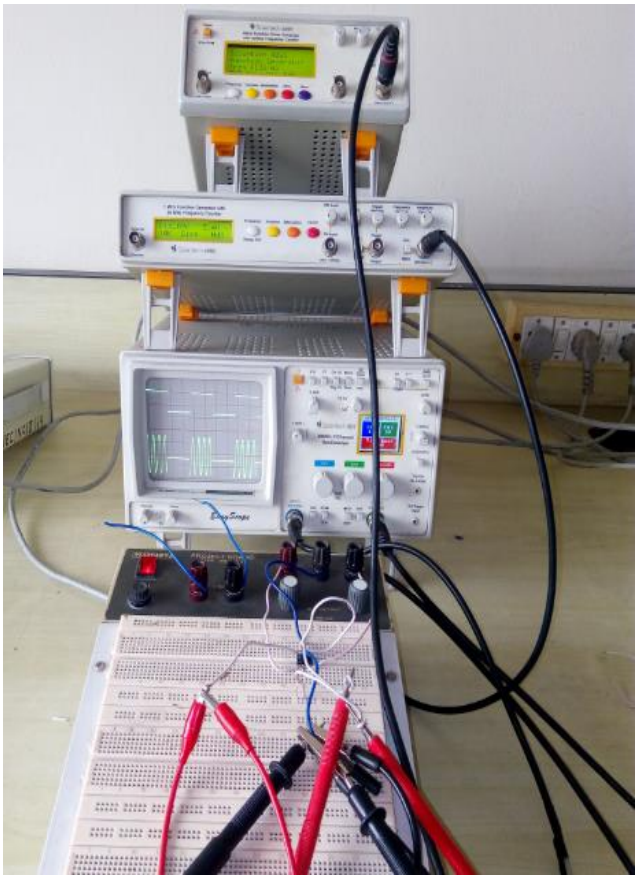

(b) Implementation Digital Data Input and ASK Output Waveform

Figure 9. ASK Waveform Generation

G. Generation of Frequency Shift Keying (FSK) Waveform

FSK modulation realized using a LF 398 IC and a 39 KΩ resistor is similar to ASK generation but here two carrier waves of different frequencies are applied from function generators to modulate binary bit 1 and binary bit 0.

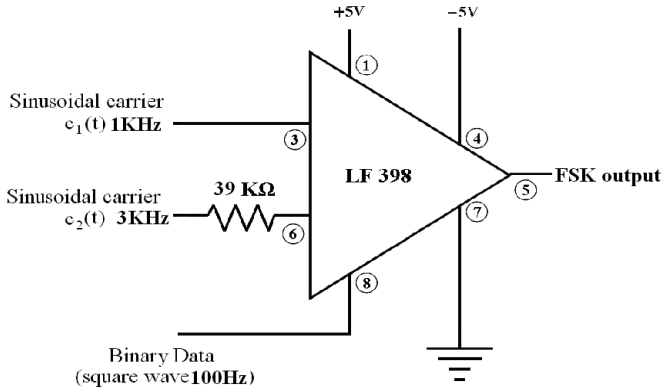

(a) FSK Generation circuit

(b) FSK Implementation and Its Output Waveform

Fig. 10. FSK Waveform Generation

H. Phase Shift Keying (PSK)

PSK modulation realized using an op-amp 741 IC inverter followed by LF 398 IC and a 39 KΩ resistor.

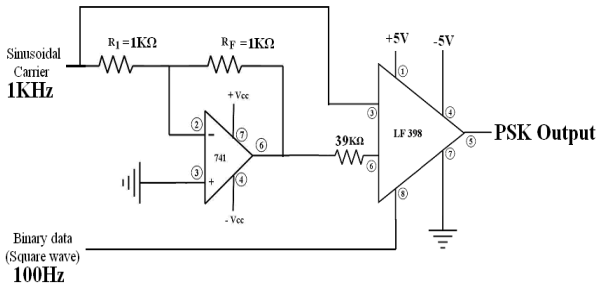

(a) PSK Generation Circuit

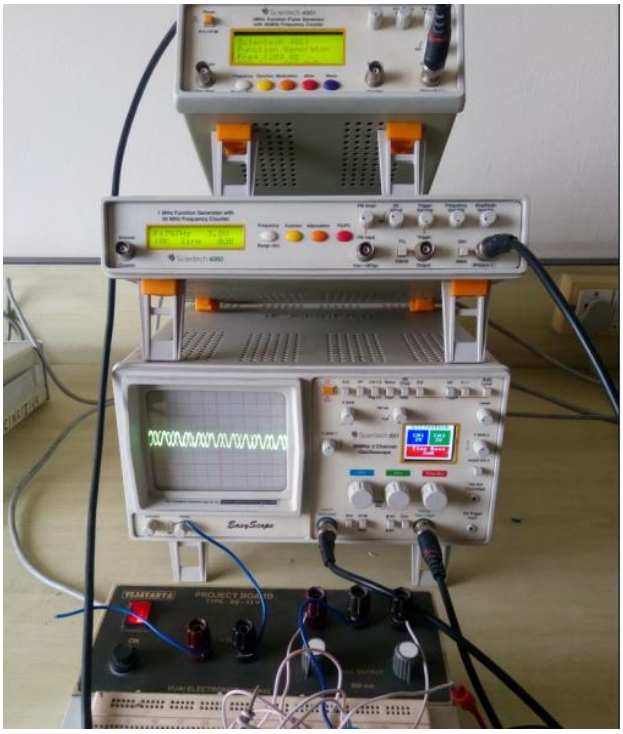

(b) PSK Implementation and Its Output Waveform

Figure 11. PSK Waveform Generation

I. Generation of Pulse Width Modulation (PWM) waveform

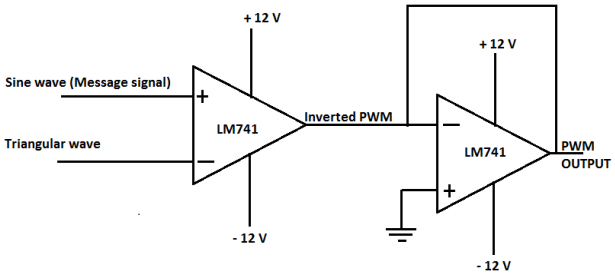

(a) Pulse Width Modulation (PWM) Circuit

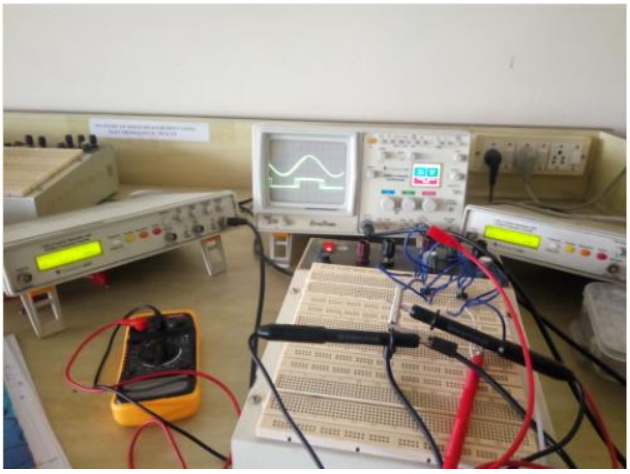

(b) PWM Implementation

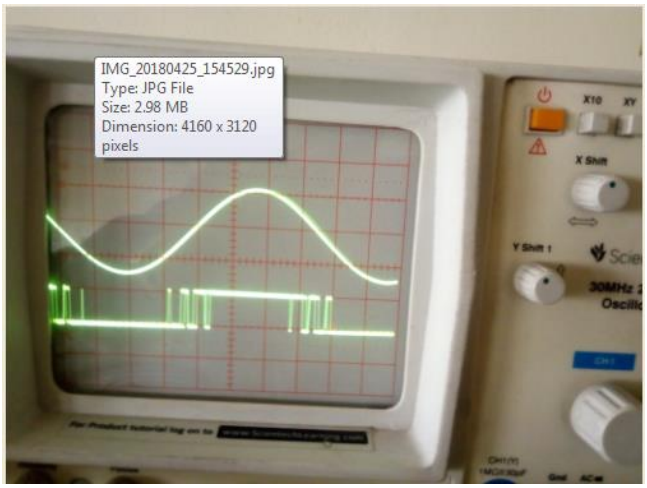

(c) Output Waveform of PWM

Figure 12. PWM Waveform Generation

IV. RESULTS

The circuit used for generation of sample and hold, PAM, natural sampling, Flat top sampling, PAM-TDM, ASK, FSK and PSK experiments had been arranged on project board. Message signals, binary inputs data and carrier waves were applied from the function generator/s, their amplitude and frequencies were adjusted suitably. Finally, the resultant output digital communication particular application wave has been obtained and observed on the cathode ray oscilloscope (CRO) as shown in fig. 4 to fig.12. Tabulated results have been shown in table-I to table-VII.

SAMPLE AND HOLD RESULTS

S.No.	Analog input message signal (Sine Wave)	Control switching input (Square Wave)
	Amp.	Freq.	Amp.	Freq.
1	4 V(pp)	316 Hz	4 V(pp)	4.35 KHz
2	8 V(pp)	316 Hz	8 V(pp)	3.28 KHz

PAM RESULTS

S.No.	*Analog input message signal (sine wave)*		*Sampling signal(square wave)*	
	Amp.	Freq.	Amp.	Freq.
1	4 V(pp)	316 Hz	4 V(pp)	3.27 KHz
2	8 V(pp)	316 Hz	8 V(pp)	3.28 KHz
3	8 V(pp)	316 Hz	4 V(pp)	8.09 KHz
4	8 V(pp)	316 Hz	2.5 V(pp)	8.08 KHz

NATURAL SAMPLING RESULTS

S.No.	*Analog input message signal(sine wave)*		*Sampling signal frequency(square wave)*	
	Amp.	Freq.	Amp.	Freq.
1	8 V(pp)	318 Hz	8 V(pp)	3.01 KHz
2	8 V(pp)	316 Hz	8 V(pp)	764 Hz
3	8 V(pp)	316 Hz	8 V(pp)	7.90 KHz
4	8 V(pp)	316 Hz	8 V(pp)	30.57 KHz
5	8 V(pp)	318 Hz	8 V(pp)	1.00 KHz

FLAT TOP SAMPLING RESULT

S.No.	*Analog input message signal(sine wave)*		*Sampling signal frequency(square wave)*	
	Amp.	Freq.	Amp.	Freq.
1	8 V(pp)	318 Hz	8 V(pp)	2.65 KHz
2	8 V(pp)	225 Hz	8 V(pp)	2.65 Hz
3	8 V(pp)	225 Hz	8 V(pp)	1.91 KHz

PAM-TDM RESULTS

S.No	*Message 1 (sine wave) input*		*Message 2 (triangular wave) input*		*Sinusoidal carrier signal(square wave)*	
	Amp.	Freq.	Amp.	Freq.	Amp.	Freq.
1	4V(pp)	415 Hz	2.4V(pp)	788 Hz	4V(pp)	3.87K Hz
2	6V(pp)	415 Hz	2.5V(pp)	788 Hz	4V(pp)	3.87K Hz
3	8V(pp)	415 Hz	4.2V(pp)	788 Hz	4V(pp)	3.87K Hz

DIGITAL MODULATION SCHEMES Results

Digital Modulation Techniques	*Binary data (square wave) input*		*Sinusoidal Carrier1*		*Sinusoidal carrirer2*	
	Amp.	Freq.	Amp.	Freq.	Amp.	Freq.
ASK	4V(pp)	100 Hz	4V(pp)	1KHz	-----	-----
FSK	4V(pp)	100 Hz	4V(pp)	1KHz	4V(pp)	3KHz
PSK	4V(pp)	100 Hz	4V(pp)	1KHz	-----	-----

PWM Results

S.No.	*Analog input message signal (sine wave)*		*Triangular wave*	
	Amp.	Freq.	Amp.	Freq.
1	4 V(pp)	50 Hz	2.3 V(pp)	600 Hz
2	6 V(pp)	82 Hz	2.1 V(pp)	1.36 KHz
3	8 V(pp)	100 Hz	2.6 V(pp)	1.36 KHz

V. CONCLUSION

The circuit used for generation of sample and hold, PAM, natural sampling, flat top sampling, PWM, PAM-TDM, ASK, FSK and PSK are arranged, realized and demonstrated using LF 398 IC and few other circuit passive components. All waveforms are observed on CRO has been justified the results. In this paper, we reduces the value of desired resistor and DC supply voltage from 15V to a pencil cell upto 5-9V, these advantages enhances a very low cost and simple circuitry based generation of digital communication laboratory experiments. Thus these circuits surely become the first choice in optical fiber and microwave link modulation schemes. These circuits are also help full for digital communications laboratory purposes for graduate and post graduate students. LF 398 IC is not limited to only these digital modulation applications but we can also generate analog modulations DSB-SC AM, FM, PM waves too. LF 398 IC could also be used to produce sample and hold circuit for reconstruction of sampling and natural sampling, and flat-top sampling in conjunctions with few filter circuits and other simple ICs. Pulse amplitude modulation and Time Division Multiplexing circuits have been also be implemented and verified those omits the use of very costly kits available in the laboratory. So we conclude that by the use of LF 398 IC, we can replace our communication laboratory economic and hands-on rather than using costly kits.

VI. REFERENCES

[1] S. Haykin, "Digital Communications", reprint, John Wiley & Sons, 2001.

[2] B. Kamini, "An alternate approach to the lboratory implementation of communication experiments", Digital signal processing education workshop & IEEE, 2011.

[3] A. Goyel, " Generation of ASK, FSK & PSK using sample and hold IC LF 398", in Proc IEEE xplore, International conference on signal processing & communication (ICSC), Delhi, 2016, pp. 51-54.

[4] J. Milliman and C. C. Halkias, "Integrated Electronics," 2 ed., Tata McGraw Hill, 1991.

[5] D. R. Choudhury & S. B. Jain, " Linear Integrated Circuits", 4 ed., New Age International Publication, 2012.

[6] J. G. Prokis, " Digital Communications", 4 ed., McGraw Hill, 2000.

[7] B. P. Lathi, " Modern Digital and Analog Communication systems", 3ed., Oxford University Press, 1998.

[8] A. B. Carlson and P. B. Crilly, "Communication Systems", McGraw Hill, 5 ed., 2010.

[9] W. Tomasi, "Electronics Communication Systems Fundamentals Through Advanced", 5 ed., Printice Hall India, 2008.

[10] A. K. Varshney,"Digital and Analog Communication", 1 ed., International Book House publication, 2011.

[11] I. Xilinx, "Design Suit", 2012.

[12] National Semiconductors, LF 398 data sheet.

[13] National Semiconductors, LM 741 data sheet.

[14] A. Sharma, S. Majumdar and A. Naugarhiya, "Verilog based simulation of ASK, FSK , PSK, QPSK digital modulation techniques", International conference on I-SMAC, 2017.

[15] S. Haykin, “Communicztion Systems”, 2 ed.”, Wiley Estern Limited, 1983.

[16] G. Kennedy, “Electronic Communication Systems”, 3 ed., Tata McGraw Hill, 1989.

[17] A. Varshney, “A Cost Effective Generation of Digital Modulation Techniques(ASK, FSK & PSK) Using LF 398 IC”, Recent trends in analog devices and circuits, vol. 1, issue 1, HBRP, 2018.

[18] B Kanmani, “Digital Communication Using Labview”, MITE-2013, IEEE International Conference on MOOC, Innovation and Technology in Education (MITE), Jaipur, 20-22 December, 2013.

[19] Zanming Xia, Chunhua Wang, Jie Jin, Sichun Du,Hairong Lin, Huai Yang “Novel AM/FM/ASK/PSK/QAM signal generator based on digitally programmable CDTA”,circuits syst signal process, 2015, pp 1635-1653.

Themed Section : Engineering and Technology
© 2018 IJSRSET | Volume 5 | Issue 3 | Print ISSN: 2395-1990 | Online ISSN: 2394-4099

Investigation of Performance Analysis of QoS in the Internet of Things (IoT)

S. Balamurugan[1], Dr. A. Ayyasamy[2], Dr. K. Suresh Joseph[3]
[1]Research Scholar, Department of CSE, Annamalai University, Tamilnadu, India
[2]Assistant Professor, Department of CSE, Annamalai University, Tamilnadu, India
[3]Assistant Professor, Department of Computer Science, Pondicherry University, Tamilnadu, India
chella40978@gmail.com[1], samy7771@yahoo.co.in[2], ksjoseph.csc@gmail.com[3]

ABSTRACT

With the coming out of the new era, Internet of Things (IoT) is essential to describe best models, which can sort out IoT applications and establish the Quality of Service (QoS) factors needed to fulfil the needs of those services. Quality of Service in IoT is one of the decisive features which desires investigate and stabilization for QoS execution, administration and optimizations. On the different approach, as Wireless Sensor Networks (WSN) comprises a major factor of the IoT, they be converted into a key issue regarding QoS condition. In addition, regarding QoS needs, we also classify best models for the IoT and representation their achievability through a classification of IoT applications. The review is done to afford a summary of different QoS ideas and for various qualities of service parameters of IoT.

Keywords: Internet of Things, Quality of Service, Service Oriented Architecture, Wireless Sensor Networks, Protocol

I. INTRODUCTION

Internet of Things (IoT) intends to allow the interconnection of a huge quantity of smart devices using a grouping of networks and computing technologies. But an entry of interconnected devices constructs a larger requires on the fundamental communication networks and concerns the quality of service (QoS). Devices such as security alarms, cameras, etc, produce delay sensitive information that must be converse in a real time. Such devices have diverse features with partial buffer capacity, storage and processing power. Therefore the commonly used model cannot be a good-looking mechanism to pleasure delay sensitive traffic. Based on the systematic model different simulation results are cause in instruct to scrutinize the backlog length and the blocking probability of high and low priority traffic for system with various capacities[2].

Now-a-days the different communication technologies are used for the transfer of information, more number of issues in security and privacy sectors. IoT finds its application in the all the fields, since new mode of communication between the different systems and devices. Internet of Things (IoT) also called the internet of everything or industrial network is a wide technology which is been viewed as a global network of machines and devices capable of interacting with each other [4]. The IoT allows things to be controlled remotely across existing network infrastructure, provide opportunities for more direct integration of the physical world into computer-based systems, and resulting in improved

efficiency, accuracy and economic benefit in addition to reduced human intervention [5].

II. REVIEW OF LITERATURE

An extensive range of research results have been reputable for QoS support in traditional networks, but, only a small number of research efforts are found with IoT it provides an stimulating and capable idea for effortlessly connecting the fundamental world of information to the real world. Dores et al. have discussed the circumstances of the art technologies such as Next Generation Networks (NGN), Internet of Things (IoT), Wireless Sensor Networks (WSN), Body Sensor Networks (BSN) and Cloud Computing and have suggest the necessitate for the incorporation of the technologies in making the future internet a reality [11]. The authors have also execute a QoS test in conditions of delay and jitter and have recommended that more explore work is required to enhance QoS with varied characteristic which will assure certain quality of services to users and the providers.

Mohamed et al. have illustrated the requirement of put together IoT paradigms and the different issues involved in this context [12]. They have presented ever growing connected devices allocate a lot of data which cannot be locally or temporarily accumulate on the devices and the required foreseen is hire storage space and the well-organized consumption of the data and the resources. The authors have said that the active prioritization of the demand is necessary along with the QoS requirements such as bandwidth, delay, jitter and packet loss.

Ren et al have projected a QoS architecture for IoT as the consequence of their thorough analysis of the active QoS mechanism with view to the description of IoT in a layered basis, such as application layer, network layer and perception layer which insisted the require for the trustworthy QoS design.[13]. The authors, illumination the functions of each layer of their planned work they did suggest that the research work is further essential to comfort an end to end quality in availing and providing services in smart environment as IoT is integrated with heterogeneous networks. The existing research on IoT and Quality of Service is the necessity for dynamic prioritization of the demand along with the QoS requirements which are capable of delivering real time services and applications with guaranteed quality. Hence, in this discussion a novel Quality of Service design for the Internet of Things is proposed [14].

III. KEY ELEMENTS INVOLVED IN IOT

A. Sensing

The first step in IoT workflow is gathering information at a “point of activity.” The information collected may be information collected by the appliance or any devices. The sensing can be biometric, biological, environmental, visual or audible.

B. Communication

IoT devices need a channel for sending collected information at the device level to the Cloud-based service for further processing. This expects either Wi-Fi (wireless LAN based communications) or WAN communications.

C. Cloud Based Capture & Consolidation

Collected data is sent to the cloud based service where the data is combined with other data to produce useful information to the user. Collected information may be forming any sources [1]. Data processing is always required for analysing.

D. Delivery of Information

Delivery of Information is the last step where the useful information is sent to the user. That may be a consumer, a commercial or an industrial user. The aim is to provide information in a simple and transparent manner.

IV. PROTOCOLS AND NETWORK TECHNOLOGIES

IoT mainly uses the standard protocols and networking technologies. The most important technologies and protocols of IoT are RFID [9], NFC, low-energy Bluetooth, low-energy wireless, low-energy radio protocols, LTE-A, and Wi-Fi Direct. These technologies hold the explicit networking functionality desirable in an IoT arrangement in dissimilarity to a typical standardized network of general systems.

A. NFC and RFID

RFID (radio-frequency identification) and NFC (near-field communication) offers simple, less energy, and flexible options for characteristics and contact tokens, connection bootstrapping, and payments [3].

B. Low-Energy

Bluetooth affords the low-power, long-use require of IoT purpose while uses a normal technology with local support across systems [16].

C. Low-Energy Wireless

These technologies return the mass power starving attribute of an IoT structure. Even though sensors and additional elements can ability following over extended periods, communication links (i.e., wireless) must remain in listening mode. Low-energy wireless diminish consumption [8] thus extends the existence of the device. The following list shows the protocols involved in internet of things devices and applications as shown in Figure 1.

D. CoAP

CoAP is designed to enable low-power sensors to use RESTful services while meeting their power constrains.

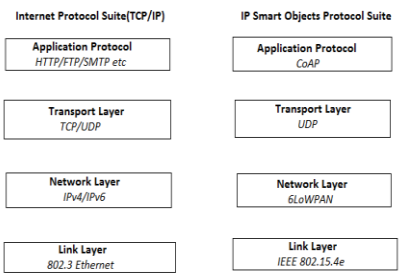

Figure 1. Comparison of Internet Protocol Suite with IP Smart object protocol suite

It is built over UDP, instead of TCP commonly used in HTTP [21] and has a light mechanism to provide reliability. CoAP architecture is divided into two main sub layers: messaging and request/response. The messaging sub layer is responsible for reliability and duplication of messages while the request/response sub layer is responsible for communication.

E. 6LoWPAN

IPv6 over Low power Wireless Personal Area Network (6LoWPAN) is the first and most commonly used standard in this category [15]. It efficiently encapsulates IPv6 long headers in IEEE802.15.4 small packets, which cannot exceed 128 bytes.

F. MQTT

It is designed to provide embedded connectivity between applications and middleware's on one side and networks and communications on the other side[14].

G. Radio Protocols

ZigBee, Z-Wave, and Thread are radio protocols used for establishing low-rate private area networks technologies not only use low-power but also offer high throughput. This increases the power of small local device networks without the typical costs.

H. LTE-A

LTE-A, or LTE Advanced, provides an important boost to LTE technology by increasing not only its coverage, but also reducing its latency and raising its throughput. It gives IoT an enormous power by increasing its range, with its most noteworthy applications being vehicle, UAV.

I. Wi-Fi Direct

Wi-Fi Direct removes the need of an access point [10]. It allows P2P (peer-to-peer) connections retaining the speed of Wi-Fi, but with lower latency. Wi-Fi Direct removes an element of a network that often marsh it down and it does not compromise on speed or throughput.

V. QOS ARCHITECTURE VISUALIZATION OUTLINE

There are numerous concepts and implementation factors incorporated in defining and designing IoT architectures [7] such as:

(i) Essential the architecture basing the facility components for providing the services in IoT using applicable protocols and access networks for execute the IoT systems - service oriented architectures.

(ii) Maintenance of the framework or situations of the application systems as the base for designing the architecture - context aware architectures.

(iii) The plan of architectures build approximately the middleware (software components) as the base to employ the IoT systems [6].

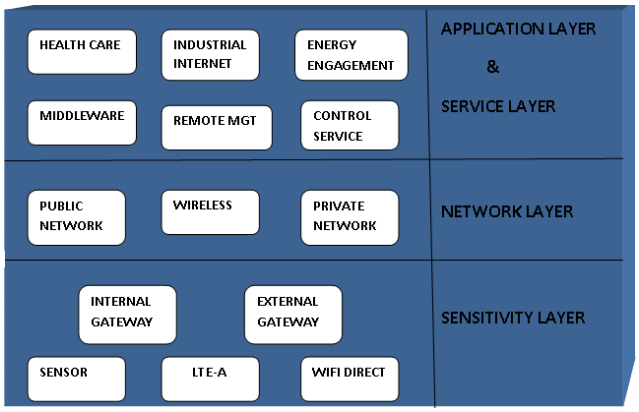

Figure 2. Three Layer Conceptual architecture embedding the QoS architecture and cross layer QoS components.

The works of three-layer architecture for our conceptual IoT systems are

A. Application Layer and Service Layer

This layer consists of helpful modules for application systems and users which utilise the actual world data for analysis, computation, and for a real world action.

End Users / Applications: The application layer has systems or users or machines or an environment for consuming / using the data sensed by the real world object or situation. The application functional modules will be particular to application domains which consume data received from lower layers indicating the real situation for needed functions [17].

IoT data specific modules: It incorporates the functions like optimization [6] of duplicate and redundant data from field devices, functions of storing/retrieval of data for future references, and retrieval of data for adaptive and dynamic decisions etc. Some of these components are distributed between application and perception layers for achieving effective QoS.

B. Network Layer

The network layer is involved in routing [20] the data from lower layer to upp1er layer and vice versa. The essential components and modules of this layer would include:

i. Diverse class of access networks, protocols

ii. Communication devices vital for connectivity and communication.

iii. Routing functionality/modules

C. Perception Layer

The sensing layer functional modules will comprise of the essential data sensing / data gathering from real world objects which would consist of all the real world objects, machines and people [19]. Also the functions may contain controlling of field devices/actions based on data sensed and control commands received by upper layers and application systems/users of the domain.

Edge Nodes: These are smart embedded devices which has the minimum computing, storage and communication capabilities. (System on Chip - SoCs, Microcontrollers etc.)

D. Field Devices

These are the devices where the real world data is sensed with or without intelligence and are capable of sensing data/information for a specific purpose. Example sensors, RFID, ECP, actuator and other objects accessible directly or indirectly and providing the field data in the IoT environment by enabling IoT application for actions with real world data/situation (can include devices, machines and objects with computing capabilities and participating in IoT data [20].

VI. CONCLUSION

The QoS parameters directly map to IoT layers, some of the QoS parameters are applicable across the layers and parameters are defined and schemes are implemented to achieve various organisations by different researches. The QoS parameters of application layer are service time, services availability, service delay, service accuracy, service load, service priority, information accuracy, cost of network deployment, and cost of service usage and maximum of resources available per unit price & penalties for service degradation and fault tolerance.

VII. REFERENCES

[1] John AS. Research Directions for the Internet of Things, Internet of Things Journal2014; 1: 3-9.

[2] Gubbi J, et al. Internet of Things (IoT): A vision, architectural elements, and future directions, Future Generation Computer Systems, 2013; 29: 1645-1660.

[3] Ling Li, et al. QoS-Aware Scheduling of Services-Oriented Internet of Things, IEEE Transactions on Industrial Informatics, 2014; 10: 1497-1505.

[4] Saima A and Kun Y. A QoS Aware Message Scheduling Algorithm in Internet of Things Environment, IEEE Online Conference on Green Communications (Online Green Comm) 2013; 175-180.

[5] Tingxun SHI, et al. Quality Driven Design of Program Frameworks for Intelligent Sensor Applications, 20th Asia-Pacific Software Engineering Conference 2013; 442-449.

[6] Duan R, et al. A QoS Architecture for IOT, IEEE International Conferences on Internet of Things, and Cyber, Physical and Social Computing 2011; 717-720.

[7] Medha S and Kulkarni DB. Enabling QoS Support for Multi-Core Message Broker in Publish/Subscribe System, Advance Computing Conference (IACC) IEEE International 2014; 774-778.

[8] Rafael P, et al. A RFID QoS Mechanism for IoT Tracking Applications, Wireless and Pervasive Computing (ISWPC), International Symposium on 2013; 1-4.

[9] Marie AN, et al. Enabling QoS in the Internet of Things, CTRQ: The Fifth International Conference on Communication Theory, Reliability, and Quality of Service 2012.

[10] Vermesan O, et al. Internet of Things Strategic Research Roadmap, European Research cluster on the Internet of Things, Cluster Strategic Research Agenda 2011.

[11] Dores, C., Reis, L.P., Lopes, N.V. 2014.

[12] Internet of Things and Cloud Computing.

[13] Mohammad, A., Khan, I., Abdullah, A.A.,

[14] Huh, E.N. 2014. Cloud of Things: Integrating Internet of Things and Cloud Computing and the Issues Involved. Proceedings of the 11th International Bhurban Conference on Applied Sciences & Technology (IBCAST). IEEE.

[15] Ren, D., Chen, X., and Xing, T. 2011. A

[16] QoS Architecture for IoT, International Conferences on Internet of Things, and Cyber, Physical and Social Computing, IEEE.

[17] Zhou Ming and Ma Yan. A Modelling and Computational Method for QoS in lOT, Software Engineering and Service Science (ICSESS), IEEE 3rd International Conference 2012.

[18] Jia-Ming L, et al. An Energy-Efficient Sleep Scheduling With QoS Consideration in 3GPP LTE-Advanced Networks for Internet of Things, IEEE Journal on Emerging And Selected Topics in Circuits and Systems 2013; 3: 13-22.

[19] Jeffrey GA. Seven Ways that HetNets Are a Celluar Paradigm Shift. IEEE Communications Magazine, 2013; 51: 136-144.

[20] Giuseppe C, et al. Objects that Agree on Task Frequency in the IoT: a Lifetime-Oriented Consensus Based Approach, IEEE World Forum on Internet of Things (WF-IoT) 2014; 383-387.

[21] Chien-LF and Christine J. Challenges of Satisfying Multiple Stakeholders: Quality of Service in the Internet of Things 2012.

[22] Shancang Li, et al. Distributed Consensus Algorithm for Decision Making in Service-Oriented Internet of Things, IEEE Transactions on Industrial Informatics, 2014; 10: 1461-1468.

[23] Andreas N. Internet of Things – Architecture IoT-A European Commission within the Seventh Framework Programme (2007-2013).
[24] Xian rong Z, et al. Cloud Service Negotiation in Internet of Things Environment A Mixed Approach, IEEE Transactions on Industrial Informatics 2014;10: 1506-1515.

Themed Section : Engineering and Technology
© 2018 IJSRSET | Volume 5 | Issue 3 | Print ISSN: 2395-1990 | Online ISSN: 2394-4099

Performance of Mobile sink Node based Geographic routing protocol in Wireless Sensor Networks

Baranidharan.V[1], Kiruthiga Varadharajan [2], Mahalakshmi.G[3]

[1]Assistant Professor, Bannari Amman Institute of Technology, Sathy, Tamil Nadu, India
[2]PG Scholar, Annamalai University, Chidamabara, Tamil Nadu, India
[3]UG Scholar, Bannari Amman Institute of Technology, Sathy, Tamil Nadu, India
baranidhar@hotmail.com[1], kiruthivarathan6896@gmail.com[2],mahalakshmi.ec15@bitsathy.ac.in[3]

ABSTRACT

The sensor nodes in wireless sensor networks are very tiny, smaller in size, low cost and low energy consumption. They may prone to many failures. To ensure reliable multi-hop multipath communication between all the other nodes the routing protocols between all other nodes, the routing protocols are used in WSN. The geographic routing protocols is more capable routing protocols among the various others routing protocols in WSN due to its simplicity and scalability. The aim of this paper is to analyse the mobility sink in geographic routing and to observe its performance metrics such as Average energy consumption, End-to-End delay and Packet delivery ratio through the extensive simulations and graphical representation.

Keywords: Geographic Routing, Lifetime, Initial Battery Capacity and End To End Delay

I. INTRODUCTION

Recent innovations in the technology led to the use of many battery and low cost sensor nodes and have a diverse field of the application of WSN. Those sensor nodes are mainly involved in the collecting the data related to the environmental temperature, humidity soil fertility of the boilers in chemical industries etx. In these areas, the human interventions are very less. These nodes are placed/deployed in a phase which is not easily accessed by the human directly. These sensor networks provides a solution to any real time problems in the areas of infrastructure maintenance, disaster management, military sensing, traffic management etc.

The sensor nodes are deployed in an ad-hoc manner in the area of the concern and somewhere nearby the networks also contains a mobile sink nodes that collects the data from the all others sensor nodes for the further analysis. The deployment of all the sensor nodes will result into an unknown and unusual topology, which will be a problematic issue, there are some factors that govern the design of various sensor nodes like geographic area, cost for production, construct in hardware, scalability, fault tolerance etx, Sensor networks many have either static or mobile nodes the static nodes are placed in a predefined position the mobile nodes are placed randomly. Reliability and power consumption are the key concern of wireless sensor networks. The main aim of the paper is to analyse the scenarios with mobility sink through an extensive simulation of widely used approach called geographic routing this routing shows the various factor affecting the functioning of the entire networks.

The rest of the paper has been organized as follows, the Section I explains the introduction and various

challenge the WSN. Section II summarizes the concept of geographic routing with mobility based sink and its routing protocols. In section III shows the results and simulation based on concerned protocols. The paper is concluded in section IV with future work.

II. GEOGRAPHIC ROUTING WITH MOBILITY BASED SINK

As described in Introduction, the sink receives & collects the data information from all the other sensor nodes for further analysis consider the mobile based NPF is a scenario of the sink to route the packets from the source to destination, the geographical routing will takes location in to an consideration this geographic routing is approach to the sensor networks the data aggregation is an important process in the sensor networks the data aggregation is a helpful way to decrease the number of transmission packets of various source nodes.

A. Routing Protocols

In a WSN setup, the ore energy is consumed by the communication unit in the sensor nodes. In practice the multi-hop transmission from the source to destination requires a maximum energy. In greedy forwarding strategies, the data transmission for the one to other nodes depends upon the distance. ie. The node sends the packets to the neighbours, the far away in border area of the transmission range will leads to greater probability mobility of the packets due to the signal attenuation.

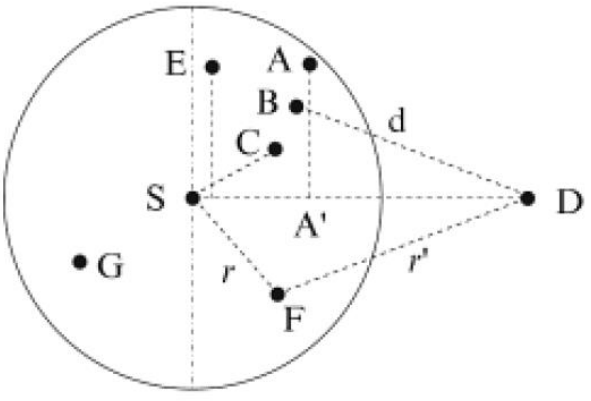

Figure 1. Sensor Network Scenario

The distance between a node S and projection A of the neighbour node A on to the line connecting S and destination D is defined Here the node A is the neighbour of the node S with most forward progress the neighbour having a positive progress are having a tremendous nodes in forward direction. In the above figures, the neighbours A, B, C, D, E and F are in forward direction the G nodes is in backward direction.

B. Problems with Geographic Routing Protocols

The chief energy consumed in sensor is communication unit multi hop communication is very much essential for transmitting data from the source to destination (sink) the energy consumption increases with decrease the communication distance. The communication distance can be reduced by using mobility based sink by programming the each sensor nodes. Programming of the each sensor nodes to route the data from the node to this sink for further transmission. There is a big issue in being a multiple dynamic/mobility sink is that the deployment to be decided. The data relying load can be balanced by the nodes. This type of problem is called as facility location problem, where the given number of facilities and customs the optimal of the facilities to be equally burdened. These protocols are also have a node probability induced error known and Link and Loop problems.

III. CONCERNED PARAMETERS

The paper is analyzed effects of various parameters on the whole network and vary the changes in the other parameters are also analysed. Average energy consumption, End to end delay and Packet delivery ratio are taken into the account of parameters. Sink position, is a simulator position of the sink as X and Y coordinates. Lifetime threshold is defined as the initial energy that the nodes will possesses and varies from

01 to 10. Sensor numbers define the total number of sensors present in the given topology, while transmission time defines the time taken in the network for data transmission from the source to its destination.

IV. SIMULATION AND GRAPHS

Through some extensive simulations we have analysed effect of the specific parameters on the given sensor networks and how the variations in these parameters change the performance and what their consequences are is measured. The simulator takes the consideration that uses the NFP algorithm this simulator takes into the consideration of various factors and parameters mentioned in section 3 the graphs are explains the effect of these parameters on each other.

A. Average Energy Consumption

Energy consumption is the most critical concern in the WSNs. One of the main purposes in this paper is to achieve energy conservation while balancing the energy consumption among sensor nodes, so as to extend the lifetime of the network. In the literature, several definitions about the lifetime of the WSN has been proposed, including the time until the first sensor node dies, the time until half of the sensor nodes die and the time until the last sensor node dies. As the communication range of the sensor nodes is limited and much smaller compared with the sensing area, the WSN is disconnected if all the key nodes in the vicinity of the sink drain their energy. Therefore, this paper defines the lifetime of the network as the time until all the key sensor nodes in the vicinity of the sink die.

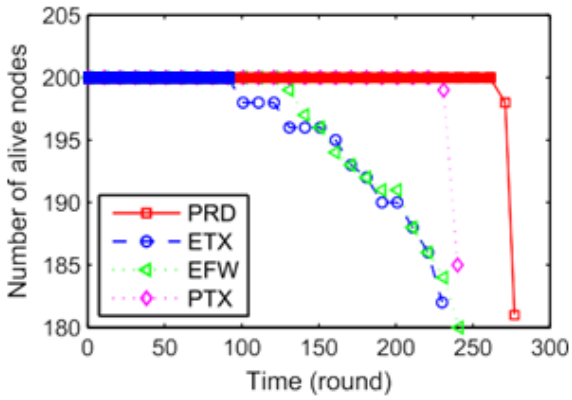

Figure 2. Average energy consumption

B. Packet Delivery Ratio (PDR)

Packet delivery ratio is the ratio of the number of packets successfully received by the sink to the total number of packets sent by the sensor nodes. It is important to guarantee packet delivery ratio when designing a WSN.

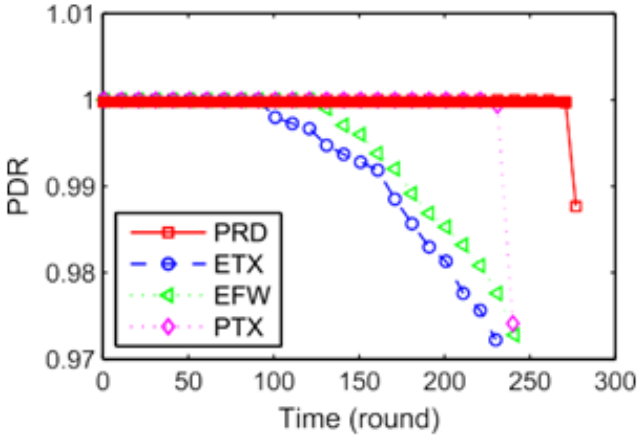

Figure 3. Packet Delivery Ratio (PDR)

As all the four metrics select sensor nodes with the best link quality to act as father nodes, the packet delivery ratio is nearly 100% at the beginning of the lifetime in the simulations. Then the packet delivery ratio decrease distinctly in all the four metrics. However, both of the packet delivery ratios in ETX and EFW show a much earlier decrease than the ones in PRD and PTX.

C. End-to-End Delay

The end-to-end delay is the total delay of a data packet from the source node to the sink, including the processing delay, the queuing delay, the transmission delay, and the propagation delay. In the WSN, as the data packet size is small and the distance between two pair of sensor nodes is very short considering that the propagation speed is almost the velocity of light, we can assume that the time spent for each attempt to transmit one packet to the next hop is a constant. We define *cycle* as the time needed to transmit one packet to the next hop. This paper uses the cycles needed to transmit one packet of data from its source to its destination, including the retransmissions, to measure the end-to-end delay in the simulations. In the real WSNs, the end-to-end delay can be measured with time stamp counter.

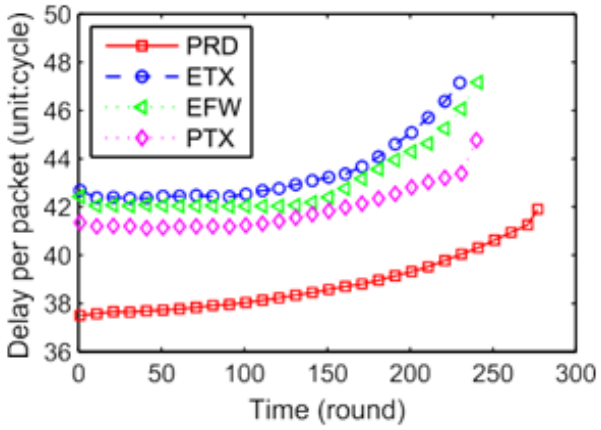

Figure 4. End-to-End Delay

The average end-to-end delay needed to deliver one packet data to the sink during the network lifetime. The end-to-end delay keeps almost stable at the beginning of the network lifetime, and then increase slowly. In ETX and EFW, the end-to-end delay increases mainly because that the length of the routing path increases when some of the sensor nodes die. The increase of the end-to-end delay is that sensor nodes tend to choose father sensor nodes with higher residual energy, whereas in PRD sensor nodes with higher residual energy as well as lower end-to-end delay are preferred to be selected as father nodes. When some sensor nodes that are the optimal choices in the routing path consume most of their energy, they change to be suboptimal, resulting the increase of the length of the routing path and thus the increase of end-to-end delay. The end-to-end delays of ETX, EFW and PTX are similar with each other in each round, because none of them attempt to select paths with lower delay. Nevertheless, PRD effectively chooses paths with the lowest delay, contributing to the best performance of end-to-end delay compared with ETX, EFW and PTX. Moreover, the performance of end-to-end delay in PRD is improved by about 11% compared with ETX.

V. CONCLUSION

This paper proposes a novel link-delay aware energy efficient routing metric called PRD for the routing path selection tailored for WSNs deployed in harsh environments, where the networks are exposed to extremely long end-to-end delay and unbalanced energy consumption among sensor nodes. PRD captures the *predicted remaining deliveries* within one unit of delay, which reflects the ability of each sensor node to forward packets. PRD also takes the end-to-end delay into consideration. The main purposes of PRD are to balance the energy consumption of the sensor nodes and extend the network lifetime, as well as controlling the end-to-end delay. Large-scale simulations are conducted to evaluate the performance of PRD. The results indicate that PRD outperforms traditional metrics such as ETX, EFW and PTX in terms of end-to-end delay, energy consumption and network lifetime performance, while guaranteeing high packet delivery ratio.

VI. REFERENCES

[1] R. C. Carrano, D. Passos, L. C. S. Magalhaes, and C. V. N. Albuquerque, "Survey and taxonomy of duty cycling mechanisms in wireless sensor networks," *IEEE Commun. Surveys Tuts.*, vol. 16, no. 1, pp. 181–194, 1st Quart., 2013.

[2] P. Huang, L. Xiao, S. Soltani, M. W. Mutka, and N. Xi, "The evolution of MAC protocols in wireless sensor networks: A survey," *IEEE Commun. Surveys Tuts.*, vol. 15, no. 1, pp. 101–120, 1st Quart., 2013.

[3] S. Qaisar, R. M. Bilal, W. Iqbal, M. Naureen, and S.

Lee, "Compressive sensing: From theory to applications, A survey," *J. Commun. Netw.*, vol. 15, no. 5, pp. 443–456, 2013.

[4] J. Yan, M. Zhou, and Z. Ding, "Recent advances in energy-efficient routing protocols for wireless sensor networks: A review," *IEEE Access*, vol. 4, pp. 5673–5686, 2016.

[5] N. A. Pantazis, S. A. Nikolidakis, and D. D. Vergados, "Energy-efficient routing protocols in wireless sensor networks: A survey," *IEEE Commun. Surveys Tuts.*, vol. 15, no. 2, pp. 551–591, 2nd Quart., 2013.

[6] O. Gnawali, R. Fonseca, K. Jamieson, D. Moss, and P. Levis, "Collection tree protocol," in *Proc. 7th ACM Conf. Embedded Netw. Sensor Syst.*, 2009, pp. 1–14.

[7] D. S. De Couto, D. Aguayo, J. Bicket, and R. Morris, "A high-throughput path metric for multi-hop wireless routing," *Wireless Netw.*, vol. 11, no. 4, pp. 419–434, 2005.

[8] R. Draves, J. Padhye, and B. Zill, "Routing in multi-radio, multi-hop wireless mesh networks," in *Proc. ACM 10th Ann. Int. Conf. Mobile Comput. Netw.*, 2004, pp. 114–128.

[9] G. Mao, B. Fidan, and B. D. O. Anderson, "Wireless sensor network localization techniques," *Comput. Netw.*, vol. 51, no. 10, pp. 2529–2553, 2007.

[10] S. Lin, J. Zhang, G. Zhou, L. Gu, J. A. Stankovic, and T. He, "ATPC: Adaptive transmission power control for wireless sensor networks," in *Proc. ACM 4th Int. Conf. Embedded Netw. Sens. Syst.*, 2006, pp. 223–236.

[11] R. Khoshkangini, S. Zaboli, and M. Conti, "Efficient routing protocol via ant colony optimization (ACO) and breadth first search (BFS)," in *Proc. IEEE Int. Conf. Cyber, Phys. Soc. Comput.*, 2014, pp. 374–380.

[12] B. Pitchaimanickam and S. Radhakrishnan, "A hybrid bacteria foraging using particle swarm optimization algorithm for clustering in wireless sensor networks," in *Proc. IEEE Int. Conf. Sci. Eng. Manag. Res.*, Nov. 2014, pp. 1–6.

Themed Section : Engineering and Technology
© 2018 IJSRSET | Volume 5 | Issue 3 | Print ISSN: 2395-1990 | Online ISSN: 2394-4099

A Unified Anti-Windup Scheme For PID Controllers

T. Bhuvanendhiran[1], Dr. S. Abraham Lincon[2]

[1]Research Scholar, Department of Electronics & Instrumentation Engineering, Annamalai University, Chidambaram, Tamil Nadu, India

[2]Professor, Department of Electronics & Instrumentation Engineering, Annamalai University, Chidambaram, Tamil Nadu, India

tbhuvanendhiran@yahoo.co.in[1], linsun_2k5@yahoo.co.in[2]

ABSTRACT

This paper presents an anti-windup scheme for PID controllers. The designed work is based on back-calculation and conditional integration schemes. A combined anti-windup scheme is used to eliminate the drawback of back- calculation and conditional integration schemes. Particularly, this scheme it can ensure a better performance for processes with various normalised delay times, an extra tuning parameters are not necessary. Thus, it is more appropriate for execution of industrial regulators due its simplicity.

Keywords: Anti-Wind Up, PID Controller, Normalised Delay Time, Saturation

I. INTRODUCTION

Proportional- Integral- derivative (PID) controllers are most widely used in various industrial settings in spite of several devised control strategies have been developed in the field of automatic control system. On the other hand the PID controller performances are affected in the presence of saturation actuators, which cause the integrator windup [1]. To design the controller to eliminate the integrator windup problem, the actuator constraints has to be taken in to the account, and prevent the degradation of PID performance, subsequently to include an anti-windup compensation scheme. In this scenario a number of schemes have been work out to design the compensator [2, 3]. Mainly they belong to two altered approaches, that is to say, conditional integration and back calculation [4]. Also the conditioning scheme presented in [5, 6]. However, due to a considerable delay time in the process, these schemes are not suitable. They might need an additional tuning attempt, which is objectionable for industrialized regulators. for that reason, a combined anti-windup scheme are implemented to the first order process with various normalised delay times, since the integrator windup occur in lower order process.

II. ANTI- WINDUP SCHEMES FOR PID CONTROLLERS

A. Generalities

The PID controller is described in the Laplace domain:

$$U(s) = Kp\left(E(s) + \frac{1}{T_i s}E(s) - \frac{sTd}{1+s(Td/N)}Y(s)\right) \qquad (1)$$

Where K_P is the proportional gain

T_i is the integral time constant

T_d is the derivative time constant and

N is generally set the value between 5 and 33 [7].

The integrator windup occurs, when a step change in input causes the actuator to saturate. Then the system error decrease more slowly than in the ideal one. Consequently, the value of the integral term becomes huge. As a result, the value of output reaches that of input, the controller still saturates due to the integral term and usually leads to big overshoots and settling times. In general, the integrator windup mainly occurs when a step is applied to the reference set point signal rather than the manipulated variable [8].when the process is a lower order the integrator windup mostly takes place. For these reasons, the first order plus delay time systems are consider in this work.

B. Conditional Integration Scheme

To avoid integrator windup, the Conditional Integration can be adopted. In this Scheme, the integral term is increased only when certain conditions are satisfied, otherwise it is kept constant.

The diverse cases can be described as follows:

1. The integral term is limited to a selected value
2. The integration is stopped when the system error is large, i.e. when $|e| > \bar{e}$ where $\bar{e}$ is a selected value
3. The integration is stopped when the controller saturates, i.e. when $u \neq u_s$
4. The integration is stopped when the controller saturates and the system error and the manipulated variable have the same sign, i.e. when $u \neq u_s$ and $e \times u > 0$.

The above methods have been implemented and compared, fourth case is the best one [4, 9].figure .1 Shows the conditional integration anti-windup scheme.

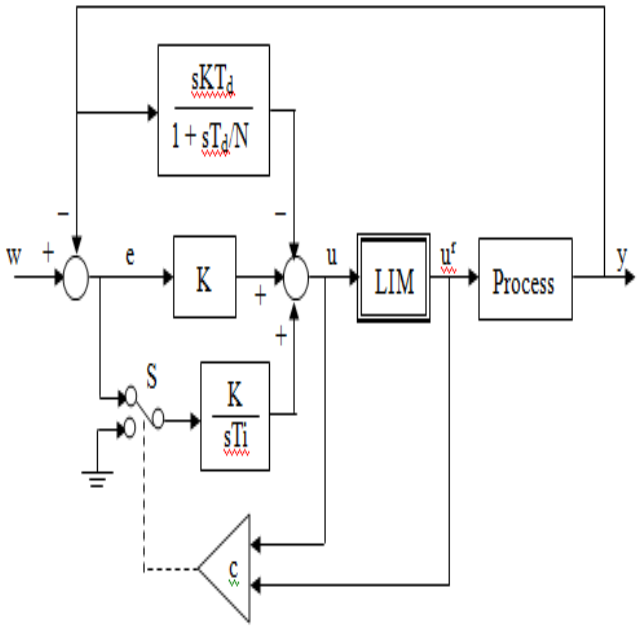

Figure 1. Anti-Windup Scheme of Conditional Integration.

C. Back- Calculation scheme

The back calculation scheme is the substitute approach of conditional integration scheme. Once the controller saturates, it recomputed the integral term. Whenever the difference occurs between saturated and unsaturated control signal, eventually the integral value is decreased by means of feedback, as shown in Figure 2. The integrator input (e_i), as shown in equation (2). Where T_t is called tracking time constant, it determines the rate at which the integral term is reset and its choice of value gives the performances of the complete control scheme.

$$e_i = \frac{K_p}{T_i} e + \frac{1}{T_t}(u_s - u) \qquad (2)$$

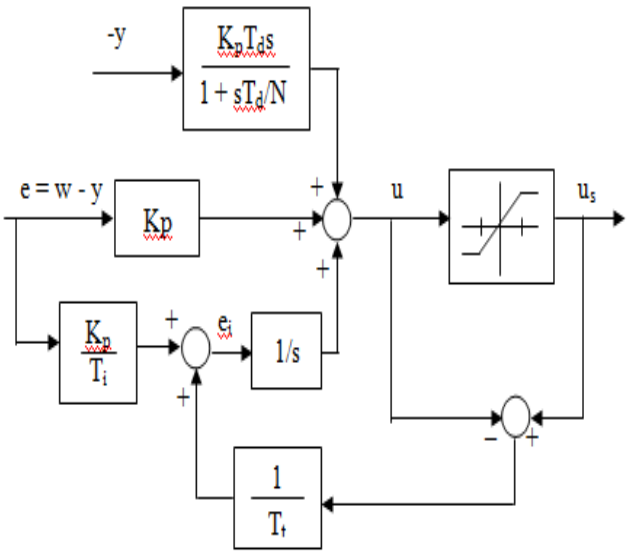

Figure 2. Anti-Windup scheme of Back-Calculation

D. Combined Scheme

A simple modification is made in combined scheme, to overcome the drawbacks between conditional integration and back calculation scheme. In particular, the back-calculation works when the controller Saturates, the system error has the same sign of the manipulated variable and the system output has left from before reference value. This can be stated as:

$$e_i = \begin{cases} \frac{K_p}{T_i} e + \frac{1}{T_t}(u_S - u), & \text{if } u \neq u_S \text{ and } u \times e > 0 \\ \frac{K_p}{T_i} e & \text{otherwise} \end{cases} \quad (3)$$

The intension of (3) is to permit an increase in the integral term, while the process output (transient) has not started due the delay time. The combined scheme basically performs as the standard back calculation scheme when delay time is small. In any case, it is possible to set a single value for T_t for various cases. And this value can be considerably lesser than T_i allowing improved performance for small normalized delay times.

III. SIMULATION RESULTS

Different anti-windup schemes are designed and incorporated to the various processes with different normalized delay times θ_1=0.2 and θ_2=0.4, which is depicted in following:

$$P_1(s) = \frac{1}{10s+1} e^{-2S} \quad (4)$$

$$P_2(s) = \frac{1}{10s+1} e^{-4S} \quad (5)$$

For both processes, Ziegler-Nichols formula has been applied, to get the PID parameters tuning values, the values are described in Table 1.

Parameter	$P_1(s)$	$P_2(s)$
K_p	6	3
T_i	4	8
Td	1	2
N	10	10

Table 1.PID Tuning Parameters Values

A positive unit step input has been applied to the system and output of the system with different anti-windup schemes for process $p_1(s)$ and $P_2(s)$ are shown in figure 3, figure 4, figure 5 and figure 6. And also without anti-windup scheme for process $P_1(s)$ and $P_2(s)$ are shown in figure 7 and figure 8. The observations made from responses and performance criteria, the combined scheme provided better performance for both first order processes with various normalized delay times. Particularly the overshoot and settling times are very less when compared to without anti-windup schemes. The table 2 and 3 shows the performance criteria of process $P_1(s)$ and $P_2(s)$.

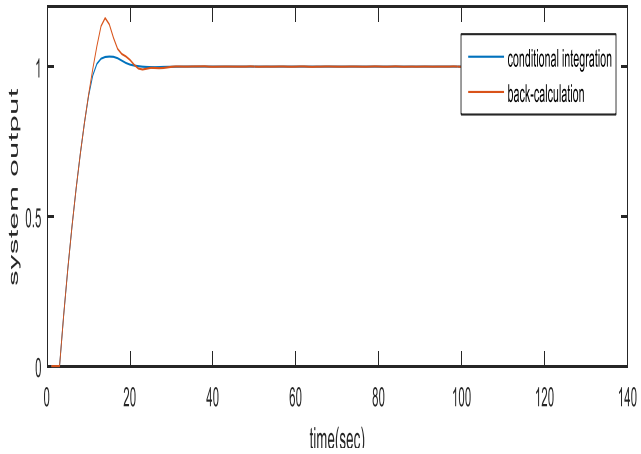

Figure 3. Step Response for P1(S) For the Considered Anti-Windup Schemes

Conditional integration 2. Back-calculation with Tt=Ti

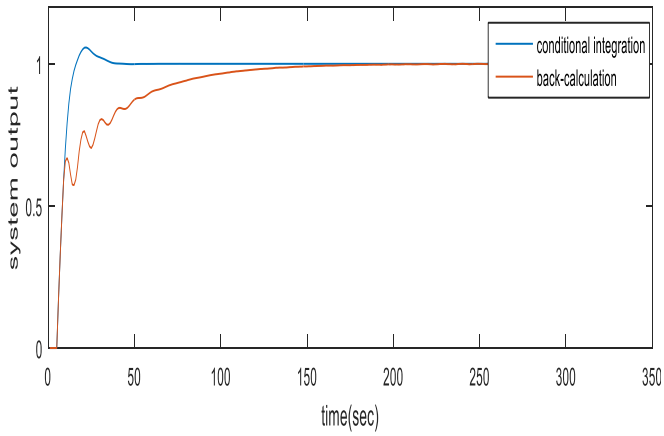

Figure 4. Step Response for $P_2(S)$ For the Considered Anti-Windup Schemes

1. Conditional integration 2. Back-Calculation with $T_t=T_i$

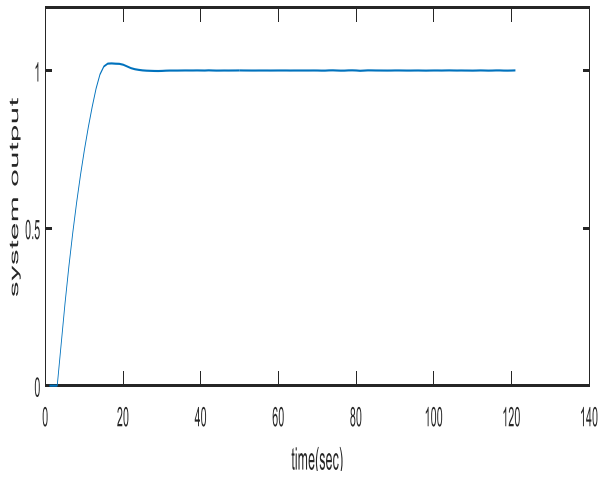

Figure 5. Step Response for $P_1(S)$ For the Combined Anti-Windup Schemes

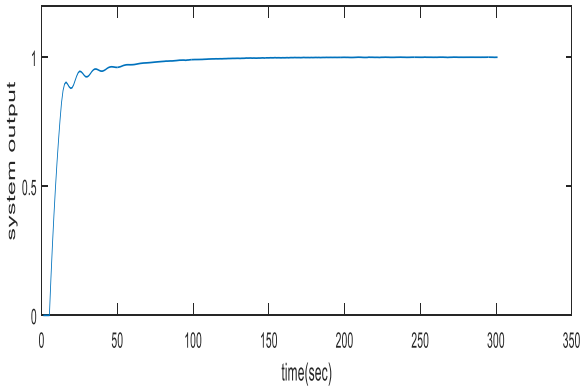

Figure 6. Step Response for $P_2(S)$ For the Combined Anti-Windup Schemes

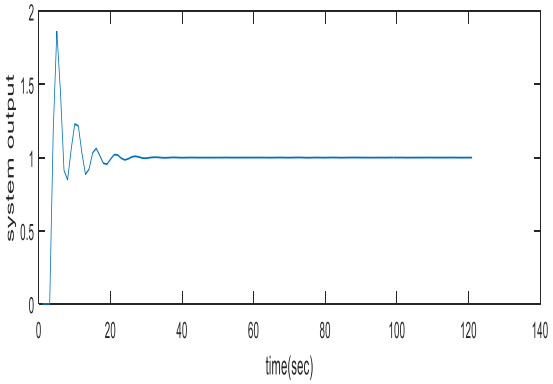

Figure 7. Step Response for P1 (S) For Without Anti-Windup Schemes

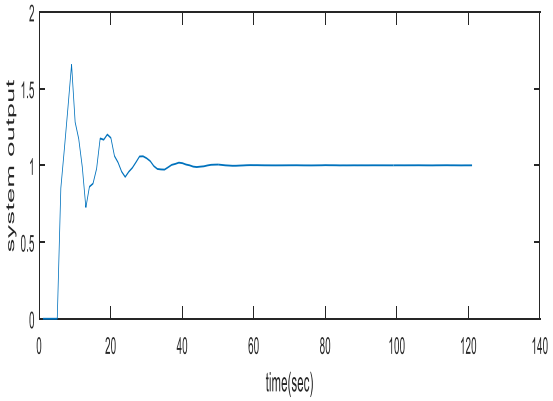

Figure 8. Step Response for P2 (S) For Without Anti-Windup Schemes

Table 3. Comparison Criteria for Process $P_1(s)$

Schemes	**ISE**	**IAE**	**Settling Time (t_s) in secs.**	**% over shoot (% M_p)**
Without anti-windup	3.03	4.85	21.10	86.47

Conditional Integration	4.82	6.75	18.02	3.36
Back Calculation	4.791	7.09	22.42	11.43
Combined Scheme	4.82	6.76	19.27	2.20

Table 4. Comparison Criteria for Process $P_2(s)$

Schemes	**ISE**	**IAE**	**Settling Time (t_s) in secs.**	**% over shoot (% M_p)**
No anti-windup	4.95	7.78	35.52	65.75
Conditional Integration	6.24	8.39	31.11	5.75
Back Calculation	9.75	22.8	118.02	0.05
Combined Scheme	6.95	12.16	72.67	0.01

IV. CONCLUSION

Combined anti-windup scheme for PID controller has been implemented to the first order process with delay time, this combined scheme offer good performance over a wide range of processes without any extra tuning effort from the control system engineer. And it is very suitable to adopt the industrial regulators due to its overall simplicity.

V. REFERENCES

[1] SCOTTEDWARD HODEL, A., and HALL, C.E: 'variable-structure PID control to prevent integrator windup', IEEE Trans.ind.electron.2001, 48, (2), pp.442-451

[2] BOHN, C., and ATHERTON, D.P.: 'An Analysis package comparing PID anti-windup strategies', IEEE control sys, mag., 1995,pp.34-40

[3] PENG, Y., VRANCIC, D., and HANUS, R.: 'Anti-windup, bumpless, and conditioned transfer techniques for PID controller', IEEE control syst. Mag., 1996,pp.48-57

[4] ASTROM, k., and HAGGLUND, T.: 'PID controllers: theory, design and tuning' (ISA press, Research Triangle park, North Carolina, 1995)

[5] HANUS, R., KINNAERT, M., and HENROTTE, J.: L.: 'Conditioning technique, a general anti-windup and bump less transfer method', Automatica, 1987,23, (6), pp.729-739

[6] WALGAMA, K.S., RONNBACK, S., and STERNBY, J.: 'Generalization of conditioning technique for anti-windup compensator', IEE proc., control theory Appl., 1991,139, (2), pp.109-118

[7] VISIOLI, A 'practical PID control' Springer, London, UK, 2006.

[8] VRANCIC, D.: 'Design of anti-windup and bump less transfer protection'. PhD thesis, university of Ljubljana, Ljubljana,Slovenia,1997.

[9] HANSSON, A., GRUBER, P., and TODTLI, J.: 'Fuzzy anti-reset windup for PID controllers', Control Eng. Pract., 1994,2,(3),pp.389-396

Themed Section : Engineering and Technology
© 2018 IJSRSET | Volume 5 | Issue 3 | Print ISSN: 2395-1990 | Online ISSN: 2394-4099

Spectrum Allocation for Downlink 4G Networks

P.Sakthibalan[1], J.Brindhadevi[2], Dr. K.Devarajan[3]
[1]Research Scholar, Annamalai University, Chidambaram, Tamil Nadu, India
[2]M.E, Communication Systems, Annamalai University, Chidambaram, Tamil Nadu, India
[3]Assistant Professor, Annamalai University, Chidambaram, Tamil Nadu, India
balan1109@gmail.com[1], j.jothini@gmail.com[2], devarajan_lecturer@yahoo.com[3]

ABSTRACT

The rapid growth of 4G network give more wireless services to many users at a time in network. Many services are providing by service providers but it can face many problems in network like traffic congestion, call dropping and call blocking during handover process. In this paper, we are introducing a spectrum allocation in 4G network, which can reserve some amount spectrum from the network resource. By using adaptive CAC is reserved spectrum resource are allocated for handoff calls and new calls during users handover. It used to regulate the traffic, improved QoS, efficient spectrum efficiency and reduce spectrum degradation. The results are shown in numerical result and analytical study that the adaptive call admission control is guarantee the allocation of spectrum is used to regulate the calls by providing efficient QoS in the network resources.

Keywords: CBP, CDP, Handoff calls, new calls, 4G, QoS

I. INTRODUCTION

The enormous growth of cellular network was introduced by the 3rd generation partnership project (3GPP) 4G -long term evolution (LTE). To provide high data rate, more desired spectral efficiency and increase wide area coverage to large number of users. These objectives are achieved by only reducing traffic, delay, loss and also give effective quality of services to the users. The radio resources management (RRM) provide solution to above objectives by one of its fundamental techniques known as (CAC) call admission control. The CAC scheme gives opportunity to new call and handoff call when handover occur. It also regulates the QoS of existing calls without degrading any call drops. This scheme satisfy the users by providing continuation of calls when handover occur, its achieved by reserved some amount of bandwidth in the network resources. So the scheme provides effective network resources allocation and excellent QoS to the users.

In this scheme some amount of bandwidth is dynamically reserved for handoff cal and new call using time varying status. But there is some disadvantage due to reservation of bandwidth, because reserved network resource is unutilized or wasted when there is no handover occurred and it become inefficient use of network resources. We introduced an adaptive call admission control with reservation spectrum to overcome the inefficient use of the network utilization. In this paper it will provide three important makeovers they are

- Reducing (CBP) call blocking probability for new calls and (CDP) call dropping probability for handoff calls.
- Maximize the throughput by reducing inefficient use of network resources.

- Improving quality of services by regulating calls in network, even under heavy traffic intensity.

The next section of this paper is, we provide the overview of the related works in II section, the introduction of the system model of our proposed scheme in section III, the Analytical study is illustrated in section IV, Numerical result and discussion in section V. Finally, conclusion of this paper is given in section VI.

II. RELATED WORKS

In [3] proposed work was a channel borrowing scheme which is borrowed the bandwidth from the available network resources and its reserved for high priority calls from the best effort traffic (BE). This scheme is dynamically reserved bandwidth using time varying status for handoff calls.

In [4] this paper shown the lot of momentum in LTE network based on reservation of CAC scheme relies on allocation of adaptive multilevel bandwidth for non–real time (NRT) calls. The disadvantage of this scheme is ignored the high CBP due to allocation of bandwidth which cause low utilization of network resources.

In [5] this proposed work scheme based on cognitive radio network for an interference aware spectrum handover. Which is maximised the network capacity and reduce the usage of spectrum. The spectrum handover problem is solved by heuristic algorithm.

In [6] this paper present the multiple sectors in cellular network for overlapping region is used by channel reservation and pre-emption (CRP). Here its reducing the CDP for handoff calls by using directional antennas are installed on enodeB which is coverage area is divided into equal sized sectors.

In [7] this work investigated about the effect of vertical handoff in heterogeneous networks. Congestion game problem is solved by this scheme. In [8] this paper showed the achievement of efficient resources utilizations by calculating total throughput of QoS performance in CAC algorithm.

In [9] the scheme of wireless broadband cognitive network work designed framework and an optimization techniques is formulated to considering the demands for each service providers and cognitive subscriber. In [10] this paper shown the CAC reservation algorithm has two kinds of applications known as narrow band and wide bands. But it has poor resources utilization to reserve and predict for avoid QoS degradation.

In [11] proposed scheme have statically and dynamically reserves network resources due to sustain the undetectable quality fluctuations throughout the handover process in LTE networks, which is based on prior knowledge for dynamically reserve resources. But it increases the system complexity and inefficient network resources.

The above-related works show the benefits and challenges of CAC scheme in network resources. We proposed the spectrum reservation by adaptive call admission control in cellular networks in the next sections.

III. PROPOSED SYSTEM

In this proposed work, there is an improvement of reservation scheme in network resources than the traditional CAC scheme. Normally CAC scheme is based on the BE traffic which reserved bandwidth for high level priority call. Due to borrowing period it cannot admitted into the network throughput which is lead to starvation. So there will be increase in CBP and CDP. It makes ineffective usage of network resource due to repeated occurrences of handoff calls and new calls, which is lead to unutilization of spectrum available in the network. In this paper our proposed work will be increase the efficient use of spectrum utilization in network resource by adjusting

the available spectrum to increase the number of admitted calls with adaptive QoS, avoid starvation in BE traffic, adaptive CAC scheme is use different traffic loads to admit new users according to the priority of the calls and its employs the different adaptive threshold value by QoS requirement according to the consideration of user traffic to increase the efficient spectrum utilization in the network.

According to the priority of calls, the real time traffic (RT) has high priorities for handover process. Spectrum requirement for handoff call or new call in the network resources can be described in equation as

$$a_i = SW_i^{max} \quad (1)$$

The call admission criteria for call i is denoted as a_i while the maximum spectrum for call i is denoted as SW_i^{max}

The spectrum requirement of handoff or new call belongs to NRT or BE traffic, which is calculated as follows:

$$a_i = SW_i^{min} \quad (2)$$

Where SW_i^{min} denote the minimum spectrum requirement for call i. Furthermore, when the available spectrum cannot be enough to admit new call, spectrum degradation approach is applied to RT traffic since they were assigned enough; this will save the BE traffic from starvation. Therefore, to compute spectrum degradation for each class j considers the given equation below:

$$SW_j^{degraded} = SW_j^{max} - D_j^{level} \quad (3)$$

Where $SW_j^{degraded}$ denote degraded spectrum for class j, SW_j^{max} represent available spectrum and D_j^{level} is the present degradation level. However, Equation (3) must satisfy Equation (4) as given below:

$$SW_j^{max} - D_j^{level} \geq SW_j^{min} \quad (4)$$

Therefore, the maximum spectrum degradation size is derived as follows:

$$SW_j^{degsize} = \frac{SW_j^{max} - SW_j^{min}}{D_j^{level}} \quad (5)$$

Where $SW_j^{degsize}$ represent maximum spectrum degradation size of class j. To accept a new call or handoff into the network using the proposed criterion, the spectrum allocated to an admitted new call or handoff is represented as $SW_{i,handoff(t)}$ and $SW_{new\ call(t)}$ over time. A handoff call *handoff* - $call_{accept(t)}$ is accepted into the network when the following condition is satisfied.

$$\text{Handoff} - call_{accept}(t) = (SW_{i,handoff} + SW_{handoff\ call}(t) + SW_{newcall}(t) \leq SW_{total}) \quad (6)$$

Where $SW_{i,handoff}$ is the admission criterion for call i. A threshold value is introduced, to change the reservation spectrum using various traffic loads for handoff calls. The threshold block new request when the number of call is higher than the threshold value.

$$th_{adaptive} = (\tau \text{ handoff} * K) * SW_{req} \quad (7)$$

Where $th_{adaptive} = \frac{\lambda_{RT}}{\mu_{RT}}$ represent the traffic load, λ_{RT} and μ_{RT} denote the arrival rate and mean service of handoff call respectively. Moreover, SW_{req} is the required spectrum for each handoff call, while K is the reservation spectrum factor, K ϵ (0,1) . A new call $new - call_{accept}(t)$ is accepted into the network when the below condition is satisfied.

$$\text{New-}\ Call_{accept} = (SW_{i,new} + SW_{handoffcall}(t) + SW_{newcall}(t) \leq SW_{total} - th_{adaptive} \cap (SW_{i,new} \leq SW_j^{degraded})) \quad (8)$$

Where $SW_{i,new}$ is the new admission criterion for call i, and $SW_j^{degraded}$ is the degradation level for each call. The first term on the right-hand side (RHS) aims that existing and new calls are not above total

spectrum for the new call. While the last term at the RHS ensures that new calls are admitted even when there is inadequate number of spectrum.

IV. ANALYTICAL STUDY

In this section we described the analytical model for our proposed CAC scheme. Using this model we derive CDP and CBP for the different traffic classes and extensive experimental simulation is carried out to verify its accuracy. In this model, we have one base station called evolved NodeB (eNodeB) and several UEs, as illustrated in Fig.1 some UEs are within the cell and are requesting for the new call, while others are outside the cell hence requesting for handoff call.

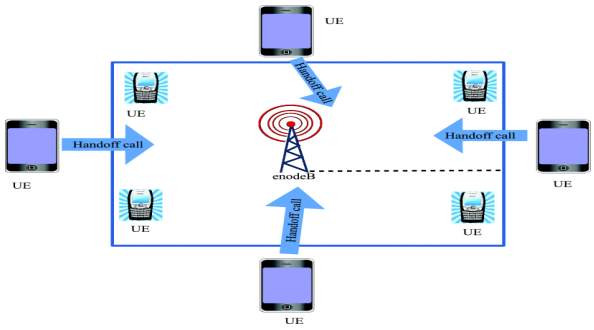

Figure 1. Simulation Topology

When there is an incoming handoff or new call the UEs request for the available bandwidth from the eNodeB. We have two different types of calls in our model: (a) Handoff call, an example is RT traffic with highest priority (b) New call consists of NRT traffic and BE traffic with lowest priority respectively. Each of this traffic has different QoS requirements and therefore. The QoS guarantees to enable them a request for the new call or handoff call. At the eNodeB, a CAC mechanism is employed which admits new call and reserves bandwidth for handoff calls, when there is unused bandwidth, while admitted calls are degraded to their lowest level. Otherwise, neither of the calls is admitted. Accordingly, the user call might either be effectively handed off to a new base station or just dropped when it is about to depart the current cell.

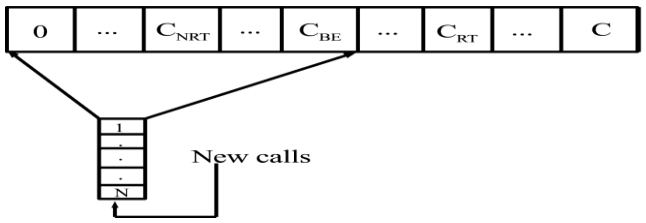

Figure 2. System Architecture

In Fig .2 we describe the model of the proposed scheme. The new call CBP and the handoff CDP are used as evaluation measure for the proposed scheme. The handoff calls have priority over new calls since the termination of handoff call in progress is more frustrating, less tolerable and less desirable than blocking anew call. This can be achieved by limiting a new call into the cell when the total number of user calls or the total occupied bandwidth is greater than the threshold value.

Furthermore, to obtain CDP, CBP, global balance equation, and a steady probability of the proposed scheme let makes the following assumptions. The arrival rate of handoff call (λ_{RT}),new calls (λ_{NRT}) and BE traffic (λ_{BE}) used Poisson distribution while their mean service uses exponential distribution with parameters as $C_{RT}\,\mu$, $C_{NRT}\,\mu$ and $C_{BE}\,\mu$ respectively while the queue size of new calls is represented as N. These probabilities are obtained by modelling the proposed using two level Markov chain transition diagram as shown in Figure. 3.

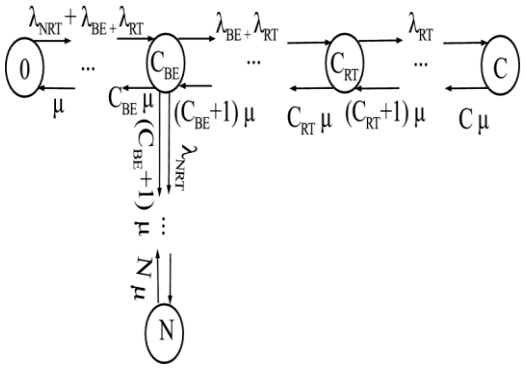

Figure 3. Markov Chain State Transition Diagram

The state space of the proposed model is based on the number of calls accepted and the degraded level of new call. The possible states of our model is represented as S = $(0; C_{BE}; C_{RT}; C_g)$. When the

number of channels in Fig. 4. Is busy then the probability P (i) can be obtained from the transition diagram. The global balance equations can be derived as follows:

$$i_\mu P_{(i)} = (\lambda_{NRT} + \lambda_{BE} + \lambda_{RT})\ P\ (i-1), 0 \leq\ i \leq C_{BE} \quad (9)$$

$$i_\mu P_{(i)} = \lambda_{NRT} P\ (i-1), C_{BE}\ < i \leq N \quad (10)$$

$$i_\mu P_i = (\ \lambda_{BE} + \lambda_{RT})\ P(i-1), C_{BE} < i \leq C_{RT} \quad (11)$$

$$i_\mu P_{(i)} = \lambda_{RT} P(i-1), C_{RT} < i \leq C \quad (12)$$

The steady probability P (i) can be derived as:

$$P_i = \begin{cases} \frac{(\lambda_{NRT}+\lambda_{RT}+\lambda_{BE})^i}{i^! \mu^i} p(0) & 0 \leq i \leq C_{BE} \\ \frac{(\lambda_{NRT})^{i-C_{BE}}(\lambda_{NRT}+\lambda_{BE}+\lambda_{RT})^{C_{BE}}}{i^! \mu^i} P(0), & C_{BE} < i \leq N \\ \frac{(\lambda_{NRT}+\lambda_{RT})^{i-C_{BE}}(\lambda_{NRT}+\lambda_{BE}+\lambda_{RT})^{C_{BE}}}{i^! \mu^i}\ P(0) & C_{BE} < i \leq C_{RT} \\ \frac{(\lambda_{RT})^{i-N}(\lambda_{NRT}+\lambda_{BE}+\lambda_{RT})^{C_{BE}}}{i^! \mu^i}\ P(0) & C_{RT} < i \leq C \end{cases} \quad (13)$$

The summarized steady-state probability of the propose model is $\delta\ 0, C_{BE}, C_{RT}$, C and characteristic function is given as $\pi\ (0, C_{BE}, C_{RT}\ )$. Equations 14 below avoid the model being in an invalid state.

$$\pi(0, C_{BE}, C_{RT}, C) = \begin{cases} 1, & (0, C_{BE}, C_{RT}, C) \in S \\ 0, & otherwise \end{cases} \quad (14)$$

Furthermore, normalized condition for the proposed model is given as:

$$\sum(0, C_{BE}, C_{RT}, C) \in S\delta(0, C_{BE}, C_{RT}) = 1 \quad (15)$$

Therefore, the CDP and CBP are computed as:

$$\text{CDP} = \sum_{i=0}^{C_{RT}} P(i) \quad (16)$$

$$\text{CBP} = \sum_{i=0}^{C_{BE}+N} p(i) \quad (17)$$

Thus the global balanced equation is used to obtain CDP and CBP from the probability of the proposed scheme.

V. NUMERICAL RESULTS AND DISCUSSION

The performance of the proposed scheme is measured in terms of CBP, CDP, and throughput and degradation ratio. The simulation scenario consists of one hexagonal cell with 500 m radius. The total spectrum used is 5 MHz with 25 resource block per slot of 12 subcarriers spacing. The call request can be classified into different classes based on their QoS requirement and call types. Based on QoS requirements the call scan is categorized as HC and NC. The HC these are RT traffic with the highest priority and the best example is live streaming. On the other hand, the NC is differentiated into two types of traffic: NRT traffic example YouTube and the BE traffic example email. The arrival rate for both RT and NRT is in the form of a Poisson distribution with the service mean exponentially distributed. The total simulation time is 1000s, while the results are obtained by taken the average over 20 times of simulation.

Table 1.Simulation Parameters

Parameters	Value
System bandwidth	5MHz
Numbers of RBs	25
TTI	1ms
Call arrival	Poisson process
Simulation period	1000s
Speed of the user	4.16 m/s for moving user
Transmission scheme	2X2 MIMO, OLS
Cyclic prefix used	Normal cyclic prefix
UE Distribution	Uniform
$\lambda_{NRT}, \lambda_{BE}, \lambda_{RT}$	1

In proposed system the energy consumption is reduced when its compared to the existing system. Due to the low traffic intensity (arrival rate 1-2.4), the improvement was done by avoid starvation. In figure, 5 shown 86.15% of energy consumption is used in proposed scheme.

In this system using reserved spectrum with CAC algorithm they were reserved some spectrum for HC and NC. So spectrum efficiency is increased due to the adaptive threshold value. In figure 6 shown the percentage 95.65% are efficiently used in the network.

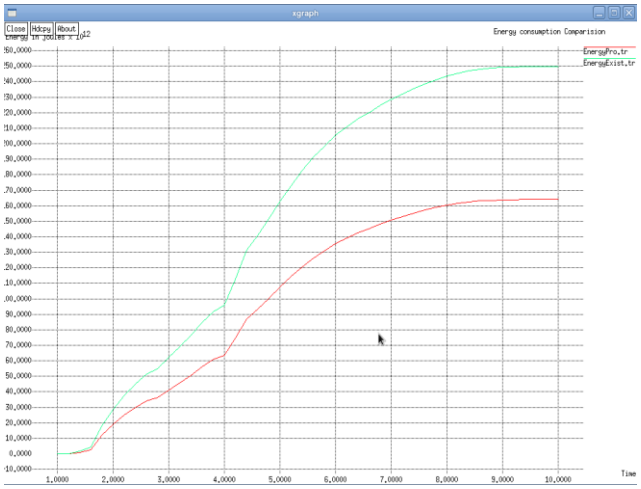

Figure 4. Energy Consumption

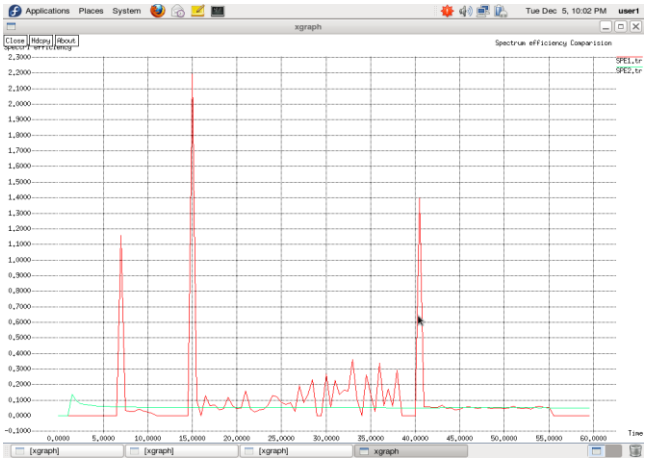

Figure 5. Spectrum Efficiency

VI. CONCLUSION AND FUTURE ENHANCEMENT

Spectrum allocation with adaptive call admission control in 4G cellular Networks to prevent starvation of user traffic and improved the effective usage of network resources. The new scheme introduced adaptive CAC criteria to avoid starvation of user traffic. The criteria use spectrum degradation to admit many users when there are insufficient network resources to accommodate new users. The proposed scheme in addition to its spectrum degradation included an adaptive threshold value which adjusted the network conditions to enable efficient use of network resources. Simulation results and numerical results are in total agreement with negligible differences.

Results also show the outstanding performance of the proposed scheme as it was able to achieve an improvement of data throughput, reduces CBP, CDP and degradation ratio as compared to the Reservation-Based scheme and other spectrum degradation schemes. This further indicates that the proposed scheme achieves higher resource utilization and provides effective QoS assurance for cellular networks. In the future, we intend to look at how to manage the energy efficiency of user traffic and eNodeB for an effective handover.

VII. REFERENCES

[1] Y. Xiao, C. P. Chen, and B. Wang, "Bandwidth degradation Qos provisioning for adaptive multimedia in wireless/mobile networks," Comput.Commun, vol. 25, no. 13, pp. 1153–1161, 2002.

[2] S. K. Das, S. K. Sen, K. Basu, and H. Lin, "A framework for bandwidth degradation and call admission control schemes for multiclass traffic in next-generation wireless networks," IEEE J. Sel. Areas Commune., vol. 21,no. 10, pp. 1790–1802, Dec. 2003.

[3] M. Ghaderi and R. Boutaba, ``Call admission control in mobile cellular networks: A comprehensive survey,'' Wireless Communication. Mobile compute. vol.6, no. 1, pp. 69_93, 2006.

[4] J. C. Ikuno, M. Wrulich, and M. Rupp, "System level simulation of LTE networks," in Proc. IEEE 71st Veh. Technol. Conf. (VTC-Spring),Jun. 2010, pp. 1–5.

[5] M. Tsang, K. Tsang, J. C.-K. Wong, and H. Tung, 'Call admission control for long term evolution," in Proc. IET Int. Communication. Conf. Wireless mobile Compute (CCWMC), 2011, pp.455–460.

[6] J. Vijay Franklin and K. Paramasivam, "Utility based scheduling and call admission control for LTE (3GPP) networks," J Inf. Tech. Software. Eng., vol. 2, no. 113, p. 2, 2012.

[7] M. Khabazian, O. Kubbar, and H. Hassanein, ``Call admission control with resource reservation for multi-service OFDM networks,'' in Proc. Int. Conf. Compute., Network Communication. (ICNC), 2012, pp. 781_785.

[8] S. A. Khanjari, B. Arafeh, K. Day, and N. Alzeidi, "Bandwidth borrowing based Qos approach for adaptive call admission control in multiclass traffic wireless cellular networks," Int. J. Communication. Syst., vol. 26, no. 7, pp. 811–831, 2013.

[9] D.-H. Kim, D. Zhang, N. Bhushan, R. Pankaj, and S.-J. Oh, ``Admission control for cellular networks with direct QoS monitoring,'' Wireless Network., vol. 19, no. 2, pp. 131_144, 2013.

[10] M. Shehada, B. Fu, S. Thakolsri, and W. Kellerer, "QoE-based resource reservation for unperceivable video quality fluctuation during handover inLTE," in Proc. IEEE Consume. Communication. Network. Conf. (CCNC), Jan. 2013, pp.171–177.

Themed Section : Engineering and Technology
© 2018 IJSRSET | Volume 5 | Issue 3 | Print ISSN: 2395-1990 | Online ISSN : 2394-4099

A Clustering Based Hyper Spectral Image (HSI) Classification and Segmentation for Satellite Remote Sensing

C. Rajinikanth[1], Dr. S. Abraham Lincon[2]
[1]Research Scholar, Department of Electronics & Instrumentation Engineering, Annamalai University, India
[2]Professor, Department of Electronics & Instrumentation Engineering, Annamalai University, India
[1]rajini_tamil@yahoo.co.in

ABSTRACT

In this paper, a new algorithm has been designated for classification of satellite remote sensing of hyperspectral image. The classification process is based on the three main categories: (1) image fusion, performed using morphological process of both spatial and spectral information available in the remote sensed images. (2) Clustering, which performed in supervised techniques using thresholding effect of image pixel intensity and (3) segmented and texture based image analysis, in this process to achieve a new textural based image clustering to overcome the problem of multi-label images in satellite remote processing. Finally, it gets clustered and result in segmented output. The proposed research contribution is validated by classification experiments using Airborne Visible/Infrared Imaging Spectrometer (AVIRIS) image sensors from the results the overall accuracy of single and multi-label of Salinas's dataset.

Keywords : Hyper Spectral Image, Satellite Remote Sensing, Clustering, Classification, Segmentation

I. INTRODUCTION

Digital image processing supports strong research in the areas of image segmentation, enhancement and image based pattern recognition. Nowadays, these areas are widely applied in remote sensing, medical image processing, radar, sonar, acoustic image processing and robotics. Among these areas Image segmentation is used everywhere to simplify and to change the representation of image in to something that is more meaningful and easier to analyse. In traditional segmentation, a general pixel clustering process is presented based on thresholding effect of image pixel intensity. In this type of segmentation, cluster separation is extracted by using mean feature of image pixel. Modern segmentation process is performed based on individual features of image pixels. Min Wang et al [1]. Discussed the several appropriate model of region line association constraint with manmade object and natural objects. They including the parallel straight line (PLSL) neighborhood, the perpendicular straight line (PPSL) neighborhood, and the PLSL methods. The structural constraints is giving a hard-boundary-constrained segmentation method (HBC-SEG) [11] for multiscale image segmentation. The proposed method has validated the error decreasing in over segmentation and insignificant increasing in under segmentation methods. The improved object-based image analysis methods can help to identify the clear object for improved constraint-based image segmentation methods, including HBC-SEG [1],[11],HBCIPSL [1],[11], and HBC-XXSL[1], [11].Yongyue Hu et al [2]. Suggested a new approaches for determination of region-growing criteria, edge-guided image object detection, and assessment of edges in multiscale segmentation. The image target detection is designed for overcoming the difficulties of the classical image

object detection in multiscale segmentation. H.Gökhan Akçay et al [3]. Discuss the generic method for the modelling and detection of compound structures that involve arrangements of an unknown number of primitives in large scenes of remote sensing. The modelling process are investigates via Markov random field and the detection task has formulated as the selection of multiple subsets of candidate regions from a hierarchy segmentation. Where each set of selected regions has been constituted an instance of the compound structure. The combinatorial selection problem of hierarchy segmentation is solved by the joint sampling of groups of regions by maximizing the likelihood of their individual appearances and relative spatial arrangements of remote sensing images. Yanfei Zhong et al [4] have developed a new technique of highly efficient Multiscale and Multi feature Normalized (MMN) cut algorithm for HSR imagery segmentation. The MMN cut is much less sensitive to image boundaries and also preserves the multi scale information. Normalized Cuts (NC), as a commonly used for the method of natural image segmentation of remote sensing images. It can also acquire a globally optimized segmentation result equivalent to the optimized partitions of a super pixel graph. These graph which can provide powerful indication to guide the HSR imagery segmentation. Guiyun Zhou el al [5]. Suggested a appropriate method for terrestrial laser scanning in planner segmentation of satellite segmentation. The planner segmentation is parameterized by its normal vector and the distance from the origin. It is multiple standpoints can be used for such applications as plane-based registration and 3-D reconstruction of buildings has been presented. F. A. Ávila Rodrigues et al [6]. Investigated on Synthetic Aperture Radar (SAR) [6], [12] image roughness due to the presence of speckle noise in remote sensing problems. In this method is estimated roughness parameters of SAR images, instead of directly processing the speckled images. SAR image algorithms based on thresholding and level set applied to synthetic and real SAR images. Due to speckle the SAR image segmentation can be hard to achieve using thresholding-based techniques and it can be suitable when applying these techniques to the estimated roughness parameters for single-look SAR images. Zhang Chunsen et al [7]. Stated that appropriate method for classification accuracy of hyper spectral image is improved by using a probabilistic weighted strategy for multi featured function. In this technique concentrate on weighted for different features and rewriting the SVM classification of P-fusion for makes full use of every single spectral–spatial feature. The probabilistic weighted strategy is compared with the VS-SVM and P-fusion, effectively improves the classification accuracy by giving feature weights based on the performance of different features. Junping Zhang et al [8]. Developed a method for object-based mid-level representation for semantic classification for high resolution remote sensing images. The mid-level representation method is how to boost the relatively low classification accuracy caused by using pixel-based image classification approaches and low-level visual structure. The method of low-level visual features and high-level semantics are not well define in semantics images. The object-oriented semantic classification algorithm that combines bag-of-visual-words (BOV) with the optimal segmentation scale intends to overcome the defect of conventional BOV in lacking of relationship between image patches and to give more thorough description. Ribana Rosche et al [9]. Presented a shapelet-based spatial–spectral classification of hyperspectral image data. The shapelet-based approach varies from earlier suggested sparse representation- based classifiers for hyperspectral image data. In this method that sophisticated prior knowledge about the spatial nature of an image is exploited by applying a constructed highly adapted patch-specific based classification procedures by means of the representation error. The shapelet-based spatial–spectral classification approach shows greater outcomes in comparison to sparse-representation-based classifiers that use only limited spatial information. Erlei Zhang et al [10].

II. STUDY AREA

The Salinas hyperspectral datasets is selected for classification Experiments. The Salinas datasets captured by the Airborne Visible/Infrared Imaging Spectrometer (AVIRIS) sensor with 224 spectral band and the dataset has a pixel value of 512 × 217 and spatial resolution of 3.7m of Fig.1 shows the RGB colour composition and ground truth reference map and colour code of Salinas's dataset. Training Data: A training set is a set of data used to discover potentially predictive relationship. Test Data: A test set is a set of data used to assess the strength and utility of a predictive relationship. In our process, the images are Train Data for 77% of different Dataset and its corresponding Test Data for 23% of the different Dataset.

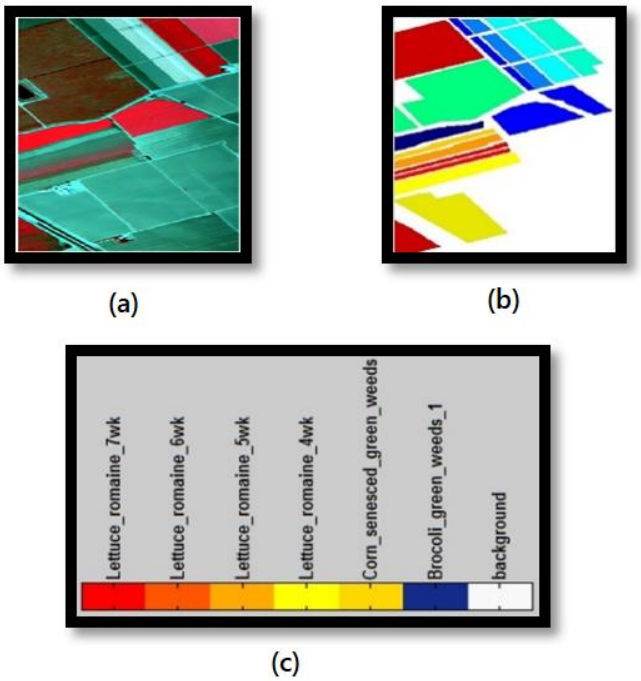

Figure 1. Dataset of Salinas (a) RGB image composite, (b) Ground- truth map, (c) Color code of different classes

III. RELATED WORKS

A. Cellular Automata

The Cellular Automata (CA) is simple method and synchronous transition technique. The remote sensed digital image like Salinas is considered as 3×3 bidirectional array. Thus, each pixel is characterized by the triplet variables as (i, j, k) .Where (i, j) represent the position of the pixel and k is the associated colour. The, k is assumed as to be 2^8 colour resolution. The CA follows two different rules for filtering depending on the location of the pixels in the images. The rule for the filtering pixel within the boundary involves the averaging neighbourhood pixels. The neighbour pixels are taken by using Moore or Neumann structure [13] format. The rule for the filtering boundary or contour pixels involves using the threshold value.

B. Histogram Equalization

The filtered image is enhanced using the histogram equalization. This histogram equalization involves in the assignment of the minimum value of the pixel intensity is considered as 0 and maximum value of the pixel intensity as 255, as the colour intensity is 2^8 bit resolution.

IV. PROPOSED METHOD

In this section has been elaborated the proposed system strategy of HSI classification of remote sensing image as shown in Fig.2.The proposed approach consist of three prevalent techniques, including image fusion, image clustering and segmentation. The image fusion has been performed based on pre-processing by using CA based image filtering. This provide smoothness to the image pixel and the image enhancement has been performed by using Histogram Equalization (HE). HE is provide clear depth information of the image. The image clustering is achieved through Spectral Spatial (SS) supervised HSI classification. Finally, it is clustered and result in segmented output.

A. Proposed SSTBA Methods

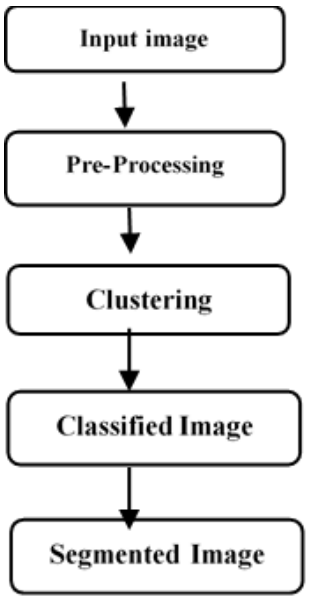

Figure 2. Block diagram of Proposed System

In this section introduces the concepts of and strategy employed to Spectral Supervised Tree Baggar Algorithm (SSTBA) for remote sensing. Proposed a supervised SSTBA classification including a new construction approach for hyper spectral image classification applied to neural networks. The SSTBA algorithm efficiently handle to multi feature learning of HSI. The SS Supervised techniques consist of grouping of samples of recognized labels to assign unclassified pixels to one of several informational classes based on available labelled data. Supervised method implements the steps such as feature extraction, training and labelling. Finally, in section (A), we introduce the SSTBA algorithm, which is the SS, supervised hyperactive spectral classification algorithm and employed to the neural networks parameters. It is described for finding the labelled image "Lb" by which the input of image pattern "P" and "L" is the optimal selection of image cluster. Moreover the clustering technique has been considered the "Lb" of each cluster by the out labelled image in clustering. At the outset the proposed clustering algorithm can estimate max and min of the selected average value, expressed as

$$M = \max(T) \qquad (1)$$

After identifying the maximum (M) and minimum (N) of the average selected pattern in image cluster, the proposed clustering algorithms has estimated the difference between each feature of image pattern. Furthermore the difference of each feature "H" can be described as

$$H = \sqrt{(P_i + P_j)^2} \qquad (3)$$

Where "P" is the pattern of image. Then P_i and P_j indicate the coordinates of the image pattern. The SS based proposed classifier has been estimated the number of class labels as well as the training of input image pattern. Finally the proposed clustering algorithms has estimated for labelled image in colour image format moreover labelled output represents segmentation result for the high resolution remote sensing data input.

B. Spectral Supervised Tree Baggar Algorithm (SSTBA):

Input: Pattern of image 'P' and Optimal selection of clusterset 'L', Output: Labeled Image, 'Lb'.

Step 1: $T = P(L)$

Step 2:$M = \max(T)$;

Step 3: P'$H = \sqrt{(P_i - P_j)^2}$

Step 4: $Lm = \{1\ to\ N\}$//

Step 5:$R = T(M - N) * Lm$ // image pattern //

Step 6: end

V. RESULTS AND DISCUSSION

The image in Fig.1 presents the Salinas dataset and Fig.1 (a)-(c) shown false colour composition, reference data and colour code. The MATLAB programming is used to input the hyper spectral image as in Fig. 3(a) and is filtered and enhanced as shown in Fig. 3(b) and (c) respectively. The proposed algorithm is designed and developed to get the classified and segmented image as shown in Fig. 3(f)

and evaluates the each stage of the proposed SSTBA algorithm for the Salinas dataset.

1) Contingency Table Matrix Parameters Analysis.
Determination of accuracy of HIS based on the proposed SSSTBA can be done by two method.

a) Contingency matrix or Error matrix
b) Kappa coefficient

Contingency matrix and Kappa coefficient is techniques for calculation of Accuracy assessment with SSTBA based HSI classification. It is based on the data providing the assumption on the classes of reference datasets. The datasets are classified two-manner 1) reference data value and 2) ground truth data value. Moreover, The Salinas dataset confusion matrix parameters, True Positive (TP) value of 118, True Negative (TN) value of 42 and Kappa co-efficient of 0.9087 in Table 1. Moreover, the FAR value 3.6145, GAR value 96.3855 has been presented in Table 2 and depicted in Fig.4 and Fig.5. The proposed method of SSTBA performance using Contingency matrix values have been compared with statistical parameter of TP, TN and moreover for other parameters are listed in Table1. The proposed SSTBA systems has been provided for better Kappa coefficient for the given dataset is listed in Table1.

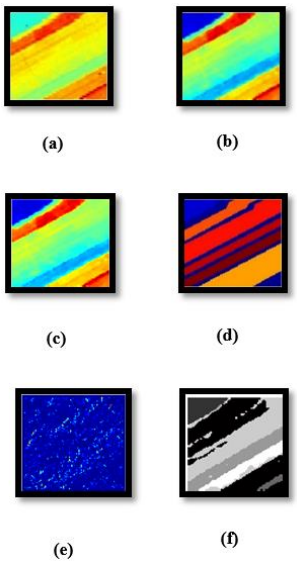

Figure 3. Output images of proposed SSTBA clustering. (a) Input image (b) Filtered image (c) Enhanced image(d) classified image (f) Segmented image

Table 1 Contingency Matrix Values

S.No	Parameters used	Proposed
1	T_P	118
2	T_N	42
3	F_P	0
4	F_N	6
5	Sensitivity	95.1613
6	Specificity	100
7	Precision	100
8	Recall	95.1613
9	Jaccard Coefficient	96.3855
10	Dice Coefficient	98.1595
11	Kappa Coefficient	0.9087
12	Accuracy	96.3855

Table 2 FAR and GAR Analysis

S.No	FAR	GAR
1	3.6145	96.3855
2	0	100

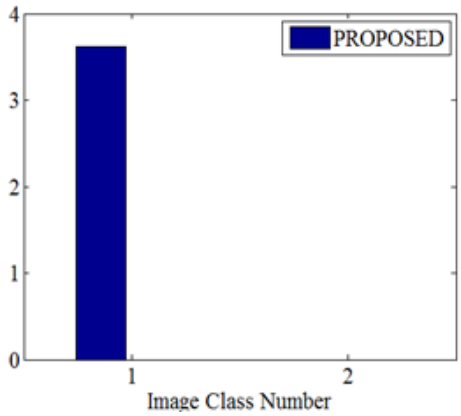

Figure 4. FAR Graph

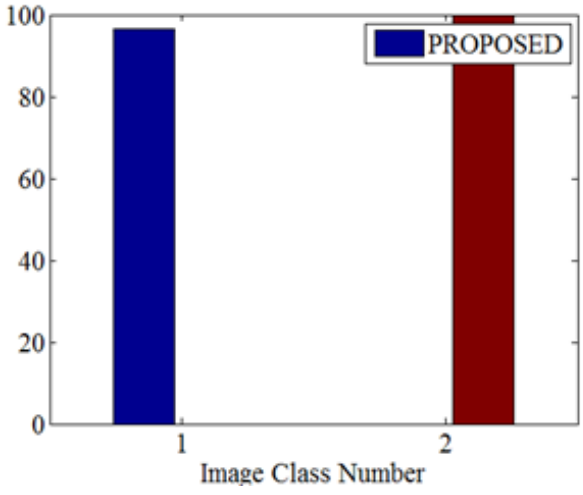

Figure 5. GAR Graph

VI. CONCLUSION

Paper contribute, a novel dictionary learning method called SSTBA for HSI classification has been proposed. The SSTBA representation show the outstanding ability to give better description of the HSI classification, especially exploiting SSSTBA in NN as classifier. The experiments conducted for Salinas's datasets prove the better performance of the proposed method compared with multilabeling image extraction methods at different HSI classification procedure.

VII. REFERENCES

[1] Min Wang, Jiru Huang, and Dongping Ming. "Region-Line Association Constraints for High-Resolution Image Segmentation," IEEE Journal of Selected Topics in Applied Earth Observations and Remote Sensing, 2016, 10 (2), pp. 628-637.

[2] Yongyue Hu, Jianyu Chen, Delu Pan, and Zengzhou Hao, "Edge-Guided Image Object Detection in Multiscale Segmentation for High-Resolution Remotely Sensed Imagery" IEEE Transactions on Geoscience and Remote Sensing, 2016 ,54(8),pp. 4702-4711.

[3] H. Gökhan Akçay and Selim Aksoy, "Automatic Detection of Compound Structures by Joint Selection of Region Groups from a Hierarchical Segmentation" IEEE Transactions on Geoscience and Remote Sensing,2016, 54 (6),pp. 3485-3501.

[4] Yanfei Zhong, Rongrong Gao, and Liangpei Zhang,"Multiscale and Multifeature Normalized Cut Segmentation for High Spatial Resolution Remote Sensing Imagery" IEEE Transactions On Geoscience And Remote Sensing, 2016,54(10),pp.6061-6075.

[5] Guiyun Zhou, Shuai Cao, and Junjie Zhou, "Planar Segmentation Using Range Images From Terrestrial Laser Scanning", IEEE Geoscience And Remote Sensing Letters, 2016,13(2),pp.257-261.

[6] F. A. Ávila Rodrigues, J. F. S. Rocha Neto, R. C. Pinheiro Marques, F. N. Sombra de Medeiros, and J. Santos Nobre. "SAR Image Segmentation Using the Roughness Information" IEEE Geoscience and Remote Sensing letters, 2016, 13(2),pp.132-136.

[7] Zhang Chunsen, Zheng Yiwei, and Feng Chenyi, "Spectral–Spatial Classification of Hyperspectral Images Using Probabilistic Weighted Strategy for Multifeature Fusion" IEEE Geoscience and Remote Sensing letters,2016,13,pp.1562-1566.

[8] Junping Zhang, Tong Li, Xiaochen Lu, and Zhen Cheng, "Semantic Classification of High-Resolution Remote-Sensing Images Based on Mid-level Features" IEEE Journal Of Selected Topics in Applied Earth Observations and Remote Sensing, 2016, 9(6),pp.2343-2353.

[9] Ribana Rosche, and Björn Waske, "Shapelet-Based Sparse Representation for Landcover Classification of Hyperspectral Images" IEEE Transactions on Geoscience and Remote Sensing, 2016, 54(3),pp.1623-1634.

[10] Erlei Zhang, Licheng Jiao, Xiangrong Zhang, Hongying Liu, and Shuang Wang, "Class-Level Joint Sparse Representation for Multifeature-Based Hyperspectral Image Classification" IEEE Journal of Selected Topics in Applied Earth Observations and Remote Sensing, 2016, 9(9),pp.4160-4177.

Themed Section : Engineering and Technology
© 2018 IJSRSET | Volume 5 | Issue 3 | Print ISSN: 2395-1990 | Online ISSN : 2394-4099

Spectrum Allocation with Full Duplex by Using Effective DF Cognitive Radio Networks

P.Divya[1], Dr.P.Kailasapathi[2]
[1]PG Scholar, Annamalai University, Tamil Nadu, India.
[2]Professor and Head, Annamalai University, Tamil Nadu, India

ABSTRACT

The enormous growth of the radio frequency (RF),wireless powered cooperative cognitive radio network (CCRN) has drawn a rapid increase of interest for improving the spectrum utilization with encourage to motivate joint information and energy cooperation between the primary and secondary systems. Dedicated energy beam forming is have the intension of achieving of wireless power transfer at relieves the low efficiency, which nonetheless evoke out-of-band EH phases and thus low cooperation efficiency. To address this issue, in this paper, we consider a novel CCRN aided by full-duplex (FD)-enabled energy access points (EAPs) that can support to wireless charge the secondary transmitter while simultaneously receiving primary transmitter's signal in the first transmission phase, and to perform decode-and-forward relaying in the second transmission phase. We examine a weighted sum-rate maximization problem subject to transmitting power constraints as well as a total cost constraint using successive convex approximation techniques. A zero-forcing-based suboptimal scheme that need only local channel state information for the EAPs to acquire their optimum receiving beam forming is also solved. Various tradeoffs between the weighted sum-rate and other system parameters are provided in numerical results to statement the effectiveness of the proposed solutions against the benchmark ones.

Keywords: Cognitive Radio, Cooperative Communication, Full-Duplex, Decode-And-Forward, D.C. Programming, Successive Convex Approximation, Power Splitting, Energy Harvesting.

I. INTRODUCTION

The rapid development of wireless services and applications, the demand for frequency resources has dramatically increased. How to accommodate these new wireless services and applications within the limited radio spectrum becomes a big challenge facing the modern society [1].

The compelling need to establish more flexible spectrum regulations motivates the advent of cognitive radio (CR)[2].Cooperative cognitive radio networks (CCRNs) further pave way to improve the spectrum efficiency of a CR system by advocating cooperation between the primary and secondary systems for mutual benefits. As Compared with classical CR start to deal with [3], CCRN make it possible for cooperative gains on top of CR in the sense that the secondary transmitter (ST) helps to provide the diversity and enhance the performance of primary transmission via relaying the primary user (PU)'s message while being allowed to access the PU's spectrum. Inspite of the conventional CCRN advantage from information-level cooperation, its implementation in real world might be limited due to STs' power constraints, especially when the STs are low-power devices.

With the advent of various energy harvesting (EH) technologies, CCRN has now been envisioned to

improve the overall system spectrum efficiency by enabling both information level and energy-level cooperation [4]. Apart from the natural energy sources such as solar and wind that is intermittent due to the environmental change, radio frequency (RF) signal has recently been exploited as a new viable source for wireless power transfer (WPT) (see [5] and references therein). RF-enabled WPT has many preferred advantages. For example, compared with other induction-based WPT technologies, it can power wireless devices to relatively longer distance (e.g., commercial chips available for tens of microwatts (μW) RF power transferred over 12m [6]), while the associated transceiver designs are more flexible with the transmitting power, waveforms, and resource blocks fully controlled to accommodate different physical conditions. Joint information and energy cooperation in CR networks has thus been explored in much wireless energy harvesting (WEH)-enabled scenarios, e.g., [7]–[10]. The benefit of RF-powered CCRN is nevertheless compromised by the low WPT efficiency mainly due to the severe signal attenuation over distance. One way to improve the WPT efficiency is to employ multiple antennas at the ST, which can improve the EH efficiency of the secondary system [8]. The other way to boost the WPT efficiency is to power the ST via the dedicated energy/hybrid access point (EAP/HAP) [9] in addition to the PU. However, previous works all assume that the involved devices operate in half-duplex (HD) mode, which transfers wireless power at the expense of some spectrum efficiency. In continuous effort to address this issue, full duplex (FD)-enabled communications with wireless information and power transfer has sparked an upsurge of interest (see [11]–[15] and references therein).

In this paper, we consider a spectrum sharing decode and- forward (DF) relaying CR network consisting of one pair of primary transmitter (PT) and primary receiver (PR), and one pair of multiple-input multiple-output (MIMO) secondary users (SUs). A number of multi-antenna FD EAPs are coordinated to transfer wireless power to the ST while simultaneously retrieving information sent from the PT in the first transmission phase, decode and forward the PT's message to the PR in HD mode in the second transmission phase. The ST is required to assist the primary transmission and earn the rights to access the PU's spectrum in return; the EAPs are paid by the system as an incentive to support the cooperative WPT and wireless information transfer (WIT). We assume that there is no direct link between the PT and the PR due to severe path loss [14], and the perfect1 global channel state information (CSI) known at a coordination point who is in charge of acquiring global CSI from the dedicated nodes2 and implementing the algorithm accordingly in every transmission block (assumed to be equal to the channel coherence time.

Compared with [7] investigating joint opportunistic EH and spectrum access, we focus on overlay CR transmission, which allows for primary messages known at the ST a priori due to the first-slot transmission, so that the ST can precancel the interference caused to the secondary receiver (SR) by some non-linear precoding techniques, e.g., dirty-paper coding (DPC). Furthermore, although overlay cognitive WPCN has been considered in [9] with dedicated WPT, the HAP was only equipped with one antenna, and therefore their transmission policy is not applicable to ours with multi-antennas. In [8], the multi-antenna ST received information from the primary transmitter (PT) and was fed with energy by the PT. However, the energy received by the ST was not intended for WPT and thus the RF EH capability was limited. By contrast, the deployment of cooperative FD-enabled EAPs intended for WPT in ours breaks this bottleneck. A wireless powered communication network (WPCN) with an FD enabled HAP under the assumption of perfect self-interference (SI) cancellation was investigated in [15], which is nevertheless not achievable in practice even with the state-of-the-art FD technique [18]. A similar setup was considered in [19], whereas our work differs from it mainly in two folds. First, the considered EAPs in this paper are FD empowered so

that they fundamentally improve the spectral efficiency of the CCRN system of interest. Second, compared with the non-cooperative EAPs whose power levels are binary (on or off) in [19], we exploit EAP-assisted cooperation in both WPT and WIT phases via continuous power control, which is an extension to the non-cooperative model.

II. RELATED WORK

In this paper [2], RF band is the set of radio etiquettes in, protocols, air interfaces, spatial and temporal patterns that intense the use of the radio spectrum. Cognitive radio ranges Software radios for multiband multimode personal the software radio with radio-domain model-based reasoning about such etiquettes are emerging as platforms.

In this paper [3], to achieve the ergodic capacity and the outage capacity of the secondary user-fading channel under different types of fading channel models and power constraints, we consider the case known as the optimal power allocation and spectrum sharing strategies.

In this paper [4], to enabled wireless communication by investigating a new joint communication and energy cooperation approach, we pursue a unified study on smart grid and coordinated multipoint (CoMP).

In this paper [5] wireless powered communication, networking (WPCN) is a new networking paradigm by use of microwave wireless power transfer (WPT) technology. So, the battery of wireless communication devices can be remotely replenished.

In this paper [7], from ambient radio frequency (RF) signals by energy harvesting, the Wireless networks can be self-sustaining. Recently, researchers have attention on designing.

In this paper [5], we attentively at wireless powered efficient circuits and devices for Radio Frequency energy harvesting appropriate for low-power wireless applications.

In this paper [8], Cooperation between the primary and secondary systems can improve the spectrum efficiency in cognitive radio networks. The efficient idea is to boost secondary system that helps the primary system's performance by relaying, and, in return, the primary system provides more opportunities for the secondary system to access the spectrum.

The cognitive WPCN is work under bandwidth sharing in primary wireless communication systems by using technique of cognitive radio which is enabled in secondary WPCN is shown in [9].

In paper [11], it has shown that the WPCN allocate the optimal network resources. Here to set distribution users in the downlink (DL) to operate full duplex in one hybrid access point, simultaneously it receive information from the users through TDMA in the uplink.

III. PROPOSED SYSTEM

The Main Contribution of this Paper:

- The weighted sum-rate of the FD EAPs–aided CCRN system is maximized using successive convex approximation (SCA) techniques subject to per-EAP power constraints for WPT and WIT, respectively, the STs transmitting power constraint, and a practical cost budget that constraints the payment made to the EAPs for their assistance.
- The centralized optimization enables cooperation among the EAPs to effectively mitigate the interference with STs Information decoding (ID), and the self-interference (SI) that degrades EAPs, reception of the PTs signal.
- A low-complexity suboptimal design locally nulling out the SI at the EAPs is also developed in order to reduce the complexity of the iterative algorithm, and is validated by computer

simulation to yield performance with little gap to that achieved by the proposed iterative solutions.

This paper, we consider a WEH-enabled CCRN that consists of one primary transmitter-receiver pair, one secondary transmitter-receiver pair, and a set of FD-enabled EAPs denoted by $K = \{1,\ldots, K\}$ as shown in Fig. 1. The PT and the PR are equipped with one antenna each, while the ST and the SR are equipped with N and M antennas, respectively. The number of transmitting and receiving antennas at the kth EAP are denoted by NT,k and NR,k, respectively, $\forall k \in K$, and $Nk = NT,k + NR,k$.

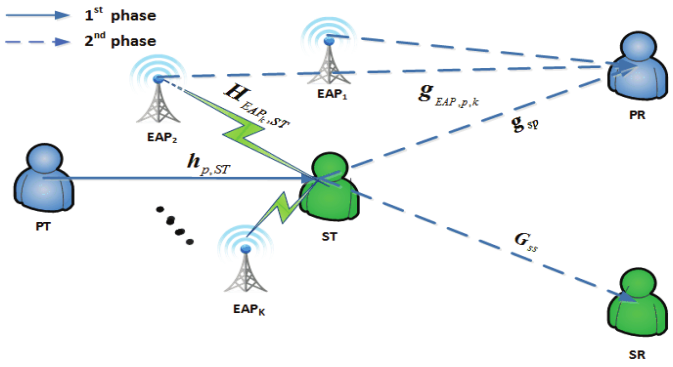

Figure.1 System model for the wireless powered CCRN.

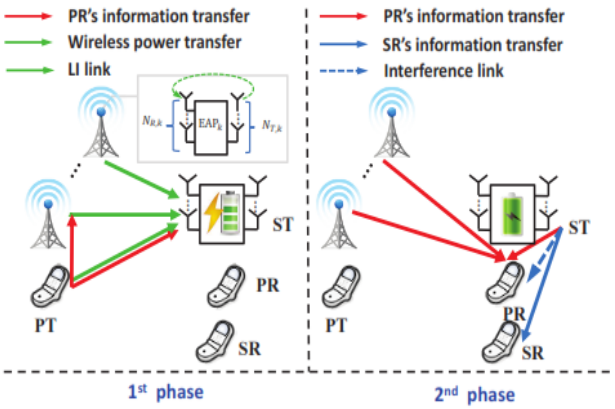

Figure 2. Transmission Protocol for the Wireless Powered CCRN

We assume that the ST is battery less, and thus it resorts to WEH as its only source of power for information transmission.3 .As illustrated by Fig. 2, a two-slot (with equal length) transmission protocol is assumed to be adopted. In the first time slot, the PT transfers the energy-bearing primary user's signal to the ST. Concurrently, the EAPs operating in FD mode cooperate to transfer wireless power to the ST using NT,k 's antennas, while jointly receiving information from the PT using *NR,k* 's antennas. In the secondary time slot, the ST decodes and forwards PT's message and superimposes it on its own to broadcast to the PR and the SR. Meanwhile, the decoded PT's information is also forwarded to the PR by the EAPs that employ *Nk* antennas each for information transmission. Let s denote PT's transmitting signal that follows the circularly symmetric complex Gaussian (CSCG) distribution, denoted by $s \sim CN(0, 1)$, and $\boldsymbol{x} \sim CN(\mathbf{0}, \boldsymbol{X})$, the energy signals4 coordinately transmitted by K EAPs, where $\boldsymbol{X}$ is the covariance matrix of $\boldsymbol{x}$. On the other hand, x can also be alternatively expressed by $x = [x_k]_{k=1}^{k}$, where $x_k \in C^{N_{T,k} x l}$ is the energy signal transmitted by each individual EQP and is subject to per-EAP power constraint given by $E\left[\|x_k\|^2\right] \le P_0 \forall k \in K$.

IV. RESULTS AND DISCUSSION

A. Performance Merits

The simulation result shows the comparison between the existing system and proposed system. In existing system, there are two transmitters and receivers are works under the one base station, namely primary and secondary. This primary and secondary users are communicate with each other by using one base station will leads to occur collision and packet loss. To overcome this issue, the proposed system is designed, in this proposed system both the transmitters and receivers are works under two Energy Access Point (EAP1 & EAP2) for communication. Like, primary transmitter and receiver uses the energy access point1 (EAP1) and secondary transmitter and receiver uses energy access point 2 (EAP2) which provides efficient spectrum, traffic less, and efficient packet delivery.

B. Simulation

Figure 3. Shown that the network formation of existing system and proposed system. In existing

system shows that one base station for each user, which causes collision. In proposed system, there is two energy access points splited for primary users and secondary users, which provides efficient spectrum.

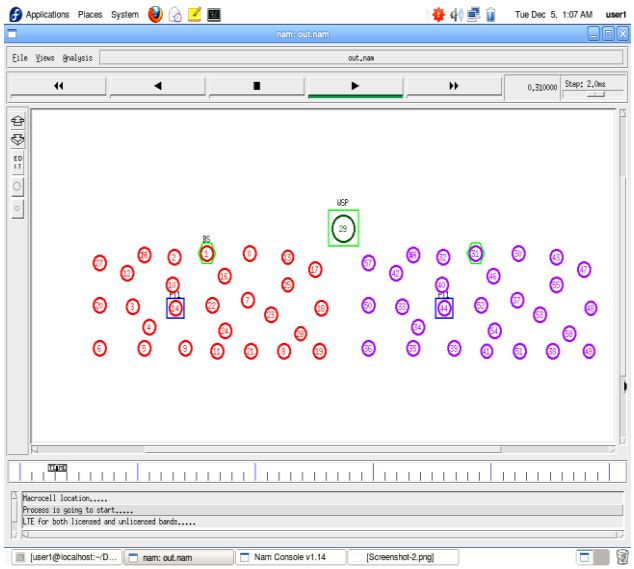

Figure 3. Packet Drop at Heavy Traffic

Figure 4, shows that, to overcome existing issues, replace the energy access points instead of one base station, to provide efficient spectrum, traffic less and good packet delivery.

Figure 4. Efficient Spectrum for Communication

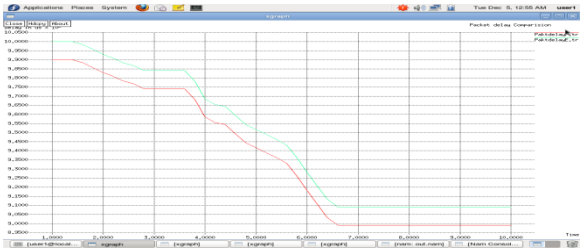

Figure 5. Packet Delay

Figure 5. Shown that comparison of packet delay, where red sign shows proposed system, which the packet delay is less, whereas the existing system shows the sign of green, which the packet delay is high.

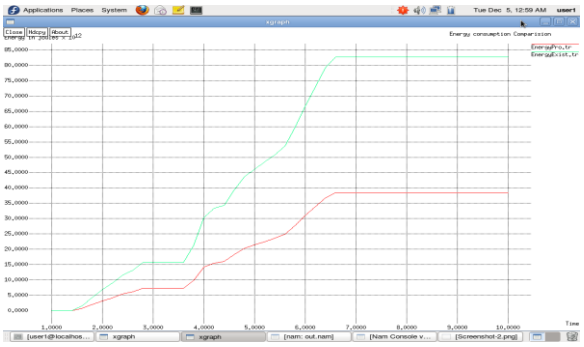

Figure 6. Energy Consumption

Figure 6, shows the comparison of energy consumption, as same as above red sign shows proposed system, and energy is less as compared to existing system as shown in green sign.

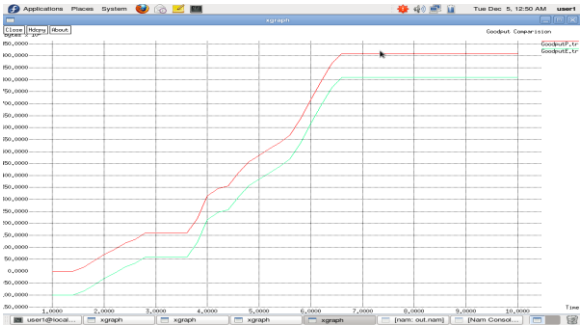

Figure 7. GoodPut

Figure 7 shows the comparison of goodput, as same as above red sign shows proposed system, and good put is high as compared to existing system as shown in green sign.

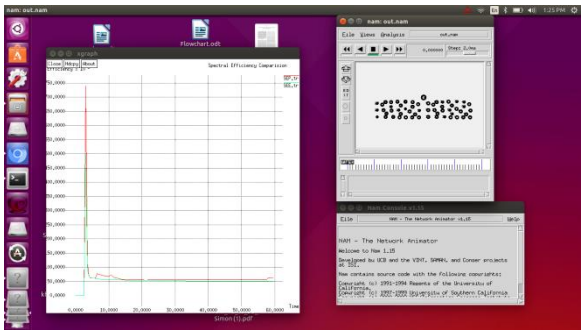

Figure 8. Spectral Efficiency

Figure 8. Shown the comparison of spectral efficiency as same as above red sign shows proposed system, and goodput is high as compared to existing system as shown in green sign.

IV. CONCLUSION

This paper investigated two techniques to fundamentally improve the spectrum efficiency of the RF EH-enabled CCRN, namely, dedicated EB and FD relaying both provided by multi antenna EAPs. Specifically, assuming a two-equal-slot DF relaying protocol, the EAPs jointly transfer wireless power to the ST while decoding PT's message in the first transmission phase, the EAPs cooperate to forward PT's message and the ST superimposes PT's message on its own to broadcast in the second transmission phase. The EAPs' EBs as well as their receiving and transmitting beam forming for PT's message, and ST's PS ratio as well as its transmitting beam forming were jointly optimized to maximize the weighted sum-rate taking both energy and cost constraints into account. The proposed algorithms using SCA techniques were proved to converge with the KKT conditions satisfied. The EB design based on ZF was also shown to be promising. Other benchmark schemes were also provided to validate the effectiveness of the proposed ones.

V. REFERENCES

[1] FCC, "Spectrum policy task force," Federal Communications Commission, ET Docket No. 02-135, Tech. Rep., Nov. 2002.

[2] J. Mitola and G. Q. Maguire, "Cognitive radio: Making software radios more personal," IEEE Pers. Commun., vol. 6, no. 6, pp. 13–18, Aug.1999.

[3] X. Kang, Y.-C. Liang, A. Nallanathan, H. K. Garg, and R. Zhang, "Optimalpower allocation for fading channels in cognitive radio networks:Ergodic capacity and outage capacity," IEEE Trans. Wireless Commun.,vol. 8, no. 2, pp. 940–950, Feb. 2009.

[4] J. Xu and R. Zhang, "Comp meets smart grid: A new communicationand energy cooperation paradigm," IEEE Transactions on VehicularTechnology, vol. 64, no. 6, pp. 2476–2488, Jun. 2015.

[5] S. Bi, Y. Zeng, and R. Zhang, "Wireless powered communication networks: an overview," IEEE Wireless Commun., vol. 23, no. 2, pp.10–18, Apr. 2016.

[6] Wireless Power Solutions-Power cast Corp. [Online]. Available: http://www.powercastco.com

[7] S. Lee, R. Zhang, and K. Huang, "Opportunistic wireless energy harvesting in cognitive radio networks," IEEE Trans. Wireless Commun.,vol. 12, no. 9, pp. 4788–4799, Sept. 2013.

[8] G. Zheng, Z. Ho, E. A. Jorswieck, and B. Ottersten, "Information andenergy cooperation in cognitive radio networks," IEEE Trans. SignalProcess., vol. 62, no. 9, pp. 2290–2303, May 2014.

[9] S. Lee and R. Zhang, "Cognitive wireless powered network: Spectrum sharing models and throughput maximization," IEEE Trans. Cogn.Commun. Netw., vol. 1, no. 3, pp. 335–346, Sept. 2015.

[10] C. Zhai, J. Liu, and L. Zheng, "Cooperative spectrum sharing with wireless energy harvesting in cognitive radio networks," IEEE Trans.Veh. Technol., vol. 65, no. 7, pp. 5303–5316, Jul. 2016.

[11] H. Ju and R. Zhang, "Optimal resource allocation in full-duplex wireless powered communication network," IEEE Trans. Commun., vol. 62,no. 10, pp. 3528–3540, Oct. 2014.

[12] C. Zhong, H. A. Suraweera, G. Zheng, I. Krikidis, and Z. Zhang,"Wireless information and power transfer with full duplex relaying,"IEEE Trans. Commun., vol. 62, no. 10, pp. 3447–3461, Oct. 2014.

Themed Section : Engineering and Technology
© 2018 IJSRSET | Volume 5 | Issue 3 | Print ISSN: 2395-1990 | Online ISSN : 2394-4099

Fuzzy C-Means Clustering based Dynamic Spectrum Allocation in Mobile Communication

Ganesan R[1], Pradeep S[2]

[12]Assistant Professor, Department of ECE, Bharathiyar College of Engineering & Technology, Karaikal, Puducherry, India

ganesanr.ece@gmail.com[1], s.pradeeponline@gmail.com[2]

ABSTRACT

In mobile networks, the efficiency of a point-to-point communication link has several limitations. The only way to improve the network capacity is by node density. This research discusses similar issues in current LTE macro based system. In existing system, the spectrum efficiency utilization is made by handling the traffic for indoor users to reduce the load on macro cells. Traditionally, the Dynamic Spectrum Allocation (DSA) aims to increase the capacity and to reduce the interference by (de)activating the available LTE frequency carriers. To avoid such issues we need to allocate the spectrum dynamically with respect to the user demand. To implement this several current survey is made and a new spectrum allocation is proposed. It is based on evaluating the DSA potential of achieving some improvement and to identify the traffic conditions. In this proposed scheme, the spectrum sharing has processed and identified throughout by using Fuzzy C-Means (FCM) clustering algorithm. It is named as Fuzzy C-Means Clustering based Dynamic Spectrum Allocation (FCM-DSA). The experimental results prove that the proposed scheme attains maximum throughput of 105Mbps when comparing with traditional adaptive co-existence spectrum sharing schemes.

Keywords: Mobile Communication, Macro Cells, Spectrum Allocation, Spectrum Sharing, Fuzzy C-Means Clustering

I. INTRODUCTION

A large majority of the algorithms were developed for networks based on the demand. Nowadays the process is combined with the multiple applications on a single IP-based infrastructure with high Quality of Service (QoS). In addition to that, there is a need to satisfy end-users' Quality of Experience (QoE). To satisfy this process, Third-Generation Partnership Project (3GPP) is used to represent the QoS framework for Long Term Evolution (LTE) based networks. Since, the problems exist due to the some demand made by the user such as data rate and bandwidth. This type of processing may results in pushing the researchers to think about some intelligent techniques. Hence, during network congestion the Mobile Network Operators (MNOs) need to think about some techniques to manage network traffic in the transport layer. Tabany and Guy (2015) solved this issue by implementing a new Delay-Aware QoS Scheme (DAQS). Since, the problem exists such as complexity and performance degradation.

The reliable data transmission is important in various aspects such as quality of-service requirements. Mostly the communication network provides effective way in many applications such as

content sharing, video streaming and mobile multimedia communications. When analysing wireless applications the task is critical because also gets increased inters of channel variation, system robustness and interference.

Traditionally, the 3GPP has introduced LTE macro cells to handle the traffic for indoor users and to reduce the load on the Macro cells. But still these processes have some limitations on current LTE macro based system. For Mobile Network Operators (MNOs) it is critical to use the LTE spectrum assets, as well as the installed network infrastructure, in the most cost efficient way.

The main contribution of this method is spectrum sharing based on the macro cell capacity, then it is processed and its capacity is identified and grouped between the cells with the help of FCM. It results in the improvement in network capacity and performance.

The main objective of this research is to improve the performance, lifetime and minimize the energy. These processes are made by Fuzzy C-Means (FCM) clustering algorithm based spectrum sharing. The main advantages of this method is

- It is efficient for overlapped data set.
- In FCM the data point is assigned to each cluster center, this may results in utilizing the data point to more than one cluster.

This research investigates the potential gain from DSA for a LTE macro-cellular network covering a geographical area with Fuzzy C-Means based non-uniform spatial traffic distribution. The remaining of the paper is organised as follows. Some existing methodologies are illustrated in Sect. 2. The problem identification is made in the section 3. The potential DSA performance and its overall process are described in section 4 as research model. The evaluation of the proposed FCM based optimised DSA algorithm with traditional adaptive Co-existence spectrum allocation is made in the section 5. Finally, the paper is summarized in the section 6.

II. LITERATURE SURVEY

Hu and Qian (2014) explored a system framework of cooperative green heterogeneous networks for 5G wireless communication systems. Initially, they made a survey about Spectrum Efficiency (SE), Energy Efficiency (EE), and Quality of Service (QoS) based mobile association and power control. They also presented the system framework of cooperative green heterogeneous networks. Their major objective is to balance and optimize the SE, EE, and QoS in heterogeneous wireless networks.

In cellular and future communication systems, the flexibility and efficiency is improved by using Multi-Input Multi-Output Orthogonal Frequency Division Multiplexing (MIMO-OFDM). Patel et al., (2016) presented a resource Allocation Problem for spectrum sharing in wireless communication system with key element energy efficiency. They proposed an algorithm that process subcarrier and power allocation simultaneously under data rate constraint.

Bao and Liang (2014) studied joint spectrum allocation in heterogeneous cellular networks with several base stations. For this concept they applied the geometric approach to derive the average downlink user data rate in a closed-form expression. They combined the optimizing spectrum allocation and user association in order to solve the optimization problem. A computationally efficient Structured Spectrum Allocation and User Association (SSAUA) are designed. If the density of users is low then there is performance degradation. A Surcharge Pricing Scheme (SPS) is represented here to make Nash equilibrium. They compared the SSAUA approach with the SPS.

Christodoulopoulos et al., (2013) considered the problem of serving traffic in a spectrum-flexible optical network. Here the problem is identified in the

spectrum allocation. While allocating the spectrum an end-to-end connection may change to adapt the time-varying transmission rate. While considering the route with appropriate Routing and Spectrum Allocation (RSA) algorithm, the spectrum utilizes around the reference frequency to expand and contract to match source rate fluctuations. They proposed and analyzed the three Spectrum Expansion/Contraction (SEC) policies for modifying the spectrum allocated to each connection.

Velasco et al.,(2014) solved the routing and spectrum allocation related optimization problems with the help of Off-Line to In-Operation Flexgrid Network Planning. Chatterjee et al., (2015) focused on different node architectures, and compare its performance in terms of scalability and flexibility. They reviewed and classified the Routing and Spectrum Allocation (RSA) approaches with some merits and demerits. It includes various aspects, namely, fragmentation, modulation, survivability, energy saving and networking cost.

With the recent developments, the spectrum aggregation is introduced by 3GPP with LTE-advanced standard. Hence, the LTE-A needs some update function to enhance the features of the carrier aggregation. Lee et al., (2014) reviewed some techniques based on the challenges.

Pai et al., (2016) made a Game Theoretic Optimization of Spectrum Allocation in Cognitive Radio. They have been used the energy detection, it is a spectrum sensing method that detects the presence or absence of a signal by measuring the received signal power. It is used for solving the complex problems and identifies the practical issues. It is noticed that the imperfect knowledge of the noise power results in unwanted detection. Hence to avoid these issues the perfect method is to be needed.

Huang et al., (2016) analyzed the system model of the cognitive radio network based video monitoring system. Here, the cognitive radio network is introduced into the wireless video monitoring system to improve the spectrum utilization. In some conditions the cognitive radios have disabled the interference to licensed users. Initially, they recalled the concept of wireless video monitoring system and then the centralized cooperation spectrum is made with the sensing algorithm. Then the priority and channel ranking is made with the help of the spectrum allocation algorithm.

Akyildiz et al., (2006) made a detail survey about dynamic spectrum access approaches. They listed several challenges and some complex problems. Leaves et al., (2001) focused on spatial and temporal DSA in a multi radio network consisting of a Universal Mobile Telecommunications Service (UMTS) and Digital Video Broadcasting-Terrestrial (DVB-T) system. They made a temporal DSA based load prediction. Finally, the perfect and imperfect load predictions are compared to show that DSA has 30% higher spectrum efficiency compared to fixed channel assignment. Rodriguez et al. (2006) extends the previous DSA concept with spectrum bidding which is formed as different cells from the participating DVB-T and UMTS systems. Further, Kovács and Vidács (2006) proposed a spatial and temporal DSA where called Regional Spectrum Brokers (RSB) coordinates the temporal DSA. The RSB solves the spectrum assignment problem with the help of integer linear programming to reduce the interference.

Hoffmann et al., (2015) evaluated the Self-Optimised Network (SON) based on DSA algorithm. Madan et al., (2010) proposed new paradigms for design and operation of such heterogeneous cellular networks. It focussed on cell splitting, semi-static resource negotiation on third-party backhaul connections and range expansion. It also manages the fast and dynamic interference management for QoS through the-air signalling. Finally, they represented DSA is made with simple, lightweight and extremely low overhead.

III. PROBLEM STATEMENT

In the real time wireless technology or a wireless system the environment parameters changes may be permanent to communicate efficiently by avoiding the interference with the users. Some ancient strategies square measure created to assign the spectrum with many objectives like Spectrum utilization potency Degree of quality and Distance from primary user to the secondary users. The DSA is a process of allocating different dynamic frequency channels that are encountered in many communication systems. Since in adaptive co-existence spectrum the main purpose is to make LTE allocate time resource adaptively based on the traffic load of WLAN system. It is necessary to improve the throughput of the spectrum allocation models. In this research, we made a comparison for FCM based DSA and adaptive co-existence spectrum to verify the effectiveness.

IV. RESEARCH MODEL

A. Adaptive Co-existence Mechanism

Before entering in to adaptive co-existence methodology, the following details are needed. The LTE varies with several categories when comparing with the LAN. It is processed by allocating the bandwidth resources on physical medium. The major difference between LTE and Wireless Local Area Network (WLAN) is that LTE just reduces its transmission speed while WLAN holds its transmission in the case of channel interference. The wireless local area network could be a competition primarily based system and relies on Carrier Sense Multiple Access with Collision Shunning (CSMA/CA), that is, terminals and Access Points (AP) contend along for an equivalent band. If the LTE and local area network deployed in an exceedingly same frequency then the considering the distinction in bandwidth allocation, the bulk of a network/WLAN/wireless fidelity/ WiFi nodes square measure probably to be blocked by LTE once LTE and local area network networks are deployed within the same waveband as a result of LTE interference levels are typically higher than the brink that local area network uses to work out whether or not the channel is idle. Therefore, medium access controls (MAC). The adaptive Co-existence algorithm is shown in the figure 1:

Input: Calculate the ratio during reallocation cycle named as $T_c > 0$ and maximum instant.
Output: LTE sub-frame configuration modes
if (condition) then
LTE spares single sub-frame to WLAN
else if (condition) then
:
:
end if

Figure 1. Adaptive Co-existence Algorithm

From the algorithm, it is noticed that the adaptive co-existence algorithm deals with the selection of LTE frames. It is totally depends on the sub frames with several nodes. Xing et al., (2015) investigated the research with the help of selecting an initial LTE carrier deployment within the allocated spectrum. They have utilized the typical European LTE operator with 20MHz spectrum available in the band of 1800MHz. In terms of evaluating the DSA nodes the investigation is based only on the two scenarios namely, a hexagonal cell layout and a site-specific urban cell layout. In these conditions, they made a traffic hotspot cell which is called as one macro cell at the middle of the investigated area. Based on the cell density the process is made with the hexagonal layout were chosen that may proves the similarity between site specific network under several areas. The inter-site distance within the hexangular layout was chosen such the ensuing cell density is analogous to the one within the site-specific network layout within the thought of space. In many cases, the requested traffic from the users is considered within the network, because the offered traffic to the network. The offered traffic levels within the hotspot cell and also the encompassing cells square measure varied consistent with abstraction traffic intensity maps that square measure scaled otherwise among the hotspot cell and also the encompassing cells so as to come up with

totally different load ratios and interference things to the world served by the hotspot cell. During this process the traffic intensity maps the value with some of the assumed characteristics and resulted in minimum throughput. To make the system effective the bounded interval is managed and processed with the help of the cell alignment. It is one of the methods that use different networks to co-exist within the same radio spectrum. The simple example of Co-exist spectrum allocation is digital televisions.

The traditional dynamic spectrum allocation is processed by activating the cell. It is triggered under high load condition. Here, the value is assumed as pre-configured cells. The cells are separated with the help of the cluster information. It is assumed that each cell has a preconfigured Cluster of interfering cells. For adaptive allocation they considered some hotspot cells to coordinate the cluster. In these cases, the high capacity cells are processed or grouped in one group and other low capacity cells are grouped as another one. The high capacity cells are mostly used for spectrum sharing.

B. Fuzzy C-Means Clustering

Dunn (1973) initiates the FCM and further it is modified according to the application. Bezdek et al., (1984) extended the k-means algorithm to Fuzzy C-Means Clustering algorithm. Normally, the Fuzzy C-means is checked by assigning the membership value to each data point which is equivalent to each cluster centre. In fuzzy based set the process is carried through the distance between each cluster with respect to the data point. If the data rate is high then there is number membership value towards the particular cluster center. From the equation it is noticed that the summation of membership of each data point should be equal to one. With respect to the iteration the location of the cluster head is updated as mentioned in the equation. In fuzzy clustering, the clustering process is made by allowing the cell to be a member of any cluster. The objective function for clustering is represented below.

$$Obj(\mathrm{X},\mathrm{Y}) = \sum_{iw=1}^{n}\sum_{jw=1}^{c}\left(\mu_{iwjw}\right)^{m}\left|\left|x_{iw}-v_{jw}\right|\right|^{2} \quad (1)$$

Where obj is defines the objective function , X = (μij)n*c is the fuzzy membership matrix, $n \rightarrow$ number of cells, $c \rightarrow$ the number of cluster center, $\mu_{iwjw} \rightarrow$ the membership of iw^{th} cell to jw^{th} cluster center, $m \rightarrow$ the fuzziness index m € [1, ∞], $\left|\left|x_{iw}-v_{jw}\right|\right| \rightarrow$the Euclidean distance.

With a certain degree of membership the feature vector assign to a centroid and features be inclined to overlap. Initially, the centroids are chosen randomly. So, various initial centroids generate various results and these make FCM to be sensitive to initial centroids. Through an iterative process, the objective function value can be attained where membership and cluster centroids are updated according to given below equations

$$\mu_{ij} = 1/\sum_{k=1}^{c}\left(\frac{d_{ij}}{d_{ik}}\right)^{\left(\frac{2}{m-2}\right)} \quad (2)$$

$$v_j = \frac{\sum_{i=1}^{n}\left(\mu_{ij}\right)^{m}x_i}{\sum_{i=1}^{n}\left(\mu_{ij}\right)^{m}}, \forall j = 1,2,..,c \quad (3)$$

C. Proposed FCM based Dynamic Spectrum Allocation

By means of combining the traditional methods namely, k-means and fuzzy, many researchers were focussed and implemented it in the clustering concepts. In that FCM is termed as the best method because it has best result for overlapped data set. The FCM process is considered for spectrum allocation because the clustering is efficient and similar to that the channels are randomly deployed. The main motive of this clustering is to select the proper channel and initiate the exact slot by satisfying the application module requirement. The algorithm is illustrated below:

Input: Initialize a set of N cell capacity from network
Output: C- Clusters formation

Membership value initialized for cells.
Calculate the vectors

$$C^{(k)} = [c_j] \; with \; U^{(k)}$$

Compute the fuzzy centroid
Update the fuzzy membership value as

$$U^{(k)}, U^{(k+1)}$$

check If updated membership value < previous membership value stop, else
Return to initialization.
Repeat until the centroid no longer move

Figure 2. Algorithm for proposed FCM based DSA

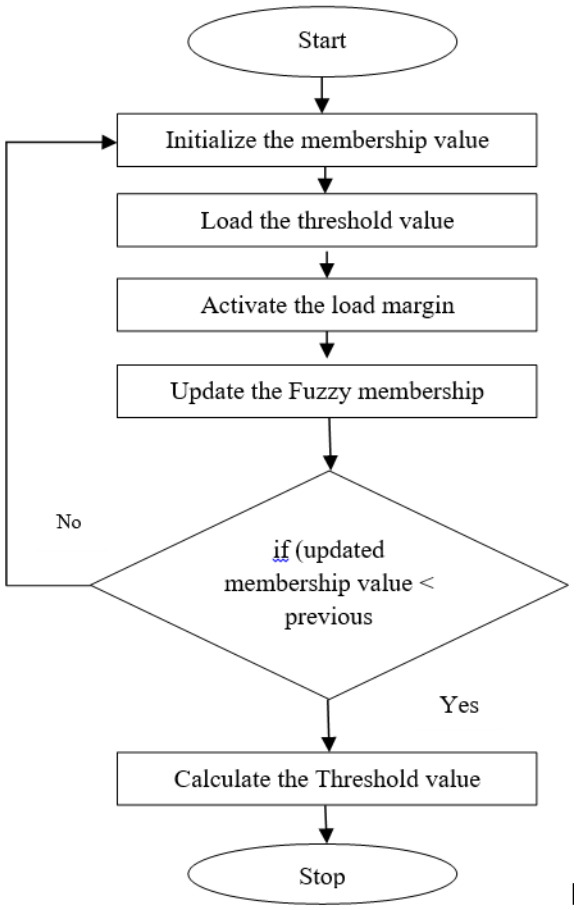

Figure 3. Flow chart for Proposed Fuzzy C-Means based Dynamic Spectrum Allocation

The FCM algorithm is considered here to activate the spectrum allocation with respect to the congested nodes. It is initially, starts with the concept of load threshold activation. The selections of cells are considered here with respect to the level of the bandwidth level. The main advantage of this method is, it faces more challenges and results in the maximum load level with high throughput. The neighbour node or a cell gives the exact location of the spectrum. The process of FCM in allocation is based on the load levels of the neighbour node update value.

There is a need for activating the load value with respect to the threshold activation. While looking it into the cell perspective, the threshold value deals with this concept and process it through the nearby nodes. If the threshold value of the cell is low then the cell allows its cluster neighbours to enable higher bandwidth configurations. While looking it in the cluster based approach, the maximum load among the cell is fixed with the neighbours cluster information.

The main objective of spectrum allocation is to manage the spectrum in a radio system. It shares the radio networks over space and time, to increase overall the spectrum efficiency. In traditional methods the DSA is compared with the absence of cluster throughput with the hexagonal layout and uniform traffic intensity. If the coverage is to long then the cell sizes will be varied with respect to the hexagonal layout.

V. Experimental Result

The evaluation of Dynamic spectrum allocation is important to verify the functionality and its characteristics. The overall evaluation is made in MATLAB. Here the green colour nodes are congested users with 25 users. While red color indicates the non-congested users, which is less than the 25 users. Figure 4 shows the initialization of users under random process. It helps to allocate the spectrum sharing resources. Under different load situations, the neighbouring cells and the hotspot cell can result in some interference situations. It is used her to increase the system performance level. The neighbouring nodes are represented with respect to the carried traffic levels to manage the users. With different iterations, the channels are represented in the figure 5. Furthermore, the optimal FCM-DSA configuration depends only on the traffic ratio between the surrounding cells and the hotspot cell. The figure 6 results show that DSA can provide significant gains only in non-uniform traffic distributions.

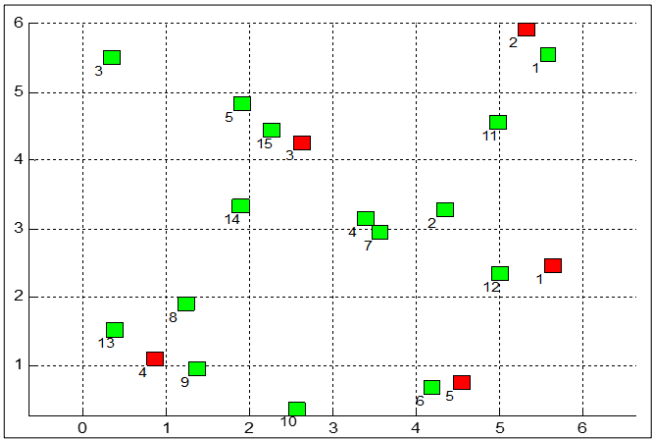

Figure 4. Initialization of Channels

- Congested Channel
- Non Congested Channels

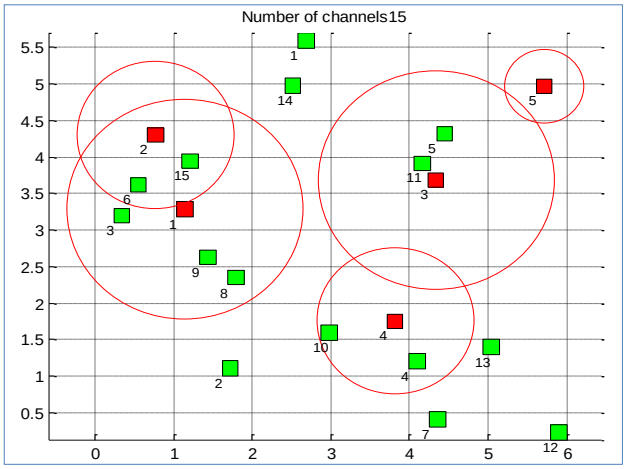

Figure 5. Representation of Channels

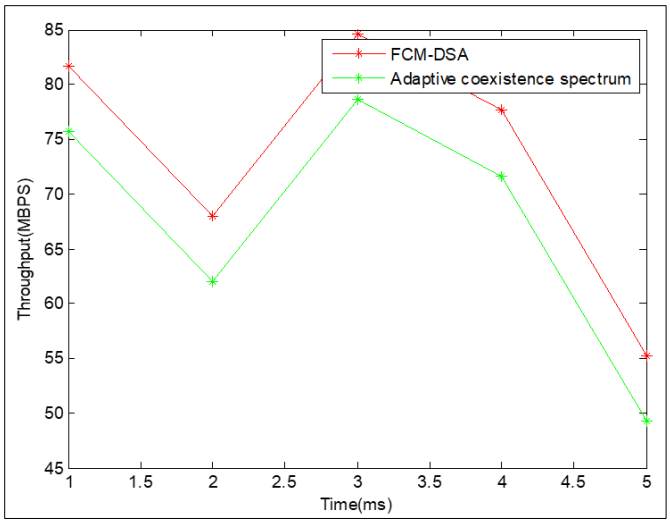

Figure 6. Representation of Throughput

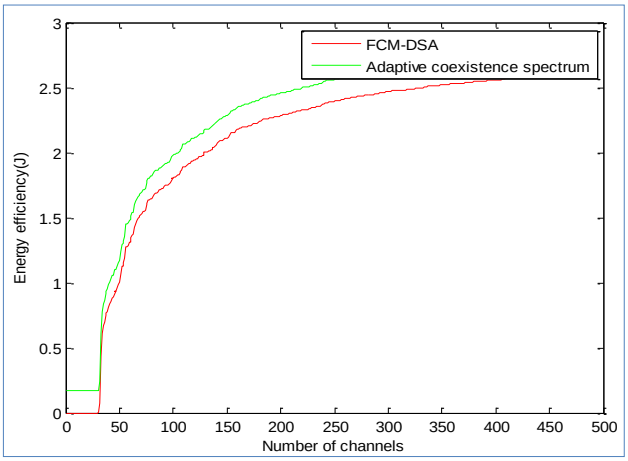

Figure 7. Comparison of Adaptive Co-Existence Spectrum and Proposed FCM-DSA

Table I Experimental Result

Time (ms)	Throughput (Mbps)	
	Adaptive Co-existence Spectrum	FCM-DSA
1	76.2	82.5
2	61.9	69.4
3	77.3	84.2
4	71.2	78.1
5	49.1	55

The throughput of the adaptive Co-existence spectrum is very minute when comparing with the proposed FCM-DSA method. It has 7% difference of throughput. Hence, from this we cannot able to justify it is better. Next parameter is energy efficiency, it is considered here to validate the result with respect to the number of channels. If the number of channels is increased then the energy efficiency is also gets increased. The comparison table I shows that simulated value with respect to the time and throughput values.

VI. CONCLUSION

In the fast growing demand of mobile broadband services, the spectrum allocation faces more issues when comparing with other concepts. Hence, this paper investigated the various concepts for allocating the spectrum with LTE domains. The dynamic spectrum allocation based on Fuzzy C-Means Clustering is considered in this research to cover the

geographical area by means of non-uniform spatial traffic distribution. The overall experimental results were carried out with the MATLAB simulations and generating 25 minimum congested channels verify it. The comparison result proves that the simulation results of the proposed Fuzzy C-Means based Dynamic Spectrum Allocation throughput is improved by 6% and 2 Joules improve the energy efficiency. Hence, proposed FCM-DSA shows more efficient than the traditional Adaptive Co-existence module. In future, extent this research to incorporate the effect of correlation in the design of the user-group assignments in real time applications.

VII. REFERENCES

[1] Tabany, M. R., & Guy, C. G. (2015, July). Design and implement delay-aware QoS scheme for 3GPP LTE/LTE-A networks for mixed traffic flow. In Computers and Communication (ISCC), 2015 IEEE Symposium on (pp. 38-44). IEEE.

[2] Hu, R. Q., & Qian, Y. (2014). An energy efficient and spectrum efficient wireless heterogeneous network framework for 5G systems. IEEE Communications Magazine, 52(5), 94-101.

[3] Patel, H., Gandhi, S. D., & Vyas, D. (2016). A Research on Spectrum Allocation Using Optimal Power in Downlink Wireless system.

[4] Bao, W., & Liang, B. (2014, April). Structured spectrum allocation and user association in heterogeneous cellular networks. In INFOCOM, 2014 Proceedings IEEE (pp. 1069-1077). IEEE.

[5] Christodoulopoulos, K., Tomkos, I., & Varvarigos, E. (2013). Time-varying spectrum allocation policies and blocking analysis in flexible optical networks. IEEE Journal on Selected Areas in Communications, 31(1), 13-25.

[6] Velasco, L., Castro, A., Ruiz, M., & Junyent, G. (2014). Solving routing and spectrum allocation related optimization problems: From off-line to in-operation flexgrid network planning. Journal of Lightwave Technology, 32(16), 2780-2795.

[7] Chatterjee, B. C., Sarma, N., & Oki, E. (2015). Routing and spectrum allocation in elastic optical networks: A tutorial. IEEE Communications Surveys & Tutorials, 17(3), 1776-1800.

[8] Lee, H., Vahid, S., & Moessner, K. (2014). A survey of radio resource management for spectrum aggregation in LTE-advanced. IEEE Communications Surveys & Tutorials, 16(2), 745-760.

[9] Pai, V., Prabhu, A., & Menon, A. (2016, August). Game Theoretic optimization of spectrum allocation in cognitive radio. In Computing Communication Control and automation (ICCUBEA), 2016 International Conference on (pp. 1-5). IEEE.

[10] Huang, X. L., Zhai, Y. B., Sun, S. Y., Sun, Q. Q., & Hu, S. Q. (2016, August). Spectrum Sensing and Spectrum Allocation Algorithms in Wireless Monitoring Video Transmission. In International Conference on Machine Learning and Intelligent Communications (pp. 402-411). Springer, Cham.

[11] Akyildiz, I. F., Lee, W. Y., Vuran, M. C., & Mohanty, S. (2006). NeXt generation/dynamic spectrum access/cognitive radio wireless networks: A survey. Computer networks, 50(13), 2127-2159.

[12] Leaves, P. A. U. L., Ghaheri-Niri, S., Tafazolli, R., Christodoulides, L., Sammut, T., Staht, W., & Huschke, J. (2001). Dynamic spectrum allocation in a multi-radio environment: Concept and algorithm.

[13] Rodriguez, V., Moessner, K., & Tafazolli, R. (2006). Market driven dynamic spectrum allocation over space and time among radio-access networks: DVB-T and B3G CDMA with heterogeneous terminals. Mobile Networks and Applications, 11(6), 847-860.

[14] Kovács, L., & Vidács, A. (2006, August). Spatio-temporal spectrum management model for dynamic spectrum access networks. In Proc., First International Workshop on Technology

and Policy for Accessing Spectrum (TAPAS 2006).

[15] Hoffmann, H., Ramachandra, P., Kovács, I. Z., Jorguseski, L., Gunnarsson, F., & Kürner, T. (2015). Potential of dynamic spectrum allocation in LTE macro networks. Advances in Radio Science: ARS, 13, 95.

[16] Madan, R., Borran, J., Sampath, A., Bhushan, N., Khandekar, A., & Ji, T. (2010). Cell association and interference coordination in heterogeneous LTE-A cellular networks. IEEE Journal on Selected Areas in Communications, 28(9), 1479-1489.

[17] Xing, M., Peng, Y., Xia, T., Long, H., & Zheng, K. (2015, May). Adaptive spectrum sharing of LTE co-existing with WLAN in unlicensed frequency bands. In Vehicular Technology Conference (VTC Spring), 2015 IEEE 81st (pp. 1-5). IEEE.

[18] Bezdek, J. C., Ehrlich, R., & Full, W. (1984). FCM: The fuzzy c-means clustering algorithm. Computers & Geosciences, 10(2-3), 191-203.

[19] Dunn, J. C. (1973). A fuzzy relative of the ISODATA process and its use in detecting compact well-separated clusters.

Themed Section : Engineering and Technology
© 2018 IJSRSET | Volume 5 | Issue 3 | Print ISSN: 2395-1990 | Online ISSN : 2394-4099

MEMS Cantilever Sensor in Food Processing Industry

Beulah Sujan K[1], T Shanmuganantham[2]

[1] PG Scholar, Department of Electronics Engineering, Pondicherry University, Pondicherry, India

[2]Assistant Professor, Department of Electronics Engineering, Pondicherry University, Pondicherry, India

beulahsujanacademic@gmail.com[1], shanmugananthamster@gmail.com[2]

ABSTRACT

MEMS (Micro Electro Mechanical systems) cantilever sensor is designed which is used in food processing industry to detect toxic substances or bacteria present in the food which is packed. In this paper, MEMS cantilever sensor of dimensions 400 μm ×50 μm ×1μm is designed to detect the presence of bacteria in food obtained from cattle by using MZN (metronoidazole) molecules. The MEMS cantilever sensor designed by using the software INTELLISUITE version 8.7 and also the MEMS cantilever is designed with different sensing materials. The cantilever sensitivity is found for different sensing layer in order to find good sensor.

Keywords: MEMS, Cantilever, INTELLISUITE, MZN

I. INTRODUCTION

Now-a-days in this modern world we consume food which is packed such as milk, meat etc. In order to find any toxic substances or bacteria in food we use MEMS cantilever sensor as detectors in food processing industry. MEMS usually which are micro fabricated devices has wide area of applications. In medical field MEMS are used to detect diseases [2]. In Bio-medical field MEMS are used for drug discovery and drug development [3]. MEMS can be used as switches at Radio frequency range. This usage of MEMS has been extended to the food processing industries as detectors. In this paper, we detect the bacteria or toxic materials present in food obtained from cattle because of excessive feeding with additives which promote growth [1]. Usually MZN is used as antibody which reacts with bacteria and stops further growth.

The MEMS cantilever sensor works as detector based on adsorption phenomenon [4]. According to adsorption phenomenon, the surface of MEMS cantilever is coated with sensing layer. On the top of this sensing layer the molecules which react with the food sample is placed [1]. When food sample is added to the cantilever, the reaction takes places between food sample and molecules on the surface of cantilever. As reaction occurs, there is increase in mass due to which the cantilever beam deflects [5]. Thus the cantilever is used as a detector. The figure1 shows the adsorption phenomenon.

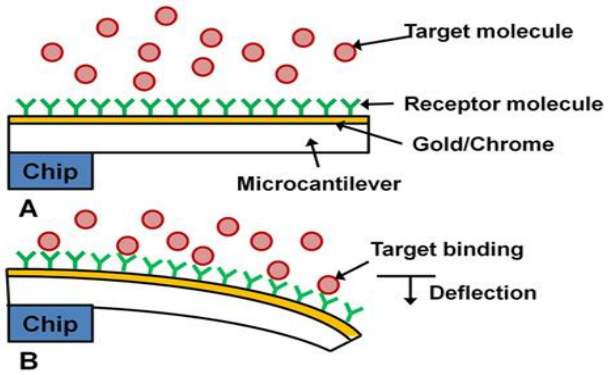

Figure 1. Adsorption Phenomenon

The analysis, which are carried for micro cantilever sensor, are:

1. Static analysis

2. Dynamic analysis

A. Static Analysis

Static analysis mainly determines the displacement undergone by MEMS cantilever sensor when it is subjected to pressure [4].

B. Dynamic Analysis

Dynamic analysis mainly determines the frequencies of cantilever when cantilever beam vibrates [4]

A.

The organization of this document is as follows. In Section 2, it discusses about design of cantilever. The section 3 presents the simulated results and discussions and Section 4 concludes the work.

II. MICROCANTILEVER DESIGN

A basic cantilever sensor which has one fixed end and other end is made free. A micro cantilever is designed with length of 400µmts, width of 50µmts and thickness of 1µmts. On the surface of this cantilever beam a sensing layer and antibody MZN of mass 1.45g/cm3 is considered. Food sample is considered for detection and food sample is added on the surface of cantilever. If there is presence of bacteria in food sample, the bacteria reacts with MZN molecule as a result the mass of cantilever beam increases and beam deflects. Thus we can detect the presence of bacteria in food which is packed [6].

The sensing layers, which are considered, are:

1. Tungsten
2. Tantalum
3. Chromium mono silicide
4. Glass pyrex sensor

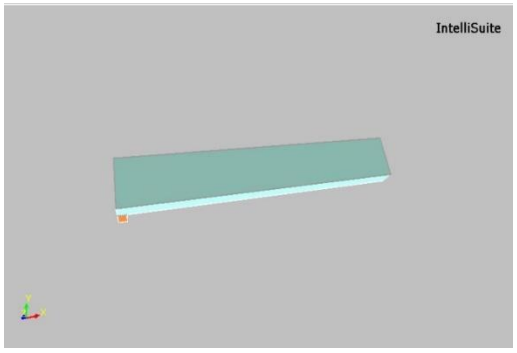

Figure 2. Design of Cantilever Sensor

III. SIMULATED RESULTS AND DISCUSSION

The cantilever is designed with different sensing layers

1. Tungsten
2. Tantalum
3. Chromium mono silicides
4. Glass pyrex

A. Simulation Result of Micro Cantilever Beam with Tungsten as Sensor

a. Static analysis

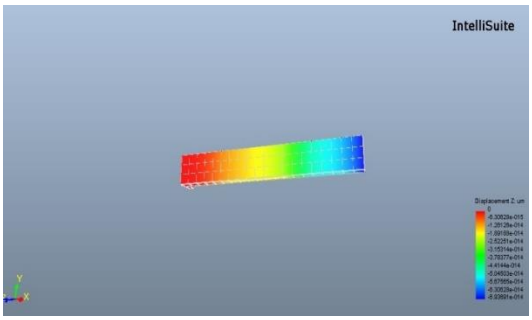

Figure 3. Static Analysis of Tungsten Sensor

B. Dynamic Analysis

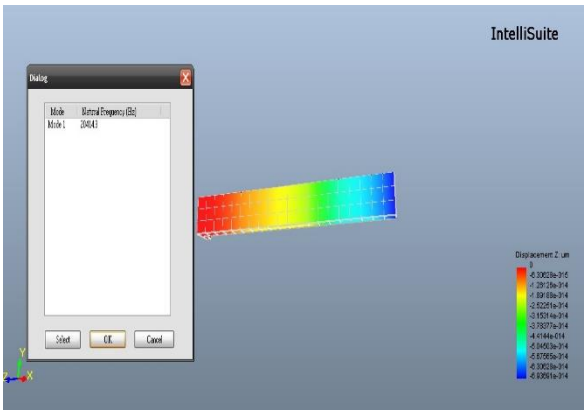

Figure 4. Dynamic Analysis of Tungsten Sensor

B. Simulation Result of Micro Cantilever Beam with Tantalum as Sensor

a. Static analysis

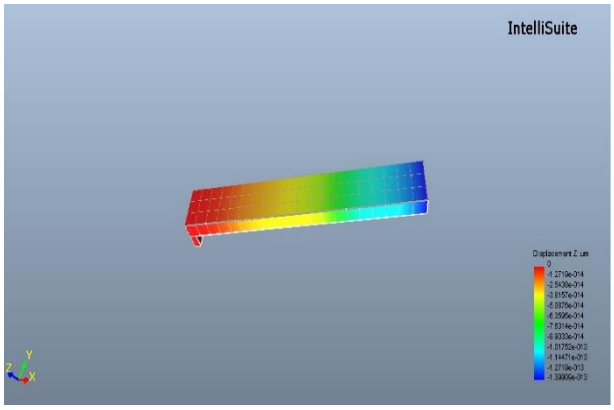

Figure 5. Static Analysis of Tantalum Sensor

b. Dynamic Analysis

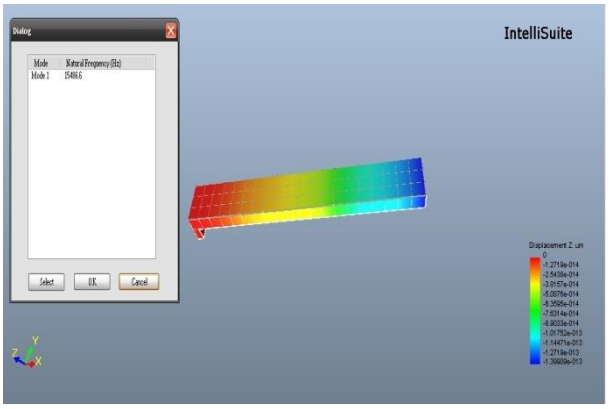

Figure 6. Dynamic Analysis of Tantalum Sensor

C. Simulation Result of Micro Cantilever Beam with Chromium Mono Silicide as Sensor

a. Static Analysis

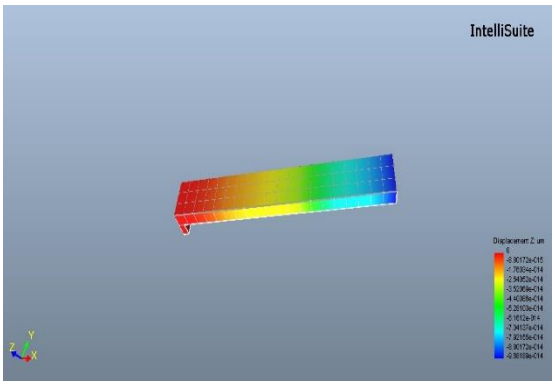

Figure 7. Static Analysis of Chromium Mono Silicide Sensor

b. Dynamic Analysis

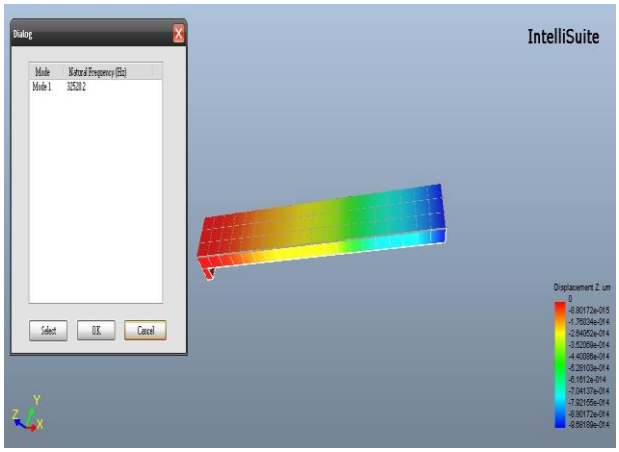

Figure 8. Dynamic Analysis of Chromium Mono Silicide Sensor

D. Simulation Result of Micro Cantilever Beam with Glass Pyrex as Sensor

a. Static analysis

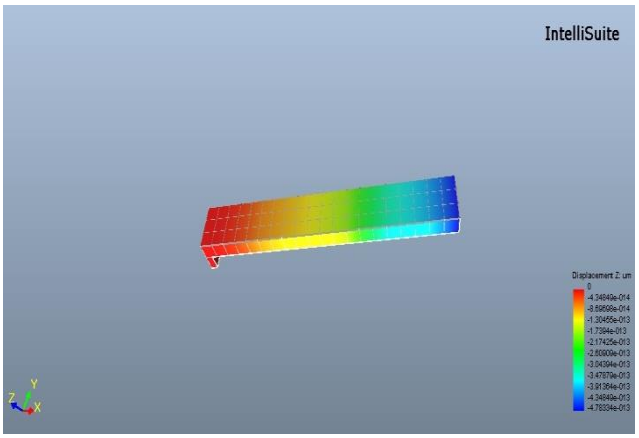

Figure 8. Static Analysis of Glass Pyrex Sensor

b. Dynamic analysis

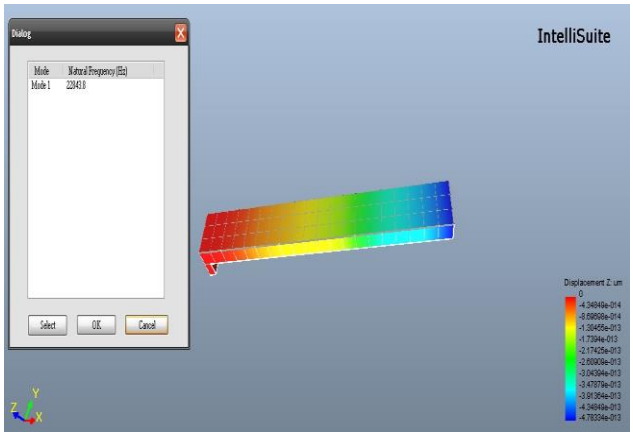

Fig.9 Dynamic Analysis of Glass Pyrex Sensor

TABLE I Frequency Response of Different Sensing Layers

Material	Density(kg/m3)	Frequency(kHz)
Tungsten(W)	19250	20.414
Tantalum(ta)	16600	15.486
Chromium mono silicide(crsi)	5440	32.5202
Glass pyrex	2230	22.8438

TABLE II Sensitivity of Different Sensing Layers

Material	Max. displacement (picomts)	Min. displacement (picomts)	Applied pressure (picopa)	Sensitivity (mts/pa)
W	0.069	0.00630	14.21	0.0044264
ta	0.1399	0.0127	14.21	0.008951
crsi	0.0981	0.0088	14.21	0.006284
Glass pyrex	0.47	0.0434	14.21	0.030021

IV. CONCLUSION

As four different sensing layers are used, the sensing layer with maximum frequency response is considered as fast detector if accuracy is not major concern. Therefore from values which are tabulated above we can conclude that chromium mono silicides (crsi) is fast detector with less delay response compared with other sensing layers considered. If accuracy is major concern then a layer with maximum sensitivity is considered as good sensor with accurate results. Therefore from values which are tabulated above glass pyrex is considered as good sensor compared with other sensing layers considered.

V. REFERENCES

[1] Dhinesh kaarthi. K, S. K. Sathya Lakshmi Preeth, R. Kumar "MEMS Cantilever based identification of Carcinogenic MZN", International Conference on Electrical, Instrumentation and Communication Engineering (ICEICE2017), April 2017.

[2] Muhammad Ahsan Saeed, Shahbaz Mahmood Khan, Umair Rao "Design and analysis of capacitance based Bio-MEMS cantilever sensor for tuberculosis detection," IEEE conference paper, January 2016.

[3] K.S.N.Murthy, G.R.K.Prasad, N.L.N.V.kiran T.V.S.Manoj "Design and simulation of MEMS Biosensor for the detection of Tuberculosis", Indian journal of science and technology, vol 9(31), August 2016.

[4] Monika Chaudary, Amita Gupta, "Microcantilever-based Sensors", Defence Science Journal, Vol.59, No.6, November 2009.

[5] Frometa, Nardo Ramriez. "Cantilever biosensor methods" Biotechnological Aplicada,(2006).

[6] K. Beulah Sujan, T. Shanmuganantham, "Bio-MEMS cantilever sensor design and analysis for detecting multiple diseases", IEEE International Conference on Circuits and Systems, 2017.

Themed Section : Engineering and Technology
© 2018 IJSRSET | Volume 5 | Issue 3 | Print ISSN: 2395-1990 | Online ISSN: 2394-4099

SRR Loaded CB-CPW Fed Antenna for Wearable WBAN and Interfacing Applications

Sajith.K[1], J.Gandhimohan[2], T.Shanmuganantham[3]
[1]Electronics Engineering, Pondicherry Central University, Pondicherry, Puducherry, India
sajithrajan999@gmail.com[1], shanmuga.dee@gmail.com[3]

ABSTRACT

In this paper introduced the split ring resonator (SRR) loaded, conductor backed coplanar wave guide (CB-CPW) fed wearable antenna for glaucoma monitoring application and also used for interfacing with other wireless networks. The main drawbacks of existing antennas are the lower gain and poor radiation efficiency. This is SRR loaded antenna; hence, it had high gain, bandwidth and radiation characteristics. The designed SRR loaded technique exceptionally essential part for wearable transceiver module for healthcare monitoring. This antenna designed to fine-tune at resonating frequency 2.4GHz and 3.5GHz. The simulated results for the magnitude of reflection coefficient are -36dB at 2.46GHz, -14dB at 3.5GHz for non-SRR loaded structure,-36dB at 3.52GHz for SRR loaded with bio-tissue layered antenna, 35dB at 2.4GHz and 30dB at 3.56GHz for SRR loaded antenna without any bio-tissue layer respectively. The antenna required characteristic like such as far-field configuration, magnitude of reflection coefficient, VSWR and gain of the proposed antenna is presented.

Keywords: SRR, Bio-Compatible Substrate, CB-CPW, Specific Absorption Rate (SAR), Wireless Body Area Network (WBAN).

I. INTRODUCTION

The designed antenna consists of asymmetrical conductor backed coplanar waveguide (CPW) fed, two ground plane and central conductor are laid in same plane with different dimension. It is placed on the top of biocompatible substrate called Teflon. The split ring resonator loaded at bottom side of this substrate. The problem of existing antenna is lower gain, poor radiation characteristics and compatibility. However, this proposed SRR loaded antenna overcomes these problems. The main advantage of SRR loaded antenna had high gain and bandwidth, as compared to the conventional antenna. The designed SRR loaded antenna was negative permeability at the main resonance. The Teflon substrate material can solved by biocompatibility issue, since it used for glaucoma and other health care monitoring applications [11].The wearable device can easily interface with WI-FI Bluetooth, WIMAX, WLAN and other wireless communication technology as shown in Fig.1. The medical WBANs network communication are classified as on-body/wearable communication, implantable /in-body communications, and off-body/external communication respectively [1], [2].

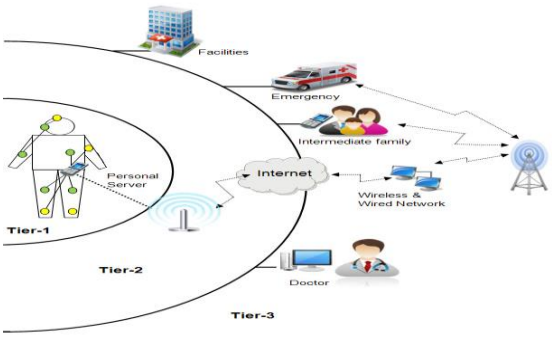

Figure 1: Interface in wearable WBAN & other wireless networks [1]

In this paper organized as Section II includes the explanation of the geometrical design of proposed antenna. The segment III indicated the geometrical revelation of proposed structure. The section IV of this paper point out on the simulation results and descriptions. Part V is the conclusion part of the paper.

II. MODELING AND DESCRIPTION

The conductor backed coplanar wave guide is the one of the quasi mode transmission line using in microwave printed circuits as well as in fabricated antennas, as signal carrying element. It consists of two identical ground plane and one middle metallic strip conductors are in the same plane. The effective dielectric constant and characteristic impedance of this line is given by [3].

$$\varepsilon_{reff,sub} = p(\varepsilon_r - 1) + 1 \quad (1)$$

$$z_o = \frac{30\pi y}{\sqrt{\varepsilon_{reff,sub}}} \quad (2)$$

The letter p is called the filling fraction, the expression for m depends on the shape of geometry and y is elliptical integrals [4],[5].

$$\varepsilon_{ref,sub} = \frac{\varepsilon_{r,sub}+1}{2} + \frac{\varepsilon_{r,sub}-1}{2}\left[1+12\frac{h}{w}\right] \quad (3)$$

The equation (3) indicates effective dielectric constant of substrate. This proposed antenna used a biocompatible substrate-Teflon with dielectric constant is 2.1 , thickness 1.6 mm, so as to resonate at 3.5GHz, then the width of single element of rectangular patch is given by[2],[6],[7].

$$W = \frac{c}{2 f_{op}}\sqrt{\frac{2}{\varepsilon_{r,sub}+1}} \quad (4)$$

From equation (4) width of antenna 20mm obtained. Finally the effective length of a SRR loaded proposed antenna is calculated analytically [12].

$$L_{eff} = \frac{c}{2 f_{op}\sqrt{\varepsilon_{r,sub}}} \quad (5)$$

From equation (5) the effective length of a SRR loaded proposed antenna is 20mm obtained. The relationship between permeability, permittivity and frequencies is given by equation (6) and (7).

$$\mu_b(\omega) = \mu_{ob}\left[1 - \frac{\omega_{pm,b}^2}{\omega_b\left(\omega_b - j\gamma_{m,b}\right)}\right] \quad (6)$$

$$\mu_b(\omega) = \mu_{ob}\left[1 - \frac{\omega_{pm,b}^2}{\omega_b\left(\omega_b - j\gamma_{m,b}\right)}\right] \quad (7)$$

III. LAYERED DESIGN

The electrical characteristic (effective dielectric constant) of the tissue is 53.65 at 2.4GHz, and conductivity is 0.91(s/m) at 2.4GHz [11]. The proposed antenna layered structure mention in Figure: 2, Figure: 3.The patch dimension is shown in Figure: 4, Figure: 5 and Table I respectively. The Comparison results of other wearable antennas as shown in Table II.

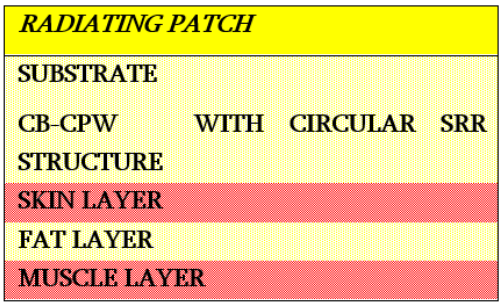

Figure 2. The Proposed Antenna Layers

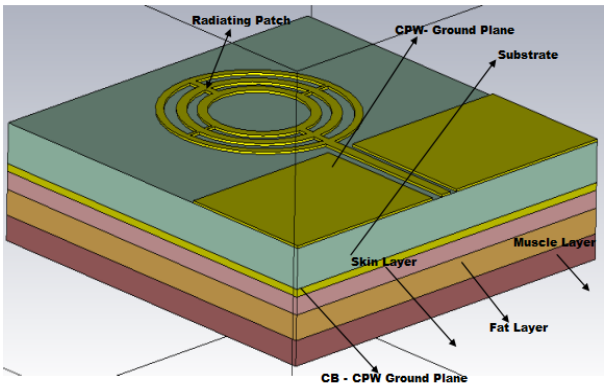

Figure 3: The Proposed Antenna Layered Structure

TABLE I: THE PROPOSED DIMENSION FOR GIVEN STRUCTURE

ANTENNA DIMENSION	VALUE(MM)
W	20
W_1	9.1
Q	6.7
R	5
E	8
D	1
N	10.7
L	20
L_1	6.4
N_1	3.6
H	0.8
H_1	1
M_1	6.5

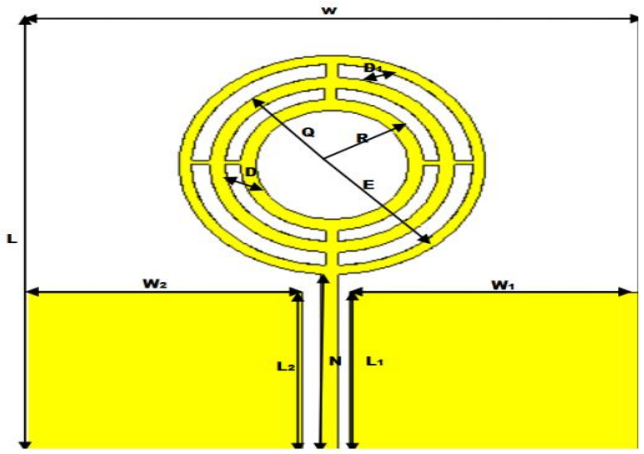

Figure 4. Geometrical Representation of SRR Loaded Proposed Antenna

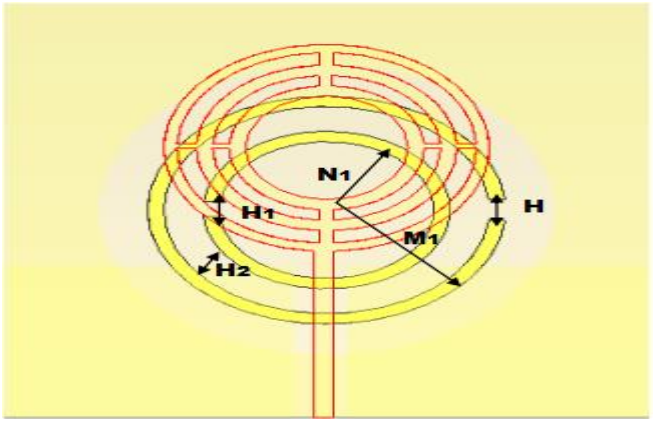

Figure 5. Geometrical Representation of SRR Structure for Proposed Antenna

IV. RESULTS AND DISCUSSIONS

The antenna is computer-generated while implement on body for wearable health monitoring or glaucoma inter ocular pressure (IOP) monitoring. The premeditated antenna is implementing on the skin, fat and muscle layer. Few antenna parametric results are discussed as give below.

A. Magnitude of Reflection Coefficient

The give designed antennas resonate at a resonating frequencies and it's corresponded magnitude of reflection coefficient are -36dB at 2.46GHz, -14dB at 3.5GHz for non-SRR loaded structure,-36dB at 3.52GHz for SRR loaded with bio-tissue layered antenna, 35dB at 2.4GHz and 30dB at 3.56GHz for SRR loaded antenna without any bio-tissue layered structure respectively. This magnitude of reflection coefficient parameter values are helped to interfacing between ISM band and other wireless network band. The magnitude of reflection coefficient for the proposed wearable antenna was shown in the Figure: 6, 7.

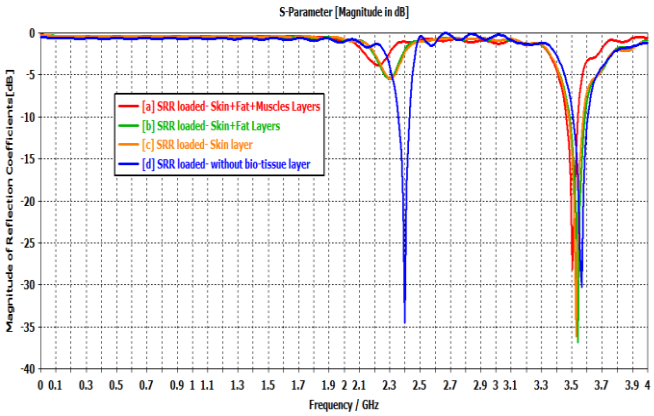

Figure 6. Magnitude of reflection coefficient versus frequency plot [a] Skin layer with SRR [b] Skin and fat layer, [c] Skin, fat and muscle layer, [d] SRR loaded antenna without any bio-tissue layers.

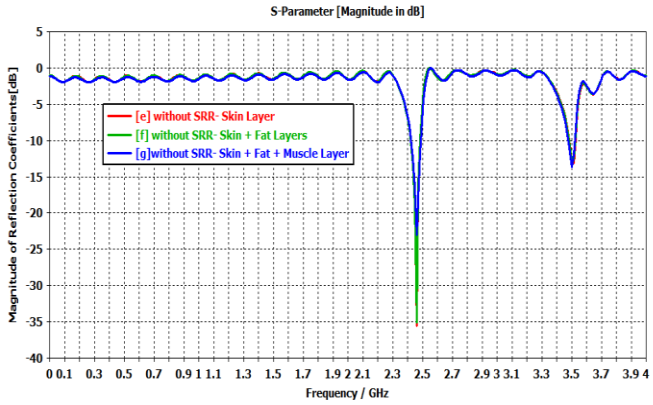

Figure 7. Magnitude of reflection coefficient versus frequency plot [e] Skin layer with SRR [f] Skin and fat [f] Skin, fat and muscle layer.

B. Voltage Standing Wave Ratio

The VSWR values are 1.05 at 2.46GHz, 1.55 at 3.5GHz for without SRR loaded antenna, 1.04 at 3.52GHz for SRR loaded, 1.03 at 2.4GHz and 1.1 at 3.56GHz for SRR loaded without any bio-tissue layered antenna was shown in the Figure: 8,9.

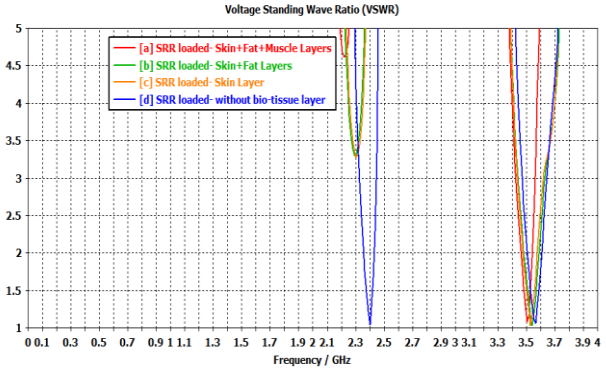

Figure 8. Voltage standing wave ratio - Frequency plot [a] Skin layer with SRR [b]skin and fat layer [c] Skin, fat and muscle layer[d] SRR loaded antenna without any bio-tissue layers.

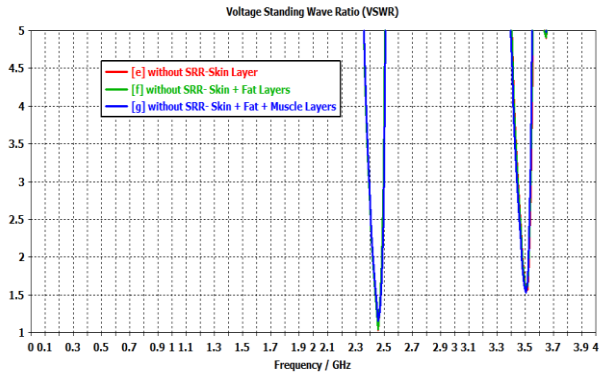

Figure 9. Voltage standing wave ratio - Frequency plot [a] Skin layer without SRR [b]skin and fat layer [c] Skin, fat and muscle layer.

C. Far Field Gain

The some amount of radiated power is absorbed by human tissue. This absorption rate is called SAR value, due to wearable antenna gain is reduced some amount [9].This absorption is related to the operating frequencies are shown in Figure: 10-12. The designed antenna directive gains are 2.3dBi at 2.46GHz, 4.2dBi at 3.5GHz for non-SRR loaded proposed structure, 5dBi at 3.52GHz for SRR loaded, 2.5dBi at 2.4GHz and 4.4dBi at 3.56GHz for SRR loaded without any bio-tissue layered proposed structure.

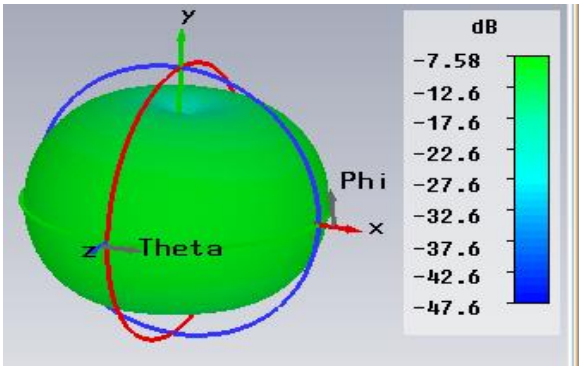

Figure 10. 3D- plot of gain at 2.46GHz

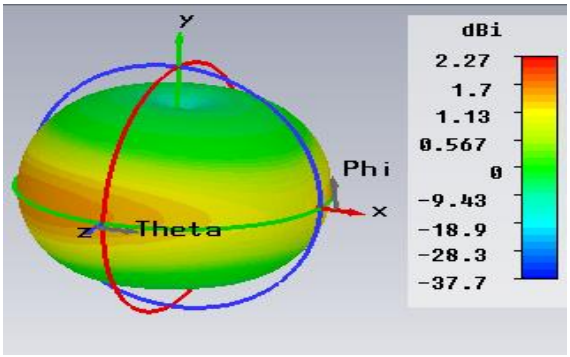

Figure 11. 3D-plot of directive gain at 2.46GHz

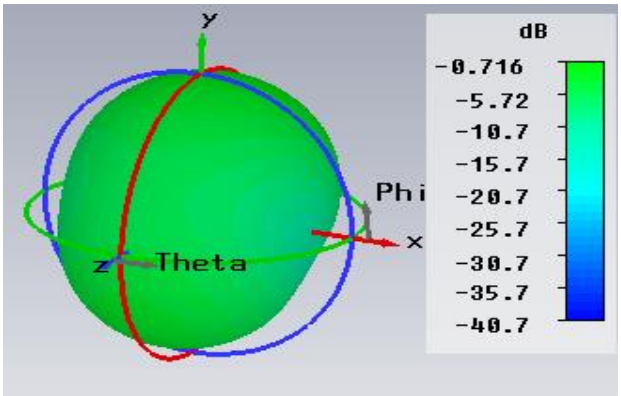

Figure 12. 3D- plot of gain at 3.5GHz

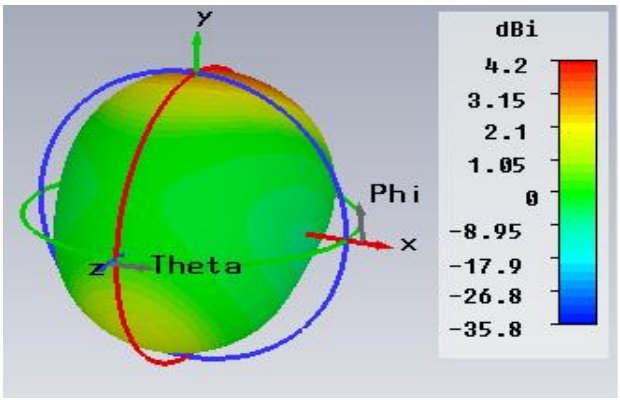

Figure 13. 3D-plot of directive gain at 3.5GHz

D. Radiation Pattern

It is a graphical representation or mathematical representation of radiation characteristic at far field as function of time as well as space [8], [10].the radiation pattern of proposed antenna are shown in Figure:14-16.

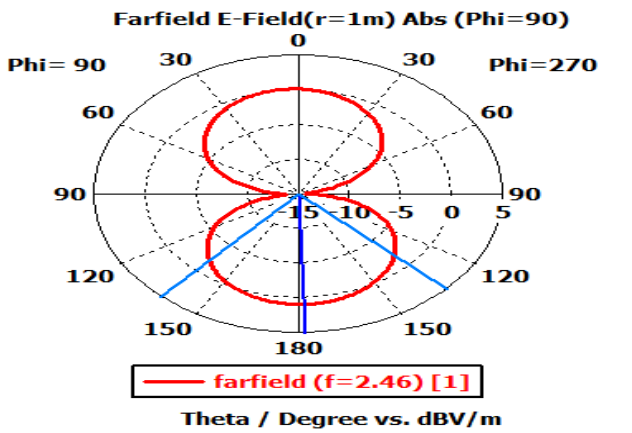

Figure 14. Shows polar plot of E-field at 2.43GHz

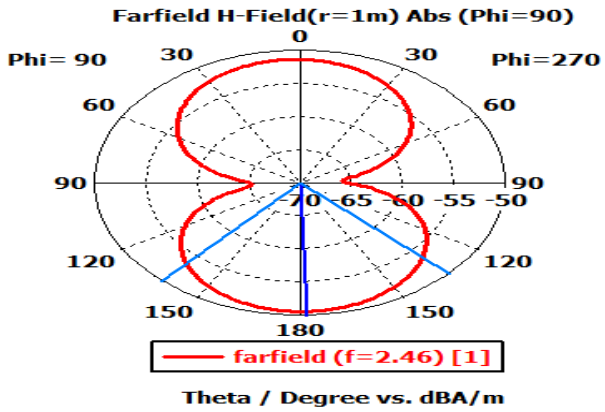

Figure 15. Shows Polar Plot of E-field at 2.43GHz

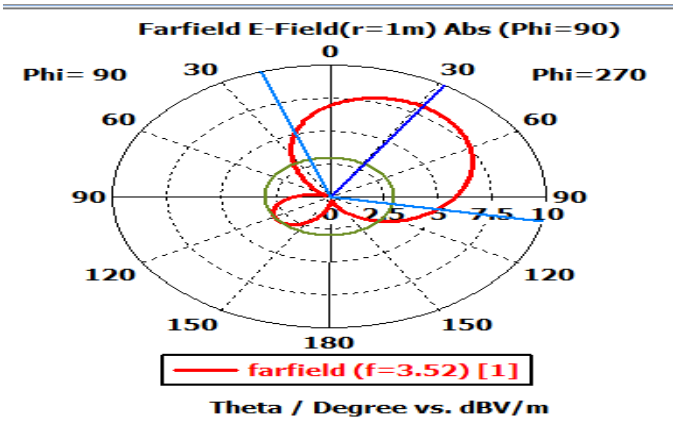

Figure 16. Shows Polar Plot of E-field at 3.5GHz

Reference	Dimension [mm³]	Gain [dB]	10dB-BW [MHz]	Dielectric Materials
[4]	15240	-16	12	ARLON1000
[5]	10240	-	20	Rogers3120
[6]	6480	-	20	RT/duroid6002
[11]	1265.6	-25	142	Rogers3120
Prop. Ant. with SRR-skin layer f=3.52GHz	640	-2	100	Teflon
Prop. Ant. without SRR- skin layer f=2.46GHz	640	-8	60	Teflon
Prop. Ant. without SRR- skin layer f=3.5GHz	640	-1	40	Teflon
Prop. Ant. without SRR without bio-tissue f=2.4GHz	640	-	80	Teflon
Prop. Ant. without SRR without bio-tissue f=3.56GHz	640	-	100	Teflon

V. CONCLUSION

The SRR asymmetrical CB-CPW fed multilayered dual band antenna is designed in this paper used for wearable WBAN applications. The designed antenna overall dimension is 20x20x1.6mm³, and

simulated results for the magnitude of reflection coefficient are -36dB at 2.46GHz, -14dB at 3.5GHz for non-SRR loaded structure,-36dB at 3.52GHz for SRR loaded with bio-tissue layered antenna, 35dB at 2.4GHz and 30dB at 3.56GHz for SRR loaded antenna without any bio-tissue layer respectively. These are ISM band, WIMAX band and WLAN band, since these antennas are applicable for IOP monitoring through the various wireless networks. The proposed antenna simulation results and design methodology can believe for helpful to coming antenna researchers.

VI. REFERENCES

[1] Samaneh Morassaghi, Mehran Abolhasan, Justin Lipman "Wireless body Area Networks: A Survey" IEEE communication surveys and tutorial, vol.16, pp.1658-1686, March 2013.

[2] S. Ashok Kumar, T. Shanmuganantham, J.Navin Sankar, "Design and development of implantable CPW fed monopole L-Slot antenna at 2.45 GHz ISM band for biomedical applications", International Journal for RF Technologies: Research and Applications, vol.7, pp.201-208, August 2016.

[3] T. Shanmuganantham, "Design and performance of implantable CPW fed Apollian Shaped Antenna at 2.45 ISM band for Bio-medical Applications" transaction on electrical and electronic material, vol.16, pp.250-253, October 2015.

[4] S. Ashok Kumar, T. Shanmuganantham "Design and analysis of implantable CPW fed bowtie antenna for ISM band applications" AEU: International Journal of Electronics and Communication, (Elsevier), vol.68, issue 2, pp.158-165, February 2014.

[5] S. Ashok Kumar, T. Shanmuganantham "design of clover slot antenna for biomedical application" Alexandria Engg. Journal, 2016.

[6] S. Ashok Kumar, T. Shanmuganantham, M. Arun Raj "analysis and design of CPW fed antenna at ISM band for biomedical application"` Alexandria Engg. Journal, 2017.

[7] Bose anundhimeena, P.T. Selvan, S Raghavan "compact meta materials Antenna with high directivity for bio-medical systems" circuits and systems, vol.7, October 2016, pp.4036-4045.

[8] S. A. Kumar, T. Shanmuganantham, R sanmuga sundaram, "CPW-fed small meta-material inspired antenna for WiMax and WLAN applications" IEEE Cof. On Indian ant. Week 2016.

[9] C.M Cynthia, Raghavan S "a flexible conformal loop antenna for intramuscular implantable myoeletric sensors" GCCT conf. on 2015.

[10] C.A. Balanis "antenna theory analysis and Design" fourth edition, John Wiley & Sons 2016.

[11] Sajith k, Gandhimohan, and T. Shanmuganantham "A novel SRR loaded CPW-fed antenna for implantable ISM band applications" IEEE Conf. on Indian ant. Week 2017.

[12] Deepanshu kaushal, Sajith k, T. Shanmuganantham "dual band characteristics in a micro-strip rectangular patch antenna using Novel Slot" IEEE Int. Conf. on (ICICICT), July 2017.

Themed Section : Engineering and Technology
© 2018 IJSRSET | Volume 5 | Issue 3 | Print ISSN: 2395-1990 | Online ISSN : 2394-4099

Hybrid Multimodality Medical Image Fusion based on Guided Image Filter with Pulse Coupled Neural Network

B.Rajalingam[1], Dr. R.Priya[2]
[1]Research Scholar, [2]Associate Professor
Department of Computer Science & Engineering, Annamalai University, Chidambaram, Tamilnadu, India
rajalingam35@gmail.com[1], prykndn@yahoo.com[2]

ABSTRACT

Multimodal medical image fusion technique is a fast and effective fusion method proposed for creating a highly integrating and informative fused medical image to acquire a more complete and accurate description of the same object. A multimodality medical image fusion technique plays an important role in biomedical research and clinical disease diagnosis. This paper, proposed an efficient hybrid multimodal medical image fusion approach based on combining the multi-level decomposition of an image into a bottom layer containing huge level variations in strength and a feature layer capturing minute level information with pulse coupled neural network fusion rule. The proposed work combines the guided image filtering and pulse coupled neural network for fusion process. Experimental results demonstrate that the proposed method can obtain magnetic resonance imaging (MRI), positron emission tomography (PET) and single photon emission computed tomography (SPECT) are the source images as experimental images. Hybrid fusion algorithms are evaluated using several quality metrics. Compared with other existing techniques the experimental results demonstrate the better processing performance in both subjective and objective evaluation criteria.

Keywords: Multimodal Medical Image Fusion, Guided Filter, Multi-Level Decomposition, DCHWT, MRI, SPECT, GIF, DWT and PCNN

I. INTRODUCTION

Image fusion is the mixture of two or more different images to form a novel image by using certain techniques. It is extracting information from multi-source images, improves the spatial resolution for the original multi-spectral image, and preserves the spectral information. Image fusion can be done in three levels: Pixel level fusion, Feature level fusion and Decision level fusion. Pixel-level fusion having a large portion of the remarkable data is protected in the merged image. Feature-level fusion performs on feature-by-feature origin, such as edges, textures. Decision-level fusion refers to make a final merged conclusion. The image fusion decrease quantity of information and hold vital data. It make new output image that is more appropriate for the reasons for human/machine recognition or for further processing tasks. Image fusion is classified into two types' single sensor and multi sensor picture combination consolidating the pictures from a few sensors to shape a composite picture and their individual pictures are converged to acquire an intertwined image Ex: Multi focus and Multi Exposure fusion.

Multi sensor image fusion merging the images from several sensors to form a composite image and their individual images are merged to obtain a fused image. Ex: medical imaging, military area. multimodality medical images categorised into several types which include computed tomography (CT), magnetic resonance angiography (MRA), magnetic resonance imaging (MRI), positron emission tomography (PET), ultra sonography (USG), nuclear magnetic resonance(NMR) spectroscopy, single photon emission computed tomography (SPECT), X-rays, visible, infrared and ultraviolet. MRI, CT, USG and MRA images are the structural therapeutic images, which afford lofty resolution images. PET, SPECT and functional MRI (fMRI) images are functional therapeutic images, which afford low-spatial resolution images with functional information. Anatomical and functional therapeutic images can be incorporated to obtain more constructive information about the same object. Medicinal image fusion reduces storage cost by storing the single fused image instead of multiple-input images. Multimodal medical image fusion uses the pixel level fusion. Different imaging modalities can only provide limited information. Computed Tomography (CT) image can display accurate bone structures. Magnetic Resonance Imaging (MRI) image can reveal normal and pathological soft tissues. The fusion of CT and MRI images can integrate complementary information to minimize redundancy and improve diagnostic accuracy. Combined PET/MRI imaging can extract both functional information and structural information for clinical diagnosis and treatment. Image fusion having several applications like medical imaging, biometrics, automatic change detection, machine vision, navigation aid, military applications, remote sensing, digital imaging, aerial and satellite imaging, robot vision, multi focus imaging, microscopic imaging, digital photography and concealed weapon detection. Multimodal medical imaging plays a vital role in a large number of healthcare applications including medical diagnosis and treatment. Medical image fusion combining multiple images into form a single fused modalities. Medical image fusion methods involve the fields of image processing, computer vision, pattern recognition, machine learning and artificial intelligence.

The research paper is organized as follows. Sec. 2 describes the literature survey on related works. Sec. 3 discusses the proposed research work method both traditional and hybrid multimodal medical image fusion techniques, performance evaluation metrics is briefly reviewed. Sec. 4 describes the implemented medical image fusion experimental results and performance comparative analysis. Finally, Sec. 5 contains the conclusion.

II. RELATED WORKS

B. Rajalingam, Dr. R. Priya. [1] Proposed a multimodal medicinal image fusion approach based on traditional and hybrid fusion techniques and performance are evaluated using quality metrics. B. Rajalingam, Dr. R. Priya.[2] Proposed a novel multimodal medicinal image fusion approach based on hybrid fusion techniques. Magnetic Resonance Imaging (MRI), Positron Emission Tomography (PET) and Single Photon Emission Computed Tomography (SPECT) are the input multimodal therapeutic brain images and the curvelet transform with neural network techniques are applied to fuse the multimodal medical image. B.Rajalingam, Dr. R.Priya [3] proposed a novel neuro-fuzzy hybrid multimodal medical image fusion technique to improve the quality of fused multimodality medical image.

Xiaojun Xua, Youren Wang, et al. [4] proposed a multimodality medicinal image mixture algorithm based on discrete fractional wavelet transform. The input therapeutic images are decomposed using discrete fractional wavelet transform. The sparsity character of the mode coefficients in subband images changes. Xingbin Liu, Wenbo Mei, et al.[5] proposed a new technique namely Structure tensor and non subsampled shearlet transform (NSST) to extract geometric features. A novel unified optimization model is proposed for fusing computed Tomography (CT) and Magnetic Resonance Imaging (MRI) images. K.N. Narasimha Murthy and J. Kusuma[6] proposed Shearlet Transform (ST) to fuse two different images Positron Emission Tomography (PET) and Magnetic Resonance Imaging (MRI) image by using the Singular Value Decomposition (SVD) to improve the information content of the images. Satishkumar S. Chavan, Abhishek Mahajan,et al.[7] introduced the technique called Nonsubsampled Rotated Complex Wavelet Transform (NSRCxWT) combining CT and MRI images of the same patient. It is used for the diagnostic purpose and post treatment review of neurocysticercosis. S. Chavan, A. Pawar, et al.[8] innovated a feature based fusion technique Rotated Wavelet Transform (RWT) and it is used for extraction of edge-related features from both the source modalities (CT/MRI). Heba M. El-Hoseny, El-Sayed M.El.Rabaie,et al.[9] proposed a hybrid technique that enhance the fused image quality using both traditional and hybrid fusion algorithms(Additive Wavelet Transform (AWT) and Dual Tree complex wavelet transform (DT-CWT)). Udhaya Suriya TS, Rangarajan P [10] implemented an innovative image fusion system for the detection of brain tumours by fusing MRI and PET images using Discrete Wavelet Transform (DWT). Jingming Yang, YanyanWu,et al.[11] described an Image fusion technique Non-Subsampled Contourlet Transform (NSCT) to decompose the images into lowpass and highpass subbands. C.Karthikeyan, B. Ramadoss[12] proposed the fusion of medical images using dual tree complex wavelet transform (DTCWT) and self organizing feature map (SOFM) for better disease diagnosis. Xinzheng Xu,Dong Shana,et al.[13] introduced an adaptive pulse-coupled neural networks (PCNN), which was optimized by the quantum-behaved particle swarm optimization (QPSO) algorithm to improve the efficiency and quality of QPSO. Three performance evaluation metrics is used. Jyoti Agarwaland Sarabjeet Singh Bedi, et al.[14] innovate the hybrid technique using curvelet and wavelet transform for the medical diagnosis by combining the Computed Tomography (CT) image and Magnetic Resonance Imaging (MRI) image. Jing-jing Zonga and Tian-shuang Qiua[15] proposed a new fusion scheme for medical images based on sparse representation of classified image patches In this method, first, the registered input images are separated into confidential patches according to the patch geometrical route, from which the corresponding sub-dictionary is trained via the online dictionary learning (ODL) algorithm and the least angle regression (LARS) algorithm to sparsely code each patch; second, the sparse coefficients are combined with the "choose-max" fusion rule; Finally, the fused image is reconstructed from the combined sparse coefficients and the corresponding sub-dictionary. Richa Gautam and Shilpa Datar[16] proposed a method for fusing CT (Computed Tomography) and MRI (Medical Resonance Imaging) images based on second generation curvelet transform. Proposed method is compared with the results obtained after applying the other methods based on Discrete Wavelet Transform (DWT), Principal Component Analysis (PCA) and Discrete Cosine Transform (DCT). Jiao Du, Weisheng Li, Bin Xiao,et.al.[17] proposed an approach union Laplacian pyramid with multiple features for accurately transferring salient features from the input medical images into a single fused image. Zhaobin Wang, Shuai Wang,Ying Zhu,et al.[18] described the statistical analysis PCNN and some

modified models are introduced and reviewed the PCNN's applications in the field of image fusion. Zhaobin Wang, Shuai Wang, et al.[19] Proposed a novel guided filtering based weighted average technique to make full use of spatial consistency for fusion of the base and detail layers. B. K. Shreyamsha Kumar [20] proposed a discrete cosine harmonic wavelet transform (DCHWT) based image fusion to retain the visual quality and performance of the merged image with reduced computations.

III. PROPOSED RESEARCH WORK

A. Traditional Multimodal Medical Image Fusion Techniques

This paper implements different traditional image fusion algorithms for different types of multimodality medical images as shown in Fig .1

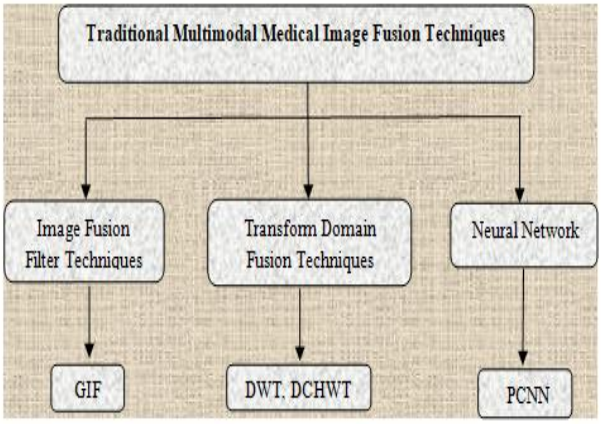

Fig. 1 Traditional multimodal medical image fusion techniques

i) Image Fusion with Guided Filtering

Currently, in medical image processing energetic research topic is edge preserving filter technique. Image processing has several edge preserving smoothing filtering techniques such as guided filter, weighted least squares and bilateral filter. Among the several filter techniques the guided image filter is giving better results and less execution time for fusion process. This image fusion filter method is based on a local linear form, creating it eligible for other image processing methods such as image matting, up-sampling and colorization. A multi-level representation is utilized by average smoothing filter. Subsequently, based on weighted average fusion technique, the guided image filter fuses the bottom and feature layers of multi-modal medical images.

(a) Multi level Image Decomposition

The average filter used to decompose the input multimodal medical images into multilevel representations. The bottom layer of each input image is represented by.

$$\mathbf{E}_n = S_n * K \quad (1)$$

Where the n^{th} input image is denoted as S_n, average filter is represented by K and the 31×31 conventional matrix is set to average filter size. First the bottom layer is found then the feature layer can be simply computed by subtracting the bottom layer from the input medical images.

$$\mathbf{F}_n = S_n - E_n \quad (2)$$

The aim of the multi-level decomposition step is to separate each input medical images into bottom and feature layer. A bottom layer contains the huge level variations in strength and a feature layer contains the minute level information.

(b) Guided Image Filter with Weight Map Construction

The Gaussian filtering is applied on both the input multimodality medical images

to get the high pass multimodal medical image R_n.

$$\mathbf{R}_n = S_n * M \quad (3)$$

Where the Gaussian filters is represented by M with 3 × 3 matrix. Construct the saliency maps P_n using the local average value of R_n.

$$P_n = |R_n| * v_{r_v \sigma_v} \quad (4)$$

Where Gaussian low pass filter is denoted by v and $(2r_v + 1)$ $(2r_v + 1)$ is the size of low pass filter and the r_v and σ_v parameters of the Gaussian filters. The calculated saliency weight maps are giving good description and detail information of the saliency intensity. After that, the saliency weight maps are compared to establish the weight maps are represented by,

$$T_x^k = \begin{cases} 1 \text{ if } P_1^k = \max(P_1^k, P_2^k \dots\dots, P_X^k \\ 0 \qquad\qquad\qquad\qquad \text{otherwie} \end{cases} \quad (5)$$

Where the number of input multimodal medical images is represented by X, the saliency value of the pixel k in the n^{th} image is P_x^k. But, the artifacts of the merged image which may produce the weight maps with noisy and not associated with object limitations. The effective way to solve the above problem is to use spatial consistency. Spatial consistency is two adjacent pixels have identical clarity or color, they will be apt to have comparable weights. The formulating an energy function is based on spatial consistency fusion approach. To get the essential weight maps this energy function can be minimized globally. But, the optimization based methods are often somewhat incompetent. Guided image filtering is performed on every weight map T_n with the equivalent input image S_n serving as the supervision image.

$$W_n^E = V_{r_1 \varepsilon_1}(T_n, S_n) \quad (6)$$

$$W_n^F = V_{r_1 \varepsilon_1}(T_n, S_n) \quad (7)$$

Where the guided image filtering parameters are represented by $r_1, \varepsilon_1, r_2, \text{and } \varepsilon_2$, the weight maps of the bottom and features layers denoted by W_n^E and W_n^F. N is normalized weight maps value and each pixel k is sum to one. The inspiration of the weight maps construction technique is represented in the following expression. The eqn.1, eqn. 3 and eqn. 4 derived the local variance point i is referred by its value very small and the supervision image having pixel in very large, then a_k will become close to 0 and the filtering output R will equal to $\overline{T_k}$. If the local variance of pixel i having very large value, then the i is represent the pixel edge area, next a_k will become far from zero. As established in, $\nabla R \approx \bar{a} \nabla S$ will turn into accurate, which means that only the weight map in one side of the edge will be averaged. In both situations, those pixels with identical color or clarity tend to have comparable weights. In contrast, sharp and edge-aligned weights are preferred for merging the feature layers because details may be lost when the weights are over-smoothed. Hence, a large filter size and a large blur degree are chosen for merging the bottom layers, while a minute filter size and a minute blur degree are chosen for the feature layers.

(c) Multi level Image re-enactment

Multi level image reconstruction contains the following two steps. Initially, the bottom and

feature layers of different input multimodal medical images are combined together using weighted averaging filtering

$$\bar{E} = \sum_{n=1}^{N} W_n^E \mathbf{E}_n \quad (8)$$

$$\bar{F} = \sum_{n=1}^{N} W_n^F \mathbf{F}_n \quad (9)$$

Next, the merged output multimodal medical image R is obtained by combining the merged bottom layer $\bar{E}$ and the merged feature layer $\bar{F}$

$$R = \bar{E} + \bar{F} \quad (10)$$

(d) Procedural steps for image fusion using Guided Image Filtering:

1) Take the two input multimodal medical images.

2) Resize both images into 512 x 512 dimensions.

3) Decompose the input multimodal medical images using average filtering.

4) Separate the input multimodality medical images into bottom layer and feature layer based on multi scale representation.

5) Apply the Gaussian laplacian filters for to construct the weight map and saliency map.

6) Perform the image reconstruction and get the final fused multimodal medical image.

ii) Discrete Wavelet Transform (DWT)

Wavelet transform is applied in two domains namely continuous and discrete. CWT (Continuous Wavelet Transform) is the correlation between the wavelet at different scales (inverse of frequency) and the signal and is figured by changing the size of the investigation window each time, moving it, increasing it by the flag. Scientific condition is given by

$$\varphi_x(\tau, R) = \frac{1}{\sqrt{R}} \int X(t).\, \varphi * \left(t - \frac{\tau}{R}\right) dt \quad (11)$$

In the above expression τ (translation) and R (scale) are variables required for transforming the signal x (t). Psi (Ψ) is the transforming function known as mother wavelet. In DWT (Discrete Wavelet Transform) a 2D signal (image) I(x, y) is first filtered through low pass and high pass finite impulse response filters (FIR), having impulse response h[n] in horizontal direction and then decimated by factor of 2. This gives first level decomposition. Further the low pass filtered image is again filtered through low pass and high pass FIR filters in vertical direction and then again decimated by 2 to obtain second level decomposition. Filtering operation is given by the convolution of the signal and impulse response of signal.

$$X[n] * h[n] = \sum_{k=-\infty}^{\infty} X[k].\, h[n-k] \quad (12)$$

Now to perform inverse wavelet transform, first up sample the sub band images by factor of 2 column wise and then filter them through low pass and high pass FIR filters. Repeat the same process in next step row wise. Now add all the images to get the original image.

(a) Procedural steps for image fusion using DWT algorithm

1) Take the two input multimodal medical images.

2) Resize both images into 512 x 512 dimensions.

3) Convert both the images into gray scale if required.

4) Apply 2D-DWT on both the images and obtain its four components.
5) Now apply the fusion rule as per the requirement.
a) Most extreme pixel determination governs (all maximum): By choosing every single greatest coefficient of both the input images and merging them.
b) Mean: By taking the normal of the coefficients of both the images.
c) Blend: By taking the normal of the estimated coefficients of both the input images and choosing the most extreme pixels from detail coefficients of both the input data.
6) Now apply IDWT to obtain the fused output image.

iii) Discrete cosine harmonic wavelet transforms (DCHWT)

A DCT expresses a predetermined order of data indicated in terms of a sum of cosine functions alternate at different frequencies. The discrete cosine transform generate the signal in the symmetric cyclic order and remove the discontinuity symmetric signal to move from one step to next step efficiently. The extension of the symmetric signal make the length into double for the original signal and giving better frequency resolution for factor of two.
$A_E(t)$ and $\psi_E(t)$ are denoted as real symmetric signal and real symmetric wavelet function respectively.

$$R_c(x,y) = \frac{|x|^{\frac{1}{2}}}{2\pi}\int_{-\infty}^{\infty} A_E(\sigma)\,\Psi_E(x\sigma)\cos(\sigma y) \quad (13)$$

Where the cosine transforms are represented by $A_E(\sigma)$ and $e(\sigma)$ of wavelet functions $A_E(t)$ and $\psi_E(t)$, respectively. The wavelet transform $R_c(x,y)$ used in the cosine domain moderately than the Fourier domain. Consequently, Eq. 13 can be modified as

$$R_c(x,y) = |x|^{\frac{1}{2}} \quad {}^{-1}[R_E(\sigma)\Psi_E(x\sigma)] \quad (14)$$

In Eq.14 cosine transform functions $A_E(\sigma)$ and $e(\sigma)$ are used to compute the cosine wavelet coefficients $R_c(x,y)$ for a particular scale x. The harmonic wavelet function is denoted as $\Psi(\sigma)$ in harmonic wavelet transform, the cosine harmonic wavelet function s(σ) is easy and it is zero for all frequencies apart from the small frequency band where it is stable, It is referred by.

$$\Psi_E(\sigma) = \begin{cases} 1, \sigma_c - \sigma_0 < \sigma < \sigma_c + \sigma_0, \\ -\sigma_c - \sigma_0 < \sigma - \sigma_c + \sigma_0, \\ 0, \quad \text{elsewhere} \end{cases} \quad (15)$$

The equivalent wavelet $\varphi_E(t)$ in time domain is converted into.

$$\Psi(t) = \frac{\sigma_0}{\pi}\frac{\sin\sigma_0 t}{\sigma_0 t}\cos(\sigma_c t) = \frac{\sigma_0}{\pi}\sin c(\sigma_0 t)\cos(\sigma_c t) \quad (16)$$

The Shannon scaling function is a cosine modulated edition of the protect wavelet. The symmetric rectangular function and for a discrete signal, it is zero apart from on symmetric finite bands [π/c, π/d] and [–π/c, –π/d] where c, d can be real numbers for the spectral weighing in cosine harmonic transform. The cosine harmonic transform too suffers from the difficulty of poor time localization and the result of spectral weighing to restrict in time period by wavelet

functions other than rectangular outputs in non orthogonal wavelets due to spectral overlap similar to the Fourier based harmonic wavelet transform. In discrete cosine harmonic wavelet transform the multimodal medical image is decomposed by cluster the discrete cosine transform coefficients in a method similar to that of discrete Fourier transform coefficients except for the conjugate procedure in inserting the coefficients symmetrically. The inverse discrete cosines transform of these collection results in discrete cosine harmonic wavelet coefficients. The discrete cosine transform of these progression subbands results in subband DCT coefficients, which are relocated in their equivalent spot to recover the overall DCT range at the unique sampling rate.

(a) Procedural steps for image fusion using DCHWT algorithm

1) Take the two source multimodal medical images.
2) Resize both images into 512 x 512 dimensions
3) Divide the first 2D image into rows and link them together in a chain form to have a 1D row vector R.
4) Divide the second 2D image into columns and link them together in a chain form to have a 1D column vector C.
5) Apply DCHWT on both R and C separately and then apply averaging operation on the vectors.
6) Apply inverse DCHWT on the resulting vector.
7) Convert 1D vector into 2D image to obtain the fused output medical image

iv) PCNN Model

Pulse coupled neural network system (PCNN) is a novel visual cortex roused neural system portrayed by the worldwide coupling and heartbeat synchronization of neurons. The basic PCNN demonstrate is appeared in Figure. 2, which incorporates three sections: open field, modulation field and heartbeat generator. The equation for streamlined PCNN can be communicated as

$$E_{ij}(r) = T_{ij} \quad (17)$$

$$S_{ij}(r) = e^{-a^L} S_{ij}(r-1) + X^L \sum_{kj} Y_{kj} R_{ijkl}(r-1) \quad (18)$$

$$V_{ij}(r) = E_{ij}(r)[1 + \beta S_{ij}(r)] \quad (19)$$

$$\theta_{ij}(r) = e^{-a^\theta} \theta_{ij}(r-1) + X_{ij}^{\theta} R_{ij}(r-1) \quad (20)$$

$$R_{ij}(r) = \text{step}\left(V_{ij}(r) - R_{ij}(r)\right) = \begin{cases} 1, & U_{ij}(r) > \theta_{ij}(r) \\ 0, & \text{otherwise} \end{cases} \quad (21)$$

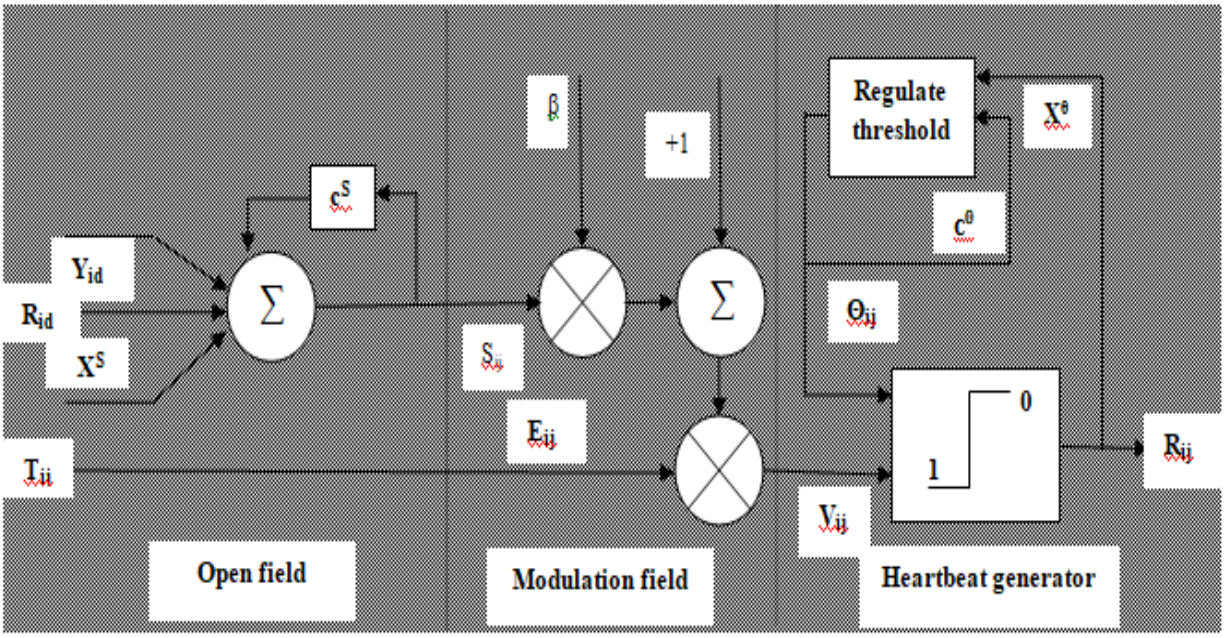

Fig. 2 Simplified PCNN model

In Fig. 2, the open field contains two input compartment: the feeding E_{ij} and the connecting S_{ij} (see (17) and (18)). Each neuron receives the output R_{ij} of neighborhood neurons and the peripheral stimuli T_{ij}, where T_{ij} represent the gray value of the input image. In the modulation field, the domestic state signal V_{ij} is created by connecting input signal S_{ij} and the feeding input E_{ij} via connecting coefficient β. Then, if V_{ij} is superior to the threshold value θ_{ij} of the neuron, the heartbeat generator will produce a pulse, namely, it is called a fire. After the neuron outputs a pulse, the threshold of the neuron will get higher rapidly by feedback. If θ_{ij} is superior to V_{ij}, the heartbeat generator stops generating the pulse, the threshold starts to reduce until θ_{ij} is less than V_{ij} again. Y_{id} denotes the connecting weight, the decay coefficients c^{S}, c^{θ} and potentials coefficients X^{S},

X^{θ} undertaking the periodicity of the pulse output of the PCNN model.

B. Hybrid Multimodal Medical Image Fusion Techniques

Traditional medical image fusion techniques lack the ability to get high-quality images. So, there is a bad need to use hybrid fusion techniques to achieve this objective. The basic idea of the hybrid technique is to combine the guided image filter fusion technique with neural network fusion techniques to improve the performance and increase fused image quality.

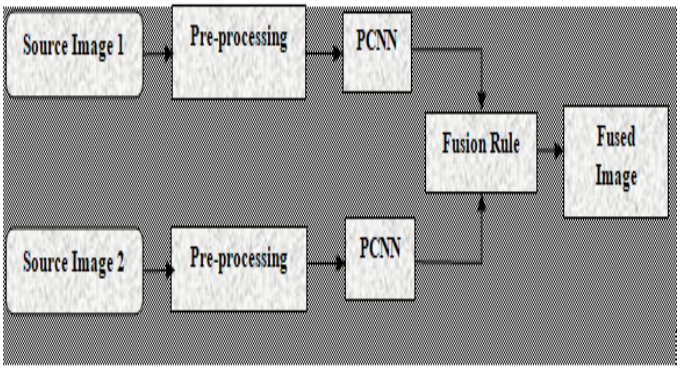

Fig. 3 Image Fusion Process of PCNN

Another possibility is applying two stage transformations on input images before fusion process. These transformations provide better characterization of input images, better handling of curved shapes and higher quality for fused details. The overall advantages of

the hybrid techniques are improving the visual quality of the images, and decreasing image artifacts and noise. Each image size is 512*512 dimensions. Fig. 4 illustrates the schematic diagram of the proposed hybrid multimodal medical image fusion techniques.

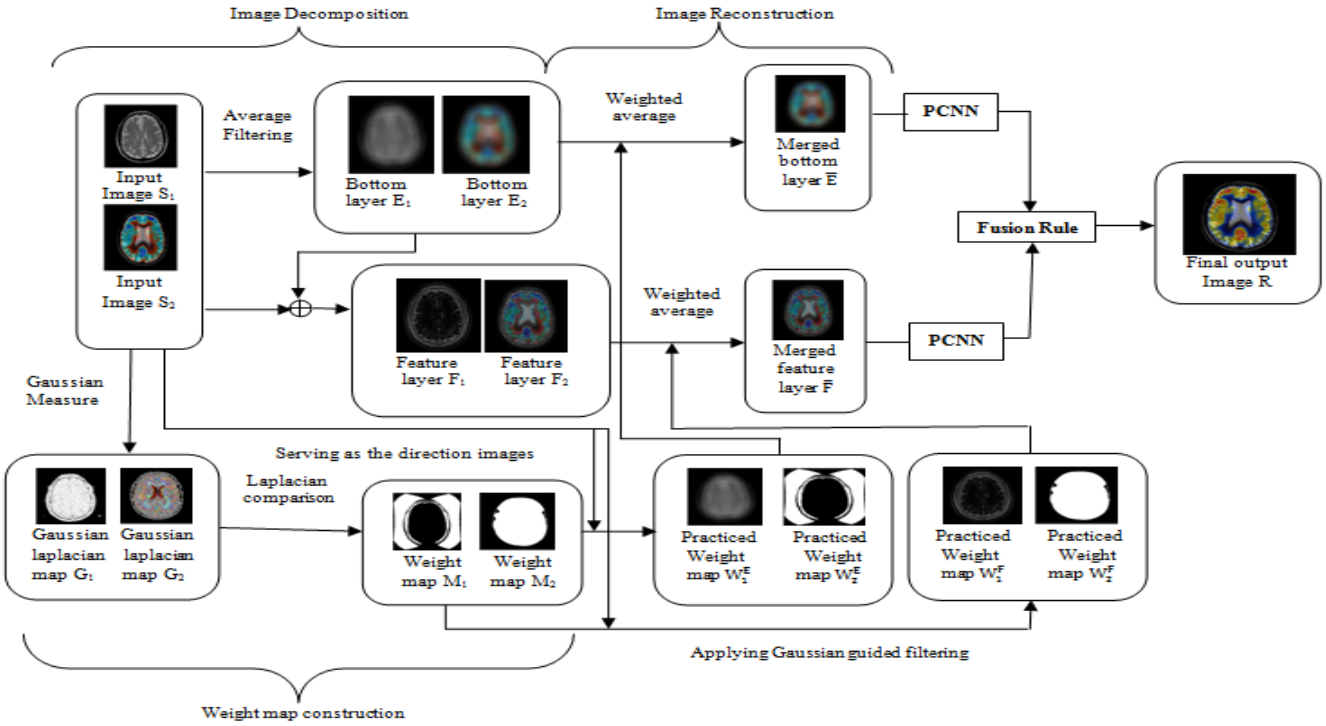

Figure 4: Schematic diagram for the proposed hybrid multimodal medical image fusion

i) Proposed hybrid multimodal image fusion algorithm (GIF-PCNN)

In this work both GIF and PCNN are applied on the input source multimodal medical images.

Input: X and Y are the two inputs of multimodal medical images which need to be processed.

Output: Multimodality medical image, which is getting fused.

Step 1: The input source images are decomposed into multi-level representations by average filtering.

Step 2: Resize both images into 512 x 512 dimensions

Step 3: Variables I1 and I2 are multimodal images in matrix form where each pixel gray level value is in the Range from 0 to 255.

Step 4: Compare rows and columns of both input multimodal medical images.

Step 5: Apply the Gaussian laplacian filtering for weight map construction.

Step 6: Perform the reconstruction operation on the both bottom layer and feature layers of different input images.

Step 7: Now apply the PCNN pre-processing steps on the guided filter processed source images.

Step 8: Apply the pulse coupled neural network fusion rule for the accurate medical image fusion.

Step 9: Fused final output multimodal medical image is displayed.

C. Evaluation Metrics

Fusion quality metrics are utilized in this work to evaluate the efficiency of the fusion algorithms. These metrics are:

i) Average Gradient (g)

The average gradient represents the amount of texture variation in the image. It is calculated as:

$$g = \frac{1}{(R-1)(S-1)} \sum_{i=1}^{(R-1)(S-1)} \frac{\sqrt{(\frac{\partial f}{\partial x})^2 + (\frac{\partial f}{\partial x})^2}}{2} \quad (22)$$

Where R and S are the image dimensions of images x and y respectively.

ii) Standard Deviation (STD)

It is used to establish how much difference of the data is from the average or mean value. The input data is said to be clearer if its STD value is bigger. STD is deliberate using the equation:

$$STD = \frac{\sqrt{\sum_{i=1}^{R} \sum_{j=1}^{S} |f(i,j) - \mu|^2}}{RS} \quad (23)$$

Where R and S represent the dimensions of the image f(i,j), and the mean value is represented by μ .

iii) Local Contrast (C_{local})

It is an index for the image quality and purity of view. It is calculated using the equation:

$$C_{local} = \frac{|\mu_{target} - \mu_{background}|}{\mu_{target} + \mu_{background}} \quad (24)$$

Where μ_{target} is the mean gray-level of the target image in the local region of interest and $\mu_{background}$ is the mean of the background in the same region. The larger value of C indicates more purity of the image.

iv) Structural Similarity Index Metric (SSIM)

It is a measure of the similarity between two regions w_x and w_y of two images x and y.

$$SSIM(x, y|w) = \frac{(2\bar{w}_x \bar{w}_y + C_1)(2\sigma w_x w_y + c_2)}{(\bar{w}_x{}^2 + \bar{w}_y{}^2 + C_1)(\sigma^2 w_x + \sigma^2 w_y + c_2)} \quad (25)$$

Where C_1 and C_2 are small constants. $\bar{w}_x$, $\bar{w}_y$ are the mean values of w_x and w_y. $\sigma^2 w_x$, $\sigma^2 w_y$ are the variance of w_x and w_y. $\sigma w_x w_y$ is the covariance between the two regions

v) Xydeas and Petrovic Metric ($Q^{AB/F}$)

This metric is used to measure the transferred edge information amount from source images to the fused one. A normalized weighted performance form of that metric can be calculated as following

$$Q^{AB/F} = \frac{\sum_{m=1}^{M} \sum_{n=1}^{N} (Q_{(m,n)}^{AF} W_{(m,n)}^{AF} + Q_{(m,n)}^{BF} W_{(m,n)}^{BF})}{\sum_{m=1}^{M} \sum_{n=1}^{N} W_{(m,n)}^{AF} + W_{(m,n)}^{BF}} \quad (26)$$

Where $Q_{(m,n)}^{AF}, Q_{(m,n)}^{BF}$ is the edge information preservation value and $W_{(m,n)}^{AF}, W_{(m,n)}^{BF}$ are their weights

vi) Mutual Information (MI)

MI is an index that calculates the quantity of dependency between two images (R, S), and it gives the joint distribution detachment between them using the subsequent equation:

$$I(r, s) = \sum_{y \epsilon R} \sum_{r \epsilon R} p(r, s) \log\left(\frac{p(r,s)}{p(r)p(s)}\right) \quad (27)$$

Where p(r) and p(s) are the marginal probability distribution functions of the both images, and p(r,s) is the joint probability distribution function.

$$MI(r, s, f) = \frac{I(r,s) + I(r,f)}{H(r) + H(s)} \quad (28)$$

Where H(r), H(s) are the entropies of images r and s.

vii) Feature Similarity Index Metric (FSIM)

It represents edge similarity between input images and the fused image, and it can be calculated from the following equation:

$$FSIM = \frac{\sum_{x\in\Omega} S_L(x).PC_m(x)}{\sum_{x\in\Omega} PC_m(x)} \quad (29)$$

Where, Ω is the image spatial domain, $S_L(x)$ is the total similarity between the two images, and $PC_m(x)$ is the phase congruency value.

viii) Processing Time

It represents the time required for the fusion process in seconds according to the computer specifications.

IV. EXPERIMENTAL RESULTS AND DISCUSSIONS

The implementations are based on four set of source images and the proposed technique is compared with existing techniques i.e. DWT, DCHWT and PCNN. The implementation is executed in MATLAB R2013b on windows 7 laptop with Intel Core I5 Processor, 4.0 GB RAM and 500 GB Hard Disk. The processed multimodality therapeutic input images are gathered from harvard medical school [21] and radiopedia.org [22] medical image online database. The size of the image is 512 × 512 for execution process.

A. Dataset 1

The MRI and PET are the input source images as shown in Figure-5A, B respectively. Figure-5G is the fused final output image of the proposed technique. The Existing techniques are DWT, DCHWT, Guided Filtering and PCNN outputs as shown in Figure-5C to F respectively.

B. Dataset 2

The MRI and SPECT are the input source images as shown in Figure-6A, B respectively. Figure 6G is the fused final output image of the proposed technique. The Existing techniques are DWT, DCHWT, Guided Filtering and PCNN outputs as shown in Figure-6C to F respectively.

C. Dataset 3

The MRI and SPECT are the input source images as shown in Figure-7A, B respectively. Figure 7G is the fused final output image of the proposed technique. The Existing techniques are DWT, DCHWT, Guided Filtering and PCNN outputs as shown in Figure-7C to F respectively.

D. Dataset 4

The MRI and SPECT are the input source images as shown in Figure-8A, B respectively. Figure 8G is the fused final output image of the proposed technique. The Existing techniques are DWT, DCHWT, Guided Filtering and PCNN outputs as shown in Figure-8C to F respectively.

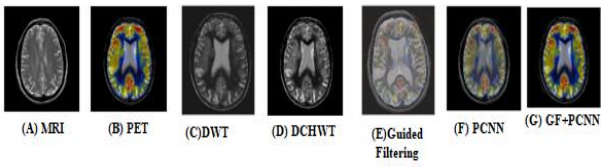

Fig. 5: Results of Dataset 1

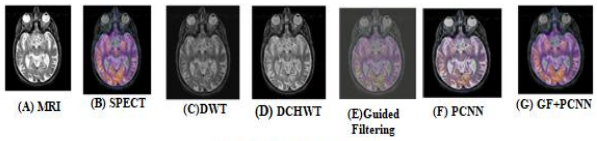

Fig. 6: Results of Dataset 2

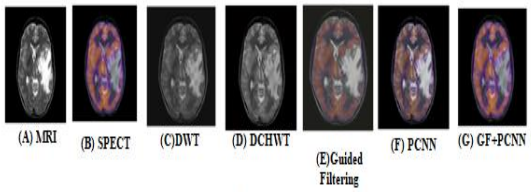

Fig. 7: Results of Dataset 3

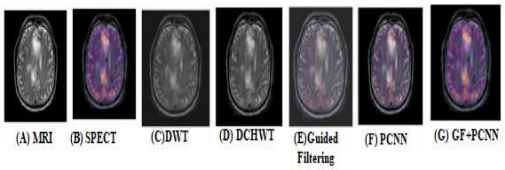

Fig. 8: Results of Dataset 4

Table1. Performance Metrics Obtained For Different Medical Image Fusion Algorithms

Method	Metrics	DWT	DCHWT	GIF	PCNN	Proposed Method (GF+PCNN)
Dataset 1	AG	0.0693	0.0735	0.0798	0.0881	**0.0939**
	STD	0.698	0.713	0.859	0.899	**0.974**
	C_{local}	0.596	0.767	0.876	0.898	**1.071**
	SSIM	0.826	0.859	0.865	0.883	**0.939**
	$Q^{AB/F}$	0.8491	0.8796	0.8810	0.8993	**0.9870**
	MI	0.8343	0.8487	0.8682	0.8816	**0.9657**
	FSIM	0.9381	0.9487	0.9526	0.9689	**0.9899**
	PT	2.596	2.473 sec	2.295	2.189	**1.894 sec**
	AG	0.0633	0.0775	0.0858	0.0899	**0.0963**
	STD	0.5627	0.6179	0.6659	0.6987	**0.7852**
	C_{local}	0.6862	0.6943	0.7012	0.7145	**0.8981**
Dataset 2	SSIM	0.6858	0.6489	0.6258	0.6058	**0.7879**
	$Q^{AB/F}$	0.5665	0.5869	0.4968	0.5386	**0.6432**
	MI	1.0842	1.1854	1.2712	1.1763	**1.3513**
	FSIM	0.8831	0.8483	0.8526	0.8891	**0.9054**
	PT	2.396	2.297 sec	2.671	2.957	**2.191 sec**
Dataset 3	AG	0.0797	0.0785	0.0814	0.0831	**0.0915**
	STD	0.953	0.936	0.962	0.982	**1.014**
	C_{local}	0.628	0.673	0.691	0.714	**0.816**
	SSIM	0.7659	0.7172	0.6932	0.7869	**0.8325**
	$Q^{AB/F}$	0.6756	0.6239	0.6544	0.6878	**0.7456**
	MI	1.2539	1.0177	1.2248	1.4724	**1.9746**
	FSIM	0.9381	0.9487	0.9526	0.9689	**0.9899**
	PT	2.996	3.273 sec	3.695	2.889	**2.294 sec**
Dataset 4	AG	0.0683	0.0715	0.0758	0.0821	**0.0979**
	STD	0.728	0.742	0.789	0.799	**0.864**
	C_{local}	0.656	0.687	0.736	0.798	**0.8471**
	SSIM	0.956	0.939	0.985	0.999	**1.039**
	$Q^{AB/F}$	0.5391	0.5692	0.5710	0.5399	**0.5970**
	MI	1.043	1.187	1.368	1.882	**1.5657**
	FSIM	0.8881	0.9187	0.9376	0.9689	**0.9917**
	PT	3.896	2.373 sec	3.295	2.689	**2.094 sec**

The above table present the performance metrics of the evaluated results for experimental datasets. Table 1 demonstrates the experimental results of the traditional fusion algorithms and hybrid fusion algorithms on the dataset 1, 2, 3 and 4. To evaluate the performance of the proposed image fusion approach MRI, PET and SPECT image are selected as the input source images. It can be seen that because of different imaging standards, the source images with various modalities contain integral data. The performance metrics are compared with the traditional methods like Discrete Wavelet Transform (DWT), Discrete Cosine Harmonic Wavelet Transform (DCHWT), Guided Image Filtering (GIF) and Pulse Coupled Neural Network (PCNN) to the hybrid method (Guided Image Filtering-PCNN). The evaluations of performance metrics for hybrid techniques results are better than other existing traditional techniques as shown in Table 1. By means of objective criteria analysis, the proposed algorithm not only preserves edge information but also improves the spatial detail information. Therefore, the proposed method of multimodal medical image fusion is an effective method in both subjective and objective evaluation criterion. The experimental results are shown in Figure 5, 6, 7, 8 and Table 1.

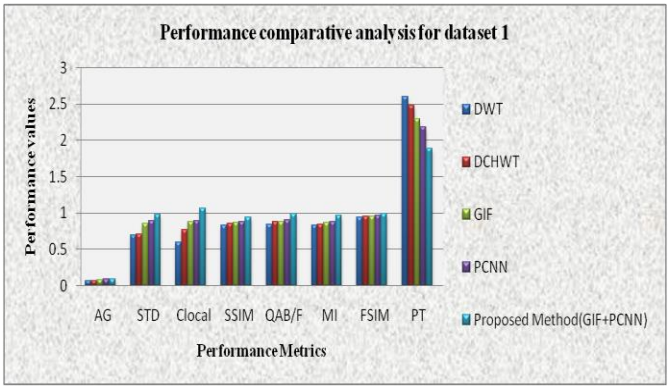

(A)

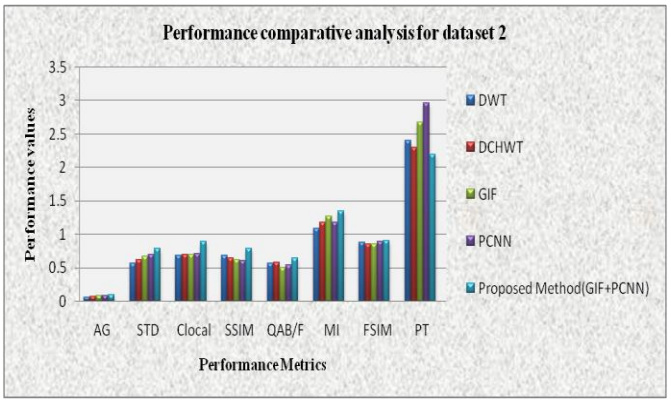

(B)

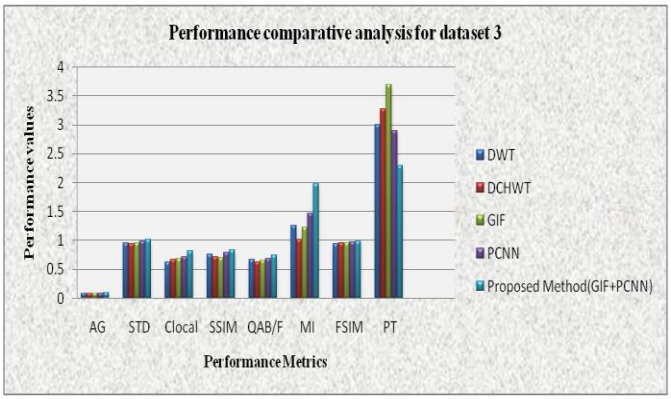

(C)

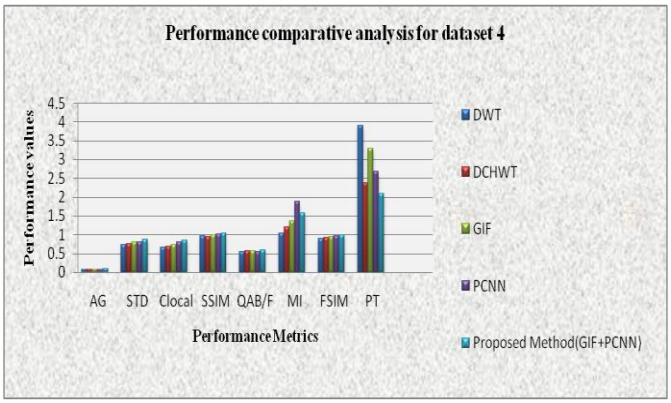

(D)

Figure 9. Performance Comparative analysis for 4 datasets (A-D)

The evaluated performance metrics output results are shown in Table 1. Note that the superior performance value in each column of Table 1 is shown in bold. The graphs for all the values of Table 1 are shown in the Fig. 9A, B,C and D. From the Table 1 and Fig. 9, it is clear the proposed technique outperform the existing techniques for all the performance metrics.

V. CONCLUSION

This work investigated the performance of both the traditional and hybrid multimodal medical image fusion techniques using several evaluation metrics. It has been shown that the best medical image fusion technique was implemented using proposed hybrid technique. This hybrid technique (guided image filtering-PCNN) introduced a superior performance compared to all the other traditional techniques. It gives much more image details, higher image quality, the shortest processing time and a better visual inspection. All these advantages make it a good choice for several applications such as for assisting medical diagnosis for an accurate treatment

VI. REFERENCES

[1] B.Rajalingam, Dr. R.Priya, "Multimodality Medical Image Fusion Based on Hybrid Fusion Techniques" International Journal of Engineering and Manufacturing Science. Vol. 7, No. 1, 2017.

[2] B.Rajalingam, Dr. R.Priya, "A Novel approach for Multimodal Medical Image Fusion using Hybrid Fusion Algorithms for Disease Analysis" International Journal of Pure and Applied Mathematics. Volume 117 No. 15 2017.

[3] B.Rajalingam, Dr. R.Priya, "Hybrid Multimodality Medical Image Fusion Technique for Feature Enhancement in Medical Diagnosis" International Journal of Engineering Science Invention (IJESI), Volume 2, Special issue, 2018, pp. 52-60

[4] Jiao Du,WeishengLi n,BinXiao,QamarNawaz "Union Laplacian pyramid with multiple features for medical image fusion" Elsevier, Neuro computing 194, 2016.

[5] xingbin Liu, Wenbo Mei, Huiqian Du "Structure tensor and nonsubsampled sheasrlet transform based algorithm for CT and MRI image fusion" Elsevier, Neurocomputing, 2017.

[6] K.N. Narasimha Murthy and J. Kusuma "Fusion of Medical Image Using STSVD" Springer,

Proceedings of the 5th International Conference on Frontiers in Intelligent Computing: Theory and Applications, Advances in Intelligent Systems and Computing, 2017.

[7] Satishkumar S. Chavana, Abhishek Mahajanb, Sanjay N. Talbarc, Subhash Desaib, Meenakshi Thakurb, Anil D'cruzb "Nonsubsampled rotated complex wavelet transform (NSRCxWT) for medical image fusion related to clinical aspects in neurocysticercosis" Elsevier, Computers in Biology and Medicine, 2017.

[8] S. Chavan, A. Pawar and S. Talbar "Multimodality Medical Image Fusion using Rotated Wavelet Transform" Advances in Intelligent Systems Research. Vol. 137, 2017

[9] Heba M. El-Hoseny, El-Sayed M. El.Rabaie, Wael Abd Elrahman, and Fathi E Abd El-Samie "Medical Image Fusion Techniques Based on Combined Discrete Transform Domains" 34th National Radio Science Conference, IEEE , 2017

[10] Udhaya Suriya TS , Rangarajan P, "Brain tumour detection using discrete wavelet transform based medical image fusion" Biomedical Research, 2017

[11] Periyavattam Shanmugam Gomathi, Bhuvanesh Kalaavathi "Multimodal Medical Image Fusion in Non-Subsampled Contourlet Transform Domain" Scientific Research Publishing, Circuits and System, 2016

[12] C.Karthikeyan and B. Ramadoss "Comparative Analysis of Similarity Measure Performance for Multimodality Image Fusion using DTCWT and SOFM with Various Medical Image Fusion Techniques" Indian Journal of Science and Technology, Vol 9, June 2016.

[13] Xinzheng Xua, Dong Shana, Guanying Wanga, Xiangying "Multimodal medical image fusion using PCNN optimized by the QPSO algorithm" Elsevier, Applied Soft Computing , 2016.

[14] Jyoti Agarwal and Sarabjeet Singh Bedi "Implementation of hybrid image fusion technique for feature enhancement in medical diagnosis",springer, Human-centric Computing and Information Sciences, 2015.

[15] Jing-jing Zonga, Tian-shuang Qiua, "Medical image fusion based on sparse representation of classified image patches" Elsevier, Biomedical Signal Processing and Control, 2017.

[16] Richa Gautam and Shilpa Datar "Application of image fusion techniques on medical images" International Journal of Current Engineering and Technology, 2017.

[17] Xiaojun Xu, Youren Wang, Shuai Chen "Medical image fusion using discrete fractional wavelet transform" Elsevier, Biomedical Signal Processing and Control 27, 103–111-2016

[18] Zhaobin Wang, Shuai Wang,Ying Zhu, Yide Ma "Review of image fusion based on pulse-coupled neural network" Springer, Arch Computer Methods Eng, 2015.

[19] Shutao Li, Xudong Kang S And Jianwen Hu "Image fusion with guided filtering" Transactions on Image Processing, Vol. 22, No. 7, July 2013.

[20] B. K. Shreyamsha Kumar "Multifocus and multispectral image fusion based on pixel significance using discrete cosine harmonic wavelet transform" Springer-Verlag London Limited, 2012.

[21] https://radiopaedia.org.

[22] http://www.med.harvard.edu

Themed Section : Engineering and Technology
© 2018 IJSRSET | Volume 5 | Issue 3 | Print ISSN: 2395-1990 | Online ISSN: 2394-4099

Design of Double Sided Cantilever Automation for Agriculture Field

N. Kalaiyazhagan[1], T.Shanmuganantham[2], D. Sindhanaiselvi[3]
[12] Department of Electronics Engineering, Pondicherry University, Puducherry, India
[3]Departmentof Electronics & Instrumentation Engineering, Pondicherry Engineering College, Puducherry, India
kalaiyazhaganece@gmail.com[1],shanmugananthamster@gmail.com[2]

ABSTRACT

In order to change our agriculture to be simplified that reduces manpower in the agriculture field by means of digital technology is the basic idea of this paper. For this automation, the first step to design a sensor which detects both humidity and temperature. And this sensor is designed to work in both wired and wireless environment. This type of sensors is mainly designed for agriculture usage but user can also apply for different domain like boiler, chemical industry, oil refineries, medical, and etc. The sensor is simulated and derived in various levels of observation. Simulation is done with the help of Intellisuite software with finite element method for a sensor.

Keywords: Finite Element Method (FEM), Humidity Sensor, Temperature Sensor, MEMS, Double Sided Cantilever.

I. INTRODUCTION

The structure of double sided cantilever that detects both high and low values of temperature and humidity. To sense humidity level surface tensile technique is used and to sense temperature bimorph technique can be implemented [1].Array of MEMS sensors is equal to one normal conventional sensor efficient wise. To relax cantilever film stresses initially it uses thermal annealing process which changes the overall bimorph sensitivity. When compared with gold, Al/Ti metals show superior sensitivity [2]. This work is to analysethe deformation of bimorph material by means of varying temperature. If deformation occurs then the dimension varies, also it tends to thermal strain in the cantilever. This process of thermal induced deformation makes microstructure cantilever into thermal actuator [3]. If cantilever thickness is less that tends deflection to be more with very less input pressure (smaller than kilo-Pascal level) [4]. Every pressure sensor won't act as a differential sensor but differential sensor can act as pressure sensor [5].

Double sided cantilever structure gives two ideal measurement for both humidity and temperature with different material properties. To sense humidity, Platinum and Poly-silicon and to sense temperature gold and copper are used as sensing layer.

II. THEORITICAL ANALYSIS

A. Relative Humidity

The ratio of water vapour pressure to saturated water vapour pressure at gas temperature
Where,

$$RH = \frac{Pw}{Pws} \times 100\% \quad (1)$$

To have sufficient accuracy between 0 to 373 degrees Celsius of water vapour saturation pressure.

$$V = 1 - \frac{T}{Tc} \quad (2)$$

$$In\left(\frac{Pws}{Pc}\right) = \frac{Tc}{T}(c_1 v + c_2 v^{1.5} c_3 v^3 c_4 v^{3.5} c_5 v^4 c_6 v^{7.5}) \quad (3)$$

Temperature in K (T), saturation pressure hectopascal (HPa), the critical temperature as 647.096 (Tc), constant critical pressure of water vapors Pc=220 to 640 HPa and co-efficient (Ci).

From equation (1),

$$Pw = Pws \times \frac{RH}{100} \quad (4)$$

For example, take 50%RH

$$Pw = 4.24\ KPa \times \frac{50}{100} \quad (5)$$

Finally,
Pw=2.12KPa

Then the dew point temperature detection occurs that can be compared with regular time intervals,

$$Td = \frac{Tn}{\log 10\frac{Pw}{A} - 1} \quad (6)$$

$Td = 14℃$

TABLE I

Dew Point Calculation		
Relative Humidity	**Dew Point (Rh)**	**(Pw) with Pws=30 (Degree Celcius)**
RH%	℃	As ambient temperature
10	32	0.424
20	24	0.848
30	20	1.272
40	16	1.696
50	14	2.12
60	12	2.544
70	10	2.968
80	08	3.392
90	06	3.816
100	05	4.24

$$A = C.\frac{Pw}{T} \quad (7)$$

$$A = 2.16679 \times \frac{0.424}{(273+30)} \quad (8)$$

$$A = 32g/m^3$$

$$Pws = A.10^{\left(\frac{m.T}{T+Tn}\right)} \quad (9)$$

The saturation pressure level of water vapour over water A, m, Tn is constant.

Generally displacement co-efficient Δz is to calculate the maximum deflection of the cantilever beam.

$$\Delta z = \frac{3(1-v)\,\delta s\,(\frac{l}{2})}{E} \quad (10)$$

Where δs implies applied input pressure towards the cantilever beam with E and V as the material properties of cantilever beam using young's modulus and Poisson ratio's. Then the aspect ratio of cantilevers bending moment is,

$$(M) = WL \quad (11)$$

Where the deflection of the cantilever at load will be,

$$(L) = \frac{1}{3}\frac{W(L+r_n)^3}{E} + \frac{W(L+r_n)}{\frac{5}{6}AG} \quad (12)$$

Where W= leaver arm distance and length (L)

The force acting on opposite direction with applied input pressure at the cantilever beam will produce

maximum deflection. The aspect ratio of the beam decides the dimension and maximum deflection of cantilever beam.

$$R_A = P + WL - R_B \quad (13)$$

$$R_A = P + WL - \left(\frac{(P_1+WL)}{2} + \frac{M}{L}\right) \quad (14)$$

$$R_A = \frac{(P_1+WL)}{2} - \frac{M_1}{L} \quad (15)$$

With different input value, reaction force changes when the aspect ratio and deflection of the cantilever is changed.

B. Thermal Expansion

By two different material with dissimilar coefficients of thermal expansion where connected together to vary temperature that causes change in structure of cantilever to deform in desired way.

Radius of a curvature with deformed structure expressed as,

$$\frac{1}{r} = \frac{6w_1w_2E_1E_2t_1t_2(t_1t_2)(a_1-a_2)\Delta T}{(W_1E_1t_1^2)^2+(W_2E_2t_2^2)^2+2W_1W_2E_1E_2t_1t_2(2t_1^2+3t_1t_2+2t_2^2)} \quad (16)$$

$$\delta = r - r\cos\theta \cong \frac{1}{2}r\theta^2 \quad (17)$$

$$\theta = \frac{arc\ length\ (L)}{radius\ (r)} \quad (18)$$

The angle of 'θ' is calculated for micro-cantilever at maximum deflection from the point of right angle triangle, considering as arc-angleθ.

$$d = r - r\cos\theta \quad (19)$$

If overall bending angle is small then the magnitude of vertical displacement can be estimated by replacing$\cos\theta$with above equation.

$$d = r - r(1 - \frac{1}{2}\theta^2 + O(\theta^4)) \quad (20)$$

$$d = \frac{1}{2}r\theta^2 \quad (21)$$

Vertically free cantilever displacement is derived from the above equation (17).

C. Thermal resistance

The electrical resistivity can be calculated with significant change in the temperature sensitivity.

$$R_T = R_o(1 + a_R(T - T_o)) \quad (22)$$

R_TWill be electrical resistance with temperature T and $R_o$same as$R_T$but$R_o$is based on$T_o$temperature co-efficient of resistance (TCR)a_R.

$$\sigma_x = E\varepsilon_x \quad (23)$$

$$\sigma_x = -EKY \quad (24)$$

Where,

$$K = \frac{1}{\rho} = 8.33 \times 10^{-3}m^{-1} \quad (25)$$

$$\delta = \rho(1 - \cos\theta) \quad (26)$$

$$\rho = \frac{\delta}{(1-\cos\theta)} \quad (27)$$

Due to bending σ_x leads to compression or tension and subjected by longitudinal line of the cantilever beam, if material is linear elastic.

III. DESIGN PROCEDURE WITH ASSIGNING BOUNDARY CONDITION

The cantilever beam is designed by the 3D builder and by using theoretical dimensional values. With respect to the application, cantilever dimensions and shape is designed. Materials are selected with respect to properties like elasticity, young's modulus, Poisson ratio and density. Each layer have different material characteristic because layer1 is substrate, layer2 is dielectric and top layer will be sensing layer. To

increase sensitivity two (or) more materials combined together.

And next step is finite element method (FEM) of thermo-electro mechanical system. For application purpose the parameter changes for sensing temperature and humidity. The displacement, stress misses, stress in Z-axis and reaction force are common. The ultimate aim of finite element method is to subdivide a larger components into smaller and simple parts.

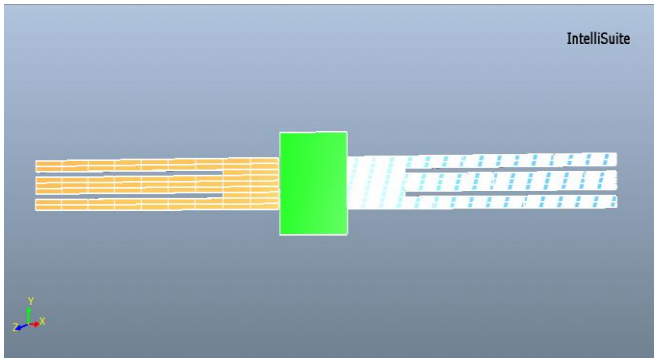

Figure 1. Double Sided Cantilever

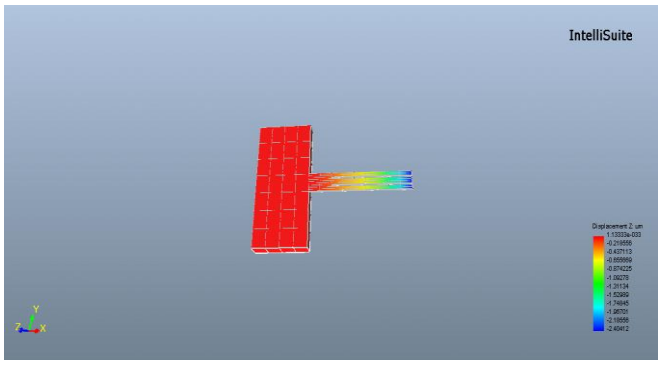

Figure 2. Simulated Result of Pressure Sensor with 10 Kpa Input

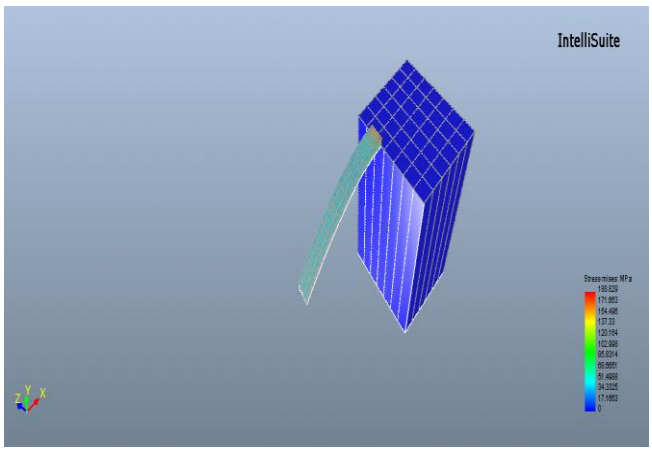

Figure 3. Simulated Result of Temperature Sensor with 10 Degree Celsius Input

IV. RESULTS AND DISCUSSION

When compared with analytical and simulation results are close to each other. By changing the main input temperature and humidity on top of the sensing layer of the sensor we can get different values. With mechanical mesh in micro-meter is given before to the input feeding to partition the sensor into micro-meter range. The applied input values are directly proportional to the deflection coefficient of the cantilever beam.

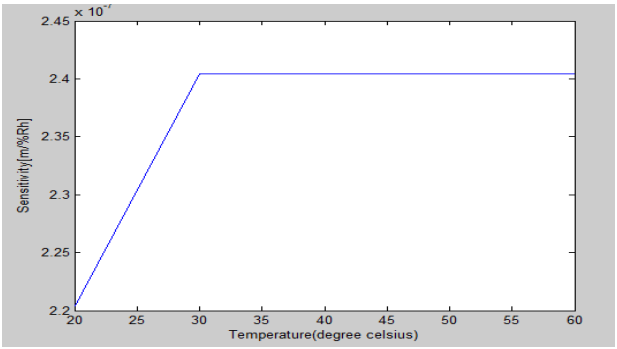

Figure 4. Temperature vs Sensitivity

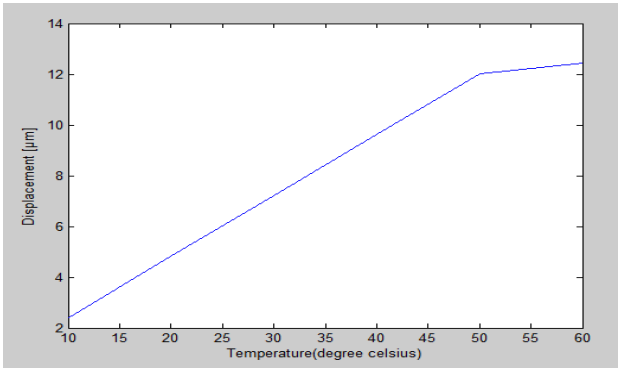

Figure 5. Temperature vs displacement

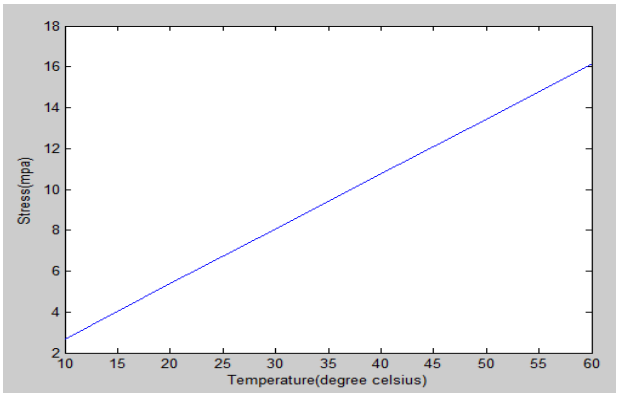

Figure 6. Temperature vs stress

From figure (4) there is a gradual increase of sensitivity and temperature but after reaching 2.4, the sensitivity level and displacement will be maintained constant because of material property. When temperature increases, stress on the layer also increases because both are depend with each other. Here for temperature both the stress and displacement will be proportional. Also sensitivity is derived from displacement of the sensor. Layers aspect ratio will vary whenever the thickness of the cantilever is changed.

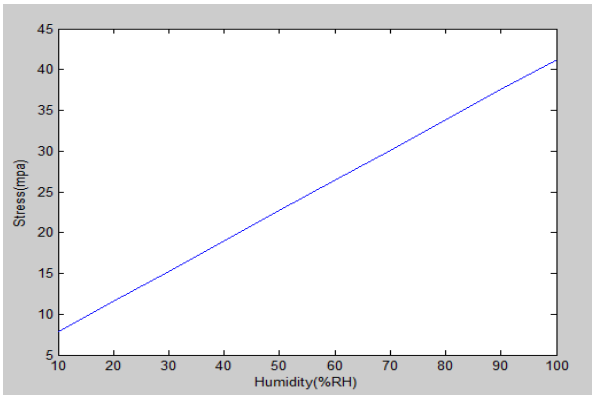

Figure 7. Humidity vs Stress

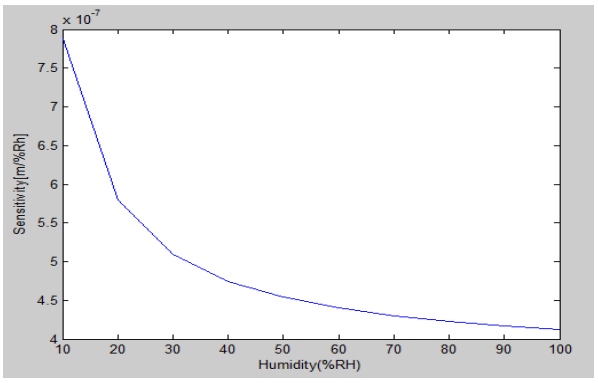

Figure 8. Humidity vs Sensitivity

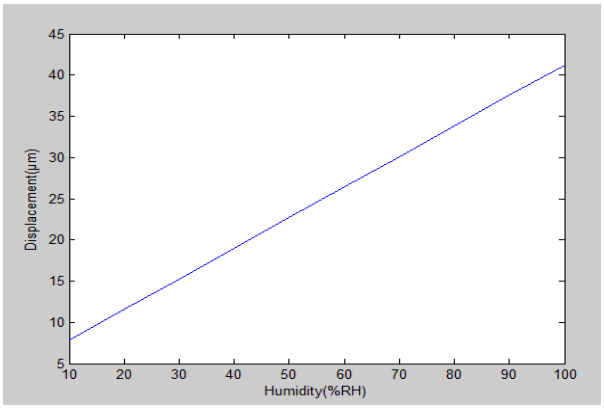

Figure 9. Humidity vs Displacement

A. For Humidity Sensing

TABLE III

Layers	Dimensions And Thickness Of Layers		
	Layer Name	Dimension	Thickness (um)
0	Substrate (Silicon)	20x40	25
1	Dielectric (Sio2)	150x20	0.4 0.2 0.3
2	Sensing (Platinum)	150x20	0.4 0.2 0.25
3	Sensing (Poly-silicon)	150x20	0.2 0.15 0.1

Where silicon has young's modulus value of 170 (Gpa), Poisson ratio of 0.26 and density of 2.32 (gm/cc) as material properties. Every layer has their individual material property (young's modulus, Poisson ratio, density) to give produce its own characteristics. The substrate of sensor is to give physical strength.

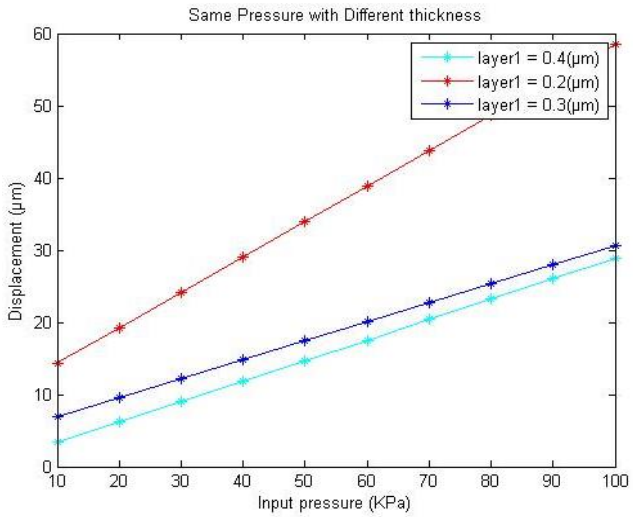

Figure 10. By Changing Various Thicknesses for Layer 1

The dielectric layer has material property as young's modulus of 61 (GPA), Poisson ratio 0.24 and density 2.1 (gm/cc). With same input thickness of the layer 2 and layer 3 is constant, layer 1 varies with minimum, maximum and moderate deflection. Layer 2 is to be sensing layer that has more sensing properties compare with other layers because this layer will be directly contacted with atmosphere. Two sensing layers are used because to increase the sensitivity and deflection one has more deflection property and other give more elasticity.

With same input thickness of the layer 1 and layer 3 is constant, layer 2 varies with minimum, maximum and moderate deflection.

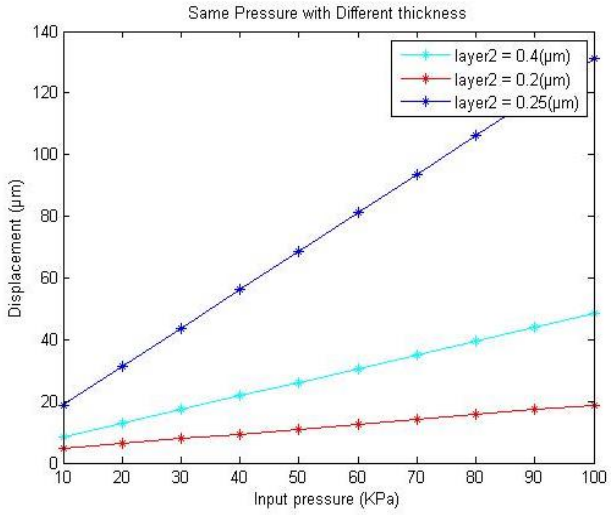

Figure 11. By Changing Various Thicknesses for Layer 2

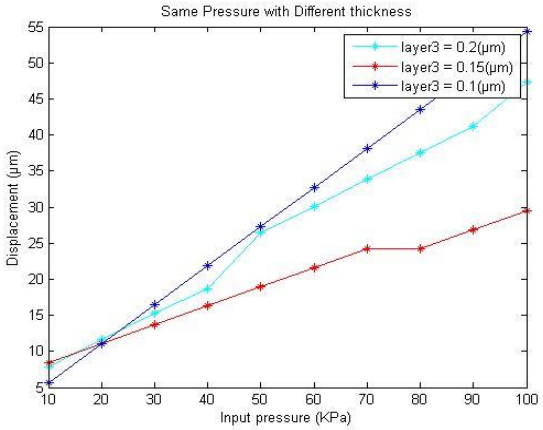

Figure 12. By Changing Various Thicknesses for Layer 3

Platinum has high Poisson ratio and density gives more elasticity. Poly-silicon gives more deflection because young's modulus is 160 (Gpa).

With same input thickness of the layer 1 and layer 2 is constant, layer 3 varies with minimum, maximum and moderate deflection. The sensing layer 2 and 3 has highest material property for humidity sensing. For each layer only the thickness is varied to detect moderate deflection because minimum has more deflection which leads to breakage of cantilever. If thickness is maximum then it leads to less deflection and would not sense lowest pressure in atmosphere.

B. For Temperature Sensing

TABLE IIIII

Layers	Dimensions And Thickness Of Layers		
	Layer name	Dimension	Thickness (μm)
0	Substrate (Silicon)	20x40	25
1	Dielectric (Platinum)	150x20	0.1 0.15 0.2
2	Sensing (Au)	150x20	0.15 0.1 0.05

3	Sensing (Cu)	150x20	0.2 0.15 0.1

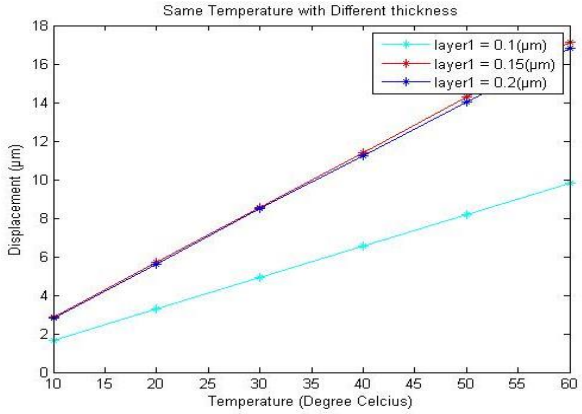

Figure 13. By changing various thicknesses for layer 1

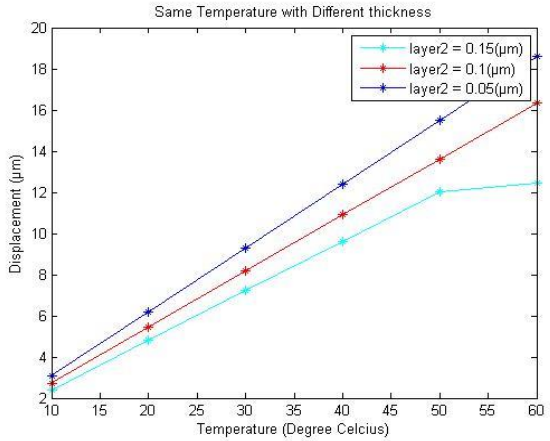

Figure 14. By Changing Various Thicknesses for Layer 2

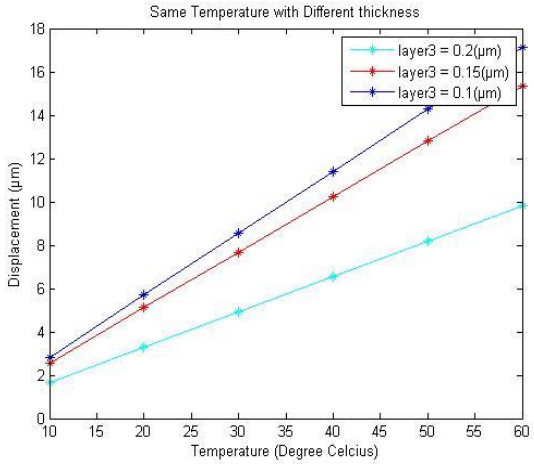

Figure 15. By Changing Various Thicknesses for Layer 3

V. CONCLUSION

This sensor is designed mainly for automation in agriculture and also to implement MEMS concept. The basic need for automation is to connect natural environment with digital environment as conversion of mechanical into digital or other. For this process we need sensors, basically for agriculture farmer to sense temperature, humidity, moisture, fertilizers and pesticides. If farmer knows temperature and humidity they can take safety precautions of their land in case of irregular environmental climate change cause negative impact on land and leads nutrition leach. To avoid this, designing a sensor is necessary which detects both temperature and humidity simultaneously.

VI. REFERENCES

[1] N. Kalaiyazhagan, T. Shanmuganantham, "Design and Analysis of MEMS Sensor for Agriculture Applications", International Conference on Circuits and System (ICCS)-2017, December 2017.

[2] N. Namioka, Y. Takei, N. Minh-Dung, T. Usami, N. Thanh-Vinh, H. Takahashi, T. Takahata, K. Matsumoto and I. Shimoyama, "Measurement of Vacuum Pressure With Cantilever-based Differential Pressure Sensor Utilizing Vapor Pressure and Narrow Gap of Cantilever," MEMS, 2016 IEEE 29th International conference at Shanghai, China.

[3] Teng-Chuan Cheng and Tsung-Heng Tsai, "Differential π-shaped CMUTs with Improved Linearity and Sensitivity," 2016 International Conference on Consumer Electronics, IEEE 2016.

[4] N. Kalaiyazhagan, T. Shanmuganantham, "MEMS Sensor Based Cantilever for Intracranial Pressure Measurement", SPRINGER, International Conference on Microelectronics, electromagnetics and Telecommunication, (ICMEET) 2018.

[5] Hidetoshi Takahashi, Nguyen Minh Dung, Kiyoshi Matsumoto and Isao Shimoyama, "Differential Pressure sensor using piezo-resistive cantilever,"

Journal of Micromechanics and Microengineering 2012.

[6] M. Shanmugavalli, G. Uma, M. Umapathy, "Uncertainty Analysis Of Micro Differential Pressure Sensor Using Interval Analysis," International Journal On Smart Sensing And Intelligent Systems, Vol. 2, No. 3, September 2009.

Themed Section : Engineering and Technology
© 2018 IJSRSET | Volume 5 | Issue 3 | Print ISSN: 2395-1990 | Online ISSN : 2394-4099

Quality of Service Aware Routing Protocol in Mobile Ad-Hoc Network

S. Kanchanamalai[1], Dr K Devarajan[2]
[1]PG Scholar, Annamalai University, Chidambaram, Tamil Nadu, India
[2]Assistant Professor, Annamalai University, Chidambaram, Tamil Nadu, India

ABSTRACT

A Mobile Ad-hoc NETwork (MANET) is a collection of wireless mobile nodes forming an infrastructure less network that has no centralized manager. Recently the work on quality of service guaranties in ad-hoc networks have attracted more attention. Routing is challenging task in MANETs due to the dynamic behavior. Multipath routing allows load balancing to use of multiple paths for routing between a source-destination pair. Load balancing is a general technique that is applied to achieve Quality of Service (QoS) in MANETs. Multipath routing can increase end-to-end throughput and provide quality of service in networks. It exploits the resource redundancy and diversity in the underlying network to provide benefits such as fault tolerance, load balancing, increase throughput, and improvement in QoS metrics such as delay and packet loss. In this work, a modified Dynamic Source Routing (DSR) and Ad-hoc On-demand Distance Vector (AODV) protocol is purposed which extend the existing DSR and AODV protocol. The proposed work is implemented in Network Similator-2 (NS2), evaluates its performance, and compared with existing protocol.

Keywords: MANET's, QoS Quality of Service, DSR Dynamic Source Routing, AODV Ad-Hoc On-Demand Distance Vector Routing

I. INTRODUCTION

MANET is a self-organized, infrastructure less, decentralized and self configuring multi-hop wireless network. The dynamic nature of MANETs makes network open to attacks and un-reliability. Routing is always the most significant part for any networks. Each node should not only work for itself, but should also be cooperative with other nodes. Due to in built characteristics of MANETs, such as periodic change in topology, nodes mobility makes QoS routing is the hardest task. QoS (Quality of Service) refers to a broad mobilization of networking technologies and techniques. The goal of QoS is to accommodate guarantees on the capability of a network to deliver predictable results.. QoS routing is the task of routing data packets from source to destination. All mobile nodes perform functioning of routers that search and maintain routes to other nodes in the network. Routing is the method of moving the information from a source to a destination in an intermediate network. Mainly two type of routing protocols are used. Pro-active protocols like DSR and AODV are used to maintain updated information of the network, by continuously evaluate the known routes and attempt to discover new ones. Reactive protocols initiate a route only when a node wants to start communication with another node. Route request and Route reply messages are used to initialize and finalize the route found between source to destination. After finding the route, a suitable shortest path is discovered by the source node for the transmission of data packets. Route discovered by reactive algorithms having problems like congestion problems as the

centre of network carry more traffic. This causes poor performance in reactive protocol like DSR and AODV. To remove all these flaws and drawback, multi-hop forwarding routing algorithm have been proposed. Multi-hop forwarding Routing algorithm is the act of moving information from a source to a destination in an intermediate using multiple paths.

II. RELATED WORK

Sanjeev Kumar et.al., [1] have proposed a new protocol Modified Dynamic Source Routing (MDSR) to provide data transmission with higher end-to-end reliablity in wireless ad hoc networks, the objective to provide a reliable route for packet transmission with a minimum network overhead.

Mamoun Hussein Mamoun et.al., [2] fined problems in QoS routing in MANET and introduce new routing algorithm (NRRA).

A.Valarmathi et.al., [3] defines modification to original DSR protocol. DSR was modifying to monitor the occurrence of congestion by using multiple resource utilization thresholds as Quality of Service.

Ramesh et al., [4] have proposed proposes a congestion aware multi-path Dynamic Source Routing Protocol. The resultant protocol will generate set of highly disjoint paths and calculate the correlation factor between the paths to decrease the end to end delay.

Dhirendra Kumar Sharma et al.,[5] enhances the performance of SMR protocols by using route update mechanism. The MANET, routing protocols are used to provide the specific path for sending the data packets. Multipath routing provides the multiple paths in the MANET. So, in this paper we enhance the performance of Split Multipath Routing protocols by using route update mechanism. This proposal is useful in route recovery process.

Venkata Subramanian et al., [6] have suggested a Mobile ad- hoc networks, the unstable transport layer and inhibited amount of traffic being carried out by the network is owing to the high packet loss rates and frequent topological changes. Develops a Qos-based Robust Multipath Routing (QRMR) protocol for mobile ad hoc networks. Multipath allot weights to individual links depending on the metrics link quality, channel quality and end-to-end delay.

Mujing Jin ZhaoweiQu et al., [7] exploits that in Ad Hoc network, the multi-hop networks as the characteristics of the dynamic changing of the interconnection topology make the routing very important. They defines an optimized scheme of SMR. Which allows the SMR having better performance in low-speed environment especially can decrease the end-to-end delay and also expands the range.

Zafare et al., [8] have suggested that Multipath routing in mobile ad-hoc networks allows the establishment of multiple paths for routing between a source-destination pair. Itprovides benefit of fault tolerance, load balancing, bandwidth aggregation and the improvement in quality-of-service.

David B et al., [9] have suggested that the Dynamic Source Routing protocol (DSR) is a simple and efficient routing protocol designed specifically for use in multi-hop wireless ad hoc networks of mobile nodes.describes stable tradeoffs between delay and routing load. Scheme uses two routes for each session; the shortest delay route and the one that is maximally disjoint with the shortest delay route.

Johnson, et.al [10] describes Dynamic Source Routing protocol (DSR) is a simple and efficient routing protocol. The protocol is composed of the two mechanisms of Route Discovery and Route Maintenance, which work together to allow nodes to discover and maintain source routes to arbitrary destinations in the ad hoc network.

Linifang Zhanget al., [11] have suggested a load-balancing scheme define load-balancing scheme for performance improvement of the multipath routing protocol. End to end delay improve and network resource utilized efficiently. In order to analyze the effect on the distribution of input traffic.

III. A NEW TECHNIQUE: MODIFIED AODV

A. Multi-Hop Packet Forwarding Process

The proposed algorithm is based on MAODV and MDSR. AODV and DSR enables "active, dynamic, multipath routing between mobile nodes wishing toestablish and maintain an ad hoc network". AODV and DSR allows for the construction of routes to specific destinations and does not require that nodes keep these routes when they are not in active communication. AODV or DSR avoids the "counting to infinite" problem by using destination sequence numbers. This makes AODV and DSR loop-free.

AODV defines 3 message types:

- Route Requests (RREQs) intilialize the route finding process
- Route Replies (RREPs) finalize the routes based on request
- Route Errors (RERRs) RERR alert the network of a link failure in an active route.

In this Algorithm, the Route is selected based on the trust Index of all nodes.

Let
Z = {N1, N2,….Nn} be the network of nodes.
Tibe the trust index of node Ni,
Tinc be the value of trust increment, Trust Based Multi-Hop Forwarding Scheme for Data
Security in Mobile Ad Hoc Networks
Te be the value of Trust node energy,
Tc be the trust node cost.
Nk be the node which forwards a data packet Pk.
p be positive constant for trust increment and decrement.

Algorithm 1

Initially, each node maintains a lookup table, which includes sequence numbers, source and destination IP addresses and port numbers, and the address of the next hop.

Node Ni receives the data packet Pk.
If Pk is a retransmitted packet, then Node i decrements trust index of Nk by
Te = Te – 2*p
Compare Ti-1 with Tc.
If T0 < Ti-1 < Tc,
Packet is dropped.
Else
Packet is forwarded to node Ni+1.
Ni updates the lookup table with current trust values.
End if
Else
If Pk is an acknowledgement packet, then
If Nk originally forwarded Pk, then
Ni
increments trust index of Nk by
Tinc= Tinc + p
End if
End if

B. Load Balancing Technique

Load balancing is a networking method to shell out assignment across multiple network links, central processing unit, disk drives. Load balancing is partioning the amount of work that a network has to do between two or more networks so that more work is done in the same amount of time and, in general, all users are furnished quicker. Load balancing can be implemented with hardware, software, or a combination of both. Typically, load balancing is the main reason for computer server aggregate.

IV. RESULT AND DISCUSSION

In order to demonstrate the effectiveness of Ad hoc On Demand Distance Vector (AODV), Modified

AODV. The performance of protocol proposed is compared with the performance of Dynamic Source Routing (DSR), Modified DSR. The proposed protocol is implemented using the Network Simulator (NS-2). In this simulation to compare the four on–demand ad-hoc routing protocol to implement the best performance. However, the traditional routing protocols, such as AODV, MAODV, DSR and MDSR, may find their limitations in industrial installations due to the harsh environmental conditions, interference issues, and other constraints. In MANETs, transmission breakage will result in lost or procrastinating of process or restrict data, and lost the process or restrict deadline is normally impossible for industrial applications, as it may cause discord in industrial automation or possibly end the automation, ultimately results in economic failure. The sensed data should be continuously and accurately transmitted to the sink node, and the programming or re tasking data for sensor node operation, command, and query should be reliably delivered to the target nodes. It is also required that these networks can operate for years without replacing the device batteries.

Since the varying wireless channel conditions and sensor node failures may cause network topology and connectivity changes over time, to forward a packet reliably at each hop, it may need multiple retransmissions. These result in undesirable delay as well as additional energy consumption. Opportunistic routing (OR) has been proposed as an effective cross-layering technique to combat fading channels, thus improving the robustness and energy efficiency in wireless networks. The aim of opportunistic routing is to catch the advantage of the broadcast nature of wireless communication, associate the multiple neighbors of the sender into local forwarding. Since the wireless medium is shared, each node can overhead the data packets sent by its neighbors. In the network layer, a set of forwarding candidates are list in the data packet and these nodes will follow the assigned priorities to relay the packet. Essentially, only one node is chosen as the actual forwarder at the MAC layer in an a posteriori manner. Reactive routing protocols are designed to decrease the bandwidth and storage cost consumed in table driven protocols. These protocols apply the on-demand procedures to dynamically build the route between a source to destination. Routes are generally desinged and maintained by two different phases, namely: route discovery and route maintenance. Route discovery usually maintain on-demand by flooding an RREQ (Route Request) through the network, i.e., when a node has data to send, it broadcasts an RREQ. When a route is initiate, the destination returns an RREP (Route Reply), which contains the route information (either the hop-by-hop information or complete addresses from the source to the destination) traversed by the RREQ.

V. PERFORMANCE METRICS

Performance in throughput: It is defined as the total number of packets delivered over the total simulation time. The throughput comparison shows that the three algorithms performance margins are very close under traffic load of 50 and 100 nodes in MANET scenario and have large margins when number of nodes increases to 200. It is defined as Mathematically: Throughput= N/1000 Where N is the number of bits derived successfully by all destinations.

Performance in packet delivery ratio: Packet delivery ratio is defined as the ratio of data packets received by the destinations to those generated by the sources. Mathematically, it is defined as: PDR= S1÷ S2 Where, S1 is the sum of data packets received by the each destination and S2 is the sum of data packets generated by the each source.

Performance in packet loss: When one (or) more packet of data travelling across a network fail to reach their destination. It is measured as percentage of packet loss with respect to packet sent.

Performance in energy consumption: Energy consumption of a node at time t is defined as the summation of the number of packets transmitted by

the node at time t (Nt) with the number of packets received by the node at time t (Nr).

Performance in routing overhead: The routing load is defined as the total number of routing control packets normalized by the total number of received data packets.

VI. SIMULATION RESULT

The simulation results are presented and analysed, focusing on metrics like Throughput, Packet Delivery Ratio, Packet loss, Energy Consumption and Routing Overhead. The results of the Ad-Hoc On demand Distance Vector (AODV), Modified Ad-Hoc On demand Distance Vector (MAODV), Dynamic Source Routing (DSR) and Modified Dynamic Source Routing (MDSR) model are compared to choose the best model.

A. Packet Delivery Ratio

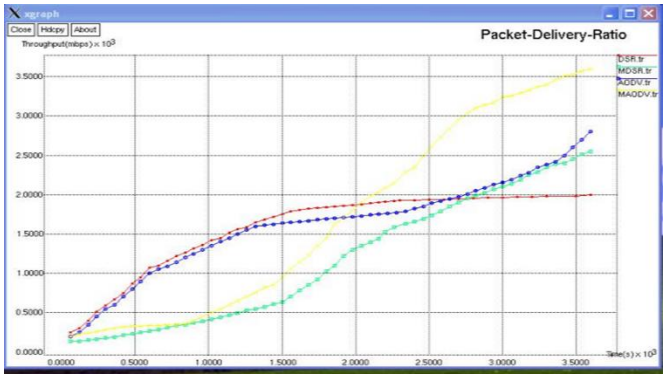

Figure 1. Packet Delivery Ratio Vs. Time

This figure 1, it can inferred that the Packet Delivery Ratio for four on demand routing protocol DSR, MDSR, AODV, and MAODV. This graph shows the Time Vs Throughput comparison of four reactive routing protocol. From this comparison AODV and MAODV routing protocol shows the better performance when compared to DSR and MDSR routing protocol.

B. Packet Loss

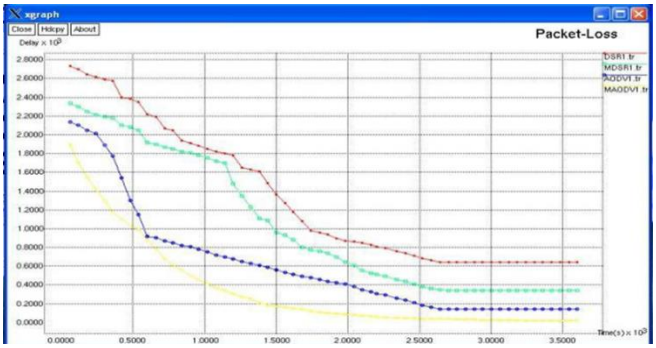

Figure 2. Packet Loss Vs Time

This figure 2, shows the Packet Delivery Ratio for four On-demand routing protocol DSR, MDSR, AODV and MAODV. This graph shows the Time Vs shows the Packet Delivery Ratio for four On-demand routing protocol DSR, MDSR, AODV and MAODV. This graph shows the Time Vs Delay comparison of four reactive routing protocol. From this comparison AODV and MAODV routing protocol shows the better performance when compared to DSR and MDSR routing protocol.

C. Routing Overhead

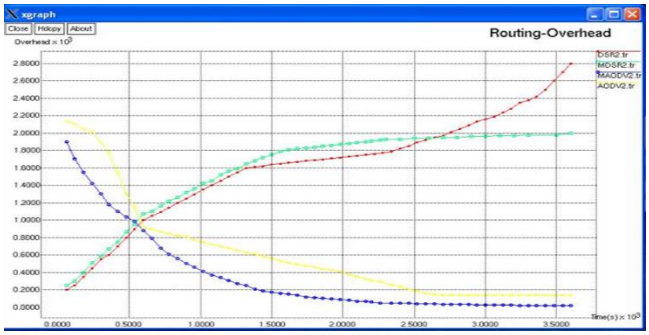

Figure 3: Routing Overhead Vs. Time

From figure 3, it can inferred that the Routing Overhead for four On-demand routing protocol DSR, MDSR, AODV and MAODV. This graph shows the Time Vs Overhead comparison of four reactive routing protocol. From this comparison AODV and MAODV routing protocol shows the better performance when compared to DSR and MDSR routing protocol.

VII. CONCLUSSION

In this work, we presented AODV, MAODV, which can augment most existing reactive routing protocols in MANETs to provide reliable and energy-efficient packet delivery against the unreliable wireless links. We introduced a biased back off scheme in the route discovery phase to find a robust virtual path with low overhead. Without utilizing the location information, data packets can still be greedily progressed toward the destination along the virtual path. Therefore, AODV, MAODV provides very close routing performance to the geographic opportunistic routing protocol. We extended AODV, MAODV to demonstrate its effectiveness and feasibility. Simulation results showed that, as compared with other protocols, AODV, MAODV can effectively improve robustness, end-to-end, energy efficiency and latency.

VIII. REFERENCES

[1] Sanjeev Kumar, Yogesh Chaba, "Quality of Service Aware – Modified DSR Protocol in Mobile Ad-Hoc Network", International Journal of Advanced Research in Computer Science and Software Engineering, Volume 4, Issue 10, October 2014, pages.876-882

[2] Mamoun Hussein Mamoun, "A New Reliable Routing Algorithm for MANET", International Journal of Research and Reviews in Computer Science, 3, June 2011, pages.638-642

[3] Valarmathi, R.M. Chandrasekaran, "Performance of improved dynamic source routing algorithm for military communication logistics", International Journal of Enterprise Network Management, November 3/2011, pages.302-310

[4] Ramesh, V. Subbaiah, P. Chaitanya, N. S. Supriya, "Performance Comparison of Congestion Aware Multi-Path Routing (with Load Balancing) and Ordinary DSR", IEEE 4th International Conference, 15-17 Dec. 2010, pages. 1 - 5

[5] Dhirendra Kumar Sharma, Sanjay Kumar Biswash, Chiranjeev Kumar "Enhancement of Split Multipath Routing Protocol in MANET", International Journal on Computer Science and Engineering, 03, 2010, pages. 679-685

[6] Venkatasubramanian, S.Gopalan, N.P., "A QoS-Based Robust Multipath Routing Protocol for Mobile Ad hoc Networks", First Asian Himalayas International Conference, 3-5 Nov. 2009, pages. 1 – 7

[7] Mujing Jin Zhaowei Qu, "Improvement for Split Multipath Routing Protocol in Ad Hoc Network", IEEE International Conferences, 16-18 Oct. 2009, pages. 299 – 302

[8] Zafar, H. Harle, D. Andonovic, I. Khawaja, "Performance evaluation of shortest multipath source routing scheme", Communications. IET, May 2009, pages. 700 - 713

[9] Rookhosh, F.; Haghighat, A.T.; Nickmanesh, S., " Disjoint Categories in Low Delay and On-Demand Multipath Dynamic Source Routing Ad hoc Networks", First International Conference on, 21-22 Oct. 2008, pages. 207-213

[10] David B. Johnson David A. Maltz Josh Broch, "DSR: The Dynamic Source Routing Protocol for Multi-Hop Wireless Ad Hoc Networks", Proceedings of INMC 2004. 8th International, 24-26 Dec. 2004, pages. 516 – 521.

[11] Linifang Zhang, Zenghua Zhao, Yantai Shu, Lei Wang, Yang, O.W.W., "Load Balancing of Multipath Source Routing in Ad Hoc Networks", Communications, 2002. ICC 2002. IEEE International Conference, 2002, pages. 3197 - 3201 vol.5

[12] R.Leung, Jilei Liu; E.Poon, A-L.C Chan, Baochun Li, "MP-DSR: A QoS-aware Multi-path Dynamic Source Routing Protocol for Wireless Ad-Hoc Networks", Proceedings LCN 2001. 26th Annual IEEE Conference, 2001, pages. 132 - 141

[13] Lee, S.-J., Gerla, M., "Split Multipath Routing with Maximally Disjoint Paths in Ad hoc Networks", ICC 2001. IEEE International Conference, 2001, pages. 3201 - 3205 vol.10

[14] Kui Wu Harms, "Performance Study of a Multipath Routing Method for Wireless Mobile

Ad Hoc Networks", Proceedings Ninth International Symposium, 2001, pages. 99 – 107

[15] A. Nasipuri, R. Castaeda, and S. R. Das, "Performance of multipath ad hoc networks", in ACM/Baltzer Mobile Networks and Applications (MONET) Journal, 2001, pages. 339–349. vol. 6

[16] Lei Wang, Yantai Shu, Miao Dong, Lianfang Zhang, Yang, O.W.W., "Adaptive Multipath Source Routing in Ad Hoc Networks", ICC 2001. IEEE International Conference on; 2001, pages. 867 - 871 vol.3

[17] Lei Wang, Lianfang Zhang, Yantai Shu, Miao Dong, "Multipath source routing in wireless ad hoc networks", Proceedings of Canadian Conference on Electrical and Computer Engineering, 2000, pages.479-483, vol. 1.

Themed Section : Engineering and Technology
© 2018 IJSRSET | Volume 5 | Issue 3 | Print ISSN: 2395-1990 | Online ISSN: 2394-4099

Train Track Monitoring cum Bridge Overload Detection System

S. Mangalapriya, V. Violetjuli, C. Rajanandhini
Department of Electronics and Communication Engineering, Periyar Maniammai Institute of Science and Technology, Thanjavur, Tamilnadu, India

ABSTRACT

Communication-based train control (CBTC) systems use wireless local area networks (WLANs) to transmit train status and control commands. Since WLANs are not originally designed for applications with high mobility, random transmission delays and packet drops are inevitable, which could result in unnecessary traction, brakes or even emergency brakes of trains, loss of line capacity, and passenger satisfaction. In this paper, we study the packet drops introduced by random transmission errors and handovers in CBTC systems, analyze the impact of random packet drops on the stability and performances of CBTC systems, and propose two novel schemes to improve the performances of CBTC systems. Unlike the existing works that only consider a single train and study the communication issues and train control issues separately, we model the system to control a group of trains as a networked control system (NCS) with packet drops in transmissions. Extensive field test and simulation results are presented. We show that our proposed schemes can provide less energy consumption, better riding comfort ability, and higher line capacity compared with the existing scheme.

Keywords: Communication-Based Train Control, Networked Control System, CBTC Systems.

I. INTRODUCTION

Consumer electronics are electronic equipment intended for everyday often in entertainment, communications and office productivity. Radio broadcasting in the early 20th century brought the first major consumer product, the broadcast receiver. Later products include computers, telephones, MP3players, audio equipment, televisions, calculators, GPS automotive electronics, digital cameras and players and recorders using video media such as DVDs, VCRs or camcorders. Increasingly these products have become based on digital technologies, and have largely merged with the computer industry in what is increasingly referred to as the consumerization of information technology.

Rail-Guided transport systems have attracted much attention since they can provide greater transport capacity, superior energy efficiency, lower carbon emission, and outstanding features of punctuality and safety when compared with other mass transit methods. In traditional rail systems, a track circuit is commonly used to coarsely determine the location of a train and to transmit unidirectional ground-train control information. The coarse train positioning and low unidirectional communication throughput lead to low line capacity of the track-based train control (TBTC) system. The typical minimum headway, which is the time interval between two neighboring trains, of TBTC is several minutes. As a modern successor to TBTC, communication-based train control (CBTC) systems use continuous high-capacity bidirectional train–ground communications to transmit status and control commands of trains and to realize automatic train control functions. The line capacity can be increased. The typical minimum Headway of CBTC is 90 s or even less. For urban transit systems, wireless local area networks (WLANs)

are commonly used due to the open standards and the available commercial-off-the-shelf equipment.

The project relates to the location of singular points in the automatic control of railway tracks. According to a possible embodiment, the railway carriage carrying the control equipment's is provided with sensor orientated to detect the crack and fire sensor used to detect the fire. This project pertains to a process for monitoring the condition of rail on train tracks and more specifically has the object of the identification of defects detected by monitoring equipment on the tracks to be checked to allow maintenance crews to subsequently find these defects. When we give the supply to the device, the DC motor gets start through relay driver circuit.

The equipment Track Detection Electronics System (TDES) are placed in the track with the interval of two distances. The TDES has one voltage generator, one comparator and one RF Module. The Voltage generator generates the dc voltage and supply through the track to the next TDES. The comparator compares the input voltage from previous TDES with the reference voltage. If the voltage does not match, i.e., the track was broken the TDES send the signal to Control System through the RF Module.

The load cell measures the load of the train, compares the values with the reference from control system, and informs to control system, if the train is overloaded. The train receives the signal from control system to stop the train, if any crack was found on the track or the bridge overloaded.

II. PROPOSED SYSTEM

Owing to the crucial repercussions of this problem, this paper presents an implementation of an efficient and cost effective solution suitable for large scale application. With the advent of powerful digital signal processors, Image Processing techniques have been explored to formulate solutions to the problem of railway crack detection. Though it provides good accuracy, this method uses techniques like image segmentation. The usage of microwave antennas in Crack detection investigated in research. Another important technique for crack detection is infrared sensing which seemed to more suitable but later it became inaccurate.

Hence this paper proposes a cheap, novel yet simple scheme with sufficient ruggedness suitable to the Indian scenario that uses an Weighting Machine to calculated the efficiency of Bro IR-Photo diode arrangement to detect the crack in railway lines, which proves to be cost effective as compared to the existing methods.
In our project we have three modules. They are TDES module, Load cell Module, Train Module and a common monitoring system i.e., control system.

A. Block Diagrams

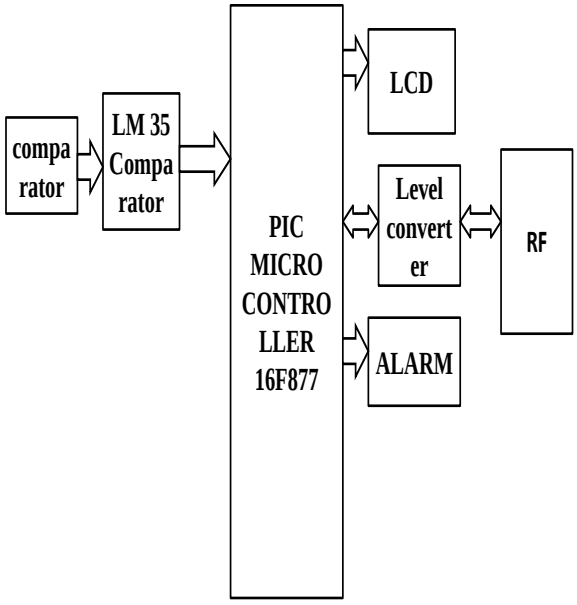

Figure 1. TDES Block Diagram

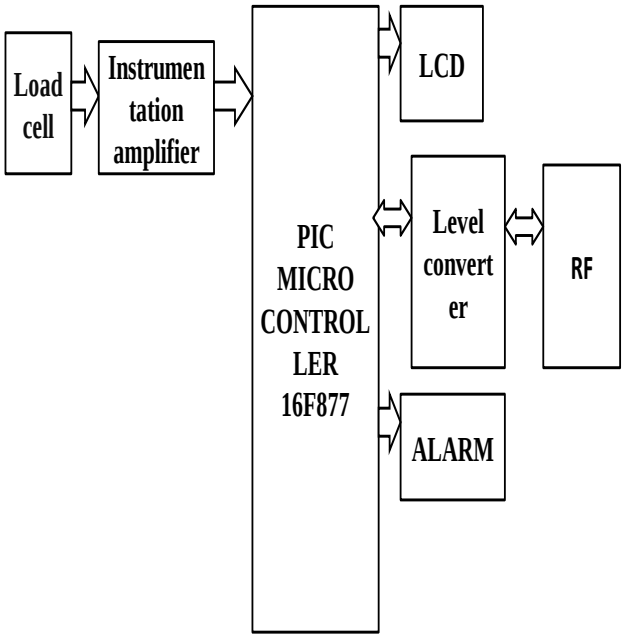

Figure 2. Bridge Section

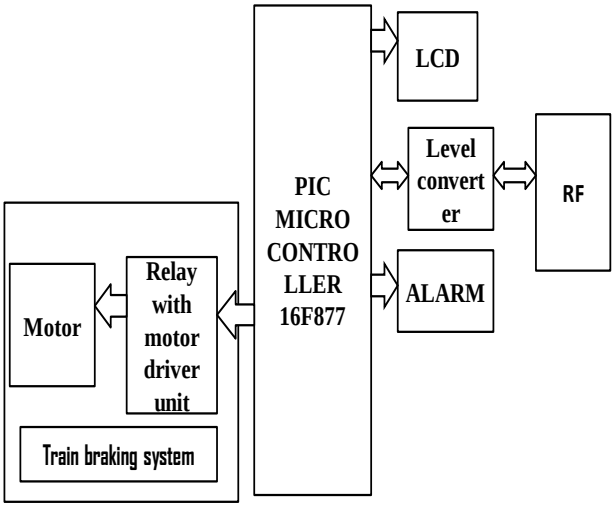

Figure 3. Train Module

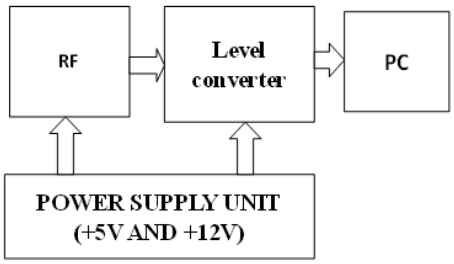

Figure 4. Monitoring Unit

Track detection electronic system has the major components like voltage generator, voltage comparator and RF module. The voltage generator generates 5V DC supply and sends it through the track to another TDES, which is placed with the distance of few kilometres. The second TDES receive the voltage from first one, and compare it with the reference value. LM35 comparator and PIC 16F877 microcontroller is used to compare the values.

The PIC microcontroller validates the output of comparator. If the crack is available in the track, the output of the comparator is "0", else the output is "1". Then the microcontroller sends the stop signal to monitoring system to stop the train, if the comparator output is "0".

We are using RF module to send the signal to monitoring system. The level converter is used to establish the serial communication between microcontroller and RF module.

In Bridge section, we are placed one load cell on the track few kilometers before bridge. This load cell calculates the total load of the train and compares this value with the reference from monitor unit. If the load of the train is more than the reference value, this module sends the stop signal to monitor unit.

In Train section, we are placed one load cell on the track few kilometres before bridge. This load cell calculates the total load of the train and compares this value with the reference from monitor unit. If the load of the train is more than the reference value, this module sends the stop signal to monitor unit.

In monitoring unit, the monitoring unit organizes the entire system and control the train. In this module one PC connected with RF module receives the data from TDES and load cell. The corresponding command (STOP Command) to send the train if any crack was found in the track or bridge overloading is occurs.

III. RESULT AND DISCUSSION

The PC based monitoring system continously monitor the bridge section,TDES and train also, If the temprature in train may rise the control PC generally

notified COOL TERM software used to monitor the entire the system with virtual terminal.

If the continuity of the track was broken the PC given analog and notification message as shown in the figure. If the load cell output is more than the reference value the system, generate the error message to stop the train.

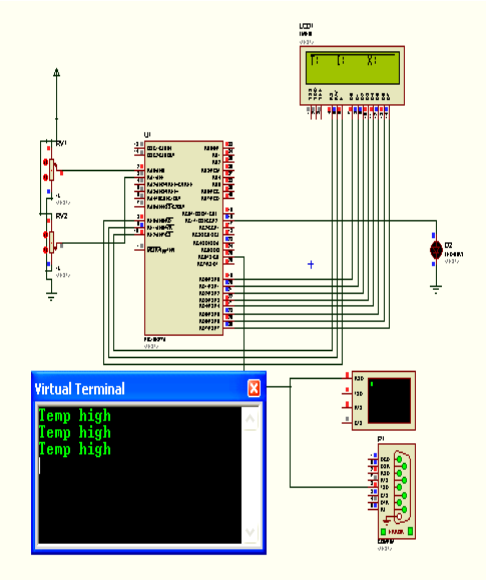

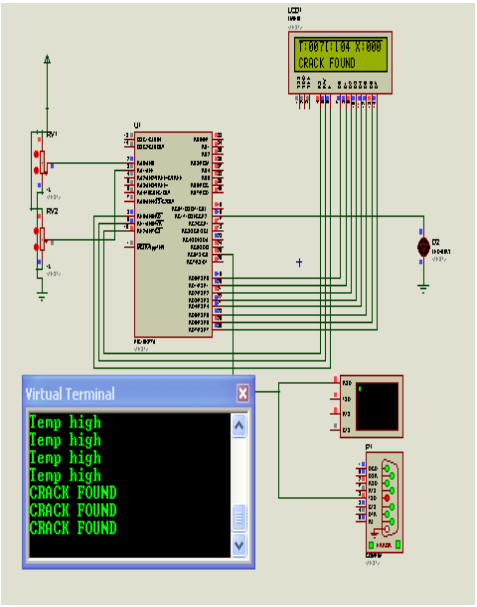

IV. CONCLUSION

The railway environment monitoring system is erupted for finding the problem on the track as well as the inside train information's by using of the sensor networks in addition using to monitoring bridge weight by using of load cell. It's used to monitoring the bridge health status such as sensor is transmitted to a master station (or) monitoring. Control from the train this is developed mainly on to prevent the precaution effect at the railway networks.

In future the reference value for Bridge Load Cell is monitors automatically by an efficient electronics system incorporated with civil measurements. The entire project will be speed up with OFC connection by the help of RailTel Corporation to improve our work.

V. REFERENCES

[1] Richard J. Greene, John R. Yates and Eann A. Patterson, "Crack detection in rail using infrared methods"

[2] High speed detection of broken rails, rail cracks and surface faults, Prof. M Dhanasekar, Wirtu,L Bayissa.

[3] The most advanced system for broken rail detection.

[4] http://www.tc.gc.ca/media/documents/railsafety/technologies.pdf

[5] http://en.wikipedia.org/wiki/GSM.

Themed Section : Engineering and Technology
© 2018 IJSRSET | Volume 5 | Issue 3 | Print ISSN: 2395-1990 | Online ISSN : 2394-4099

An Overview of Thermal Image Processing and Its Various Applications

P.Kanimozhi[1], Dr. S. Sathya[2]

[1]Assistant Professor, Aries Arts and Science College, Karunkuzhi, Tamil Nadu, India

[2]Assistant Professor, Department of Computer Science and Engineering, FEAT, Annamalai University, Chidambaram, Tamil Nadu, India

ABSTRACT

Recent development in technology is focusing on modern and simple methods for diagnosing of fatal and incurable diseases using thermal image processing. Thermal Imaging is a type of imaging that determines an image based on the absolute temperature of the subject. The image is formed based on the heat signature of objects. Thermal imaging method is non-invasive and non-destructive method used even when the equipment is running, in production and on load. The image produces fast, accurate and immediate temperature measurement and helps in fault detection. The technique uses infrared radiations and includes most of the thermal radiation emitted by objects near room temperature. Using these images deadly diseases like tuberculosis, cancer, inflammatory diseases, complex pain syndromes can be identified. Diseases diagnosed early can be treated well and cured as quickly as possible.

Keywords: Thermal Images, Invasive, Inflammatory, Syndromes

I. INTRODUCTION

The expansion of software that could identify objects of interest sensed with thermal imaging video equipment, which the previous research specified with the use of infrared video cameras .Unlike traditional methods , video recording provides a real-time archive of what was observed and could be conducted at remote locations.[1] Thermal image processing concerns with infrared radiation. Infrared (IR) light is electromagnetic radiation with a wavelength longer than that of visible light, measured from the nominal edge of visible red light at 0.7 -300 micrometres. Thermal images use the heat emitted by any object captured by the infrared cameras which produces images usually grey scale in nature. Hot objects are indicated by white colour while cold objects with black. Different temperatures are identified by various colours which is seen later in this paper.

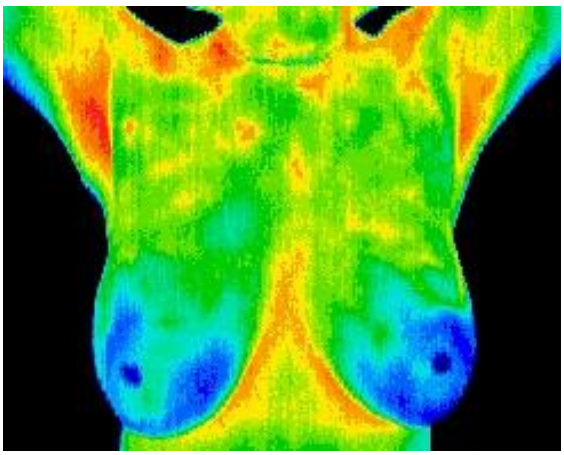

Figure 1. Ordinary Thermal Image

Good thermal symmetry with no suspicious thermal findings. These patterns represent a baseline that won't alter over time and can only be changed by pathology.

II. DEFINITION FOR THERMAL IMAGE

A thermal image (thermo gram) is a digital representation of a scene and a measure of the thermal radiation emitted by the pictured objects. Thermal images are captured via thermo graphic cameras, which are devices capable of sensing this radiation in the form of infrared light. A thermal image remotely senses the temperature of an object or at least accurately tell its temperature relative to its environment. The objects can be seen in the dark as well as perceive the temperatures of many objects remotely.

Thermal Imaging is the conversion of radiated or reflected heat into real-time pictures or images. A thermal image is an analogue visual representation of temperature differences. All objects above absolute zero (-273 degrees) emit radiation waves that are infrared. Depending on temperature and emissivity, most objects in the world can be thermally imaged. Human beings emit the heat pattern captured by the thermal IR sensors and images are created. According to their temperature and characteristics different objects emit different range of Infra-red energy. The temperature of the human body varies between 35.5°C to 37.5°C [2].

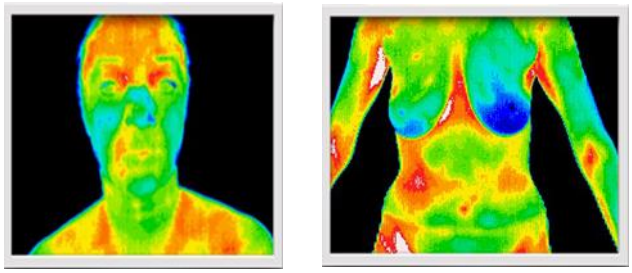

Figure 2. Different Thermal Images

The problems related with difference in temperature can be easily detected using thermal imaging. A variety of heat detection tasks uses thermal imaging for checking any leakages , any abnormal body temperatures when naked vision is not possible. Thermal infrared images have detectors and lens combination that provides a visual representation of objects.

The most common tool used for thermal imaging today is the thermal infrared camera. Thermal infrared cameras can be used to detect and display the presence of anything radiating heat above absolute zero. They supply visual representation of the infrared energy emitted by all objects.

The advantages of thermal imaging are

- Non-invasive and non-destructive so used for any applications
- Fast ,accurate, helps in fault detection
- Easy installation of cameras at convenient times
- Real time applications and low light conditions
- Passive usage of cameras independent of light

III. MECHANISM BEHIND THERMAL IMAGE

As thermal images allow to "see" in the dark, images are received clearly even in poor light conditions. The technique used is based on 'blackbody radiation 'where most objects emit electromagnetic radiation as a function of its temperature. In room temperature this radiation is at infrared wavelengths. As temperature grows light emitted is in visible spectrum releasing energy in ultraviolet wavelengths. Infrared light consists of long wavelengths in the visible spectrum is absorbed by the objects soon increasing its kinetic energy thereby creating thermal image.

Thermal cameras are used to capture the images depicting thermal scenes by detecting IR radiation from an object, is a part of the thermal radiation which is the function of the objects temperature. An array of micro bolometers act as simple sensor in the cameras to detect long IR wavelengths of objects temperature by absorbing thermal radiation and changes resistance as result. This can be electrically measured and determine the images thermally.

A few thermal properties which are used in accurate producing of images are

Absorption—understanding absorption is more important because various materials absorb and emit certain wavelengths of light at varying levels affecting thermal energy.

Transmission—materials not only transmit light wavelengths of the objects alone but also some EM radiation is transmitted into the camera which affects the image

Emission-- For a given temperature, different materials emit thermal radiation at widely varying levels. Understanding two dissimilar materials at

different temperature to sense the object emissivity is important.

Reflectivity—the radiation can be reflected based on the surface conditions of an object bounce and strike the camera sensors, similar to directly emitted radiation.

IV. APPLICATIONS OF THERMAL IMAGES

A thermal imaging camera can scan entire areas and objects all at once, never missing any overheating hazards. This enables the viewer for instant diagnostic insights showing the full extent of the problem. This property is used for various applications in certain areas like building Surveyors to detect moisture, identify energy loss & poor insulation. Electrical/Mechanical Engineers use thermal image to find electrical faults and use as fire prevention. Industrial/Civil Engineers use to identify water ingress in aeroplanes. Environmental Engineers use to detect anomalies in solar panels.

The study of temperature has widespread applications across science and medicine. [3]The human body is homoeothermic, i.e. self-generating and regulating the essential levels of temperature for survival. The association between human body temperature and disease is almost as old as medicine itself. So thermal images are used to study a number of diseases where skin temperature can reflect the presence of inflammation in underlying tissues, or where blood flow is increased or decreased due to a clinical abnormality. In principle, thermal imaging can be applied in medicine either as a diagnostic test or as outcome measure for clinical trials.

A. Diagnosis of Diseases

Most of the diseases could be cured if diagnosed in the early stage. This reduces the death rate in many dangerous and malignant diseases like cancer and contagious diseases like tuberculosis.

B. Breast Cancer Screening

Early-stage cancer detection could reduce breast cancer death rates significantly in the long-term. The most critical point for best prognosis is to identify early-stage cancer cells. Investigators have studied many breast diagnostic approaches, including mammography, magnetic resonance imaging, ultrasound, computerized tomography, positron emission tomography and biopsy.[4] However, these techniques have some limitations such as being expensive, time consuming and not suitable for young women. Moreover involves high radiation levels for some method and low specificity leading to over diagnosis.

Improving screening practice in order to reduce breast cancer mortality has been developed. Many established risk factors for breast cancer, including being a woman, aging, breast density, family history, genetics, or a prior breast cancer diagnosis, cannot be modified. Breast cancer screening, referred to as secondary prevention, is the routine testing of individuals without symptoms that aims to detect breast cancer at its earliest stages so effective treatment can be offered[5] .Thermal imaging enhances screening of breast cancer.

This quick and easy test starts with medical history being taken before the scanning to be performed. When doing a breast series, this first session provides the initial portion of the person's baseline in developing "thermal thumbprint". A subsequent session in 3 months assures that the patterns remain unchanged and with these two sessions baseline is established. Standard region of interest exams take approximately 15 minutes and a full body 30 minutes.

In this method there is no invasive problem, no radiation effect. This method is also painless and for this test there is no contact with the body.

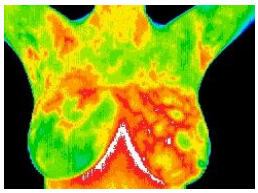

Figure 4. Thermal Image of Cancer Affected Patient

Fibrocystic Significant vascular activity in the left breast. Women at any age can begin utilizing thermography as a safe means of screening for breast disease. Thermography is not dependent on the density of a women's breast or do implants or surgical procedures affect the process of detecting thermal pattern. Thermography is especially appropriate for younger women between 30 & 50 whose denser breast tissue makes it more difficult for mammography to pick up suspicious lesions. This test can provide a 'clinical marker' to the doctor or mammographer that a specific area of the breast needs particular close examination

C. Tuberculosis Identifying Using Thermal Image

Even if a person has symptoms of TB, it is often difficult to diagnose TB, and is particularly difficult to diagnose rapidly. Though there are various methods to diagnosis tuberculosis, there are certain disadvantages. Chest x-ray, sputum, skin test and culture methods are used in the hospitals to check if the patients are affected by mycobacterium tuberculosis. The problems faced are need of sophisticated infrastructure and trained professional. Time delay and negative results lead to fatal effects.

Thermal images provide thermo gram, a representation in colour of radiation differences in affected areas. Thermal cameras uses infrared radiation related to temperature to realize the differences in heat emitted by the affected portion. The software of the thermal cameras emits a visible alarm to the PC when a higher level of temperature is detected. High accuracy is assured in this method.

Figure 5. Thermal Images

Affected areas are shown by orange colour; other parts are shown by blue colour to indicate normal status.

V. CONCLUSION

Thermal imaging has developed for multiple applications because of practical technology, more reliable and portable mode. Standard software and devices when used in this technology is used for many applications in image processing. Thermal imaging applications are widely spread because of the advantages of thermal cameras. This technique is used for diagnosing dangerous diseases. There is a scope for working on development of innovative, efficient & fast interpreting algorithms which will help doctors in detecting the deadly disease

VI. REFERENCES

[1] CA Duberstein DJ Virden S Matzner J Meyer VI Cullinan AR Maxwel-Automated Thermal Image Processing for Detection and Classification of Birds and Bats- FY2012 Annual Report Offshore Wind Technology Assessment

[2] VS. Elanthendral1 , R.K.Rekha2 , M. Rameshkumar3- Thermal Imaging for Facial Expression – Fatigue Detection- CSE Department, Veltech Multitech Dr.Rangarajan Dr.Sakunthala Engineering College Chennai, Tamil Nadu

[3] E F J Ring 1,3 and K Ammer -Infrared thermal imaging in medicinal Imaging Research Unit, Faculty of Advanced Technology, University of Glamorgan, Pontypridd, CF37 1DL, UK 2 Institute for Physical Medicine and

Rehabilitation, Hanuschkrankenhaus, Vienna, Austria

[4] Lulu Wang-Early Diagnosis of Breast Cancer-1,2 1 School of Instrument Science and Opto-Electronics Engineering, Hefei University of Technology, Hefei 230009, China; luluwang2015@hfut.edu.cn 2 Institute of Biomedical Technologies, Auckland University of Technology, Auckland 1142, New Zealand; luwang@aut.ac.nz

[5] Earlier Detection and Diagnosis of Breast Cancer: A Report from It's About Time! A Consensus Conference

[6] Amalric R, Altschuler C, Giraud D and Spitalier J M- 1984 Value of infrared thermography in the assessment of malignant melanoma of the skin Recent Advances in Medical Thermology ed E F J Ring and B Phillips (New York: Plenum) pp 623–9

[7] Amarja Adgaonkar , Aditi Atreya , Akshay D. Mulgund , Juhi R. Nath -Identification of Tuberculosis bacilli using Image Processing K.C. College Of Engineering And Management Studies And Research

[8] HarshalTalathi, Jinal Patel, KakoliLaha - Mrs.J.M.Kundargi -Identification of Tuberculosis Bacilli using image Processing , Department Of Electronics and Telecommunication ,K.J.Somaiya College of Engineering, Mumbai, India.

[9] Mohebian, M.R.; Marateb, H.R.; Mansourian, M.; Mañanas, M.A.; Mokarian, F. A hybrid computer-aided-diagnosis system for prediction of breast cancer recurrence (HPBCR) using optimized ensemble learning. Comput. Struct. Biotechnol. J. 2017, 15, 75–85. [CrossRef] [PubMed]

[10] U.S. Breast Cancer Statistics 2017. Available online: http://www.breastcancer.org/symptoms/understand_ bc/statistics (accessed on 2 July 2017).

[11] Mark D. Perkins, MD; Marcus B. Conde, MD; Marneili Martins, MD; Afranio L. Kritski, MD, PhD-Serologic Diagnosis of Tuberculosis Using a Simple Commercial Multiantigen Assay*-

[12] Grange JM, Lazlo A. -Serodiagnostic tests for tuberculosis: a need for assessment of their operational predictive accuracy andacceptability.BullWorldHealthOrgan1990;68:571–576

Themed Section : Engineering and Technology
© 2018 IJSRSET | Volume 5 | Issue 3 | Print ISSN: 2395-1990 | Online ISSN: 2394-4099

A Study on Deep Learning in Agriculture

Abhishek Pandey[1], Dr. V. Ramesh[2]
[1]Research Scholar, SCSVMV University, Kanchipuram, Tamil Nadu, India
[2]Assistant Professor, SCSVMV University, Kanchipuram, Tamil Nadu, India

ABSTRACT

We have seen in recent years an amazing improvement in applications using Deep learning. It started with speech recognition then moved on to computer vision, object recognition and natural language processing. Deep learning constitutes a recent, modern technique for image processing and data analysis, with promising results and large potential. Deep learning are machine learning algorithms based on learning multiple level of abstraction. As deep learning has been successfully applied in various domains, it has recently entered also the domain of agriculture. In this paper, we explored the platforms that employ deep learning techniques, applied to various agricultural and food production challenges. We examine the particular agricultural problems under study, the specific models and frameworks employed the sources, nature and pre-processing of data used, and the overall performance achieved according to the metrics used at each work under study. Moreover, we study comparisons of deep learning with other existing popular techniques, in respect to differences in classification or regression performance. Our research findings indicate that deep learning provides high accuracy, outperforming existing commonly used image processing techniques.

Keywords: Deep Learning, Classification, Regression

I. INTRODUCTION

It is expected that global population will reached 9 billion in 2050.it means we require more agricultural production in order to meet food demands. Otherwise we will be suffering from food security problems. So we have to increase our per unit area production. In agriculture we emphasis on yield. For increasing yield, our farm enterprises require new and innovative technologies to face and overcome these difficult challenges. So we are using different methodologies, technologies, and different processes for higher yield per unit area. In methodological approaches we can use different simulation models, but nowadays deep neural network or deep learning is also used in modern countries. Deep learning is a discipline of Computer Science that deals with giving ability to the machines that it seems to behave like, that it has human intelligence. There is a lot of scope of deep learning in many fields of life like in Agriculture that it can monitors crop conditions, like water scarcity conditions, plant population in field and soil moisture content etc. Deep learning is working in almost all disciplines of agriculture. In Irrigation it can control irrigation water in the field we can optimize the use of water because it have automatic irrigation systems in it that take weather conditions and predicts amount of water to be applied. Non chemical weed control is used in discriminating between weeds and crop seedling. It is an important step towards control of weeds by nonchemical way. Drone technology is another adoption of Artificial intelligence. Drones can be used to provide detailed mapping of crops in the fields. They are also capable of delivering customized fertilizers pesticides, insecticides based upon the requirement of each crops.

Artificial intelligence and deep learning algorithms has been found useful in almost every field of work

and study. It being deployed in every field makes it the next big thing and breakthrough for a smart future. In India, especially in Punjab increasing agriculture output to meet ever increasing population's demand is one of the major issues being faced today. Agricultural experts would tell that factors like climate, soil, rain along with other factors affect the output of a crop. Farmers feel immense pressure in such situations and lack of knowledge to counter the problems faced and modern techniques of farming only add further to the problem. There have been various sorts of efforts to implement deep learning and check the innumerable effect it has on different aspects like production time, assistance, output etc. We have seen field of medical science specifically benefitting from the implementation of deep neural networks. Researchers are constantly working of technologies like machine learning, deep neural network to aid artificial intelligence as a product for human use.

II. RELATED WORK

If we look specifically towards the field of farming, quite a lot of research is being conducted. Research on topics like hydration characteristics of Wheat, applying machine learning to agricultural data show that farming activities can greatly benefit from deep learning. Every research being done aims to improve the control of input variables such as fertilizer, seed, chemicals or water with respect to the desired outcomes of increased profitability, reduced environmental risk or better product quality. Research on some specific important crops like wheat are being carried out to because crops like wheat, rice need high output to meet the mass demand and any case of crop failure means huge loss. So deep learning can reduce chances of crop failure due to improper farming activities. This all data is learned and used by deep learning. Hence, a lot of research is being conducted for the same.

III. DEEP AGRICULTURE FRAMEWORK

In this paper we explore applications of deep learning to provide business leaders with an understanding of current and emerging trends, and present representative examples of popular applications. The most popular applications of Deep Learning in Indian agriculture appear to fall into three major categories:

i. Crop and Soil Monitoring – Companies are leveraging sensors and various IoT-based technologies to monitor crop and soil health.
ii. Predictive Agricultural Analytics – Various AI and machine learning tools are being used to predict the optimal time to sow seeds, get alerts on risks from pest attacks, and more.
iii. Supply Chain Efficiencies– Companies are using real-time data analytics on data-streams coming from multiple sources to build an efficient and smart supply chain.

Here we explore various Deep and machine learning frameworks that helps our farmers to strengthen their crop production.

A. Intello Labs – Using Deep Learning for Image Analysis

Bengaluru-based Intello Labs was started by IIT-Bombay alumnus Milan Sharma in May 2016. The company claims to provide advanced image recognition technology that can recognize objects, faces, flora and fauna and tag them in any image. The company claim to use deep learning algorithms on which a new generation of intelligent applications are being built for applications including agriculture, e-commerce, advertising, manufacturing, and curation. Small farmers around the world follow traditional farming practices due to lack of access to scientific understanding of crop lifecycle, pests, quality metrics and the latest micro-fertilizers. Intello Labs Image based solutions provide insights on the crops' health during the growing season. Intello Labs claims to provide Agricultural Product Grading: Automated quality analysis of images of food products is an

accurate and reliable method for grading fresh products (fruits, grains, vegetables, cotton etc.) characterized by color, size and shape. Their solution reads the image that a farmer has taken on his phone and determines the product quality in real time, without any manual intervention. Alerts on Crop Infestation: Farmers can click an image of their crop and use their solution to understand the pests, diseases, and foreign plants (weeds) growing in their farms. The solution uses deep learning and image processing models to identify any crop diseases or pest infestation in the crops. Along with the parameters, it gives recommendations on how that disease can be cured and prevented from increasing further.

B. Microsoft India – AI-Based Sowing App

Determining the right time to sow crops is often one of the biggest challenges for Indian farmers where drought and excess rainfall can be equally serious challenges. Microsoft in collaboration with ICRISAT (International Crops Research Institute for the Semi-Arid Tropics), developed an AI Sowing App that uses machine learning and business intelligence from the Microsoft Cortana Intelligence Suite. The app sends sowing advisories to participating farmers on the optimal date to sow. The best part – the farmers don't need to install any sensors in their fields or incur any capital expenditure. All they need is a feature phone capable of receiving text messages.

Figure 1. A Photo of A Text Message From The Microsoft India AI Sowing

To calculate the crop-sowing period, historic climate data (spanning over 30 years from 1986 to 2015) for the specific area in Andhra Pradesh was analysed using AI. To determine the optimal sowing period, the Moisture Adequacy Index (MAI) was calculated. MAI is the standardized measure used for assessing the degree of adequacy of rainfall and soil moisture to meet the potential water requirement of crops. Microsoft has also partnered with United Phosphorous (UPL), India's largest producer of agrochemicals, to create the Pest Risk Prediction App that again leverages AI and deep learning to indicate in advance the risk of pest attack. Today, these farmers across the Indian states of Andhra Pradesh and Karnataka wait to get a text message before sowing the seeds. As per the report cited above, in a few dozen villages in Telangana, Maharashtra, and Madhya Pradesh, farmers receive automated voice calls alerting them whether their crops are at risk of a pest attack based on weather conditions and stage of the crop. No specific numbers on the results were reported.

C. Gramophone (Agstack Technologies) – Image Recognition for Soil Science

Based in the Indian state of Madhya Pradesh, Gramophone claims to leverage the power of image recognition and soil science to help farmers with timely information, technology, and right kind of inputs to achieve better yields. This technology platform uses deep learning to predict pest and disease, forecast commodity prices for better price realizations and recommends products to farmers. Gramophone use temperature, humidity and pathology/entomology data to give accurate advisory to the farmers. Gramophone primary focus is to digitize agriculture science and convert it into actionable information for the farmers to provide personalized farm management solution, which would guide farmers across the cropping cycle.

IV. CONCLUSION

Given the huge potential of agriculture in India, it's imperative that deep and intelligent technology is used to the maximum so that both farmers and consumers can make the most of it. With recent advancements in technology coupled with conducive

government policies, we have seen many agtech startups emerge in the country which is a great starting point for the penetration of advanced technologies like AI in agriculture. AI and deep learning comes as a great boon to the agricultural sector which is heavily dependent on climatic conditions which are often unpredictable. Throughout the paper, we have seen instances of how companies are using sensors for crop and soil monitoring, as well as AI and deep learning tools for predictive analytics. More and more use cases of deep learning in agriculture are likely to show up in the near future because of the immense value it can add.

V. REFERENCES

[1] McKinion, J. M., and H. E. Lemmon. "Expert systems for agriculture." Computers and Electronics in Agriculture 1.1 (1985): 31-40.

[2] Jat, Avnish Singh, Suma Dawn, Abhinav Mishra, and Amit Kumar. "Asperger's Disorder: Application for its Treatment through Emotion Detection."

[3] D. Toppeta, ''The Smart City Vision: How Innovation and ICT can build Smart, Livable, Sustainable Cities'', iThink, Report 005, 2010.

[4] Verma Kunal, Pabbi Dinesh, ''Agriculture Advancement Using Artificial Intelligence'', International conference on recent innovations in science, technology, management and enironment , 2016.

Themed Section : Engineering and Technology
© 2018 IJSRSET | Volume 5 | Issue 3 | Print ISSN: 2395-1990 | Online ISSN: 2394-4099

Certain Investigation on Hyper Spectral Remote Sensing Image

C. Rajinikanth[1], Dr. S. Abraham Lincon[2]
[1]Research Scholar, Department of Electronics & Instrumentation Engineering, Annamalai University, India
[2]Professor, Department of Electronics & Instrumentation Engineering, Annamalai University, India
rajini_tamil@yahoo.co.in[1]

ABSTRACT

In this paper, a technique has been designated for classification of satellite remote sensing of hyperspectral image. The classification process is based on the three main categories: (1) Clustering, which performed in supervised techniques using Thresholding effect of image pixel intensity and (2) segmented and texture based image analysis, in this process to achieve a new textural based image clustering to overcome the problem of multi-label images in satellite remote processing. Finally, it is clustered and result in segmented output.

Keywords : Hyper Spectral Remote Sensing Image, Image Classification

I. INTRODUCTION

Digital image processing supports strong research in the areas of image classification and image based pattern recognition. Recently, these areas are broadly applied in remote sensing, medical image processing, and robotics. Between these areas Image classification is used everywhere to shorten and to change the representation of image in to something that is more significant and easier to analyse. In traditional classification, a general pixel clustering process is presented based on thresholding effect of image pixel intensity. Presented a shapelet-based spatial–spectral classification of hyperspectral image data. The shapelet-based approach varies from earlier suggested sparse representation- based classifiers for hyperspectral image data. In this method that sophisticated prior knowledge about the spatial nature of an image is exploited by applying a constructed highly adapted patch-specific based classification procedures by means of the representation error. The shapelet-based spatial–spectral classification approach shows greater outcomes in comparison to sparse-representation-based classifiers that use only limited spatial information [1]. Developed a method for object-based mid-level representation for semantic classification for high resolution remote sensing images. The mid-level representation method is how to boost the relatively low classification accuracy caused by using pixel-based image classification approaches and low-level visual structure. The method of low-level visual features and high-level semantics are not well define in semantics images. The object-oriented semantic classification algorithm that combines bag-of-visual-words (BOV) with the optimal segmentation scale intends to overcome the defect of conventional BOV in lacking of relationship between image patches and to give more thorough description [2]. Discuss the generic [5] method for the modelling and detection of compound structures that involve arrangements of an unknown number of primitives in large scenes of remote sensing. The modelling process are investigates via Markov random field and the detection task has formulated as the selection of multiple subsets of candidate regions from a hierarchy segmentation. Where each set of selected regions has been constituted an instance of the compound

structure. The combinatorial selection problem of hierarchy segmentation is solved by the joint sampling of groups of regions by maximizing the likelihood of their individual appearances and relative spatial arrangements of remote sensing images. Ddeveloped a new technique of highly efficient Multiscale and Multi feature Normalized (MMN) [4] cut algorithm for HSR imagery segmentation. The MMN cut is much less sensitive to image boundaries and also preserves the multi scale information. Normalized Cuts (NC), as a commonly used for the method of natural image segmentation of remote sensing images. It can also acquire a globally optimized segmentation result equivalent to the optimized partitions of a super pixel graph. These graph which can provide powerful indication to guide the HSR imagery segmentation. Suggested a appropriate method for terrestrial laser scanning in planner segmentation of satellite segmentation. Its normal vector and the distance from the origin parameterize the planner segmentation. It is multiple standpoints can be used for such applications as plane-based registration and 3-D reconstruction of buildings has been presented [3].

II. WORK AREA

The Salinas hyperspectral datasets is selected for classification Experiments. The Salinas datasets captured by the Airborne Visible/Infrared Imaging Spectrometer (AVIRIS) sensor with 224 spectral band and the dataset has a pixel value of 512 × 217 and spatial resolution of 3.7m of Fig.1 shows the RGB colour composition and ground truth reference map and colour code of Salinas's dataset. In our process, the images are Train Data for 77% of different Dataset and its corresponding Test Data for 23% of the different Dataset.

III. RELATED WORKS

A. Filtering Technique

The Cellular Automata is simple method and synchronous transition technique. The remote sensed digital image like Salinas is considered as 3×3 bidirectional array.

B. Enhancement Technique

The filtered image is enhanced using the histogram equalization. This histogram equalization involves in the assignment of the minimum value of the pixel intensity of input image.

IV. RESULTS AND DISCUSSION

The MATLAB programming is used to input the hyper spectral image as in Fig. 3(a) and is filtered and enhanced as shown in Fig. 3(b) and (c) respectively and evaluates the each stage of the proposed SSTBA algorithm for the Salinas dataset.

A. Comparison Matrices Analysis

Confusion matrix and Kappa coefficient is a techniques for calculation of Accuracy assessment with SSTBA based HSI classification. It is based on the data providing the assumption on the classes of reference datasets. The datasets are classified two manner 1) reference data value and 2) ground truth data value. Moreover the FAR value 3.6145, GAR value 96.3855 has been presented in Table 1.

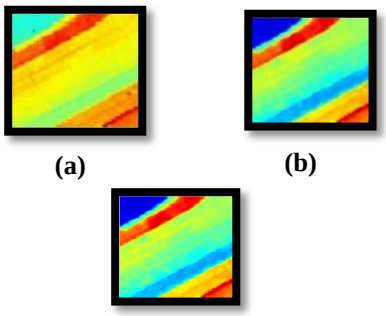

Figure 3. Output images of SSTBA clustering. (a) Input image (b) Filtered image (c) Enhanced image

Table 1 FAR and GAR Analysis

S.No	FAR	GAR
1	3.6145	96.3855
2	0	100

V. CONCLUSIONS

Paper contribute, a novel dictionary learning method called SSTBA for HSI classification has been proposed. The SSTBA representation show the outstanding ability to give better description of the HSI classification, especially exploiting SSSTBA in NN as classifier. The experiments conducted for Salinas's datasets prove the better performance of the proposed method compared with multi-labeling image extraction methods at different HSI classification procedure.

VI. REFERENCES

[1] Erlei Zhang, Licheng Jiao, Xiangrong Zhang, Hongying Liu, and Shuang Wang, "Class-Level Joint Sparse Representation for Multifeature-Based Hyperspectral Image Classification" IEEE Journal of Selected Topics in Applied Earth Observations and Remote Sensing, 2016, 9(9),pp.4160-4177.

[2] Ribana Rosche, and Björn Waske, "Shapelet-Based Sparse Representation for Landcover Classification of Hyperspectral Images" IEEE Transactions on Geoscience and Remote Sensing, 2016, 54(3),pp.1623-1634.

[3] Guiyun Zhou, Shuai Cao, and Junjie Zhou, "Planar Segmentation Using Range Images From Terrestrial Laser Scanning", IEEE Geoscience And Remote Sensing Letters, 2016,13(2),pp.257-261.

[4] Yanfei Zhong, Rongrong Gao, and Liangpei Zhang,"Multiscale and Multifeature Normalized Cut Segmentation for High Spatial Resolution Remote Sensing Imagery" IEEE Transactions On Geoscience And Remote Sensing, 2016,54(10),pp.6061-6075.

[5] H. Gökhan Akçay and Selim Aksoy, "Automatic Detection of Compound Structures by Joint Selection of Region Groups from a Hierarchical Segmentation" IEEE Transactions on Geoscience and Remote Sensing, 2016, 54 (6), pp. 3485-3501.

Themed Section : Engineering and Technology
© 2018 IJSRSET | Volume 5 | Issue 3 | Print ISSN: 2395-1990 | Online ISSN: 2394-4099

Robust Medical Image Watermarking Scheme Based On RDWT-SVD

Ravisankar[1], Kanimozhi[2]
[1]PG Scholar, ECE Annamalai University, Tamil Nadu, India
[2]Assistant Professor, ECE Annamalai University, Tamil Nadu, India
lravisankar21@gmail.com[1]

ABSTRACT

In the modern era, digital image watermarking is a successful method to protect the multimedia digital data for example copyright protection, content verification, rightful ownership identification, tamper detection etc. In this system, for improving the robustness and security, a Dual watermarking approach using Redundant Discrete Wavelet Transform (RDWT) and block based singular value decomposition (SVD) is presented. After applying RDWT to both cover and watermark images, we apply SVD to the LL sub bands of them. Then modify singular values of the cover image using singular values of the visual watermark. The advantage of the proposed technique is its robustness against most common attacks. In the existing system, the original images is split into the blocks and proceed DFT transform after that by using Arnold scrambling produce. Analysis and experimental results show higher performance of the proposed method in comparison with the DWT-SVD method.

Keywords: Medical Image Watermarking, Redundant Discrete Wavelet Transform, Singular Value Decomposition

I. INTRODUCTION

Watermarking (data hiding) is the process of embedding data into a multimedia element such as image, audio or video for security purposes or copyright protection. This embedded data can later be extracted from, or detected in the multimedia. A watermarking algorithm consists of an embedding algorithm, and an extraction, or detection algorithm. The type of information needed by the detector is an important criterion in classification of watermarking schemes:

- Non-blind schemes require both the original image and the secret key(s) for watermark embedding.
- Semi-blind schemes require the secret key(s) and the watermark itself.
- Blind schemes require only the secret key(s) [1].

Watermarking can be performed in the spatial or transform domain. Spatial domain methods are less complex but are not as robust as transform domain methods against various attacks [2]. One of the most common techniques in transform domain watermarking is to modify the coefficients obtained from singular value decomposition (SVD) of the cover image. The SVD based watermarking algorithm was first presented by Liu et al. [3]. In this algorithm, the authors after applying singular value decomposition to the cover image modify these coefficients by adding the watermark. They apply SVD transform

again on the resultant matrix for finding the modified singular values. These singular values were combined with the known component to get the watermarked image. In another similar work, Chandra et al. [4], embed singular values of the watermark in the singular values of entire host image.

The most important drawback of SVD-based algorithms is quality degradation of the watermarked image. In addition, the extracted watermark is not robust enough against common attacks in SVD based algorithms. Thus researchers, usually combine SVD with other algorithms such as DCT and DWT.

In [5], authors combined DWT with SVD technique. In that paper, after decomposing the host image into four sub-bands, applied SVD to each sub-band and embedded singular values of the watermark into the sub-bands. In [6] DWT is combined with SVD technique to hide singular values of watermark in high frequency band (HH) of an image. When DWT is combined with SVD technique the watermarking algorithm outperforms the conventional DWT algorithm with respect to robustness against Gaussian noise, compression and cropping attacks [7]. Despite good performance of DWT methods in Watermarking, they suffer from drawbacks which are mentioned in section 2. To over come the drawbacks of DWT based watermarking, one solution is the use of Redundant Discrete Wavelet Transform (RDWT).A New Robust Watermarking Scheme Based on RDWT-SVD.

A. RDWT

One of the most common methods used for watermarking is DWT, but one of the main drawbacks of this method is that because of the down-sampling of its bands, it does not provide shift invariance. This causes a major change in the wavelet coefficients of the image even for minor shifts in the input image. The shift variance of DWT causes inaccurate extraction of the cover and watermark image [8],since in watermarking, we need to know the exact locations of where the watermark information is embedded, to overcome this problem, researchers have proposed using Redundant Discrete Wavelet Transform.

3. SVD

SVD efficiently represents intrinsic algebraic properties of an image, where singular values correspond to brightness of the image and singular vectors reflect geometry characteristics of the image. Since slight variations of singular values of an image may not affect the visual perception, watermark embedding through slight variations of singular values. The singular value decomposition of a matrix is a factorization of the matrix into a product of three matrices.

II. PROPOSED SYSTEM

In this system, trying to realize a new algorithm by combining both DWT and SVD. Generally wavelet domain allows us to hide data in regions that the human visual system (HVS) is less sensitive to, such as the high resolution detail bands (HL, LH and HH), Hiding data in these regions allow us to increase the robustness while maintaining good visual quality. Integer wavelet transform maps an integer data set into another integer data set. In discrete wavelet transform, the used wavelet filters have floating point coefficients so that when we hide data in their coefficients any truncations of the floating-point values of the pixels that should be integers may cause the loss of the hidden information which may lead to the failure of the data hiding system.

To avoid problems of floating point precision of the wavelet filters when the input data is integer as in digital images, the output data will no longer be integer which doesn't allow perfect .reconstruction of the input image [10] and in this case there will be no loss of information through forward and inverse transform [9]. Due to the mentioned difference between integer wavelet transform (IWT) and discrete wavelet transform (DWT) the LL sub band in the case of IWT appears to be a close copy with smaller scale of the original image while in the case of DWT the resulting LL sub band is distorted. Lifting

schemes is one of many techniques that can be used to perform integer wavelet transform it is also the scheme used in this system.

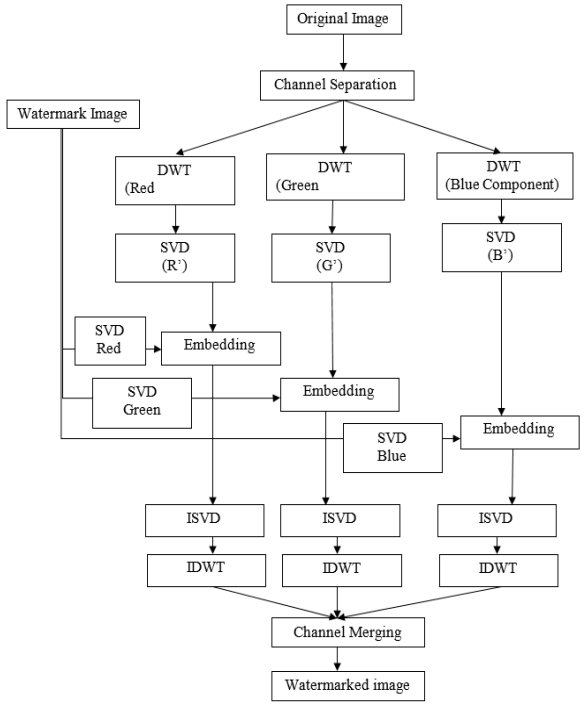

Figure 1. Watermark Embedding Process

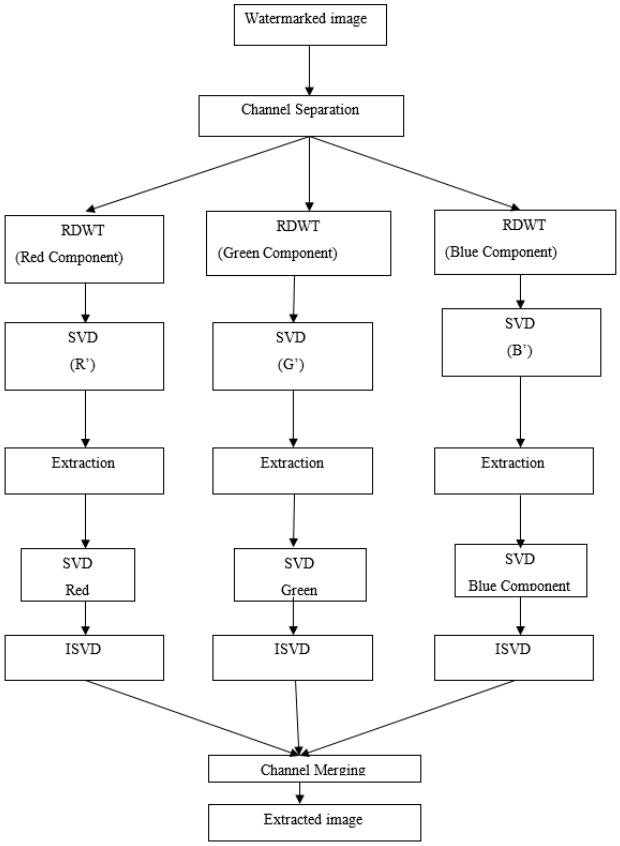

Figure 2. Watermark Extraction Process

III. CONCLUSION

The image is divided into two different watermarks are inserted into the horizontal and vertical sub-bands of wavelet coefficients. In this system, a new blind digital image-watermarking scheme using SVD in RDWT domain is presented. The transparency and robustness of the proposed method is investigated with extensive experiments. The experimental results show that the proposed method offers good transparency for the watermarked images, which is evaluated by PSNR. The performance of the proposed method against different attacks of the watermarked image is evaluated by correlation coefficients of extracted watermark logos and some subjective image tests. The experimental results show that the proposed method can effectively resists against geometric and non-geometric attacks.

IV. REFERENCES

[1] Lai, C.C.; Tsai, C.C. Digital image watermarking using discrete wavelet transform and singular value decomposition. IEEE Trans. Instrum. Meas. 2010, 59, 3060–3063.

[2] Lai, C.C. A digital watermarking scheme based on singular value decomposition and tiny genetic algorithm. Digit. Signal Process. 2011, 21, 522–527.

[3] Gupta, A.K.; Raval, M.S. A robust and secure watermarking scheme based on singular values replacement. Sadhana 2012, 37, 425–440.

[4] Yang, X.S. Multiobjective firefly algorithm for continuous optimization. Eng. Comput. 2013, 29, 175–184.

[5] Yavuz, E.; Telatar, Z. Comments on "A digital watermarking scheme based on singular value decomposition and tiny genetic algorithm". Digit. Signal Process. 2013, 23, 1335–1336.

[6] Su, Q.T.; Niu, Y.G.; Wang, Q.J.; Sheng, G.R. A blind color image watermarking based on DC component in the spatial domain. Opt. Int. J. Light Electron. Opt. 2013, 124, 6255–6260.

[7] Makbol, N.M.; Khoo, B. E redundant discrete wavelet transform and singular value decomposition. AEU Int. J. Electron. Commun. 2013, 67, 102–112.E. Robust blind image watermarking scheme based on

[8] Guo, J.M.; Prasetyo, H. False-positive-free SVD-based image watermarking. J. Vis. Commun. Image Represent. 2014, 25, 1149–1163.

[9] Mishra, A.; Agarwal, C.; Sharma, A.; Bedi, P. Optimized gray-scale image watermarking using DWT-SVD and firefly algorithm. Expert Syst. Appl. 2014, 41, 7858–7867.

[10] Hai, T.; Li, C.M.; Zain, J.M.; Abdalla, A.N. Robust image watermarking theories and techniques: A review. J. Appl. Res. Technol. 2014, 12, 122–138.

[11] Nyeem, H.; Boles, W.; Boyd, C. Digital image watermarking: Its formal model, fundamental properties and possible attacks. EURASIP J. Adv. Signal Process. 2014, 1, 1–22.

[12] Su, Q.T.; Wang, G.; Jia, S.L.; Zhang, X.F.; Liu, Q.M.; Liu, X.X. Embedding color image watermark in color image based on two-level DCT. Signal Image Video Process. 2015, 9, 991–1007.

[13] Ali, M.; Ahn, C.W. Comments on “Optimized gray-scale image watermarking using DWT-SVD and firefly algorithm”. Expert Syst. Appl. 2015, 42, 2392–2394.

[14] Fazli, S.; Moeini, M. A robust image watermarking method based on DWT, DCT, and SVD using a new technique for correction of main geometric attacks. Opt. Int. J. Light Electron. Opt. 2016, 127, 964–972.

[15] Keshavarzian, R.; Aghagolzadeh, A. ROI based robust and secure image watermarking using DWT and Arnold map. AEU Int. J. Electron. Commun. 2016, 70, 278–288.

[16] Ansari, I.A.; Pant, M.; Ahn, C.W. Robust and false positive free watermarking in IWT domain using SVD and ABC. Eng. Appl. Artif. Intell. 2016, 49, 114–125.

[17] Zhang, H.; Wang, C.Y.; Zhou, X. Fragile watermarking for image authentication using the characteristic of SVD. Algorithms 2017, 10, 27.

[18] Singh, D.; Singh, S.K. DWT-SVD and DCT based robust and blind watermarking scheme for copyright protection. Multimed. Tools Appl. 2017, 76, 13001–13024.

[19] Singh, D.; Singh, S.K. DWT-SVD and DCT based robust and blind watermarking scheme for copyright protection. Multimed. Tools Appl. 2017, 76, 13001–13024.

[20] Liu, R.Z.; Tan, T.N. An SVD-based watermarking scheme for protecting rightful ownership. IEEE Trans. Multimed. 2012, 4, 121–128. Future Internet 2017, 9, 45

Themed Section : Engineering and Technology
© 2018 IJSRSET | Volume 5 | Issue 3 | Print ISSN: 2395-1990 | Online ISSN: 2394-4099

Differential Drive 2 Wheel Odometry

Ankit Deo[1], Raaghavi Ravisankar[2]

[12]Dept. of Electronics & Instrumentation Engineering, Vellore Institute of Technology, Tamilnadu, India
r.raaghavi2016@vitstudent.ac.in[2]

ABSTRACT

Things that we used:

- We used a 2 wheel differential drive robot for indoor mapping of an environment.
- Used MATLAB PRM path planner to find an obstacle free path in the environment
- Used image processing to find obstacles in the environment.
- In cases where image processing failed to give the exact location of the obstacle, we used an ultrasonic sensor as an interrupt to avoid collision

What did we get:

- As we increased no. Of nodes the probability of getting an obstacle free path increased but at the same time no. Of combination between the nodes increased ${}^{n}C_{2}$ times this caused a lot of lag in the MATLAB software as data to be processed increased at a rapid rate.
- Connection distance and look ahead distance: distance between two nodes cannot be less than the dimension of the bot so we need to set the connection distance between two nodes to be atleast 1.25 times of the dimension of the bot.

Keywords: Robot, Differential Drive, MATLAB

I. INTRODUCTION

Industrial robots generally have their base fixed [1-4] .The have several limitations including localization and Path planning. In this paper, we present the specifications, Equations, Procedure for simulations and their results.

Robot Specification:

- 2 wheel differential drive robot
- wheel encoders intact with it to give the runtime RPM of the bot
- Magnetometer intact with it to give change in orientation of the bot.

Procedure followed:

Differential drive odometry can be used even in multiple wheels. The RPM of one set of wheels can be varied with respect to the other to follow any trajectory on the plane.

Using image processing a binary grid like structure of the environment is developed. In the grid 1 is for obstacle and 0 is for free space.

Using MATLAB probabilistic road map planner we get an obstacle free path by tuning the number of nodes and connection distance between two nodes.
The more the number of nodes we define more accurate obstacle free path we get but at the same time the processing speed is a constraint since we have ${}^{n}C_{2}$ combinations for the nodes.

Again, we need to tune the connection distance more 1.25 times the bot dimensions. In rare cases our bot

might collide with the obstacle due to errors. The best way to ensure that this doesn't happen is using an ultrasonic sensor whenever the bot is about to collide, the reading becomes less than a particular value which we can define as threshold. We called a function to move right or left for a small duration as an interrupt to avoid collision.

Equations used could be widely seen in all open literature including the one in our references [1-4].

$$\begin{cases} \dot{x} = v\cos\phi \\ \dot{y} = v\sin\phi \\ \dot{\phi} = \omega \end{cases}$$

Design for this model!

$$v = \frac{R}{2}(v_r + v_\ell) \Rightarrow \frac{2v}{R} = v_r + v_\ell$$

$$\omega = \frac{R}{L}(v_r - v_\ell) \Rightarrow \frac{\omega L}{R} = v_r - v_\ell$$

$$\begin{cases} \dot{x} = \frac{R}{2}(v_r + v_\ell)\cos\phi \\ \dot{y} = \frac{R}{2}(v_r + v_\ell)\sin\phi \\ \dot{\phi} = \frac{R}{L}(v_r - v_\ell) \end{cases}$$

$$v_r = \frac{2v + \omega L}{2R}$$

$$v_\ell = \frac{2v - \omega L}{2R}$$

II. SIMULATIONS OBTAINED

We present the following results Simulation with the obstacle present, Probalistic road map.

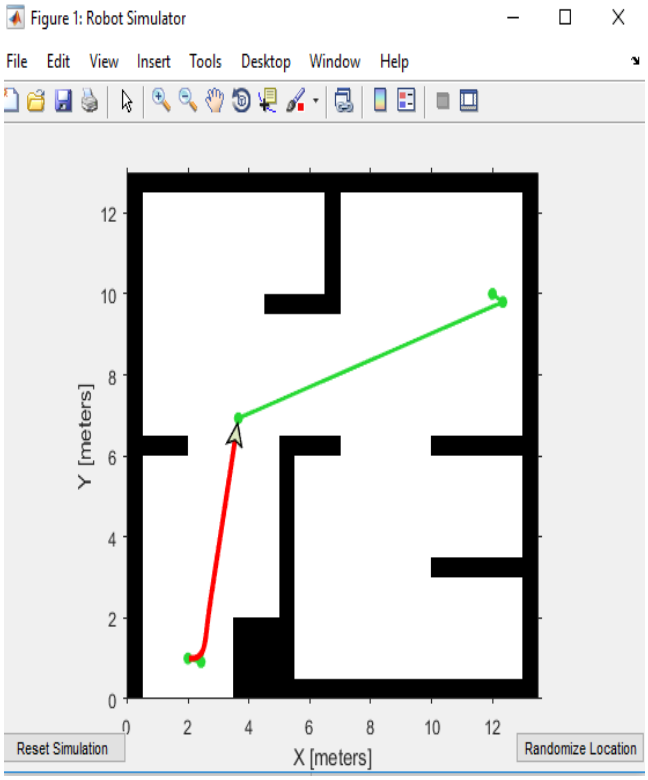

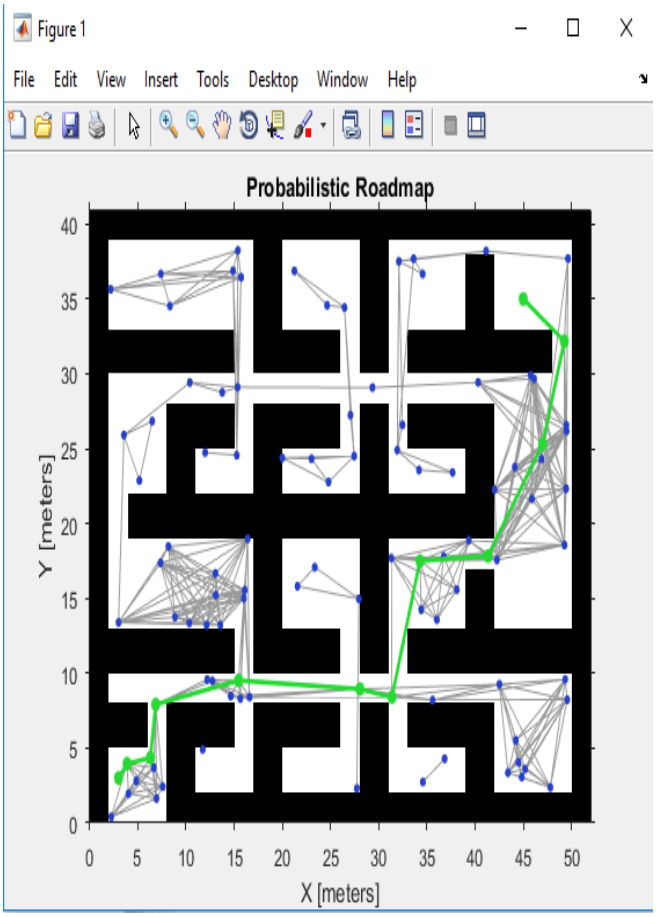

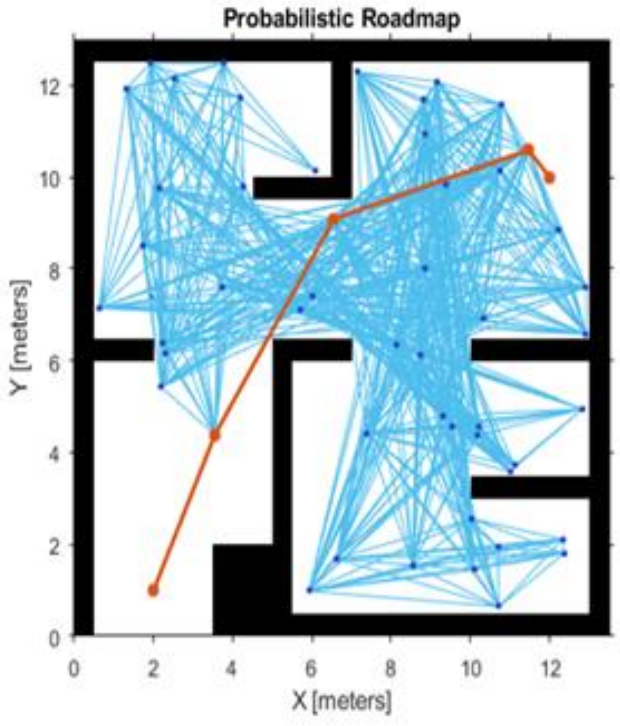

III. APPLICATIONS

A. Encoders

Encoders are used to generate rotary or linear motion into digital signal. This is used for controlling motion parameters such as speed, rate, distance, direction.

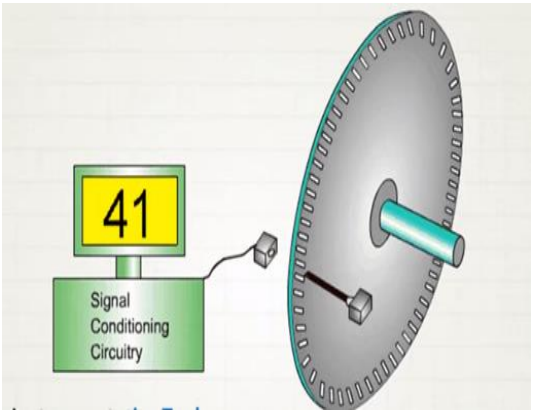

The Encoders typically consists of rotating and stationary electronic circuit. The rotor disc in absolute optical encoder uses opaque and transparent segments arranged in a Gray Code pattern. The stator has corresponding pairs of LEDs and phototransistors arranged so that the LED light receives through the transparent sections of the rotor disc and detected by phototransistors on the other side. After the electronic signals are amplified and converted, they are then available for the evaluation of the position of speed of the disc.

B. Ultrasonic Sensors

An Ultrasonic sensor is a device that can measure the distance to an object by using sound waves. It measures distance by sending out a sound wave at a specific frequency and listening for that sound wave to bounce back. By recording the elapsed time between the sound wave being generated and the sound wave bouncing back, it is possible to calculate the distance between the sonar sensor and the object.

IV. CONCLUSION

This can be used in unmanned mapping of terrain of unknown alien planet. Since planets are generally spherical in shape, a sphere has no starting and ending points. The coordinate from which our rover started is considered to be 0,0 and all the other coordinates are calculated with respect to it using image processing we can define the starting and ending points of the rover for the terrain to be mapped and the obstacles will be detected. We have used encoders here to get the rpm and distance traversed. Here, in our work we set a threshold if it crosses the, then interrupts are used to move it away from the obstacle and continue in its desired path.

ACKNOWLEDGEMENTS

We would like to thank our Authorities for motivating us in initiating this work. We would like to thank the (Organizer of the National Conference ETRES'18 on 26-27th April 2018) Dr.R.Gayathri, Dept of ECE, Annamalai University. We dedicate this work to our Beloved Parents.

V. REFERENCES

[1] http://rossum.sourceforge.net/papers/DiffSteer/
[2] https://robotics.stackexchange.com/
[3] Evangelos Papadopoulos and Michael Misailidis, "On Differential Drive Robot Odometry with

Application to Path Planning,", Proceedings of the European Control Conference 2007 Kos, Greece, July 2-5, 2007.

[4] D. Fox, W. Burgard, and S. Thrun, "The dynamic window approach to collision avoidance", IEEE Robotics & Automation Magazine, 4(1):23–33, March 1997.

Themed Section : Engineering and Technology
© 2018 IJSRSET | Volume 5 | Issue 3 | Print ISSN: 2395-1990 | Online ISSN: 2394-4099

Optimal Placement of SVC using Firefly Algorithm

N.Karthik[1], A.K.Parvathy[2], R.Arul[3], Jayapragash.R[4]

[12]Department of Electrical and Electronics Engineering, Hindustan Institute of Technology & Science, Chennai, Tamilnadu, India

[34]School of Electrical Engineering, Vellore Institute of Technology, Chennai, Tamilnadu, India

nkarthik@hindustanuniv.ac.in[1]

ABSTRACT

This paper presents an application of Firefly Algorithm (FFA) to recognize the optimal placement of Static Var Compensator (SVC) in a power system network. A circuit model of SVC is utilized to regulate the bus voltage magnitudes and line power flows for improvement of voltage profile and real power loss minimization respectively. The key reason for the voltage instability is the insufficient reactive power at the load buses of the system. Here IEEE 57 bus system is taken into consideration for finding the optimal location and sizing of SVC using FFA. To validate the proposed algorithm, simulation is performed on standard IEEE 57 bus system using MATLAB software package. The simulation results obtained from FFA are compared with Particle Swarm Optimization (PSO) and found to be better.

Keywords: Firefly Algorithm (FFA), Loss Minimization, SVC, Optical Location, Particle Swarm Optimization (PSO), Voltage Profile.

I. INTRODUCTION

Reactive Power Compensation is a static non-linear programming problem, which optimizes a certain objective function while fulfilling a set of operational, and physical constraints imposed by equipment and equipment limitations [1, 2]. It is also a large-scale static optimization problem with both continuous and discrete decision variables [3]. Several classical optimization techniques such as linear programming, non-linear programming and quadratic programming [4] and the interior point method [5] have been applied to solve the optimal power flow problem. All the above classical optimization have some drawbacks such as getting trapped in local optima or they are suitable for taking into consideration of a explicit fitness function in the optimal power flow problem. These disadvantages can be overcome if meta-heuristic optimization techniques are utilised to solve the optimal power flow problem. Classical optimization techniques used in optimal power flow problem are based on linear programming and non-linear programming. Fast Quadratic Programming has also been employed for large scale reactive power optimization. The most important disadvantage of these optimization techniques comprises local minima criterion and the time consumption. In order to overcome these shortcomings, meta heuristic optimization algorithms for instance Differential Evolution [6],Ant colony search Algorithm [7], Genetic Algorithm [8], PSO Algorithm and its several modifications such as hybrid PSO[9, 10] were proposed. Recent works on optimal power flow problem includes various meta heuristic optimization techniques like Harmony search Algorithm (HSA) [11] Biogeography-Based optimization (BBO) [12], and

teaching learning based optimization (TLBO) [13] for minimization of real power loss. Dr. Xin-She Yang [14] developed Firefly Algorithm at Cambridge University, which is based on the flashing behaviour of fireflies in 2007. The fitness function of the optimization problem is associated with that of the brightness of firefly and depending on the movement of the fireflies towards the brighter one in the given population thus solving the optimization problem. The rest of this paper is structured as follows. The power flow model of SVC is presented in Sect. 2. The statistical formulation of the optimal power flow problem is presented in Sect. 3. In Sect. 4, firefly algorithm and its performance in reactive power optimization is demonstrated in detail. Simulation results on IEEE 57 bus system and the association with the results provided by particle swarm optimization (PSO) algorithm is shown.

II. POWER FLOW MODEL OF SVC DEVICE

The Static Var Compensator performs similar to a shunt connected variable reactance. SVC either absorbs or generates reactive power so as to control the magnitude of the voltage at the point of connection to the AC network. Fig.1 shows the equivalent circuit of variable susceptance model which is utilized to obtain the SVC non-linear power flow equations and the liberalized equations required by the Newton's method. The linearized equation of the SVC device is given by the subsequent equation, where the total susceptance B_{svc} is considered to be the state variable.

$$\begin{bmatrix}\Delta P_i \\ \Delta Q_i\end{bmatrix}^k = \begin{bmatrix}0 & 0 \\ 0 & \frac{\partial Q_i}{\partial B_{svc}}\end{bmatrix}^k \begin{bmatrix}\Delta\theta \\ \Delta B_{svc}\end{bmatrix}^k \quad (1)$$

The variable shunt susceptance, B_{svc} is modified at the ending of every iteration (k),

$$B_{svc}^{k+1}=B_{svc}^{k}+\Delta B_{svc}^{k} \quad (2)$$

Reactive power drawn by SVC device, which is also reactive power injected, Q_{svc} at bus i, is

$$Q_{svc}=Q_i=-V_i^2 B_{svc} \quad (3)$$

The current drawn by SVC depending on the equivalent circuit of SVC is

$$I_{svc}=jB_{svc}V_i \quad (4)$$

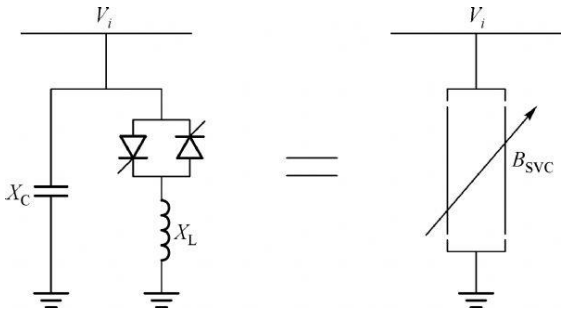

Figure 1. Model of SVC

III. FORMULATION OF REACTIVE OPTIMIZATION PROBLEM

The FACTS devices are to be installed at suitable positions with best possible parameters that curtail the real power loss for better deployment of the existing power system. This paper aims to build up a strategy that executes optimal placement of SVC with an intention of curtailing active power loss and enhancing voltage profile.

A. Formulation of Objective Function

The goal of using FFA is to curtail active power loss, which can be calculated from the load flow solution [14], and described as

$$\text{Min } P_{loss}=\sum_{l=1}^{nl} G_l(V_{i2}+V_{j2}-2V_iV_j\cos\delta_{ij}) \quad (5)$$

B. Operating Constraints for the Optimal Placement Problem

The optimal power flow problem is subject to the subsequent equality and inequality constraints

(i) Power flow Constraints

$$P_i=V_i \sum_{j=1}^{N} V_j(G_{ij}\cos \theta_{ij} + B_{ij} \sin \theta_{ij})=0 \quad (6)$$

$$Q_i=V_i \sum_{j=1}^{N} V_j(G_{ij} \sin \theta_{ij} + B_{ij} \text{ Cos } \theta_{ij})=0 \quad (7)$$

Where 'i' and 'j' are buses and N is number of buses

(ii) Operating limits of the voltage

$$V_{imin} \leq V_i \leq V_{imax} \quad (8)$$

(iii) Reactive Power Generation Limit

$$Q_{Gimin} \leq Q_{Gi} \leq Q_{Gimax} \quad (9)$$

(iv) SVC size limit

$$-200\text{MVAR} \leq Q_{SVC} \leq 200\text{MVAR} \quad (10)$$

IV. FIREFLY ALGORITHM

The firefly algorithm is a nature inspired swarm intelligence technique, enthused by the sporadic activities of fireflies. It is analogous to other meta-heuristic optimization algorithms utilizing swarm intelligence for instance PSO. The main intention for a firefly's flash is to function as a indication structure to exert a pull on other fireflies. The intensity (I) of flashes diminishes as the distance (r) augments and thus the majority of the fireflies can correspond barely up to quite a few hundred meters.

The Firefly Algorithm was based on the subsequent idealized activities of the flashing features of fireflies:

1. All fireflies are unisexual, so that one firefly will be engrossed to all other fireflies;
2. The degree of attractiveness depends on their brightness, and for any two fireflies, the firefly with lesser brightness will be engrossed by the firefly with higher brightness; on the other hand, the brightness can reduce as their distance increases.
3. It will move indiscriminately if there are no fireflies brighter than a given firefly.

The pseudo code of the FFA can be formulated depending on these three idealized conventions.

Pseudo Code of the Firefly Algorithm:

Define Objective function
Generate initial population of fireflies;
Define light intensity;
Describe absorption coefficient γ;
While (TG<Max No. of Generations)
For r = 1 to n (all n fireflies);
For s=1 to n (all n fireflies)
If ($I_r > I_s$), move firefly i towards j;
End if
Determine new solutions and update the
value of light intensity;
End for s;
End for r;
Rank the fireflies and find the current best;
End while;
Post process results and visualization;
End procedure;

The brightness of the firefly is found out by the fitness function. FFA has two major advantages over other optimization techniques: ability of dealing with multimodality and the automatic subdivision. Initially, FFA depends on attraction and attractiveness decreases with distance. Secondly, this subdivision permits the fireflies to be capable of finding all optima concurrently if the size of the population is adequately superior to the number of modes. FFA primarily creates a swarm of fireflies positioned arbitrarily in the search space. Preliminary allocation is generally formed from a standardized indiscriminate allocation and the location of each firefly in the search space exemplifies a probable solution of the optimization problem.

V. SIMULATION RESULTS

The Firefly Algorithm has been applied to determine the suitable location of the FACTS device for IEEE 57-bus system using MATLAB software. Simulation results obtained are compared with PSO. The standard IEEE 57-bus system has 41 transmission lines and six generator buses (Bus No 2, 3, 6, 8, 9 and 12). Table 1 shows the application results in terms of the position and size of the SVC device and the ensuing transmission losses. For the appropriate position and size of FACTS device, the reactive power generation is lesser in FFA method when compared to PSO. Table II shows the voltage profile under different load conditions determined using FFA and PSO and it is observed that there is an improvement of voltage profile of the system after reactive power compensation by means of Firefly Algorithm. The system load was increased gradually from the base case for this purpose. The system was loaded from its base case up to load factor (L.F) of 1.4 in FFA and PSO. The total active and reactive power losses, total active and reactive power generation of the system, reactive power generation of each generator, size and bus position of SVC device are presented in Table I. In FFA algorithm, the reactive power generation is lesser than the PSO algorithm for the appropriate size and location of FACTS device. The transmission line losses in FFA method are relatively lesser than the PSO method.

TABLE I. Reactive Power Optimization Results Under Different Load Conditioned In FFA & PSA Algorithm

	L.F	Q_{g2} (MVAR)	Q_{g3} (MVAR)	Q_{g6} (MVAR)	Q_{g8} (MVAR)	Q_{g9} (MVAR)	Q_{g12} (MVAR)	Q_{gT} (MVAR)	Q_{TLoss} (MVAR)	P_{gT} (MW)	P_{TLoss} (MW)	Size of SVC (MVA)	Location (Bus No)
	1	0.891	-0.97	10.124	72.75	-	145.89	345.81	158.78	1224.69	24.69	43.676	7
	1.1	8.342	-0.679	-6.783	64.85	2.014	124.73	365.91	181.46	1231.46	28.036	99.352	12
FFA	1.2	9.147	43.568	20.136	80.14	-	152.47	487.48	287.10	1262.76	62.368	129.458	16
	1	0.775	-0.47	4.369	63.52	-	121.58	324.78	155.83	1223.56	27.76	52.374	9
	1.1	7.437	-0.445	-3.301	50.14	1.854	110.56	341.41	177.90	1226.94	31.142	115.785	15
PSO [15]x `	1.2	7.132	39.175	12.047	77.47	-	136.71	463.01	283.02	1260.80	65.006	150.766	15

TABLE II. Voltage Profile at Different Buses in FFA and PSO Algorithm under Different Load Conditions

Bus No	L.F = 1		L.F = 1.1		L.F = 1.2	
	PSO[15]	FFA	PSO[15]	FFA	PSO[15]	FFA
1	1.04	1.04	1.04	1.04	1.04	1.04
2	1.01	1.01	1.01	1.009	1.01	1.01
3	0.985	0.984	0.985	0.983	0.985	0.978
4	0.9786	0.9775	0.9785	0.9767	0.976	0.965
5	0.9758	0.9747	0.9756	0.9732	0.973	0.969
6	0.98	0.977	0.98	0.979	0.98	0.976
7	0.9832	0.9830	0.992	0.990	0.992	0.984
8	1.005	1.003	1.005	1.002	1.005	1.002
9	0.98	0.975	0.98	0.978	0.97	0.965
10	0.988	0.976	0.9886	0.9868	0.97	0.959
11	0.9771	0.9761	0.9772	0.9765	0.962	0.955
12	1.015	1.0132	1.015	1.009	0.995	0.984
13	0.9821	0.9813	0.9837	0.9821	0.967	0.948
14	0.9748	0.9722	0.9774	0.9769	0.962	0.958
15	0.9909	0.9901	0.9924	0.9913	0.982	0.971
16	1.0134	1.0124	1.0126	1.0124	0.99	0.987
17	1.0175	1.0165	1.0163	1.0159	0.999	0.995
18	0.9777	0.9697	0.9776	0.9765	0.972	0.969
19	0.9612	0.9572	0.9694	0.9679	0.957	0.949

20	0.9639	0.9628	0.9777	0.9759	0.965	0.958
21	1.0227	1.0216	1.0487	1.0468	1.038	1.027
22	1.0263	1.0234	1.0538	1.0527	1.043	1.039
23	1.0242	1.0145	1.0583	1.0546	1.049	1.038
24	1.0045	1.0021	1.1507	1.1490	1.173	1.168
25	0.9713	0.9697	1.0824	1.0817	1.091	1.087
26	0.9632	0.9642	1.0906	1.0870	1.11	1.105
27	0.9816	0.9743	1.0428	1.0411	1.049	1.037
28	0.9951	0.9871	1.0324	1.0317	1.035	1.029
29	1.0076	1.0069	1.0309	1.0299	1.0318	1.0295
30	0.9579	0.9567	1.0583	1.0578	1.0623	1.0591
31	0.9475	0.9469	1.0199	1.0178	1.014	1.009
32	0.9857	0.9843	1.0141	1.0125	1.0021	1.0017
33	0.9835	0.9829	1.0119	1.0112	0.9995	0.9981
34	1.0217	1.0203	0.9964	0.9958	0.9752	0.9749
35	1.031	1.029	1.0014	1.0009	0.9808	0.9799
36	1.0264	1.0259	1.0098	1.0089	0.9905	0.9894
37	1.0265	1.0234	1.0184	1.0175	1.0006	1.0039
38	1.0311	1.0294	1.0464	1.0435	1.0331	1.0289
39	1.0241	1.0235	1.016	1.0156	0.9976	0.9864
40	1.0226	1.0216	1.0061	1.0049	0.9863	0.9755
41	1.0117	1.0127	1.0053	1.0028	0.9865	0.9814
42	0.9879	0.9866	0.9792	0.9763	0.9553	0.9497
43	1.0161	1.0129	1.0143	1.0129	0.998	0.993
44	1.032	1.029	1.0442	1.0439	1.0315	1.0295
45	1.0446	1.0435	1.051	1.047	1.0432	1.0387
46	1.0691	1.0595	1.0753	1.0689	1.0613	1.0598
47	1.0465	1.0395	1.0561	1.0514	1.0416	1.0399
48	1.0418	1.0438	1.053	1.049	1.0384	1.0376
49	1.0478	1.0469	1.0558	1.0539	1.0389	1.0358
50	1.032	1.029	1.0367	1.0323	1.0151	1.0124
51	1.0555	1.0499	1.0568	1.0557	1.036	1.028
52	0.9703	0.9692	0.9871	0.9852	0.9779	0.9758
53	0.9569	0.9487	0.9704	0.9691	0.9569	0.9553
54	0.9879	0.9797	0.9952	0.9940	0.9824	0.9793
55	1.0279	1.0236	1.0295	1.0278	1.0193	1.0175
56	0.9938	0.9925	0.9843	0.9839	0.9608	0.9597
57	0.9932	0.9879	0.9833	0.9829	0.9595	0.9573

VI. CONCLUSION

In this paper firefly algorithm has been applied to recognize the best possible locations of SVC device and their parameter with the purpose of minimizing the voltage deviations to improve the load bus voltage profile. Application results reveal that the recognized size and location of SVC device reduce the network real power loss. It is feasible that with the application of firefly algorithm can result in the minimization of the active power losses and proper implementation of power system planning and operation.

VII. REFERENCES

[1] Stephen Frank, Ingrida Steponavice, Steffen Rebennack,"Optimal power flow: a bibliographic survey I Formulations and deterministic methods", Springer Journal of Energy Systems, Vo1. 3, No. 3, pp.221-258, 2012.

[2] Abbas Rabiee, Maziar Vanouni, Mostafa Parniani, "Optimal reactive power dispatch for improving voltage stability margin using a local voltage stability index", International Journal of Energy Conversion and Management, Vol. 59, pp.66-73, 2012.

[3] Youcef Amrane, Mohamed Boudour , Messaoud Belazzoug, "A new Optimal reactive power planning based on Differential Search Algorithm", International Journal of Electrical Power and Energy Systems, Vol. 64, pp. 551-561, 2015.

[4] K.L. Lo, S.P. Zhu, "A decoupled quadratic programming approach for optimal power

dispatch", Electric Power System Research., Vol. 22, pp.47-60, 1991.

[5] Edimar J. Oliveira, Leonardo W. Oliveira, J.L.R. Pereira, Leonardo M. Honório, Ivo C. Silva Junior, A.L.M. Marcato, "An optimal power flow based on safety barrier interior point method", International Journal of Electrical Power and Energy Systems,Vol.64, pp.977-985, 2015.

[6] Youcef Amrane, Mohamed Boudour, Ahmed Amine Ladjici, Ali Elmaouhab, "Optimal VAR control for real power loss minimization using differential evolution algorithm", International Journal of Electrical Power & Energy Systems, Vol. 66, pp.262-271, 2015.

[7] Abbas Ketabi, Ahmad Alibabaee, R. Feuillet, "Application of the ant colony search algorithm to reactive power pricing in an open electricity market," International Journal of Electrical Power & Energy Systems, vol.32, pp. 622-628, 2010.

[8] D. Devaraj, J. Preetha Roselyn, "Genetic algorithm based reactive power dispatch for voltage stability improvement", International Journal of Electrical Power & Energy Systems, Vol. 32, pp. 1151-1156, 2010.

[9] Bhaskar Kanna, Sri Niwas Singh,"Towards reactive power dispatch within a wind farm using hybrid PSO", International Journal of Electrical Power & Energy Systems, Vol. 69, No. 7, pp.232-240, 2015.

[10] Gonggui Chen, Lilan Liua, Peizhu Songd, Yangwei Dua, "Chaotic improved PSO-based multi-objective optimization for minimization of power losses and L index in power systems", International Journal of Energy Conversion and Management, Vol. 86, pp.548-560, 2014.

[11] R. Arul , G. Ravi, S. Velusami, "Solving Optimal Power Flow Problems using Chaotic Self-adaptive Differential Harmony Search Algorithm", Electric Power Components and Systems, Vol.41, pp.782-805, 2013.

[12] A. Ananthi Christya, P. Ajay D. Vimal Raj," Adaptive biogeography based predator–prey optimization technique for optimal power flow", International Journal of Electrical Power & Energy Systems, Vol. 62, pp.344-352, 2014.

[13] Mojtaba Ghasemia, Mahdi Taghizadeha, Sahand Ghavidela, Jamshid Aghaeia, Abbas Abbasianb, "Solving optimal reactive power dispatch problem using a novel teaching–learning-based optimization algorithm", Engineering Applications of Artificial Intelligence, Vol. 39, pp.100-108, 2015.

[14] X. S. Yang, "Nature-Inspired Meta-Heuristic Algorithms", 2nd ed., Beckington, Luniver Press, 2010.

[15] Subramanian Annamalai, Ravi Govinthasamy, "Voltage Collapse Enhancement and Loss Reduction by Reactive Power Reserve", International Journal of Computer Applications, Vol.12, Issue.12, pp. 32-42, 2011.

[16] N.Karthik, R.Arul, A.K.Parvathy, "Firefly Algorithm based Reactive Power Optimization", International Journal of Applied Engineering Research, Vol.10, Issue.77, pp. 514-520, 2015.

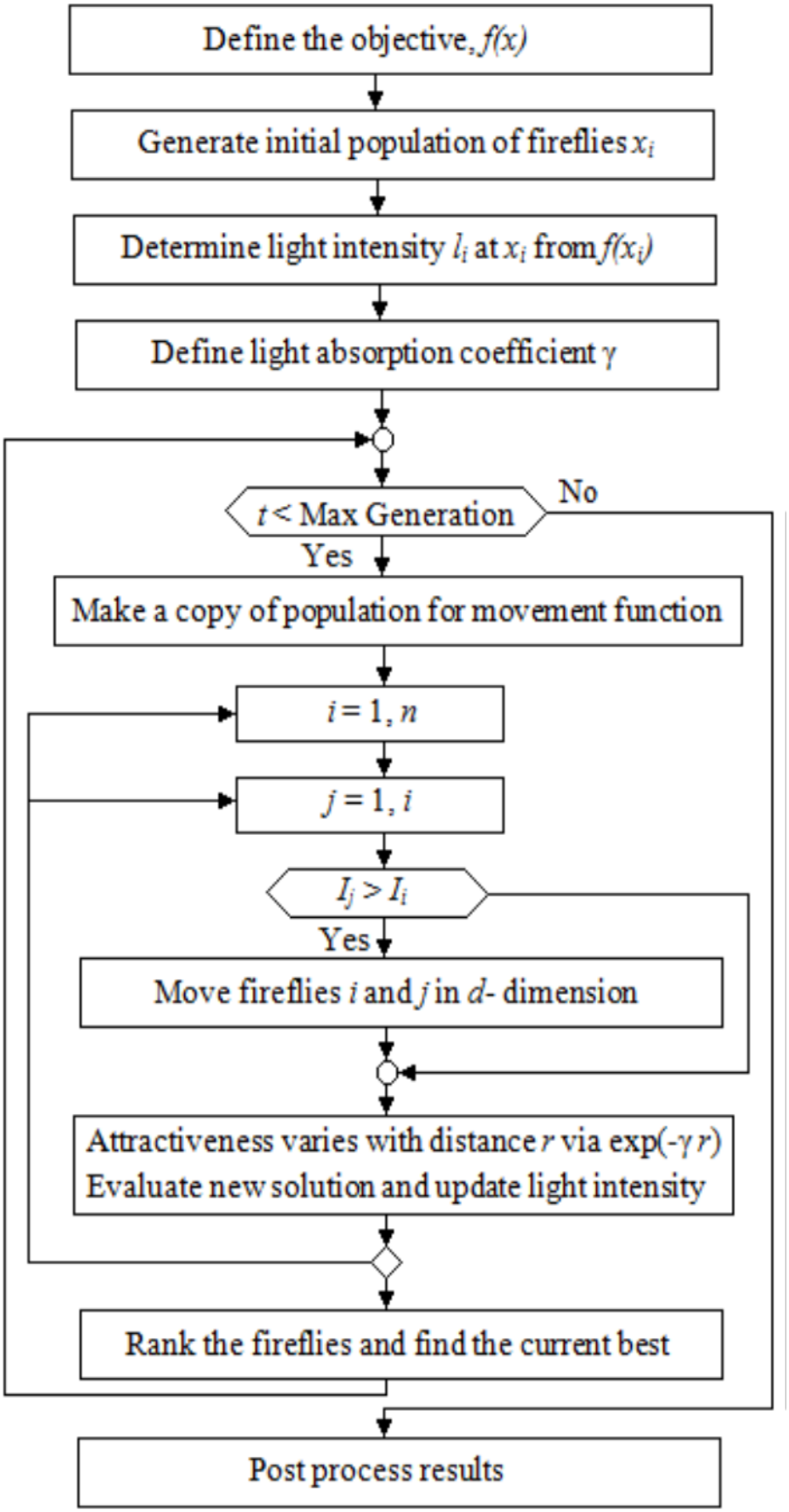
Define the objective, f(x)
Generate initial population of fireflies x_i
Determine light intensity l_i at x_i from $f(x_i)$
Define light absorption coefficient γ
t < Max Generation
No
Yes
Make a copy of population for movement function
i = 1, n
j = 1, i
$I_j > I_i$
Yes
Move fireflies i and j in d- dimension
Attractiveness varies with distance r via exp(-γ r)
Evaluate new solution and update light intensity
Rank the fireflies and find the current best
Post process results

Themed Section : Engineering and Technology
© 2018 IJSRSET | Volume 5 | Issue 3 | Print ISSN: 2395-1990 | Online ISSN: 2394-4099

Internet of Things for Smart Cities

B.Sreenidhi[1]
[1]Department of Electronics and Communication Engineering, Velammal Institute of technology, Panchetti, India

ABSTRACT

With the development of smart meters, similar to the Sophisticated Metering Infrastructure (SMI), and the Internet of Things (IoT), each smart city is outfitted with different sorts of electronic gadgets. Along these lines, hardware and innovations empower the different parts of urban communities more available and relevant. The objective of the present paper is to give a comprehensive audit on the idea of the smart city besides their diverse applications, advantages, and points of interest. In addition, the vast majority of the possible IoT advancements are presented, and their abilities to converge into and apply to the diverse parts of smart cities are talked about. The potential use of smart cities regarding innovation improvement in the future gives another significant discourse in this paper. In the mean time, the key boundaries to its usage are thoroughly expressed.

Keywords: Cloud Platform; Internet of Things (IoT); Smart City; Exact Response

I. INTRODUCTION

In view of the quick ascent of the population density inside urban situations, substructures and administrations have been expected to supply the necessities of the citizens. As needs be, there has been an amazing development of advanced gadgets, for example, sensors, actuators, cell phones and brilliant machines which drive to huge business goals of the Internet of Things (IoT), on the grounds that it is conceivable to interconnect all gadgets and make interchanges between them through the Internet. The IoT archetype is in the power of smart and self-configuring devices, which are well linked together by global grid infrastructures. IoT can be typically defined as a real object, largely dispersed, with low storage capabilities and processing capacities, while aiming at enhancing reliability, performance and security of the smart cities as well as their infrastructure.

The IoT archetype is in the power of smart and self-configuring devices, which are well linked together by global grid infrastructures. It can be typically defined as a real object, largely dispersed, with low storage capabilities and processing capacities, while aiming at enhancing reliability, performance and security of the smart cities as well as their infrastructure. On this basis, in the present paper, a survey of the IoT-based smart cities information from related reports is conducted. The IoT consists of three layers, including the perception layer, the network layer, and the application layer. The perception layer includes a group of Internet-enabled devices that are able to perceive, detect objects, gather and exchange information with other devices through the Internet communication networks. Radio Frequency Identification Devices (RFID), cameras, sensors, Global Positioning Systems (GPS) are some examples of perception layer devices. Forwarding data from the perception layer to the application layer under the constraints of devices' capabilities, network limitation

and the applications' constraints is the task of the network layer. IoT systems use a combination of short-range networks communication technologies such as Bluetooth and ZigBee, which are used to carry the information from perception devices to a nearby gateway, based on the capabilities of the communicating parties. Internet technologies such as WiFi, 2G, 3G, 4G, and Power Line Communication (PLC) carry the information over long distances based on the application. Since applications aim to create smart homes, smart cities, power system monitoring, demand-side energy management, coordination of distributed power storage, and integration of renewable energy generators, the last layer which is the application layer, is where the information is received and processed. Accordingly, we are able to design better power distribution and management strategies.

II. IoT TECHNOLOGIES IN SMART CITIES

The IoT is a broadband network which employs standard communication protocols, whereas the Internet would be its convergence point. The major idea of the IoT is the extensive presence of objects which are able to be measured and inferred, as well as it is able to modify the situation. Accordingly, IoT is employed by the expansion of several things and communication equipment. Things in the IoT involve smart equipment such as mobile phones and other facilities including foodstuff, appliances and landmarks that can collaborate to achieve a joint objective. The main characteristic of the IoT is its effect on consumers life. In the concept of IoT, since the cabling cost for millions of sensors is expensive, the communication between sensors should be wireless. Low-power standard communication is suitable for interconnection among many devices. According to location and distance coverage, some networks are introduced as follows.

Home Area Networks (HAN) which use short-range standards like, ZigBee, Dash7, and Wi-Fi. All monitoring and control components in a home are connected by the HAN.

Wide Area Networks (WAN), provide communication between customers and distribution utilities which require much broader coverage than HAN and for implementation needs fiber cable or broadband wireless like 3G and LTE.

1)Radio-Frequency Identification (RFID)

RFID including readers and tags has a vital task in the framework of the IoT. Employing the technologies on each related thing, accomplishing their automatic identification and dedicating the single digital identity to any of the things will be possible, to include the network associated with the digital information and services. RFID provides some applications in smart grids, including tracking and localization of objects, healthcare applications, parking lots and asset management. Each tag can be as a sensor because they have not only data which is written manually but also capture data like environmental information.

2)3G and Long Term Evolution (LTE)

3G and LTE are standards for wireless communication for mobile phones and data terminals. Regarding the development and expansion of wireless communication infrastructures, LTE and 3G are available everywhere, even in third world countries. This technology is for broadband connectivity and designed for short-range uses. Hence, it is applied for WANs, which require longer distance ranges. Nevertheless, there are some barriers to their implementation that should be addressed. High data cost due to providing this service by the service providers, and inability to use them for communication among billion devices are some of the problems of these services.

3)ZigBee

In the sensor nodes, ZigBee is applied as a low-power and low-cost wireless communication technology. It is suitable for creating wireless

personal area networks (WPAN) such as home automation, medical device collection and other low power, low-bandwidth. Some of its applications include wireless light switches, electrical meters, and traffic management systems. ZigBee is suitable for limited ranges, coverage of city region and supporting billions of devices. With the ZigBee-based network, a mechanism for transmission of IPv6 packets is specified. To apply ZigBee, additional equipment usually is required involving a coordinator, router and ZigBee end-devices.

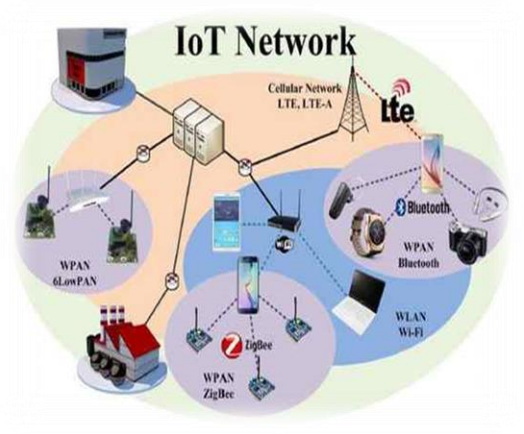

Figure 1: IoT Network

III. SMART CITIES PLATFORM AND STANDARDS

The relationship between the physical and IT infrastructure constructs a novel machine-to-machine (M2M) communication for smart cities which along with new features of network drives smart cities communication platforms. These platforms help to cover the communication requirements between heterogeneous access technologies and application suppliers. Moreover, these platforms help form the IoT with real world sensors and communication networks

Figure 2: IoT for Smart City

IV. ACTUAL APPLICATIONS OF IOT IN SMART CITIES

The IoT utilizes the Internet to combine different heterogeneous things. In like manner and for giving ease access, every single existing thing must be connected to the Internet. The justification behind this is smart urban communities incorporate sensor systems and association of insightful machines to the web is fundamental to remotely screen their treatment, for example, control use checking to enhance the power utilization, light administration, aeration and cooling system administration. To get this point, sensors can be stretched out at different areas to assemble and investigate information for usage change . Figure 3 shows the significant uses of the IoT for a shrewd city. The key points in this field of information are communicated in the accompanying subsections.

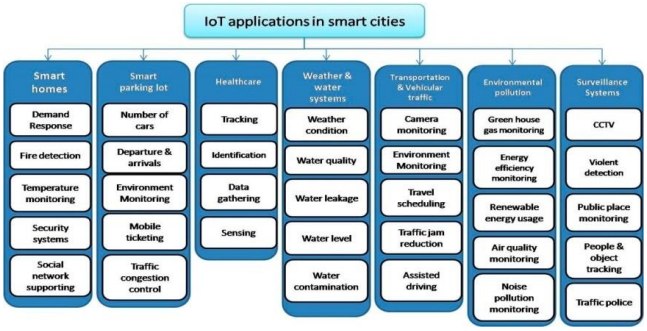

Figure 3. Significant Applications of IoT in Smart Cities

A. Smart Homes

IoT innovation prompts having brilliant houses and applications including smart TV's, home security framework, lighting control, fire discovery, and temperature checking. The sensors of this apparatuses screen the conditions and condition and send reconnaissance information to a focal controller at home which empowers the householder to persistently screen and control the home even from outside and settle on the best choice under each situation. In like manner, these observation information help to anticipate future occasions to be set up ahead of time by taking an effective estimation to counteract losing accommodation, security, solace and elevated

requirement of living. Besides, smart houses in an area can be associated together through Neighbor Area Network (NAN). For this situation, houses can share some survey information like outside camera to discover report occasions to a police headquarters. Human services, overseeing shared assets, and empowering bolster person to person communication are different uses of the brilliant groups. Consequently, this idea isn't just association of neighbors yet in addition expansion and improvement of a thorough brilliant city which can monitor and control entire activities in a smart city.

B. Smart Parking

By empowering keen stopping, arriving and withdrawing times of various transports are followed everywhere throughout the city. In this manner, these parking garages must be arranged in such an approach to consider various vehicles in each location. Besides, new parking garages must be set up where there are more vehicles. Appropriately, the information of smart parking areas can give benefits to the customers and traders day-by-day lives in the smart urban areas. This administration works in light of street sensors and smart presentations, which lead drivers to the best way to park in the city. A few advantages of this administration are finding a parking area faster, which implies less CO emanations from the vehicles, lesser movement blockage, and more contented citizens. It can be coordinated into urban IoT frameworks. Besides, by short-run correspondence innovations like RFID and NFC, it is conceivable to understand an electronic confirmation of stopping grants and considers offering better administrations to nationals.

C. Surveillance Systems

Surveillance is the most noteworthy component of the smart cities from the resident's perspective. To this end, the whole city must be continually checked and watched, yet assessing the data and finding criminal acts are profoundly testing. Conventional Closed Circuit Television (CCTV) frameworks give a foundation to brilliant observation frameworks duals activities to locate any brutal demonstration and even identify the general population. Hence surveillance system plays a vital role in smart cities.

D. Smart Energy and Smart Grids

The usage of the IoT allows smart management and control of energy distribution as well as consumption in diverse conditions. The IoT node has various capabilities like sensing and networking that increase the probability of optimum development of energy providers. This management can be developed for emergency circumstances. Applying these methods will lead to reliability improvement, power quality enhancement and profit growth.

Figure 4: Various Applications of IoT for Smart Cities

V. CONCLUSION

Although a conclusion may review the main points of the paper, do not replicate the abstract as the conclusion. A conclusion might elaborate on the importance of the work or suggest applications and extensions. Authors are strongly encouraged not to call out multiple figures or tables in the conclusion these should be referenced in the body of the paper.

VI. CHALLENGES

This section presents the current challenges for the implementation of IoT-based smart cities.

Figure 5: Challenges in IoT

(i)Sensor Networks

Sensor network can be considered as an extraordinary innovation for empowering the IoT. They can shape the world by giving the capacities of estimating, deriving, and understanding ecological lists. Current advancement and change in advances have given productive and modest gadgets to applying to expansive scale remote detecting uses. Besides, cell phones contain different sorts of sensors and, therefore, they enable various types of versatile utilizations in various territories of the IoT. For this reason, the principle testing activity can be done by the means by which the extensive scale data of the sensors with respect to vitality and system limitations are protected.

(ii)Security and Privacy

When all the information is gathered and evaluated in the same IoT platform, the system may confront numerous attacks such as cross-site scripting, and side-channels. Moreover, the system can be subjected to significant vulnerabilities. In addition, its multi-tenancy may lead to the security problems as well and result in data leakage. Therefore, cities must adopt serious measures to ensure the privacy and security of citizen data. Without this guarantee, citizens cannot trust to government, and the colection of the information will be difficult. All systems should be resistant against cyber-attacks, particularly the critical infrastructure like smart meters. As a result, for successful implementation of IoT, cities should place privacy and security as a top priority. Some aspects of security in IoT including privacy, trust and data confidentiality as well as their solutions are presented.

(iii)Legal and social aspects

The IoT framework likely is an administration as per the client gave information. For such terms, the specialist organizations must be founded on different neighborhood and universal standards. Similarly, the candidates are looked with adequate information to go to a predefined situation and information gathering. It would be more agreeable if the open door were given to the candidates to pick and take an interest in the enlistment data that demonstrates an occasion for safe interactions.

VII. CONCLUSION

The significance of thinking about how new ideas and innovations (particularly the IoT) advantage brilliant urban areas is obvious. The point of this audit article was to investigate variation particulars and highlights of IoT frameworks, alongside the proficient motivators for using them. Since the achievement of the IoT substructures can empower a volume of chances for smart cities, to begin with, the most critical research inspirations were communicated and thereafter, a few fundamental and accommodating applications clarified. It was delineated how day by day exercises could be expanded and enhanced through utilizing them. In like manner, the difficulties emerging from actualizing the IoT framework were appropriately delineated. Regarding this matter, the joining of the IoT stage into other autonomous and smart systems to give a smart and far reaching usage is a standout amongst the most intriguing future inclinations. Also, furnishing an approach to adapt to some essential difficulties, for example, the protection privileges of the clients/inhabitants, is as yet a territory of research intrigue. A portion of the improvements in the real usage of smart over the world were introduced, which can be considered as tests or pilot ventures for future exhaustive smart cities. The IoT through its usefulness and determinations ought to without a doubt utilize savvy frameworks and sensors to guarantee consumers rights.

VIII. REFERENCES

[1] Jaradat, M.; Jarrah, M.; Bousselham, A.; Jararweh, Y.; Al-Ayyoub, M. The Internet of Energy: Smart Sensor Networks and Big Data Management for Smart Grid. Procedia Comput. Sci. 2015, 56, 592–597

[2] Rathore, M.M.; Ahmad, A.; Paul, A.; Rho, S. Urban planning and building smart cities based on the Internet of Things using Big Data analytics. Comput. Netw. 2016, 101, 63–80

[3] Zhu, C.; Leung, V.C.M.; Shu, L.; Ngai, E.C.H. Green Internet of Things for Smart World. IEEE Access 2015, 3, 2151–2162

Themed Section : Engineering and Technology
© 2018 IJSRSET | Volume 5 | Issue 3 | Print ISSN: 2395-1990 | Online ISSN : 2394-4099

Audio Transmission through Free Space Optics using Visible Light

M. Mohana Krishnan[1], G. S. Sudharsana Prasad[1], Dr. M. Gulam Nabi Alsath[1], R.Balaji[1], S.Logesh[1]
[1]Electronics and Communication Engineering, Sri Sivasubramanya Nadar College of Engineering, Kancheepuram, Tamil Nadu, India

ABSTRACT

With FSO communication, maximum data transfer rates up to 2.5 Gbps is possible, unlike the maximum data transfer rates of 622Mbps offered by RF communication systems. Using air as a medium FSO technology can transmit voice, video and data. Transmission using FSO technology is relatively simple. In this paper, we propose a prototype of audio transmission system using inexpensive commercially available LASER. Experimental result shows that high quality audio can be transmitted with maximum distance of 6 m. Careful considerations can make it an attractive alternative to introduce in the market for applications like communication among buildings within a large campus and other indoor and short distance outdoor places without the complexities of cables.

Keywords: Visible Light Communication, LASER, Audio Broadcasting System, Attractive Alternative Communication

I. INTRODUCTION

FSO provides point to point and point to multipoint transmission of communication information by using air as medium and optical signal as it carrier. It has drawn attention in telecommunication industry, due to its cost effectiveness – easy installation, quick establishment of communication link. The range of frequencies where it operates makes FSO communication free from licensing. G. Anandhi et al [1] first analyzes various issues with current wireless communication systems, and discusses how visible light communications can resolve these issues. G. Subba Rao et al [2] has theoretically investigated the transmission performance of the FSO system. It is shown that the system can be used for providing high speed data rate and for free space optical communication networks, extending broadband connectivity to remote areas. Luanxia Yang et al [3] has proposed FSO communication systems using OOK and source information transformation. It was shown that such systems can achieve good BER performance without the need for knowledge of the instantaneous CSI and PDF of the turbulence model. They have derived an analytical expression for the PDF of the detection threshold and developed a tight upper bound on the average BER. Manish Sharma et al [4] have evaluated the performance of a ground-to ground FSO. The average bit error rate of their configured architectures is also evaluated under different turbulence conditions. The performance of these reconfigured architectures slightly degrades in comparison to the basic architecture.

M. J. Lok et al [5] - theoretical and numerical analyses have been carried out to study the capability of FSO communication system under atmospheric turbulent channel. It possesses advantages over RF technology such as lower power consumption. It also reveals the relationship between the scintillation index and the strength of turbulence. Modulation and signaling formats have been verified to FSO system

performance by measuring the BER during the propagating along FSO channel under atmospheric turbulence. Under weak turbulence, PSK modulation format offers the best performance by obtaining the lowest BER at the lowest. Thus FSO technology facilitates an optimal solution, bandwidth scalability, speed of deployment (hours versus weeks or months), re-deployment and portability, and cost- effectiveness (on average, one-fifth the cost of installing fiber-optic cable).

II. FSO OPERATION

A Free Space Optical transmission system is one form of wireless communication system designed for the interconnection of two points which have a direct line of sight. The carrier that is used for the transmission of this signal is Infrared and it can be generated by either high power LED or laser diode. The basic principles for the transmission of a signal along a fiber are the same as for transmission through free space.

III. FSO OVER OTHER MODES OF COMMUNICATION

The increasing demand for high bandwidth in metro networks and service providers' pursuit of a range of applications, including metro network extension, firm LAN-to-LAN connectivity, wireless backhaul and many more are relentless. This imbalance is often referred to as the "last mile bottleneck." Service providers are put in the situation where they have to provide services quickly and cost-effectively. But the last mile bottleneck is only part of a larger problem. Similar issues exist in other parts of the metro networks. The connectivity bottleneck is everywhere in metro networks.

Parameters	FSO	Optical Fiber	Microwave Radio	Coaxial Cable
Installation	Moderate	Difficult	Difficult	Moderate
Data Rate	Gbps	Independent	Mbps	Mbps
Security	Good	Very Good	Poor	Good
Connectivity	P2P, P2MP Short And Long Reach	P2P, P2MP Short And Long Reach	P2P Short Reach	Multidrop Short Reach
Maintenance	Low	Low	Low	Moderate
Spectrum License	Not Required	Required	Required	Required

Table 1 represents comparison of FSO over other modes of Communication. Firstly, the most obvious choice is fiber-optic cable. Without a doubt, fiber is the most reliable means of providing optical communications. But the digging for laying fiber and associated costs to lay fiber to establish connection often make it economically prohibitive.

Second option is the radio frequency (RF) technology. Though RF based communication for long distance communication, RF-based networks require large capital investments to acquire spectrum license. RF technologies cannot scale and the bandwidth is limited to 622 megabits.

The third alternative is wire and copper based technologies. The biggest hurdle is bandwidth scalability. Copper technologies may ease some short-term pain, but the bandwidth limitations of 2 to 3 Megabits, which makes them a marginal solution.

Fourth and finally, the most viable-alternative is FSO. The technology facilitates an optimal solution, bandwidth scalability, speed of deployment and cost-effectiveness (on average, one-fifth the cost of installing fiber-optic cable).

IV. WORKING OF FSO

The Figure 1 represent general block diagram of FSO. The transmitter consists of electrical input, which is the input from the user, followed by modulator; the modulation scheme is selected by the user based on the

application. Now the signal is converted from electrical to optical and is transmitted by using light source (i.e.) LED or Laser. The receiver consists of photo detector which detects the transmitted signal and converted the received optical signal into electrical signal for processing. The converted electrical signal is given to demodulator to get back the original signal that is transmitted.

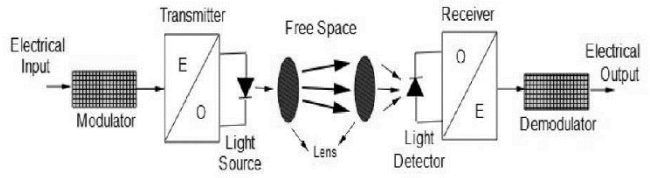

Figure 1. FSO Block Diagram

[Reference article : Loss Calculation in Free Space Optical Communications , Mr.G.Subba Rao et al. Int. Journal of Engineering Research and Application, Vol. 6, Issue 6, (Part -4) June 2016, pp.49-51]

V. DESIGN AND IMPLEMENTATION

Figure 2 represents the block diagram of FSO audio transmitter and receiver. The voice input from the mobile is given to 2N3904, the output of the previous section is amplitude modulated and converted into optical signal using optical source.

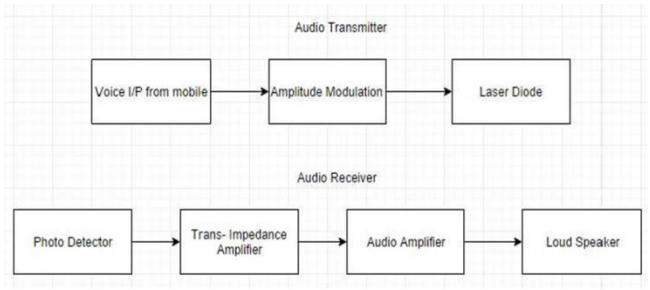

Figure 2. Block diagram of FSO Audio Transmitter and Receiver

The optical source used in this work is a laser diode that emits optical radiation at 635nm. Thus Amplitude Modulation technique is been applied to modulate the instantaneous power of the optical signal. We can even use a plano - convex lens after the Laser for better performance and mostly for low power Lasers with conventional beam divergence of 0.6 mrad. The modulated optical signal then passes through the atmosphere as a coherent beam. Figure 3 shows the Audio Transmitter circuit.

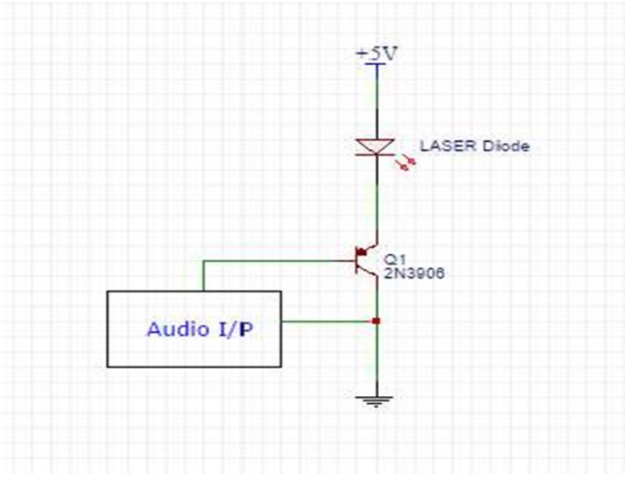

Figure 3. Audio Transmitter Circuit

The optical receiver, which is responsible for converting the optical signal into electrical equivalent and removing the effects of different noise sources through transmission and obtaining an exact replica of the transmitted signal, contains a photo detector. Figure 4 represents audio receiver circuit. The output from the optical detector should be amplified by a pre-amplifier. LM 741 is used for this purpose. The output of the previous section is given to LM386 an audio amplifier, and then this amplified signal is given to the loud Speaker.

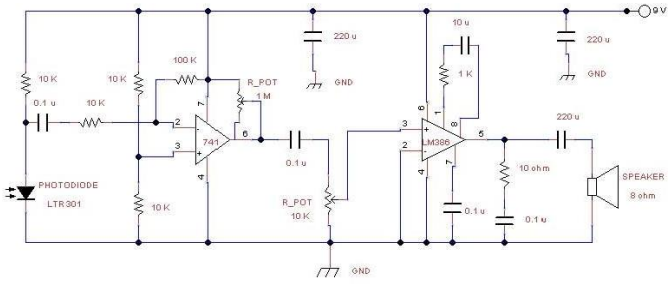

Figure 4. Audio Receiver Circuit

VI. HARDWARE IMPLEMENTATION

Figure 5 shows the hardware setup of FSO Audio Transmission System. It has to be noted that laser diode used has wavelength of 635 nm. In the setup shown above the transmitter uses simple BJT2N3904 which modulates the input voice signal from the mobile fed through the audio jack. The receiver

consists of a photodiode (LTR301); one of the common features of this photodiode is high sensitivity and wide range of collector current. Thus the received optical signal from the transmitter through air interface is converted from optical signal to its equivalent current signal. This is then given to IC741 which acts as a trans-impedance amplifier (current to voltage converter). The IC741 also boost the signal to certain level and it is given to the Audio amplifier - LM386 which further boosts the signal and the audio is played by the Loud speaker. The 10K potentiometer is connected between the output of IC741 and non-inverting input of LM386, by tuning this potentiometer we can able to vary the gain of the audio amplifier which in turn controls the volume of the Loud speaker.

VII. CONCLUSION AND FUTURE WORK

The proposed wireless technology which transmits data or sound signals from one point to another through a laser beam will be used in many applications in the near future. The system is safe since no hazardous radiation is emitted. The possibility of transmitting audio is presented in this work using simple, cheap and available elements. The (FSO) distance (range) between a working transmitter and receiver is 6 meters indoor, thus the designed system acts as a demonstration system which uses the benefits of the wireless laser communication. To increase the range of communication system, one can use beam expander, more powerful lasers and/or more sensitive detectors. The produced picture wasn't obvious because of the noise sources (internal noise and external noise).

Thus FSO can be used in:

Outdoor wireless access: it can be used by wireless service providers for communication and it requires no license to use the FSO as it is required in case of microwave bands.

Fiber backup: FSO can also be used as a backup link in case of failure of transmission through fiber link

Service acceleration: it can also be used to provide instant service to customers when their fiber infrastructure is being deployed in the meantime.

Military access: Since FSO System is a secure and undetectable system it can connect large areas safely with minimal planning and deployment time and is hence suitable for military applications. It can be used to communicate between point-to-point links and point to multipoint links.

VIII. REFERENCES

[1] G. Anandhi, J. Meera , I. Irudhayasuji , P. Anandhi, "Design of an intelligent data transmission technique over free space optics" in *International Journal of Advanced Research in Electronics and Communication Engineering* (IJARECE), vol. 4, Issue 4, Apr. 2015.

[2] G. Subba Rao, Hinsermu Alemayehu, Temesgen Bailie, Hari Hara P Kumar, "Loss calculation in free space optical communications" in *International Journal of Engineering Research and Application*, ISSN : 2248-9622, vol. 6, Issue 6, part 4, pp. 49-51, Jun. 2016.

[3] Luanxia Yang, Bingcheng Zhu, Julian Cheng, and Jonathan F. Holzman, "Free-space optical communications using on–off keying and source information transformation" in *Journal of Lightwave Technology*, vol. 34, no. 11, Jun. 1, 2016.

[4] Manish Sharma, D. Chadha, and Vinod Chandra, "High-altitude platform for free-space optical communication: performance evaluation and reliability analysis" in *Journal of Optical Communication Network*, vol. 8, no. 8, Aug. 2016.

[5] M. J. Lok, I. E. Lee, Z. Ghassemloo, and G. C. Chung, "Investigation on the error performance of modulation formats in free-space optical communication links with turbulences" in *10th International Symposium on Communication Systems, Networks and Digital Signal Processing* (CSNDSP), Apr. 2016.

Themed Section : Engineering and Technology
© 2018 IJSRSET | Volume 5 | Issue 3 | Print ISSN: 2395-1990 | Online ISSN: 2394-4099

Design of Shared Aperture Microstrip Patch Antenna Array For Conformal 5G Communications

G. S. Sudharsana Prasad*, K.Arun, M.Gulam Nabi Alsath
Electronics and Communication Engineering, Sri Sivasubramanya Nadar College of Engineering,Kalavakkam, Tamil Nadu, India
sudharsana14112@ece.ssn.edu.in[1]

ABSTRACT

This paper presents a conformal shared aperture microstrip 2 x 2 array antenna designed for dual-band operation at 38 and 60 GHz frequencies on a flexible substrate (Rogers RO4003c). The window shaped slot is designed to operate at 38 GHz and the patches placed inside the window shaped slot are designed to operate at 60 GHz. Corporate feeding is employed to excite the patches operating at 60 GHz. The proposed antenna can bend to fit any shape of wearable device since it is designed on a flexible substrate. Application of this SAA is in wearable devices operating in 5G communication system. The antenna design has been simulated using CST microwave studio and finally the simulation results are presented.

Keywords: Shared aperture, 5G communication, Conformal antenna.

I. INTRODUCTION

Presently, Wireless Communication is the fastest growing field of the Communication field. There are many government and commercial applications where weight, size, cost, performance, ease of installation, aerodynamic profiles are the major constraints. In the last few years, the development of 5G technology represented one of the principle interests in the information and Communication field. Also, in today's environment, technology demands antennas which can operate on different wireless bands and should have different features like low cost, minimal weight, low profile and are capable of maintaining high performance over the operating frequency ranges.

The technological developments in the communication and biomedical fields have increased the demand for wearable devices such as smart watches, smart bands, On-body health monitoring devices etc. This has led to the idea of flexible electronics where the devices are designed in order to comfortably fit on various body parts. In order to satisfy the demand for wearable devices, conformal antennas are also required. The developed conformal antenna design can be employed for wearable devices that work in 5G communication band.

The objective of the work is to develop an antenna for 5G communication. The upcoming 5G communication systems are designed to work in mmwave frequencies like 28 GHz, 37 GHz, 38 GHz and 60 GHz[1][2]. The attenuation due to water molecules in atmosphere is significant for signals at 38 GHz since water molecules absorb these signals. Similarly attenuation due to absorption of signal by atmospheric oxygen is high at 60 GHz. Thus both these frequencies can be used together to increase the

signal strength to a better level compared to that obtained using one single frequency band.

The paper is aimed at developing a conformal shared aperture microstrip 2 x 2 array antenna designed for dual-band operation at 38 and 60GHz frequencies on a flexible substrate (Rogers RO4003c). Two different radiators, viz. window shaped slot and square patch antenna share a common aperture. Thus, the proposed antenna operates at both 38 GHz and 60GHz frequencies which will aid in the increased signal strength required for 5G communication systems.

The organization of the paper is as follows. Section II of this paper describes the steps involved in design of the antenna and Section III illustrates the simulated antenna performance. Finally in Section IV, the conclusion is presented.

II. DESIGN

The basic design [3][4][5][6] is shown in Fig 1. The V-band patches are placed inside the K_a-band slot. This can be done since the ratio between 60 GHz and 38 GHz is such that the K_a-band slot can accommodate V-band patches inside it (frequency ratio between 60 and 38 GHz is about 1.57). In this case the K_a-band slot is large enough to house a 2 x 2 V-band array. The V-band patches are connected using corporate feeding technique which is then excited in the middle using coaxial probe. The K_a-band patch is excited using a coaxial probe again. The dimensions of the single array element is fixed to be 10 x 10 mm^2 in which 6.4 x 6.185 mm^2 is the area of the K_a-band slot and 1.26 x 1.26 mm^2 is the area of each V-band element inside the K_a-band slot. The radiators are designed on a 0.203-mm-thick lossy RO4003c substrate with dielectric constant 3.55 and dissipation factor 0.0027.

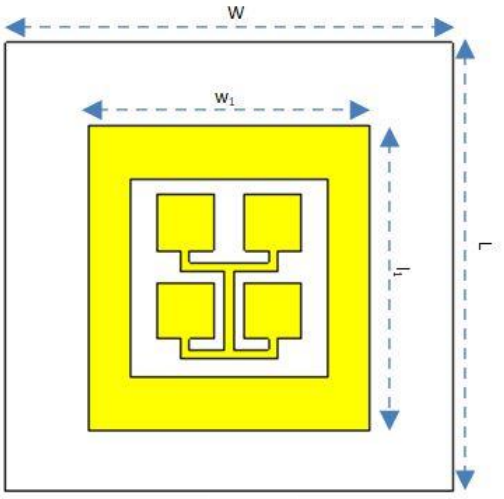

(a)

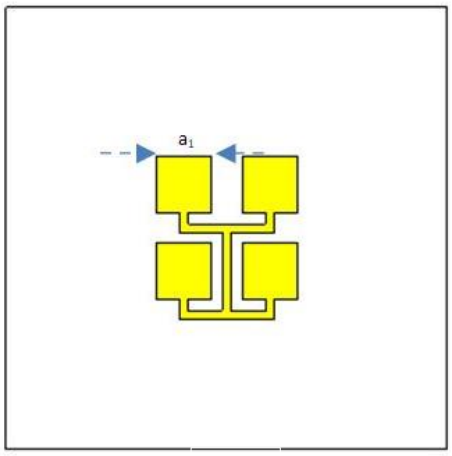

(b)

Figure 1. Proposed SAA element. (a) Array element consisting of K_a-band slot and 2 x 2 array of V-band patch. (b) 2 x 2 array of V-band patch corporate fed. L=10 mm, W = 10 mm, l_1 = 6.4 mm, w_1 = 6.185 mm, a_1 = 1.26 mm.

The antenna shown in Fig. 1 is then replicated to form a 4 x 4 array as shown in Fig. 2. This array is then bent in the form of a cylinder, to compare the characteristics of the antenna with the array element. Since the antenna is designed on a flexible substrate, the antenna's performance changes only by a small amount. The total area of the 2 x 2 antenna array is 20 x 20 mm^2.

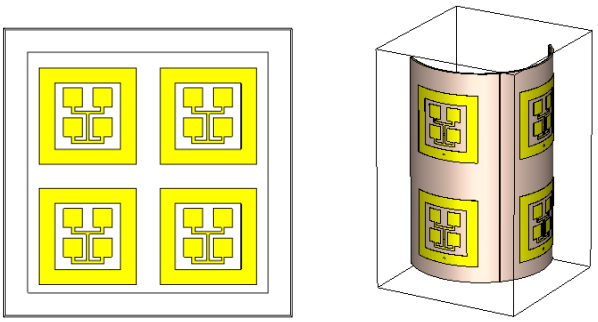

(a) (b)

Figure 2. Proposed Shared Aperture Antenna (SAA) array. (a) 2 x 2 Shared Aperture array before performing bend operation. (b) Array antenna after performing bend operation.

III.SIMULATION RESULTS

The proposed antenna was designed using CST microwave studio and the results obtained are discussed below. The slot radiating at 38 GHz was designed and simulated, the S-parameter characteristics for which is shown in Fig. 3

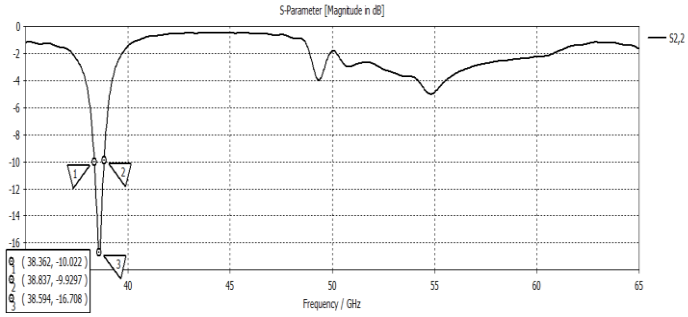

Figure 3. Simulated S-parameter characteristics of the Ka-band slot.

Similarly for the element radiating at 60 GHz, initially it was fed directly using coaxial probe and simulated to view its S-parameter plot. Then corporate feeding technique was employed in order to optimize the design and then simulated to observe its S-parameter characteristics. The S-parameter plot for the patch is shown in Fig. 4.

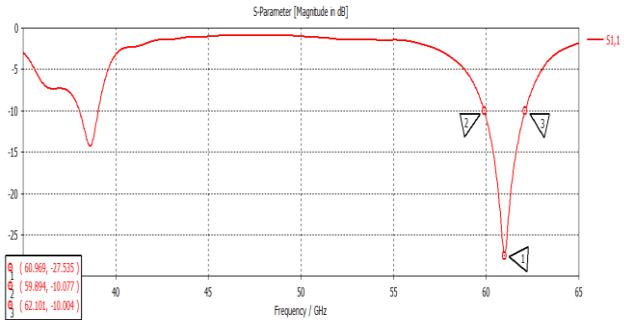

Figure 4. S-parameter characteristics of the 2 x 2V-band patch array

A. S-parameter characteristics of the proposed Shared Aperture Antenna array element

The optimum result was achieved after many design trials. The S-parameter characteristics of the array element are shown in Fig. 5. The Far-field radiation pattern shown in Fig. 6 and 7 show the radiation pattern of the antenna at 38 GHz and 60 GHz respectively.

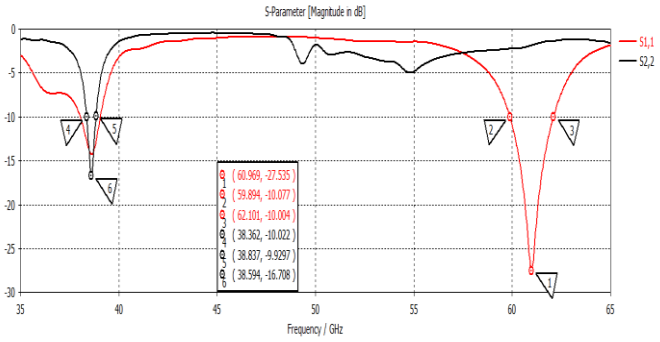

Figure 5. S-parameter characteristics of the radiating element of Shared aperture antenna array

B. Farfield Radiation Pattern Of A Single Array Element

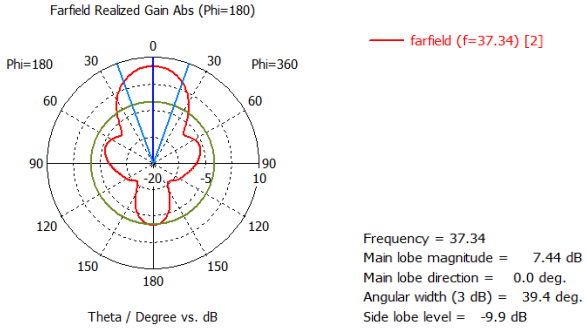

Figure 6. Farfield radiation pattern at 38 GHz

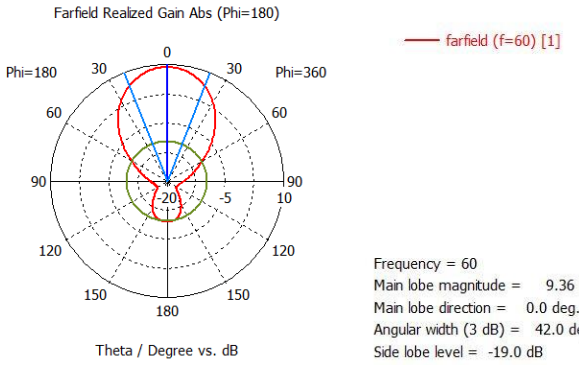

Figure 7. Farfield radiation pattern at 60 GHz

C. S-Parameter Characteristics Of Proposed Conformal Shared Aperture Antenna Array

At 38GHz, the return loss is below the acceptable value of -10dB from 38GHz to 39.1GHz and at 60GHz it is between 60 GHz to 62 GHz approximately.

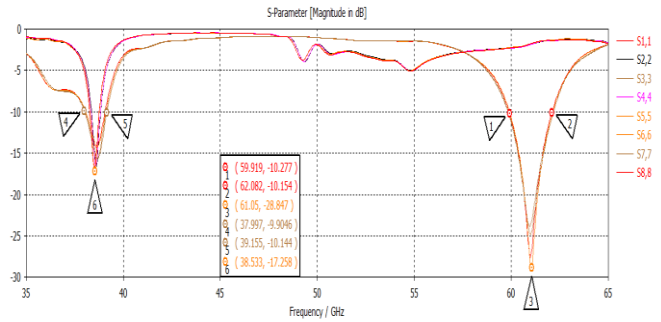

Figure 8. S-Parameter measured for Shared Aperture Array Antenna

D. Farfield Radiation Pattern Of The Array Antenna

The Farfield realized gain is around 7 dB at 38GHz and around 10 dB at 60GHz.

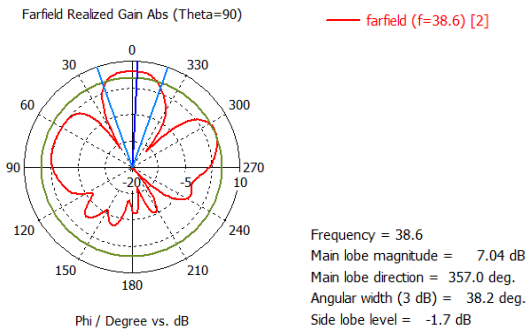

Figure 9. Farfield radiation pattern at 38 GHz

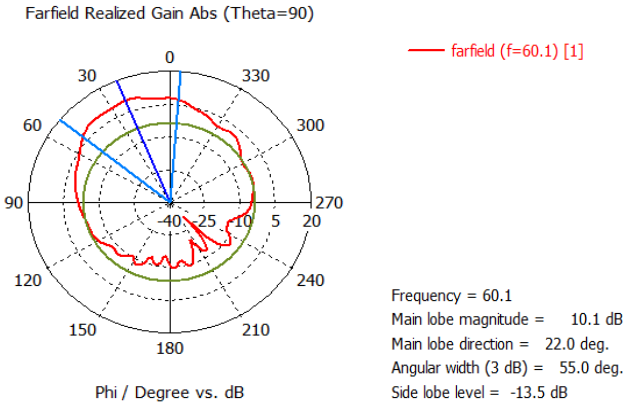

Figure 10. Farfield radiation pattern at 60 GHz

IV.CONCLUSION

Thus a Shared-Aperture Microstrip Patch Antenna Array for Conformal 5G Communications for wearable devices is developed on a flexible substrate (Rogers O4003c). The rapid advancements in wearable devices in terms of technology, functionality, size and more real-time applications have increased the demand for flexible antennas. The proposed design can be a potential aid in designing a conformal antenna for wearable devices. In future, we are planning to implement proximity feeding technique in order to reduce the spurious radiation further and Specific Absorption Rate (SAR) calculations for various human body parts when exposed to the designed antenna.

V. REFERENCES

[1] Xu, H., Rappaport, T. S., Boyle, R. J., &Schaffner, J. H. (2000) 'Measurements and models for 38-GHz point-to-multipoint radiowave propagation', IEEE Journal on Selected Areas in Communications, Vol.18, No.3, pp.310-321.

[2] Rappaport, T. S., Ben-Dor, E., Murdock, J. N. and Qiao, Y. (2012, June) '38 GHz and 60 GHz angle-dependent propagation for cellular & peer-to-peer wireless communications', Communications (ICC), IEEE International Conference on pp.4568-4573.

[3] Constantine A. Balanis, "Microstrip Antennas," in Antenna theory analysis and design, IIIrded. New Jersey, USA.

[4] Granholm, Johan, and Niels Skou. (2000) 'Dual-frequency, dual-polarization microstrip antenna development for high-resolution, airborne SAR', Microwave Conference, Asia-Pacific.

[5] Shafai, L. L., Chamma, W. A., Barakat, M., Strickland, P. C. and Seguin, G. (2000) 'Dual-band dual-polarized perforated microstrip antennas for SAR applications', Transactions on Antennas and Propagation, Vol.48, No.1, pp. 58-66. IEEE.

[6] Wang, Z., Xiao, L., Fang, L. and Meng, H. (2014, November) 'A design of E/Ka dual-band patch antenna with shared aperture', Microwave Conference (APMC), Asia-Pacific pp.333-335. IEEE.

Themed Section : Engineering and Technology
© 2018 IJSRSET | Volume 5 | Issue 3 | Print ISSN: 2395-1990 | Online ISSN : 2394-4099

Review on 2D to 3D Conversion Techniques and other Dimensions

B. Gnana Priya[1], Dr. M. Arulselvi[2]

[1]Lecturer, Department of Computer Science and Engineering, Annamalai University, Tamil Nadu, India

[2]Assistant Professor, Department of Computer Science and Engineering, Annamalai University, Tamil Nadu, India

ABSTRACT

In modern era there has been a rapid progress in the field of 3D image processing. Many 2D to 3D conversion algorithm have been developed, which works by constructing depth maps. Also we are all familiar about 4d ,5d, 7d ,9d movies, gaming and various shows in malls and theme parks. The measure of spatial extent like length, height and width is called dimension. Though we hear about various dimensions in image processing, mathematically there are only three dimensions in which we can work with. The other dimensions are created with special effects , seat movements ,interactivity and so on.. This paper explores the various ways to create 3d content, explains the 3d file format and present a brief outline behind other dimensional technologies.

Keywords : Image Processing, 3-D Cameras, Local Point Transformation Function, PIC, KNN

I. INTRODUCTION

Nowadays 3D hardware popularity is increased and many of us intent to buy 3D capable hardware such as TVs, Cameras, smart phones ,gaming consoles and much more. 3D content used widely in medicine, engineering, earth science, architecture, video games, movies, printing and much more. The term stereoscopic vision[1] refers to the human ability to view with both eyes in similar, but slightly different ways. Eyes of any person are a few inches apart and this is called the interocular distance. This allows humans to judge distance, which develops their ability to have true depth perception. For people and animals that have stereoscopic vision, each eye sees a similar, but slightly different image. These positional differences are referred to as horizontal disparities or binocular disparities. The brain processes these images in a way that allows the person or animal to slightly see around an obstacle without having to physically move. This process is accomplished by matching the different images and then taking into account the differences in the two images. Although the visual differences are small, the end result is a significantly improved depth perception of one's surroundings. The 3D effect is created by taking two images from two lenses, creating a parallax effect. Parallax occurs from viewing an object along two lines of sight.

II. 3D TECHNOLOGY

3D image can be created using a 3D camera or 2D to 3D image convertor software can be used. 3D camera in current scenario are of two types. One with two lenses and two image sensors are available for simultaneous exposure of a stereo pair. The two lenses are set approximately the same distance apart as a pair of human eyes mimicking the sense of depth that we get when we view things

with our own eyes. The twin lenses capture two images simultaneously similar to how your right and left eye would see two different images and the 3D processor converts these two images into a single 3D image file. By layering the two 2D images on top of one another, the camera is able to create one single stereoscopic 3D image with depth. These cameras are more expensive due to the additional hardware and limited demand. Panasonic and Fujifilm markets double-lens 3-D cameras. Fujifilm FinePix Real 3D W3 and Panasonic Lumix 3D1 with 10 and 12 megapixels of resolution are the most popular of 3D cameras available. Recent trend adds 3-D assist capabilities to conventional cameras. The other type made inexpensively by taking two pictures with the same camera, but moving the camera a few inches either left or right. Nikon and Sony 3D cameras allow the photographer to shoot one scene, then shift the camera assisted by a translucent image on the camera display. After the subject is aligned, the camera exposes the second image, using the same exposure and focus. Sony SLT-A58K and DSLR Samsung NX300 with 2D/3D Lens are examples.

It is not the creation of 3D images that is problematic, but more the displaying of them. Today's 3-D cameras capture the images and do not perform any of the decoding functions needed to view the photos three-dimensionally. Images taken with any 3D camera can be viewed on a 3D TV, using special 3D prints or on the back of the camera as in Fujifilm. Active decoding viewing uses battery-powered glasses to sync polarized images with a 3-D television. Viewing 3-D TV without glasses can be accomplished through the use of lenticular screens, but the field of view for these TVs is limited, and the lenticular screen reduces image resolution. Other method make use of glasses to view the 3d image. Passive decoding technology uses either anaglyphic viewing the red and cyan lensed glasses or polarized viewing, which uses gray lenses with different polarizing directions. Some of the drawbacks include : 3D TVs are expensive; 3D prints are time consuming to produce and expensive; Its not possible to view 3D image on our camera except Fujis Finepix. Other challenges are : some of the camera will work only in landscape orientation. Images taken with the camera in a vertical orientation are more difficult as your eyes cannot adjust to the parallax . Images with some depth will work better for examples medium distance photo shots. While others like macro shots, night time images and compositions where the subject is near the edge of the frame will not be as effective.

A. 3D Conversion Software

There are many 2d to 3d open source convertor software available. The convertor tool adds depth information to the 2d image fed to it. Different algorithms and techniques are used by different convertors to convert a given 2d image into a 3d image. some of the popular software available are Blender, Make3d, 3dShade, 123d catch, Insight3d, ConvertImage, etc. Some of them are fully automatic , have programs that automatically estimates depth for an image. Most of the convertors will get a 2d image captured from a normal camera and stored in PC in standard image format as input and adds depth using some techniques. Others are semi automatic, we have to assign depth to various parts of the image. We need to define few parameters like width , depth, position of object explicitly.

Some software make use of a single 2d image to create its 3d counterpart. The software creates picture of two colours, manipulate the color mixture and overlaps the two images(same image) that gives us the illusion of depth. Some of them calculates color intensities in picture and produce depth information with quite accurate perspective.

The software also allows us to select tones from hundreds of tones available in their database and render it with our image. The second method is to use series of 2d image of the scene, the software will automatically match them and measure position in space. Some of them are design tools, wherein the user draws the image as object in the screen. The camera angle, directional light are set by default and object converted into 3d image. Some of standard features includes allows us to customize shade, view or color special effects like crop, resize, rotate material finishing like wax, sandstone, steel possible to export and import the 3D files.

The software available will convert 2d formats like jpeg, png, gif, bmp, tif, pdf into 3d files. But cannot be guaranteed to achieve complete accuracy.

III. 2D TO 3D IMAGE CONVERSION METHODS

2D to 3D image conversion can be done in two ways. They are automatic and semiautomatic methods. In semiautomatic conversion method we need to assign depth to various parts of the image. Based on this sparse depth assignment, a computer algorithm estimates dense depth over the entire image or video sequence. In automatic methods, no human intervention is needed and a computer algorithm automatically estimates the depth for a single image or video. Automatic methods estimates depth from shading, perspective geometry, structure from motion , depth from models or depth from defocus.

A. Learning Depth from examples

A scene depth can be learned from a large database of images and depth pairs[2]. J.Konard proposed an automatic conversion of 2D to 3D image by machine learning techniques. The method relies on repository of images and depth pairs available. The assumption here is two images that are photo metrically similar are likely to have the same depth. While analyzing the available 3D pairs we may likely get a match for our 2D input image. The k-nearest neighbor algorithm is used to find the closest 3D image for any given input image. Euclidean distance function used to find difference between histograms of oriented gradients. Median filtering used for depth fusion of k images to compute the output. This method yields good depth quality but seldom have distortions.

B. Learning Based 2D to 3D Image Conversion

Janusz Konard[3] came up with other automatic 2D to 3D algorithm which has two methods. (i) Learning by a local point transformation function (ii) Learning by global

Figure 1. Original 2D Image

Figure 2. 3D Image using PIC 3D Software

Figure 3. 3D Image using Convert Image Software

nearest neighbor (KNN) algorithm. Local attributes like color, spatial position are used for learning a point transformation. We can estimate the transformation function by training the database. We can have separate transformation for each attribute and finally they are linearly combined to find the final depth. Advantage here is computational efficiency and reduced complexity.

C. Multiple Depth Cues

An image have various attributes and the depth perception arises from a variety of depth cues. Wang[4] proposed an automatic 2D to 3D conversion algorithm that uses multiple depth cues. Perspective geometry, defocus and visual saliency(subjective perceptual quality that makes an object distinct from background and other object in an image) are depth cues used here. The given color image is converted into grayscale. Then depth is detected from any of the three steps. (i) Vanishing point detection: If image are of perspective geometry, intersection tend to aggregate to one cluster. If predominant cluster exists

the scene contains an vanishing point. In this case a cone depth model and saliency map used to estimate depth. If no vanishing point we can estimate depth by defocus. Here two dimensional discrete cosine transformation used and results remapped to depth range 0-255. If image does not have vanishing point or defocus, depth extraction done using depth models. Spherical, Cylindrical and plane model used in this method.

D. Random Walks and Graph Cuts

This is a semi automatic method wherein user assigns a rough estimate of depth values to a few points in the image. The depth values for rest of the image determined by the system[5]. With the resulting depth map we can produce a 3D image. This method is based on the Random walker algorithm for image segmentation. The algorithm works by assigning small number of pixels called seeds with labels. The unlabelled pixels have a random walker and probability computed to find which seed it reaches first and is labelled. Graph cuts have hard segmentation and smoothness provided by random walks. Depth maps using graph cuts are generated with user defined depth values to generate depth prior. The depth prior and user stroke are integrated into Random walks as additional feature to determine edge weights. To produce quality depth maps Random walks are combined with Graph cuts.

IV. 3D CONTENT

What does a 3D file contains? is an important thing we need to know before handling them. The content of a 3D file can be classified into three categories- such as geometry, appearance and scene information.

A. Geometry

The geometry of a model is stored as a set of 3D points. There are various ways to represent surface information of a 3D image. A set of Polygons may be used to represent the surface of the model . These polygonal meshes are convenient and quick to render 3D content. This method is very simple and is widely used in 3D printing. Here use of more vertices yields better results but this may lead to larger storage space. Use of polygons not feasible for smooth surfaces. We can use Non uniform Rational B-spline patches to create smooth surfaces. Here, a number of control points each with its own weights and parameters known as knots are stored. We can easily edit the 3D model because we need to work only with control points to achieve transformation in a particular part of an image. But, the method is quiet time consuming. Now the latest method is to use constructive solid geometry, CSG. All the image elements are not treated as the same. Instead assign different 3D shapes to different objects based on their appearance. Simple primitive shapes like cylinder, sphere and cubes are taken and Boolean operations like addition and subtraction are performed to built 3D shapes. We must save each of the operations and shape information for future editing. Conversion from CSG format to other mesh type formats is a challenging task and is a subject under study. Constructive solid geometry is a user friendly and time saving method.

B. Appearance

Assigning texture to the surface of the model is more important, as in 3D we need to have a feel of the model. The texture and color for each vertices (or) knots (or) shapes need to be assigned by mapping each 3D vertex to a corresponding point in the 2D image. Light source plays a vital role in the appearance of an object. Colour of the object we perceive depends on the light source. Most of 3D file formats support texture mapping. The extra information may be stored in the same file or in a separate file.

C. Scene

Layout of the 3D model with respect to camera, light source and nearby objects is referred as the scene information of the 3D image. The direction of camera, its magnification, principal point and up

direction are needed to define the view of the camera. In order to define the scene the position of the light source, its intensity and colour need to be known. A single 3D image may have several parts. In such case we need to know how to layout the several parts and separate transformation matrix for each part need to be stored. Most of 3D file formats currently available does not support scene information.

V. 3D FILE FORMATS

3D file formats are used to store information about 3d models. Unlike 2d image files ,a 3D image file not only stores pixel values but some additional information are also added. This includes geometry, appearance and information about the scene. Table list some of popular 3D image formats available. Most of the 3D formats are optimized for use on the specific software alone. Different formats stores different attributes about the image. Therefore difficult to exchange files and view them on different software. 3D image created using one software cannot be viewed using another software. .BLEND file created by Blender cannot be viewed using AutoCad software. Some open source formats to solve this interoperability problem are also available. Neutral formats like STL and CoLLADA(.STL and .DAE extension respectively) may be used to exchange and view the 3D models. First convert 3D file into .DAE file and export it. Use other 3D software and import the .DAE file and convert them into the software respective format. Some of the 3D file formats are : .3D, .3D2, .3D4,.3DM, .3DX, .ANIM, .BLEND, .C3D, .D3D, .MESH, .P3L, .P3M, .STC, .U3D , .X3G.

VI. OTHER TECHNOLOGIES

A. 4D Technology

4D technology involves the use of already existing 3D tech with an additional dimension. For the most part 4D applications are simply a matter of marketing. For now a real 4D object, as defined in mathematics or physics, does not exist. 4D in 4D cinemas is simply 3D plus an additional dimension or element. This additional element is usually a simulation or group of simulations of environmental occurrences based on what is being projected. With 3d videos we use special seat effects. Movement to any direction as per the film, sways ,wave motion , tilts, jumping, bending, racing, tumbling all in sync with screen activity. In addition to these leg ticklers, back ticklers, neck blast are also added.

B. 5D Technology

5D techniques include

i) Seat effects

All the effects like 4D are used. A high grade chair with a driver unit and air tank aids in seat movement.

ii) Special effects

Effects like smoke, rainfall, snow, bubble, wind, and lightning are added.

iii) Sound effects

Surround sound components, speakers with special processors and amplifiers are used.

iv) Screen and projection

Two high quality projectors are used for viewing the 3D movie on display which can be viewed by special 3D glasses that offer passive polarization effect. This 3D projection is controlled by a special 3D computer that keeps streaming both the left and right eyes simultaneously for the effect. We also need customized silver screens that offer an image bouncing effect which is necessary for creating the 3d effect.

v) Control system

A motion control personal computer that syncs the chairs with the screen action is used. The control system also syncs the video and the special effects.

C. 7D Technology

7D is an interactive cinema where we can use the toy gun to shoot the target. The equipment included in 7d theatre are a Master System , projection system , sound system ,6 DOF dynamic seat system , environment , interactive simulation system . The main control system is mainly in the computer software and it controls the operation of the entire theatre, Projection systems, including the screen and projector.

D. 9D Technology

Now, the 9D is the newest technology in the world. Like our 9d virtual reality, viewers just need to wear VR glasses and then go into the world of the movies. It breaks the limit of virtual and real world and takes viewers amazing experience. It consists of three revolutionary new products: Interactive cinema with 360° rotation function, Immersive Glasses, Breakthrough VR entertainment content platform.

VII. CONCLUSION

3D technology gives us a realistic view of things and in near future will be a very common application in many fields. Glasses free 3D display using plastic films help us to view 3D content without much difficulty. The other dimensional technologies are becoming much popular and most of us excited to view such shows. This paper reviews the basic concepts in 3D processing and rather explains the techniques behind how other dimensions are implemented in real time.

VIII. REFERENCES

[1] https://en.wikipedia.org/wiki/Stereoscopy

[2] J. Konrad, M. Wang, and P. Ishwar, "2D-to-3D image conversion by learning depth from examples," in Proc. IEEE Computer. Soc. CVPRW, Jun. 2012, pp. 16-22.

[3] J. Konrad, M. Wang, and P. Ishwar,C.Wu,D. Mukharjee, "Learning based, automatic 2D-to-3D image and video conversion," in Image Processing IEEE Trans on,vol.22,no.9,pp.3485-96,Sept. 2013 Jun. 2012, pp. 16-22.

[4] P.Ji,L.Wang,D. Li, M. Zhang, "An automatic 2D to 3D conversion algorithm using multi-depth cues," IEEE Conf.Audio,Language and Image Processing,pp.546-50,July 2012.

[5] R. Phan, R. Rzeszutek, and D. Androutsos, "Semi-automatic 2D to 3D image conversion using scale-space random walks and a graph cuts based depth prior," in Proc.18th IEEE Int. Conf. Image Process., Sep. 2011, pp. 865– 868.

[6] Kenton McHenry and Peter Bajcsy "An Overview of 3D Data Content and Viewers", National Centre for Supercomputing Applications, 2008.

[7] http://edutechwiki.unige.ch/en/3D_file_format

[8] http://convertimage.net

[9] http://pic3d.egedsoft.com

Themed Section : Engineering and Technology
© 2018 IJSRSET | Volume 5 | Issue 3 | Print ISSN: 2395-1990 | Online ISSN : 2394-4099

IoT Based Toxic Gases Monitoring System in Underground Sewages Using Wristband

R.Vijayalakshmi[1], Dr.D.Sengeni[2]

[1]PG Student, M.E, Applied Electronics, Department of Electronics and Communication Engineering, CK College of Engineering and Technology, Cuddalore, Tamilnadu, India

[2]Associate Professor, Department of Electronics and Communication Engineering, CK College of Engineering and Technology, Cuddalore, Tamilnadu, India

vijiramaraj111@gmail.com[1], sengeni67@gmail.com[2]

ABSTRACT

Most of the cities adopted the underground drainage system and its the duty of Municipal Corporation to maintain cleanliness, healthy and safety of cities. If the drainage system is not properly managed then pure water gets contaminate with drainage water and infectious diseases may get spread. Drainage cleaning people are not aware of risk of sudden attack of poisonous gas since the gases are odorless if exposed for long time which may cause serious health problems. Due to the lack of using proper gas leakage detection system, a number of dangerous accidents occurred during the last few decades. To overcome all these problems effective monitoring system is needed in the drainage channels. The detected system is proposed with three gas sensors like Carbon Monoxide, Hydrogen sulphide sensors and Methane, one Ultrasonic sensor used for detect obstacle, one Heat Beat sensor used to Calculate the pulse rate of Human. Carbon Monoxide, Hydrogen sulphide, Methane gases are highly toxic to human hence the proposed system will gives alert through the LCD Display after reaching the thershold level of each gas sensors then people gets alerts through the LED glow. Heart Beat sensor will calculate the range of the Pulse rate then output at the abnormal range will give alert through Buzzer and notification message through an GSM . Ultrasonic sensor gives alert through LED glow when obstacles occured. These sensors will be placed at the wristband and performance of varies sensors operations are monitored and stored by using application, for avoiding the future dangerous accidents.

Keywords: Carbon Monoxide Sensor; Hydrogen Sulphide Sensor; Methane Gas Sensor; Ultrasonic Sensor; Wristband; Heart Beat Sensor; LCD; LED; Drainage Channel; Thershold Limit

I. INTRODUCTION

Sewer system is an underground system of pipes commonly used to transport wastewater from homes and businesses either to a treatment facility, where the water is treated and released into natural water bodies like lakes and streams or in any river to permanently drain out from the area. Sewer manhole is one of the most important parts of the sewer system. Sewer manhole is a structure through which a person can gain access to the underground wastewater collection system. Manholes are not designed for someone to work in regularly, but workers may need to enter inside the manhole to complete their jobs such as cleaning, repair, inspection etc.

The lack of prior caring of sewage work is the witness for the deaths of thousands of sewage cleaners throughout the year from accidents and various

diseases such as hepatitis and typhoid due to sudden or sustained exposure to hazardous gases like carbon monoxide, hydrogen sulphide, methane. A better knowledge related to hazards in the surroundings is necessary for the prevention of poisoning of gases. These gases have to be keep on track so that enormous rise in the normal level of effluents should be known and corrective measures can be taken. In contrary, the existing systems available are not much portable and are not affordable. Also it is hard to implement.In the previous the designed Surveillance rover detects the presence of carbon monoxide (CO) gas for monitoring system MATLAB is used. The device consists of a processing section which takes input, processes it and provides output.This system requires base station should near to the sensors.

In this paper an embedded system is designed with ARM Microntroller and various gas sensors for the purpose of detection and altering that helps in eliminating the lives of human which is being endangered. The system is affordable to implement at well-defined monitored. In the existing system, a number of jobs related with gas detection and ensure security system. It has been implemented among these some were theoretical research approach and some were demonstrated in practical field to detect the gas but both approaches were effective manhole gas sensing unit has been developed which is capable to detect the toxic and explosive gases individually within a minute and generate LED glow at the various levels if any of the gas is beyond its threshold limit it gives an alert through LED glow and LCD Display. Harmful gases like carbon monoxide detection, Methane gas detection, and Hydrogen Sulphide gas detection these gases are very toxic to the human. Ultrasonic sensor to determine obstacles in the drainage channel and Heart Beat sensor this will be fixed on the workers wristband who enter into the manholes based on this Heart Beat sensor the alert system Buzzer and Message Notification will be sends to outside workers and Municipal Officers.

II. SYSTEM DESIGN

A) ARM7 Microcontroller (LPC 2148)

ARM Microcontroller (LPC 2138) is needed to continuously sense the sensor output. Also this is used to store some information which can be used for further processing. Interfacing an 5 different sensors such as carbon monoxide sensor, Hydrogen sulphide sensor, Methane gas sensor, Ultrasonic sensor, Heart beat sensor these sensors to be connected in I/O pins and the alert systems such as Buzzer, LED, LCD this to be connected in another I/O pins.The total pin is 64 and 48 I/O pin (port 0 and port 1).sIt has an programming language of Embedded C.

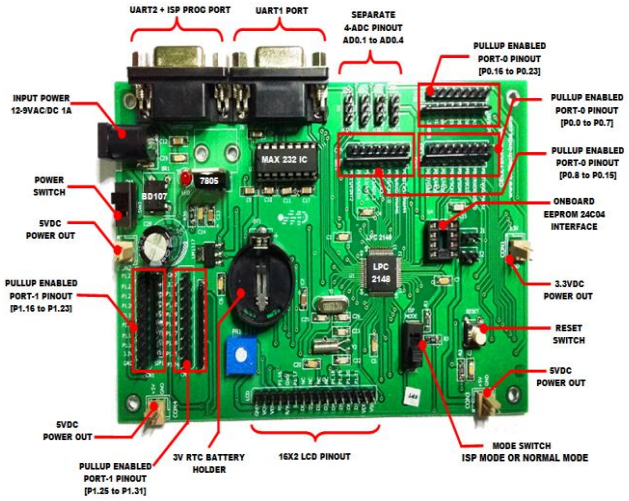

Figure 1. ARM Microcontroller (LPC 2148)

B) System Description

Smart Drainage System helps to alert an workers of various gas levels presents inside the drainage and it measures the distance of Obstacle presents the sensor performance measures and stores by using system application for reduce the future accidents in drainage channel. Efficient Monitoring, High performance, Alert system and safe manner. From the fig:1,The main toxic gases present in drainage is carbon monoxide gas, Hydrogen sulphide gas, Methane gas in ppm range, Ultrasonic sensor and Heart Beat sensor in input block and Output block is an alert system such as LED, LCD Buzzer and messege notification (GSM) these blocks are interfaced with ARM Microcontroller. The block diagram of the complete system. The detailed functioning of the systems will be discussed here with the description of

all the subsystems. The functioning of every subsystems built with the necessary components will be.This paper based on open drains.so, In future looking forward to closed drains and wireless gas sensors at cheaper and easier ways to clean then without the help of mankind.

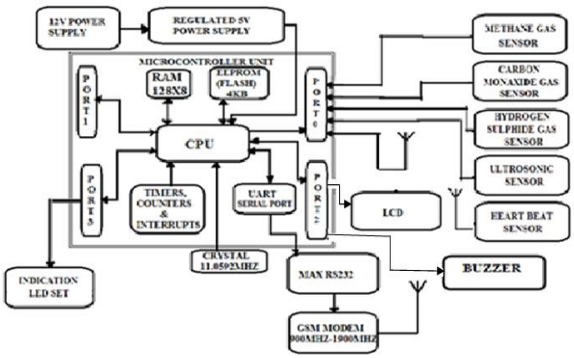

Figure 2. Block Diagram of Proposed System

a) System Modules

A sensor is a device that measures a physical quantity and converts it into a signal which can be read by observer or by an instruments .There are three types of Harmful gas sensor used such as Carbon Monoxide sensor, Hydrogen sulphide sensor and Methane gas sensors. Ultrasonic sensor in drainage channel and heart beat sensor will fixed on workers hand.

The detection range of various harmful gas sensors like carbon monoxide, Hydrogen sulphide and Methane.It can be varied depends on level of gas presents in drainage total detection range of sensor are noted below the table:1 based on sensor used detection will be varied.

Table 1: Detection Range of Gas Sensors

Sensor Name	Detection Range
Carbon monoxide sensor	20-2000 ppm
Hydrogen sulphide sensor	1-200 ppm
Methane sensor	150-10000ppm

The thershold limit of various harmful gas sensors like carbon monoxide, Hydrogen sulphide and Methane.It can be varied depends on level of gas occured in drainage if the gases are beyond thershold limit,workers may have death.so,thershold limit is measured and it shown in Table: 2 based on gas levels low, medium, high.The maximum gas value such as high level is said to be an thershold limit.

Table 2: Threshold Limit For Gas Sensors

SENSOR NAME	THERSHOLD LIMIT
Carbon Monoxide Sensor	35ppm
Hydrogen sulphide sensor	40 ppm
Methane sensor	750ppm

i) Carbon Monoxide Sensor (MQ-9)

Carbon Monoxide (CO) sensor is a simple-to-use, suitable for sensing CO concentrations in the air. From this fig:2, If the CO gas not occured there is no gas affected in LCD display. Then, if the CO gas is occured gas is affected then the LCD display shows Carbon monoxide Gas Leakage and green LED will glow.The gas levels to be divided into three such as Low , Medium, High.Depends on the CO gas presents in drainage value will be displayed in LCD display and LED will glow. If Low level gas is occured 10ppm will display and Green LED will glow, if Medium level gas is occured 20ppm will display and Yellow LED will glow and if High level gas is closed 35ppm will display and Red LED will glow.

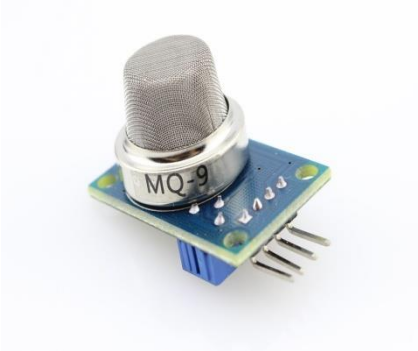

Figure 3. Carbon Monoxide Sensor (MQ-9)

ii)Hydrogen Sulphide Sensor Module(MQ-135)

A hydrogen sensor is a gas detector that detects the presence of hydrogen.From this fig:2, If the H2S gas not occured there is no gas affected in LCD display. Then, if the H2S gas is occured gas is affected then the LCD display shows Hydrogen Sulphide Gas Leakage and green LED will glow.The gas levels to be divided into three such as Low , Medium, High.Depends on the CO gas presents in drainage value will be displayed in LCD display and LED will glow. If Low level gas is occured 10 ppm will display and Green LED will glow, if Medium level gas is occured 25 ppm will display and Yellow LED will glow and if High level gas is occured 40ppm will display and Red LED will glow.

Figure 4. Hydrogen Sulphide Sensor Module (MQ-135)

iii)Methane Sensor Module(MQ-5)

MQ-5 gas sensor modules are used in gas leakage detecting equipments in family and industry, are suitable for detecting of CH4, Natural gas. LNG, avoid the noise of alcohol and cooking fumes and cigarette smoke. High sensitivity to CH4, Natural gas, Small sensitivity to alcohol, smoke, Fast response, Stable and long life, Simple drive circuit

From this Fig :4, If the CH4 gas not occured there is no gas affected in LCD display. Then, if the CH4 gas is occured gas is affected then the LCD display shows Methane Gas Leakage and green LED will glow. The gas levels to be divided into three such as Low , Medium, High. Depends on the CH4 gas presents in drainage value will be displayed in LCD display and LED will glow. If Low level gas is occured 150ppm will display and Green LED will glow, if Medium level gas is occured 450ppm will display and Yellow LED will glow and if High level gas is occured 750 ppm will display and Red LED will glow.

Figure 5. Methane Gas Sensor Module (MQ-5)

iv)Ultrasonic Sensor Module

Ultrasonic sensor is a device that can measure the distance to an object by using sound waves. It measures distance by sending out a sound wave at a specific frequency and listening for that sound wave to bounce back.Fig :5,If there is no obstacle in drainage channel intially the LED is off state and displays No obstacles and if there is an Obstacle in drainage then LCD display shows obstacle detected and corresponding LED will glow.

Figure 6. Ultrasonic Sensor

v)Heart Beat Sensor

A heart rate monitor is a personal monitoring device that allows one to measure one's heart rate in real time or record the heart rate for later study. From this Fig:6 ,Initial Heart Beat sensor rate should be in

(65-75) normal condition and if the heart beat rate is below 65 said to be abnormal condition then it shows an output in LCD display shows Attention needed and performance of sensor messege alert through the IoT.

Figure 7. Heart Beat Sensor

vi) LCD Display Module 2X16 and LED Module

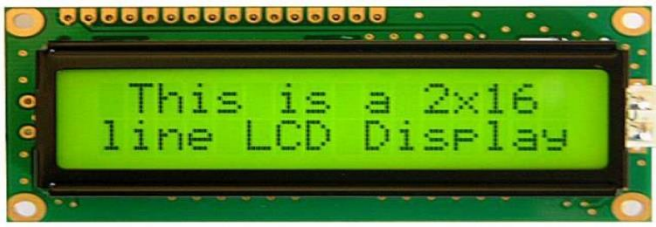

Figure 8. LCD Display Module

Liquid Crystal Display (LCD) is a flat display used in digital watches, cameras and many portable computers. LCD displays utilize two sheets of polarizing material with a liquid crystal solution between them advantage of having a low power consumption than the LED. From fig: 7 The gas sensors, Ultrasonic sensor and Heart Beat sensor performance and displayed in LCD. From Table: 3, Gas levels such as low, medium, high value also displayed.

Table 3: Level of Gas Sensors

Sensor Name	Low	High	Medium
Carbon Monoxide	10ppm	20ppm	35ppm
Hydrogen Sulphide	10ppm	25ppm	40ppm
Methane	150ppm	400ppm	750ppm

A light-emitting diode (LED) is a semiconductor device that produces light in different colors. From Table :4, Different gas level Low, Medium, High based on gas levels presents in drainage channels LED will glow.From fig: 8 different color of LED is interfaced with ARM Microntroller based on the gas occured i drainage channel corresponding LED will glow.

Table 4. Gas Level LED Color

GAS LEVEL	LED DISPLAY
Low	Green
Medium	Yellow
High	Red

III. RESULTS AND DISCUSSION

Design and Implementing this project with interfacing of hardware tool. The various devices are arranged in the block diagram. The placing different components as embedded system . The output can run in LCD, LED, Buzzer, Messege notification and sensor performance is measured in system application in the form of graphical representation. The representation shows how the Hydrogen Sulphide gas variation,Carbon monoxide variation, Methane gas variation ,Heart beat sensor variation and Ultrasonic sensor variation. These variations can be identified with the help of Logical representation in software.

The automation technique involving the automatic motoring of all the processes which includes the monitoring and inspection needs provides for a very efficient system. The automation process helps the workers for the to avoid the sudden attack of toxic gases for safety purpose to reduce the amount of errors that occur, reduction in the human resources, increased efficiency and most importantly very cost effective.

i) Carbon Monoxide Gas Levels

Carbon Monoxide (CO) sensor is a simple-to-use, suitable for sensing CO concentrations in the air. Depends on the CO gas presents in drainage value will be displayed in LCD display and LED will glow. MQ-9 gas sensor has high sensitity to Carbon Monoxide. The sensor could be used to detect different gases contains CO and combustible gases, it is with low cost and suitable for different application. From the fig; 9 , If Low level reached 10ppm will display and Green LED will glow, if Medium level reached 20ppm will display and Yellow LED will glow and if High level reached 35ppm will display and Red LED will glow.

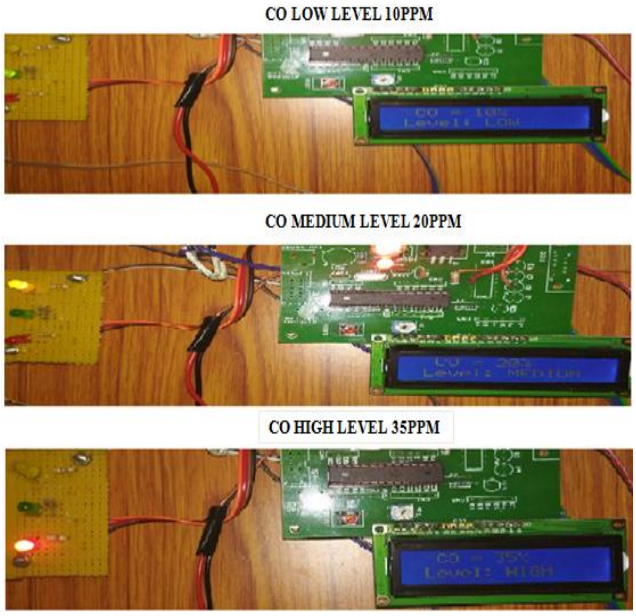

Figure 9. When the CO gas reaches a certain level in drainage channel and display Carbon Monoxide gas and level of gas.If Low level reached then LCD display shows the 10ppm , Medium level reached then LCD display shows 20ppm ,High level reached then LCD display the level 35ppm and corresponding LEDs will glow as per the level of gas persent inside the drainage channels.

ii) Hydrogen Sulphide Gas Levels

H2S Gas detectors can be used to detect combustible, flammable and toxic gases, and oxygen depletion. Depends on the H2S gas presents in drainage value will be displayed in LCD display and LED will glow. This type of device is used widely in industry and can be found in locations, such as on Drainage channels, oil rigs, to monitor gas levels. Form the fig 10, If Low level reached 10ppm will display and Green LED will glow, if Medium level reached 25ppm will display and Yellow LED will glow and if High level reached 40ppm will display and Red LED will glow.

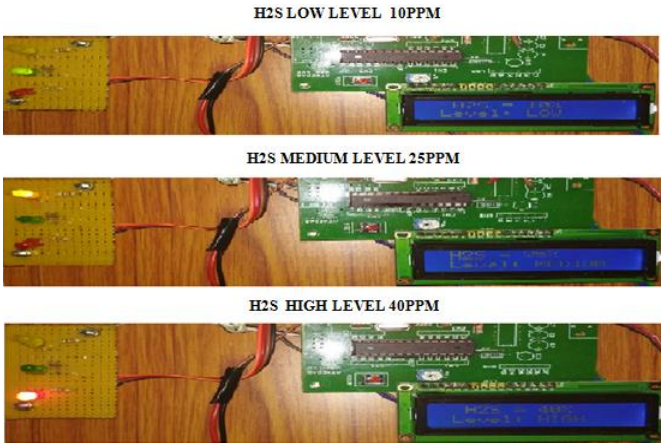

Figure 10. When the H2S gas reaches a certain level in drainage channel and display Hydrogen sulphide and level of gas. If Low level reached then LCD display shows the 10ppm , Medium level reached then LCD display shows 25ppm ,High level reached then LCD display the level 40ppm and corresponding LEDs will glow as per the level of gas persent inside the drainage channels.

iii) Methane Gas Levels

MQ-5 gas sensor modules are used in gas leakage detecting equipments in family and industry, are suitable for detecting of CH4,Natural gas. Depends on the H2S gas presents in drainage value will be displayed in LCD display and LED will glow. High sensitivity to CH4, Natural gas, Small sensitivity to alcohol, smoke, Fast response, Stable and long life. From fig 11, If Low level reached 150ppm will display and Green LED will glow, if Medium level reached 400ppm will display and Yellow LED will glow and if High level reached 750ppm will display and Red LED will glow.

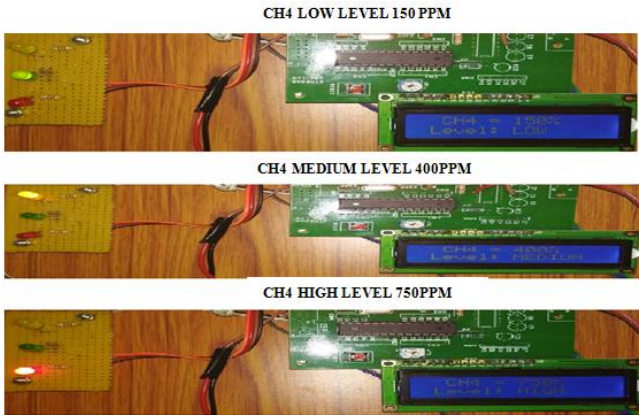

Figure 11. When the CH4 gas reaches a certain level in drainage channel and display Methane gas and level of gas. If Low level reached then LCD display shows the 150ppm , Medium level reached then LCD display shows 400ppm ,High level reached then LCD display the level 750ppm and corresponding LEDs will glow as per the level of gas persent inside the drainage channels.

iv) Ultrasonic Sensor

Ultrasonic sensor is a device that can measure the distance to an object by using sound waves. It measures distance by sending out a sound wave at a specific frequency and listening for that sound wave to bounce back. This performance to be monitored in LCD. It is used to sense the obstacles in drainage channel. From fig 12, LCD display shows obstacles detected then the blue LED is in ON state.

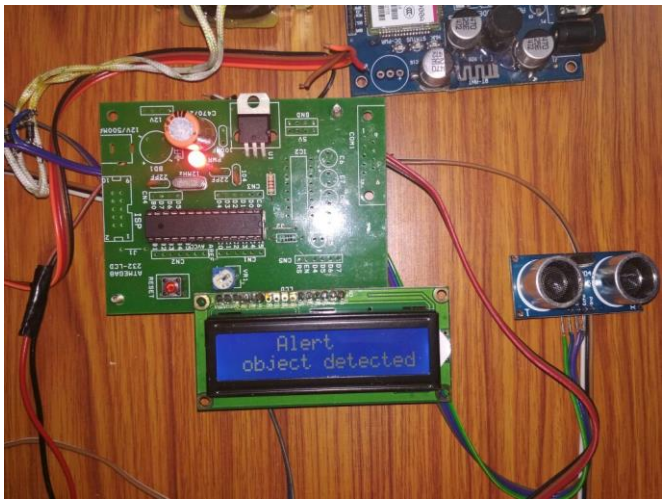

Figure 12. When the input of the Ultrasonic sensor is Low and LCD display shows Obstacle detected and blue LED glow.

v) Heart Beat Sensor

It is used to measure the pulse rate of human. It has an digital input signals Low and High. From Fig:19,If the input signal is Low pulse rate is normal, if the input signal is High there is pulse rate is abnormal then the alert message sends to the municipal officers and outside workers will shows pulse rate in LCD display.

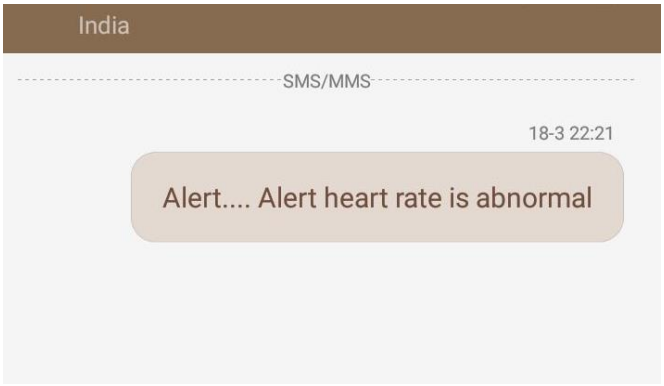

Figure 13. When Heart Beat sensor reaches abnormal range and alert message sends to the municipal officer and outside workers.

IV. HARDWARE IMPLEMENTED

The main aim of the design which is to both automatic and manually read and regulate various sensors and stores and display it on system application was however been achieved. Also all types of sensors are designed in the Emdedded system. There may be other software used for designing system but proteus is the simplest and hardware design in embedded system using different components. The five sensors Hydrogen sulphide gas, Carbon monoxide gas, Methane gas, Ultrasonic sensor and Heart beat sensor are continuously monitored with the help of ARM Microcontroller. Different types of parameter are designed to safeguard the Drainage channel. Improving the sensors efficiency even slightly input voltage varies. Improvement in sensors efficiency can be achieved. In order to automate a alert system and

minimize human intervention, there is a need to develop a proteus software design and implemented in Embedded design system and helps to reduce the errors caused by humans.

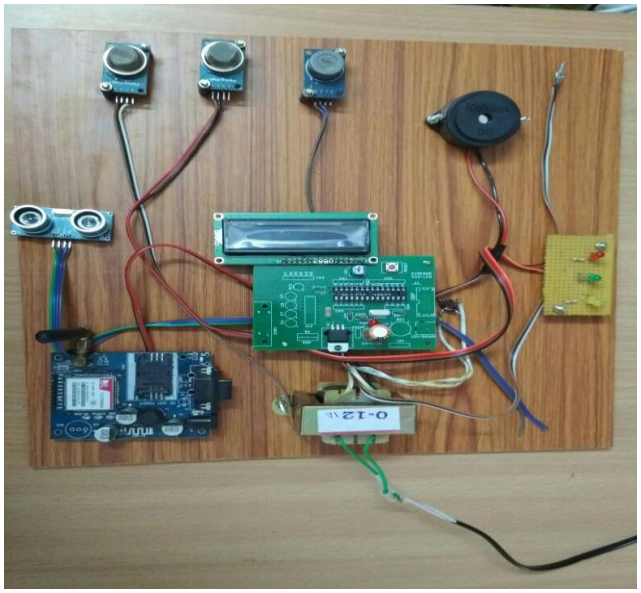

Figure 14. Hardware Implemented

V. CONCLUSION

Smart Drainage Detection system designed and implemented for continuous monitoring and alert system to the drainage-cleaning people. Further it can be monitored in Real time data is acquired by the system and for alert displayed on the LCD , LED ,Buzzer and Messege notifications.

1. Various sensors performs measured by interfacing with ARM Microcontroller (LPC 2148) it will proccess and control programmed in Embedded C and alert by using various alert system to the workers under working in draiange .
2. Various level of gas sensors is measured by using an switches and for alert LED will be used.
3. Obstacle is detected in drainage channel and heartbeat will be measured to the workers.

ACKNOWLEDGMENT

I Would like to express deepest gratitude and appreciation to Guide Dr.Sengeni. For her excellent guidance, caring, patience, suggestions and encouragement with much appeciation to all those who gave us me to complete this project .Last but not least, again I would like to say many thanks go to my guide . Dr.Sengeni., who are given as full effort guiding me to make the goal as well as the panels especially in my presentation that has improved my presentation that has improved my presentation skills by their comment and tips.

VI. REFERENCES

[1] Ali Adid Amb, Sheikh Afrin , F.M Fahad and Hasan U. Zaman, “Acost Effective Way to Build a Web Controlled Search and CO Detector Rover” , IEEE Transcation (2017).

[2] Sugato Ghosh ,Indranil Das, Deepajana Adak, Nillohit Mukherjee, Raghunath Bhattacharrya, Hiranmay Saha “Development of Selective and sensitive Gas Sensor for Manhole Gas Detection” , International Conference on Sensing technology 978-1-5090-0795-0/15/$31.00 ©2016

[3] Sindhoor.S , “IoT Based Garbage Gas Detection System”, Tinternational Journal of Computer Science and Mobile Computing ,vol 5 Issues 9, September-(2016).

[4] Chandler Kemp, Aravind P.Ravikumar and Adam R.Brandt ,“Comaparing natural gas leakage detection technologies using an open-souce virtual gas field simulator” ,Environmental science and technology, vol.4, issues 12, March(2016).

[5] K.Krishnakumari, B.Suganthi, M.Yuganthi P.S.Pooja, “Review of Natural Gas Leakage through gas Pipelines and Various Methods to Detect the Leakage” Internation Conference on Explorations and Innovations in Engineering and technology -2016.

[6] Saransh sharma ,Raja Datta and mrigant Sharad “Avoiding Event Driven Energy Drainage in Wireless Acoustic sensor Nodes for security Applications” International Conference on Communication and Signal Processing, pg no:1991-1996April 6-8, 2016.nishMathew (2012), ‘Internal Model Control of pressure process using ARM

Microcontroller',International Conference Computing, Electronics and Electrical Technologies (ICCEET).

[7] B.Hossain, Saruar J.Shourov, M.Rana, S.Anower ,"Matlab Guidance Based Smart Gas leakage Detection and Security System Using Analog to Digital Technique", International Jounal of Smart Home,vol 9.No 4 .pp.13-24 (2015).

[8] Ali.M.Sadighioon, Nicole metje, David N.Chapman and Carl J.Antony, "Smartpipes:Smart Wireless Sensor Networks for leak Detection in Water Pipelines" Internation Journal of sensors and Actuator Networks, Actuator Netw. , 3, 64-78. 2014.

[9] Sindhu S Kale, Amairullah khan ,"Develpement on Gas Leak Detection and Loation System Based on Wireless Sensor Networks: A Review", International Journal of Engineering Trends and Technology ,vol 12 Number 6- june(2014).

[10] Ashish Shrivastava, Ratnesh Prabhaker, Rajeev Kumar and Rahul verma, "GSM Based Gas Leakage Dection System", International Journal of Technical Reasearch and Application, vol 1, Issue 2 (may-june 2013).

[11] V.Divya, S.Dharanya, S.Shaheen and A.Umamakeswari "Amphibious Surveillance Robot with Smart Sensor Nodes" Indian Journal of Science and Technology" Vol 6 (5) May (2013).

[12] Sheikh Rafik Manihar, Komal Prasd Dewagan, Jayant Rajpurohit,"Multiple gas Analyzer and Indicator",International Journal of Modern Engineering Research, vol.2,Issues 4, July-Aug. (2012).Gowri Shankar (2008),'Controlof Boiler Operation using PLC &SCADA', International Multi Conference of Engineers and Computer Scientists(IMEC).

[13] Jiangwen Wan , Yang YU, yinfeng Wu, Renjein Feng and Ning Yu, "Hierachical Leak Detection and Localization Method in Natural Gas Pipeline Monitoring Sensor Networks" Journal of Sensors, Sensors, 12, 189-214.2012

[14] N.L.T.Lile,M.H.M.Jaafar, M.R.Roslam,M.S.Muhamad Azmi, " Blockage Detection in Circular Pipe Using Vibration Analysis", International Journal on Advancced Science Engineering Information technnology, vol.2,No.3 (2012).

[15] Sidra Rashid, Saad Qaisar, Husnain Saeed and Emad Felemban, " A Method for Distributed Pipeline Burst and Leakage Detection in Wireless Sensor Networks Using Transform Analysis", International Journal of Distributed Sensor Networks, volume , Article ID 9396557, 14 Pages (2012).

[16] Menglong CONG, Shuxu GUO, Yiding WANG, "A novel Methane Detectin System Based on InGaAsP distributed feedback", state Key Laboratory on Intergrated Optoelectronics vol. XLI, No 3 (2011).

[17] Sofian M.kanan,Oussama M.EI-kadri, Imad A.Abu –Yousef and Marsha C.Kanan, "Semiconducting Metal Oxide Based Sensors for Selective Gas Pollutant Detection" Journal of Sensors, Sensors, 9, 8158-8196.2009.

[18] Fei Lei, Lei Yao, Deng Zhao ,Yucong Duan , "Energy –Efficient Abnormal Nodes Detection and Handlings in wireless Sensor Networks" IEEE paper Accepted for Publications.(2006).

[19] Feng Yun,Serguei A.Chevtchenko ,Yong-tae Moon, "GaN Resistive Hydrogen Gas Sensor ", Electrical and Computer Engineering Publications, Applied Physics Letters, 87, 073507 (2005).

[20] Javid Huseynov, Shankar Baliga, Micheal Dillencournt, Lubomir Bic ,Nader Bagherzadeh, "Gas- Leak Localization Using Distributed Ultrasonic Sensors" General Monitors Transnational, Proc. of SPIE Vol. 7293 72930Z1.

[21] Michael B.Frish, "Currect and Emering Laser Sensors For Greenhouse gas sensing and leak Detection'' Physical Sciences Inc.,

[22] Zipeng Zhu, Yuhui Xu and Binqing Jiang , "A One ppm NDIR Methane Gas Sensor with Single frequency Filter Denoising Alogorithm", IEEE control system magzine, pp.80-84 (1898).

Themed Section : Engineering and Technology
© 2018 IJSRSET | Volume 5 | Issue 3 | Print ISSN: 2395-1990 | Online ISSN : 2394-4099

Design of Low Noise Amplifier for X band Application

Makesh Iyer[1], T Shanmuganantham[2]
[1]PG Student, Department of Electronics Engineering, Pondicherry University, Puducherry, India
[2]Assistant Professor, Department of Electronics Engineering, Pondicherry University, Puducherry, India
makwave.26791@gmail.com[1], shanmugananthamster@gmail.com[2]

ABSTRACT

In this work various low noise amplifiers are designed for X band applications which ranges from 8 GHz to 12 GHz and the center frequency considered is 10.5 GHz. This frequency is used for Police Speed RADAR Application. For improving the stability of the amplifier inductive source degeneration methodology is used which not only improves the stability of the amplifier but also increases the signal strength i.e. improves the gain with minimum change in the noise figure. With the help of this technique a high power gain of 13.051 dB and optimum noise figure of 1.468 dB and minimum VSWR of 1.007 at the source side and 1.022 at the load side of the amplifier.

Keywords: LNA, ADS, Power Gain, Noise Figure, X band

I. INTRODUCTION

In the microwave spectrum of electromagnetic waves 8 GHz to 12 GHz frequency range is classified under X band by IEEE. There are various applications operating under this band like traffic light, detection system, Police Speed RADAR, Radio Navigation, Amateur Radio, etc. The main advantage of using X band frequencies for these sensitive applications is its high immunity towards atmospheric attenuation and being robust even in harshest weather conditions. Even in rain, sand storm and other much worse weather conditions there is high link available for the users.

Christina Lessi, Evangelia Karagianni designed an X band LNA for Marine Navigation RADAR and obtained a power gain of 15 dB and noise figure of 5 dB [1]. Tumay Kanar, Gabriel M. Rebeiz, designed cascaded low noise amplifiers using SiGe HBT for X band and K band applications obtaining a noise figure of 1.2 dB for X band and 2.2 dB for K band LNA with a power gain of 24.2 dB and 19 dB respectively [2]. Mohammad Fallahnejad, Yasaman Najmabadi, et al, designed different low noise amplifiers for 10 GHz applications using GaAs HEMT with lumped matching components obtaining a power gain of 15.049 dB and noise figure of 0.806 dB and to further improve the noise immunity RF chokes were used and could achieve less noise figure of 0.775 dB and gain of 14.77 dB [3]. Toahera Abdullah, Apratim Roy, et al, designed a wide band CMOS based LNA with gain flattening method obtaining a power gain of 11 dB, noise figure of 2.3 dB and VSWR of 3.5 at source side and 9.5 at load side of the amplifier [4]. Nan Li, Weiwei Feng, and Xiuping Li, designed a CMOS UWB LNA for 3–12-GHz using the load effect of common gate configuration which is applied with the dual resonance load network for noise figure flatness and wide-band matching which resulted in the power gain

of 13.8 dB and noise figure of 3.5 dB [5]. Murat Davulcu, Can Caliskan, et al, designed high dynamic range SiGe BiCMOS LNA for X band applications obtaining a power gain of 15 dB and noise figure of 2.7 dB [6]. Jyh Chyurn Guo and Ching Shiang Lin designed an UWB CMOS LNA using resistive feedback under forward body bias condition and obtained the noise figure of 3.95 dB, gain of 10.55 dB [7]. Abdelkader Taibi, Mohamed Trabelsi, et al, designed low noise amplifiers with different techniques like connecting an inductor Li as a coupling device between the first and the second amplifier stage where they obtained a noise figure of 5 dB and power gain of 10 dB without Li and 15 dB with Li. Another technique is using a Microstrip band pass filter with the LNA in which power gain of 16 dB and 4.5 dB is achieved [8]. The main parameters of consideration for analysis of the efficient working of a low noise amplifier are power gain, noise figure, VSWR and scattering parameters.

II. DESIGN ASPECTS

Advanced Design System (ADS) simulation tool is used for designing the low noise amplifier. There are two different types of device libraries available in the ADS software namely S – parameter library and RF Transistor library. S – Parameter library works on fixed bias i.e. these parameters of the device are fixed for a particular bias point of the device. In this work, the S – parameter library device is used.

The low noise amplifiers are designed with the help of the S - parameters of the active device being used. These parameters are responsible for determining the stability of the device and hence the amplifier. The step by step procedure for designing a low noise amplifier is described in [9].

The active device used in this work is ATF – 36163 which is a surface mount pseudomorphic high electron mobility transistor (pHEMT) of Hewlett Packard. The range of operation of this device is between 1.5 – 18 GHz.

In a low noise amplifier, the vital parameters to be considered are, maximum gain provided by the active device which is termed as MAG (maximum available gain) and NFmin (minimum intrinsic noise) figure which in turn depends on the S parameters of the device.

Theoretically, the stability of the device is checked using Rollet K - $|\Delta|$ test which is described in [10].
Also, B is another parameter that is calculated for checking stability which should be positive for stable operation given by,

$$B = 1 + \left|S_{11}\right|^2 - \left|S_{22}\right|^2 - \left|\Delta\right|^2 \quad (1)$$

And Δ is given by,

$$\Delta = S_{11}\, S_{22} - S_{12}\, S_{21} \quad (2)$$

The condition for stability is that if $K > 1$, $|\Delta| < 1$ and B = +ve, then the device is unconditionally stable and if $K < 1$ then device is potentially unstable. This condition will tend the device to oscillate and the maximum available gain will be no more valid due to unstable condition.

Hence, the maximum gain produced by the device will now be said as MSG (maximum stable gain) which is mathematically expressed as,

$$MSG = \frac{|S_{21}|}{|S_{12}|} \quad (3)$$

If the device is unconditionally stable i.e. $K > 1$, then the gain obtained will be maximum available gain which is expressed as,

$$MAG = \frac{|S_{21}|}{|S_{12}|}(K \pm \sqrt{K^2 - 1}) \quad (4)$$

There is another parameter introduced to check the stability of the active device for stable operation given by,

$$\mu = \frac{1-|s_{11}|^2}{|S_{22}-\Delta S_{11}^*|+|S_{12}S_{21}|} \quad (5)$$

For the device to operate in unconditionally stable region the value of μ should be greater than 1 (μ > 1) and if it's less than 1 then the device is potentially unstable. This condition will tend the device to oscillate which degrades the noise immunity and distort the signal.

Hence, to improve the stability of the active device there are various techniques available which are described in [11]. One such technique is to connect an inductor in series to the source terminal of the active device i.e. here pHEMT and this technique is said to be inductive source degeneration technique. This technique not only improves the stability of the amplifier but also improves the signal strength i.e. the power gain without much affecting the noise immunity [12]. Here, the circuit is designed both using the lumped elements and distributed components i.e. transmission line equivalent of the lumped components and in this work the fact that lumped components are not suitable to be used at high frequencies is understood due to the reason that is described in [13].

The substrate used for designing the Microstrip matching components is RT Duroid 5880 of Rogers Corporation which has following parameters shown in table 1.

TABLE I

RT Duroid 5880 parameters

Parameters	Values
ε_r	2.2
tanδ	0.0009
substrate height (h)	1.6 mm
metal thickness (t)	0.035 mm
conductivity (σ)	5.8 x e7

Voltage Standing wave ratio (VSWR) is another parameter which determines the amount of reflections that occurs in a microwave circuit due to improper impedance matching. It is represented in the form of reflection co-efficient which is mathematically described in [14].

The VSWR values ranges from 1 < VSWR < ∞ for the corresponding reflection co-efficient of 0 < Γ < 1 theoretically.

III. PROPOSED DESIGNS

The low noise amplifier is designed with source inductive degeneration for this application using lumped matching network components is shown in fig. 1.

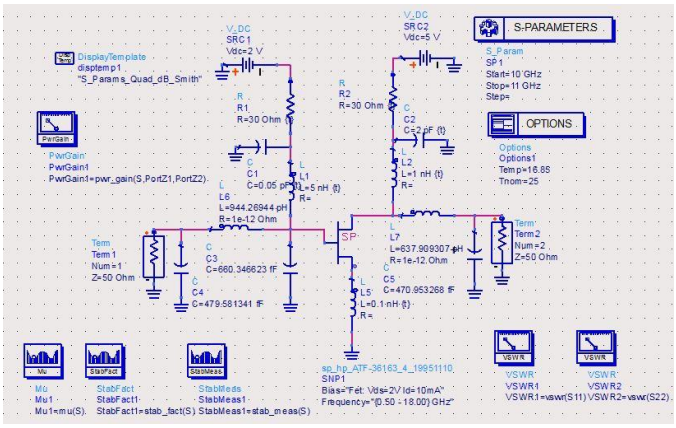

Figure 1. LNA Using Lumped Components

The Rollet's stability factor K, μ and |Δ| obtained for the complete designed amplifier including the matching network is shown above in fig. 2 which is obtained as 1.279, 1.083 and 0.446 respectively.

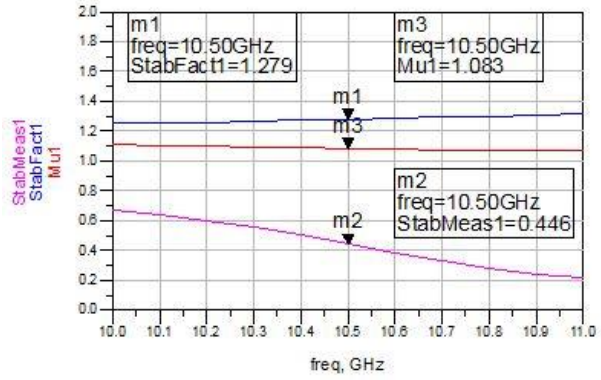

Figure 2. Stability check

Therefore, the above obtained values of K > 1, |Δ| < 1 and μ > 1 proves that the device is unconditionally stable.

The VSWR obtained for the source (VSWR1) and load (VSWR2) matching is shown in fig. 3 which are 1.009 and 6.049 at input and output side respectively. Though the source side VSWR is less, the load side VSWR is very high which signifies that the amount of reflections is very high and hence maximum input power cannot be transferred to the output side of the amplifier.

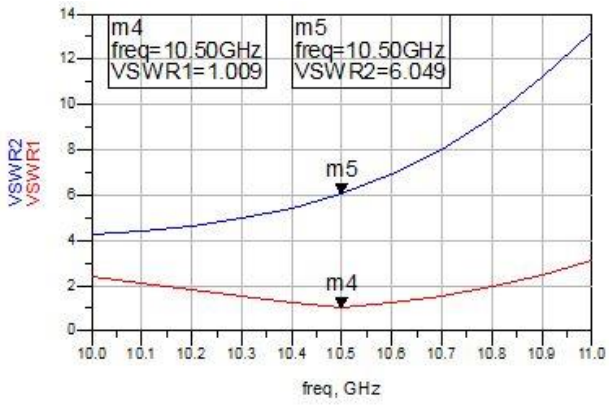

Figure 3. VSWR

The second LNA designed is using distributed Microstrip components for the input and output matching network which is shown in fig.4.

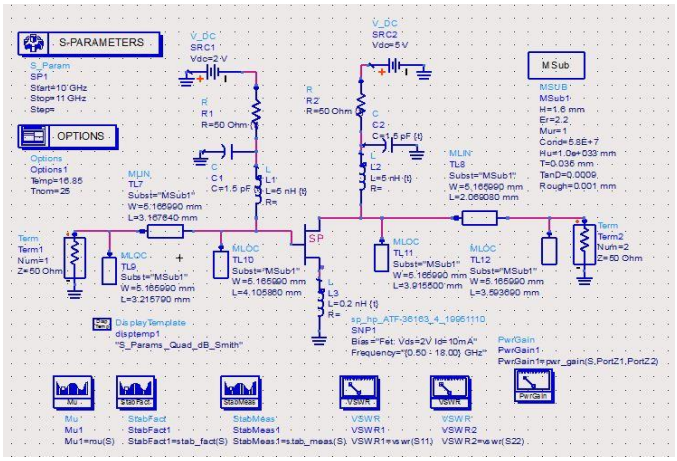

Figure 4. LNA Using Microstrip Components

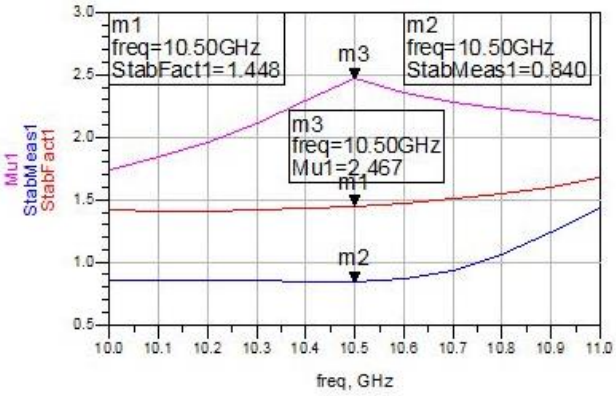

Figure 5. Stability check

The Rollet's stability factor K, μ and |Δ| obtained for the complete designed amplifier including the matching network is shown above in fig. 5 which is obtained as 1.448, 2.467 and 0.840 respectively.

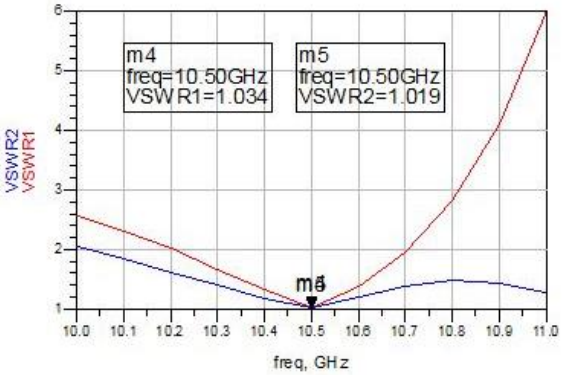

Figure 6. VSWR

The VSWR obtained for the source (VSWR1) and load (VSWR2) matching is shown in fig. 6 which are 1.034 and 1.019 at input and output side respectively. These minimum values of VSWR signifies that the amount

of reflections is very less and hence maximum input power can be transferred to the output side of the amplifier.

The third low noise amplifier is designed using RF chokes connected both at the gate and drain terminal of the active device because of the fact described in [15]. The designed LNA is shown in fig. 7.

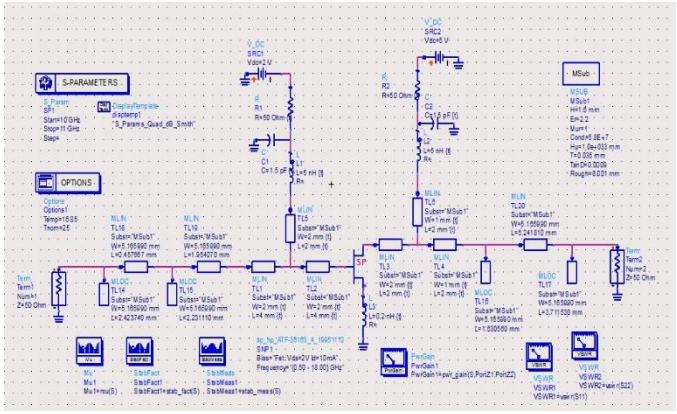

Figure 7. LNA using RF choke

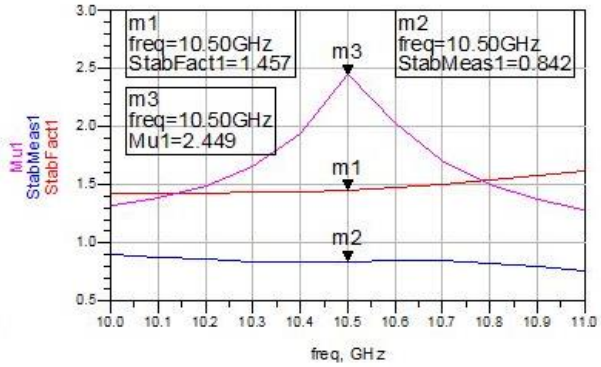

Figure 8. Stability check

The Rollet's stability factor K, μ and |Δ| obtained for the complete designed amplifier including the matching network is shown above in fig. 8 which is obtained as 1.457, 2.449 and 0.842 respectively.

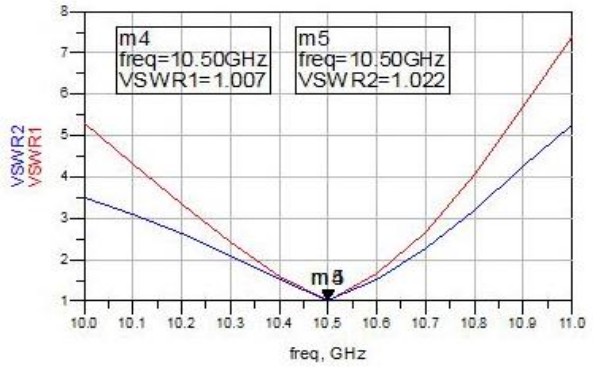

Figure 9. VSWR

The VSWR obtained for the source (VSWR1) and load (VSWR2) matching is shown in fig. 9 which are 1.007 and 1.022 at input and output side respectively. These minimum values of VSWR signifies that the amount of reflections is very less and hence maximum input power can be transferred to the output side of the amplifier.

IV. SIMULATED RESULTS AND DISCUSSION

The power gain and noise figure obtained for the source degenerative LNA using lumped components are 8.327 dB and 1.902 dB as shown in fig. 10 and 11 respectively.

Figure 10. Power Gain

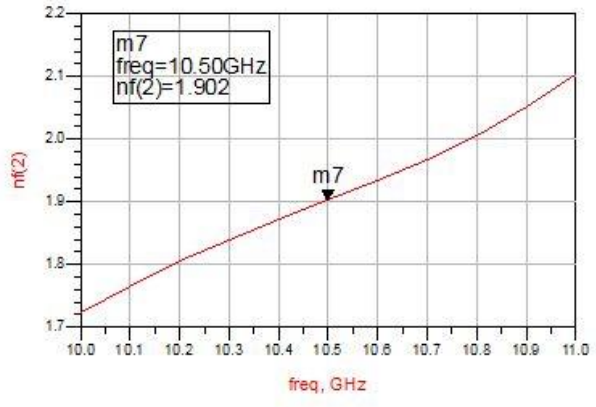

Figure 11. Noise Figure

These values of gain and noise figure shows that the lumped components are not suitable for highter frequency applications due to its low noise immunity.

The S - parameters obtained for lumped component LNA is shown in fig. 12. The values obtained are S_{11} as -46.647 dB, S_{12} as -22.029 dB, S_{21} as 8.327 dB, and S_{22} as -2.899 dB.

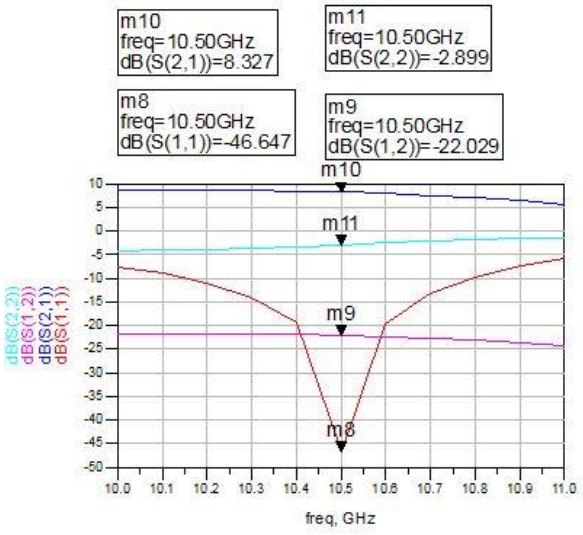

Figure 12. S parameters

The power gain and noise figure obtained for the source degenerative LNA using Microstrip components are 13.014 dB and 1.484 dB as shown in fig. 13 and 14 respectively.

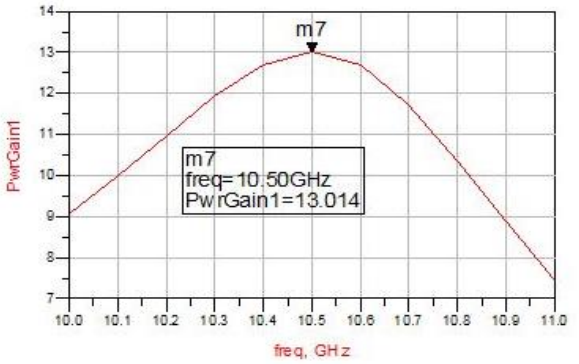

Figure 13. Power Gain

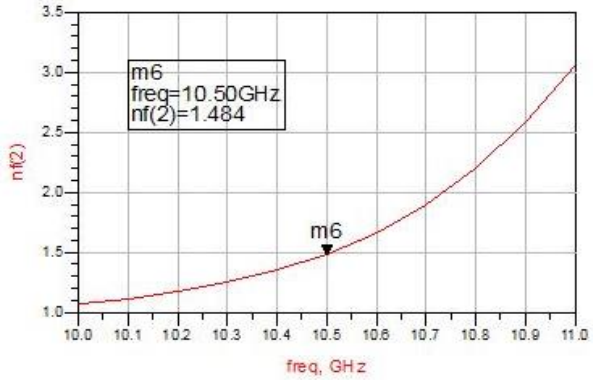

Figure 14. Noise Figure

The S - parameters obtained for Microstrip component LNA is shown in fig. 15. The values obtained are S_{11} as -35.613 dB, S_{12} as -20.995 dB, S_{21} as 13.014 dB, and S_{22} as -40.430 dB.

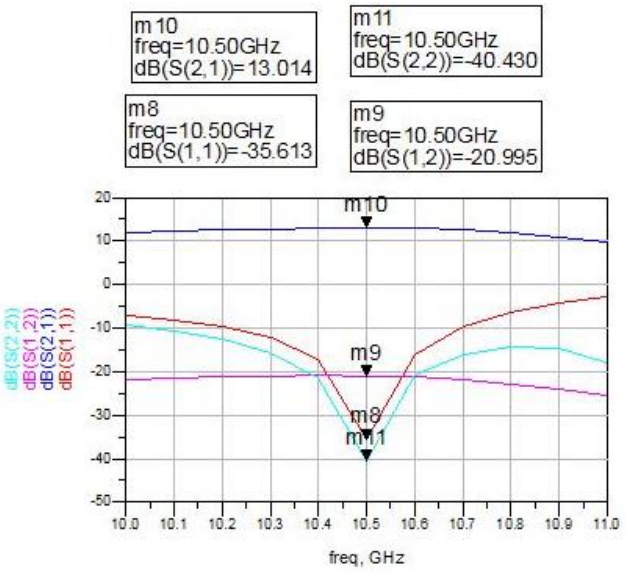

Figure 15. S parameters

The power gain and noise figure obtained for the source degenerative LNA using RF chokes are 13.051 dB and 1.468 dB as shown in fig. 16 and 17 respectively.

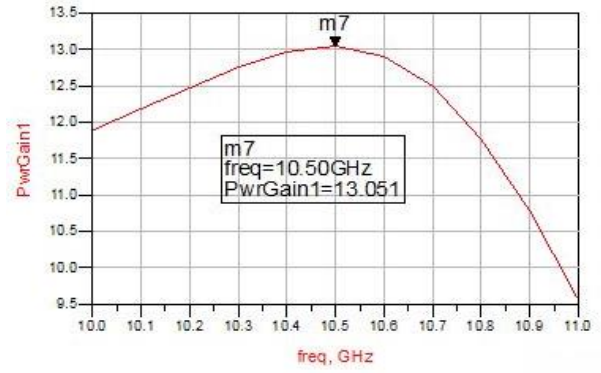

Figure 16. Power Gain

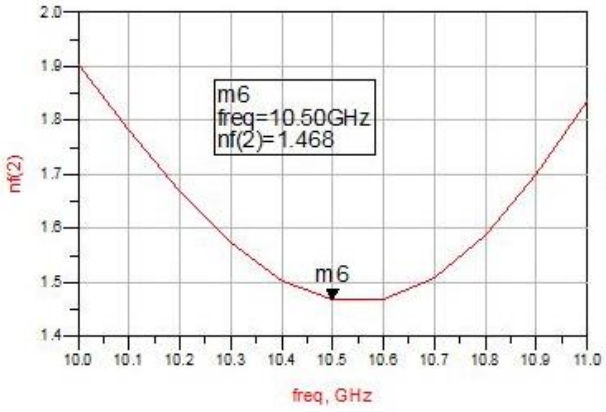

Figure 17. Noise Figure

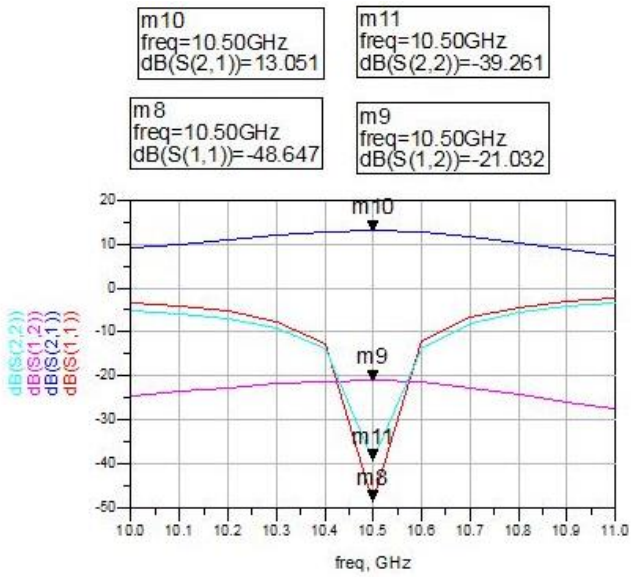

Figure 18. S parameters

The S - parameters obtained for RF choke LNA is shown in fig. 18. The values obtained are S_{11} as -48.647 dB, S_{12} as -21.032 dB, S_{21} as 13.051 dB, and S_{22} as -39.261 dB.

TABLE II

Comparison results of various LNA's

Parameters	Lumped Component LNA	Microstrip Component LNA	RF Choke LNA
K	1.279	1.448	1.457
|Δ|	0.446	0.840	0.842
μ	1.083	2.467	2.449
S_{11} (dB)	-46.647	-35.613	-48.647
S_{21}/G* (dB)	8.327	13.014	13.051
S_{12} (dB)	-22.029	-20.995	-21.032
S_{22} (dB)	-2.899	-40.430	-39.261
NF# (dB)	1.902	1.484	1.468
VSWR	1.009 (I) 6.049 (O)	1.034 (I) 1.019 (O)	1.007 (I) 1.022 (O)

G* - power gain, NF# - noise figure

IV.CONCLUSION

In this work various low noise amplifiers are designed and the results are obtained in ADS software. Different components like lumped components, distributed components, and RF choke are used for getting better noise immunity, gain and minimum VSWR while source degenerative technique is used for improving the stability of the amplifier and considering the overall comparison results from section 4 we can conclude that the RF choke designed low noise amplifier is providing better performance by providing a power gain of 13.051 dB, 1.468 dB noise figure, source side VSWR of 1.007 and load side VSWR of 1.022 which shows that minimum reflections will occur both at the input and output side of the amplifier resulting in maximum power transfer from source to load. The bandwidth constraint in these designs can be solved by implementing multistage cascading and cascoding techniques in LNA design.

V. REFERENCES

[1] Christina Lessi, Evangelia Karagianni, "An X-Band Low Noise Amplifier Design for Marine Navigation Radars," *International Journal of Communications, Network and System Sciences*, vol. 7, March 2014.

[2] Tumay Kanar, Gabriel M. Rebeiz, "X- and K-Band SiGe HBT LNAs with 1.2- and 2.2-dB Mean Noise Figures," *IEEE Transactions on Microwave Theory and Techniques,* vol. 62, no. 10, October 2014.

[3] Mohammad Fallahnejad, Yasaman Najmabadi, et al, "Design and Simulation of Low Noise Amplifier at 10 GHz By Using GaAs High Electron Mobility Transistor," *IOSR Journal of Electrical and Electronics Engineering,* vol. 10, Issue 5, Sep – Oct. 2015.

[4] Toahera Abdullah, Apratim Roy, et al, "A Wideband 6.9-17.7 GHz CMOS Low-Noise Amplifier with a Gain Flattening Technique," *16th International Conference on Computer and Information Technology*, March 2014.

[5] Nan Li, Weiwei Feng, and Xiuping Li, "A CMOS 3–12-GHz Ultra wideband Low Noise Amplifier by Dual-Resonance Network," *IEEE Microwave and Wireless Components Letters*, vol. 27, no. 4, April 2017.

[6] Murat Davulcu, Can Caliskan, et al, "X-Band High Dynamic Range Flat Gain SiGe BiCMOS Low Noise Amplifier," *Proceedings of the 10th European Microwave Integrated Circuits Conference,* September 2015.

[7] Jyh-Chyurn Guo, Ching-Shiang Lin, "Low Power UWB CMOS LNA Using Resistive Feedback and Current-Reused Techniques Under Forward Body Bias," *Proceedings of the 47th European Microwave Conference,* October 2017.

[8] Abdelkader Taibi, Mohamed Trabelsi, et al, "Efficient UWB low noise amplifier with high out of band interference cancellation," *IET Microwaves, Antennas & Propagation Journal*, vol. 11, Issue. 1, 2017. Doi: 10.1049/iet-map.2016.0187

[9] Makesh Iyer, T Shanmuganantham, "Design of LNA for C band Applications," *IEEE International Conference on Circuits and Systems,* March 2018.

[10] Makesh Iyer, T Shanmuganantham, "Design of LNA for Satellite Uplink," *Elsevier's SSRN Journal of Information Systems & eBusiness Network,* March 2018.

[11] Makesh Iyer, T. Shanmuganantham, "Optimum LNA for WAVE Application," Proceedings of *International Conference on Micro-Electronics, Electromagnetics and Telecommunications*, February 2018.

[12] M.H. Misran, M.A. Meor Said, et al, "Design of Low Noise Amplifier for WiMAX Application," *IOSR Journal of Electrical and Electronics Engineering*, vol. 6, Issue 1, June 2013.

[13] Makesh Iyer, T Shanmuganantham, "LNA Design for Airport Surveillance RADAR Receiver System," *IEEE International Conference on Recent Advances in Engineering and Technology,* December 2017.

[14] Makesh Iyer, T Shanmuganantham, "LNA design for WLAN Applications," *IEEE International Conference on Circuits and Systems,* March 2018.

[15] Makesh Iyer, T. Shanmuganantham, "Design of LNA for RADAR Altimeters," *Proceedings of International Antenna Test and Measurement Society Conference (ATMS),* March 2018.

Themed Section : Engineering and Technology
© 2018 IJSRSET | Volume 5 | Issue 3 | Print ISSN: 2395-1990 | Online ISSN : 2394-4099

Deep Learning based Bird Audio Detection

E. Sophiya[1], S. Jothilakshmi[2]

[1]Department of Computer Science and Engineering, Annamalai University, Annamalainagar, Tamilnadu, India

[2]Department of Information Technology, Annamalai University, Annamalainagar, Tamilnadu, India

venus.sophiya@gmail.com [1], jothi.sekar@gmail.com [2]

ABSTRACT

Audio event detection (AED) is defined as analyzing a continuous acoustic signal in order to extract the sound events present in the acoustic scene. Sound events are best labels for an auditory scene, because they help in describing and understanding a recognizable event present in the sound. In this work, Bird audio detection is carried out to determine whether birds sound is present in the given environmental audio. The system is designed with machine learning algorithm using Tensorflow. The proposed model learns spectrogram features from audio and predicts the presence of bird sounds with an accuracy of 80.76%.

Keywords: Audio processing, Audio scene analysis, Audio event detection, Bird audio detection, Deep learning, Tensorflow, Audio features.

I. INTRODUCTION

Automatic detection of animal vocalizations, such as singing birds, has a scientific challenge in itself, can be helpful for monitoring biodiversity. Various researches are involved in bioacoustics, the recent field named ecoacoustics that gathers ever-growing quantities of recordings that need to be manually analyzed. Automatic tools that label the recordings accurately are very much in demand to ease the time-consuming task of listening to hours of them [1]. Monitoring birds by their sound is important for many environmental and scientific purposes. A variety of crowdsourcing and remote-monitoring projects now record these sounds, and analyze the sound automatically. Still there are many issues to solve, as indicated by the number of projects that are yet to be fully automated.

Bird audio detection is one of intensive research given by Detection and Classification of Acoustic Scenes and Events (DCASE 2018), due to the fact that birds are more easily detectable through the audio modality rather than vision. Bird audio detection (BAD) aims to detect the presence or absence of bird calls in an audio recording. BAD is an Audio event detection (AED) task, which aims to identify all the audio events and their occurrence time in a mixed audio recording. BAD have many applications in environmental science, such as monitoring the density and the migration of birds in depopulated zone. Bird audio detection (BAD) is defined as identifying the presence of bird sounds in a given audio recording. Figure 1 shows the Bird audio detection system.

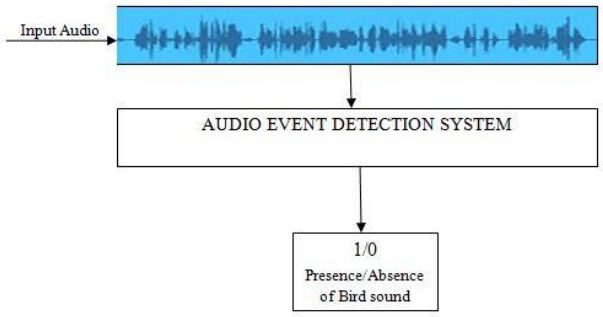

Figure 1. Audio Event Detection System for Birds Sound

In many conventional, remote wildlife-monitoring projects, the event detection process is not fully automated and requires heavy manual labor to label the obtained data [2], [3]. In certain cases such as dense forests and low illumination, automated detection of birds in wildlife can be more effective through their sounds compared to visual cues. The challenge provides three bird audio datasets recorded in different acoustic environments. Bird sounds can be broadly categorized as vocal and non-vocal sounds. In this research work, since non-vocal bird sounds are harder to associate with birds without any visual cues, the research on BAD has been mostly focused on vocal sounds. The challenge provided annotated and non-annotated bird call recordings. The former is utilized as the training dataset and the latter are recordings from a completely different geographical location and employed as the test dataset.

Different locations also mean different acoustic environments leading to a variety of sound sources. Furthermore, each of these bird species has unique calls, resulting in a wide variety of bird calls. Labeling such a wide variety of calls into one class weakens the classifier and can result in misclassification of similar sounding non-bird sounds. The problem is further intensified in the dataset used because each of the bird calls has been recorded with different devices that add their own system noise. A bird audio detection method which can work across such a wide range of species and environments is termed as a generic method. BAD have many difficulties.

First, in an audio clip only the presence or the absence of birds is known but not knowing the time stamps of the bird calls and other sounds. Detecting the presence of bird calls in audio recordings can serve as a basic step for wildlife and biodiversity monitoring. To help advance the state of the art in automating this task, Bird audio detection challenges were organized by DCASE. Specifically, participants were asked to build algorithms that predict whether a given 10-second recording contains any type of bird vocalization, regardless of the species. Use of passive acoustic monitoring to estimate animal population density and there is increasing interest in using acoustic indices for biodiversity assessments.

In this work, the bird audio detection using simple convolutional neural networks (CNNs) is proposed. The CNN architecture exploits the combined modeling of fully connected four layers. CNN architecture has also been proposed in automatic speech recognition and music classification [4]. Bird species identification has been the target of several international evaluation campaigns such as LifeCLEF (BirdCLEF), a yearly contest including bird species identification in various audio recordings. A variety of machine learning techniques have been explored for this task. The winning solutions of last year BirdCLEF edition were based on deep convolutional neural networks (CNNs) [5]. Indeed, the success of deep learning (DL) and deep neural networks (DNN) in many domains involving classification tasks, offers new and appealing perspectives. In the context of the BAD challenge, concerned with the detection of bird sound in short duration recordings, the evaluation reported is based on CNNs, more specifically on densely connected CNNs, also called denseNets [6].

The rest of the paper is organized as follows. The related work of bird audio detection is reviewed in Section 2. The proposed framework is explained in

Section 3. Experimental results obtained by proposed method are discussed in Section 4. Finally, Section 5 concludes the paper.

II. Related Works

Sharath Adavanne, Konstantinos Drossos, et al [7] proposed the novel method for detection of bird calls in audio segments using stacked convolutional and recurrent neural networks. Data augmentation using blocks mixing and domain adaptation using the test mixing is implemented to make the method robust for unseen data. Thomas Pellegrini [1] proposed to detect bird sounds in audio recordings automatically and monitoring biodiversity based on audio field recordings. The author experimented several types of convolutional neural networks to estimate how accurate the state-of-the-art machine learning approaches and the bird audio detection challenges are reported in the framework. Emre Cakir, Sharath Adavanne, et al [8] proposed the convolutional recurrent neural networks on the task of automated bird audio detection in real-life environments. The convolutional layers extract high dimensional, local frequency shift invariant features, while recurrent layers capture longer term dependencies between the features extracted from short time frames. Qiuqiang Kong, Yong Xu, et al [9] implemented Bird audio detection (BAD) to detect whether there is a bird call in an audio recording or not. They applied joint detection and classification (JDC) model on the weakly labeled data (WLD) to detect and classify an audio clip at the same time. Anshul Thakur, R. Jyothi, et al [10] describes the bird activity detector which utilises a support vector machine (SVM) with a dynamic kernel. Bird activity detection is the task of determining if a bird sound is present in a given audio recording. Dynamic kernels are used to process sets of feature vectors having different cardinalities. Probabilistic sequence kernel (PSK) is one such dynamic kernel. Thomas Grill and Jan Schlüter [11] present and compare two approaches to detect the presence of bird calls in audio recordings using convolutiona neural networks on mel spectrograms. Comparing multiple variations of the systems, find that despite very different architectures, both approaches can be tuned to perform equally well. Dan Stowell, Mike Wood, et al [12] reviews the state of the art in automatic bird sound detection, and identifies a widespread need for tuning-free and species-agnostic approaches.

III. Proposed Work

Deep learning refers to a machine learning techniques that uses supervised or unsupervised algorithm to automatically learn multiple levels of representations in deep architectures. Inspired by the human biological neurons for processing natural signals, deep learning has reached much attention in various research domains such as speech recognition, computer vision, and image analysis. Figure 2 shows Deep Neural Network (DNN) architecture.

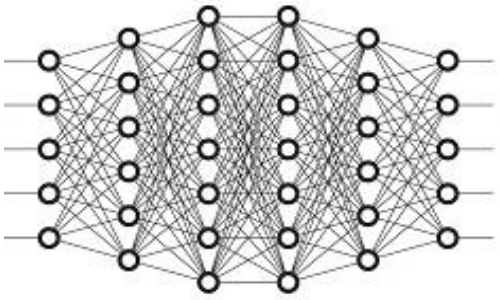

Figure 2. Architecture of DNN

Tensorflow is used to implement complex DNN structures without getting complex mathematical details, and availability of large datasets. Tensorflow has a high-level machine learning API which makes easy to configure, train, and evaluate a large number of machine learning models. Keras, a high-level deep learning library, is used on top of Tensorflow. It supports various DNNs like RNNs, CNNs, and a combination of the two architectures.

In the proposed work spectrogram features are learned from the audio signals to detect the bird audio.

The machine learning model is designed with CNN with three hidden layers. This network is implemented in keras. In this system, the official dataset of IEEE AASP Challenge (2018) on Detection and Classification of Acoustic Scenes and Events (DCASE) is used. The dataset consists of 10sec long wav files with 44.1 khz mono PCM. The data files are manually labeled with a 1 and 0 to indicate the presence/absence of any birds audio within that audio clip.

For each input audio signal, Short Term Fourier Transform (STFT) magnitude spectrogram with a window size of 10ms is extracted over 40 ms audio frames of 50% overlap, windowed with hamming window. Librosa library is used in the feature extraction process.

The spectrogram is a representation of the audio signal in time-frequency domain. The relevant information content of spectrogram will be high in a time domain of a signal. Thus the proposed work can easily detect the bird audio event within an audio clip. Figure 3 and Figure 4 shows the visual representation and spectrogram representation of audio with and without birds sound. The preprocessed data is then mapped to the training and test data. The dataset has audio files with and without bird sounds. So applying normalization will improve the prediction of events within the audio. The features are then normalized using scikit learn preprocessing function.

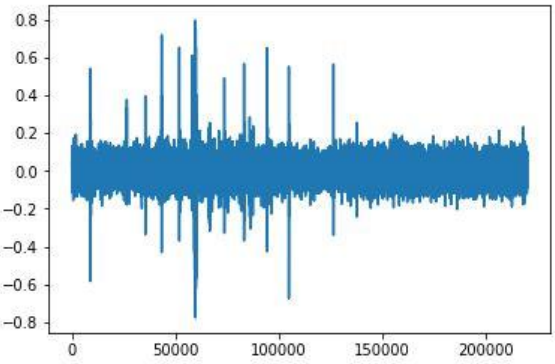

Figure 3 (a). Representation of Audio with Bird sound

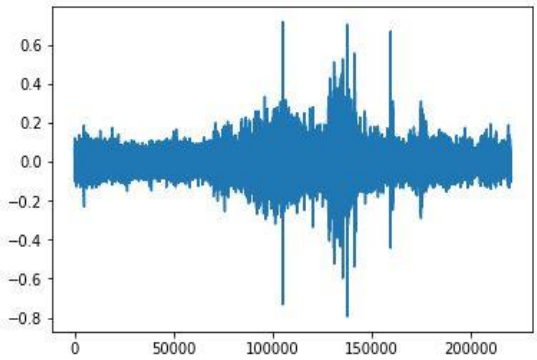

Figure 3 (b). Representation of Audio without Bird sound

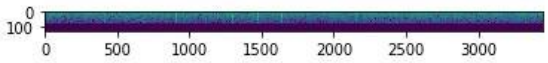

Figure 4 (a). Spectrogram of Audio with Bird sound

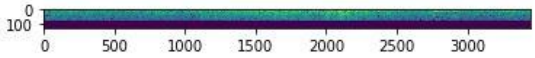

Figure 4 (b). Spectrogram of Audio without Bird sound

The preprocessed data is then mapped to the training and test data. The dataset has audio files with and without bird sounds. So applying normalization will improve the prediction of events within the audio. The features are then normalized using scikit learn preprocessing function. The machine learning model used in this work is CNN and the network is implemented with keras. The keras library will support best function to try various network architectures. The architecture of model consists of four dense layers with 128, 32, 32, and 2 units that detect the bird audio. Each convolution layer is mapped with Relu activation function and output layer is mapped by softmax function.

IV. Experimental work and Results

The objective of the feature learning in the network is to get the estimated bird audio event closer to binary target outputs, where target output is 1 if any bird sound is present in a given recording and 0 vice versa.

For the prediction of birds audio, the dataset is randomly partitioned into 60% for Training, 20% for

Validation, 20% for Testing. The proposed model is evaluated using three cross fold validation scheme.

TABLE I
Development dataset for Bird audio detection

Dataset	Bird Sound	
	Present	Absent
freefield1010	5755	1935

The network is trained with back-propagation through time using Adam optimizer and binary cross-entropy as the loss function. Keras deep learning library has been used to implement the network. The scores for validation and test dataset are presented in Table 2. The proposed network outputs a probability of 80.76% for birds sound in these recordings.

TABLE III
SCORES FOR VALIDATION AND TEST DATA WITH SPECTROGRAM FEATURE

Feature	Accuracy (%)	
	Validation	Test
Spectrogram	90.9	80.76

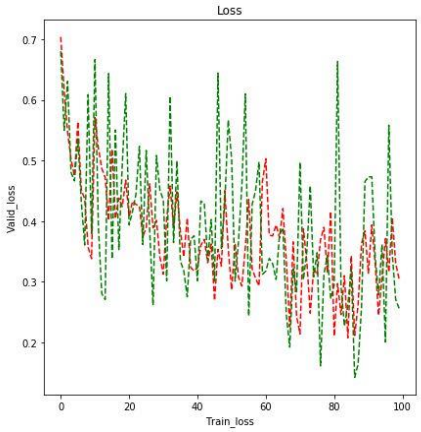

Figure 5(a). Loss

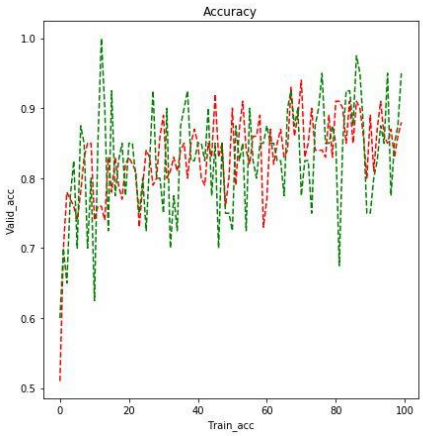

Figure 5(b). Accuracy

V. CONCLUSION

In this work a bird audio detection is carried out based on deep learning algorithm using Tensorflow. The objective of the model is to estimate the presence/ absence of birds sound in a given audio. The audio detection system outputs a zero if none of the target species are detected, and as one otherwise. The datasets are collected from DCASE 2018 challenge. CNN network with spectrogram features were used to model the system. The proposed work thus predicts the bird audio by achieving an accuracy of over 80.76%. In future, this work will be extended with different network architecture and the model can also be hyper tuned with parameters to predict the events better with higher accuracy.

VI. REFERENCES

[1] Thomas Pellegrini "Densely Connected CNNs for Bird Audio Detection" 25th European Signal Processing Conference (EUSIPCO), 2017.

[2] R. T. Buxton and I. L. Jones, "Measuring nocturnal seabird activity and status using acoustic recording devices: applications for island restoration," Journal of Field Ornithology, vol. 83, no. 1, pp. 47–60, 2012.

[3] T. A. Marques, L. Thomas, S. W. Martin, D. K. Mellinger, J. A. Ward, D. J. Moretti, D. Harris, and P. L. Tyack, "Estimating animal population density using

passive acoustics," Biological Reviews, vol. 88, no. 2, pp. 287–309, 2013.

[4] E. C. akır, G. Parascandolo, T. Heittola, H. Huttunen, and T. Virtanen, "Convolutional recurrent neural networks for polyphonic sound event detection," in IEEE/ACM TASLP Special Issue on Sound Scene and Event Analysis, 2017

[5] E. Sprengel, Y. Martin Jaggi, and T. Hofmann, "Audio based bird species identification using deep learning techniques," Working notes of CLEF, 2016.

[6] G. Huang, Z. Liu, K. Q. Weinberger, and L. van der Maaten, "Densely connected convolutional networks," arXiv preprint arXiv:1608.06993, 2016.

[7] Sharath Adavanne, Konstantinos Drossos, Emre Cakır, Tuomas Virtanen "Stacked Convolutional and Recurrent Neural Networks for Bird Audio Detection" 25th European Signal Processing Conference (EUSIPCO), 2017

[8] Emre Cakir, Sharath Adavanne, Giambattista Parascandolo, Konstantinos Drossos and Tuomas Virtanen "Convolutional Recurrent Neural Networks for Bird Audio Detection" 25th European Signal Processing Conference (EUSIPCO), 2017

[9] Qiuqiang Kong, Yong Xu, Mark D. Plumbley "Joint Detection and Classification Convolutional Neural Network on Weakly Labelled Bird Audio Detection" 25th European Signal Processing Conference (EUSIPCO), 2017

[10] Anshul Thakur, R. Jyothi, Padmanabhan Rajan, A.D. Dileep "Rapid Bird Activity Detection Using Probabilistic Sequence Kernels" 25th European Signal Processing Conference (EUSIPCO), 2017

[11] Thomas Grill and Jan Schlüter "Two Convolutional Neural Networks for Bird Detection in Audio Signals" 25th European Signal Processing Conference (EUSIPCO), 2017

[12] Dan Stowell, Mike Wood, Yannis Stylianou and Herve Glotin "Bird Detection In Audio: A Survey and a Challenge" IEEE International Workshop On Machine Learning For Signal Processing, Salerno, Italy, Sept. 13–16, 2016

Themed Section : Engineering and Technology
© 2018 IJSRSET | Volume 5 | Issue 3 | Print ISSN: 2395-1990 | Online ISSN : 2394-4099

CPW Fed Multiple Hexagonal Shaped Antenna for IoT Application

Vyshnavi Das S K[1], T Shanmuganantham[2]
[1]PG Scholar, Dept. of Electronics Engg. Pondicherry University, Pondicherry, India
[2]Assistant Professor, Dept. of Electronics Engg. Pondicherry University, Pondicherry, India
vyshnadassk@gmail.com[1],shanmugananthamster@gmail.com[2]

ABSTRACT

A CPW fed antenna of multiple hexagonal shapes is proposed for Internet of Things (IoT) application. The substrate of the antenna is taken as FR4 epoxy of relative permittivity 4.4 and dielectric loss factor 0.02. The operating frequencies of the antenna are found to be 4.84GHz and 5.88GHz with impedance bandwidth of 80MHz and 70MHz respectively. The gain of radiation of the antenna is 1.4 dBi and 7.43 dBi respectively at the respected resonant frequencies. The operating bands of the antenna are in the ranges of WiFi network with the required specifications of IoT applications.

Keywords: CPW, Multiple hexagonal shapes, Internet of Things, FR4 epoxy, Relative permittivity, Dielectric loss factor

I. INTRODUCTION

The wireless communication has vigorous impact in our daily life. As the demand increases the flexibility of the system should also be increased. Development in combining two or more technology in to a single stream is widely considered in these days. The Internet of Things (IoT) is such a technology which is an integration of Wireless Sensor Network (WSN), Wireless communication network, Software, Actuators etc,. [1]. The virtual mapping of things to things or communication between the physical things without the human interaction is possible through this technology.

The each things or the device which is recognized in an IoT domain is provided with a unique IP address. These devices should also embed with sensors thus they can be identified by the conditions given by the users [2]. This WSN interconnects with wireless communication network such that the mapping of virtual world to physical world and vice versa is possible. The integration of softwares and actuators enables the practical implementations of this technology in the real world. The antenna which is used for IoT domain should works according to some prerequisites such that the operation frequency of the antenna should matched with the frequency ranges of any of the wireless communication network like Bluetooth, WiFi, WiMAX, etc,. [3].

Since IoT is an emerging technology. There should be a limit for the amount of data that has to be transferred through this technology. Otherwise the memory requirement and area of the device must be enlarged in order to compensate power handling which leads to incompatibility of the IoT module with the real world [4]. Thus as per these concerns only

few bytes of data is transferring through this technology so the bandwidth requirement of the antenna is also limited within 1GHz.

The organization of this document is as follows. In Section 2, the dimension and theoretical parameters of the antenna is given. The section 3 presents the simulated results and discussions and Section 4 concludes the work.

II. ANTENNA DESIGN

The substrate of the antenna is chosen as FR4 epoxy material of relative permittivity 4.4 and dielectric loss tangent 0.02. The conductor backed CPW fed antenna having the dimension of 25 × 30 × 1.6 mm^3 .The geometrical shape of the antenna is given in Figure 1.

A conductor backed CPW feeding technique is used for the proposed antenna where third ground plane acts as the third return conductor which covers the entire back side of the substrate [5]. The radiating patch of the antenna is a combination of five hexagons and one circle. The continuous disturbance in the geometry of the antenna alters the distribution of the surface current which makes deviations in the phase of the current [6]. This enables the antenna to exhibit more than one resonant frequency of operation [7].

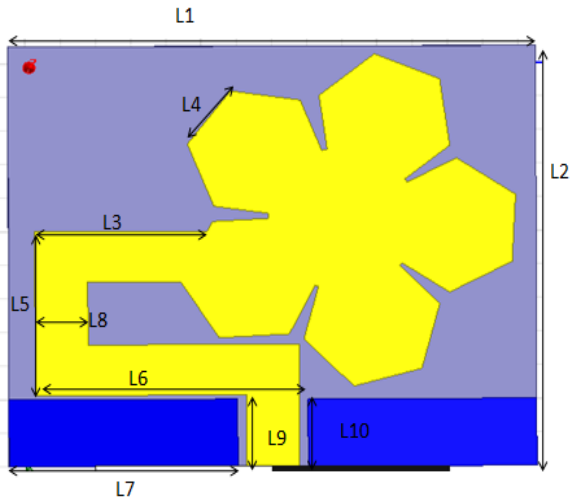

Figure 1. The structure of the antenna

The parametric dimensions of the antenna is given in the Table I.

TABLE I

The dimensions of the antenna

Parameter	Dimension(mm)	Parameter	Dimension(mm)
L1	25	L6	15
L2	30	L7	13
L3	13.5	L8	3.75
L4	10	L9	5
L5	9.75	L10	4

III. SIMULATED RESULTS AND DISCUSSION

The characteristics of an antenna is depending upon certain parameters like reflection coefficient, radiation pattern, VSWR, gain, directivity, radiation efficiency etc, These parameter values are discussed here for the proposed antenna.

A. Reflection Coefficient

Reflection coefficient is simply gives the idea of how much power is reflected back due to the impedance mismatch in the transmission medium. Generally the impedance bandwidth of the antenna is selected in the range of frequencies at which have the reflection coefficient or S_{11} value less than -10dB. The simulated graph of reflection coefficient Vs frequency is given in Figure 2.

The operation frequency bands of the antenna are (4.79-4.88) GHz and (5.84-5.91) GHz with impedance bandwidth of 80MHz and 70 MHz respectively. The resonance frequencies are 4.84 GHz and 5.88 GHz is in the ranges of the WiFi bands with the peculiarities of IoT applications.

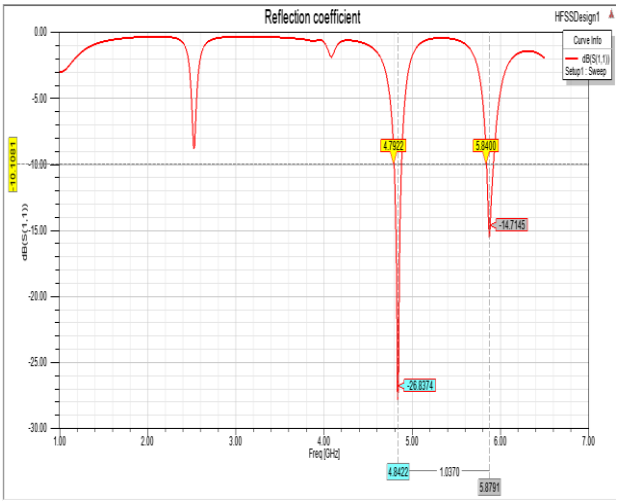

Figure 2. The S_{11} value in dB Vs frequency graph

B. Voltage Standing Wave Ratio (VSWR)

The VSWR value of the antenna gives how much efficiently the power is transmitted. The value of VSWR is less than 2 for perfect impedance match between the antenna and the transmission line. The simulated result of VSWR is shown in the Fig .3

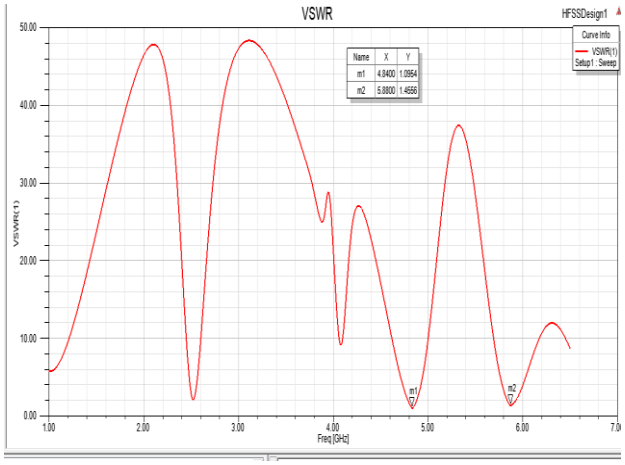

Figure 3. The VSWR value Vs frequency graph

The simulated results shows that the antenna exhibits perfect impedance match in the resonating frequencies 4.84 GHz and 5.88 GHz with the VSWR values of 1.09 and 1.45 respectively.

C. Radiation Pattern

The Radiation Pattern of the antenna illustrates about the radiation of the antenna in space. The primary sweep of the radiation pattern is the elevation angle. For the two values of azimuthal angle, 0 degree and 90 degree the radiation pattern is simulated and illustrated in the Figure 4 and Figure 5 for the respected resonant frequencies.

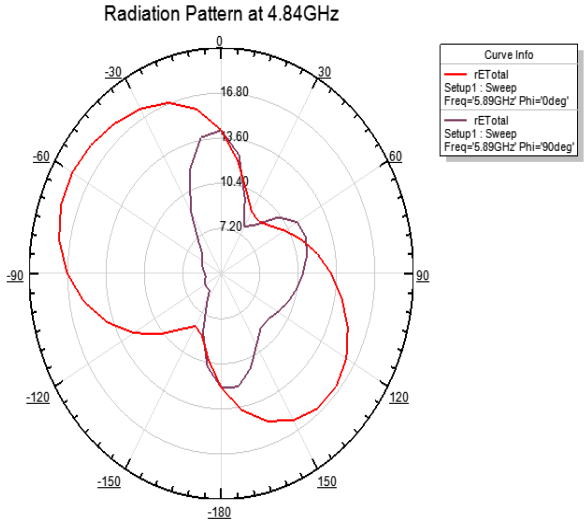

Figure 4. The Radiation pattern of the antenna at 4.84 GHz

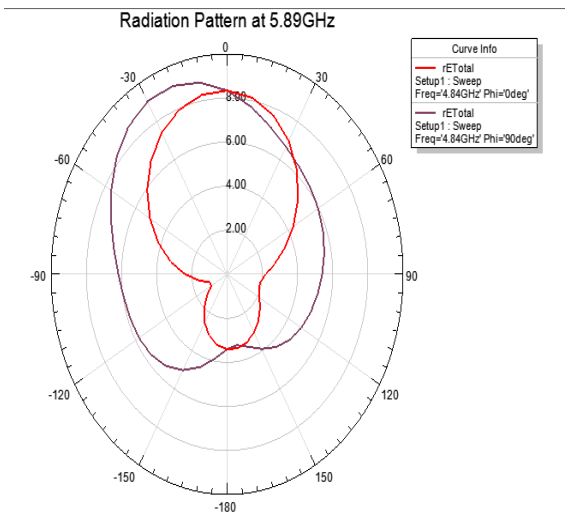

Figure 5. The Radiation pattern of the antenna at 5.88 GHz

D. Gain of the Antenna

The gain of the antenna is the parameter which describes the performance of the antenna in the far field. The simulated results of the gain of the antenna

at resonant frequencies are given in the Figure 6 and Figure 7.

The antenna proposed antenna is radiating in the far field with the gain of 1.4 dBi and 7.43 dBi at 4.84 GHz and 5.88 GHz respectively.

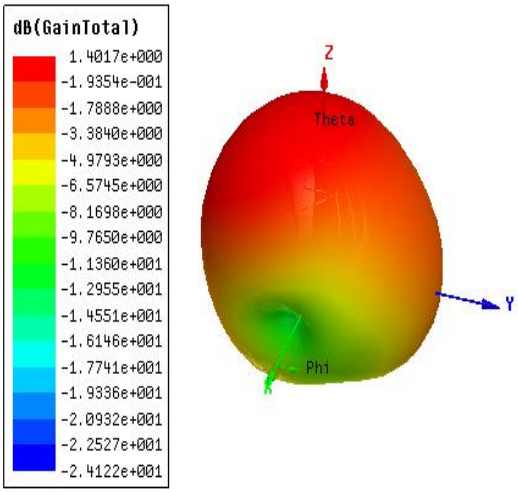

Figure 6: The Gain of the antenna at 4.84 GHz

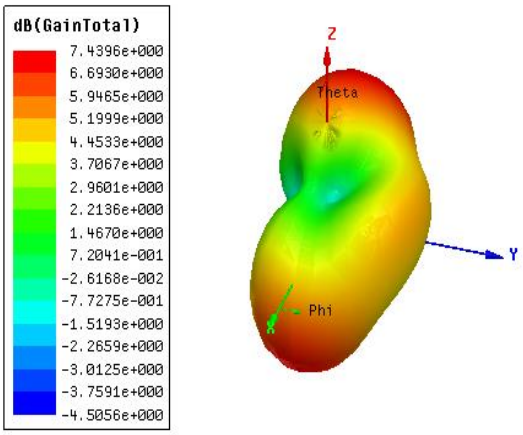

Figure 7. The Gain of the antenna at 5.88 GHz

The total performance of the antenna is shown in the Table II and comparison with the existing model in the current scenario is also provided Table III.

TABLE II

The overall performance of the proposed antenna

Parameter	**Value at 4.84 GHz**	**Parameter**	**Value at 5.88 GHz**
Bandwidth	80MHz	Bandwidth	70MHz
VSWR	1.09	VSWR	1.45
Gain	1.4dBi	Gain	7.43dBi
Reflection Coefficient	-26.8dB	Reflection Coefficient	-14.7dB

TABLE III

The overall performance of the antenna [8]

Parameter	**Value at 4.72 GHz**	**Parameter**	**Value at 5.73 GHz**
Bandwidth	890MHz	Bandwidth	720MHz
VSWR	1.15	VSWR	1.16
Gain	1.8dBi	Gain	2.5dBi
Reflection Coefficient	-22.7dB	Reflection Coefficient	-22.1dB

According to the comparison table the proposed antenna is providing better reflection coefficient and VSWR value at first resonant frequency and better gain at second resonant frequency.

.

IV.CONCLUSION

A CPW fed dual band antenna for IoT application with multiple hexagonal shape is introduced in this work. The resonant frequencies of the antenna found as 4.84 GHz and 5.88 GHz with impedance bandwidth of 80 MHz and 70 MHz respectively. The working ranges of the antenna at respected frequencies are (4.79 GHz-4.87 GHz) and (5.84 GHz-5.91 GHz) with gain of 1.4dBi and 7.43 dBi respectively.

V. REFERENCES

[1] Vikram N, Kashwan K. R, "Design of ISM Band RFID Reader Antenna for IoT Applications", IEEE International Conference on Wireless Communication, Signal Processing and Networks (2016)

[2] Andrea Zanella, Nicola Bui, Angelo Castellani, Lorenzo Vangelist, and Michele Zorzi, "Internet of Things for Smart Cities", IEEE Internet of Things journal, Vol. 1,No.1, F(2014)

[3] S. Lemey , O. Caytan , D. Vande Ginste , P. Demeester , H. Rogier , and M. Bozzi, "SIW Cavity-backed Slot (Multi-)Antenna Systems for the Next Generation IoT Applications", IEEE, (2016)

[4] J. W Cervanres-Solis, C Baber, "Towards the definition of a modeling framework for meaningful Human- IoT interactions", British Human Computer Interaction Conference, (2017).

[5] Vyshnavi Das S K, T Shanmuganantham, "Design of Multiband Microstrip Patch Antenna for IoT Applications", IEEE International Conference on Circuits and Systems (ICCS), (2017,)978-1-5090-6480-9

[6] Vyshnavi Das S.K, T Shanmuganantham, "Design of Polygon Shaped Patch Antenna for IoT Application", International Conference on Communication, Networks and Computing (CNC), (In press) ,(2018)

[7] R Kiruthika, T Shanmuganantham, Rupak Kumar Gupta, " A fan shaped triple microstrip patch antenna with DGS for X- band application", Control, Instrumentation, Communication and Computational Technologies (ICCICCT), (2016)

[8] Vyshnavi Das S K, Dr. T Shanmuganantham, "CPW fed Dual band Antenna for IoT Application", International Journal of Engineering and Technology,(In press),(2018).

Themed Section : Engineering and Technology
© 2018 IJSRSET | Volume 5 | Issue 3 | Print ISSN: 2395-1990 | Online ISSN : 2394-4099

Home Automation Using Py-Ardomotics

[1]K.Anu, [2]R.Hemalatha, [3]K.Rajesh, [4]M.Shenbagapriya, [5]C.Gomathi
[1] UG Scholar, Knowledge Institute of Technology, Salem, Tamilnadu, India
[2,3,4,5] Assistant Professor, Knowledge Institute of Technology, Salem, Tamilnadu, India

ABSTRACT
According to the present world scenario, the word automation extending all over the countries, but in India it doesn't reach the level till yet. Home automation is becoming popular due to its numerous benefits. Home automation refers to the control of home appliances and domestic features by local networking or by remote control. The main objective of this work is to bring automation in the domestic level without using the GSM or GPS. Domestic automation can be done by using microcontroller arduinos which can be used for applications. Ngrok is software used to convert a local host into a public server and the interfacing can be done by using the Python language. It has numerous applications in the fields of home automation, apartment automation, medicinal fields

Keywords: Python, Arduino, Automation, Ngrok, Local host, GSM, GPS

I. INTRODUCTION

Automation is a technique, method, or system of operating or controlling a process by electronic devices with reducing human involvement to a minimum. The implementation of automation in domestic apartments, houses, institutions increasing day by day. Industrialist and researchers are working to build efficient and affordability automatic systems to monitor and control different machines like lights, fans, AC based on the requirement. Automation makes not only an efficient but also an economical use of the electricity and water and reduces much of the wastage.

IoT grant to people and things to be connected Any-time, anyplace, with anyone, ideally using any network and any service. Automation is another important application of IoT technologies. It is the monitoring and reduces the energy consumption and controlling the environment in buildings, schools, offices and museums by using different types of sensors and actuators that control lights, temperature, and humidity. As the automation can be done by creating our own server it will be more reliable and easy to change it as per our

The Smart home which can be also called as automated home, with the use of new technology, to make the domestic activities more convenient, comfortable, secure and economical. The home automation system includes main components which are:

1. **User interface:** as a monitor, computer, or Phone, for example, that can give orders to control System.
2. **Mode of transmission**: wired connections (example Ethernet) or Wireless (radio waves, infrared, Bluetooth, GSM) etc.
3. **Central Controller:** It is hardware interface that communicates with user interface by controlling domestic services

4. **Electronic devices**, a lamp, an AC or a heater, which is compatible with the transmission mode, and connected to the Central control system.

The Figure.1 shows the projected trends in smart home in previous years.

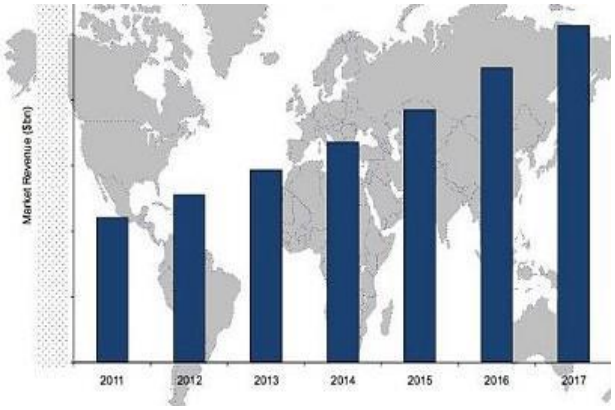

Figure 1: Popularity of Smart home in market.

II. LITERATURE SURVEY

The Figure 2 shows the basic architecture of Remote Home Automation.

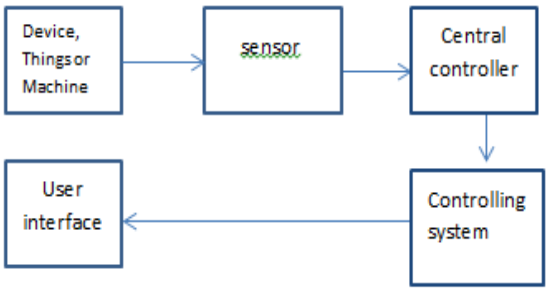

Figure 2: Basic Block Diagram of Home Automation

The home automation system that uses Wi-Fi technology, here the system consists of three main components; web server, which presents system core that controls, and monitors users' home and hardware interface module(Arduino PCB (ready-made), Wi-Fi shield PCB, 3 input alarms PCB, and 3 output actuators PCB.), which provides appropriate interface to sensors and actuator of home automation system. The System is better from the scalability and flexibility point of view than the commercially available home automation systems. The User may use the same technology to login to the server web based application. .If server is connected to the internet, so remote users can access server web based application through the internet using compatible web browser.

The application has been developed based on the android system. An interface card has been developed to assure communication between the remote user, server, raspberry pi card and the home Appliances. The application has been installed on an android Smartphone, a web server, and a raspberry pi card to control the shutter of windows. Android application on a smartphone issues command to raspberry pi card. An interface card has been realized to update signals between the actuator sensors and the raspberry pi card.

Cloud-based home appliance monitoring and controlling System is design and implement a home gateway to collect metadata from home appliances and send to the cloud-based data server to store on HDFS (Hadoop Distributed File System), process them using MapReduce and use to provide a monitoring function to Remote user. It has been implemented with Raspberry Pi through reading the subject of E-mail and the algorithm. Raspberry Pi proves to be a powerful, economic and efficient platform for implementing the smart home automation

2.1 DRAWBACKS OF EXISTING SYSTEMS:

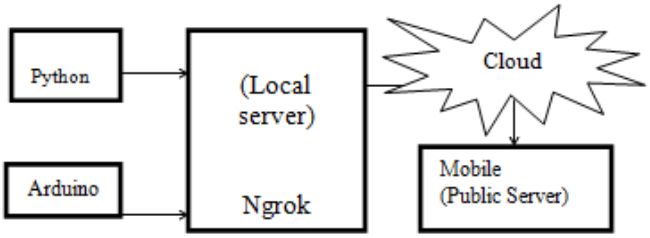

As our existing systems have higher amount of dependability for example if we take \home security apps, the person who installed the only can access the home so it will lead will to failure sometimes, in some other case it will be costly because of the usage of electronic devices like GSM, GPS, Advanced microcontroller.

III. METHODOLGY

3.1 Ngrok

Ngrok is one of the software used to convert the local server to a public server can be accessible by the mobile phone. This software produces the specific URL which can be accessible by the mobile devices from anywhere while connected to the internet

3.2 Arduino

Arduino is a microcontroller which is similar to a Personal Computer or a CPU but instead of interacting with human beings they interact with other machines. Basically, Microcontrollers were developed for making process automated. It works on the basis of result taken from the sensor and other output devices.

3.3 Python

Python is an interpreted high level programming language for general purpose programming. Python has a designed philosophy that emphasizes code readability, and syntax that allows the programmers to express concepts in fewer lines of codes .It constructs the enables clear programming on both small and large scales

3.4 Energia:

Energia is an open source electronic prototyping software and community driven Integrated Development Environment and software framework. Based on wiring framework, it provides an intuitive coding environment for coding an microcontroller. The Energia IDE is cross platform and supported on Mac OS, window, and Linux.

3.5 BLOCK DIAGRAM

This block diagram in Figure 3 shows the working principle of the developed method.

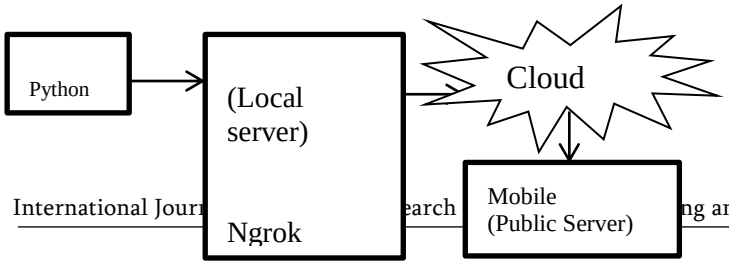

Figure 3: Block diagram of Py-Ardomotics

IV. METHODS AND MATERIAL

For this work, HTML based webpage should be created as per user desire and requirements. Then the coding should be written in the Energia software to command what should be done while switching on and off the device. It should contain the port and number of inputs and number of outputs. If the user requires large number of applications, they should insert large output and input pins. Ngrok software must be used to convert the local host address can be accessed by mobile phones anywhere only with the presence of internet. Python is the high level programming language used to interface the Arduino with the Ngrok. Once when all these procedures are done, Ngrok software should be opened in the presence of Wi-Fi or any form of internet accessibility. Once when the Ngrok shows online, it will create two addresses one its own physical internet protocol Address and the another one IP address can be used by any other device like mobile phones which can be used to control all the devices in the home. The encryption keys were included to safeguard our server. The user can see the options what they choose already. For instance, user can know whether the light is on or off already by this the user can get acknowledged for the actions done for the day.

These are the outputs came when implemented this work in real time.

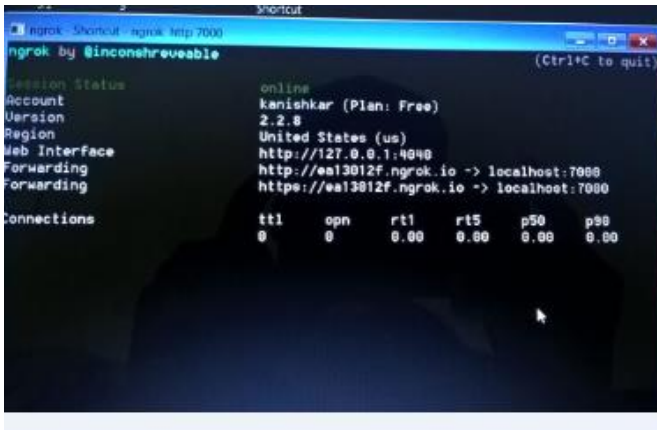

Figure 4: Running of Ngrok software

Here when the software is running, it form a tunnel to public server from local server and creates the IP address.

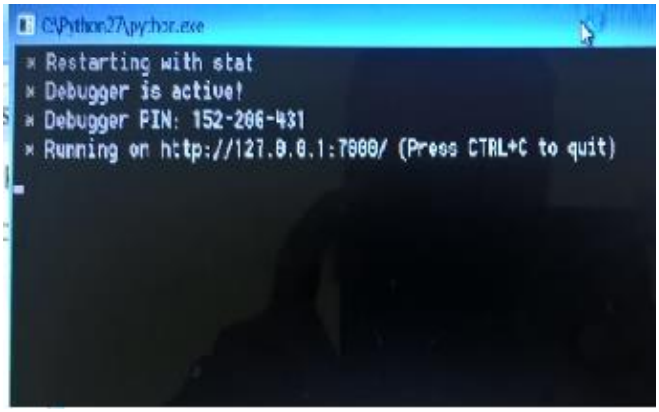

Figure 5:Ready for execution

In the Figure 5, when the server is connected with online it is ready to execute the further actions.

Figure 6: Final execution in mobile.

V. CONCLUSION

As on now, this Ngrok technology is used by some of the industrial resource persons and technocrats. When this software used in home automation it will create major turning point for the automation. In future, it will be accessed by all the domain of the mankind where the need of automation is present. This work helps to access our entire home through our mobile phone without the usage of GPS, GSM, and Bluetooth. In future some of us need to send the acknowledgement for the working of the device. For that a sensor will keep near the light to discover whether the device is on or not.

VI. REFERENCES

[1] Ahmed ElShafee, Karim Alaa Hamed, "Design and Implementation of a Wi-Fi Based Home Automation System", International Journal of Computer, Electrical, Automation, Control and Information Engineering Vol: 6, No: 8, 2012.

[2] Hayet Lamine and Hafedh Abid , "Remote control of a domestic equipment from an Android application based on Raspberry pi card", IEEE transaction 15th international conference on Sciences and Techniques of Automatic control & computer engineering - STA'2014, Hammamet, Tunisia, December 21-23, 2014.

[3] YunCui, MyoungjinKim, YiGu, Jong-jinJung, and HankuLee, "Home Appliance Management System for Monitoring Digitized Devices Using Cloud Computing Technology in Ubiquitous Sensor Network Environment", Hindawi Publishing Corporation International Journal of Distributed Sensor Networks Volume 2014, Article ID 17409.

[4] Jain Sarthak, Vaibhav Anant and Goyal Lovely , "Raspberry Pi based Interactive Home Automation System through E-mail.", IEEE transaction,2014 International Conference on

Reliability, Optimization and Information Technology ICROIT 2014, India, Feb 6-8 2014.

[5] Ardam H. and Coskun I., "A remote controller for home and office appliances by telephone", IEEE Transactions on Consumer Electronics, vol. 44, no. 4,pp. 1291-1297, 1998.

[6] Greichen, J.J., "Value based home automation or today's market," IEEE Transactions on Consumer Electronics, vol. 38, no. 3, pp.34-38, Aug. 1992

[7] Baki Koyuncu, "PC Remote Control of Appliances by Using Telephone Lines", 1995, IEEE Transactions on Consumer Electronics,Vol. 41(1), pp. 201-209.

Themed Section : Engineering and Technology
© 2018 IJSRSET | Volume 5 | Issue 3 | Print ISSN: 2395-1990 | Online ISSN : 2394-4099

Design and Dynamic Analysis of Switched Reluctance Generator System

Jayapragash R[1], Arul R[2], Sumathi V[3], Chellamuthu C[4]

[123]Associate Professor, School of Electrical Engineering, Vellore Institute of Technology, Chennai, Tamil Nadu, India

[4]Professor, Department of Electrical and Electronics Engineering, R.M.K. Engineering College, Kavaraipettai, Tamil Nadu, India

ABSTRACT

This paper discusses the design and dynamic analysis of Switched Reluctance Generator (SRG) system. A 1 Hp, 4 phase, 8/6, SRG machine is modelled in MATLAB/Simulink software, using the torque and flux linkage characteristics obtained from analytical model. Single Switch per Phase Converter (SSPC) with separate source bus and load bus in order to minimize the current drawn from the excitation battery which is used to energize the stator windings of the SRG. The transient response of SRG system is obtained at various load level and the results are reported. The feasibility check is performed on SRG to act as a Wind Generator (WG).

Keywords: Switched Reluctance Generator, Single Switch per Phase Converter, Wind Generator

I. INTRODUCTION

SRM has several merits over conventional machines in both generating mode and motoring mode operations. It is a worth candidate for many industrial applications. Over a long period of time the research was focused on the motoring operation only. As the machine has got reversible power flow tendency, a few scholars took research on generating mode of SRM. This led to an idea that this machine will be good solution for worldwide increase in demand of electrical energy. The problems of the conventionally used generators has changed the researchers attention to the more simple and robust variable speed SRG which exhibits the qualities of a generator [1].

SRG as seen shows a very rugged construction associated with no permanent magnets or conductors in the rotor. The manufacturing of SRG is easy at low price and it possesses the capability of operating at high speed. The torque generated by SRG is not depending upon the current direction and therefore converter allows current in one direction itself enough to operate the machine. The machine accelerates at fast rate due to low inertia of the rotor as the machine and the power converter are very robust [2]. The machine can tolerate faults as the phase windings of SRG are both electrically and magnetically independent from other windings.

Increased use of fossil fuel leads to air contamination, increase in earth atmosphere temperature and there is a necessity to focus on non-conventional resources to minimize these problems. The power generated from wind is one of the available renewable energy power source which also helps in reduction of carbon dioxide emissions to the atmosphere. Generator operates with wind energy input is one of the major component in wind energy conversion system and permanent magnet generator is the widely used one. It needs more torque to run and not advisable to use

in high temperature places. Therefore, we emphasize more on SRG as it is simple in structure, tough, highly efficient and easy to use in adverse environments [3]. This article is prepared with the following sections. Section 2 gives steps involved in the modelling of SRG machine. Section 3 briefs the power converter topology and section 4 presents the static and dynamic response of SRG system.

II. SWITCHED RELUCTANCE GENERATOR

For achieving generator mode operation of the machine, windings are excited as the rotor is moving away from the stator poles, [4].

In generating mode, the SRG generates opposite torque which opposes the movement and extract energy from the prime mover [5]. A controller with rotary position sensor is augmented so that the feedback is utilized to integrate the pulses of stator current and position of the rotor. The cross-sectional view of SRG is shown in Figure 1 and theoretical graphs of various parameters/phase of SRG are shown in Figure 2.

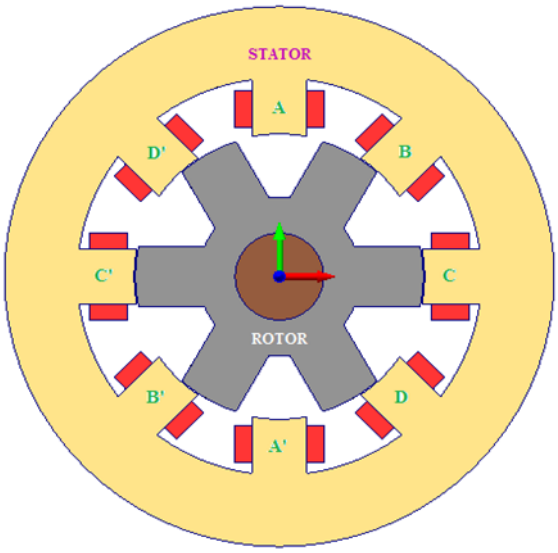

Figure 1. Cross-section of 8/6 SRG

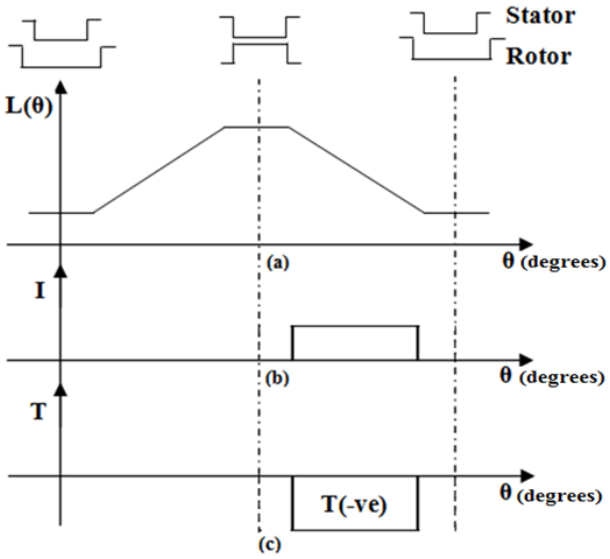

Figure 2. (a) Inductance profile (b) Current pulse (c) Torque

Torque is produced by the affinity of the rotor to settle at minimum reluctance position which favors spontaneous magnetization irrespective of current direction. Therefore, the machine contributes flux during excitation and it should be zero before the excitation of incoming phase [6].

Neglecting magnetic saturation, flux linkage is given as

$$y = L(q).i \qquad (1)$$

The magnetic energy stored (We) or co-energy (Wc) changes with position of rotor to produce torque and it is expressed as

$$W_e = W_C = \frac{1}{2} L(q).i^2 \qquad (2)$$

The electromagnetic torque is calculated using the equations given below

$$T_e = \left[\frac{\partial W_C(q,i)}{\partial q} \right]_{i=cons} \qquad (3)$$

$$T_e = \frac{1}{2} i^2 \frac{dL(q)}{dq} \qquad (4)$$

Where, i = phase current

L = self-inductance

θ = position of rotor in radians

= variation of inductance with rotor position

It is evident from equation (4) that the mode of operation of the machine is decided by the change in inductance with rotor position.

SRG is basically identified by a nonlinear operation due to saturation of magnetic field. A valid SRG model needs information regarding magnetic characteristics of the machine to determine its electrical and mechanical behaviors. The linked flux of a stator phase and developed torque, are a function of the excitation current (i) and the position of rotor (θ). For study purpose, amidst the availability of various numerical methods, FEA is the most often used method for study of electromagnetic field, [11]. This work employs MagNet 7.1.1 to develop FEA model.

Net torque developed in a SRG is a result of summation of torque produced in individual phases and is obtained as

$$T_{e(Total)} = \sum_{n=1}^{m} T_n(i,q) \qquad (5)$$

The dynamic mechanical analysis of the system is yields us with

$$T_e = T_L + Bw + J\frac{dw}{dt} \qquad (6)$$

Where Te = electromagnetic torque (N-m)

TL = applied mechanical torque (N-m)

ω = angular speed (rad/sec)

J = moment of inertia (Kg/m2)

B = Viscous friction co-efficient (N-m/rad/sec)

Angular speed is computed from equation (7) and it is expressed as

$$w = \frac{1}{J}\int (T - T_L - Bw)dt \qquad (7)$$

Rotor position is obtained by integrating the angular speed and it is given as

$$q = \int w dt \qquad (8)$$

Equation (8) is elucidated to get speed information and rotor position and the corresponding model is shown in Figure 3.

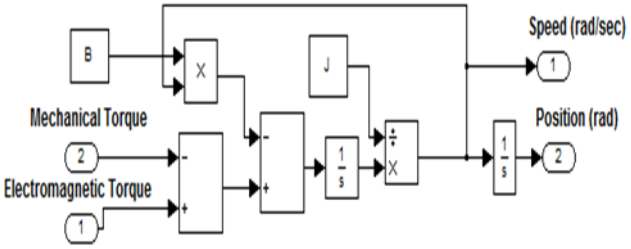

Figure 3. The dynamic model of machine

Equivalent electrical circuit of the stator windings SRG is shown in Figure 4.

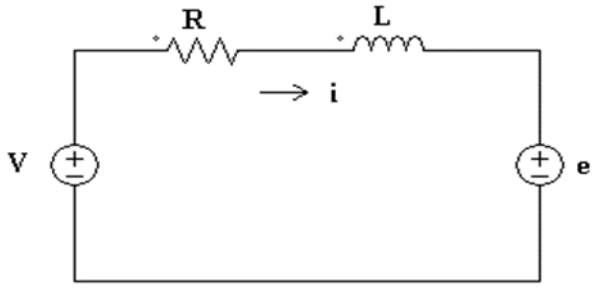

Figure 4. Electrical equivalent of the phase winding

On applying KVL, A differential equation is obtained which depends upon phase voltage v (t) given as

$$v = iR + \frac{dy(i,q)}{dt} \qquad (9)$$

Where v - DC source voltage

ψ - Flux linkage

R - Resistance of the phase winding

The flux linkage ψ, depends on of phase current (i) and position of rotor (θ). The phase winding resistance R has to be considered for low speed operations.

The flux linkage (ψ) depends on current (i) and position of rotor (θ) [7], therefore the voltage equation can be rewritten as

$$v = iR + L\frac{di}{dt} + iw\frac{dL}{dq} \qquad (10)$$

The current is calculated from the voltage drop across the inductor and it is given as

$$V_L = L\frac{di}{dt} \qquad (11)$$

The incremental inductance is modelled as controlled current source. The sub system, which implements the current calculation, is shown in Figure 5.

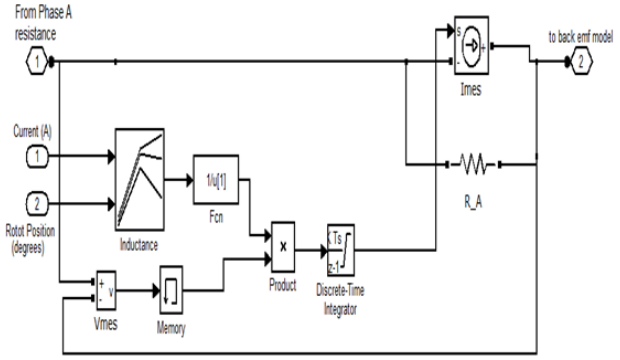

Figure 5. The model for the incremental inductance

The controlled voltage source is used to represent the back emf. The subsystem for back emf computation is presented in Figure 6.

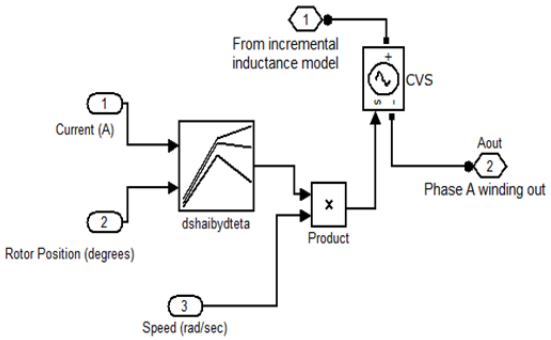

Figure 6. The back EMF model

The MATLAB/Simulink model of the terminal voltage expression is shown in Figure 7.

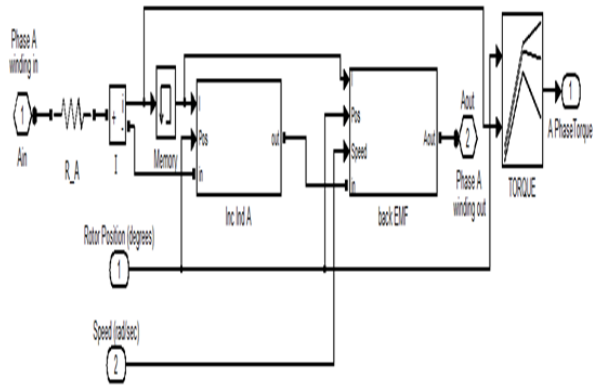

Figure 7. Simulink model of the phase voltage equation

The complete simulation model of SRG in the MATLAB/Simulink environment is shown in Figure 8. Stator windings of SRG are energized in a sequential fashion and the torque developed by the individual phases are integrated to obtain the total torque (T) produced by the machine [8]. Dynamic mechanical analysis yields a equation, which is solved in the mechanical block to obtain speed and position of rotor.

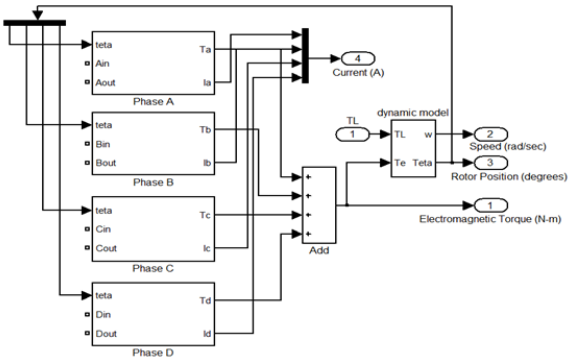

Figure 8. MATLAB/Simulink model of SRG

III. SINGLE SWITCH PER PHASE CONVERTER

Switched reluctance machines belong to a group which are obviously called as electronically commutated machine. It means that they are not able to operate on a rigid grid with a constant voltage and frequency, but they need the cooperation of converters. Therefore, it is very important to investigate how a converter topology influences the performances of this machine operation, [9]. The excitation period shown in Fig. 9 is between the θon and θoff, during which the phase winding is excited from a DC source or from a capacitor. Then there is a generation period, between θoff and θext, during which the electrical energy is generated and delivered to the load, [10]. Therefore, the values of θon, θoff and θext are very important variables affecting the output parameters of SRG.

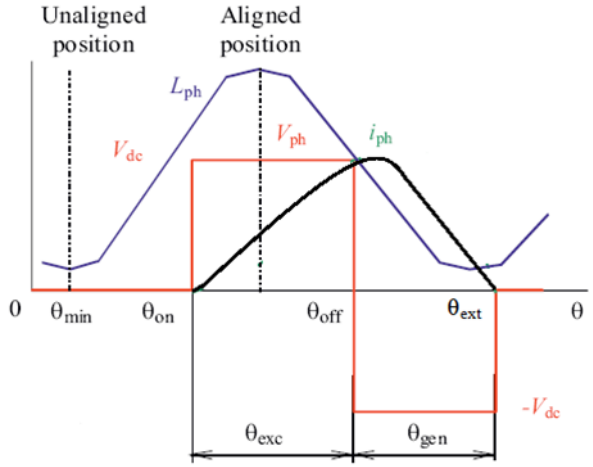

Figure 9. θon, θoff and θext variables of SRG

In order to reduce the number of devices, single switch per phase converter is used. Dedicated buses are made available for the source and load which are used to prevent absorption of high magnitude of current from the battery which is used for excitation. This converter allows feeding of the load from the grid even when SRG is not running. This is good for an unstable renewable complementary power source like wind power. Fig. 10 illustrates a circuit configuration of the single switch per phase converter.

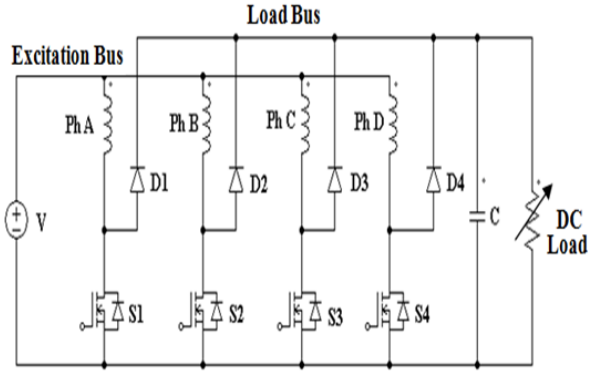

Figure 10. Single switch per phase converter for SRG

During excitation period of a phase, switch S1 connects the DC excitation bus to the winding to increase the phase current. During generation, the switch S1 is OFF. The energy in the winding is delivered to the load through the diode D1. It is clear from the circuit that the applied voltage is in series with the electromotive force.

IV. ANALYSIS OF SRG SYSTEM

SRG system normally comprises of three main components: SR machine, converter and controller. SRG and single switch per phase converter discussed in the previous section are integrated together toobtain SRG system. The complete block diagram of SRG system is shown in Fig. 11.

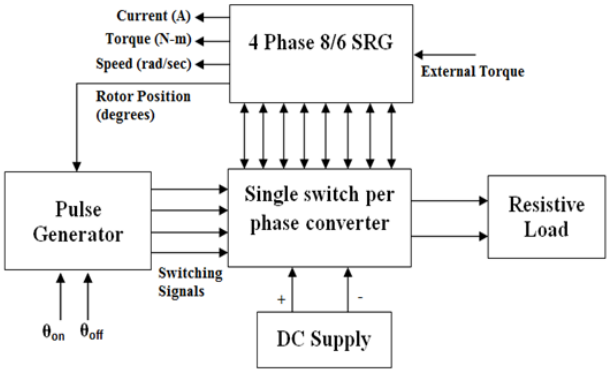

Figure 11. Block diagram of SRG System

The stator windings of SRG are energized using SSPC topology powered by DC supply. The required external torque for SRG is supplied manually to analyze the performance of SRG. For SRG based Wind Energy Conversion System (WECS), the torque

is supplied by the wind turbine. The output of SRG is supplied to the stand alone load. The MATLAB/Simulink model of SRG system is shown in Fig. 12.

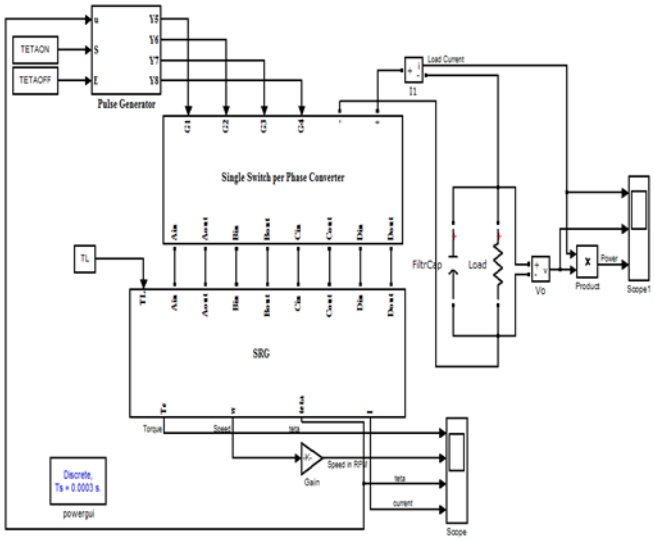

Figure 12. MATLAB/Simulink model of SRG system

The θon, θoff, converter input voltage and torque supplied to the generator are the operating variables of SRG. The steady state response of SRG drive system for the turn-on angle of 15° and turn-off angle of 27° are shown in Fig. 13.

From Fig. 13 (b & c) it is clear that phase current is aligned with the decreasing inductance slope and SRG contributes negative torque as shown in Fig. 13 (d). Therefore, the placement of turn-on angle is very important for the operation of SRG. The speed of SRG is shown in Fig. 13 (e).

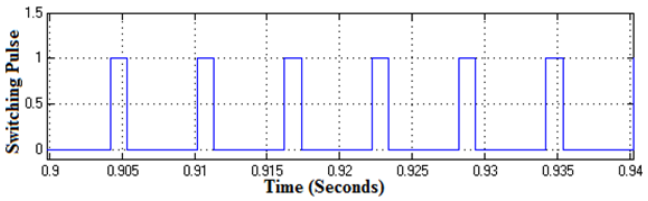

(a) Switching Pulse

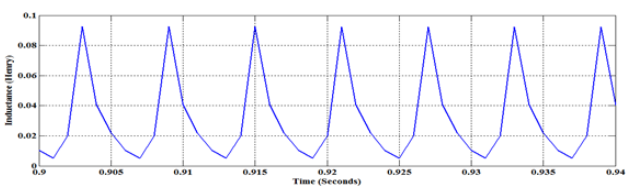

(b) Phase Inductance

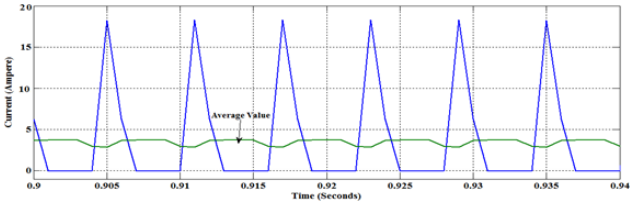

(c) Phase Current

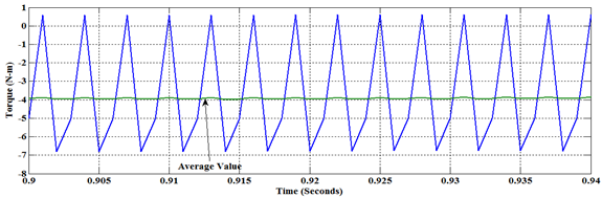

(d) Torque

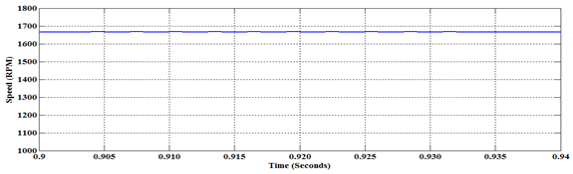

(e) Speed

Figure 13. Steady state response of SRG drive system for turn-on angle of 15°, turn-off angle of 27°

Output power of SRG is supplied to the stand alone resistive load. The transient response of SRG system is analyzed by changing the load resistance from 40Ω to 30Ω. The corresponding change in load current and power consumed by the load are shown in Fig. 14.

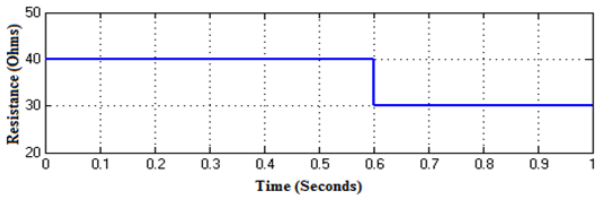

(a) Load Resistance

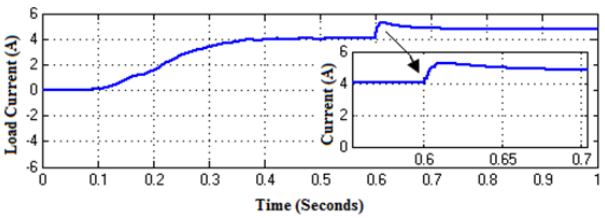

(b) Load Current

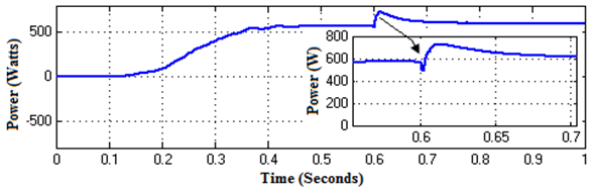

(c) Load Power

Fig. 14: Transient response of SRG system for the change in RL from 40 Ω to 30Ω

When load is increased, there is an increase in load current, decrease in terminal voltage and in turn increase in output power. The rated current of SRG is 5A and the machine is loaded till 4.77 A to calculate the efficiency and it is given below.

Mechanical power input

$$P_{in} = T_L \frac{2pN}{60} \quad (12)$$

For TL = 4N-m and speed N = 1660RPM
Pin = 694.98 watts

Electrical power output $P_{out} = V_L I_L$ (13)

The measured current and voltage are IL=4.77A, VL=125V
Pout = 596.25 watts
Percentage efficiency =85.79%

From the response of SRG system, it is clear that the switched reluctance machine gives reasonable performance in the generating mode of operation.

V. CONCLUSION

A 1 Hp, 4 phase, 8/6, machine model of SRG is developed in the MATLAB/Simulink software using the torque and flux linkage characteristics obtained from analytical model. To minimize the current drawn from the excitation battery, Single switch per phase converter has dedicated buses for source and load. This converter allows the grid to feed the load even when SRG not in operation. This is suitable for unstable renewable complementary power source like wind power. Therefore, it is found that single switch per phase converter is suitable for SRG operation. Finally, single switch per phase converter is integrated with SRG machine model and analyzed the performance of SRG system. The generating mode operation is achieved by exciting the phase winding when the rotor leaves aligned position. From the results it is clear that, phase current is aligned with the decreasing inductance region and SRG produces negative torque to extract power from the prime mover. The transient response of SRG system is analyzed by changing the load resistance from 40Ω to 30Ω and the results are reported. From the steady state and transient response of SRG system, it is found that SRG gives satisfactory performance as a generator and found suitable to act as a wind generator.

VI. REFERENCES

[1] Ion Boldea, "Variable speed generators", CRC Press, Taylor and Francis Group, Boca Raton, FL, USA, pp. 9.1-9.35, (2006).

[2] Nassereddine, M, Rizk, J & Nagrial, M, "Switched reluctance generator for wind power applications", Proceedings of world academy of science, engineering and technology, vol. 31, pp. 126-130, (2008).

[3] Susitra, D, Annie, E & Paramasivam, S, "Switched Reluctance Generator - Modeling, Design, Simulation, Analysis and Control-A Comprehensive Review", International Journal of Computer Applications, vol. 1, no. 2, pp. 10-16, (2010).

[4] Amissa Arifin, Ibrahim Al-Bahadly & Mukhopadhyay, SC, "A Comprehensive Simulation Platform for Switched Reluctance Generator System", WSEAS Transactions on Power Systems, vol. 7, no. 4, pp. 198-208, (2012).

[5] Karthikeyan, R & Arumugam, R, "Performance analysis of a soft magnetic composite switched reuctance generator", European Journal of Scientific Research, vol.83, no.4, pp.545-557, (2012).

[6] Amissa Arifin & Ibrahim Al-Bahadly, "Switched Reluctance Generator for Variable Speed Wind Energy Applications", Smart Grid and Renewable Energy- Scientific Research Publicatios, vol. 2, no. 1, pp. 27-36, (2011).

[7] Hany, M Hasanien & Muyeen, SM, "Speed control of grid-connected switched reluctance generator driven by variable speed wind turbine using adaptive neural network controller", Electric Power Systems Research, vol. 84, no.1, pp.206-213, (2011).

[8] Cornea, O & Popovici, D, "A switched reluctance motor drive model using standard simulink library components", Proceedings of eleventh International conferrence on electrical and electronic equipment, pp. 69-74, (2008).

[9] Hrabovcova, V, Pavol Rafajdus, Liptak, M & Lorand Szabo, "Performance of converters suitable for switched reluctance generator operation", Journal of Electrical Engineering, vol. 64, no. 4, pp. 201-211, (2013).

[10] Liptak, M, Hrabovcova, V, Rafajdus, P & Zigmund, B, " Switched Reluctance Machine with Asymmetric Power Converter in Generating Mode", Journal, Acta Electrotechnica et Informatica, Slovak Republic, vol.7, no.1, pp. 5-10, (2007).

[11] Srinivas, KN & Arumugam, "Analysis and Characterization of Switched Reluctance Motors: Part II- Flow, Thermal, and Vibration Analyses", IEEE Transactions on Magnetics, vol. 41, no. 4, pp. 1321-1332. (2005).

Themed Section : Engineering and Technology
© 2018 IJSRSET | Volume 5 | Issue 3 | Print ISSN: 2395-1990 | Online ISSN: 2394-4099

Investigation Study of Three In One Multiple Agricultural MEMS Sensor Using Microcantilever

B. Priyadarisshini[1], D. Sindhanaiselvi[2], T. Shanmuganatham[3]

[1]PG Scholar, Department of Electronics and Instrumentation Engineering, Pondicherry Engineering College, Puducherry, India

[2] Assistant Professor, Department of Electronics and Instrumentation Engineering, Pondicherry Engineering college , Puducherry, India

[3]Associate Professor, Department of Electronics Engineering, Pondicherry University, Puducherry, India

priyasandra94@gmail.com[1], dsindhanaiselvi@gmail.com[2],shanmuganathamstr@gmail.com[3]

ABSTRACT

MEMS based three- in- one multiple sensor with soil Temperature, soil moisture and humidity sensor proposed using simple cantilever for the agricultural applications. These parameters are the most important parameters for agricultural monitoring to control the usage of water supply to the plants. The study is to find the optimized dimension of the three- in- one multiple MEMS sensor with respect to maximum deflection for the temperature range of 0°C to 40.556°C, relative humidity and the soil moisture range of 10 % to 100%. The dimension is optimized with respect to aspect ratio parameters such as length, width and thickness of different layers.

Keywords: Microcantilever, Temperature, Humidity, Soil Moisture, Deflection.

I. INTRODUCTION

Agriculture field is influenced by chemical products into the soil, natural hazard and improper irrigation that affects the growth of the crop. Monitoring soil nutrients, soil moisture, soil temperature, humidity and soil pH gives thorough knowledge of the field condition that enriches the crop by understanding the soil health. MEMS technology acts as economical platform in designing the sensor in the diverse fields especially in the research work of agricultural sector [10]. This is an emerging technology in designing the multiple sensor in compact size, cheaper cost, and low power consumption benefits to the farmers. These advantages indicates the multiple sensor are affordable and they are highly recommended for the poor farmers for their boon.

MEMS is most broadly used technology in microscopic device with electrical and mechanical elements in it used in wide applications [6, 7, 8, 9]. Depending upon the ranges of the parameters, farmers can monitor and collect data of soil water availability, temperature that gives better understanding to perform smart irrigation system, which gives high profit in harvesting the crop.

The novelty of this project to measure the three different influential parameters using three –in- one multiple sensor such as temperature, humidity and soil moisture with advancement of MEMS technology for the. The exact soil moisture and soil temperature,

humidity gives wide knowledge about usage of water in the field and intake of nutrients from the soil for the critical growth stages of the crop. The simple cantilever is proposed to design the three in one multiple sensor. The sensor is proposed for the temperature range of 0°C to 40.556°C, Relative Humidity range of 10 % to 100 % at the temperature range of 25°C to 40°C and soil moisture range of 10% to 100%. The investigation study is carried out too find the optimized dimension for three multiple sensor in the single substrate with respect to aspect ratio such as length in (μm) , width in (μm) and thickness in (μm) and its performance is analysed. The cantilever based temperature sensor is tend to deflect when exposed to the temperature layer with higher thermal coefficient. Similarily humidity and soil moisture sensor [2] tends to deflect more when exposed to the polymer based material since it had good absorbtion of water content in the soil and in air.

II. STRUCTURE OF THREE –IN – ONE INTEGRATED SENSOR

A. Basic structure

The three in one multiple sensor on silicon substrate of dimension 600μm x 600 μm x 5μm by using bulk micromachining. In order to form the cantilever, centre of the substrate is etched using mask of dimension 500μm x 500μmx 5μm. the temperature, humidity, soil moisture based cantilever is added on the surface of the substrate by surface micromachining method. Each sensor dimension has been satisfied by

Significant design aspect ratio [5] are:

(1) Ratio of length to width (l : w)
(2) Ratio of width to thickness (w : t)

The two constraints are shown in the Equations below:

$$l: w \geq 2:1 \quad (1)$$

$$w - 8t \leq 0 \quad (2)$$

The length, width and thickness are considered to be the key factors to optimize the structure of the cantilever without any breakage of the beam and also to obtain the maximum deflection. In the temperature cantilever sensor consists of two layers such as dielectric layer and sensing layer. The humidity cantilever sensor is of three layers such as dielectric layer and sensing layer with the temperature compensation layer. Soil moisture cantilever sensor comprises of two layers such as dielectric layer and a sensing layer. The dimension of three sensors is followed with respect to Equations (1) and (2). is given in Table 1.

TABLE I

DIMENSION OF THREE- IN-ONE MULTIPLE SENSOR

PARAMETER	DIMENSION (μm)						
	L:w	*Length*	*Width*	*Thickness*			
				Substra	*Dielect ric*	*Sensing layer1*	*Sensing layer1*
Temperature	4:1	200	50	5	6.25		-
Humidity	2:1	200	100	5	12.5		
Soil Moisture	4: 1	200	50	5	6.25		-

Multiple sensor is designed by applying the first aspect ratio of the micro cantilever given in Equation (1). So the length and width is fixed in the ratio of 4:1 for the three layered sensor such as Soil Temperature and soil moisture sensor and for four layered humidity sensor [1,3] , the length and width is fixed in the ratio of 2:1. The dimension of two layered temperature and soil moisture sensor of 200μm x 50μm and the dimension of three layered humidity sensor is of 200μm x 100 μm. . Based on the width of the sensor, the thickness of the overall layer has been obtained by obeying the second aspect ratio.

Due to the mutual split up of the thickness for each layer of the sensors. Henceforth, thickness of the soil

temperature and soil moisture sensor is 6.25 µm. While thickness of the humidity sensor is 12.5µm. The three- in- one multiple sensor is shown below Fig 1:

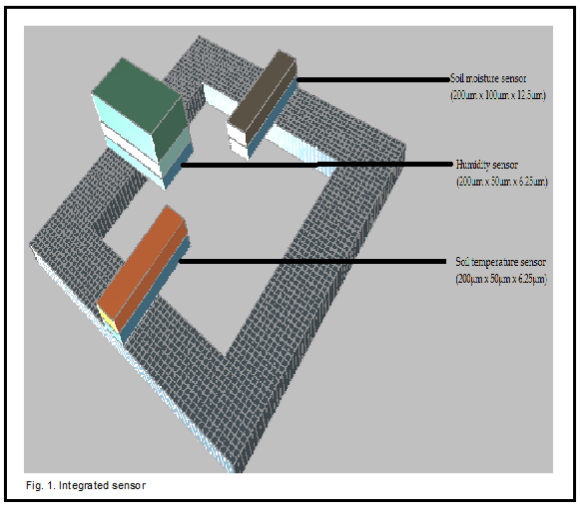

Figure 1. Structure of three- in- one multiple sensor

The soil temperature sensor and soil moisture sensor comprises of three layers such as silicon based substrate, silicon dioxide as dielectric layer and the sensing layer as in Fig. 1. Aluminium [4] as temperature sensing element and poly ether as soil moisture sensing element. Whereas humidity sensor has four layer with temperature compensation layer beneath the polymer based humidity sensing element, Polysilicon.

III. DEFLECTION ANALYSIS

Three in one multiple sensor ' s thickness has been varied in the different cases are carried out for the deflection analysis at the maximum temperature (105 °F / 40.556°C) and humidity range of 100% for 25°C and soil moisture for 100% for the optimized structure on the cantilever and it is tested . The deflection analysis is shown below in the Table II, Table III and Table IV with the thickness variation for each layer such as sensing layer1, sensing layer 2 and dielectric layer. But the silicon based substrate is kept constant with the thickness of 5µm. The optimized thickness with maximum deflection of the three in one multiple sensor is given in Table V.

TABLE III DEFLECTION ANALYSIS OF TEMPERATURE SENSOR

THICKNESS VARIATION (µM)		DEFLECTION (µm)
DIELECTRIC LAYER	SENSING LAYER 1	TEMPERATURE AT 40.566°C
0.25	6	1.35148
1	5.25	1.83464
1.25	5	1.96629
2	4.25	2.2459
2.25	4	2.29681
3	**3.25**	**2.31463**
3.125	3.125	2.24369
3.25	3	2.27488
4	2.25	2.01712
4.25	2	1.88435
5	1.25	1.10779
5.25	1	1.10018
6	0.25	0.18809

TABLE III DEFLECTION ANALYSIS OF HUMIDITY SENSOR

THICKNESS VARIATION (µm)			DEFLECTION (µm)
DIELECTRIC LAYER	SENSING LAYER 1	SENSING LAYER 2	HUMIDITY AT 100°C FOR 25°C
0.25	6	6.25	3.23499
1	5.25	6.25	3.29117
1.25	5	6.25	3.30135
2	4.25	6.25	3.30902
2.25	4	6.25	3.30473
3	3.25	6.25	3.27468
3.125	3.125	6.25	3.0259
3.25	3	6.25	3.2598
4	2.25	6.25	3.20476
4.25	2	6.25	3.18409
5	1.25	6.25	1.20281
5.25	1	6.25	3.10039
6	0.25	6.25	3.04945

TABLE IV DEFLECTION ANALYSIS OF SOIL MOISTURE SENSOR

THICKNESS VARIATION (µm)		DEFLECTION (µm)
DIELECTRIC LAYER	SENSING LAYER 1	SOIL MOISTURE AT 100%
0.25	**6**	**177.152**
1	5.25	143.26
1.25	5	124.908
2	4.25	49.0729
2.25	4	24.7669
3	3.25	0.208663
3.125	3.125	0.0146309
3.25	3	0.203307
4	2.25	0.187437
4.25	2	0.184115
5	1.25	1.14275
5.25	1	1.60853
6	0.25	0.145377

TABLE V OPTIMIZED THICKNESS VARIATION OF INTEGRATED SENSOR

THICKNESS VARIATION (µm)			DEFLECTION (µm)		
DIELECTRIC LAYER	SENSING LAYER 1	SENSING LAYER 2	TEMPERATURE AT 40.566° C	HUMIDITY AT 100°C FOR 25°C	SOIL MOISTURE AT 100%
0.25	6	-	-	-	177.152
2	4.25	6.25	-	3.30902	-
3	3.25	-	2.31463	-	-

IV. CONCLUSION

MEMS based three in one agriculture sensor is proposed as compact sensor designed using cantilever for the agricultural application. The dimension of the sensor is fixed based on the aspect ratio for 200 µm x 100 µm x 12.5 µm for cantilever based humidity sensor and 200µm x 50 µm x 6.25 µm for temperature and moisture sensor. The investigation study is carried out for maximum deflection for analysis by mutual split up of thickness among the dielectric layer and sensing layer it is found that the temperature sensor yields deflection of 2.31463µm, humidity sensor yields the deflection of 3.30902 µm and soil moisture sensor yields the deflection of 177.152 µm. further the sensitivity can be enhanced by adding of ribs and perforation.

V. REFERENCES

[1] Rong-Hua Ma, Chia-Yen Lee, Yu-Hsiang Wang, Hao-Jen Chen "Microcantilever-based weather station for temperature, humidity and flow rate measurement," Microsyst Technol, vol. 14, pp. 971-977, November 2007.

[2] Jie Liu, Mangilal Agarwal, Kody Varahramyan,Ernest S. Berney IV, Wayne D. Hodo "Polymer- based microsensor for soil moisture measuremnet," Sensors and Actuators, vol. B129, pp. 599-604, September 2007.

[3] Lung-Tai Chen, Chia – Yen Lee, and Wood-hi cheng, "MEMS-based humidity sensor with integrated temperature compensation mechanism," Sensors and Actuators, vol. A147, pp. 522-528, July 2008.

[4] Ashish, Kumari Nidhi Gupta, Dr. T.Shanmuganantham, "Design Of Temperature Sensors For Enviromental Applications", Int. Journal of Engineering Trends and Technology (IJETT) –Volume 4 Issue 10 - Oct 2013.

[5] B.Priyadarisshini, D.Sindhanaiselvi, T. shanmuganatham, "Design and dimension optimization of high sensitive microcantilever as humidity sensor," IEEE,International Conference on Emergimg Devices and Smart Systems, Mahendra Engineering College, Namakkal, Tamil Nadu, 2,3 of March 2018.

[6] D.Sindhanaiselvi, T.Shanmuganantham, "Double Boss Sculptured Diaphragm Employed Piezoresistive Mems Pressure Sensor With Silicon-On-Insulator (SOI)" Journal of

Engineering Science and Technology, School of Engineering, Taylor's University., Vol. 12, July 2017

[7] Marie Joan Syndhya, D.Sindhanaiselvi, T.Shanmuganantham, "Design and Analysis of Rectangular type Pizoresistive Microcantilever for Antigen Detection", International Journal of Control Theory and Application, International Science Press, Vol. 10, 2017.

[8] Marie Joan Syndhya, D.Sindhanaiselvi, T.Shanmuganantham, " Investigation on Piezoresistive Micro Cantilever Design for Blood Glucose Sensing", International Journal of Control Theory and Application, International Science Press , Vol. 10, 2017.

[9] D.Sindhanaiselvi, T.Shanmuganantham, "Investigation on Performance of Piezoelectric Beam Based Mems Actuator for Focussing of Micro Lens in Mobile Application", IEEE International Conference on circuits and systems, 2017.

[10] Rajul S. Patkar, Madhuri Vinchurkar, Mamta Ashwin, and V. Ramgopal Rao, "A Novel PET-Based Piezoresistive MEMS Sensor Platform for Agricultural Applications," Journal of Microelectromechanical Systems, Vol. 26, No. 4, PP. 746-748, August 2017.

Themed Section : Engineering and Technology
© 2018 IJSRSET | Volume 5 | Issue 3 | Print ISSN: 2395-1990 | Online ISSN : 2394-4099

Circular Patch FSS Antenna with different Resonating Frequencies for Satellite Applications

Daisy Sharma[1], Dr. T. Shanmuganantham[2]

[1] Department of Electronics Engineering, Pondicherry University, Puducherry, India

[2] Department of Electronics Engineering, Pondicherry University, Puducherry, India

daisy28nov@gmail.com[1],shanmugananthamster@gmail.com[2]

ABSTRACT

A compact size, flexible and low profile FSS antenna is proposed in this paper. The substrate used is FR4 epoxy with relative permittivity 4.4. The antenna is of dimension 150mm×150mm×1.6mm.The shape of the patch is circular with a radius of 20 mm. Ground plane of negligible height is present below the substrate. Microstrip line feeding is used for feeding the antenna. The proposed antenna design can be used for satellite communication. HFSS is used for simulation of the antenna and results are obtained in C band.

Keywords: FSS(Frequency selective surface), micro strip line feeding,FR4 epoxy, HFSS

I. INTRODUCTION

The use of microstrip antenna in modern days has increased in communication arena. Microstrip antennas are used in satellites, radars, WLAN, mobile communications etc.[1] Advantages of microstrip antenna include low profile, light weight, ease of fabrication etc. But microstrip antenna has low gain and power handling capacity[2]-[3]. Hence a concept called FSS is used in microstrip antennas to enhance the antenna parameters.

FSS are periodic structures which are one or two dimensional lattices designed to achieve band pass or band stop response.[4]FSS has good electromagnetic characteristics so it is used in various applications. Multiband features is a major requirement of antennas used in satellite communication. Using multilayered structure, loading multiple resonant elements, fractal elements and FSS leads to multiband characteristics. Frequency response of FSS is a function of incident angle, polarisation and frequency[5]. In 1990s, FSS were used as sub reflectors of reflectors to obtain multiband characteristics. When FSS is integrated with substrate integrated waveguide (SIW), it reduces cross polarisations, widens impedance bandwidth and increases efficiency [6].FSS can be used for chip less RFID.

FSS are used where high performance is required. The parameters controlling frequency response of FSS are dielectric substrate, element geometry, physical dimensions and periodicity [7].NASA Cassini project required multiple frequencies for communication at S, X, Ku and Ka band. There two FSS were used for band separation. To overcome side lobes, array configurations can be used. Multiband frequency antennas operate at different frequency bands.

II. ANTENNA DESIGN

The dimension of antenna proposed in this paper is 150mm×150mm. The substrate used is FR4 epoxy with relative permeability 1 and magnetic loss tangent 0.The height of the substrate is 1.6mm. Antenna is a 3×4 array consisting of 12 patches. Ground of negligible thickness lies below the substrate. The patch is fabricated above the substrate is of circular shape. The radius of the circular patch is 20mm. The patches are interconnected so that equal surface current distributions occur. Micro strip line feeding technique is used for the antenna. The material of the radiation box is air, contains the antenna setup.

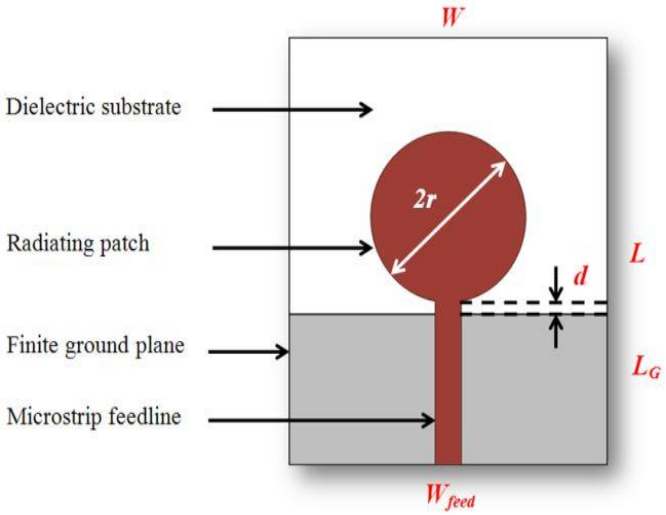

Figure 3 : Antenna elements

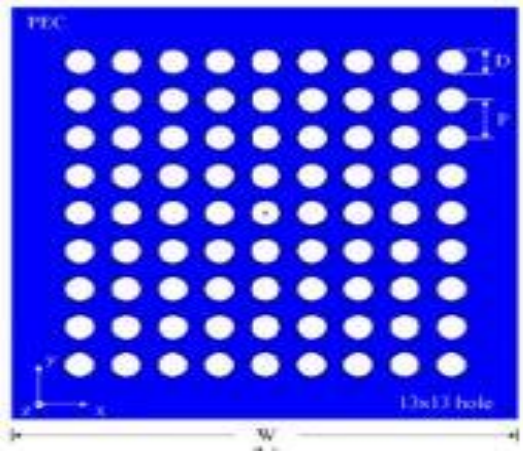

Figure 1. Array of FSS

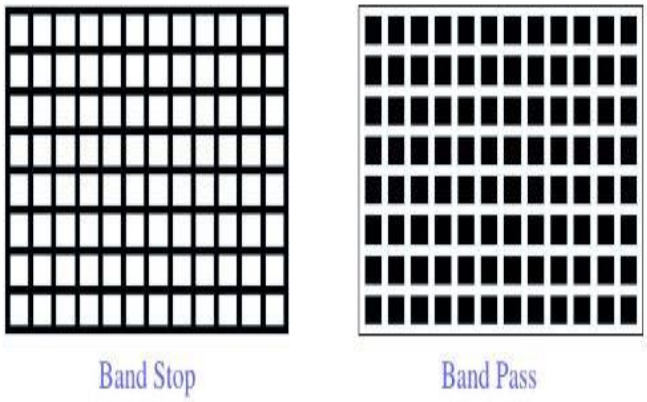

Figure 2. Characteristics of FSS

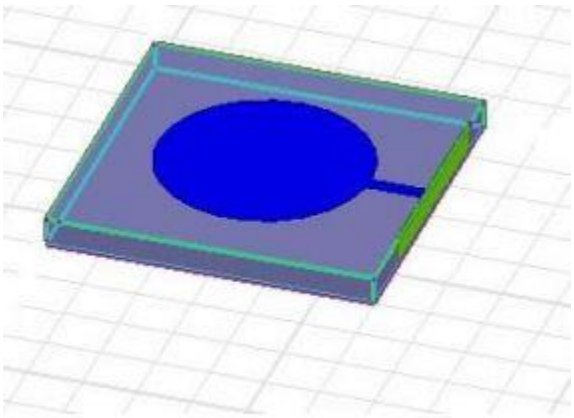

Figure 4. Circular patch

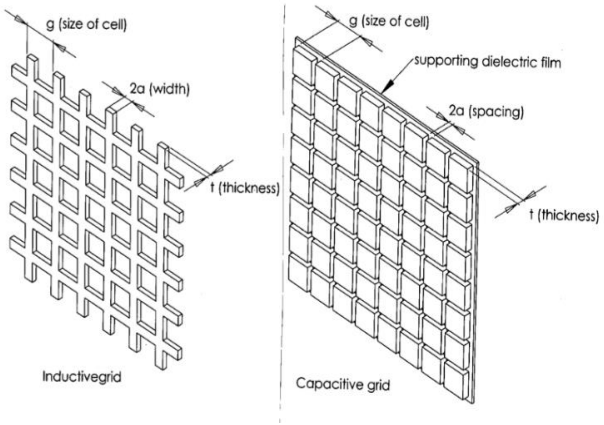

Figure 5. FSS properties

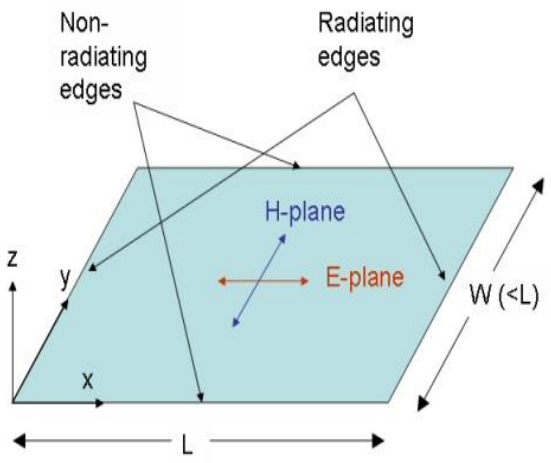

Figure 6. Patch edges

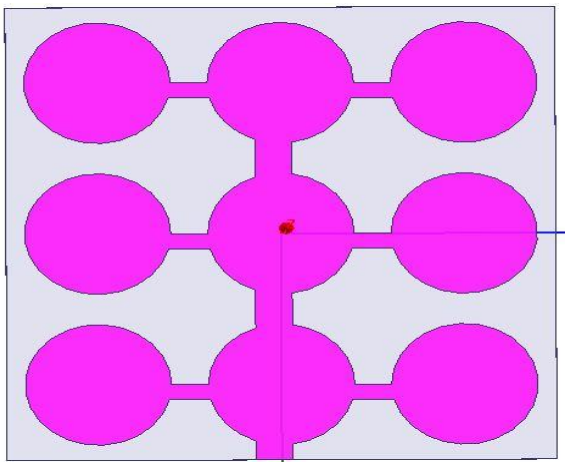

Figure 7. Proposed Antenna Design

Figure1 shows array of FSS. Figure2 illustrates characteristics of FSS. Figure 3 gives antenna elements. Figure 4 shows circular patch. Figure 5, gives FSS properties. Figure 6 shows patch edges.Figure7 shows proposed antenna design.

III. SIMULATION RESULTS AND DISCUSSIONS

Based on transmission line model, antenna parameters are calculated.

S parameters are scattering parameters, which are vector entities. They are popularly used in microwave circuit design and testing. At high frequencies, measurement of Y,H or Z parameters are difficult. S_{11} is called return loss. When it is ideal short, S_{11}= -1 and for ideal termination S_{11}=0. S_{11} is measured below -10dB and is minimised at the resonating frequencies.Figure8 shows the S_{11} parameter graph. There are six resonating frequencies. The resonating frequencies of the proposed antenna design are 4.81 GHz,5.27GHz, 5.68 GHz, 6.56 GHz, 6.72 GHz and 6.83 GHz.

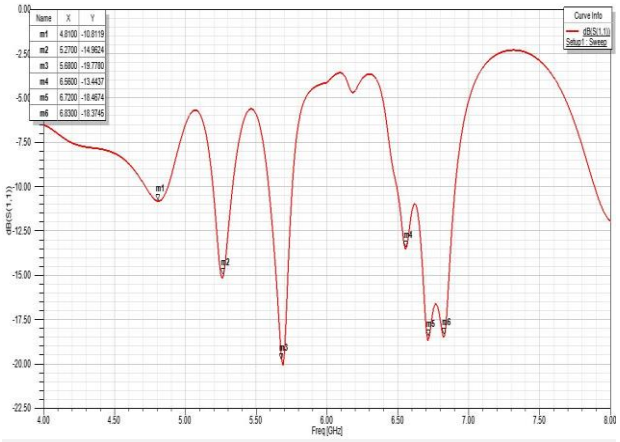

Figure 8. S_{11} parameter graph

VSWR indicates the mismatch between antenna and the feed lines connected to it. VSWR for a ideal system is 1 but practically it is below 2. If the antenna is poorly matched then VSWR value exceeds 2.Reflections are caused by mismatched impedances. The load must not have any reactance elements. Figure 9 shows VSWR graph. It is observed that at the resonating frequencies the VSWR value is below 2.

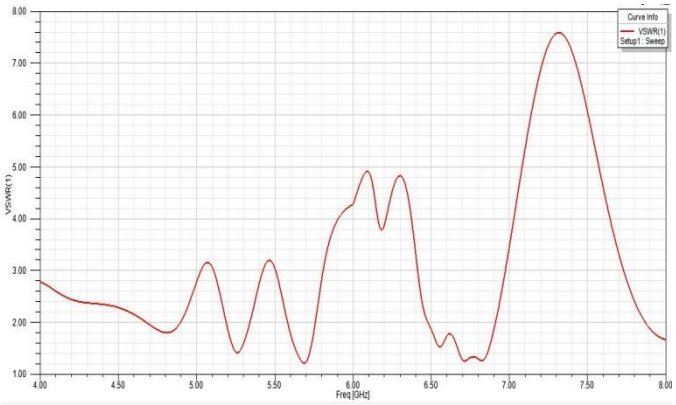

Figure 9. VSWR graph

Radiation is not uniform for all antennas in all directions. Radiation pattern is plotted in azimuth or E plane and elevation or H plane respectively.

Figure 10 gives the radiation at 4.81 GHz Figure 11 shows the radiation characteristics at 5.27 GHz Figure 12 illustrates the radiation characteristics at 5.68 GHz Figure 13 shows the radiation characteristics at 6.56 GHz .Figure 14 shows the radiation characteristics at

6.72 GHz. Figure 15 shows the radiation characteristics at 6.83 GHz . All radiation pattern are for $\varphi = 0^0$ and $\varphi = 90^0$ respective.

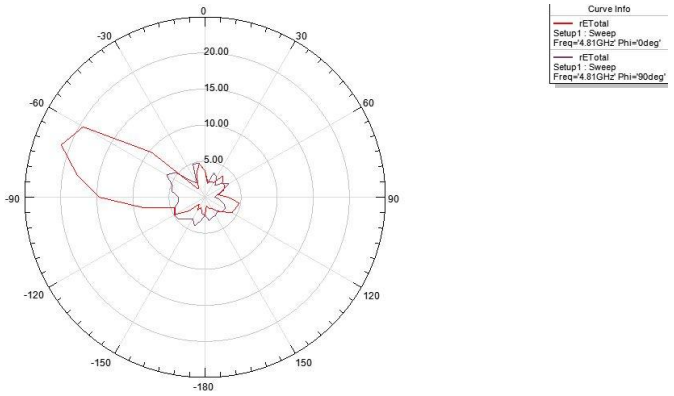

Figure 10. Radiation characteristics at 4.81 GHz

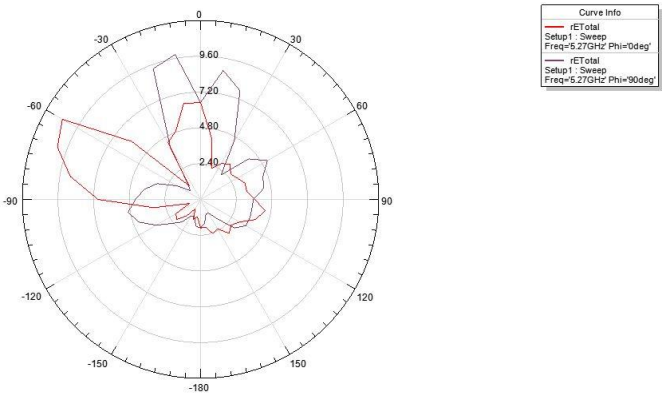

Figure 11. Radiation characteristics at 5.27 GHz

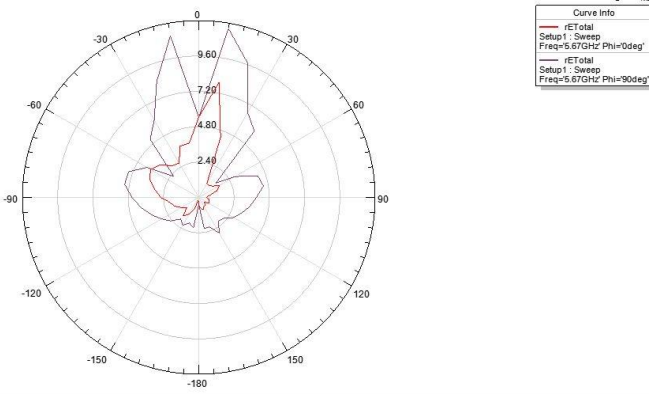

Figure 12. Radiation characteristics at 5.68 GHz

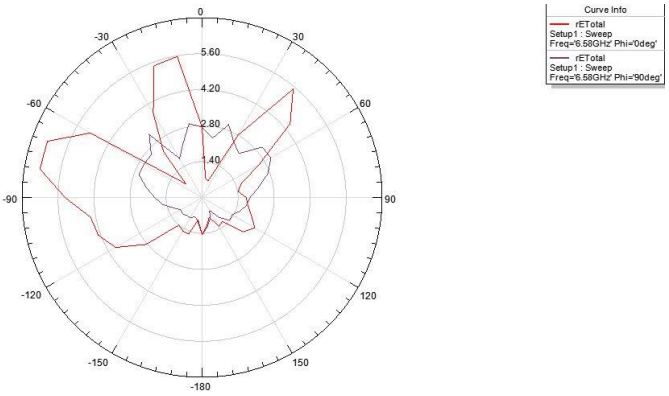

Figure 13: Radiation characteristics at 6.56 GHz

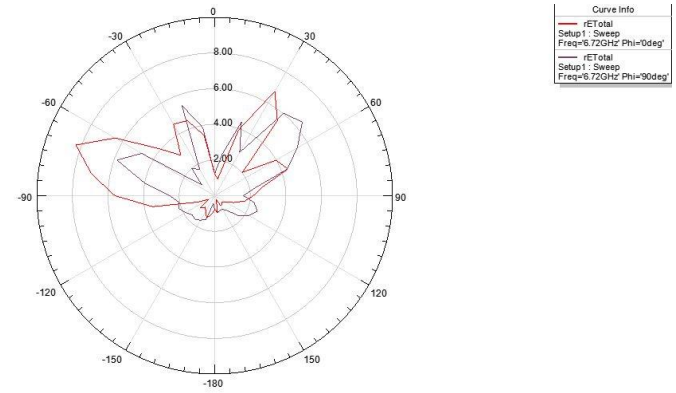

Figure 14. Radiation characteristics at 6.72 GHz

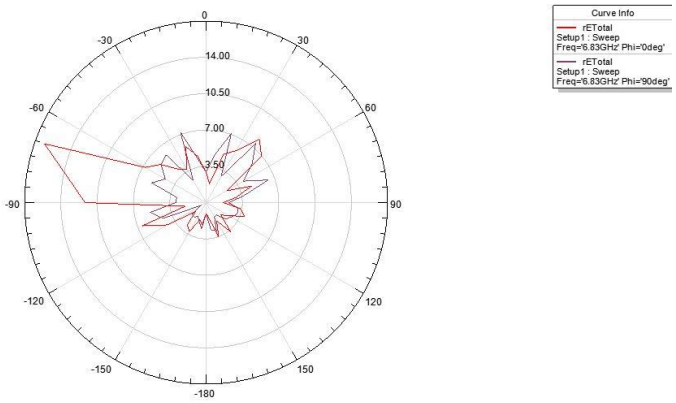

Figure 15. Radiation characteristics at 6.83 GHz

Gain of an antenna is measured in dBi or dBd. Direction of maximum radiation is referred as gain. It can be discussed as a function of angle. All the gain shown below are 3D polar plot of gain. Figure16 shows gain at 4.81 GHz. Figure17 gives gain at 5.27 GHz. Figure18 gives gain at 5.68 GHz. Figure19 gives gain at 6.56 GHz. Figure20 gives gain at 6.72 GHz. Figure21 gives gain at 6.83 GHz.

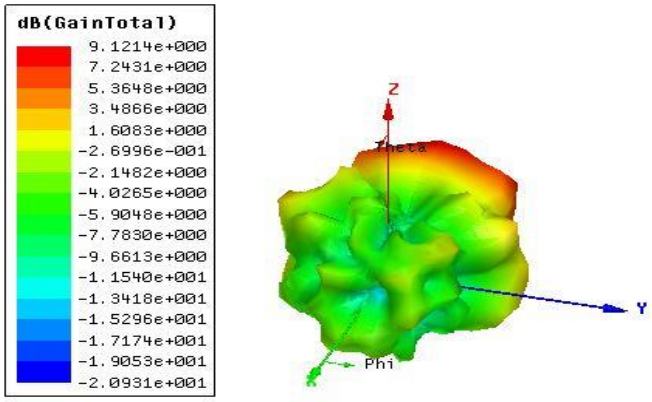

Figure 16. Gain at 4.81 GHz

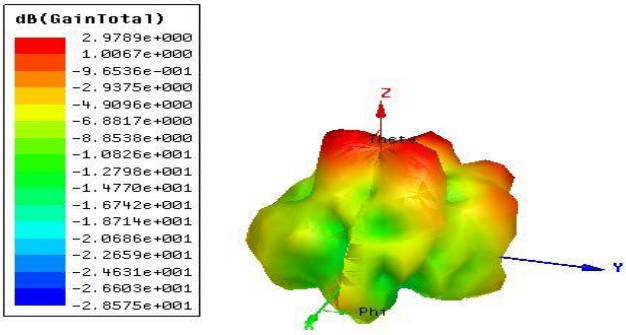

Figure 17. Gain at 5.27 GHz

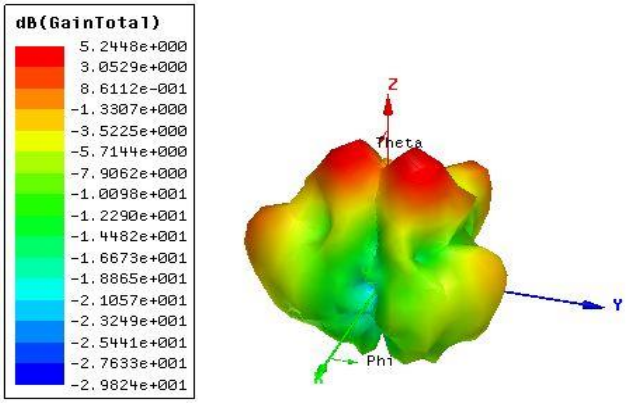

Figure 18. Gain at 5.68 GHz

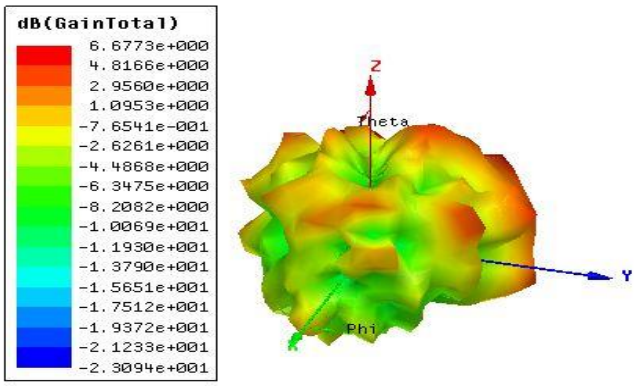

Figure 19. Gain at 6.56 GHz

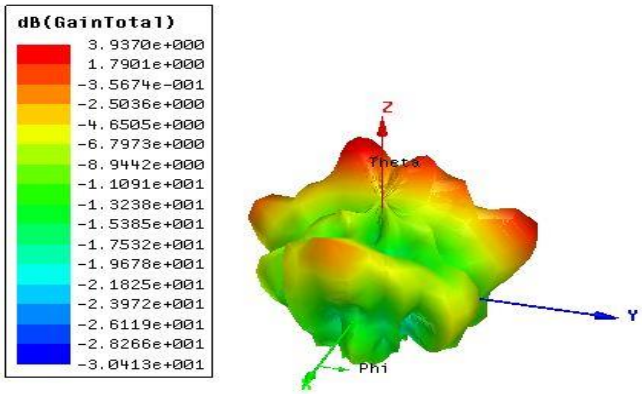

Figure 20. Gain at 6.72 GHz

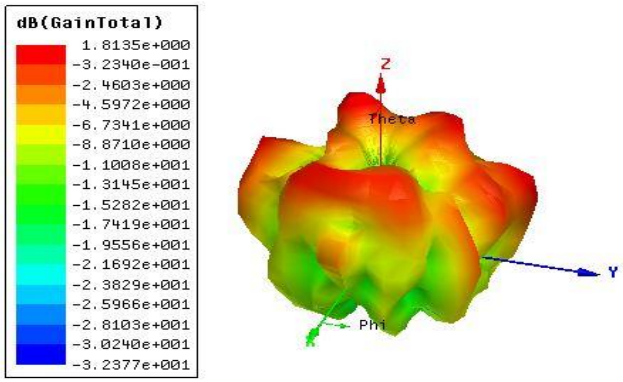

Figure 21. Gain at 6.83 GHz

Methods using current distribution curve are used to calculate antenna impedance, resistance, radiation resistance, reactance, radiation pattern etc. Figure 22 illustrates current distribution.

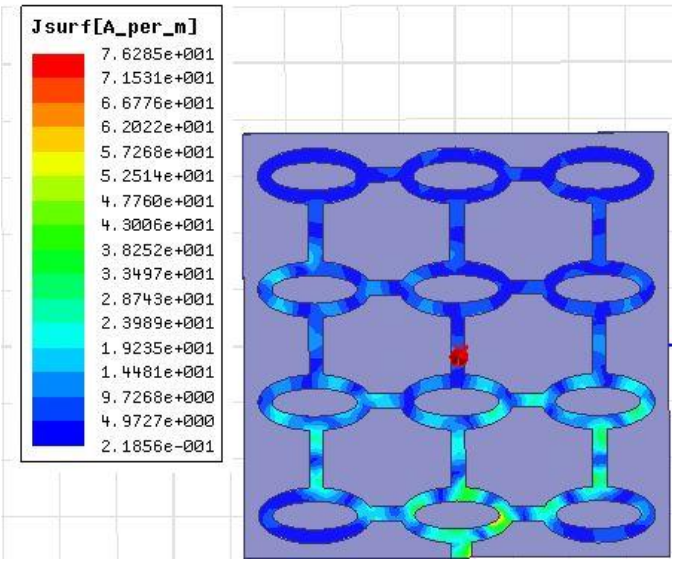

Figure 22. Current distribution of proposed antenna

IV. CONCLUSION

An antenna consisting of periodic array of circular patch was designed and simulated. It is a 3×4 array consisting of 12 patches. Desirable gain and bandwidth was achieved. The design is applicable for satellite applications. VSWR and S parameters were observed and was satisfactory. The designed antenna has multiband characteristics.

V. REFERENCES

[1] A.R. Parvathy, Thomaskutty Mathew, "*A novel aperture coupled micro strip circular patch antenna for dual band operation*", Progress in Electromagnetic Research Symposium,2017

[2] Xiao Zhang, Lei Zhu, "*Dual-Band High-Gain Circular Patch Antenna Working in Its TM11 and TM12 Modes*", IEEE Transactions on Antennas and Propagation,2018

[3] Daisy Sharma, T .Shanmuganantham, "*Design Analysis of Multiband FSS Antenna in C and Ku Band*",ICCCSP,2018

[4] Daisy Sharma, T .Shanmuganantham, "*Design of Multiband Antenna using FSS*", IEEE I2CT,2018

[5] Daisy Sharma, T .Shanmuganantham, "*Novel Design of Circular Patch FSS Microstrip Antenna for C Band Applications*", MECIT,2018

[6] Daisy Sharma, T .Shanmuganantham, "Analysis of Single and Dual Band Microstrip FSS Annular Ring Antenna for Ku Band",IEEE ICCCSP,2018

[7] Daisy Sharma, T .Shanmuganantham, *"Design of Single Band Micro strip Antenna Using FSS",*CNC,Springer,2018

Themed Section : Engineering and Technology
© 2018 IJSRSET | Volume 5 | Issue 3 | Print ISSN: 2395-1990 | Online ISSN: 2394-4099

Microcantilever Based Integrated Temperature Sensor, Humidity Sensor and Moisture Sensor – Comparitive Analysis

B. Priyadarisshini[1], D. Sindhanaiselvi[2], T. Shanmuganatham[3]

[1]PG Scholar, Department of Electronics and Instrumentation Engineering, Pondicherry Engineering College, Puducherry, India

[2]Assistant Professor, Department of Electronics and Instrumentation Engineering, Pondicherry Engineering College, Puducherry, India

[3]Associate Professor, Department of Electronics Engineering, Pondicherry University, Puducherry, India

priyasandra94@gmail.com[1], dsindhanaiselvi@gmail.com[2],shanmuganathamstr@gmail.com[3]

ABSTRACT

Microcantilever based integrtaed temperature sensor, humidity sensor and moisture sensor is proposed to reduce the cost of the device. This novel idea of integrating temperature, humidity and moisture sensor since they are inter dependent parameter in the environmental measurement. The proposed work investigates about the performance of the three sensor by placing them in a single silicon substrate. The structure which yields maximum deflection is the optimized method to fix the three sensors. The deflection analysis is carried out for temperature at 100ºC, relative humidity at 10% to 100% and the moisture range of 10 % to 100%.

Keywords: Temperture Cantilever, Humidity Cantilever, Moisture cantilever, Maximum Deflection.

I. INTRODUCTION

MEMS based cantilever sensor is simple to design and economical in manufacturing such devices using micro machining method. Now a days, more than two sensors are integrated in a single substrate to achieve the precision output with better compensation also. To achieve this MEMS technology is most widely used since the product is smaller in size, low in cost and low power consumption.

The output from the sensor has two uses. The first one is to display the data or to store the data, but it not result with automated output without any feedback. The second one is sensor are part of feedback loops to achieve the control over the measured parameter. The output of sensor is eventually used to function the actuator with or without modification. In both the cases the sensors are needed individually. However many practical functions require the concreted use of multiple sensor [1] located at different locations. One of the most prominent example is monitoring the weather conditions [2] and agricultural monitoring [11]. The integration of multiple sensors result in effective use of power supply, reduced size and computational time and increase the commercial availability of sensor with MEMS technology adopted [6, 7, 8, 9, 10].

The key idea of this proposed work is to integrate the three interdependent sensor such as temperature cantilever, humidity cantilever and moisture [3] cantilever using single silicon substrate with advancement of MEMS technology. The simple

cantilever structure is proposed for each sensor to integrate them. The sensor is proposed for the temperature range of 100°C to 40.556°C ,Relative Humidity range of 10 % to 100 % at the temperature range of 25°C to 40°C and soil moisture range of 10% to 100%. The performance is studied based on placing the three microcantilever sensor on single silicon substrate in different directions. The structure with maximum deflection is the optimized integration of three sensor. The simulation is carried out using MEMS CAD INTELLISUITE Tool.

II. STRUCTURE OF INTEGRATED SENSOR

A. Basic structure

The basic structure of the temperature cantilever, humidity cantilever and moisture cantilever is shown in Figure 1, 2. The temperature cantilever with dimension 200µm x 100µm x 0.5µm and it is comprises of three layer such as substrate, dielectric layer and sensing layer. Similarily The temperature cantilever with dimension 200µm x 100µm x 0.5µm and it is comprises of four layer substrate, dielectric layer and sensing layer 1, sensing layer 2. The temperature and humidity sensor is constructed using INTELLISUITE MEMS CAD tool.

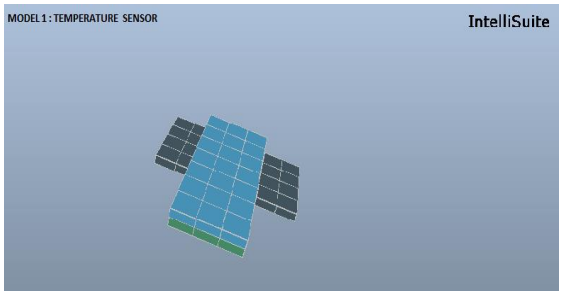

Figure 1: Temperature Sensor

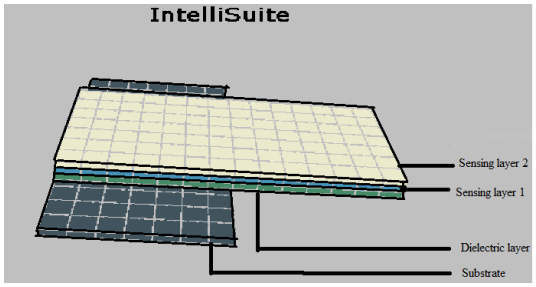

Figure 2. Humidity Sensor

B. Optimized Dimension

The maximum deflection for the dimension of temperature and humidity sensor shown in Table 1, Table 2, Table 3.

TABLE I

OPTIMIZED DIMENSION OF TEMPERATURE SENSOR

Structure Name	Dimension(µm)	Deflection(µm)
Corner perforation	**200x 100 x 0.5**	**54.9271**
Without perforation	200x 100 x 0.5	50.5893

TABLE II

OPTIMIZED DIMENSION OF HUMIDITY SENSOR

Humidity (100 %)	Dimension(µm) 200x 100 x 0.5	Deflection(µm) Without ribs	Deflection(µm) With ribs
T= 25°C	200x 100 x 0.5	28.0929	38.3051

C. Structure of Integrated sensor with respect to different placement

Silicon based Temperature sensor and humidity sensor [2, 4] is integrated in the single simple cantilever. Integrated sensor is constructed on the either side and also on the same side of the cantilever. Temeperature sensor comprises of Aluminum [5] deposited upon the dielectric layer Silicon dioxide. Aluminum is best temperature sensing element Humidity sensor is comprises of Platinum, temperature compensation layer upon the polymer based humidity sensor,

Polysilicon with the constant dimensions of length 200μm , width 100μm , height 0.5μm. The various cases of the integrated cantilever structures are shown in below:

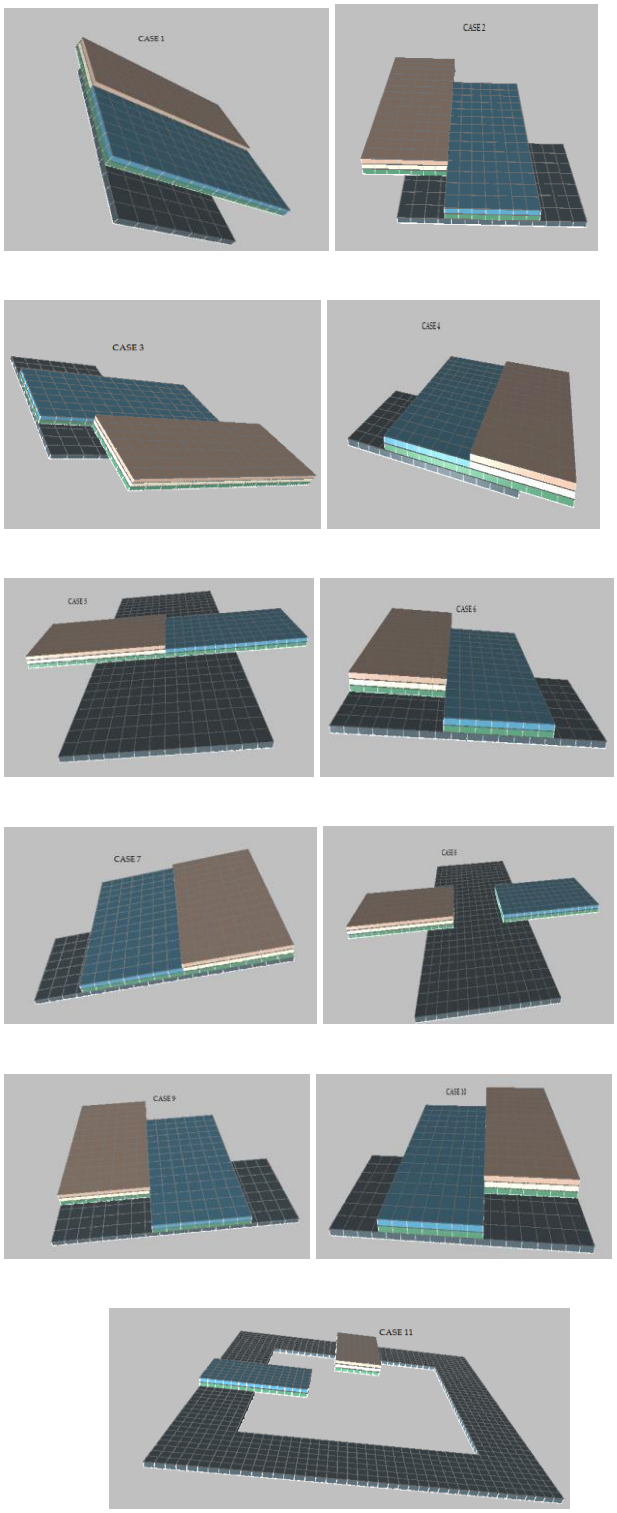

Figure 3. Varied Structure for the Integrated Temperature and Humidity Sensor

D. Deflection output

For the integrated temperature and humidity sensor, deflection analysis is carried out for the optimum temperature and humidity range for the various structure on the cantilever and it is tested and optimized The deflection analysis is shown in the Table 1.

TABLE III

DEFLECTION ANALYSIS OF VARIED STRUCTURES OF INTEGRATED SENSOR

CASE	DEFLECTION(μm)	
	TEMPERATURE FOR 100° C	HUMIDITY for 100% at 25° C
Case 1	46.9143	24.2056
Case 2	38.8155	29.066
Case 3	38.8155	29.066
Case 4	46.9143	24.2056
Case 5	52.6223	26.4591
Case 6	46.0789	21.5997
Case 7	46.0789	21.5997
Case 8	8.41255	3.5583
Case 9	38.7535	27.2908
Case 10	38.7535	27.2908
Case 11	47.5853	27.6799

E. Optimized Structure Of Integrated Sensor (Temperature And Humidity Sensor)

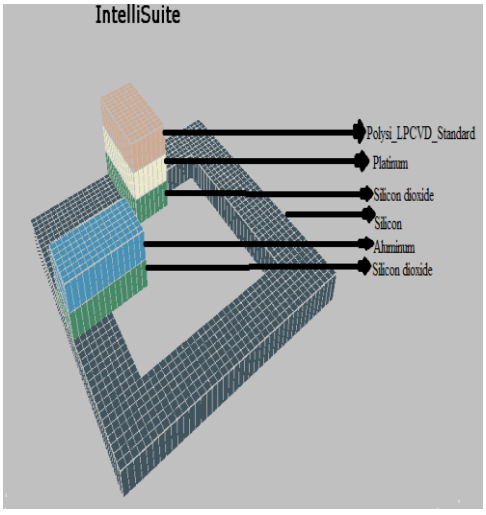

Figure 4. Optimized Integrated Temperature and Humidity Sensor

F. Structure of integrated sensor (temperature and soil moisture sensor)

The integrated sensor on silicon substrate of dimension 600µm x 600 µm x 5µm by using bulk micromachining. In order to form the cantilever, centre of the substrate is etched using mask of dimension 500µm x 500µmx 5µm. the temperature and soil moisture based cantilever is constructed on the substrate Each sensor dimension has been satisfied by significant design aspect ratio are:

(1) Ratio of length to width (l : w)
(2) Ratio of width to thickness (w: t)

The two constraints are shown in the Equations below:

$$l: w \geq 2:1 \quad (1)$$

$$w - 8t \leqslant 0 \quad (2)$$

The two-layered cantilever based temperature and soil moisture sensor is constructed with the dimension of 200µm x 50µm x 6.25µmis shown in Fig.5.

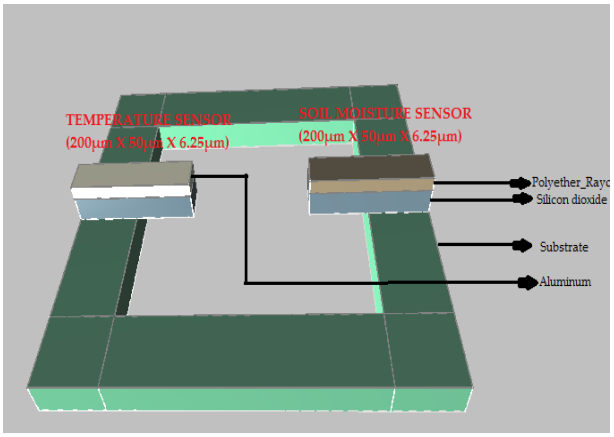

Figure 5. Optimized Integrated Temperature and Soil Moisture Sensor

TABLE IIV DIMENSION OPTIMIZATION OF INTEGRATED TEMPERATURE AND SOIL MOISTURE SENSOR

THICKNESS VARIATION (µm)		DEFLECTION (µm)	
Dielectric Layer	Sensing Layer 1	Temperature At 40.566°C	Soil Moisture At 100%
0.25	6	1.43338	177.08
1	5.25	1.72689	143.15
1.25	5	1.96608	124.511
2	4.25	2.2455	48.676
2.25	4	2.27906	24.7605
3	3.25	2.31226	0.00419557

G. Deflection output

Sensitivity analysis of integrated temperature and soil moisture sensor for the thickness variation of substrate of 5(µm) and dielectric layer of 0.25(µm) and sensing layer of 6(µm) for the dimension of [200 (µm) x 50(µm) x6.25 (µm)] is shown in Table 4, Table 5.

TABLE IIIV SENSITIVITY ANALYSIS OF INTEGRATED TEMPERATURE SENSOR

Temperature (°C)	Deflection (µm)
1.66667	0.0589055
4.44444	0.157081
7.22222	0.255256
10	0.353432
12.7778	0.451609
15.5556	0.549785
18.3333	0.647958
21.1111	0.746134
23.8889	0.844311
26.6667	0.942487
29.4444	1.04066
32.2222	1.13884
35	1.23701
37.7778	1.33519
40.556	1.43338

TABLE V SENSITIVITY ANALYSIS OF SOIL MOISTURE SENSOR

SOIL MOISTURE AT 100%	Deflection (µm)
10	17.7088
20	35.4176
30	53.1264
40	70.8353
50	88.5441
60	106.253
70	123.962
80	141.671
90	159.38
100	177.088

Sensitivity analysis of integrated temperature and soil moisture sensor for the thickness variation of substrate of 5(µm) and dielectric layer of 3(µm) and sensing layer of 3.25(µm) for the dimension of [200 (µm) x 50(µm) x6.25 (µm)] is shown in Table 6, Table 7.

TABLE VI SENSITIVITY ANALYSIS OF INTEGRATED TEMPERATURE SENSOR

Temperature (°C)	Deflection (µm)
1.66667	0.0951058
4.44444	0.253615
7.22222	0.412124
10	0.570634
12.7778	0.729144
15.5556	0.887655
18.3333	1.04616
21.1111	1.20467
23.8889	1.36318
26.6667	1.52169
29.4444	1.6802
32.2222	1.83871
35	1.99722
37.7778	2.15573
40.556	2.31426

TABLE VII SENSITIVITY ANALYSIS OF SOIL MOISTURE SENSOR

SOIL MOISTURE AT 100%	Deflection (µm)
10	0.0000041974
20	0.00389636
30	0.000584455
40	0.00167823
50	0.00209778
60	0.00251734
70	0.0029369
80	0.00335646
90	0.00377601
100	0.00419557

III. CONCLUSION

By using simple cantilever, MEMS based temperature and humidity sensing is integrated on the single free standing cantilever for the varied application. This integrated sensor will be in compact size and also can be used in the various applications as one among the other sensor. In the integrated sensor , temperature and humidity is placed on both sides also on the same side of the cantilever and the deflection analysis is carried out with respect to to temperature (°C) and relative humidity (%). Among the varied structure Case 11 has maximum deflection for the temperature sensor and humidity sensor. Even Case 5 has maximum deflection for temperature sensor but the structure is not as a typical cantilever structure. Hence case 10 has chosen as the optimized structure. Integrated temperature and soil moisture sensor has been designed in the dimension of 200µm x 50µm x 6.25µm based on the aspect ratio and the optimized thickness variation is achieved depend on the maximum deflection. For the thickness variation for substrate of 5(µm) and dielectric layer of 0.25(µm) and sensing layer of 6(µm) has maximum deflection of 177.08µm for the moisture senor . Where else , the thickness variation for substrate of 5(µm) and dielectric layer of 03(µm) and sensing layer of 3.25(µm) has maximum deflection of 2.31226 µm for the temperature senor This current study is further

develops the optimized structure with perforation and ribs for the enhanced deflection in the microcantilever .

IV. REFERENCES

[1] David J.Nagel, "Microsensor Cluster", Microelectronics Journal, 33 (2002), 107-119. (Elsivier)

[2] Rong-Hua Ma, Chia-Yen Lee, Yu-Hsiang Wang, Hao-Jen Chen "Microcantilever-based weather station for temperature, humidity and flow rate measurement," Microsyst Technol, vol. 14, pp. 971-977, November 2007.

[3] Jie Liu, Mangilal Agarwal, Kody Varahramyan,Ernest S. Berney IV, Wayne D. Hodo "Polymer- based microsensor for soil moisture measuremnet," Sensors and Actuators, vol. B129, pp. 599-604, September 2007.

[4] Lung-Tai Chen, Chia – Yen Lee, and Wood-hi cheng, "MEMS-based humidity sensor with integrated temperature compensation mechanism," Sensors and Actuators, vol. A147, pp. 522-528, July 2008.

[5] Ashish, Kumari Nidhi Gupta, Dr. T.Shanmuganantham, "Design Of Temperature Sensors For Enviromental Applications", Int. Journal of Engineering Trends and Technology (IJETT) –Volume 4 Issue 10 - Oct 2013.

[6] B.Priyadarisshini, D.Sindhanaiselvi, T. shanmuganatham, "Design and dimension optimization of high sensitive microcantilever as humidity sensor," IEEE, Accepted.

[7] D.Sindhanaiselvi, T.Shanmuganantham, "Double Boss Sculptured Diaphragm Employed Piezoresistive Mems Pressure Sensor With Silicon-On-Insulator (SOI)" Journal of Engineering Science and Technology, School of Engineering, Taylor's University., Vol. 12, July 2017

[8] Marie Joan Syndhya, D.Sindhanaiselvi, T.Shanmuganantham, "Design and Analysis of Rectangular type Pizoresistive Microcantilever for Antigen Detection", International Journal of Control Theory and Application, International Science Press, Vol. 10, 2017.

[9] Marie Joan Syndhya, D.Sindhanaiselvi, T.Shanmuganantham, " Investigation on Piezoresistive Micro Cantilever Design for Blood Glucose Sensing", International Journal of Control Theory and Application, International Science Press , Vol. 10, 2017.

[10] D.Sindhanaiselvi, T.Shanmuganantham, "Investigation on Performance of Piezoelectric Beam Based Mems Actuator for Focussing of Micro Lens in Mobile Application", IEEE International Conference on circuits and systems, 2017.

[11] Rajul S. Patkar, Madhuri Vinchurkar, Mamta Ashwin, and V. Ramgopal Rao, "A Novel PET-Based Piezoresistive MEMS Sensor Platform for Agricultural Applications," Journal of Microelectromechanical Systems, Vol. 26, No. 4, Pp. 746-748, August 2017.

Themed Section : Engineering and Technology
© 2018 IJSRSET | Volume 5 | Issue 3 | Print ISSN: 2395-1990 | Online ISSN : 2394-4099

An Elliptical Ring FSS Antenna excited with Microstrip Feed for Satellite Application

Daisy Sharma[1], Dr. T. Shanmuganantham[2]
[1]Department of Electronics and Communication, Pondicherry University, Puducherry, India
daisy28nov@gmail.com[1]
[2]Department of Electronics and Communication, Pondicherry University, Puducherry, India
shanmugananthamster@gmail.com[2]

ABSTRACT

A novel light weight FSS antenna is designed and discussed in this paper.FR4 epoxy is used as the substrate with relative permittivity 4.4 and dielectric loss tangent 0.02.The dimensions of the substrate is 150mm × 150mm with height 1.6mm.The shape of the patch used is elliptical ring which is in 3×4 array. The elliptical patches are interconnected to achieve better antenna characteristics. Microstrip line feeding technique is used for feeding the antenna. The design is proposed for satellite applications. HFSS software is used to simulate the antenna and study the antenna parameters.

Keywords : FSS (Frequency selective surface), Micro Strip Line Feeding, FR4 epoxy, HFSS

I. INTRODUCTION

FSS is a periodic array structure which consist of radiating or non-radiating elements which make them act as band pass or band stop filters.[1]FSS is a function of both frequency and angle of incidence. FSS can act as a barrier for unwanted signal and hence we can use it as spatial filters. FSS is used to enhance antenna performance as a reflector. [1]-[2]For wearable antennas, FSS is employed as sub reflector. In any planar or irregular structure, FSS can be employed as EMI shield.

Cross polar radiation components are reduced by using polarisation dependent frequency selective surfaces. Circular polarisation is generated itself by FSS. [3] For satellite communication, the necessary requirements are wide bandwidth, high gain and circular polarisation. Patch array antenna are better option for increasing gain. Designing multiple feeds is difficult in FSS. [4]- [5] Side lobes and back radiations are reduced by circular polarisation. Microstrip antenna with circular polarisations finds its application in satellite communication, radar and mobile communication because of its compact size and low profile. Circularly polarised antennas are superior in performance than linearly polarised antennas. [6]These antennas reduces Faraday rotation effect and multi path interference. Achieving 3dB axial ratio bandwidth is critical for circular polarised antenna. To realize wideband impedance bandwidth and 3dB axial ratio bandwidth of circular polarised antenna various steps can be taken. Lower the dielectric constant of substrate, higher the antenna efficiency but size of the antenna will be more.[7] Thicker substrate gives wider impedance bandwidth. Impedance bandwidth can be improved by employing proximity coupled feeding [8].

Thickness and type of substrate used has a major impact on gain improvement. If the eccentricity of the ellipse is small in a narrow frequency band, the radiation can either right hand or left hand circularly polarised [9]. Use of multiple feeds results in circular

polarisation. But for exciting circularly polarised antenna only one feed point is required.

II. ANTENNA DESIGN

The proposed design is a periodic array of elliptical ring with interconnections. The dimension of proposed antenna is 150mm×150mm. The substrate used is FR4 epoxy with relative permittivity 4.4, relative permeability 1, dielectric loss tangent 0.02 and magnetic loss tangent 0.The height of the substrate is 1.6mm.Ground lies below substrate which is of negligible thickness. Above the substrate patches are designed. The antenna design consist of 3×4 array. It consist of 12 periodic elliptical ring patches. Elliptical ring consist of two ellipses, one outer ellipse and one inner ellipse. The desired design of the patch is obtained by subtracting one ellipse from another. The outer ellipse has a major radius of 10mm and ratio is 2.The inner ellipse has a major radius of 5mm and ratio of 3. Micro strip line feeding technique is used for the antenna. The material of the radiation box is air contains the antenna setup. The antenna is simulated and results are obtained in C band. Figure 1 illustrates the proposed antenna design.

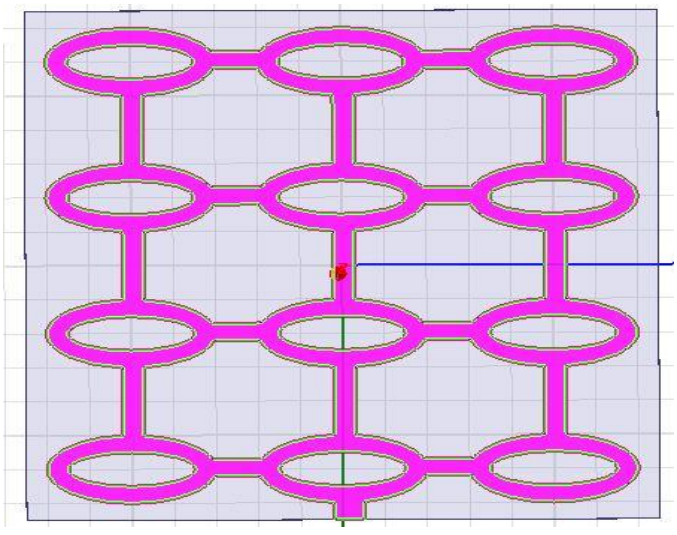

Figure 1. Proposed antenna design

Patch and feeding technique used is fabricated in the dielectric substrate. Patches are interconnected so that equal surface current distribution is there throughout radiating patches. If the patches are not interconnected, there are mutually coupled but the characteristic parameters varies. Design flexibility is provided by elliptical ring patch as the dimensions can be altered. Circular polarisation can be obtained by using single feed point on the elliptical ring patch.

The geometrical shape of elliptical patch allows to perform rigorous theoretical analysis in a standard co-ordinate system. x-y coordinates are replaced by elliptical coordinates u and v.

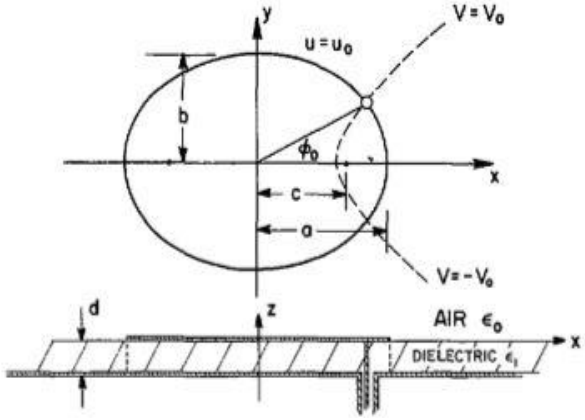

Figure 2. Ellipse with elliptical coordinates

Figure2 illustrates ellipse with elliptical coordinates

Ellipse is defined by :

u = ln $(\frac{a+b}{c})$ where

semi major axis is designated by a, semi minor axis is designated by b and foci is designated by c.

Ellipse eccentricity is given by :

e = $\frac{c}{a}$

The Maxwell's equations reduces to the following set of equations when thickness of dielectric substrate is smaller than wavelength :

$$\frac{\partial^2 E_z}{\partial u^2} + \frac{\partial^2 E_z}{\partial v^2} + {k_1}^2 c^2 (cosh^2 u - cos^2 v) E_z = 0$$

$$H_u = \frac{j}{\mu\omega c\sqrt{cosh^2 u - cos^2 v}} \frac{\partial E_Z}{\partial v}$$

$$H_v = \frac{-j}{\mu\omega c\sqrt{cosh^2 u - cos^2 v}} \frac{\partial E_Z}{\partial u}$$

$H_z = 0 \quad E_z = 0 \quad E_z = 0$

$k_1 = \omega\sqrt{\mu_0 \varepsilon}$

Maximum directivity can be calculated by :

$D = \frac{1+|r|}{1-|r|}$ where reflection coefficient is designated by r

For a particular frequency, maximum power in boresight direction($\theta = 0$) is obtained when resonant length is given by:

$l = \frac{N\lambda}{2} + (\frac{\phi_r + \varphi_g}{\pi})\frac{\lambda}{2}$ where N is integer number (=1)

Reflection coefficient phase of FSS unit cell is designated by $\emptyset_r$

Reflection coefficient phase of substrate with ground plane is designated by φ_g

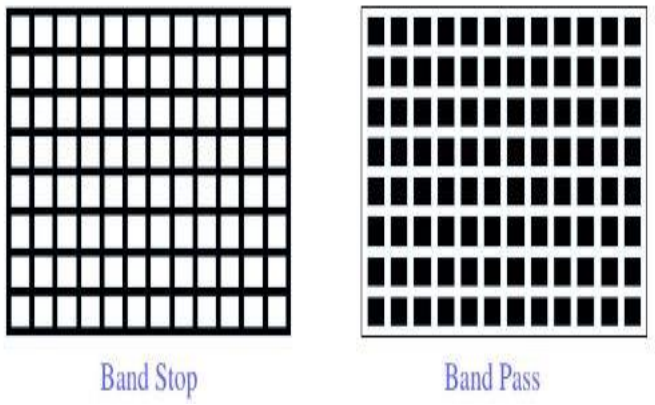

Figure 3. Characteristics of FSS

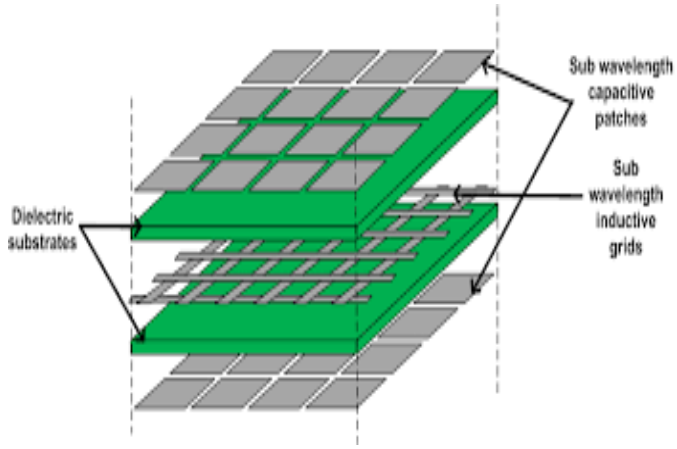

Figure 4. Structure of FSS

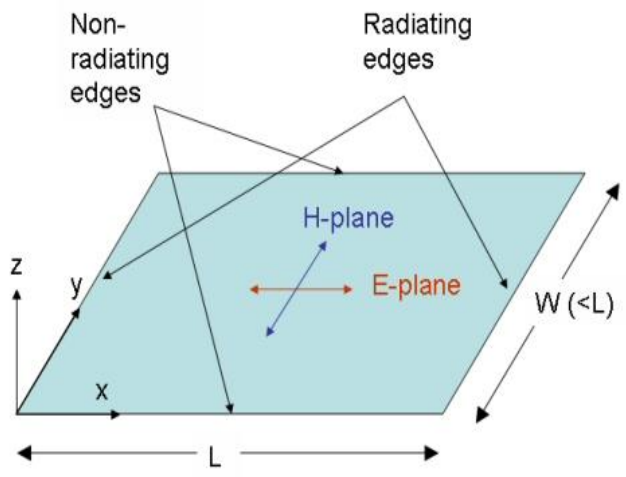

Figure 5. Patch edges

Figure3 shows characteristics of FSS. Figure 4 gives the structure of FSS. Figure 5 shows Patch edges.

III. SIMULATION RESULTS AND DISCUSSIONS

Based on transmission line model, antenna parameters are calculated. Generally elliptical antenna has elliptical polarised radiation but it is circular polarised when antenna is fed under specified condition. By limiting eccentricity of the ellipse to a range of 10 to 20 percent desired circular polarisation can be achieved.

S parameters are scattering parameters which are vector entities. They are popularly used in microwave circuit design and testing. At high frequencies, measurement of Y, H or Z parameters are difficult. Vector network analyser is used to measure S parameters. There are four scattering parameters for two port device. S_{11} and S_{22} are forward and reverse reflection coefficients respectively. When it is ideal short, S_{11}= -1 and for ideal termination S_{11}=0. S_{11} is measured below -10dB and is minimised at the resonating frequencies.Figure6 shows the S_{11} parameter graph. There are two resonating frequencies. The resonating frequencies of the proposed antenna design are 4.08 GHz and 5.45 GHz.

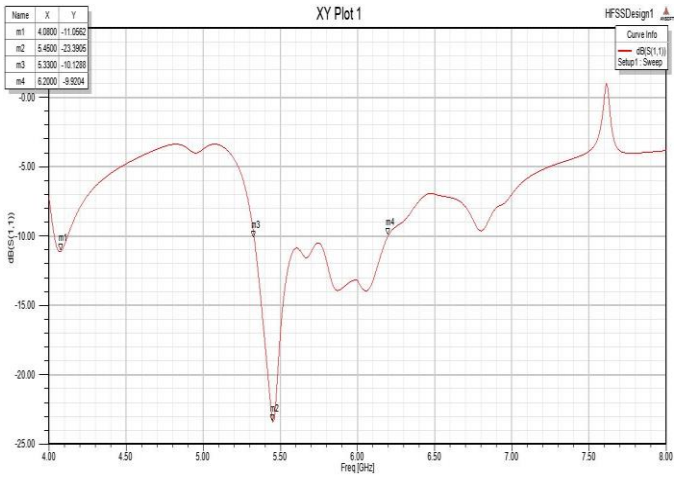

Figure 6. S_{11} parameter graph

VSWR indicates the mismatch between antenna and the feed lines connected to it. VSWR for a ideal system is 1 but practically it is below 2.When the VSWR graph is below 2, it means impedance is matched properly and reflections are less. If the antenna is poorly matched then VSWR value exceeds 2.Reflections are caused by mismatched impedances. For proper matching, the load impedance should be equal to characteristic impedance of the transmission line. The load must not have any reactance elements. Figure 7 shows VSWR graph. It is observed that at the resonating frequencies the VSWR value is below 2.The VSWR is 1.78 and 1.14 at the respective resonating frequencies.

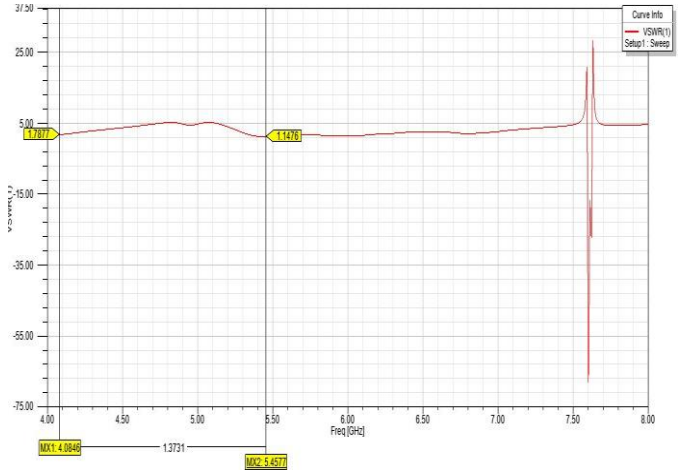

Figure 7. VSWR graph

Radiation is not uniform for all antennas in all directions. Radiation pattern is plotted in azimuth or E plane and elevation or H plane respectively.

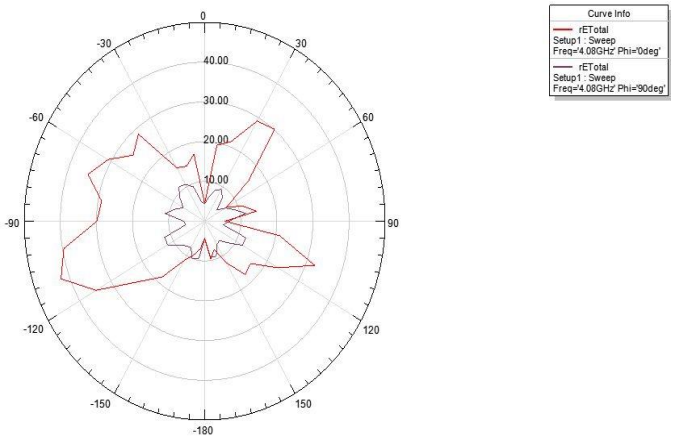

Figure 8. Radiation pattern at resonating frequency 4.08 GHz for $\varphi = 0^0$ and $\varphi = 90^0$

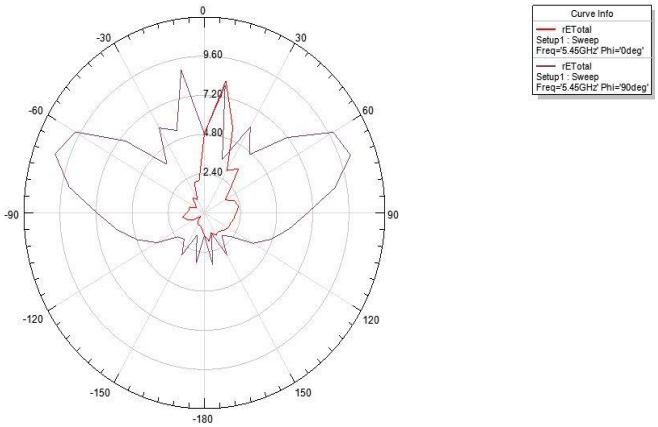

Figure 9. Radiation pattern at resonating frequency 5.45 GHz for $\varphi = 0^0$ and $\varphi = 90^0$

Figure 8 shows the radiation pattern at resonating frequency 4.08 GHz for $\varphi = 0^0$ and $\varphi = 90^0$ respectively. Figure 9 shows the radiation pattern at resonating frequency 5.45 GHz for $\varphi = 0^0$ and $\varphi = 90^0$ respectively.

Gain of an antenna is measured in dBi or dBd. Direction of maximum radiation is referred as gain. It can be discussed as a function of angle. Figure10 shows 3D polar plot of gain at 4.08 GHz resonating frequency. Figure11 gives 3D polar plot of gain at 5.45 GHz resonating frequency.

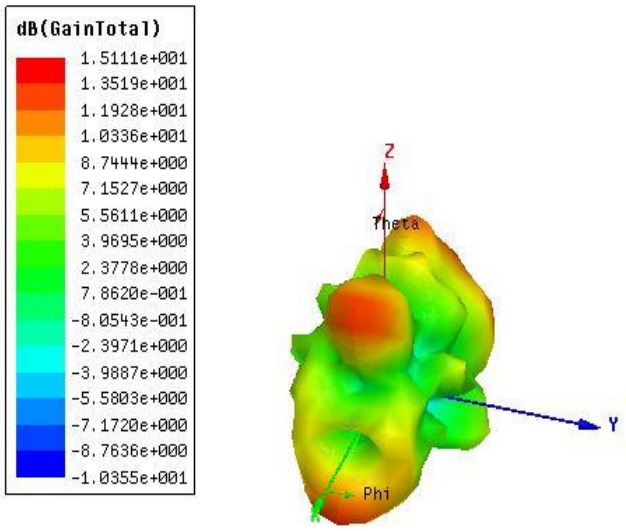

Figure 10. 3D polar plot of gain at 4.08 GHz

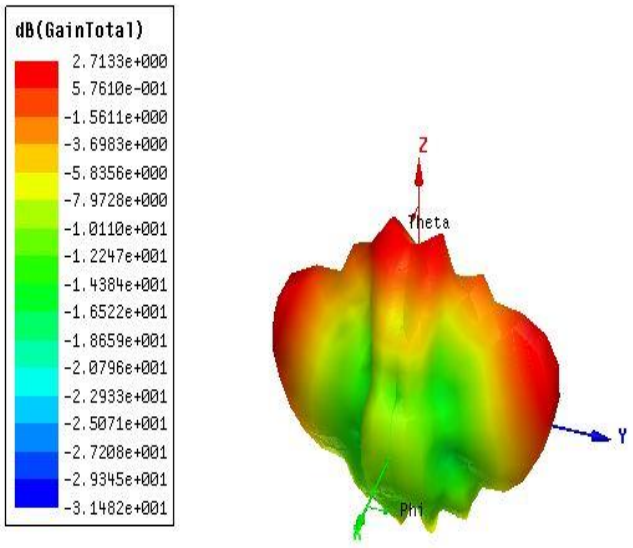

Figure11. 3D polar plot of gain at 5.45 GHz

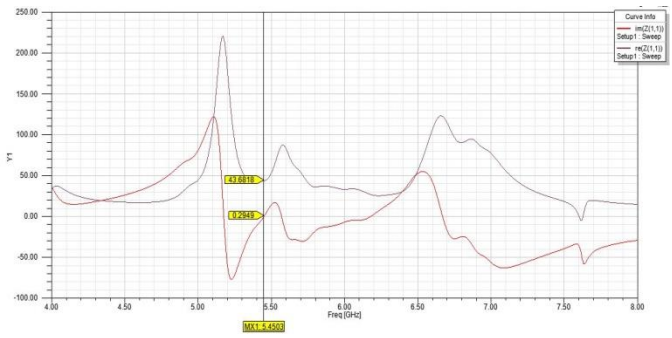

Figure 12. Input impedance Vs frequency graph

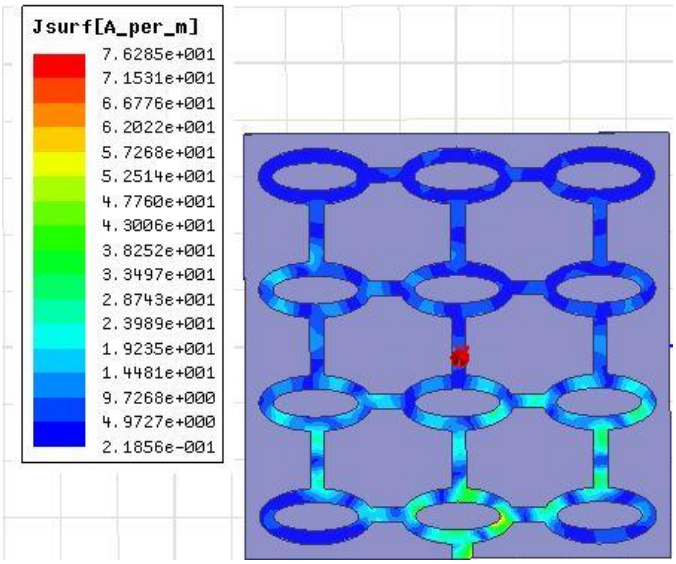

Figure 13. Current distribution of proposed antenna

Figure 12 shows input impedance Vs frequency graph. Figure 13 illustrates current distribution of proposed antenna.

Methods using current distribution curve are used to calculate antenna impedance, resistance, radiation resistance, reactance, radiation pattern etc.

IV. CONCLUSION

An interconnected elliptical ring patch FSS antenna is designed. It consist of periodic 3×4 array of twelve patches. The substrate is FR4 epoxy with dimension 150mm×150mm×1.6mm.The resonating frequencies of the proposed antenna are 4.08 GHz and 5.45 GHz. The antenna utilizes low power. Desired gain and bandwidth is achieved. The antenna finds its application in satellite communication. The results are obtained in C band using HFSS.

V. REFERENCES

[1] Liang C. Sheng, "*The Elliptical Micro strip Antenna with Circular Polarization*", IEEE Transactions On Antennas And Propagation, Vol.. AP-29, no. 1, January 1981

[2] Ali Hakam, M. I. Hussein , Mohamed Ouda, Raed Shubair and Elham Serria, "*Novel Circular*

Antenna with Elliptical Rings for Ultra-Wide-Band", Antenna and Propagation (EuCAP) ,2016

[3] Wai Yan Yong, Sharul Kamal Abdul Rahim ,Mohamed Himdi, Fauziahanim Che Seman ,Ding Lik Suong, , Muhammad Ridduan Ramli And Husameldin Abdelrahman Elmobarak, "*Flexible Convoluted Ring Shaped FSS for X-Band Screening Application*", IEEE Access, vol. 6,2018

[4] Daisy Sharma, T .Shanmuganantham, *"Design Analysis Of Multi Band Fss Antenna In C And Ku Band"*, IEEE International Conference on Computer, Communication and Signal Processing, 2018.

[5] Cahya Edi Santosa1, Josaphat Tetuko Sri Sumantyo, Ari Sugeng Budiyanta, and Achmad Munir, "*Broadband X-band Circularly Polarized Microstrip Antenna with Elliptical Patch Ring-slotted for Airborne SAR System*", Progress In Electro magnetics Research Symposium (PIERS), 2017

[6] Daisy Sharma, T .Shanmuganantham,"*Design of Multiband Antenna using FSS*", IEEE I2CT, 2018

[7] Daisy Sharma, T .Shanmuganantham, "*Design of Miniaturised FSS Microstrip Antenna for Ku Band Applications*", IEEE International Conference on Circuits and Systems,2017

[8] Daisy Sharma, T .Shanmuganantham, "*Design of Miniaturized Dual Band Antenna using FSS*", IEEE International Conference on Circuits and Systems, 2017

[9] Daisy Sharma, T .Shanmuganantham, *"Design of Single Band Micro strip Antenna Using FSS",*CNC, Springer, 2018

Themed Section : Engineering and Technology
© 2018 IJSRSET | Volume 5 | Issue 3 | Print ISSN: 2395-1990 | Online ISSN: 2394-4099

RF MEMS in-line Series switch for S band Application

Aamir Saud Khan[1], T Shanmuganantham[2]
[1]PG student, Department of Electronics Engineering, Pondicherry University, Pondicherry, India
[2]Assistant Professor, Department of Electronics Engineering, Pondicherry University, Pondicherry, India
aamir.105023@gmail.com[1],shanmugananthamster@gmail.com[2]

ABSTRACT

This paper proposed an RF (Radio Frequency) MEMS (Micro Electro Mechanical systems) cantilever beam switch for S band application. The switch shows good RF parameters over the range of (2-6) GHz along with low actuation voltage. Although RF MEMS switches are very good counterpart for solid state switches but its high actuation voltage and high switching time is matter of concern. So in this paper, we generally concentrates on reducing the high actuation voltage for that a novel design of an RF MEMS in line series cantilever beam switch was proposed and designed using the software Intellisuite 8.7v for electromechanical analysis and by EM software for RF analysis. From simulation, we get actuation voltage of (2.5V) and insertion loss of -0.2683 dB at 2.55 GHz with return loss of -16.3720 dB at 2.20 GHz and isolation loss of -29.1203 dB at 2.40 GHz.

I. INTRODUCTION

Now-a-days Radio Frequency (RF) Microelectromechanical (MEMS) switches have gained lots of attention of researchers and scientist from the different parts of the world. The allurement of these switches is that it that it offers RF performance similar to that of relay based switches and miniaturized in size and cost as similar to FET based switches. These switches show low power consumption, good return loss, low insertion loss, wider temperature range, high isolation loss, very good linearity, etc [1]. But area of concern for these switches are its high actuation voltage, high switching time, reliability, lower power handling capacity and packaging. So lots of research is going out throughout the world that how to overcome these challenges and make these switches available for the commercial purposes. In 2001, Xiaodong, Lumtao, et al. designed a compact RF MEMS switch for S band application whose actuation voltage was 25 V with insertion loss of -0.5 dB and isolation loss of -21 dB at 3 GHz [2]. In 2012, Sinha, Bansal, and Rangra proposed compact T-type switch for space application whose actuation voltage was 7.5 V with insertion loss of -0.48 dB and isolation loss of -22.12 dB up to 25 GHz [3]. In 2014, Angira, Sundaram, and Rangra designed interdigitated shunt capacitive switch for X and K band application whose insertion loss is -0.11 dB at 25 GHz and isolation loss of -40.7 dB at 21.4 GHz with an actuation voltage of 12.25 V [4]. In 2015, Ziaei, Bansropun, Martins and Baillif designed a fast high power capacitive switch for X band application whose insertion loss is -0.1 dB and isolation loss of -30 dB at 10 GHz with a high pull in voltage of 60 V [5]. In 2016, El massry, Medhat and Mostafa proposed a mobile compatible switch whose actuation voltage is 3.3 V with insertion loss of -0.05 dB and isolation loss of -21 dB at 6 GHz [6]. So this paper emphasis on the analysis and simulation of a novel RF MEMS switch design to lower the actuation voltage along with good RF parameters.

II. PROPOSED DESIGN

An ultra low voltage switch is designed and simulated in FEM software Intellisuite 8.7v, where displacement and mises stress are calculated under the influence of electrostatic actuation. Table I shows the design dimensions of the switch and Figure 1 and Figure 2 shows the top view and side view of the switch. The material used for the switch is aluminium (Al).

TABLE I

Dimensions of parameters

Parameters	Proposed design
Length of beam(μm)	210
Breadth of beam(μm)	70
Thickness of beam (μm)	1
Air gap (μm)	1.5

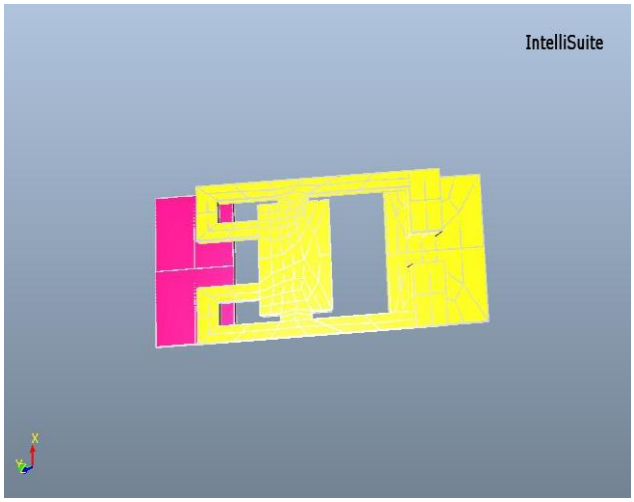

Figure 1. Top view of switch

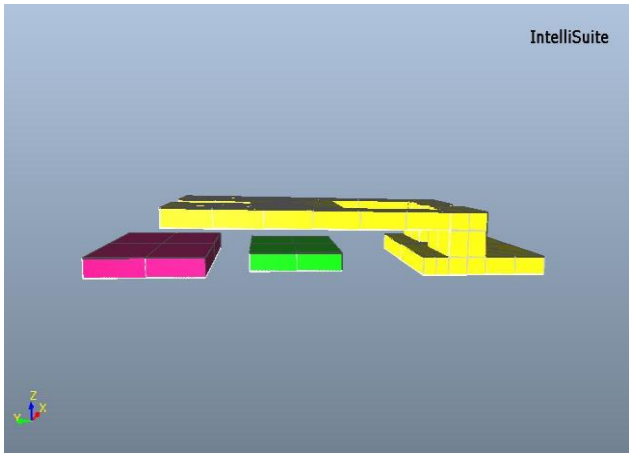

Figure 2. Side View Of Switch

The schematic representation of the switch on the Co Planar Waveguide (CPW) is shown in Figure 3

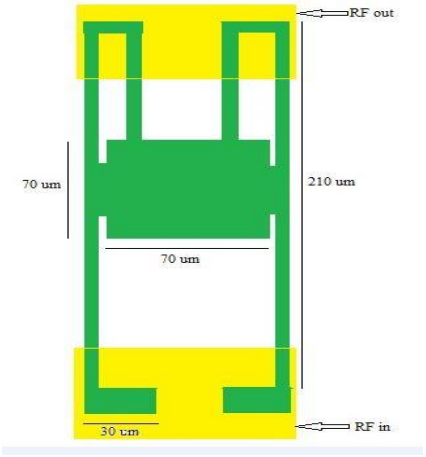

Figure 3. Schematic representation of the switch

III. MATHEMATICAL MODELING

The mathematical modelling of the RF MEMS switches has two categories: (1) Electromechanical analysis, (2) Electromagnetic analysis.

A. Electromechanical Analysis

In this analysis we generally focus on the mechanical parameters of the cantilever beam such as spring constant, Young's modulus, electrostatic force between the beam and lower electrode, actuation voltage, switching time etc,. Consider a cantilever whose one end is fixed and other is hanging freely over the t- line as shown below in Figure 4

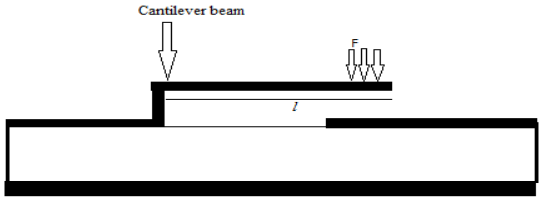

Figure 4. A simple cantilever beam

When a force F is applied at the free end of the beam it gets deflected by Δ x and is given by [7]

$$F = K \Delta x \tag{1}$$

Where K represents the spring constant of the beam and is given by [7]

$$K = 2Ew\left(\frac{t}{l}\right)^3 \frac{1-\frac{x}{l}}{3-4\left(\frac{x}{l}\right)^3+\left(\frac{x}{l}\right)^4} \tag{2}$$

where E represents beam Young's modulus. The critical stress of the beam is defined as the maximum amount of compressive stress before yielding or buckling beam occurs and is given by [7]

$$\sigma_{cr} = \frac{\pi^2 E t^2}{3l^2(1-v)} \tag{3}$$

Where *l* is beam length, *t* is beam thickness and *v* is material Poisson's ratio. The concept behind electrostatic actuation is same as the electrostatic force between the two parallel plates of capacitor. The capacitance between parallel plates is given by [8]

$$C = \frac{\varepsilon W w V^2}{g} \tag{4}$$

Where g represents beam height and ε represents the permittivity of the medium. The electrostatic force is given by [9]

$$F_e = -\frac{\varepsilon W w V^2}{2g} \tag{5}$$

Where V represents the applied bias voltage between the lower electrode and the beam and F_e is electrostatic force. So after equating linear spring force with square electrostatic force and solve for V we get actuation voltage or pull-in voltage [10]

$$V_p = V\left(\frac{2g_0}{3}\right) = \sqrt{\frac{8K g_0^3}{27 \varepsilon W w}} \tag{6}$$

Where V_p represents "pull-in voltage" and g_0 is zero bias height above the electrode. The frequency of the beam is given by [11]

$$w_0 = \sqrt{\frac{K}{m}} \tag{7}$$

where m is mass of cantilever beam. The quality factor (Q) is very important parameter for determining the switching time of the switch. From experiments it is found that if $Q \leq 0.5$, then switching time is slow and if $Q \geq 2$, then settling time is longer after release. So for better overall performance Q = 1, and switching time is given by [11]

$$t_s = 3.67\frac{V_p}{V_s w_0} \qquad \text{for } V_s \geq 1.3\ V_p \tag{8}$$

B. Electromagnetic analysis

In this we generally focus on the S parameters of the switch such as insertion loss, return loss, isolation loss etc,. RF MEMS switches are highly linear and passive two port device. When switch is in upstate (or in OFF condition) S_{21} gives isolation of the switch from that we can find C_s (series capacitance between transmission line and beam) and C_p (parasitic capacitance), and C_u is given by [12]

$$C_u = C_s + C_p \tag{9}$$

When the switch is in downstate (or in ON condition) S_{21} gives insertion loss and S_{11} gives return loss of the switch. In down state it behaves as series resistance and is given by [12]

$$R_s = R_c + 2R_{sl} + R_l \quad (10)$$

Where R_c is contact resistance, R_l is bridge resistance and R_{sl} is t-line resistance. The isolation loss of the switch is given by [12]

$$S_{21} = \frac{2jwC_u Z_0}{1 + 2jwC_u Z_0} \quad (11)$$

IV. RESULTS AND DISCUSSION

A. Electromechanical Results

The switch is designed and simulated in Intellisuite 8.7v software. The displacement of the switch is 1.5822 μm shown in Figure 5 and mises stress of the switch is 7.05611 Mpa shown in Figure 6 which is less than the critical stress which is 8.2671 Mpa (3) and the vertical displacement of the switch with applied voltage gives pull-in voltage of ~ 2.5 V as shown below in Figure 7

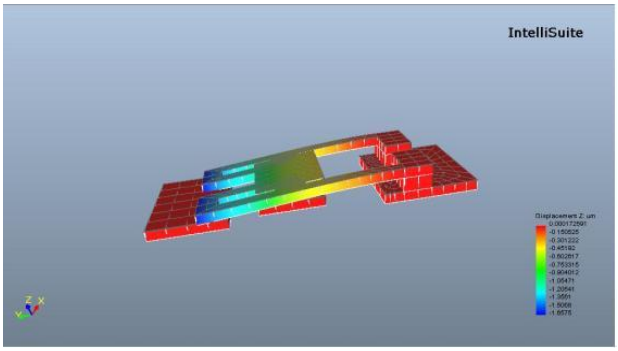

Figure 5. Switch Displacement

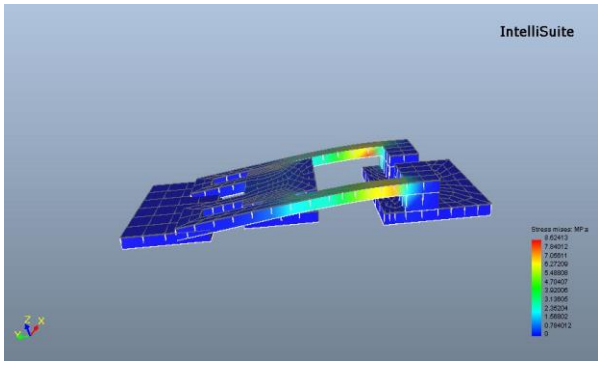

Figure 6. Switch Mises Stress

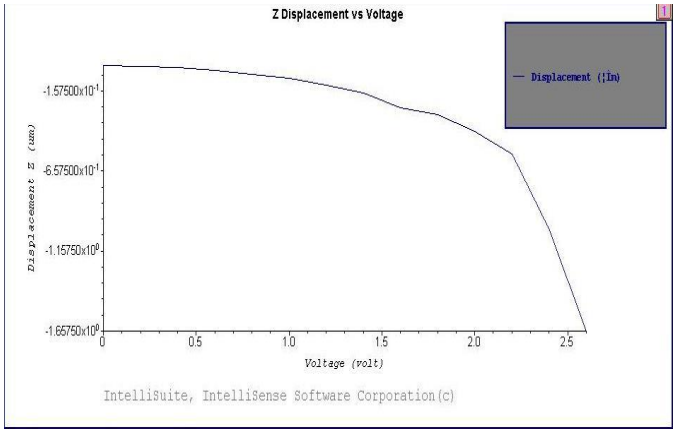

Figure 7. Voltage vs. beam vertical displacement

B. Electromagnetic results

For electromagnetic analysis the switch is designed and simulated in EM software. When the switch is in OFF condition (i.e., it will not allow power to transfer from port 1 to port 2) in that case S_{21} gives isolation loss and it is -29.1203 dB at 2.40 GHz as shown in Figure 8

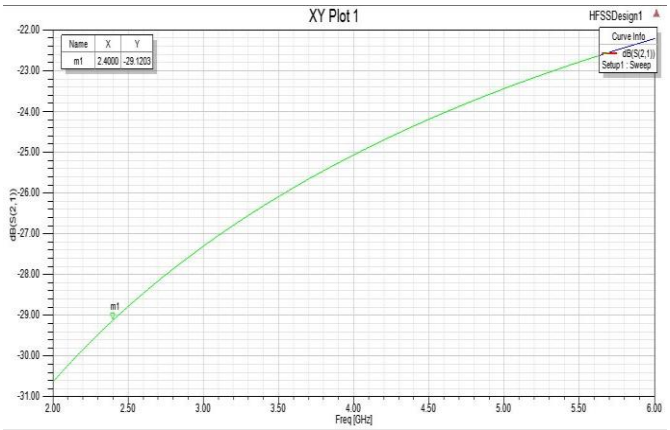

Figure 8. Isolation loss (S_{21}) in OFF condition

When the switch is in ON condition S_{21} gives insertion loss and it is -0.2683 dB at 2.55 GHz and S_{11} gives return loss of the switch and it is -16.3720 dB at 2.20 GHz as shown in Figure 9 and Figure 10.

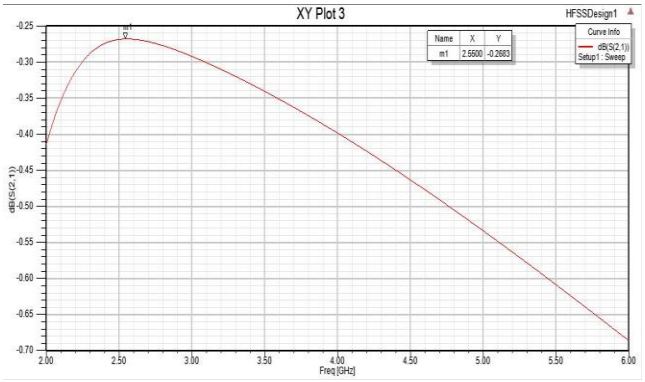

Figure 9. Insertion loss (S_{21}) in ON condition

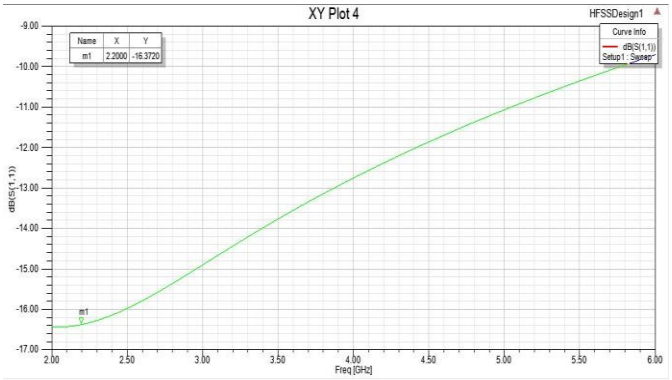

Figure 10. Return loss (S_{11}) in ON condition

TABLE II Results of proposed design

Parameters	Proposed design
Displacement (μm)	1.5822
Mises stress (MPa)	7.05611
Pull-in Voltage (V)	2.5
Isolation Loss (dB)	-29.1203 at 2.40 GHz
Insertion Loss (dB)	-0.2683 at 2.55 GHz
Return Loss (dB)	-16.3720 at 2.20 GHz

V. CONCLUSION

A novel switch was designed and simulated by software Intellisuite 8.7v which shows a low pull-in voltage of ~ 2.5 V which is well matched with today's IC technology and the electromagnetic analysis is done by EM software which shows good S-parameters such as insertion loss of -0.2683 dB at 2.55 GHz, return loss of -16.3720 dB at 2.20 GHz and isolation loss of -29.1203 dB at 2.40 GHz. In future we can work on some issues related to bandwidth, contact resistance and on the material analysis so as to get better overall performance of the switch.

VI. REFERENCES

[1] Jau Tai Wen, "RF MEMS Switches: High-Frequency Performance and Hot-Switching Reliability", High Frequency Electronics, Vol.5 No.8 (2017).

[2] Xiaodong, Lumtao, Maohui, Cuizhuo and Zhenping, "A Compact Serial RF MEMS Switch for S-band Application", "International Conference solid state", ISBN: 0-7803-6520-8/01, (2001).

[3] Sinha, Bansal, and Rangra, "RF MEMS Compact T -Type Switch Design for Switch Matrix Applications in Space Telecommunication", IEEE-International Conference On Advances In Engineering, Science And Management (ICAESM -2012), ISBN: 978-81-909042-2-3, (2012).

[4] Angira, Sundaram, and Rangra, "A Novel Interdigitated, Inductively Tuned, Capacitive Shunt RF – MEMS Switch for X and K Bands Applications", IEEE International Conference on Nano/Micro Engineered and Molecular Systems, ISBN: 978-1-4799-4726-3/14, (2014).

[5] Ziaei, Bansropun, Martins and Baillif, "Fast High Power Capacitive RF MEMS switch for X band Application", IEEE International Conference of Electromagnetic" ISBN: 978-1-4673-7135-3/15, (2015).

[6] El massry, Medhat and Mostafa, "Novel Ultra Low Voltage Mobile Compatible RF MEMS Switch for Reconfigurable Microstrip Antenna", IEEE International Conference on Circuits and Systems, ISBN: 978-1-5090-1367-8/16, (2016).

[7] Khan and Shanmuganantham (2018), "Design and Analysis of RF MEMS cantilever switches

for Parameter Enhancement," Transaction on Electrical and Electronics Materials (TRANSEEM), (in press).

[8] Khan and Shanmuganantham, "Arc-Shaped Cantilever Beam RF MEMS Switch for Low Actuation Voltage", IEEE International Conference on Circuits and Systems", ISBN: 978-1-5090-6480-9/17, (2017).

[9] Khan and Shanmuganantham (2017), "Simulation and Analysis of RF MEMS Cantilever Switch for Low Voltage Actuation", IEEE International Conference on Circuits and Systems", ISBN: 978-1-5090-6480-9/17, (2017).

[10] Khan and Shanmuganantham (2017), " Y-Shaped cantilever beam RF MEMS switch for Lower the Actuation Voltage," International Conference on Communication, Networks and Computing (CNC-2018), (in press).

[11] Rebeiz and Muldavin (2001), "RF MEMS switches and switch circuits," *IEEE Microwave Magazine*, pp(59-71).

[12] G. Rebeiz, "*RF MEMS Theory, Design and Technology*", New Jersey, J.Wiley Sons, (2003).

Themed Section : Engineering and Technology
© 2018 IJSRSET | Volume 5 | Issue 3 | Print ISSN: 2395-1990 | Online ISSN : 2394-4099

A Study of IoMT - An Advanced Application to the Current Health Scenario

Tharanee Shree Saravanan[1]
[1]Dept. of ECE, Velammal Institute of Technology, Chennai, Tamil Nadu, India
tharaneeshree@gmail.com[1]

ABSTRACT

The present study is an attempt to highlight in detail about the pros and cons of the Internet of Medical Things, which is the most effective and efficient application of information processing involving both computer hardware and software, that deals with the storage, retrieval, sharing, and use of health care information, data, and knowledge for communication and decision making. The Internet of Medical Things (IoMT) is the collection of medical devices and applications that connect to healthcare IT systems through online computer networks. Many of the innovations resulting from IoMT provide a valuable platform for the evolution of healthcare and the provision of better, personalized treatment for more patients. However, for the initiatives to succeed, both healthcare professionals and patients must buy into the changes. IoT is not just meant for improving our lives, but it is transforming our lives in a big way. Healthcare is one of the most noble causes IoT can help and it's already doing it.

Keywords: Health Care, Medical Device Application, Tele Medicine, Medical Sensors For Diagnose, Electronic Health Record, Cyber Attacks

I. INTRODUCTION

Health care is conventionally regarded as an important determinant in promoting the general physical and mental health and well-being of people around the world. A well-functioning healthcare system requires a robust financing mechanism; a well-trained and adequately paid workforce; reliable information on which to base decisions and policies; and well maintained health facilities and logistics to deliver quality medicines and technologies. Healthcare can contribute to a significant part of a country's economy. In this world of hi-tech, such an important service need an effective and efficient application of information processing involving both computer hardware and software that deals with the storage, retrieval, sharing, and use of health care information, data, and knowledge for communication and decision making, which is popularly now known as Internet Of Medical Things (IoMT).

The Internet of Medical Things (IoMT) is the collection of medical devices and applications that connect to healthcare IT systems through online computer networks. Medical devices equipped with Wi-Fi allow the machine-to-machine communication that is the basis of IoMT. IoMT devices link to cloud platforms such as Amazon Web Services, on which captured data can be stored and analyzed. IoMT is also known as healthcare IoT.

As is the case with the larger Internet of Things (IoT), there are now more possible applications of IoMT than before because many consumer mobile

devices are built with Near Field Communication (NFC) radio frequency identification (RFID) tags that allow the devices to share information with IT systems. RFID tags can also be placed on medical equipment and supplies so that hospital staff can remain aware of the quantities they have in stock.

The practice of using IoMT devices to remotely monitor patients in their homes is also known as telemedicine. This kind of treatment spares patients from travelling to a hospital or physician's office whenever they have a medical question or change in their condition.

II. A WEARABLE MEDICAL DEVICE

The Internet of Medical Things (IoMT) is a group of wearable medical devices used to collect patient physiological data. The wearable medical devices are inter-connected with the assistance of wireless networks. Most of the medical devices are connected with the use of Wi-Fi to communicate each other. The data collected on wearable medical devices are stored on a cloud database. Now-a-days, the number of wearable medical devices generates large amounts of healthcare data, including blood pressure, heart rate, body temperature, respiratory rate, blood circulation level, body pain and blood glucose level. However, the main challenge in IoMT is how to manage with respect to critical applications, where a number of connected devices generate a large amount of medical data. This large volume of data, often called big data, cannot readily be processed by traditional data processing algorithms and applications. In general, many database clusters and additional resources are required to store big data. However, storage and retrieval are not the only problems. Obtaining meaningful patterns from big data, such as that pertaining to patient diagnostic information, is also an essential problem. Presently, a number of emerging applications are being developed for various environments. Sensors are most often used in critical applications for real-time or near future. In particular, the IoMT uses an accelerometer sensor, visual sensor, temperature sensor, carbon dioxide sensor, ECG/EEG/EMG sensor, pressure sensor, gyroscope sensor, blood oxygen saturation sensor, humidity sensor, respiration sensor and blood-pressure sensor to observe and monitor the patient's health in a continuous manner. By intelligently investigating and collecting large amounts of medical data (i.e., big data), IoMT can enhance the decision-making process and early disease diagnosis. Hence, there is a need for scalable machine learning and intelligent algorithms that lead to more interoperable solutions, and that can make effective decisions in emerging IoMT.

III. CHALLENGES TO ADOPTION

Many of the innovations resulting from IoMT provide a valuable platform for the evolution of healthcare and the provision of better, personalized treatment for more patients. However, for the initiatives to succeed, both healthcare professionals and patients must buy into the changes.

That means creating a great patient experience through simple, easy-to-use devices, and clear benefits. Doctors can play an important role in advising patients on the most suitable devices for their conditions, and providing feedback to patients to demonstrate that the devices are providing improved care.

Doctors must also increase adoption rates by recognizing the benefits IoMT can bring to their practice. IoMT suppliers must provide clear use cases that doctors can assess to review the potential for their patient group. Doctors also need to have access to an end-to-end solution that enables them to access data and insights quickly and easily and receive real-time alerts when the data indicates that action is needed.

A 2013 survey by eClinicalWorks assessed healthcare providers' interest in mobile health apps linked to electronic health records (EHRs). The results show

providers want their patient engaged, and see clear benefits in health outcomes with this connection. According to the survey, 93 percent of respondents felt a mobile health app connected to EHRs delivered value.

Ninety-three percent of respondents believed that mobile health apps can improve a patient's health outcome, and 89 percent were likely to recommend a mobile health app to a patient. Respondents felt that the top three benefits of this technology were medication adherence (65 percent), diabetes management (54 percent) and preventative care (52 percent).

IV. DRIVING A CULTURE CHANGE

In many ways, IoMT represents a culture change for both patients and doctors. But that change will only take place if both parties are confident of beneficial outcomes. And any new initiatives must overcome requirements for regulatory compliance, particularly with the Health Insurance Portability and Accountability Act (HIPAA), which protects the privacy of patients' health information.

Because IoMT promotes and enables the collection and sharing of health information by a number of different parties, doctors and healthcare providers must enforce security of data.

If IoMT can overcome these initial challenges, it could prove to be the solution to rising healthcare costs that are being driven by a rising population of people over 65, which could rise to almost 20 percent of the US population by 2030, according to Administration on Aging.

As IoMT continues to evolve, it could ultimately transform US healthcare by offering broader, more accessible, and cost-effective solutions.

V. RESOURCE MANAGEMENT

IoT solutions are now used to track the location and quantity of products as a form of automated stock control. This also has application in healthcare as hospitals use the technology to monitor stock levels of essential supplies or to locate equipment in storage or in medical wards. Administrators use RFID tags fitted to the equipment to monitor and manage it.

Using the same RFID technology, hospital administrators are now able to track patients' progress through the hospital when they are visiting for consultation or staying for operations or treatment. The information enables administrators to identify bottlenecks in the system or departments where additional resources are needed.

It can also provide patients or their families more information on ER waiting times, available dates for operations, and progress of patients in recovery. This provides a more accurate basis for planning and managing hospital resources, improving efficiency, reducing costs, and improving the patient experience.

Some hospitals are taking the process further and offering patients and their families access to doctors' notes, IoMT data and other treatment information through a secure patient portal. In addition, the same principals of shared information let patients upload data that might be useful to doctors—from their own connected devices.

VI. SUPPORTING COLLABORATION

The vast amount of data available through IoMT and the ability to share findings through the cloud support collaborative treatment. In its simplest form, doctors can share information to obtain expert opinions or treatment recommendations from a specialist.

IoMT can also form the basis for a type of crowdsourcing in healthcare. Here, professionals contribute their diagnosis or opinions on rare diseases or complex medical problems. Using a form of

scientific polling based on algorithms, the participants offer a solution that speeds diagnosis and gives patients the benefit of a wide range of expert views.

That data and its related insights are available as a knowledge base that can help specialists identify and solve complex problems in the future. Commentators note that problems of liability and payment may act as barriers to the wider adoption of this form of crowdsourcing, but the application demonstrates the potential of IoMT to deliver new kinds of healthcare.

The following are five challenges of IoT in healthcare that put it at risk of failure.

Lack of EHR system integration. While the data that is collected from IoT devices can include a patient's vital signs, physical activity or glucose levels while at home, that information does not typically travel to an EHR system and, in most cases, is not centralized or made easily available to providers. This limits the information's value since it is not always presented to the provider in a clinical context.

Some EHR systems allow patients to import data into their record, but this still remains relatively limited to a few dominant EHR players and leaves many providers uncertain of how to handle information that lives outside of their records systems.

Interoperability challenges keep IoT data in different silos. Patients are likely to collect different sets of data when using different medical devices depending on each device's purpose and, in some cases, the ordering physician. A patient with diabetes may frequently collect glucose levels and report them back to their primary care physician while also potentially capturing data related to their asthma on a separate device, which may be going to their asthma and allergy care provider. In many cases, the information that the patient captures stays within the boundaries of each of the systems and IoT vendors and is not visible to other systems. Unfortunately, with the lack of wider adoption of adequate interoperability, data from different IoT devices may remain locked in each individual system and lose its potential value to the rest of a patient's care team.

IoT data alone may not be as meaningful if it is not within the context of a full health record. Many providers support the collection of meaningful patient data between visits, but this data is only valuable if it can be incorporated and viewed within the context of a full patient chart and timeline. There are still many cases where the data collected from wearables and other medical devices stays locked in the IoT vendor repository or apps, but for a physician, that data may not provide any help unless it is visible within the context of the patient's full record.

Data security causes concerns in the implementation of IoT in healthcare. From the time that the data is collected at the device level to the point that it is transmitted over to its final destination, securing that information is critical and is required under HIPAA. But with the lack of common security standards and practices, many health IT professionals have concerns about the risks associated with IoT device tampering and data breaches.

The Food and Drug Administration (FDA) is in the process of defining a common security practice and standards for medical devices as they become more frequent in the clinical setting. Earlier in 2016, the FDA released a draft of "Postmarket Management of Cybersecurity in Medical Devices: Draft Guidance for Industry and Food and Drug Administration Staff" to outline the steps manufacturers should take to continually address cybersecurity risks with their devices to better protect public health.

Constant changes in hardware and connectivity technology. Patients today need more than one device to capture the different health data their providers need. This can require more than one sensor that, in most cases, is used alongside a hub to which information is pushed that's designed to process the information. These hubs are not always compatible with the different sensors that are

available, and having a lack of common hardware or wireless connectivity standards -- such as Wi-Fi, Bluetooth or Z-Wave -- can cause patients to have extensive hardware in their homes, which can be overwhelming and costly.

Providers are hopeful that IoT will have a positive impact on supporting patient care and delivering valuable data. IoT applications offer the opportunity for providers to have visibility to what happens between visits and can provide some insights into patient medication adherence, activity levels and vital signs. But this emerging technology is threatened by the different challenges of IoT in healthcare defined here that, if left unaddressed, can get in the way of its success. Fortunately, there is traction around addressing many of these IoT challenges, and progress continues to be made toward resolving them and toward allowing IoT technologies to have a meaningful impact on healthcare.

VII. THREATS PRESENTED BY THE IOMT

The addition of connected devices to the healthcare industry has expanded the surface area for possible attacks. Further, many healthcare institutions lack adequate security capabilities. The combination of these two factors equates to an "easy win" in the eyes of cybercriminals.

Some of the more traditional forms of cyberattacks, like phishing schemes and DDoS, are still alive and well, but healthcare IT security is now faced with combating attacks on connected medical devices in healthcare facilities, as well as home health devices. These devices have, for the most part, not been designed with security as a top-of-mind concern, as developers are primarily focused on functionality and ease of use.

As a result, attackers are not only exploiting inadequate IT security to gain unfettered access to networks and data, but actual control of IP-enabled medical devices themselves. Vulnerable systems, valuable data and a wide-open surface are putting the industry in the attack spotlight and, as a result, have medical IT teams on edge.

[1]

VIII. DEFENDING AGAINST ATTACKS

With what we now know about the IoMT, it should come as no surprise that security budgets to defend against threats have been growing. "Gartner believes that the average security budget for IT, operational technology (OT) and IoT security requirements will respond to the growth of IoT devices across all business segments and scenarios, rising from less than one percent of annual security budgets in 2015 to 20 percent in 2020."

There are a number of different features healthcare IT professionals should look for when evaluating a security vendor's solutions and capabilities.

One critical consideration is that a vendor be able to provide internal segmentation firewalls (ISFWs) to defend against breaches, as the landscape of networks is typically wide open and flat. Because ISFWs operate inside the network instead of at the edge, they allow healthcare organizations to intelligently segment networks between patients, administrators, healthcare professionals and guests, as well as between types of devices – for example, between a patient information system and a life-saving heart monitor or infusion pump.

It can then prioritize interconnected medical devices that need the highest degrees of protection and monitoring, and inspect and monitor all traffic moving between segments, all without impacting performance.

A healthcare security vendor should also have a team in place that's dedicated to uncovering the latest threat intelligence, so real-time threat and mitigation updates can be made expeditiously, before cybercriminals take advantage of any weaknesses in connected IoT devices or the critical services they provide.

IX. FEW EXAMPLES FOR IoMT

1. OpenAPS - closed-loop insulin delivery

One of the most fascinating areas in IoT medicine is the open source initiative OpenAPS, which stands for open artificial pancreas system.

Dana Lewis and her husband Scott Leibrand have hacked Dana's CGM (continuous glucose monitor) and her insulin pump. Using the data feed from the CGM and a Raspberry Pi computer, their own software completes the loop and continuously alters the amount of insulin Dana's pump delivers. As of summer 2016, when Dana presented at OSCon in Austin, 59 people were using the open source software and hacking their own equipment.

This example shows how patients have been waiting for years for improved technology which the healthcare industry has not delivered.

Security concerns and lengthy development and testing periods mean that connected devices have taken some time to come to market.

Dana Lewis told e-patients.net that, in the view of OpenAPS, "the relative net risk of this [loop] feature is far outweighed by the net benefit of providing users the ability to control their own devices, as discussed here."
Reading the FAQs on the OpenAPS website gives an interesting insight into some of the issues in this part of the healthcare market.

2. **Pharma** is following, though, and developing its own connected systems to help diabetes sufferers. In 2016, Roche acquired distribution rights to an implantable long-term continuous glucose monitoring (CGM) system which uses a 90 day sensor below the patient's skin.

The sensor communicates with a smart transmitter which then sends blood glucose levels to a sister mobile app on the patient's phone.

3. Activity trackers during cancer treatment

The Memorial Sloan Kettering Cancer Center (MSK) and cloud research firm Medidata are testing the use of activity trackers to gather lifestyle data on patients being treated for multiple myeloma.
Patients will wear an activity tracker for up to a week prior to treatment and then continuously for several months over the course of multiple treatments.

The trackers will assist in logging activity level and fatigue, with appetite also being logged directly, and all data saved to Medidata's Patient Cloud ePRO app on their personal smart phones.

Using a variety of data gathered day-to-day through wearables or apps is a fairly obvious way that diagnosis and treatment can be improved for many conditions.

This is particularly the case for a disease such as cancer, for which the reaction to therapy plays an important and determinant part in prescribing the right treatment.

4. Connected inhalers

The most immediate use for IoT technology in healthcare is not to assist in diagnoses, though, but to ensure adherence. Adding sensors to medicines or delivery mechanisms allows doctors to keep accurate track of whether patients are sticking to their treatment plan.

This provides motivation but also clarity for patients. Devices connected to mobile apps allow for patients to receive reminders, as well as to check on their own adherence.

Novartis is undertaking connected inhaler research with both Qualcomm and Propeller Health, developing inhalers for chronic obstructive pulmonary disease (COPD).

Propeller's Breezhaler device connects to its digital platform via a sensor, passively recording and transmitting usage data. Novartis' own device will likely not be released until 2019, though, showing the timescales involved in this sort of research.

5. Ingestible sensors

Proteus Digital Health and its ingestible sensors are another example of digital medicine.

Again, the chief purpose of this technology, trialled with an antipsychotic and a hypertension pill, is to monitor adherence. However, in this case, the pill dissolves in the stomach and produces a small signal which is picked up by a sensor worn on the body, which again relays the data to a smartphone app.

According to a study by the World Health Organisation in 2003, 50% of medicines are not taken as directed. Proteus' system is one effort to reduce this figure.

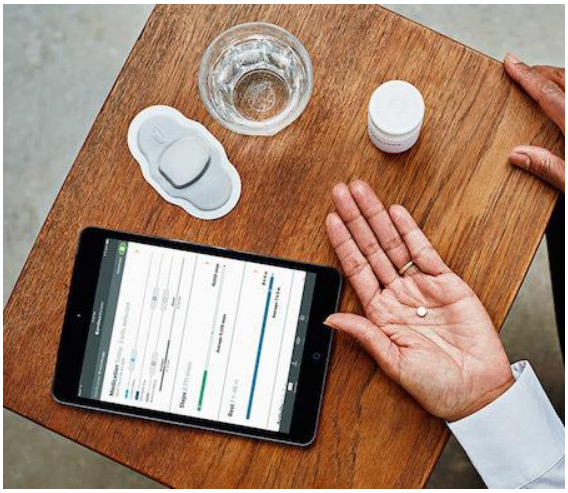

X. CONCLUSION

IoT is not just meant for improving our lives, but it is transforming our lives in a big way. Healthcare is on of the most noble causes IoT can help and it's already doing it. With the emergence of IoT (Internet of Things) and devices, the healthcare industry will benefit from seamless connectivity, improved data and information between healthcare professionals and patients.

IoT is changing healthcare in many different areas including equipment supplies, patient care and monitoring, drug delivery and management, remote surgeries and connectivity of doctors with patients. Healthcare applications are proving to be life changing not just fro primary treatments but also for patients with terminal illness. Experts believe that this is just the beginning, there are more applications which are ready to disrupt the future of healthcare.

Today's healthcare institutions should continue looking for new ways to improve the patient experience and save lives, without having to worry about dangerous cybercriminals breaching their systems. Which means that security should never be neglected during implementation or forgotten about after new devices have been activated.

Today's cybercriminals are smarter and more determined than ever, and the healthcare industry needs to be aware of the trends, capabilities and

possible avenues of attack that they are looking to exploit.

The next decade may well see a revolution in treatment and diagnosis of disease, as the Internet of Things (IoT) is brought to bear on medicine.

XI. REFERENCES

[1] "What is IoMT", http:/internet of things agenda. techtarget.com

[2] "How the IoMT is transforming Health Care", The VoIP Report, thevoipreport.com, August 31st ,2017

[3] "Emerging applications of Internet of Medical things", http:/www.journals.elsevier.com

Themed Section : Engineering and Technology
© 2018 IJSRSET | Volume 5 | Issue 3 | Print ISSN: 2395-1990 | Online ISSN: 2394-4099

Image Segmentation and Bias Correction by Using Maximum Likelihood Algorithm

Dr. P. D. Sathya[1], M.Thenmozhi[2]
[1]Assistant Professor, Annamalai University, Tamil Nadu, India
[2]ME-Communication Systems, Annamalai University, Tamil Nadu, India

ABSTRACT

This paper presents a novel optimization approach for de-noising and bias correction of MR image with intensity in-homogeneity. Intensity of inhomogeneous objects to be Gaussian distributed with different means and variances are modeled, and then a sliding window is introduced to map the original image intensity onto another domain, where the intensity distribution of each object is still Gaussian but can be better separated. The means of the Gaussian distributions in the transformed domain can be adaptively estimated by multiplying the bias field with a piecewise constant signal within the sliding window. A maximum likelihood energy functional is then defined on each of the local regional, which combines the bias field, the membership function of the object region, and the constant approximating the true signal from its corresponding object. The energy functional is then extended to the whole image domain by the Bayesian learning approach. Furthermore, the smoothness of the obtained optimal bias field is ensured by normalized convolutions without extra cost. Experiments on the real image demonstrate the superiority of the proposed algorithm to other state-of-the-art representative methods.

Keywords: Intensity in Homogeneity, Bias Correction, Brain Segmentation, Bias Field Estimation

I. INTRODUCTION

Intensity in homogeneity caused by imperfection of imaging devices and subject-induced susceptibility effects can lead to serious misclassifications by intensity-based segmentation algorithms. Medical image acquisition devices and protocols that have hugely evolved over the last decades provide a vast amount of data out of which the information essential for diagnosis, therapy planning and execution, and monitoring the progress of disease or results of treatment has to be extracted. Preprocessing step is required automatically extracting clinical useful information usually requires a preprocessing step by which various image artifacts, which may degrade the results of subsequent image analysis algorithms, are removed. Method that deal with aof preprocessing with spurious smoothly varying image intensities, i.e., with the phenomenon that is usually referred to as intensity in homogeneity, intensity non uniformity, shading or bias field. This process of images obtained by different imaging modalities, such as microscopy, computed tomography, ultrasound, and above all by magnetic resonance imaging (MRI). It manifests itself as a smooth intensity variation across the image (Fig1). Because of this phenomenon, the intensity of the same tissue varies with the location of the tissue within the image. Usually intensity in homogeneity is hardly noticeable to a human observer, many medical image analysis methods, such as segmentation and registration, are highly sensitive to the spurious variations of image intensities. This is why a huge methods for intensity in homogeneity correction of magnetic resonance (MR) images have been proposed in the past.

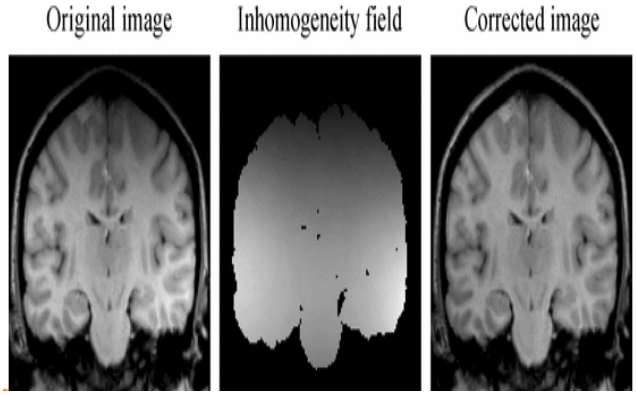

Figure 1. Intensity in homogeneity in MRI brain image

Intensity In homogeneity: Smooth spatially varying function that alters image intensities that otherwise would be constant for the same tissue type regardless of its position in an image It is the most easy form, the method assumes that intensity in homogeneity is perform multiplicative or additive, i.e., the intensity in homogeneity field multiplies or adds to the image intensities. Most frequently, the multiplicative model has been used as it is consistent with the inhomogeneous sensitivity of the reception coil. Due to induced currents in homogeneities for modeled as non uniform excitation, the multiplicative model is less appropriate. In addition to intensity in homogeneity, the MR image formation model should incorporate high-frequency noise. This noise is known to have a Rician distribution. However, as long as the signal-to-noise ratio (SNR) is not too low, noise can be approximated by a quasi-Gaussian distribution. This approximation is appropriate for image areas corresponding to tissues but not for no-signal areas, such as air.

Classification of correction methods: Intensity in homogeneity correction number of methods have been proposed in the last two decades. In the following, we propose a classification scheme, accordingly classify correction methods, and discuss the advantages and disadvantages of different correction strategies. From the very beginning, two main approaches have been applied to minimize the intensity in homogeneity in MR images, namely the prospective and retrospective approach. The first aims at calibration and improvement of the image acquisition process, while the latter relies exclusively on the information of the acquired image and sometimes also on some *a priori* knowledge. Based on the classification proposed below, we have further divided into the prospective methods into those that are based on phantoms, multi-coils, and special sequences. The retrospective methods are further classified into filtering, surface fitting, segmentation, and histogram based.

Prospective

- Phantom
- Multi-coil
- Special sequences

Reprospective

- Filtering
- Homomorphic
- Homomorphic unsharp masking
- Surface fitting
- Intensity
- Gradient
- Segmentation
- ML, MAP
- Fuzzy c-means
- Nonparametric
- Histogram
- High frequency maximization
- Information minimization
- Histogram matching

A. Prospective Methods

Phantom Based: An estimate of the intensity in homogeneity field can be obtained by acquiring an image of a uniform phantom with known physical properties and by scaling and smoothing of the

acquired phantom image or water is usually used for phantoms and median filtering is applied for image smoothing. The phantom based method, which is a major drawback of this approach because it cannot correct for patient-induced in homogeneity. The remaining intensity in homogeneity can be as high as 30%. Another limitation of this approach is the temporal and spatial variation of the coil profile that calls for frequent acquisitions of the phantom image. To reduce the number of phantom acquisitions, the authors in proposed to carefully record the orientation and position of the phantom and the coils to be able to geometrically transform the estimated in homogeneity field to any acquired image. Attempts have been made to first mathematically model the in homogeneity field by polynomials, curves [or by integration based on the Biot Savart law, and then fit the obtained model to the phantom image. A method that minimizes the dependency of the in homogeneity field on the scanner and object has been proposed , deriving a mathematical model from the equation for T1 signal generation and using a phantom image, flip angle mapping, and reference objects. However, the usefulness of this method is limited by the specific imaging conditions and sensitivity to input parameters.

Multi-coil: There are two types of coils, surface and volume are most frequently used in MRI. Surface coils usually have good SNR but induce severe intensity in homogeneity, while volume coils exhibit less in homogeneity but have poor SNR. The intensity in homogeneity field is obtained by dividing the filtered surface coil image with the body coil image and smoothing the resulting image. The main disadvantage of these methods is the prolonged acquisition time. The final in homogeneity field was modeled by a spline surface that had been fitted to a set of in homogeneity field estimates. This method could also handle multispectral images (T1, T2) if acquired by the same coils. In general, the usability of the multi-coil methods is limited by prolonged acquisition times, special coil settings, and incomplete in homogeneity correction.

Special Sequences: This group of techniques is predominantly related to specific acquisition (hardware) designs and is thus only briefly described. For certain pulse sequences, the spatial distribution of the flip angle can be estimated and used to calculate the intensity in homogeneity. The mathematical model behind this approach requires the acquisition of two images, the second one with doubled nominal flip angle of the first. Other techniques, such as sensitivity encoding by multiple receiver coils, also reduce the in homogeneity artifact but they were mainly developed to speed up the scanning process. In, echo planar imaging (EPI) phased modulation maps were estimated to remove the in homogeneity field in the original image. Another method, proposed for the in homogeneity field minimization of 4.7T images, modified certain pulses in the modified driven equilibrium Fourier transform (MDEFT) imaging. Besides, for MRI contrasts, such as diffusion weighting, magnetization transfer ratios, two point quantitative T1, and two point quantitative T2, in which the final image is a ratio, most of the multiplicative intensity in homogeneity is cancelled and the images are relatively homogeneous. This is because the sensitivity variation of the receive coil remains unchanged even if the sequence parameters are varied.

B. Retrospective Methods

Retrospective methods are relatively general as only a few assumptions about the acquisition process are usually made. These methods mainly rely on the information of the acquired images in which useful anatomical information and information on the intensity in homogeneity are integrated. *A* intensity probability distribution of the imaged anatomy is mostly used by some methods to facilitate extraction of information on intensity in homogeneity. In contrast to the prospective methods, which can correct only the intensity in homogeneity induced by

an MR scanner, retrospective methods can also remove patient dependant in homogeneity.

Filtering Methods: Assume filtering methods that can be separated from the high-frequency signal of the imaged anatomical structures by low-pass filtering. However, this assumption is valid only if the imaged anatomical structures are relatively small and thus contain no low frequencies that might be mistakenly removed by low-pass filtering. For most of the anatomical structures imaged by MR this assumption does not hold, which results in overlap of anatomy and in homogeneity frequency spectra. This limits the feasibility of filtering methods. Besides, high image contrasts generate filtering artifacts known as edge effects, manifesting themselves as a distortion of homogeneous tissues near the edges. The strongest edges that are usually at the object/background transitions can be removed by either masking out the background, replacing background pixels by average intensity values or by extrapolating tissue intensities over the background. Nevertheless, substantial intensity in homogeneity usually remains in an image after correction by these methods. Two main filtering approaches, Homomorphic filtering and Holomorphic un-sharp masking (HUM), have been proposed. Morphological filtering and simple high-pass filtering also belong to this group of methods but, in contrast to some successful applications to microscopic images, they have not been found useful for MRI.

Surface Fitting Methods: These methods fit a parametric surface to a set of image features that contain information on intensity in homogeneity. The resulting surface, which is usually polynomial or spline based, represents the multiplicative in homogeneity field that is used to correct the input image. Based on the image features used for surface fitting, this methods are further sorted into intensity and gradient based methods.

Intensity Based: A parametric surface in the form of thin plate splines was least squares fitted to intensities of a set of pixels, which were assumed to belong to the same tissue and were distributed over the entire image. Manual selection of pixels corresponding to a dominant tissue and automatic selection, which was based on neural network classification, were investigated. Although subjective and time-consuming, manual selection was shown to give better results. In, an automated iterative method was proposed, incorporating segmentation of homogeneous areas of the major tissue, followed by fitting a second order polynomial to intensities of the segmented tissue. Gaussian main tissue model, was applied to estimate the in homogeneity fields and merge several surface coil (phased array) images. The major drawback of these methods is that the in homogeneity field is estimated only from intensities of one major tissue and then blindly extrapolated over the whole image. A combination of *B*-spline surface fitting and a histogram based method was proposed in.

Gradient Based: The main assumption behind these methods is that sufficiently large homogeneous areas are evenly distributed over the entire image so that local gradients of intensity in homogeneity can be estimated by local averaging of image intensity gradients. In, a polynomial surface was least squares fitted to underlying normalized intensities of homogeneous areas. Tissue independent segmentation was used to obtain the homogeneous areas. Because these were rather sparsely distributed over the entire volume, not all image information was used to estimate the in homogeneity correction field. By a similar approach, a finite element surface model was fitted by minimizing the difference between derivatives of homogeneous areas and the corresponding surface model. Instead of surface fitting, some methods obtain the in homogeneity field by integrating derivatives estimated inside homogeneous areas. Simple polynomial models were used to extrapolate the gradients outside the homogeneous areas. The major drawback of these methods is that some adverse image information may be integrated. These methods are successful only if

homogeneous image areas are large and distinctive, such as the white matter in brain images.

Segmentation Based Methods: On the other hand, correct segmentation makes intensity in homogeneity correction rather trivial. Intensity in homogeneity correction and segmentation can thus be viewed upon as two intertwined procedures. In intensity in homogeneity correction methods segmentation based these two procedures are merged so that they benefit from each other, simultaneously yielding better segmentation and in homogeneity correction. These intensity in homogeneity correction methods are further classified according to the image segmentation method utilized.

ML, MAP Based: The maximum-likelihood (ML) or the maximum *a posteriori* probability (MAP) criterion may be used to estimate the image intensity probability distribution by parametric models. Finite mixture and more frequently finite Gaussian mixture models are used and modified to incorporate intensity in homogeneity. The models' parameters can be estimated by the expectation-maximization (EM) algorithm, iterating between classification and intensity in homogeneity correction. An additional class, named "other," which had a uniform intensity probability distribution was introduced in to model the intensities not belonging to any of the main tissues. Another similar approach uses additional mixed tissue classes to model the partial volume effect and background by Rayleigh distribution. Because the Gaussian model is only an approximation of a single tissue probability density, several Gaussians can be used per one main tissue, for example, 3 for white matter and 2 for grey matter in the brain, and much more for minor, less significant tissues. A unique approach, first published in and refined later, upgraded the EM iterative scheme by adding a special step in which the resulting in homogeneity field was scaled to minimize a new criterion, namely, the classification error rate (CER). In this way, the whole algorithm was primarily guided by the results that would be produced by a coarse segmentation. The criterion of minimum image entropy was used in to estimate the in homogeneity field, while the classical EM procedure was implemented to optimize ML in search for model parameters. To deal with the high number of searched parameters, e.g. classification and in homogeneity correction steps, or to speed up the algorithm, optimization schemes such as generalized EM (GEM) , iterative conditional modes (ICM) or expectation conditional minimization (ECM) have been proposed.

One of the main requirements of the EM based approaches is the initialization of explicitly modeled classes and spatial distribution of tissues. Initialization can be obtained by manual selection of representative points for each class, which is subjective and irreproducible. A self-adaptive vector quantization and tree-structure -means classification were implemented to estimate the initial class means, standard deviations or brain mask. Other automatic approaches used a statistical probability atlas, initially registered to the processed image, to estimate the required parameters.

Model of intensity probability do not exploit the information about spatial connectedness of neighboring pixels belonging to the same class, (hidden) Markov random fields [(H) MRF] were frequently incorporated. This resulted in improved segmentation, which was less sensitive to noise and had smoother tissue borders. Even though, to reduce over smoothing of tissue borders, spatial connectedness should not be too strong. The suggestion of authors to limit HMRF smoothing by penalizing only the neighboring intensity combinations that were implausible due to the specific topology of the imaged object.

The proposed framework, interleaving segmentation, registration and intensity in homogeneity correction to improve tissue segmentation. FGM (finite Gaussian mixture) was used as a probability model with intensity in homogeneity dependant class means. The registration step in was performed by deforming the tissue

probability maps. The ICM scheme estimated different groups of parameters, using EM to find the mixture-classification parameters and Levenberg–Marquardt optimization for in homogeneity field and registration steps. This method of algorithm, although rather tedious and time-consuming, seems promising due to the integration of segmentation, registration and intensity in homogeneity correction, which had been treated separately in the past.

Fuzzy C-Means: These methods use the standard fuzzy *c*-means (FCM) segmentation and modify the objective function to adapt to intensity in homogeneity. The main property of FCM methods is the soft classification model, which assumes that image voxels belong to more than one class. This is consistent with the partial volume effect observed in MR images and thus eliminates the explicit modeling of mixed classes, which is required by the abovementioned FGM models. The authors in proposed an adaptive fuzzy *c*-means method, which multiplies the class centroid values by a function of location, estimating the intensity in homogeneity. By using a spatial regularization terms, penalizing first and second derivatives of the in homogeneity field, were added to the objective function to preserve its smoothness. Because the weights of these regularization terms are difficult to set, they have to be tuned manually. An automatic procedure based on histogram mode searching was used to set the initial values of class centroids, while the objective function was minimized by the Jacobi iterative scheme applied on a multi-grid algorithm to speed up the process. The method was later generalized to 3-D multispectral images and accelerated by the same authors. In and refined later in, spatial information was incorporated by adding a spatial regularization term that enabled the class membership of a voxel to be influenced by its neighbors. This approach proved tolerant to salt and pepper noise, resulting in smoother segmentation. By tuning repeatedly a regularization parameter determining the smoothness of segmentation and, implicitly, also the in homogeneity field. Another approach was proposed in where the in homogeneity field was modeled by a *B*-spline surface, while the spatial voxel connectivity was implemented by a dissimilarity index, which enforced the connectivity constraint only in the homogeneous areas. In this way the tissue boundaries were better preserved. Yet another method that performed local fuzzy *c*-means classification and thereby completely avoided the need for modeling the intensity in homogeneity function was presented in.

Nonparametric: Nonparametric segmentation based in homogeneity correction methods were proposed in and, using nonparametric max shift or mean shift clustering. The methods did not require any *a priori* knowledge on the intensity probability distribution, e.g., tissue class means and variances, but blindly classified the voxels according to the main modes of the feature space that combined voxel intensities and corresponding second derivatives. The latter were incorporated to exploit the spatial voxel connectivity, i.e., to incorporate spatial information into classification. In homogeneity correction by a parametric polynomial model is based on iterative minimization of class square error, i.e., within class scatter, of the intensity distribution that is due to intensity in homogeneity.

Histogram Based Methods: The method of histogram based on operate directly on image intensity histograms and need little or no initialization and/or *a priori* knowledge on the intensity probability distribution of the imaged structures. This makes these methods fully automatic and highly general so that they can usually be applied to various images with or without pathology. A numerous segmentation based methods also operate on image intensity histograms, the distinction between the segmentation based and histogram based methods is that the latter provide no segmentation results.

High-Frequency Maximization: A well-known intensity in homogeneity is a well-known correction method, known as the N3 (nonparametric non

uniformity normalization), was proposed in. The method is iterative and seeks the smooth multiplicative field that maximizes the high frequency content of the distribution of tissue intensity. The method is fully automatic, requires no *a priori* knowledge and can be applied to almost any MR image. Interestingly, no improvements have been suggested for this highly popular and successful method.

Information Minimization: These methods are based on the assumption that intensity in homogeneity corruption introduces additional information to the in homogeneity-free image. The removal of intensity in homogeneity is, therefore, based on constrained minimization of image information, which is estimated by image entropy. Image entropy can be computed from the original intensity distributions or from the log-transformed distributions. In the first case, multiplicative correction model has to be constrained so as to avoid uniform scaling of image intensities (contrast changing), which would otherwise result in completely uniform image with no anatomical information.By the use of other method, in log-transformed intensity domain, the multiplicative correction model becomes additive and thereby requires no scaling constraints. However, numerical computation of entropy becomes far more difficult due to the nonlinear log-transformation of image intensities and associated problems with histogram binning. Nevertheless, the information minimization methods can be widely applied to different types of MR images because they use solely the information that is present in an image, without making assumptions on spatial and intensity distributions.

An information minimization based intensity in homogeneity correction method was first considered in 1995. Refined applications on microscopic and MR images followed in year 2000 and latter. The method in utilized fast annealing to minimize a three part energy function, consisting of image entropy, field smoothness constraint and a mean preserving regularization term. In, image correction was performed by a linear model consisting of multiplicative and additive components, which were modeled by a combination of smoothly varying basis functions that were constrained to preserve the global intensity statistics. An interesting attempt to extent the information minimization method was proposed in, optimizing the first-order conditional entropy. Inter-volume in homogeneity correction, removing only the differences between two in fields to allow inter-volume comparisons, was solved by minimization of joint volume entropy. Proposed an iterative correction strategy in which intensity in homogeneity correction forces, reducing the global entropy of the feature space, were estimated for each voxel. Besides intensities, spatial information in the form of second order derivatives was incorporated in the feature space. This method was further extended in with the aim to integrate spatial and intensity information from multispectral MR images, i.e., from T1, T2, and proton density (PD) weighted images. The advantage of this method was its ability to incorporate complementary information of the multispectral images and their derived features for better in homogeneity correction.

Integration of complimentary information from multispectral images requires that images are well registered, which is usually the case for multispectral MR images. In general, however, integration of multispectral images, e.g., computed tomography (CT) and MR images, requires multimodal image registration, which is also often solved efficiently in information theoretic framework, e.g., by maximizing mutual information. Therefore, the problem of registration and in homogeneity correction, one concerned with transforming an image in spatial domain to achieve spatial correspondence and the other concerned with transforming an image in intensity domain to restore intensity homogeneity, may both be solved simultaneously in an information theoretic framework. For example, by transforming a reference image, both in the spatial domain and in the intensity domain, such that mutual information of the reference and target images is maximized will bring the two images, being mono-modal or multimodal, in

spatial and in intensity correspondence. This suggests that simultaneous information theoretic registration and in homogeneity correction are well worth further exploration.

Histogram Matching: The image is divided into a small sub-volumes in proposed histogram matching method which intensity in homogeneity was supposed to be relatively constant. Local intensity in homogeneity was estimated by least square fitting of the intensity histogram model to the actual histogram of a sub-volume. The model of histogram was a finite Gaussian mixture with seven parameters, initialized from the global histogram of the image. No segmentation was required as only intensity in homogeneity estimation was needed for each sub-volume. These local estimates were then tested for outliers and interpolated by a *B*-spline surface to produce the final in homogeneity field. Another method found the Legendre polynomial in homogeneity model by nonlinear optimization based on a special valley function, which was shaped by the *a priori* given mean intensities and standard deviations of the main tissue classes. As histogram matching methods require several input parameters and a tissue model, they are far less general as, for example, the information minimization methods.

Other Methods: Three methods that cannot be easily classified into any of the above categories are briefly described. By the registration based method proposed in, an image undergoing intensity in homogeneity correction was registered to a reference image. Normalized mutual information and a *B*-spline deformation model were used to perform multi-scale rigid and non rigid registrations. The in homogeneity field was extracted by smoothing and dividing the two registered images. The major drawback of this approach is the requirement for an application-specific reference image. The second method relies on singularity function analysis. The main idea behind this method was to correct an image in such a way that its high frequency spectrum remained unchanged while the intensity in homogeneity corrupted low frequency part was removed and later reconstructed by a model that enforced piecewise intensity constancy in the image domain. The algorithm works on one dimensional image profiles, alternating between columns and rows. The final in homogeneity field is obtained by smoothing the quotient of the original and the reconstructed image. The method requires no *a priori* knowledge or background removal but may be sensitive to a number of input parameters. The third method combines a set of techniques for embedding the physics of the imaging process that generates a class of MR images into segmentation or registration algorithm.

This project presents a novel vibration approach to simultaneous bias correction and segmentation. By exploiting local image redundant information, we define a mapping from original image domain to another domain so that the intensity probability model is more robust to noise. We then define an ML energy functional based on the intensity distributions in each local region in the transformed domain, which combines the bias field, the membership function of each object region, and the constant approximating the true signal from its corresponding object. Finally, the ML energy functional is extended to the whole image domain, which we call the criterion of maximum likelihood in transformed domain (MLTD). The MLTD criterion achieves a global minimum with respect to each of its variables. Moreover, analysis of the MLTD criterion shows that it is a soft classification model, which assumes that each pixel intensity belongs to more than one class, while the hard classification assigns the intensity of each pixel to only one class. Therefore, the MLTD criterion obtains a better corrected bias field.

II. LITERATURE REVIEW

By utilizing the Bayesian rule, we design a nonlinear adaptive velocity and a probability-weighted stopping force to implement a robust segmentation for objects with weak boundaries. The proposed method is featured by the following three properties:

- It automatically determines the curve to shrink or expand by utilizing the Bayesian rule to involve the regional features of images.
- It drives the curve evolve with an appropriate speed to avoid the leakage at weak boundaries.
- It reduces the influence of false boundaries, i.e., edges far away from objects of interest.

[1] A. Anderson *et al.*described a new energy minimization method for simultaneous tissue classification and bias field estimation of magnetic resonance (MR) images. We first derive an important characteristic of local image intensities--the intensities of different tissues within a neighborhood form separable clusters, and the center of each cluster can be well approximated by the product of the bias within the neighborhood and a tissue-dependent constant. We then introduce a coherent local intensity clustering (CLIC) criterion function as a metric to evaluate tissue classification and bias field estimation. An integration of this metric defines an energy on a bias field, membership functions of the tissues, and the parameters that approximate the true signal from the corresponding tissues. Thus, tissue classification and bias field estimation are simultaneously achieved by minimizing this energy. The smoothness of the derived optimal bias field is ensured by the spatially coherent nature of the CLIC criterion function. As a result, no extra effort is needed to smooth the bias field in our method. Moreover, the proposed algorithm is robust to the choice of initial conditions, thereby allowing fully automatic applications. Our algorithm has been applied to high field and ultra high field MR images with promising results.

[2] L. Wang *et al.* described a new energy minimization framework for simultaneous estimation of the bias field and segmentation of tissues for magnetic resonance images. The bias field is modeled as a linear combination of a set of basis functions, and thereby parameterized by the coefficients of the basis functions. We define an energy that depends on the coefficients of the basis functions, the membership functions of the tissues in the image, and the constants approximating the true signal from the corresponding tissues. This energy is convex in each of its variables. Bias field estimation and image segmentation are simultaneously achieved as the result of minimizing this energy. We provide an efficient iterative algorithm for energy minimization, which converges to the optimal solution at a fast rate. A salient advantage of our method is that its result is independent of initialization, which allows robust and fully automated application. The proposed method has been successfully applied to 3-Tesla MR images with desirable results. Comparisons with other approaches demonstrate the superior performance of this algorithm.

[3] B. Wang *et al.* presented a novel level set method (LSM) for image segmentation. By utilizing the Bayesian rule, we design a nonlinear adaptive velocity and a probability-weighted stopping force to implement a robust segmentation for objects with weak boundaries. The proposed method is featured by the following three properties: 1) it automatically determines the curve to shrink or expand by utilizing the Bayesian rule to involve the regional features of images; 2) it drives the curve evolve with an appropriate speed to avoid the leakage at weak boundaries; and 3) it reduces the influence of false boundaries, i.e., edges far away from objects of interest. We applied the proposed segmentation method to artificial images, medical images and the BSD-300 image dataset for qualitative and quantitative evaluations. The comparison results show the proposed method performs competitively, compared with the LSM and its representative variants.

[4]X. Gao*et al.* presented a new image segmentation method that applies an edge-based level set method in a relay fashion. The proposed method segments an image in a series of nested subregions that are automatically created by shrinking the stabilized

curves in their previous subregions. The final result is obtained by combining all boundaries detected in these subregions. The proposed method has the following three advantages: 1) It can be automatically executed without human-computer interactions; 2) it applies the edge-based level set method with relay fashion to detect all boundaries; and 3) it automatically obtains a full segmentation without specifying the number of relays in advance. The comparison experiments illustrate that the proposed method performs better than the representative level set methods, and it can obtain similar or better results compared with other popular segmentation algorithms.

[5] **U. Vovk *et al.*** presented a medical image acquisition devices provide a vast amount of anatomical and functional information, which facilitate and improve diagnosis and patient treatment, especially when supported by modern quantitative image analysis methods. However, modality specific image artifacts, such as the phenomena of intensity in homogeneity in magnetic resonance images (MRI), are still prominent and can adversely affect quantitative image analysis. In this paper, numerous methods that have been developed to reduce or eliminate intensity in homogeneities in MRI are reviewed. First, the methods are classified according to the in homogeneity correction strategy. Next, different qualitative and quantitative evaluation approaches are reviewed. Third, 60 relevant publications are categorized according to several features and analyzed so as to reveal major trends, popularity, evaluation strategies and applications. Finally, key evaluation issues and future development of the in homogeneity correction field, supported by the results of the analysis, are discussed.

[6] **E. McVeigh *et al.*** described *a* receiver coil response is a major cause of no uniformities in magnetic resonance images. The spatial dependence of the sensitivity and phase of single-saddle receiver coils has been investigated quantitatively by calculating the $\mathbf{H}_1$ field and comparing the results with measurements of a uniform phantom. Agreement between the measurements and calculations is excellent. A method is developed which corrects for both the non-uniform sensitivity and the phase shifts introduced by receiver coils.

[7] **A. Simmons *et al.*** described a number of sources of non-uniformity for spin echo images at 1.5 T. Both coil tuning and crosstalk can have significant effects on image non- uniformity. For short repetition times, non-uniformity increases with decreasing TR, possibly due to gradient eddy currents. In sections of RF coils with poor RF uniformity, image non-uniformity varies with both echo time and the number of echoes in a multi-echo sequence. For the particular imager used, there are small differences between transverse and sagittal/coronal non-uniformity. The temporal stability of image non-uniformity is very good. The use of uniform oil phantoms is shown to be superior to low pass filtered images for correction of image non-uniformity.

[8] **A. Fan *et al.*** We propose a novel bias correction method for magnetic resonance (MR) imaging that uses complementary body coil and surface coil images. The former are spatially homogeneous but have low signal intensity; the latter provide excellent signal response but have large bias fields. We present a variation framework where we optimize energy functional to estimate the bias field and the underlying image using both observed images. The energy functional contains smoothness-enforcing regularization for both the image and the bias field. We present extensions of our basic framework to a variety of imaging protocols. We solve the optimization problem using a computationally efficient numerical algorithm based on coordinate descent, preconditioned conjugate gradient, half-quadratic regularization, and multi-grid techniques. We show qualitative and quantitative results demonstrating the effectiveness of the proposed method in producing de-biased and de-noised MR images.

[9] **M. Ahmed *et al.*** We present a novel algorithm for fuzzy segmentation of magnetic resonance imaging (MRI) data and estimation of intensity in homogeneities using fuzzy logic. MRI intensity in homogeneities can be attributed to imperfections in the radio-frequency coils or to problems associated with the acquisition sequences. The result is a slowly varying shading artifact over the image that can produce errors with conventional intensity-based classification. Our algorithm is formulated by modifying the objective function of the standard fuzzy c-means (FCM) algorithm to compensate for such in homogeneities and to allow the labeling of a pixel (voxel) to be influenced by the labels in its immediate neighborhood. The neighborhood effect acts as a regularization and biases the solution toward piecewise-homogeneous labeling. Such regularization is useful in segmenting scans corrupted by salt and pepper noise. Experimental results on both synthetic images and MR data are given to demonstrate the effectiveness and efficiency of the proposed algorithm.

[10] **B. Brinkmann *et al.*** presented a grayscale in homogeneities in magnetic resonance (MR) images confound quantitative analysis of these images. Homomorphic un-sharp masking and its variations have been commonly used as a post-processing method to remove in homogeneities in MR images However, little data is available in the literature assessing the relative effectiveness of these algorithms to remove in homogeneities, or describing how these algorithms can affect image data. In this study, the author address these questions quantitatively using simulated images with artificially constructed and empirically measured bias fields. The authors' results show that mean-based filtering is consistently more effective than median-based algorithms for removing in homogeneities in MR images, and that artifacts are frequently introduced into images at the most commonly used window sizes. The authors' results demonstrate dramatic improvement in the effectiveness of the algorithms with significantly larger windows than are commonly used.

[11] **P. Vemuri*et al.*** presented *a* magnetic resonance (MR) images can be acquired by multiple receiver coil systems to improve signal-to-noise ratio (SNR) and to decrease acquisition time. The optimal SNR images can be reconstructed from the coil data when the coil sensitivities are known. In typical MR imaging studies, the information about coil sensitivity profiles is not available. In such cases the sum-of-squares (SOS) reconstruction algorithm is usually applied. The intensity of the SOS reconstructed image is modulated by a spatially variable function due to the non-uniformity of coil sensitivities. Additionally, the SOS images also have sub-optimal SNR and bias in image intensity. All these effects might introduce errors when quantitative analysis and/or tissue segmentation are performed on the SOS reconstructed images. In this paper, we present an iterative algorithm for coil sensitivity estimation and demonstrate its applicability for optimal SNR reconstruction and intensity in homogeneity correction in phased array MR imaging.

[12] **R. Guillemaud *et al.*** proposed a modification of Wells et al. (ibid., vol. 15, no. 4, p. 429-42, 1996) technique for bias field estimation and segmentation of magnetic resonance (MR) images. They show that replacing the class other, which includes all tissue not modeled explicitly by Gaussians with small variance, by a uniform probability density, and amending the expectation-maximization (EM) algorithm appropriately, gives significantly better results. The authors next consider the estimation and filtering of high-frequency information in MR images, comprising noise, inter-tissue boundaries, and within tissue microstructures. The authors conclude that post-filtering is preferable to the pre-filtering that has been proposed previously. The authors observe that the performance of any segmentation algorithm, in particular that of Wells et al. (and the authors' refinements of it) is affected substantially by the number and selection of the tissue classes that are modeled explicitly, the corresponding defining parameters and, critically, the spatial distribution of tissues in the image. The authors present an initial

exploration to choose automatically the number of classes and the associated parameters that give the best output. This requires the authors to define what is meant by "best output" and for this they propose the application of minimum entropy. The methods developed have been implemented and are illustrated throughout on simulated and real data (brain and breast MR).

[13] K. Leemput *et al.* proposed a model-based method for fully automated bias field correction of MR brain images. The MR signal is modeled as a realization of a random process with a parametric probability distribution that is corrupted by a smooth polynomial in homogeneity or bias field. The method the authors propose applies an iterative expectation-maximization (EM) strategy that interleaves pixel classification with estimation of class distribution and bias field parameters, improving the likelihood of the model parameters at each iteration. The algorithm, which can handle multichannel data and slice-by-slice constant intensity offsets, is initialized with information from a digital brain atlas about the a priori expected location of tissue classes. This allows full automation of the method without need for user interaction, yielding more objective and reproducible results. The authors have validated the bias correction algorithm on simulated data and they illustrate its performance on various MR images with important field in homogeneities. They also relate the proposed algorithm to other bias correction algorithms.

[14] D. Pham *et al.* presented the fuzzy segmentation of two-dimensional (2-D) and three-dimensional (3-D) multispectral magnetic resonance (MR) images that have been corrupted by intensity in homogeneities, also known as shading artifacts. The algorithm is an extension of the 2-D adaptive fuzzy C-means algorithm (2-D AFCM) presented in previous work by the authors. This algorithm models the intensity in homogeneities as a gain field that causes image intensities to smoothly and slowly vary through the image space. It iteratively adapts to the intensity in homogeneities and is completely automated. In this paper, the authors fully generalize 2-D AFCM to three-dimensional (3-D) multispectral images. Because of the potential size of 3-D image data, they also describe a new faster multi grid-based algorithm for its implementation. They show, using simulated MR data, that 3-D AFCM yields lower error rates than both the standard fuzzy C-means (FCM) algorithm and two other competing methods, when segmenting corrupted images. Its efficacy is further demonstrated using real 3-D scalar and multispectral MR brain images.

[15] B. Likar *et al.* describes the problem of retrospective correction of intensity in homogeneity in magnetic resonance (MR) images is addressed. A novel model-based correction method is proposed, based on the assumption that an image corrupted by intensity in homogeneity contains more information than the corresponding uncorrupted image. The image degradation process is described by a linear model, consisting of a multiplicative and an additive component which are modeled by a combination of smoothly varying basis functions. The degraded image is corrected by the inverse of the image degradation model. The parameters of this model are optimized such that the information of the corrected image is minimized while the global intensity statistic is preserved. The method was quantitatively evaluated and compared to other methods on a number of simulated and real MR images and proved to be effective, reliable, and computationally attractive. The method can be widely applied to different types of MR images because it solely uses the information that is naturally present in an image, without making assumptions on its spatial and intensity distribution. Besides, the method requires no preprocessing, parameter setting, nor user interaction. Consequently, the proposed method may be a valuable tool in MR image analysis.

III. EXISTING APPROACH

Intensity in homogeneity is usually ascribed to a smooth and spatially varying field multiplying the true signal of the same object in the measured image. This spatially varying smooth field is named as bias field. Existing method Bias correction is a procedure to estimate the bias field from the measured image to reduce its side effect .In the existing bias correction approaches can be categorized into two categories, namely prospective and retrospective approaches. Prospective methods aim at calibrating and improving image acquisition processing by applying specific hardware or devising special imaging sequences. However, these methods cannot correct patient-induced in homogeneity. Comparatively, retrospective methods only rely on the acquired images and sometimes some prior knowledge. Thus, they are relatively more general, and can be used to correct patient-induced in homogeneity from different sources. The retrospective methods can be further categorized into several categories based on filtering, surface fitting, histogram and segmentation . Among various retrospective methods, segmentation based ones are most attractive, since they unify segmentation and bias correction under a single framework to benefit from each other, simultaneously yielding better segmentation and bias correction results. In these methods, parameter model based on the maximum-likelihood (ML) or maximum a posterior (MAP) probability criterion is often used, in which the corresponding parameters are often estimated by the expectation maximization (EM) algorithm. However, an appropriate initialization of the EM algorithm is critical to such algorithms, which requires either a close estimate of the bias field or a coarse segmentation. Manual selections of seed points for each class are often used, but it is subjective and irreproducible.Neighboring pixels information belonging to the same class, the segmentation results are often sensitive to noise and the tissue borders may not be smooth. Markov random fields (MRF) model can yield improved segmentation results that are less sensitive to noise.

Recently, Li *et al.* proposed a parametric method for simultaneous bias field correction and segmentation by minimizing a least square energy functional. The bias field is modeled as a linear combination of a set of orthogonal polynomial basis function. In 7T MRI even though this leads to a very smooth bias field, some bias fields cannot be well fitted by polynomials, such as the bias field. Moreover, each pixel is assigned to one tissue class. However, intensities of the partial volume voxels are composed of multiple class intensities in images, and the proportion of the partial volume voxels in low-resolution datasets can be up to 30%. Thus, the calculated bias field may be partially wrong. Li *et al.* proposed a variation level set (VLS) approach to simultaneous segmentation and bias correction. However, this method needs to alternatively iterate two partial differential equations, which is very time-consuming. Furthermore, the energy functional in the VLS method is not convex in the set of characteristic functions, making it easy to be trapped into local minima.

A. Overview of Existing Approach

There are two categories in bias correction, namely **prospective** and **retrospective approaches**.

Prospective methods

- Calibrating and improving image acquisition processing by applying specific hardware or devising special imaging sequences.
- These methods cannot correct patient-induced in homogeneity.

Retrospective methods

- Used to correct patient-induced in homogeneity.
- But it can't separate patient induced in homogeneity and device caused intensity in homogeneity.

IV. PROPOSED SYSTEM

This project presents a novel variation approach to simultaneous bias correction and segmentation. By exploiting local image redundant information, we define a mapping from original image domain to another domain so that the intensity probability model is more robust to noise. We then define an ML energy functional based on the intensity distributions in each local region in the transformed domain, which combines the bias field, the membership function of each object region, and the constant approximating the true signal from its corresponding object. Finally, the ML energy functional is extended to the whole image domain, which we call the criterion of maximum likelihood in transformed domain (MLTD). The MLTD criterion achieves a global minimum with respect to each of its variables. A soft classification model, shows that each pixel intensity belongs to more than one class, while the hard classification assigns the intensity of each pixel to only one class in MLTD criterion. Therefore, the MLTD criterion obtains a better corrected bias field. Moreover in MLTD criterion the recently proposed CLIC can be specially viewed. while the MLTD is more accurate to model in homogeneous image intensity.

A. Proposed and Related Works

Let us revisit the probability density function (PDF) of the intensity I(y) represented by (2). For the clustering center point x , we define a mapping T: I(x|αi) → I(x|αi) from original image intensity domain D(T) to another domain R(T) as follow.

Refer to the red dashed curves in Fig 3.1the overlapping tails of the distributions are suppressed to some extent. Therefore, the misclassification caused by the overlapping intensity can be alleviated to some extent in the transformed domain R(T). In the following, we will design our energy functional on the domain R(T) by means of the well-defined relationship between domain D(T) and R(T).

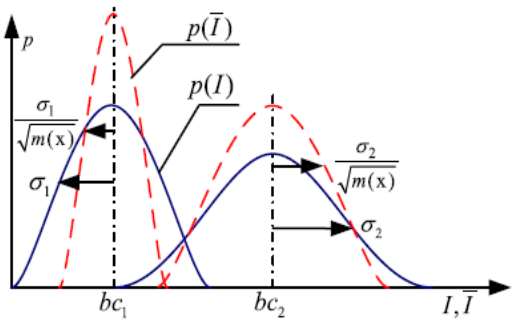

Figure 1. Original image intensity domain (blue solid curves) and the transformed domain (red dashed curves)

B. Energy Minimization

The whole minimization procedure consists of the following three steps, which are implemented iteratively.

- Keep u fixed, optimize and update the variable sets c, *b*, and *σ*.
- Keep c, *b*, and *σ* fixed, optimize and update u.
- Check whether the convergence has been reached. If not, return to 1).

Everything is detailed in Matlab Program(c,b,*σ).*

C. Advantages Of The MLTD Model

If we set to be, the membership function of region to be a truncated Gaussian window will be the same as the CLIC energy functional with except for some trivial constant factors. In addition our MLTD model the CLIC model can be specially viewed and the MLTD will be more accurate to model the image with intensity in homogeneity than the CLIC model. It is claimed that the CLIC model will yield a hard classification (the image intensity in a fixed position only belongs to one tissue). Differently, we will discuss that the proposed MLTD model leads to a soft classification (image intensity in a fixed position belongs to all tissues with a corresponding probability).

In medical imaging, partial volume voxels often have an intensity composed of multiple class intensities. For example, there is as much as 30% of

partial volume voxels in low resolution datasets. The partial volume effect severely influences the accuracy of estimated bias field if a hard classification method is adopted because the hard classification method assumes the image intensity in a fixed position only belongs to one tissue. Our proposed methods are soft classification methods which assume that intensity of each tissue is composed of multiple class intensities, thereby alleviating partial volume effect to some extent.

D. Maximum Likelihood Algorithm

The MLTD method is considered to be one of best estimation methods in statistics. For example, in adult female penguins but be unable to measure the height of every single penguin in a population due to cost or time constraints.

The unknown mean and variance of heights are normally distributed as we assumed, the mean and variance can be estimated with MLE while only knowing the heights of some sample of the overall population. The mean and variance would accomplish by MLE as parameters and finding particular parametric values that make the observed results the most probable given the model.

V. RESULTS AND DISCUSSION

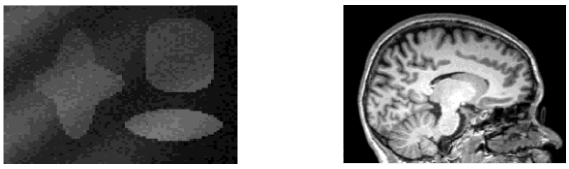

Original image

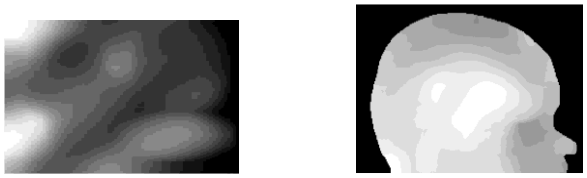

Bias field

Segmented result

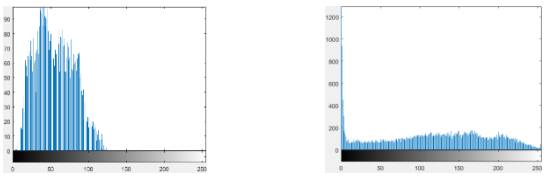

Histogram of original Image

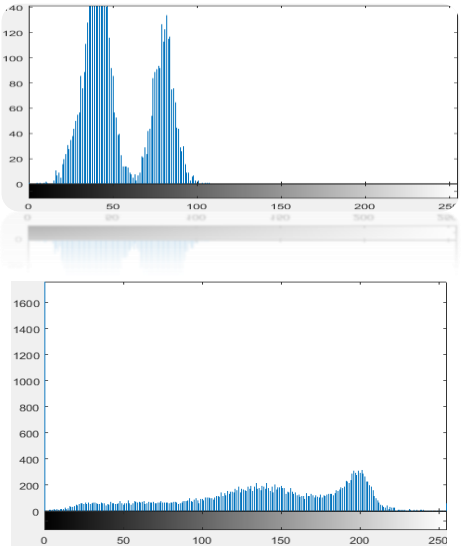

Histogram of Bias Corrected Image

In this section, compares MLTD and RMLTD methods with the CLIC and VLS methods for a synthetic image with noise. The intensity of this synthetic image is severely in homogeneous and the noise is strong in CLIC and VLS. When compared MLTD with the segmentation result by CLIC method is not visually satisfying because some background intensities are misclassified as the object intensities. Compared with their original images in Fig 6.3and6.4, it is obvious that intensity contrast between object and background is more obvious after preprocessing, which in turn results in an easier separation of the object from background. The segmentation result by VLS method is better than the CLIC method but there still exist some obvious misclassifications. In general, MLTD yields the best segmentation results among the three methods. The testing image size is 320×320. The proposed MLTD method image size is 150×120.

However, there still exist some small dot regions that are misclassified due to the strong noise.

In the sagittal slice fig. compares results by MLTD and RMLTD, CLIC and VLS on a 3-tesla MRI. The estimated bias fields, bias corrected images, and segmentation results are shown 6.7, 6.8, 6.9 respectively. The histogram of the original MRI image and the histograms of the bias corrected images by our methods, CLIC and VLS are shown. From the histograms of the bias corrected images recovered by MLTD, CLIC, and VLS, we see that the histograms of specific tissues approximately satisfy Gaussian distribution but with significantly different variances. These results validate that MLTD model is better consistent with the intensity distribution of the image with intensity in homogeneity than CLIC and VLS which do not consider the variance of intensities belonging to different tissues. Testing competing methods on Brain normal subjects (1 mm isotropic spacing, no added noise, discrete anatomical labeling) with stimulated bias fields with 0%, 20%,and 40% intensity in homogeneity, respectively. From Mc Gill Brain. The 5%, 10%, and 20% levels of Gaussian noises are then added to these images. Moreover ,the segmentation results of MLTD are much closer to the brain anatomy than CLIC and VLS.

Application to Simultaneous Segmentation and Bias Correction

Finally, show the segmentation results of MLTD method on a 7T MRI image. The original images, estimated bias fields, and the bias corrected images are shown in fig 6.1, 6.2, 6.3 respectively. Obviously, the image qualities are significantly improved and some regions whose intensity contrast is too low to be identified are able to be distinguished easily after correction.

VI. REFERENCES

[1] C. Li, C. Xu, A. Anderson, and J. Gore, "MRI tissue classification and bias field estimation based on coherent local intensity clustering A unified energy minimization framework," in Proc. Inf. Process. Med.Image, Williamsburg, VA, USA, 2009, pp. 288–299.

[2] C. Li, C. Gatenby, L. Wang, and J. Gore, "A robust parametric method for bias field estimation and segmentation of MR images," in Proc.IEEE Conf. Comput. Vis. Pattern Recognit., Miami, FL, USA, 2009,pp. 218–223.

[3] B. Wang, X. Gao, D. Tao, and X. Li, "A nonlinear adaptive level set for image segmentation," IEEE Trans. Cybern., vol. 44, no. 3, pp. 418–428,Mar. 2014.

[4] X. Gao, B.Wang, D.Tao, and X. Li, "A relay level set method for automatic image segmentation," IEEE Trans. Syst., Man, Cybern. B,Cybern., vol. 41, no. 2, pp. 518–525, Apr. 2011.

[5] U.Vovk, F. Pernus, and B. Likar, "A review of methods for correction of intensity in homogeneity in MRI," IEEE Trans. Med. Imag., vol. 26,no. 3, pp. 405–421, Mar. 2007.

[6] E. McVeigh, M. Bronskill, and R .Henkelman, "Phase and sensitivity of receiver coils in magnetic resonance imaging,"Med. Phys., vol. 13,no. 6, pp. 806–814, Nov./Dec. 1986.

[7] A.Simmons, P.Tofts, G. Barker, and S. Arridge, "Sources of intensity non-uniformity in spin echo images at 1.5 t," Magn. Reson. Med., vol. 32, no. 1, pp. 121–128, Jul. 1994.

[8] A. Fan et al., "A unified variational approach to de-noising and bias correction in MR," in Proc. Inf. Process. Med. Imag., Ambleside, U.K.,Jul. 2003, pp. 148–159.

[9] M. Ahmed, S. Yamany, N. Mohamed, A. Farag, and T. Moriarty," A modified fuzzy C-means algorithm for bias field estimation and segmentation of MRI data," IEEE Trans. Med. Imag., vol. 21, no. 3,pp. 193–199, Mar. 2002..

[10] B. Brinkmann, A. Manduca, and R. Robb, "Optimized homomorphic unsharp masking for MR grayscale in homogeneity correction," IEEE Trans. Med. Imag., vol. 17, no. 2, pp. 161–171, Apr. 1998.

[11] P. Vemuri, E. Kholmovski, D. Parker, and B. Chapman, "Coil sensitivity estimation for optimal SNR reconstruction and intensity in homogeneity correction in phased array MR images," in Proc. Inf. Process. Med.Imag, Glenwood Springs, CO, USA, 2005, pp. 603–614.

[12] R. Guillemaud and M. Brady, " Estimating the bias field of MR images," IEEE Trans. Med. Imag., vol. 16, no. 3, pp. 238–251, Jun. 1997.

[13] K. Leemput, F. Maes, D. Vandermeulen, and P. Suetens, "Automated model-based bias field correction of MR images of the brain," IEEE Trans. Med. Imag., vol. 18, no. 10, pp. 885–896, Oct. 1999.

[14] D. Pham and J. Prince, "Adaptive fuzzy segmentation of magnetic resonance images," IEEE Trans. Med. Imag., vol. 18, no. 9, pp. 737–752, Sep. 1999.

[15] B.Likar, M.Viergever, and F. Pernus, "Retrospective correction of MR intensity in homogeneity by information minimization," IEEE Trans .Med. Imag, vol. 20, no. 12, pp. 1398–1410, Dec. 2001.

Themed Section : Engineering and Technology
© 2018 IJSRSET | Volume 5 | Issue 3 | Print ISSN: 2395-1990 | Online ISSN: 2394-4099

Design of Patch Antenna operated at mm Wave Frequency for MIMO Communication

Sridevi. S[1], Mr. K. Mahendran[2]
[1]ECE, CK College of Engineering and Technology, Chidambaram, Tamilnadu, India
[2]Assistant Professor (ECE), CK College of Engineering and Technology, Cuddalore, Tamilnadu, India
sridevi10495@gmail.com[1], srimahendrancs@gmail.com[2]

ABSTRACT

In today world more than five billion wireless devices are currently being in use for voice and data transmission. With increasing the wireless devices the data rate also increasing with bandwidth. Now for minimize the error and optimize the optimize the data speed MIMO technology is used. The efficient implementation of MIMO requires efficient compact antenna. The compact microstrip patch antenna is designed for MIMO communication system using HFSS software. The designed antenna operates in mm wave frequency and implemented in hardware that provides enhanced bandwidth and data rate which is that fulfill the requirement of the 5G communication.

Keywords: MIMO, HFSS

I. INTRODUCTION

Nowadays the mobile data rate is increasing tremendous, so the fifth generation frequency is necessary to utilize the huge amount of spectrum in the millimetre wave frequency to extraordinary increase communication efficiency. The mm Wave frequency is used in communication systems undergoes high losses and blockages. These losses in mm Wave communications attains several challenges to fully exploit the potential of mm Wave frequency. To overcome these challenges, we carry out a view of existing solutions, and proposed the design for mm Wave frequency for communication.

A. Antenna

An antenna is a transducer that converts radio frequency fields in to alternating current or vice versa. Antenna plays a important role in the operation of all radio quipment. They are used in wireless local area network, mobile telephony and satellite communication.

B. Microstrip Patch Antenna

The Microstrip patch antennas are low profile, comfortable to all two dimension and nonplaintiff surface, simple and low cost to manufracture using modern printed circuit technology, it is easy to design for any structure and shape. There are many substrate that can be used for the design of patch antennas, and their dielectic constants(εr)are usually in the range of 2.2 to 22. For because of the low dielectric constant which provide better efficiency. To be reached between good antenna performance and circuit design. The microstrip antennas are also said to as patch antennas. The patch of the microstrip antenna may be the various shapes such as square, rectangle, thin strip, circular, elliptical, triangular or any other configuration.

C. mm Wave Frequency

Millimeter wave is also known as the super high frequency, it is used for the high-speed wireless and satellite communications. Millimeter wave is now

under the research only, so some of the rooms of frequency only allowed by the ITU, If the mm wave frequency is developed it can be used for the high speed data rate and wireless broadband application and it allows data rate up to 10 Gbps.

D. Metameterial Structure

Inside a dielectric material, the free space wavelength of an antenna is scaled down by a factor of, where is the relative electric permittivity and is the relative magnetic permeability of the material. Thus, the size of an antenna can be significantly reduced by choosing a high or high material. Though miniaturization can be achieved using high materials, it comes at the cost of increased dielectric losses that can significantly affect antenna efficiency.

On the other hand, materials that exhibit a high in the microwave region do not exist in nature and designers have been compelled to use lossy high materials when antenna miniaturization is a key design requirement. Fortunately materials that exhibit high, or magnetic permeability enhanced meta-materials, can now be artificially engineered to lead to smaller antennas without compromising other design criteria.

E. MIMO Communication

MIMO is an technology used in antenna design which consists of multiple antennas at receiver and transmitter for the wireless communications. The antennas at transmitter and receiver used in the communication system are combined to minimize errors and increase the data rate. MIMO technology is used in the applications such as television, wireless communication and also the mobile communication.it is also used in the modem which consists of the two frequency for the high data transmission which negotiate with the cell tower.

II. DESIGN MODELS FOR MICROSTRIP ANTENNA

The most popular model for the design analysis of microstrip patch antennas are the transmission line model which is simple and give good physical insight, in this paper the transmission line model is used to design an rectangular microstrip antenna, this design is simply based on the empirical equations governing the transmission line model. The basic parameters of the patch antenna are obtained from calculations carried out using the appropriate equations. The main aim is to obtain data for different values of frequency of operation. The parameters of interest include the effective dielectric constant (εreff), patch width(w),patch length(L) and wavelength (λ). Analysis of the different scenarios is carried out using the plots generated from the table of the calculated results. The results can be used to determine certain trade off issues that may bother on any choosed parameter at the expense of the others.

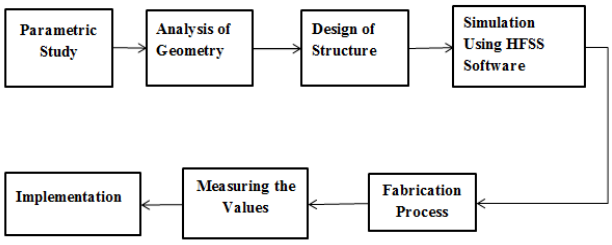

Figure 1. Design Flow

The above figure 1 represents the general design flow of the microstrip patch antenna. That consists of the flow of the design used for designing the proposed patch antenna by using the HFSS software. The proposed antenna is designed by using the desired dimensions obtained by using the given formulas.

Wavelength:

$$\lambda = \frac{c}{f_0} \quad (1)$$

c- velocity of light

fo- frequency used

Width of the patch:

$$w = \frac{c}{2f_0}\sqrt{\frac{2}{\varepsilon_r + 1}} \quad (2)$$

Effective dielectric constant:

$$\frac{\varepsilon_r + 1}{2} + \frac{\varepsilon_r - 1}{2}\left[1 + 12\frac{h}{w}\right]^{\left[\frac{-1}{2}\right]} \quad (3)$$

εr -dielectric constant
h - thickness of the substrate
w - width of the patch

Incremental length:

$$\Delta L = 0.412h * \frac{\left[(\varepsilon eff + 0.3) * \left(\frac{w}{h} + 0.264\right)\right]}{\left[(\varepsilon eff - 0.258) * \left(\frac{w}{h} + 0.8\right)\right]} \quad (4)$$

εeff- effective dielectric constant
h- thickness of the patch

Effective length:

$$L_{eff} = \frac{c}{2f_0\sqrt{\varepsilon_{reff}}} \quad (5)$$

Length:

$$L = L_{eff} - 2\Delta L \quad (6)$$

Ground:

Length: $L_g = 6h + L$ (7)

Width: $w_g = 6h + w$ (8)

Guided wavelength:

$$\lambda_g = \frac{\lambda}{\sqrt{\varepsilon_{reff}}} \quad (9)$$

Radiation box:

$$\frac{\lambda_g}{6} \quad (10)$$

Feed:

length: $L_f = \frac{\lambda_g}{4}$ (11)

width: $w_f = \frac{2h}{\pi}\left\{B - 1 - \ln(2B - 1) + \left(\frac{\varepsilon_r - 1}{2\varepsilon_r}\right)\right\} * \left\{\ln(B - 1) + 0.39 - \left(\frac{0.61}{\varepsilon_r}\right)\right\}$ (12) The rectangular shaped microstrip patch antenna is designed by using the metameterial substrate which is used to provide the negative resistance characterists and the substrate used is RT Duroid that consists of the dielectic constant is 2.2, and the feeding used here is the microstrip line feeding which is used to reduce the losses and the operating frequency is 29.5 GHz.

TABLE I DIMENSIONS OF THE PATCH ANTENNA

PARAMETERS	VALUES(mm)
W	4.01
ε_{eff}	2
H	0.41
ΔL	0.21
L_{eff}	3.59
L	3.16
Lg	5.65
Wg	6.51
Λg	7.19
Lf	1.79
Wf	1.86

The above table 1 represents the dimension of the proposed microstrip patch antenna for the frequency of 29.5 GHz.

III. RESULT ANALYSIS

Results and discussion deals with the results and discussion of the rectangular shape microstrip patch antenna. All the requirement of the design is illustrated individually and the output is given.

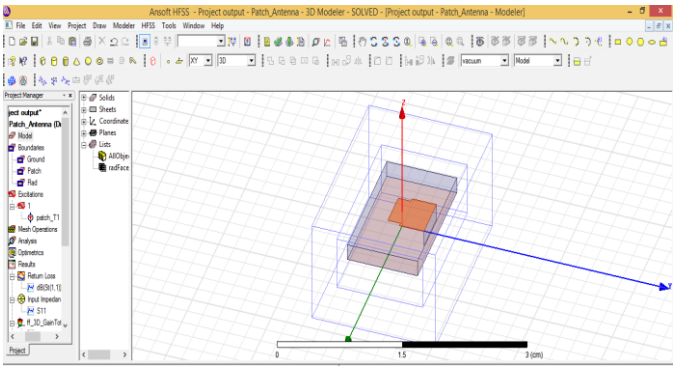

Figure 2. Design by using HFSS software

The above diagram describes the design of the microstrip patch antenna and the length and width of the antenna is selected as per the calculation depends

upon the frequency used, here the frequency used is the millimeter wave frequency.

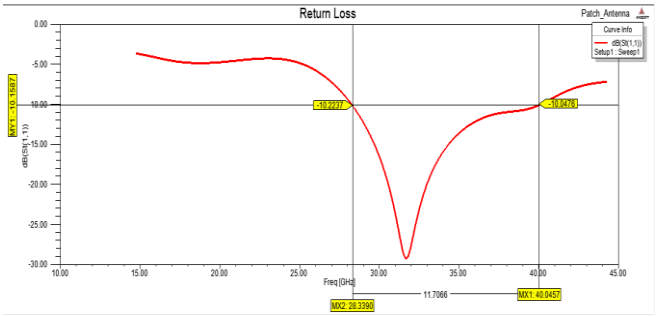

Figure 3. Return Loss

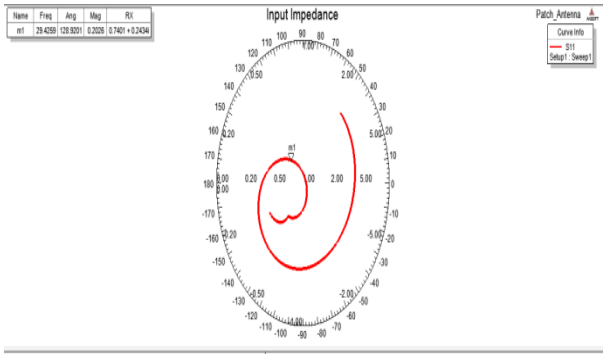

Figure 4. Input Impedence

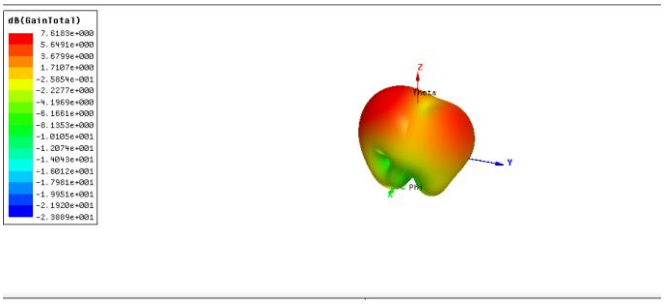

Figure 5. Gain of the Designed Antenna

IV. Hardware Design

The designed microstrip patch antenna is implemented in hardware design, which operates at the frequency of 29.5GHZ.

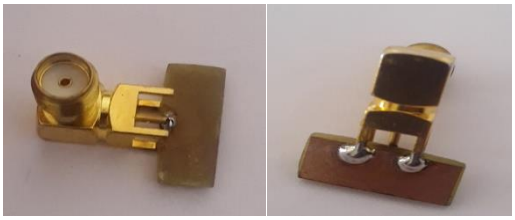

Figure 6. Hardware Design of the Antenna

V. CONCLUSION

The rectangular shaped microstrip patch antenna is designed by using the metameterial as the substrate at the frequency range of 29.5GHz to increase the bandwidth and the data rate and the data rate is increased up the 10 Gbps, so the number of users can be increased with high efficiency.

VI.REFERENCES

[1] Sourav Nandi and Akhilesh Mohan, "A Compact Dual-Band MIMO Slot Antenna for WLAN Applications", 2017. IEEE Antennas and Wireless Propagation Letters

[2] Debdeep Sarkar and Kumar Vaibhav Srivastava, "A Compact Four Element MIMO / Diversity Antenna with Enhanced Bandwidth", International Conference on Signal Processing 2017

[3] Tursunjan Yasin and Reyhan Baktur, "Bandwidth Enhancement of Meshed Patch Antennas through Proximity Coupling" IEEE, 2017.

[4] Behrouz Babakhani, and Satish K. Sharma, " Dual Null Steering and Limited Beam Peak Steering Using Triple Mode Circular Microstrip Patch Antenna", IEEE Transactions on Antennas and Propagation ,2017

[5] Manidipa Roy and Ashok Mittal, Sr. Member, "Recent Advancements in techniques to suppress surface wave propagation in Microstrip Patch Antenna", IEEE International Conference on "Computational Intelligence and Communication Technology" (IEEE-CICT 2017)

[6] Ali Foudazi1 , Thomas E. Roth, Mohammad T. Ghasr, Reza Zoughi1, "Aperture-coupled microstrip patch antenna fed by orthogonal SIW line for millimetre-wave imaging applications" IET Microwaves, Antennas & Propagation,2017

[7] R. Kiruthika, Dr. T. Shanmuganantham, Rupak Kumar Gupta, " A Fan Shaped Triple Band Microstrip Patch Antenna with DGS for X-band

Applications" International Conference on Control, Instrumentation, Communication and Computational Technologies, 2016

[8] L. Chandiea, K.Anusudha, " Pentagon Shaped Microstrip Patch Antenna With Metamaterial For UWB Application", 2016 International Conference on Control, Instrumentation, Communication and Computational Technologies 2016

[9] Rupak Kumar Gupta, Dr. T. Shanmuganantham, R. Kiruthika, "A Staircase Hexagonal Shaped Microstrip Patch Antenna for Multiband Applications" International Conference on Control, Instrumentation, Communication and Computational Technologies, 2016

[10] Nagaraj Hanchinamani, Dr. C.R. Byrareddy, "A Multiband MIMO Microstrip Patch Antenna for Wireless Applications", Volume 4 Issue IX, International Journal for Research in Applied Science & Engineering Technology September 2016.

[11] Uday kumar, Dileep Kumar Upadhyay, Babu Lal Shahu, " Improvement of performance parameters of rectangular patch antenna using metamaterial"IEEE International Conference On Recent Trends In Electronics Information Communication Technology, May 20-21, 2016.

[12] Alok Kumar, Nancy Gupta, P. C. Gautam, "Gain and Bandwidth Enhancement Techniques in Microstrip Patch Antennas ", Volume 148 – No.7, International Journal of Computer Applications (0975 – 8887), August 2016.

[13] Ekambir Sidhu, Raveena Bhatoa, Roopan , "Star shaped microstrip patch antenna design with slotted ground plane for civil/military radio location and satellite navigation applications", International Conference on Control, Computing, Communication and Materials 2016

[14] Kan Zheng, Long Zhao, Jie Mei, Bin Shao, Wei Xiang, and Lajos Hanzo, Fellow, "Survey of Large-Scale MIMO Systems", IEEE IEEE Communications Surveys & Tutorials,2015

[15] Nagaraj Hanchinamani and Dr. C.R. Byrareddy, "A Survey of Microstrip Patch Antenna for MIMO", Vol. 3, Issue 12, International Journal of Innovative Research in Computer and Communication Engineering December 2015.

[16] Yong Niu, Yong Li, Depeng Jin, Li Su, and Athanasios V. Vasilakos, " A Survey of Millimeter Wave (mmWave)Communications for 5G: Opportunities and Challenges"IEEE ,2015

[17] Md mamunur rashid and Saddam Hossain, " Antenna Solution for Millimeter Wave Mobile Communication (MWMC):5G", ISSN 2278 – 088 Volume 3, Issue 8, IEEE Antennas and Wireless Propagation Letters 1 November 2014.

[18] Priyanka Kakaria, Rajesh Nema, "Review and Survey of Compact and Broadband Microstrip Patch Antenna" IEEE International Conference on Advances in Engineering & Technology Research,2014

[19] Anisha Susan Thomas, Prof. A K Prakash, " A Survey on Microstrip Patch Antenna using Metamaterial", Vol. 2, Issue 12, International Journal of Advanced Research in Electrical, Electronics and Instrumentation Engineering December 2013.

[20] Amish Kumar Jha , Bharti Gupta, "Performance of Microstrip Antenna of Different Substrates and Geometries for S-Band", IJCSET | June 2011 | Vol 1, Issue 5,249-252 June 2011 | Vol 1, Issue 5,249-252

Themed Section : Engineering and Technology
© 2018 IJSRSET | Volume 5 | Issue 3 | Print ISSN: 2395-1990 | Online ISSN: 2394-4099

Identification of Malicious and Liar Nodes by Query Processing In Manets

R.Gangadevi[1], T.Ravichandran[2]

[1]PG Scholar, Department of ECE, Annamalai University, Tamil Nadu, India

[2]Associate Professor, Department of ECE, Annamalai University, Tamil Nadu, India

ABSTRACT

Mobile Ad-hoc Networks (MANETs) is a collection of mobile nodes sharing a wireless channel without any centralized control (or) established communication backbone. MANETs require fundamental changes to network routing protocols. These are characterized by the mobility of nodes, which can move in any direction and at any speed that may lead to arbitrary topology and frequent partition in the network. In the existing method, the malicious nodes are identified based on the grouping. In MANETs, if a normal node becomes an attacker, the malicious node tries to disrupt the operations of the system. The main drawback in the above existing method that it doesn't address the critical Liar Nodes (LNs) responsible for the network in security. In this proposed work, malicious node are identified based on the top-k-query processing methods and it is also designed to locate and identify LNs by the False Notification Attacks (FNA) using the Dynamic Source Routing (DSR) reactive routing protocol and to prevent the liar nodes from performing False Notification Attack (FNA). So that the message can be sent with more security by using the Rivest Shamir Adleman (RSA) Algorithm and Secure Hashing Algorithm 1(SHA1) methods and also with less power, thereby increasing the battery life. To analyse the following parameters such as Throughput and packet loss were simulated through Network Simulator-2 (NS-2). In the proposed work, the output produced promising results to identify and eliminate the LNs, and thus reducing the number of unwanted nodes thereby improving security due to unwanted nodes using majority of the network performance and metrices.

Keywords: Ad-Hoc Networks, Attacker, Liar Nodes, Malicious Nodes, Query Processing

I. INTRODUCTION

Mobile Ad-hoc Networks (MANETs) is a collection of mobile nodes sharing a wireless channel without any centralized control (or) established communication backbone Recently, there has been an increasing interest in MANET, which is constructed by only mobile nodes. Since such self-distributed networks do not require pre-existing base stations, they are expected to apply to various situations such as military affairs and rescue work in disaster sites. In MANETs, since each node has poor resources (i.e., the communication bandwidth and the battery life of mobile nodes are limited), it is effective to retrieve only the necessary data items using top-k query, in which data items are arranged according to a particular attribute score, and the query- issuing node acquires the data items with k highest scores in the network (the global top- k result).On the other hand, in MANETs, if a normal node becomes malicious owing to an attack from outside the network, the malicious node tries to disrupt the operations of the system. In this case, the user whose network holds the malicious node will typically continue to operate

the system normally, unaware of the threat, while the malicious node may execute a variety of attacks (e.g. Denial of Service (DoS) attack such as blackhole attack).Basically, malicious nodes attempt to disrupt query- issuing node's acquisition of the global top-k result for a long period, without being detected. However, DoS attacks in MANETs have been actively studied for long years, and as a result, using existing techniques, such attacks can be exposed by the query-issuing node or intermediate nodes. Here, a unique characteristic of top- k –query processing is that the query-issuing node does not know the unique top-k result beforehand. Therefore, even if a malicious node replaces high- score data items with its own low-score ones, when relaying the data items, it is difficult for the query-issuing to detect the attack, and it may believe that all the received data items with k highest scores are the unique top-k result. In this paper, we introduce a new type of attack called data replacement attack (DRA), in which a malicious node replaces the received data items (which we call the local top-k result) with unnecessary yet proper data items (e.g., its own low-score data items). Since DRAs are a strong attack, and more difficult to detect than other traditional types of attack, some specific mechanism for defending against DRAs are required. This method also identifies the liar nodes to prevent it from the False Notification Attack (FNA).

II. RELATED WORK

W.T.Balkey et al. [1] suggested the advantages of best top-k queries in the context of distributed peer-to-peer information infrastructures and show how to extend the limited query processing in current peer-to-peer networks by allowing the distributed processing of top-k queries, while maintaining a minimum of data traffic.

Kejun Liu et al. [2] focus on the nodes which drop the information to send forward considered as a malicious nodes. Specifically, nodes may participate in the route discovery and maintenance process but refuse to forward data packets. To detect such misbehavior and more efficient detection process, the 2ACK technique is analysed. The main idea of the 2ACK scheme is to send two-hop acknowledgement packets in the opposite direction of the routing path.

Minji Wu et al. [3] exploits the semantics of top-k query and developed an energy-efficient monitoring approach called FILA. The basic idea is to install a filter at each sensor node to suppress unnecessary sensor updates. Filter setting and query re-evaluation upon updates are two fundamental issues to the correctness and efficiency of the FILA approach. They develop a query re-evaluation algorithm that is capable of handling concurrent sensor updates and also present optimization techniques to reduce the probing cost.

R.Zhang et al. [4] suggested three schemes whereby the network owner can verify the authenticity and completeness of fine-grained top-k query results in tired sensor networks, which is the first work of its kind. This schemes are built upon symmetric cryptographic primitives and force satisfied master nodes to get both authentic and complete query results to avoid being caught.

P.Dewan et al. [5] developed reputation systems for peer-peer networks to protect the network without using any central component, and thereby harnessing the full benefits of the peer-peer network. The reputations of the peers are used to determine whether a peer is a malicious peer (or) good peer. Once detected, the malicious nodes are obstracized from the network as the good nodes do not perform any transactions with the malicious peers. This technique allows secure exchange of reputation information between the two peers participating in a transactions.

Jing Shi et al. [6] developed a two-tier sensor network with resource-rich nodes at the upper tier and resource-poor sensor nodes at the lower tier. Source node collect data from sensor nodes and answer the queries from the network owner. The reliance on

master nodes for data storage and query processing raises serious concern about both data authentication and query-result correctness.

Yao-Tung Tsou et al. [7] implies each sensor having many sensing capabilities periodically route the multidimensional sensed data to the storage node, which responds to the queries. Unfortunately, node compromises pose the great challenge of securing the data collection. The sensed data could be leaked to or could be manipulated by the compromised nodes.

Y.Sasaki et al. [8] proposed a two-phase query processing method for top-k query processing. In this method, the query-issuing node collects the information of scores of data items held by each node in the first phase. Based on the received information, it determines the threshold of the score, i.e., the estimated k-th highest score. Then, in the second round, the query-issuing node transmits a query attached with the threshold, and each node that received the query sends back only its own data items whose scores are equal to or larger than the threshold. This can further reduce the traffic and also keep high accuracy of the query result.

Baljeet Malhotra et al. [9] discussed the importance of underyling structure and proposed the use of Dominating Set Tree (DST) for processing the top-k queries. Leveraging on the properties of a DST they proposed a new algorithm, EXTOK and proved its correctness. Simulation, using real and synthetic data sets, revealed the effectiveness and superior efficiency of the combination EXTOK-DST for processing the top-k queries in WSN.

Rui Zhang et al. [10] took multidimensional range queries as an example to investigate secure cooperative data storage and query processing in UTSNs. They present a suite of novel schemes that can ensure data confidentiality against master nodes and also enable the network owner to verify with very high probability the authenticity and completeness of any query result by inspecting the spatial and temporal relationships among the returned data and the performance evaluations confirm the high efficacy and efficiency of the proposed schemes.

III. PROPOSED METHOD

In our new suggested top- k query processing method, the query issuing node first floods a query over the entire network, and each node receiving the query stores information on all possible routes to the query- issuing node. Then, each receiving node replies with data items with the k highest scores to two neighbor nodes. Each node includes, in its reply message, information on the reply message forwarding routes which consist of pairs of sender node and next node IDs. Based on this attached information, the query- issuing node can detect an attack occurring along a reply message route. In MANETs, since the network topology dynamically changes due to the mobility of nodes, radio link disconnections can occur between nodes. Therefore, if a node detects a radio link disconnection along one of its two reply routes, it sends back the data items to a different node, to which those data items have not yet been sent, to ensure that they are sent back along two different routes.

In our proposed malicious node identification method, a query- issuing node that detects a DRA narrows down the malicious node candidates based on the received reply messages. Then, the query-issuing node determines whether a given reply message sent back by a malicious node candidate includes replaced data items or not, by sending inquiries to nodes receiving reply messages from this candidate.

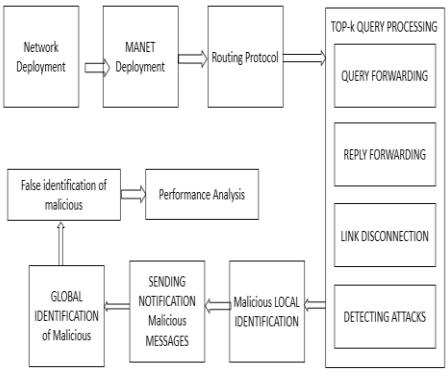

Figure 1. Architecture Diagram

In this way, the query- issuing node can detect the malicious node. Here, each node tends to identify the neighboring malicious nodes, but hardly identify the malicious nodes which are far from it. Therefore, nodes share the information on identified malicious nodes to detect the malicious nodes quickly. Specifically, after each node identifies malicious nodes, it floods the information on the identified malicious nodes within the network. When each node has received a certain number of queries, it performs malicious node identification procedures based on the received information. Specifically, it divides nodes into relevant groups based on similarities of the information on malicious nodes detected by those nodes, and then identifies malicious nodes based on the results of malicious node identifications by these groups.

Liar nodes which provides the false information can be identified by the False Notifcation Attacks (FNA).

IV. TOP- K QUERY PROCESSING

A. Query Forwarding

First, the query- issuing node floods a query over the entire network. The query consists of the node identifier of the query- issuing node (Query-issuing node ID), the query identifier of the query (Query ID), the number of requested data items (k), the query condition, and a list of the node identifiers of nodes on the path along which the query message is to be transmitted (Query path). Specifically, the query- issuing node, M_p, specifies the query condition and the number of requested data items, k. Then, M_p transmits a query message whose Query path includes its identifier, M_p, to its neighbor nodes. A node, M_q, which receives the query, transmits it. Hop count denotes the number of hops to the query- issuing node, based on the number of nodes included in the Query path. Then, M_q sets a waiting time for reply (RD) according to the following equation:

$$RD = (hop_{max} - hop_{cnt}) \cdot T_{wait} \quad (1)$$

where hop_{cnt} denotes the number of hops to the query- issuing node, hop_{max} denotes the maximum number of hops (calculated based on the area size of the network and the radio range of nodes), and T_{wait} is a positive constant. In this equation, as hop_{cnt} increases, RD decreases. When M_q receives the query later again, it stores the ID of the query sender node as its neighbor node, as well as, the Query path and the number of hops.

B. Reply Forwarding

When RD has transfered, each node sends back a reply message, which includes its own node identifier (Sender node ID), the identifier of the next node along the reply route (Dest node ID), a list of the data items (including their scores) and the node identifiers of the nodes possessing them (Data list), and a list summarizing the reply message routes, i.e., a list of the pairs of sender and next node identifiers (Forwarding Route). Node M_r sends a reply message when its RD has passed. Here, REP denotes a reply message and REP. FR denotes the forwarding route list consisting of (Sender node ID, Destination node ID), which denotes the list of sender and next node identifier pairs, and R denotes the maximum number of reply messages to be re-sent. M_r selects the next node from its neighboring nodes, which has the least hop count and least overlap between its Query path and the parent node's Query path.

C. Link Disconnection

In MANETs, the network topology changes dynamically due to the movement of nodes. When a radio link disconnection to the parent node or next node occurs, a replying node, M_r, cannot send a reply message, resulting in reduced accuracy of the query result. Therefore, if a node sends a reply message R times but does not receive an ACK from the parent or next node, the sending node detects a radio link disconnection; at which point the node sends the reply message to another neighbor node among those whose routes to the query- issuing node include the least overlap between Query path in the replay

message and their own Query path. If the sending node has no neighbor nodes which satisfy this condition, it sends the reply message to a neighbor selected in the same way as in selecting the next node in "Reply Forwarding" process among nodes which have not been sent the reply message.

D. Detecting Attacks

After the query- issuing node, Mp, obtain all the reply messages, it detects a DRA. Top- K result denotes the data items with the k highest scores, acquired by the query- issuing node, REP. Data and reply forwarding respectively denote the data list and forwarding route included in the reply message, REP, and Send route denotes the set of node identifiers along the route from the node possessing a given data item to the query issuing node (the query- issuing node can know the Send route from the forwarding route information). If the nodes which have data items in the top-k result are included in Send route (or REP.FR), but the data items in the top- k result are not included in REP. Data, the query- issuing node detects a DRA and initiates the malicious node identification process and also the liar nodes from the False Notification Attacks (FNA). If the query-issuing node does not detect a DRA, it completes the top-k query processing.

E. Global Identification

In our method, each node individually identifies malicious nodes and liar nodes using the shared information by the two steps; node grouping and malicious node identification. Each node divides nodes in the network into some groups based on the information in the notification messages received by the nodes.

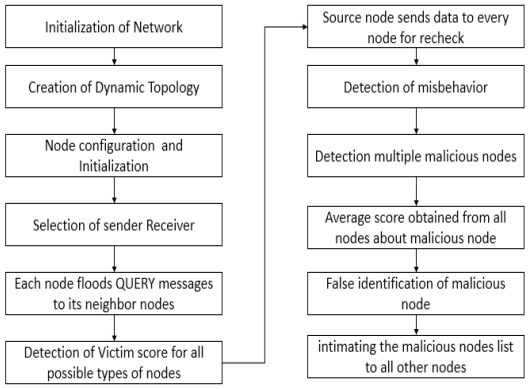

Figure 2. Flow Diagram

After the node grouping, each node conclusively determines malicious nodes and liar nodes based on the information about malicious nodes and lair nodes identified by nodes in each group. Here, there are three types of groups, i.e., a group composed of (i) only normal nodes, (ii) only malicious nodes, and (iii) both liar and malicious nodes. The nodes identified as malicious and liar nodes by all nodes in a group of (i) or (iii) are surely malicious nodes and liar nodes. Here, since liar nodes are generally minorities in the entire network, majority based judgment (and pruning) works well for malicious node and liar nodes identification. Therefore, in our method, nodes are confirmed to be malicious and liar when they are determined to the number of groups equal to or larger than a certain threshold. Malicious and Liar nodes can be identified by the following steps:

Step 1:

In our proposed system, the MANET nodes are initialized with basic configuration of node.

Step 2:

While concentrating 'Ad-hoc' network we have created dynamic topology with the nodes.

Step 3:

Nodes are initialized as per the topology as well as working behavior.

Step 4:

User can select the sender and receiver where the secured communication is important.

Step 5:

Each node floods QUERY messages to its neighbour nodes and the source node.

Step 6:

Top-k Query gives Victim score for all possible types of nodes with respect of source node.

Step 7, 8 & 9:

Source node sends data to every node for recheck the misbehaving function in the network.

Step 10, 11 & 12:

To detect falsification of malicious node, average score obtained from all nodes about malicious node list and it detects the good node from that malicious node list. Intimating the malicious nodes list to all other nodes.

V. DYNAMIC SOURCE ROUTING

Dynamic Source Routing (DSR) is a on demand reactive protocol based on the source route approach. In DSR, the protocol is based on the link state algorithm in which source initiates route discovery on demand basis. The sender determines the route from source to destination and it includes the address of intermediate nodes to the route record in the packet. DSR was designed for multi- hop networks for small diameters.

VI. ALGORITHM

A. Rivest Shamir Adleman Algorithm (RSA)

Ron Rivest, Adi Shamir, and Leonard Adleman popularized an asymmetric algorithm. Asymmetric algorithm means it uses two different keys (i.e) public and private key. Public key is given to everyone and the private key is kept private. Most importantly, RSA contrivance a public-key cryptosystem, as well as digital signatures. RSA is motivated by the published works of Diffie and Hellman.

The process of exchange the session key:

- A uses RSA asymmetric algorithm to generate their own public key (n, e) and the private key (n, d) and sends the information to B that contains the public key (n, d) and ID of A
- B gets the session key k and uses the public key encrypt the message to A, $m^e \bmod n$.
- A uses his private key to decrypt the $C^d \bmod n$, then can get K. In this way, A and B can communicate with symmetric encryption algorithm which was symmetrric and the session key K.

The RSA security depends on the computational difficulty of factoring large integers. Obviously the longer a number is the harder is to factor, and so the better the security of RSA. Strength of encryption is directly tied to key size, and key length is doubled delivers an exponential increase in strength, although it does debase performance. RSA keys are commonly 1024 or 2048 bits long, but experts believe that 1024 bit keys could be broken in the future. The main advantages in using extremely of long length is the computational overhead involved in encryption/ decryption. The main drawback is only if a new factoring technique arises that requires keys of such lengths to be used that important key length increases much faster than the average speed increase in computers utilizing the RSA algorithm.

B. Secure Hashing Algorithm

A hashing algorithm is a mathematical function that compress data to a fixed size. Hashes are convenient for situations where computers may want to identify, compare, or otherwise run calculations against files and strings of data. One of the key properties of hashing algorithms is determinism. Hashing algorithms are used in all sorts of ways – they are used for password storing, in computer vision, in databases.

SHA-0:

A retronym applied to the original adaptation of the 160-bit hash function published in 1993 under the name “SHA”.

SHA-1 :

A 160-bit hash function which is same as that of the Message Digest (MD) 5 algorithm. This was

described by the National security agency to be part of the digital signature.

SHA-2:

A family of two identical hash functions with different block sizes known as sha-256 and sha-512. They differ in word size.

SHA-3:

A hash function formerly called keycap, chosen in 2012 after a public competition among non NSA-designers.

VII. SIMULATION RESULTS

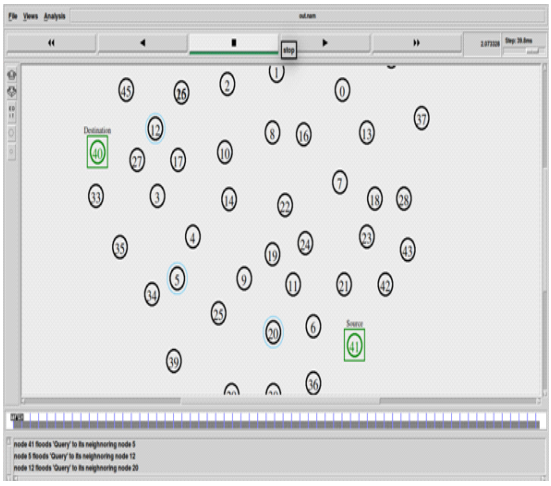

Figure 3. Selection of Source and Destination

Here the source is selected as node 0 and destination is selected as node 41 to transmit the above given message.

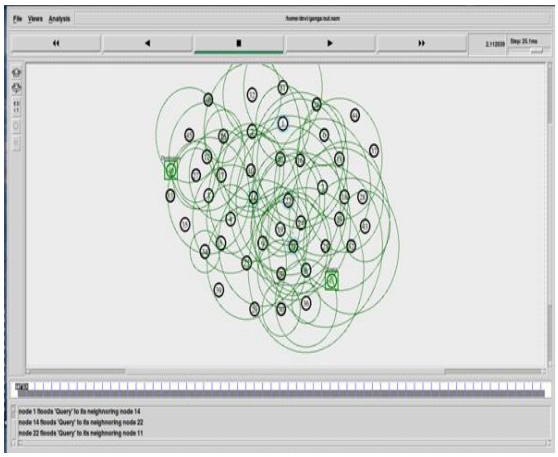

Figure 4. Node Floods Query To Neighbouring Nodes

Processing action with each and every nodes are described in the figure 4

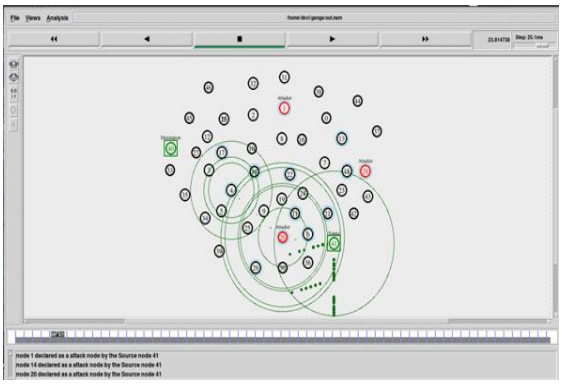

Figure 5. Identification of Malicious Nodes

Here the malicious nodes are identified one after the other using the victim score values.

Figure 6. Identification Of Liar Nodes

After the identification of malicious nodes, based on the message authentication code liar nodes are identified. Here the malicious and liar nodes are identified one after the other using two different techniques.

A. Parameter Comparison Throughput

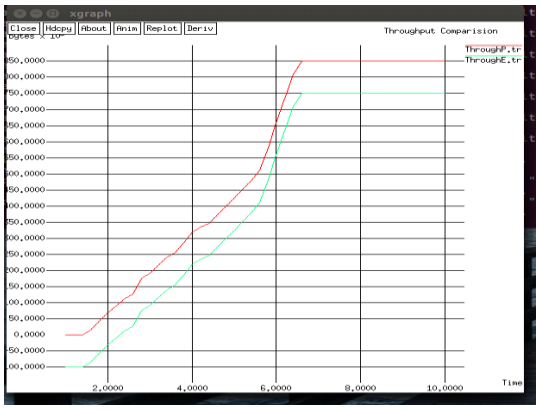

Figure 7. Throughput Comparison

Throughput is the total number of packets delivered over the total simulation time. It is found to be more in SHA algorithm than in the RSA algorithm.

B. Packet Loss

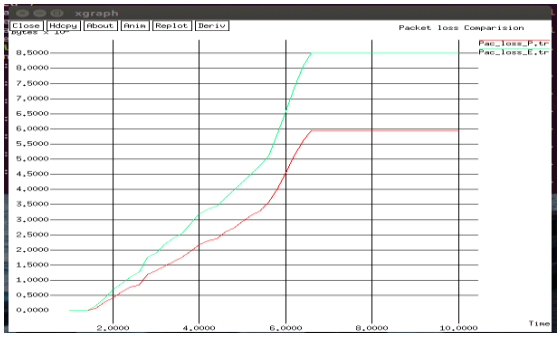

Figure 8. Packet Loss Comparison

When one or more packet of data travelling across a network fail to reach their destination. Packet loss is more in RSA algorithm than in the SHA algorithm

VIII. CONCLUSION

Malicious and liar nodes will result in the lack of security factor. So malicious and liar nodes are identified one after the other by two different techniques. In removing these nodes will improve the security factor. Then the parameters such as Throughput, packet delivery ratio, Energy consumption, packet loss were compared with RSA and SHA algorithms. SHA algorithm found to produce the better performance and results.

IX. REFERENCES

[1] W.T. Balke, W. Nejdl, W. Siberski, and U. Thaden, "Progressive distributed top-k retrieval in peer-to-peer networks," in Proc. ICDE, Apr. 2005, pp. 174–185.

[2] Kejun. Liu, J. Deng, P. K. Varshney, and K. Balakrishnan, "An acknowledgment-based approach for the detection of routing misbehavior in MANETs," IEEE Trans. Mobile Comput., vol. 6, no. 5, pp. 536–550, May 2007.

[3] Minji. Wu, J. Xu, X. Tang, and W. C. Lee, "Top-k monitoring in wireless sensor networks," IEEE Trans. Knowl. Data Eng., vol. 19, no. 7, pp. 962–976, Jul. 2007.

[4] R. Zhang, J. Shi, Y. Liu, and Y. Zhang, "Verifiable fine-grained top-k queries in tiered sensor networks," in Proc. INFOCOM, Mar. 2010, pp. 1–9.

[5] P. Dewanand, P. Dasgupta, "P2P reputation management using distributed identities and decentralized recommendation chains, "IEEE Trans Knowl. Data Eng., vol. 22, no. 7, pp. 1000–1013, Jul. 2010.

[6] J. Shi, R. Zhang, and Y. Zhang, "A Spatiotemporal Approach for Secure Range Queries in Tiered Sensor Networks," in Proc. INFOCOM, Jan.2011, pp. 945–953.

[7] C.M.Yu, Y.T.Tsou, C.S.Lu and S.Y.Kuo, "Practical and secure multi dimensional query frame work in tiered sensor networks," IEEE Trans. Inf. Forensics Security, vol.6, no.2, pp.241-245, Jun 2011.

[8] Y. Sasaki, T. Hara, and S. Nishio, "Two-phase top-k query processing in mobile ad hoc networks," in Proc. NBiS, Sep. 2011, pp. 42–49.

[9] B.Malhotra, M.A. Nascimento, and I. Nikolaidis, "Exact top-k queries in wireless sensor networks," IEEE Trans .Knowl. Data Eng., vol.23, no.10, pp. 1513–1525, Oct. 2011.

[10] Rui Zhang, Jing Shi, Yanchao Zhang and Jinyuan Sun, "Secure Cooperative Data Storage and Query Processing in Unattended Tiered Sensor Networks" , in IEEE Journal on selected

areas in communications, Vol. 30, No. 2, February 2012.

[11] Y. Yi, R. Li, F. Chen, A. X. Liu, and Y. Lin, "A digital watermarking approach to secure and precise range query processing in sensor networks," in Proc. INFOCOM, Apr. 2013, pp. 1950–1958.

[12] D. Amagata, Y. Sasaki, T. Hara, and S. Nishio, "A robust routing method for top-k queries in mobile ad hoc networks," in Proc. MDM, Jun. 2013, pp. 251–256.

[13] C.M. Yu, G.K. Ni, I.Y. Chen, E. Gelenbe, and S.Y. Kuo, "Top-k query result completeness verification in tiered sensor networks," IEEE Trans. Inf. Forensics Security, vol. 9, no. 1, pp. 109–124, Jan. 2014.

[14] T. Tsuda, Y. Komai, Y. Sasaki, T. Hara, and S. Nishio, "Top-k query processing and malicious node identification against data replacement attack in MANETs," in Proc. MDM, Jul. 2014, pp. 279–288.

[15] J. Shi, R. Zhang, and Y. Zhang, "Secure top –k – query processing in unattended tiered sensor networks," in Proc. INFOCOM, Nov 2014, pp. 945–953.

[16] Y. Zhang, G. Wang, Q. Hu, Z. Li, and J. Tian, "Design and performance study of a topology-hiding multipath routing protocol for mobile ad hoc networks," in Proc. INFOCOM, Mar. 2012, pp. 10–18.

[17] S. Chen, Y. Zhang, Q. Liu, and J. Feng, "Dealing with dishonest recommendation: The trials in reputation management court," Ad Hoc Network., vol. 10, no. 8, pp. 1603–1618, Nov. 2012.

[18] Z. Li and H. Shen, "A hierarchical account-aided reputation management system for large-scale MANETs," in Proc. INFOCOM, Apr. 2011, pp. 909–917.

[19] X. Liu, J. Xu, and W. C. Lee, "A cross pruning framework for top-k data collection in wireless sensor networks," in Proc. MDM, May 2010, pp. 157–166.

[20] M. Yiu, Y. Lin, and K. Mouratidis, "Efficient verification of shortest path search via authenticated hints," in Proc. IEEE ICDE, Long Beach, CA, USA, Mar. 2010, pp. 237–248.

[21] D. Ma, C. Soriente, and G. Tsudik, "New adversary and new threats: Security in unattended sensor networks," IEEE Netw., vol. 23, no. 2, pp. 43–48, Mar. 2009.

[22] M. Ye, X. Liu, W.-C. Lee, and D. L. Lee, "Probabilistic top-k query processing in distributed sensor networks," in Proc. IEEE ICDE, Long Beach, CA, USA, Mar. 2010, pp. 585–588.

[23] Q. Wang, K. Ren, W. Lou, and Y. Zhang, "Dependable and secure sensor data storage with dynamic integrity assurance," in Proc. IEEE INFOCOM, Rio de Janeiro, Brazil, Apr. 2009, pp. 954–962.

[24] R. Lu, X. Lin, H. Zhu, and X. Shen, "TESP2: Timed efficient source privacy preservation scheme for wireless sensor networks," in Proc. IEEE ICC, May 2010, pp. 1–6.

Themed Section : Engineering and Technology
© 2018 IJSRSET | Volume 5 | Issue 3 | Print ISSN: 2395-1990 | Online ISSN : 2394-4099

Enhancement of Signal Strength Using GSTEB Routing Protocol In WSN

[1]C.UshaDevi, [2]Dr.V.PadmaThilagam
Asst. Professor, Dept. of Electronics & Communication Engineering,
Bharathiyar College of Engineering & Technology, Karaikal, Puducherry, India
Asst. Professor, Dept. of Electrical Engineering, Annamalai University, Chidhambaram, Tamilnadu, India

ABSTRACT

A Wireless Sensor Network (WSN) composed of an enormous quantity of multifunctional wireless sensor nodes. Wireless sensor network is used to collect and send various kinds of messages to a base station .Wireless sensor networks are deployed where the physical environment is so harsh. For better performance of the network we should analyse and increase the signal strength. The current work involves comparing the signal strength of routing protocols such as LEACH, LEACH-C and GSTEB. General Self-Organized Tree-Based Energy-Balance Routing Protocol (GSTEB) is a protocol which is proposed for wireless sensor networks and is used to increase the source, channel and Destination signal strength. This protocol enhances the efficiency of the network. Among these protocols GSTEB provides higher signal strength compared to LEACH and LEACH-C.

Keywords: Wireless Sensor Network; Signal Strength; Routing Protocols

I. INTRODUCTION

A Wireless Sensor Network (WSN) has been deployed at an accelerated pace. It is reasonable to expect that whole world will be covered through the WSN in 10-15 years and access them through internet. It provides huge number of such nodes to communicate through wireless channels for information sharing as well as cooperative processing. The upcoming technologies `are built with unlimited features for numerous applications including environmental, medical, military, transportation, entertainment and smart spaces. A wireless sensor network can be referred as a group of nodes organized into a combined network. The sensor nodes are deployed randomly and densely in a targeted region. After the initial deployment of the network, sensor nodes are responsible for self-organizing an appropriate network infrastructure with multi-hop connections between sensor nodes.

Various components of a wireless sensor node includes sensing, computing, communication, actuation, and power components. These components are then incorporated on a single or multiple boards and packaged in a small number of cubic inches. A number of sensors and Analog to Digital Converters (ADC) are contained in sensing unit which are used to collect and spread environmental data. The processing unit is composed of microprocessor to store temporary data. During processing small memory storage units are used. Each node has a range between 2 to 512 kilobytes of RAM which is allocated for commercial purpose. The main function of transceiver unit is to send and receive data through a

wireless channel which is powered by batteries within the power unit.

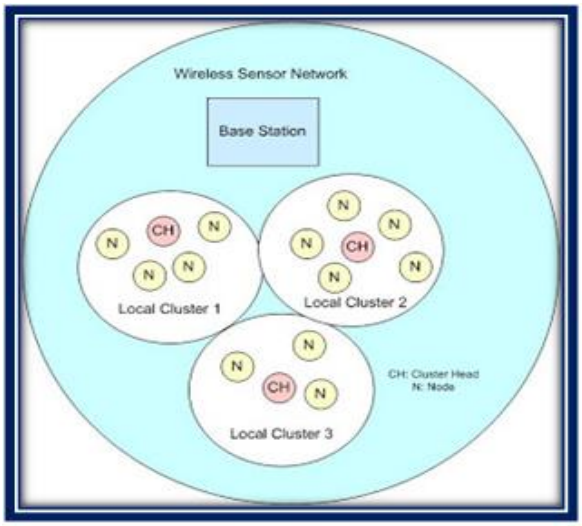

Figure 1. Architecture of WSN

Architecture of WSN is shown in Fig.1. Wireless Sensor Network comprises of a number of sensor nodes. Target node sends data to internet through Sink Node. This will broadcast to user [1]. WSNs are very useful and can be deployed to support variety of applications. These are based on growing technologies like Wireless Communication Technology, Information Technology, Semiconductors, MEMS, Micro Systems Technology, Micro-Sensors, Military Application, Health Monitoring Warehouse Management Temperature Monitoring and to check the concentration of chemicals and gases [2].

In this paper, the signal strength of LEACH, LEACH-C and GSTEB are compared. The paper is organized as follows. Section 2 describes the Methodology. In section 3 Simulation Results and discussions are presented. Section 4 concludes the paper.

II. METHODOLOGY

The Signal strength can be increased by using GSTEB protocol. This protocol is compared with LEACH and LEACH-C protocol which are used to increase the performance of the system. GSTEB protocol is based on tree structure and organizing nodes themselves automatically when signal strength decreases in root node [3].

Modules:

- Network Formation & Node Deployments
- Low Energy Adaptive clustering Hierarchal (LEACH)
- Centralized Low Energy Adaptive Clustering Hierarchal (LEACH-C)
- General Self-Organized Tree-Based Energy-Balance routing protocol (GSTEB)

A. Network Formation & Node Deployments:

Remote Sensor Network is eminent as most vital innovation in twenty-first century. A remote sensor arrangement works from huge number of sensor hubs that unite themselves to shape a remote system.Sensor hubs are in little size and battery-fueled gadgets.WSNs are utilized for some applications, for example, surge identification, home mechanization, ecological observing, woodland fire discovery and so forth. Sensor hubs are generally conveyed close to the Base station targets of enthusiasm for request to do short proximity detecting. All the sensor hubs are permitted to convey through a remote medium. The remote medium may be radio frequencies and infrared or some other medium, obviously having no wired association.

B. Low Energy Adaptive grouping Hierarchy (LEACH):

LEACH protocol is a type of hierarchical routing protocols and it is self-adaptive and self-organized in nature. LEACH protocol uses round as unit and each round is made up of cluster set-up stage and steady-state stage, for the purpose of reducing unnecessary energy costs and the steady-state stage must be much longer than the set-up stage .

i. **Set-up stage:**

In setup stage group heads are made utilizing course ask for correspondence process. Set of hubs which are not chosen as bunch head in past rounds and is later round. Hubs select themselves as CH in the interest of proposed rate and it's before record of CH. The hub that is chosen as bunch head in current round, will progress towards becoming group head again after secured all rounds. This is for uniform vitality dispersal all through the system. Chosen CHs send an ad parcel to different hubs which are not chosen as bunch go back to join their group. These hubs send joint demand to those CHs. from which they get ad parcel with most grounded flag control. After arrangement of group, CH make TDMA(Time Division Multiple Access) plan for its CM in bunch, CSMA (Carrier Sense Multiple Access) code and send TDMA plan table to its bunch individuals.

ii. **Steady state stage:**

In Steady State Phase group individuals transmits information to its CHs as per dispensed TDMA schedule openings. Bunch heads assembles information from its group individuals and totals this information to diminish measure of information that communicate to base station.

Downsides

1. LEACH does not give any thought regarding the quantity of group heads in the system.
2. Because of any reason if Cluster head passes on, the group will wind up futile in light of the fact that the information assembled by the bunch hubs could never achieve its goal i.e. Base Station [4], is the greatest drawback of LEACH.
3. Clusters are partitioned haphazardly, which brings about uneven dispersion of Clusters. For e.g. some groups have more hubs and some have lesser hubs. Some group heads at the focal point of the bunch and some group heads might be in the edge of the bunch; this wonder can cause an expansion in vitality utilization and have awesome effect on the execution of the whole system [5]

C. Centralized Low Energy Adaptive Clustering Hierarchy (LEACH-C):

Filter C is not the same as unique LEACH in bunch development yet its activity is alike unique LEACH Protocol. Drain C performs incorporated group calculation for choice of bunch heads (CHs). In LEACH-C setup stage is like unique LEACH yet Steady state stage is extraordinary. Base station (BS) gathers area information and vitality level related data from every hub. Presently base station has worldwide data of system. Base station ascertains normal hub vitality. Hubs having vitality more than normal vitality is chosen as group heads. Filter C utilize GPS or other area following strategies.

Base station sends its choice back to hubs about the selection of hubs as bunch heads. Base station communicates CHs ID(identifier) to hubs in system and hubs having the same ID are chosen as CH and the information from its group individuals utilizing TDMA plan are gathered. Concentrated LEACH utilizes a deterministic edge calculation to measure the vitality in the hub regardless of whether the hub was a bunch head in late time. The quantity of CH hubs and their position can't be guaranteed.

The focal control calculation is utilized as a part of Centralized LEACH to frame the bunches which create enhanced groups by disseminating the bunch head hubs through the system. Preferred standpoint of this convention over fundamental LEACH is the deterministic approach of picking the number of group head hubs in each round which is foreordained at the season of arrangement. Drain C causes better conveyance of bunch head hubs in the system .But LEACH-C requires current area data of all hubs utilizing GPS which isn't hearty [6] [7]

D. General Self-Organizing Tree Based Energy Balance Routing Protocol

General Self-Organized Tree-Based Energy-Balance Routing Protocol (GSTEB) [8] constructs a routing tree via a procedure in which for every single round, a root node is allocated by base station and transmits root node's choice to every nodes of sensor network. Then, every one node chooses its parent by taking into consideration simply itself as well as its neighbor's information, as a result making it a powerful protocol. It consists of four phases.

a. Initialization Phase
b. Tree constructing phase
c. Self-organized data collection and transmission
d. Information exchange phase

a. Initialization Phase:

The parameters of network are introduced in this phase. The parameters considered are such as required area, number of nodes, initial energy, radio model, packet size, maximum packet size, routing protocol and so on. Following these assumptions, Base Station (BS) sends packet to all sensor nodes in specific area to inform regarding the starting time. Each sensor nodes send its location awareness to all sensor nodes i.e., in the specific radius circle. This packet consists of node ID, Energy Level (EL) and distance of nearest nodes.

b. Tree Constructing Phase:

In tree constructing phase, each node elects parent node from its neighbors according to Energy Level (EL) and every node records its neighbors' neighbor information. The parent node is selected within the cluster by using EL. Lowest energy level nodes are acting as child nodes. These child nodes send packets to their parent node. That parent nodes send packet

to their respective CH. CH sends the packets to Base Station (BS). So distance will be reduced. EL should not be suddenly decreased.

c. Self-Organized Data Collection and Transmission:

After construction of tree, each node gathers information and it will produce data packet. The data packet of child node is send to CH through parent node. CH sends packet to Base Station. Nodes are self-organized with respect to the EL.

d. Information Exchanging Phase:

In this phase, parent node is exchanged when node exhausts its energy. After recognition of EL is reduced, the parent node exchanges in the next round of this phase. All nodes are monitoring the neighboring nodes. Automatically nodes are updating changes. It will move to next round after sending all packets.

III. SIMULATION RESULTS AND DISCUSSION

The simulation is carried out using NS2. The following Table 1 shows simulation parameter of protocols.

Number of nodes	1000*1000m
Area size	200ms
Simulation time	1118 bytes
Packet size	100 bytes
Maximum number of packets	1500
Routing protocol	LEACH, LEACH-C GSTEB
Initial energy level	20 watts
Model	Two ray model

Table 1. Simulation Parameters

IV. SIGNAL STRENGTH ANALYSIS:

Source signal strength, Channel signal strength and destination signal strength are used to evaluate the signal performance of LEACH, LEACH-C and GSTEB.

1) Source signal strength:

Fig.2 shows strength of the source over the time period. LEACH AND LEACH-C has less signal strength at source when compared to GSTEB protocol.

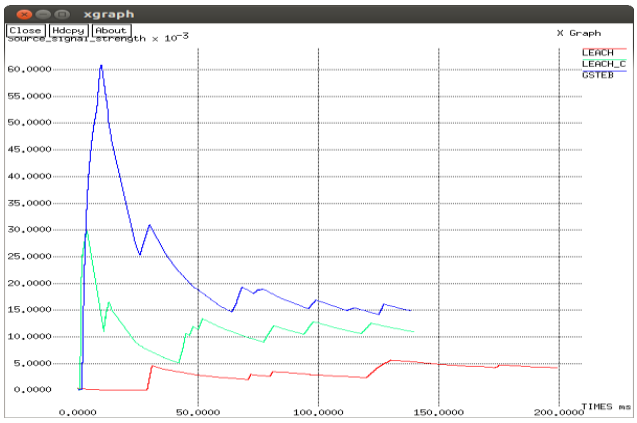

Figure. 2: Source Signal Strength Comparison

2) Channel Signal Strength:

Fig.3 shows the signal strength of the channel over the time period. LEACH AND LEACH-C has less signal strength at channel when compared to GSTEB protocol

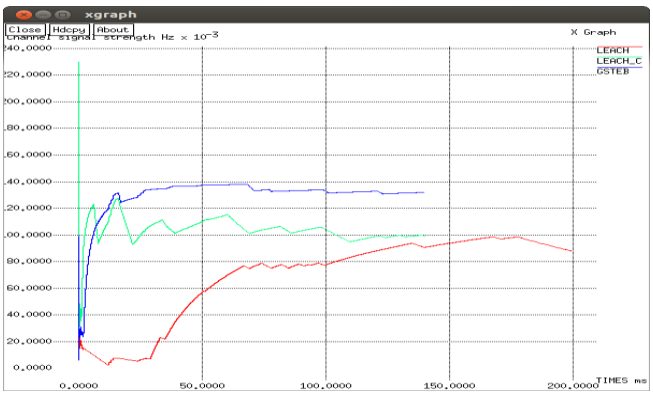

Figure 3. Channel Signal Strength Comparison

3) Destination Signal Strength:

Fig.4 shows the signal strength of the destination over the time period. LEACH AND LEACH-C has less signal strength at channel when compared to GSTEB protocol upto 75ms.

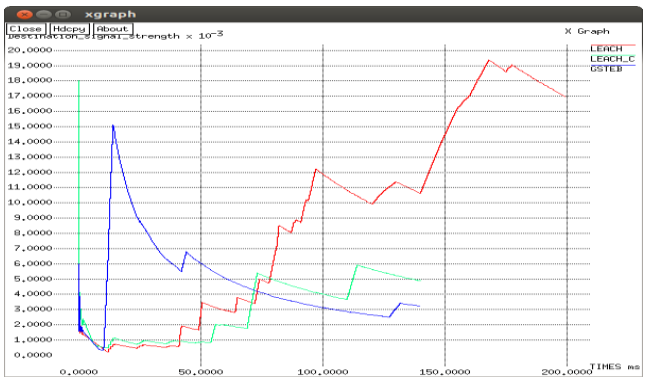

Figure 4. Destination Signal Strength Comparison

IV. CONCLUSION

The GSTEB protocol was compared with other two routing protocols (LEACH and LEACH-C). From the results obtained, it is analyzed that GSTEB provides better signal strength compared to other two protocols. Source, channel and Destination signal strength analysis are used to compare these protocols performance.

Our NS-2 simulation results show that GSTEB protocol outperforms than LEACH and LEACH-C. So we conclude that When compared , GSTEB protocol gives better performance in large area connection problem.

ACKNOWLEDGEMENT

I wish to express my sincere thanks to my Co-guide **Dr.J.Samuel Manoharan** for his guidance and suggestions. And also I extend my thanks to my family & friends who supported me to complete this paper.

REFERENCES

.

[1] Patrik Morave, Dan Komosny, Milan Simek, David Girbau, Antonio Lazaro"Energy Analysis Of Received Signal Strength Localization In Wireless Sensor Networks" Radioengineering, Vol. 20, No. 4, December 2011 "Introduction To Wireless Sensor Network," Information Processing And Routing In Wireless Sensor Networks, World Scientific Publishing Co. Pte. Ltd.

[2] "Introduction to Wireless Sensor Network," Information Processing And Routing In Wireless Sensor Networks, World Scientific Publishing Co. Pte. Ltd.

[3] Han, Zhao, Jie Wu, Jie Zhang, Liefeng Liu, and Kaiyun Tian. "A General Self-Organized Tree-Based Energy-Balance Routing Protocol for Wireless Sensor Network." (2014).

[4] Parul Kansal, Deepali KAnsal, Arun Balodi,"Compression of Various Routing Protocol in Wireless Sensor Networks", International Journal of Computer Applications Volume 5-No. 11(August 2010)

[5] M. Bani Yassein, A. AL-zou'bi, Y. Khamayseh, W. Mardini, "Improvement on LEACH Protocol of Wireless Sensor Networks", International Journal of Digital Content Technology and its Applications Volume 3- No. 2 (June 2009) http://monet.postech.ac.kr/images/introduction/image007.jpg, May 2015

[6] J.Gnanambigai, Dr.N.Rengarajan, and K.Anbukkarasi, "Leach and Its Descendant Protocols: A Survey," International Journal of Communication and Computer Technologies (IJCCT), vol. 01, issue 02, no.3, pp. 15-21, September 2012.

[7] W.Heinzelman, A.Chandrakasan, and H.Balakrishnan, "An Application-Specific Protocol Architecture for Wireless Microsensor Networks," IEEE Transaction on Wireless Communications, vol. 1, no. 4, pp. 660–670, 2002

[8] Zhao Han, Jie Wu, Member, IEEE, Jie Zhang, Liefeng Liu, and Kaiyun Tian "A General Self-Organized Tree-Based Energy-Balance Routing Protocol for Wireless Sensor Network" IEEE Transactions On Nuclear Science, Vol. 61, No. 2, April 2014

[9] X .Liu, "A survey on clustering routing protocols in wireless sensor networks." Sensors 12, no. 8 (2012): 11113-11153.

[10] Amrinder Kaur, Sunil Saini," Simulation of Low Energy Adaptive Clustering Hierarchy Protocol for WirelessSensor Network," International Journal of Advanced Research in Computer Science and Software Engineering, Volume 3, Issue7, July 2013.

[11] Ian F. Akyildiz, Weilian Su, Yogesh Sankarasubramaniam, Erdal Cayirci: "A Survey on Sensor Networks", IEEE Communication Magazine, pp. 102-114(August 2002).

[12] Rajesh Patel, Sunil Pariyani, Vijay Ukani," Energy and Throughput Analysis of Hierarchical Routing Protocol(LEACH) for Wireless Sensor

Networks", International Journal of Computer Applications Volume 20- No. 4 (April 2011)

Themed Section : Engineering and Technology
© 2018 IJSRSET | Volume 5 | Issue 3 | Print ISSN: 2395-1990 | Online ISSN: 2394-4099

A Quad-Element Frequency-Agile Pattern and Polarization Diverse Antenna Array for MIMO Applications

Yogeshwari Panneer Selvam[1], Malathi Kanagasabai[2], Gulam Nabi Alsath[3], Saffrine Kingsly[4], Sangeetha Subbaraj[5]

[1245]Department of Electronics and Communication Engineering, College of Engineering Guindy, Anna University, Chennai, Tamil Nadu, India

[3] Department of Electronics and Communication Engineering, Sri Sivasubramaniya Nadar College of Engineering, Chennai, Tamil Nadu, India

yogaindira93@gmail.com[1], mala@annauniv.edu[2], gulamnabialsathm@ssn.edu.in[3], kingsly.saffrine@gmail.com[4],sangeetha6077@gmail.com[5]

ABSTRACT

This paper presents the design of a simple frequency reconfigurable antenna. The proposed antenna comprises of a rectangular patch antenna with a rectangular slot. The regions with dense current are identified and those regions are utilized to reconfigure the frequency. The antenna performance is made agile by using three p-i-n diodes. The electrical length of the slot is varied by using the p-i-n diodes to reconfigure the application bands. The antenna resonates at 1.8 GHz, 2.4 GHz, 3.5 GHz and 5.8 GHz and finds application in GSM, Bluetooth, WiMAX and WLAN systems. The designed antenna is distributed in the horizontal plane to construct the MIMO antenna. The placement of antennas offers complementary radiation pattern resulting in patter diversity. The evaluated Cross polarization discrimination values are greater than 20 dB. This feature augments the antenna as a polarization diversity antenna. The MIMO performance metrics such as Envelope Correlation Coefficient (ECC), Diversity Gain (DG) and Mean Effective Gain (MEG) under isotropic, indoor and outdoor conditions are evaluated and presented.

Keywords: Antenna Array, Frequency Reconfigurable Antenna, MIMO, Pattern Diversity, Polarization Diversity

I. INTRODUCTION

Emerging applications require transmission and reception at high data rates. Multiple Input Multiple Output antennas fulfil such needs of communication systems by combating the destructive nature of scattering, reflection, fading and multipath propagation. Mutual coupling/Correlation between the adjacent antennas is a crucial factor to be considered as it has influence on the quality of the signal to be received and channel capacity. Increasing the isolation between the unit cells of the MIMO antenna is a mandatory requirement for the signals to be uncorrelated. A MIMO antenna having more number of unit cell radiators is more robust to the time varying channels. Locating many radiators closely in a MIMO antenna with high isolation is a difficult problem. The unit cells have to be closely placed to reduce the area occupied by the antenna and to offer a compact solution. Whereas closely packed antennas result in enhanced coupling factor.

A MIMO antenna with frequency agile characteristics is suitable candidature for time varying multipath channels. A complex environment with more obstructions and intrusions requires several transceivers operating in varying application bands at each instant. So placing more number of radiators in a MIMO antenna enhances data transmission rate and coverage area. Wireless communication applications requires antennas which cater for varying applications at each instant and with less construction complexity. Reconfigurable antennas can serve such requirements. Reconfigurable antennas integrate several radios in a single platform. Many radios are put in a single dais without employing more number of antenna components. The operation of multiple antennas can be done by a single reconfigurable antenna [1-3]. Multiple applications can be used without incrementing the area of the antenna. The antenna's performance can be made agile by using actuators like PIN Diodes, varactors, and MEMS. A MIMO antenna with polarization and pattern diversity characteristics will make the antenna more resilient to adverse channel conditions, enhances the channel capacity and coverage.

Several frequency reconfigurable antennas are reported in the literature. In [4], stepper motor is used to obtain frequency agile characteristics. U shaped slot and L shaped stub employed with MEMS is discussed in [5]. Filtering elements are designed at feed line of the antenna to tune different frequencies [6]. In some literatures, MIMO and frequency reconfiguration techniques are combined. To enhance the isolation, complex techniques are reported. MEMS switches [7], Neutralisation technique [8], EBG [9]-[10], resistive sheets [11], stacking of substrates [12] are done to reduce the mutual coupling.

In this paper, a rectangular frequency reconfigurable antenna is designed. The size of the antenna is 30 mm × 30 mm. The designed antenna operates at 1.8 GHz / 2.4 GHz / 3.5 GHz / 5.8 GHz. P-i-n diodes are utilized to make the antenna's response dynamic. The proposed antenna is then used to construct a 2 × 2 antenna array. Due to the orthogonal placement of the antenna, the obtained radiation pattern is complementary. The computed XPD values are above 20 dB. So the antenna is a pattern and polarization diversity antenna. The agile antenna can serve Global Positioning System, Bluetooth, WiMAX and WLAN applications. The proposed agile antenna array is a suitable solution for varying environments. The isolation between the radiators in the array antenna is greater than 30 dB without using any decoupling structures. The high isolation is due to the orthogonal placement of unit cell radiators. The inter-elemental spacing between the adjacent radiators is $0.125\lambda_g$. This ensures that high quality information is received. Section II presents the design of frequency reconfigurable antenna. Section III presents the construction of MIMO antenna. Section IV presents the results and discussions. Section V presents the conclusion.

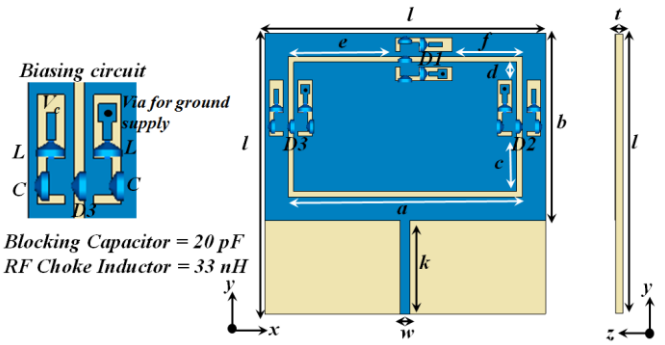

Figure 1. Proposed frequency reconfigurable antenna. (a) Front view, (b) Side view. l = 30 mm, t = 1.6 mm, w = 2 mm, k = 10 mm, a = 20 mm, b = 15 mm, c = 7.5 mm, d = 2.3 mm, e = 13 mm, f = 5 mm

II. ANTENNA DESIGN

The design of frequency reconfigurable antenna is presented in this section. The antenna consists of a low profile rectangular patch antenna with a full ground plane. Inside the patch, a rectangular slot is etched. The electrical length of the slot is dynamically

altered using the actuators. By identifying the high current accumulated region, activating/deactivating the p-i-n diodes and altering the electrical length, the required band is resonated.

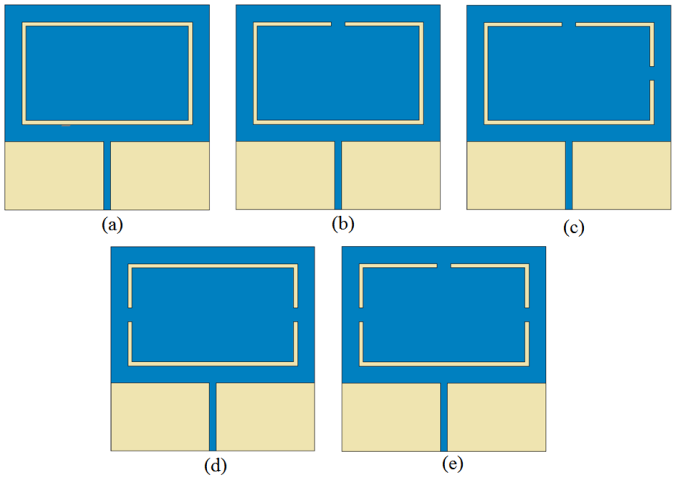

Figure 2. Different stages during the design of the proposed antenna. (a) Antenna 1 , (b) Antenna 2, (c) Antenna 3, (d) Antenna 4, (e) Antenna 5

The proposed antenna is shown in Figure 1. The proposed antenna is designed on a 1.6 mm thick FR4 substrate of loss tangent 0.025 and permittivity 4.3. The volume of the antenna is 30 × 30 × 1.6 mm^3. The performance of the antenna is made agile using 3 p-i-n diodes and the antenna has 5 operating states. The evolution of the antenna is delineated in Fig 2 and the corresponding response at each stage is shown in Fig.3

A. Frequency Reconfiguration

The frequency reconfiguration is obtained by exciting the electrical length of the different application bands in different states using p-i-n diodes. In figure 2(a), the perimeter of the rectangular slot is 70 mm (wavelength corresponding to 1.8 GHz). This slot is excited to resonate at 1. 8 GHz (GSM). This is State 1. In State 2, figure 2(b), the electrical length of the slot is made as 68 mm (wavelength corresponding to 2.4 GHz) by activating the p-i-n diode 1. Hence the Bluetooth band is excited. Then, in State 3, p-in diodes 1 and 2 are activated to adjust the electrical length of the slot as 55.5 mm (wavelength corresponding to 3. 5 GHz). So, in State 3, WiMAX band is resonated. Similarly, in State 4, to excite the WLAN band, the electrical length is made as 35 mm by activating p-i-n diodes 2 and 3. Then, in State 5, all the application bands are resonated by turning ON all the p-i-n diodes.

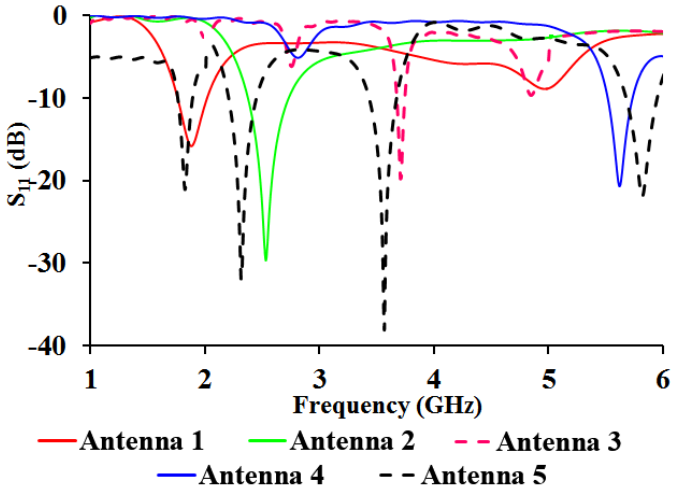

Figure 3. Reflection Coefficient Characteristics of Different Stages of Antenna during the Design of the Proposed Antenna

The different operating states of the antenna are given in Table I. The simulated reflection co-efficient characteristics are shown in Fig. 4. The results show that the antenna operates in different application bands by activating and deactivating the necessary actuators.

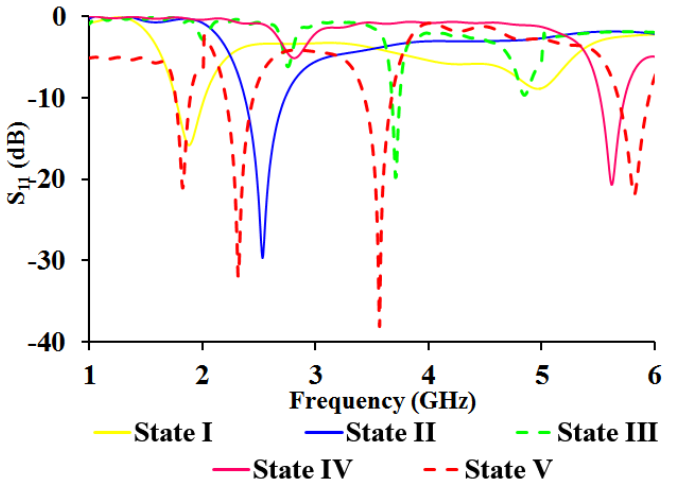

Figure 4. Reflection Coefficient Characteristics of the Proposed Antenna At Various Operating States.

TABLE I
OPERATING STATES OF THE ANTENNA

STATE	PIN DIODES			FREQUENCY
	D1	D2	D3	(GHz)
I	OFF	OF	OFF	1.8
II	ON	OFF	OFF	2.4
III	ON	ON	OFF	3.5
IV	OFF	ON	ON	5.8
V	ON	ON	ON	1.8, 2.4, 3.5, 5.8

III. IMPLEMENTATION OF QUAD ELEMENT ANTENNA ARRAY FOR MIMO TERMINALS

A planar 4-port frequency reconfigurable antenna array is implemented by orthogonally placing all the four radiators on FR4 plane of thickness 1.6 mm. The size of the FR4 plane is 70 mm × 70 mm. The edge to edge spacing between the adjacent radiators is $0.125\lambda_g$. λ_g is the guided wavelength corresponding to the lowest resonating frequency. Since four agile antennas are deployed in this antenna array, the antennas becomes more robust to the ever changing environment. The antenna array is shown in Fig 5. The isolation between the radiators is above 30 dB by placing the radiators orthogonally. The antenna does not seek the help of decoupling structures to enhance the isolation. The probability of receiving good quality signal is high because at least one agile radiator will receive signal with high SNR. This type of arrangement is resulted in a construction of polarization and pattern diversity antenna. The two properties can be related with the following features. The orthogonal arrangement lead to radiation patterns of different orientations. Polarization purity is maintained in the constructed antenna.

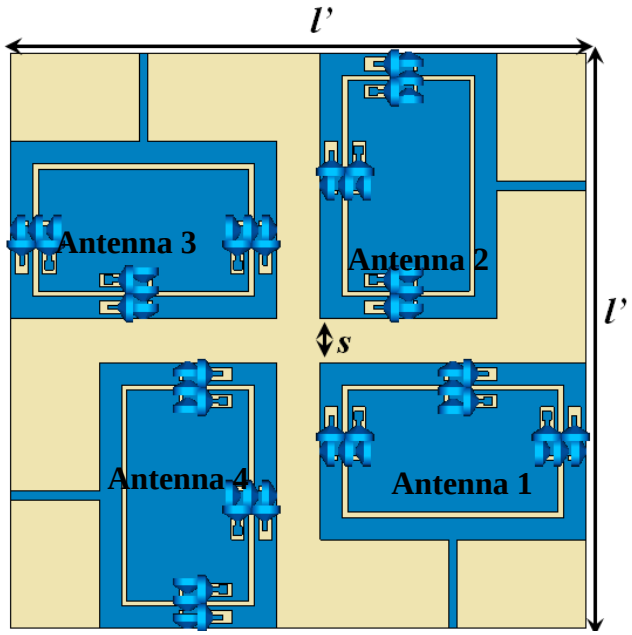

Figure 5. Proposed quad element frequency reconfigurable antenna array. (a) Front view, (b) Side view. l' = 70 mm, s = $0.125\lambda_g$.

IV. RESULTS AND DISCUSSION

All simulations were done using CST Microwave Studio 2015. The impedance, radiation characteristics and MIMO characteristics are evaluated. BAR series p-i-n diode are utilized to reconfigure the antenna. When the p-i-n diode is turned ON (forward bias), the series resistance is 2.1 Ω and series inductance is 1.8 nH. Whereas the p-i-n diode is turned OFF (reverse bias), the reverse resistance is 300 kΩ and shunt capacitance is 0.2 pF. The biasing network isolates the RF signal and DC signal. The biasing network is comprehensively designed using RF choke inductor (33 nH) and DC blocking capacitor (20 pF). At this particular value of L and C, the radiator's and bias network's characteristic impedance match. The basing lines must be of a smaller size such that the antenna's characteristics are not disturbed. The length and the thickness of the bias lines is 1 mm and 0.25 mm respectively.

A. Impedance Characteristics

The simulated S_{11} characteristics of the unit cell radiator is shown in Fig. 4. The simulated S_{11} characteristics of the antenna array is shown in Fig. 6. The bandwidth at 1.8 GHz, 2.4 GHz, 3.5 GHz and 5.8 GHz is 2.1 %, 2.2 %, 2.4 % and 3.52 % respectively.

B. Mutual Coupling Characteristics

The coupling characteristics is most important metric while designing an antenna array. Fig. 7 depicts the mutual coupling characteristics of the proposed antenna array. The inner-elemental spacing between the antennas is $0.125\lambda_g$. The coupling is obtained below -30 dB at the operating bands. Antenna 1 is the reference antenna. This reduced coupling level is because of the orthogonal placement of the antennas.

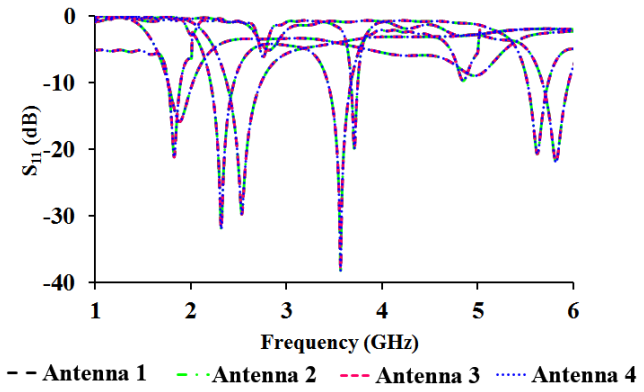

Figure 6. Reflection coefficient characteristics of the proposed antenna array

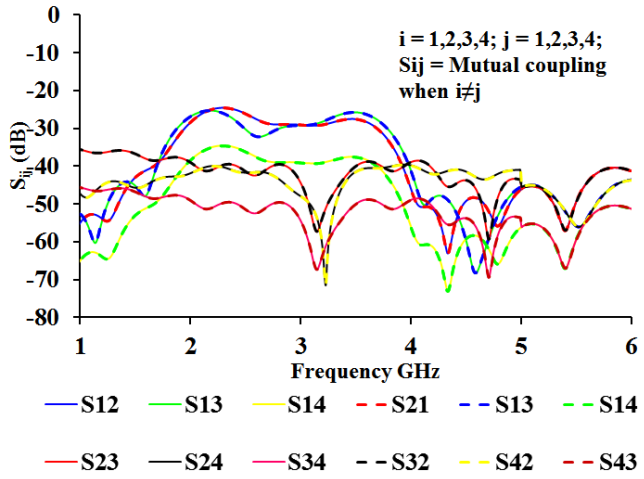

Figure 7. Mutual coupling characteristics of the proposed MIMO antenna

C. Radiation Characteristics

Table II tabulates the performance of the proposed antenna array. The radiation pattern, both xz and xy planes, are shown in Fig. 8. The simulated peak gain and percentage efficiency at State I, II, III, IV and V are 3.2 dBi & 93 %, 3.6 dBi & 80 %, 4.4 dBi & 78 %, and 5 dBi & 74 % respectively. The gain and efficiency characteristics are shown in Fig. 9. Table III tabulates the cross-polarization discrimination values. All the values are above 20 dB. This ensures the polarization discrimination between the adjacent radiators.

D. MIMO Characteristics

Envelope Correlation Coefficient (ECC) quantifies the correlation between the radiations of the antennas. ECC is given by the following far-field equation [16],

TABLE II
PERFORMANCE OF THE QUAD ELEMENT ANTENNA ARRAY

Parameter/Frequency		1.8 GHz	2.4 GHz	3.5 GHz	5.8 GHz
% BW	STATE I	2.1%	-	-	-
	STATE II	-	2.2%	-	-
	STATE III	-	-	2.4%	-
	STATE IV	-	-	-	3.52%
	STATE V	2.1%	2.2%	2.4%	3.52%
Gain (dBi)	STATE I	3.2	-	-	-
	STATE II	-	3.6	-	-
	STATE III	-	-	4.4	-
	STATE IV	-	-	-	5
	STATE V	3.2	3.6	4.4	5
Efficiency (%)	STATE I	93	-	-	-
	STATE II	-	80	-	-
	STATE III	-	-	78	-
	STATE IV	-	-	-	74
	STATE V	93	80	78	74

TABLE III

CROSS POLARIZATION DISCRIMINATION VALUES AT XZ AND XY PLANE

Frequency (GHz)	XPD(dB) (xz-plane)	XPD(dB) (xy-plane)
1.8	22	27
2.4	20	30
3.5	21	29
5.8	23	30

$$\rho_e = \frac{|\iint[\overrightarrow{F_1}(\theta,\phi).\overrightarrow{F_2}(\theta,\phi)]\,d\Omega|^2}{\iint|\overrightarrow{F_1}(\theta,\phi)|^2\,d\Omega \iint \overrightarrow{F_2}(\theta,\phi)|^2 d\Omega} \quad (1)$$

ECC between the antennas is below 0.15. This ensures less correlation is between the unit cell radiators and the antenna array is the potential choice for MIMO applications.

Similarly, Apparent Diversity Gain (ADG) and Effective Diversity Gain (EDG) are also evaluated. ADG (G_{app}) signifies the increment in the gain after adopting diversity technique. EDG (G_{eff}) takes radiation losses into account [17].

$$G_{eff} = \eta_{total} \times G_{app} = \eta_{total} \times 10 \times \sqrt{1-|\rho_e|^2} \quad (2)$$

The ADG and EDG of the proposed antenna array is greater than 9.98 dB and 7.50 dB respectively.

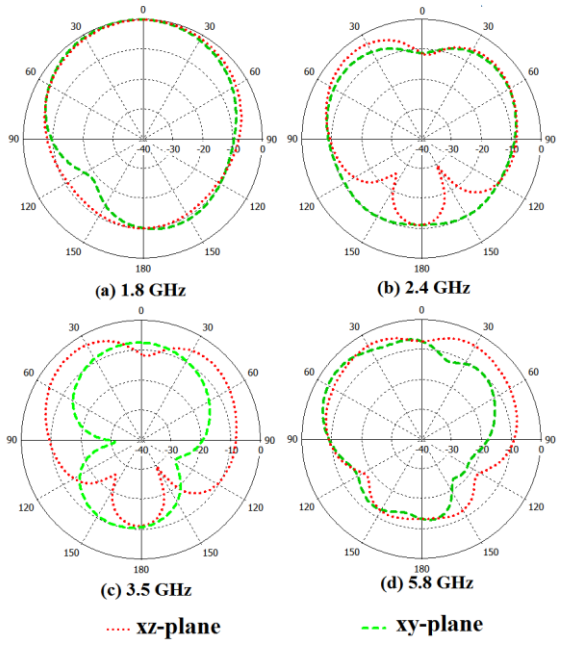

Figure 8. Simulated Radiation Pattern at Various Operating Frequencies

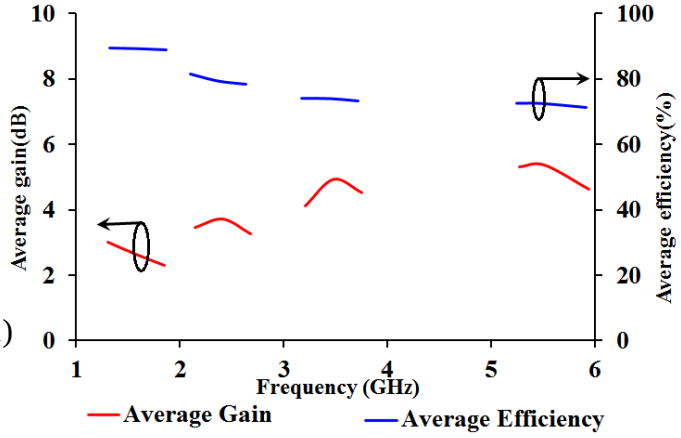

Figure 9. Simulated Average gain and Average efficiency

Mean Effective Gain (MEG) is another critical parameter to evaluate the diversity performance. The MEG difference of an array should be less than 3 dB to possess good MIMO characteristics. The estimated MEG difference between all the radiators is less than 1.3 db.

The results are evaluated in isotropic∗, outdoor∗ (XPR = 1 dB), and indoor∗ (XPR = 5 dB) scenarios. For outdoor and indoor scenarios, Gaussian power distribution for both vertical and horizontal components with mean 10° and variance 15° is assumed. In the abovementioned scenarios, the designed antenna array's performance level was good.

TABLE IV
MIMO PERFORMANCE BETWEEN ANTENNA 1 AND ANTENNA 2

Frequency (GHz)	ECC by far-field*	Isolation S_{21} (dB)	ADG* (dB)	EDG* (dB)
1.8	<0.06	>30	<10	>9.60
2.4	<0.07	>30	<9.99	>8.88
3.5	<0.12	>30	<10	>9.60
5.8	<0.15	>30	<9.98	>8.86

TABLE V
MIMO PERFORMANCE BETWEEN ANTENNA 1 AND ANTENNA 3

Frequency (GHz)	ECC by far-field*	Isolation S_{21} (dB)	ADG* (dB)	EDG* (dB)
1.8	<0.14	>30	<10	>9.38
2.4	<0.07	>30	<10	>8.86
3.5	<0.11	>30	<9.99	>8.40
5.8	<0.07	>30	<10	>7.88

TABLE VI
MIMO PERFORMANCE BETWEEN ANTENNA 1 AND ANTENNA 4

Frequency (GHz)	ECC by far-field*	Isolation S_{21} (dB)	ADG* (dB)	EDG* (dB)
1.8	.<0.13	>30	<9.99	>8.15
2.4	<0.14	>30	<9.98	>7.90
3.5	<0.14	>30	<9.98	>7.54
5.8	<0.15	>30	<9.98	>7.50

Next cumulative distribution function (CDF) [18] is calculated to validate the MIMO performance of the quad element antenna under Rayleigh channel conditions [18]. It is assumed that the receiver is exploiting Maximum Ratio Combining (MRC). The equation of MRC is (3)

$$P_{MRC}(\gamma \le x) = 1 - \sum_{i=1}^{N} \left(\frac{\lambda_i^{N-1} e^{-\frac{x}{\lambda_i}}}{\prod_{j \ne k}^{N} \lambda_i - \lambda_j} \right) \qquad (3)$$

where N is the number of unit cell radiators and λ is the value of eigen vectors acquired from the signal covariance matrix Λ_{MRC} derived using ρ_e and the equation of MEG is (4).

$$\Lambda_{MRC} = \rho_e \sqrt{MEG_i MEG_j} \qquad (4)$$

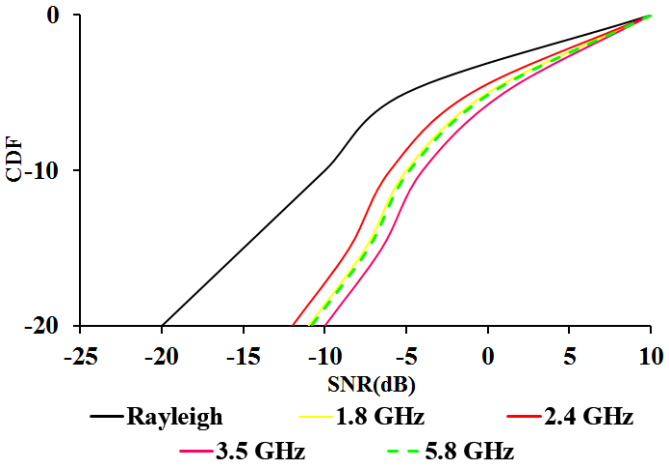

Figure 10. Cumulative Distribution Function (CDF) for the eight port antenna (a) Tri-band mode (b) UWB mode

Fig. 10 delineates the simulated curves of the CDF of the proposed quad element antenna array. With respect to the two element Rayleigh channel state, the diversity gain of the quad element antenna array in all the five states is significantly improved.

TABLE VI
COMPARISON WITH EXISTING STATE OF ART

Work	Antenna size (mm)	Reconfigu-ration	Actuators	Features		
				Frequency bands(GHz)	Gain (dBi)	η (%)
[13]	120×65	Frequency	MEMS	1.09	2.69	75-96
[14]	150×150	Frequency	PIN Diodes	2.50-2.80/ 2.40-2.96/ 1.71-1.88	3-5	55-92
[15]	80×40	Frequency	PIN Diodes	2.4/ 3.5	0.8-5	75.23-92.9
This work	70×70	Frequency	PIN Diodes	1.8/ 2.4/ 3.5/ 5.8	3.2-5	74-93

The features of the proposed antenna are the following:

1. The proposed antenna reconfigures frequency by simply, when compared to [4]-[5], utilizing PIN Diodes;
2. A low profile rectangular patch antenna is utilized for frequency reconfiguration;
3. The designed antenna reconfigures all the widely used wireless communication bands;

4. The MIMO antenna is constructed in a small area of 70 mm × 70 mm and comprises of four unit cell radiators;
5. The isolation between the radiators is above 30 dB and this isolation is achieved without using any decoupling structures;
6. The proposed MIMO antenna is constructed by placing all the four unit cells orthogonally. This helped to achieve coupling less than -30 dB with an inter-elemental spacing of $0.125\lambda_g$;
7. The proposed frequency agile MIMO antenna with pattern and polarization diversity makes the antenna more resistive to hostile environments.

V. CONCLUSION

A simple frequency reconfigurable antenna reconfiguring all the widely used communication bands is designed. The antenna makes use of low profile rectangular patch antenna. The antenna operates at 1.8 GHz, 2.4 GHz, 3.5 GHz and 5.8 GHz and finds application in GSM, Bluetooth, WiMAX and WLAN systems. The antenna's performance is made agile is using 3 p-i-n diodes. The antenna operates in 5 states. Then an array antenna is constructed by orthogonally placing four unit cells with an inter-elemental spacing of $0.125\lambda_g$. The orthogonal orientation resulted in pattern and polarization diversity antenna. The isolation between the radiators is greater than 3dB. The evaluated MIMO performance metrics such as Envelope Correlation Coefficient (ECC), Diversity Gain (DG) and Mean Effective Gain (MEG) under isotropic, indoor and outdoor conditions ensure that the proposed antenna is suitable candidature for dense MIMO applications.

REFERENCES

[1] P.-Y. Qin, Y. Guo, Y. Cai, E. Dutkiewicz, and C.-H. Liang, "A reconfigurable antenna with frequency and polarization agility," IEEE Antennas Wireless Propag. Lett., vol. 10, pp. 1373–1376, 2011.

[2] C. G. Christodoulou, Y. Tawk, S. A. Lane, and S. R. Erwin, "Reconfigurable antennas for wireless and space applications," Proc. IEEE, vol. 100, no. 7, pp. 2250–2261, Jul. 2012.

[3] Y. J. Cheng, "Substrate integrated waveguide frequency-agile slot antenna and its multibeam application," Prog. Electromagn. Res., vol. 130, pp. 153–168, Aug. 2012.

[4] Tawk, Y.; Costantine, J.; Avery, K.; Christodoulou, C.G., "Implementation of a Cognitive Radio Front-End Using Rotatable Controlled Reconfigurable Antennas," in *Antennas and Propagation, IEEE Transactions on* , vol.59, no.5, pp.1773-1778, May 2011

[5] Nikolaou, S.; Kingsley, N.D.; Ponchak, G.E.; Papapolymerou, J.; Tentzeris, M.M., "UWB Elliptical Monopoles With a Reconfigurable Band Notch Using MEMS Switches Actuated Without Bias Lines," in*Antennas and Propagation, IEEE Transactions on* , vol.57, no.8, pp.2242-2251, Aug. 2009

[6] Tawk, Y.; Costantine, J.; Avery, K.; Christodoulou, C.G., "Integrated wide-Narrowband Antenna for Muti-Standard Radio," in *Antennas and Propagation, IEEE Transactions on* , vol.59, no.7, pp.1773-1778, July 2011

[7] A. Grau, J. Romeu, M. J. Lee, S. Blanch, L. Jofre and F. De Flaviis, "A Dual-Linearly-Polarized MEMS-Reconfigurable Antenna for Narrowband MIMO Communication Systems," in *IEEE Transactions on Antennas and Propagation*, vol. 58, no. 1, pp. 4-17, Jan. 2010. 22

[8] Q. Luo, J. R. Pereira and H. M. Salgado, "Reconfigurable dual-band C-shaped monopole antenna array with high isolation," in *Electronics Letters*, vol. 46, no. 13, pp. 888-889, June 24 2010. 23

[9] Fan Yang and Y. Rahmat-Samii, "Microstrip antennas integrated with electromagnetic band-gap (EBG) structures: a low mutual coupling design for array applications," in *IEEE*

Transactions on Antennas and Propagation, vol. 51, no. 10, pp. 2936-2946, Oct. 2003. 24

[10] B. Liang, B. Sanz-Izquierdo, E. A. Parker and J. C. Batchelor, "A Frequency and Polarization Reconfigurable Circularly Polarized Antenna Using Active EBG Structure for Satellite Navigation," in *IEEE Transactions on Antennas and Propagation*, vol. 63, no. 1, pp. 33-40, Jan. 2015. 25

[11] E. Yetisir, C. C. Chen and J. L. Volakis, "Low-Profile UWB 2-Port Antenna With High Isolation," in *IEEE Antennas and Wireless Propagation Letters*, vol. 13, no. , pp. 55-58, 2014. 26

[12] M. N. Osman, M. K. Abdul Rahim, M. R. Hamid, M. F. M. Yusoff and H. A. Majid, "Compact Dual-Port Polarization-Reconfigurable Antenna With High Isolations for MIMO Application," in *IEEE Antennas and Wireless Propagation Letters*, vol. 15, no. , pp. 456-459, 2016. 27

[13] R. Hussain and M. S. Sharawi, "Integrated reconfigurable multiple-input–multiple-output antenna system with an ultra-wideband sensing antenna for cognitive radio platforms," in IET Microwaves, Antennas & Propagation, vol. 9, no. 9, pp. 940-947, 6 18 2015.

[14] A. N. Kulkarni and S. K. Sharma, "Frequency Reconfigurable Microstrip Loop Antenna Covering LTE Bands With MIMO Implementation and Wideband Microstrip Slot Antenna all for Portable Wireless DTV Media Player," in IEEE Transactions on Antennas and Propagation, vol. 61, no. 2, pp. 964-968, Feb. 2013.

[15] Jin, Z.-J.; Lim, J.-H.; Yun, T.-Y., "Frequency reconfigurable multiple-input multiple-output antenna with high isolation," in Microwaves, Antennas & Propagation, IET , vol.6, no.10, pp.1095-1101, July 17 2012

[16] M. Schwartz, W. R. Bennett, and S. Stein, *Communication System and Techniques*. New York, NY, USA:McGraw-Hill, 1965, pp.470-474.

[17] H. S. Singh, B. R. Meruva, G. K. Pandey, P. K. Bharti, and M. K. Meshram, "Low mutual coupling between MIMO antennas by using two folded shorting strips," Prog.Electromagn. Res. B. vol. 53. pp. 205-221, Jul. 2013.

[18] G. N. Alsath *et al*., "An Integrated Tri-band/UWB Polarization Diversity Antenna for Vehicular Networks," in *IEEE Transactions on Vehicular Technology*.

Themed Section : Engineering and Technology
© 2018 IJSRSET | Volume 5 | Issue 3 | Print ISSN: 2395-1990 | Online ISSN : 2394-4099

Biometric Authentication of Age and Gender prediction using GREYC Keystroke Dynamics Dataset

R. Abinaya[1], Dr. AN. Sigappi[2]
Research scholar[1], Associate Professor[2]
Department of computer Science and Engineering, Annamalai University, Chidambaram, TamilNadu, India

ABSTRACT

Keystroke dynamics allows to authenticate individuals through their way of typing on a computer keyboard. In this study, this paper interested in static shared secret keystroke dynamics (all the users type the same password). It can be combined with passphrases authentication resulting in a more secure verification system. This paper presents a new soft biometrics information which can be extracted from keystroke dynamics patterns: The Age and gender of the user when he/she types a given password or passphrase on a keyboard. This experiments were conducted on a web based keystroke dynamics database of 118 users and our experiments on keystroke authentication it exploits the features from 2D Discrete wavelet transformation (DWT) to characterize the keystroke dynamics, and provides results from classification algorithms. BPNN classifier it obtained best results achieved were 86.2% accuracy respectively.

Keywords: Biometrics, keystroke dynamics, Soft biometrics, authentication, Back Propagation Neural Network (BPNN), Discrete Wavelet Transforms (DWT).

I. INTRODUCTION

Keystroke dynamics is an interesting and a low cost biometric modality as it enables the biometric system to authenticate or identify an individual based on a person's way of typing a password or a passphrase on a keyboard [1], [2]. It belongs to the class of behavioral biometrics, in the sense that the template of a user reflects an aspect of his/her behavior. Among the behavioral biometric modalities, we can mention signature analysis, gait recognition, voice recognition, or keystroke dynamics. Generally speaking, the global performances of keystroke dynamics based authentication systems are lower than the popular morphologic modalities based authentication systems (such as fingerprints, iris, *etc*...) [3]. Besides, the main advantage of resorting to keystroke dynamics [4], [5] to authenticate a user relies in its low cost. Indeed, for this modality, no extra sensor is required. The fact that the performances of keystroke dynamics are lower than other standard biometric modalities can be explained by the variability of the user's behavior. One solution to cope with this variability is to study soft biometrics, first introduced by Jain *et al.* in [6]. In this paper "*soft biometric traits*" are defined as "*characteristics that provide some information about the individual, but lack the distinctiveness and permanence to sufficiently differentiate any two individuals*". For example, Jain *et al.* consider gender, ethnicity, and height as complementary data for a usual fingerprint based biometric system.

Soft biometrics allows a refinement of the search of the genuine user in the database, resulting in a

computing time reduction. For example, if the capture corresponds to a male according to a soft biometric module, then, the standard biometric authentication system can restrict its research area to male users, without considering female ones.

Concerning keystroke dynamics, an original approach is presented in the work of Epp *et al.* [7], strongly linked with the behavioral feature of keystroke dynamics. The authors show that it is possible to detect the emotional state of an individual through a person's way of typing. In this case, detecting anger and excitation is possible in 84% of the cases. Gender recognition is dealt in the work of Giot *et al.* in [8]: they show that it is possible to detect the gender of an individual through the typing of a fixed text. The gender recognition rate is more than 90% and the use of this information in association to the keystroke dynamics authentication, reduces the Equal Error Rate (EER) by 20%. The work of Syed-Idrus *et al.* [9] show that it is possible to detect users' way of typing by using one finger (i.e. one hand) and more than one fingers (i.e. two hands) with 80% correct recognition accuracy performed on a dataset with three passwords.

The objective of this paper is twofold. First, we present a new data collection of 118 users. This propose an extended study of soft biometrics for keystroke dynamics on this Greyc database. We are interested in the criteria that can influence the way of typing of the users. We test if it is possible to predict if the user:

1. is a male or a female?
2. belongs to a particular age category

Indeed, predicting these soft features may help an authentication system (which is not considered here) to reduce the computing burden while in search of the genuine user in the database. This paper is organized as follows. Section 2 is devoted to the description of the proposed methodology: the characteristics of the database are described, together with the data collection process, and the tools that are used for analysis purposes. In Section 3, we present the obtained results while Section 4 presents the conclusions and the future works to be addressed.

II. Proposed work of Keystroke dynamics dataset for predicting age and gender category:

In this project, the authentication of person by keystroke dynamics by Greyc Web Based Keystroke Dynamics Dataset they proposed 2D-DWT feature Transformation BPNN classifier to predict the age and gender category of the users.

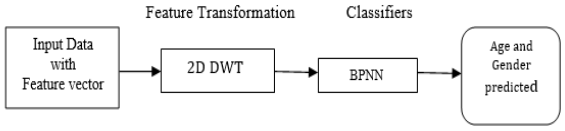

Fig.1: Flow Chart of Proposed Research Work

A. Dwt: 2d (Discrete Wavelet Transforms)

The decomposition is applied at different levels repeatedly on low frequency channel (LL) to obtain next level decomposition. The image is decomposed into four subbands LL, LH, HL, and HH subbands by applying 2D DWT on keystroke dynamics data passphrases [10]. The LL subband corresponds to low frequency components of an image and HL, LH and HH are high frequency components of a passphrases corresponds to vertical, horizontal and diagonal subbands respectively. The LL subband we obtain is half the original data. Figure 2 shows the typing speed passphrases decomposition based on wavelet scales [11], [12] 2D DWT gives dimensional reduction for less computational complexity, insensitive feature extraction, and multiresolution data approximation. The transform decomposes a typing passphrase and hence different facial expressions are attenuated by removing high frequency components. Wavelet coefficients are obtained by convolving a target

function with wavelet kernels and mathematically DWT [10]

The 2-D-DWT binary-tree decomposition. For each level, the input signal is filtered along rows and the resulted signal is filtered along columns [20]. In this way, the 2-D decomposition of an input signal, with columns and rows, is described by the following equations:

High frequency coefficient of decomposition of level j are computed as follows:

$$L_{J+1}[n] = \sum_{i=0}^{N_{L-1}} w[i] \times L_J[2_{n-i}] \quad (3)$$

$$H_{J+1}[n] = \sum_{I=0}^{N_{L-1}} h[i] \times L_J[2_{n-1-i}] \quad (4)$$

When j= {0,1…...L-1}, n= {0,1…N/2 $^{j+1}$-1} and $L_O[n]=1N[n]$

The 2D-DWT binary tree decomposition is illustration in the figure for each level the input signal is filtered along columns. In this way the 2D decomposition of an input signals 1N[M][N], with M columns and N rows is described by the following equation [17]. $L_{j+i}[row][m] = \sum_{I=0}^{N_{L-1}} w[i] \times LL_j[row][2m - i]$ (5)

$$H_{j+i}[row][m] = \sum_{I=0}^{N_{L-1}} h[i] \times LL_j[row][2m - 1 - i] \quad (6)$$

$$LL_{j+i}[n][col] = \sum_{I=0}^{N_{L-1}} w[i] \times L_j[2n - i][col] \quad (7)$$

$$LH_{J+1}[n][col] = \sum_{I=0}^{N_{H-1}} h[i] \times L_J[2n - 1 - i][col] \quad (8)$$

$$HL_{j+1}[n][col] = \sum_{i=0}^{N_{L-1}} w[i] \times H_j[2n - i][col] \quad (9)$$

$$HH_{j+1}[n][col] = \sum_{i=0}^{N_{H-1}} h[i] \times H_J[2n - 1 - i][col] \quad (10)$$

Where j={0,1…..L-1),row = {0,1….N/ $2^j - 1$ },m={0,1…M/ $2^{j+1} - 1, col = \{0,1 \ldots N/2^{j+1}$ -1}, n= {0,1…N/2^{j+1}-1},and $LL_0[n][m]$.

In the rest of this document, we use the term layer to indicate both intermediate and output signals, while level is used for each decomposition stage. In the rest of this document, we use the term layer to indicate both intermediate and output signals while level is used for each decomposition stage [13], [14].

Learning in a multilayer network proceeds the same way as for a perceptron. a training set of input patterns is presented to the network that networks computes to its output pattern and if there is an error Origin other words a difference between actual and desired output patterns – the weights are adjusted to reduce this error

In a back-propagation neural network, the learning algorithm has two phases.

- First, a training input pattern is presented to the network input layer. The network propagates the input pattern from layer to layer until the output pattern is generated by the output layer.
- If this pattern is different from the desired output, an error is calculated and then propagated backwards through the network from the output layer to the input layer. The weights are modified as the error is propagated.

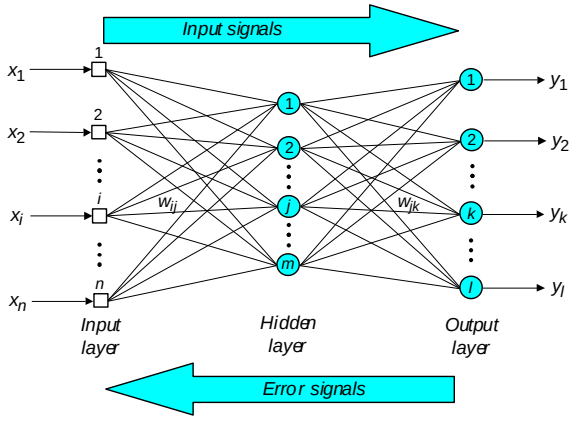

Fig: no.2 Three-layer back propagation neural network:

Step 1: initialization.

Set all the weights and threshold levels of the network to random numbers uniformly distributed inside a small range:

$$\left(-\frac{2.4}{F_I}, +\frac{2.4}{F_I}\right) \quad (12)$$

where F_i is the total number of inputs of neuron i in the network. The weight initialization is done on a neuron-by-neuron basis.

Step 2: Activation

Activate the back-propagation neural network by applying inputs $x_1(p)$, $x_2(p)$, $x_n(p)$ and desired outputs $y_{d,1}(p)$, $y_{d,2}(p)\ldots$, $y_{d,n}(p)$.

(*a*) Calculate the actual outputs of the neurons in the hidden layer:

$$y_j(p) = \text{sigmoid}\left[\sum_{i=1}^{n} x_i(p) \cdot w_{ij}\right](p) - \theta_j \quad (13)$$

where n is the number of inputs of neuron j in the hidden layer, and sigmoid is the *sigmoid* activation function.

Step 2: Activation (continued)

(*b*) Calculate the actual outputs of the neurons in the output layer**:**

$$y_k(p) = sigmoid\left[\sum_{j=1}^{m} x_{jk}(p).w_{jk}(p) - \theta_k\right] \quad (14)$$

where m is the number of inputs of neuron k in the output layer.

Step 3: Weight training

Update the weights in the back-propagation network propagating backward the errors associated with output neurons.

Calculate the error gradient for the neurons in the output layer

$$\delta_k(p) = y_k(p).[1 - y_k(p)].e_k(p) \quad (15)$$

$$e_k(p) = y_k(p).[1 - y_k(p).e_k(p)] \quad (16)$$

Calculate the weight corrections

$$\Delta w_{jk}(p) = \alpha.y_j(p).\delta_k(p) \quad (17)$$

Update the weights at the output neurons

$$w_{jk}(p+1) = w_{jk}(p) + \Delta w_{jk}(p) \quad (18)$$

Step 3: Weight training (continued)

Calculate the error gradient for the neurons in the hidden layer:

$$\delta_j(p) = y_j(p).\left[1 - y_j(p)\right] \times \sum_{k=1}^{1} \delta_k(p) w_{ij}(p)$$

$$\Delta w_{ij}(p) = \alpha.x_i(p).\delta_j(p)$$

$$\Delta w_{ij}(p+1) = w_{ij}(p) + \Delta w_{ij}(p) \quad (19)$$

Step 4: Iteration

Increase iteration p by one, go back to *Step 2* and repeat the process until the selected error criterion is satisfied.

B. Modelling Technique:

Recognition of Age and Gender Category by Keystroke Dynamics of 2d-Dwt Features with BPNN Classifier:

In BPNN classifier the Different letter password data are obtained from the dataset here 255 dimensions with 5 persons the input features are converted in to 1664 features by using 2D DWT transformation.in BPNN 20 hidden layer size with 70 training set and 30 testing for classification process getting 4class output. By different length of password for each user each layers trained the values as feed forward process. hence by BPNN the iteration value is 100 and the 4 output is Male >20 obtained 87, the male <20 obtained 86% female>20 is 87 and female<is 87 respectively by these four age and gender category male <hast highest accuracy rate by 2 hidden layers with 118 no of users as input.

Table .1: BPNN –classifier in different password data results

BPNN Classifier	TPR	FPR	Accuracy	Error detection
male above 20	86.26	13.74	87.23	87.23
Male below 20	86.24	13.76	86.53	86.53
Female above 20	86.7	13.3	87.45	87.45
Female below 20	86.17	13.83	87.45	87.45

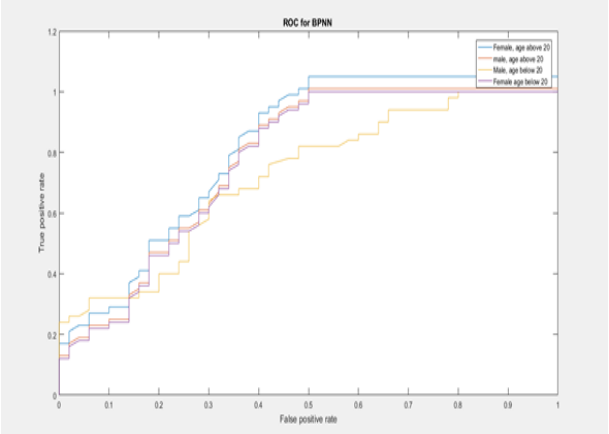

Fig. no: 3 ROC CURVE OF BPNN –classifier in different password data results

The above chart describes the different dimension level by DCT, 2D-DWT accuracy rate with various classifiers. Hence the performance matrix shown by the ROC curve.

III. Experimental Results and Discussion:

A. Dataset description:

The dataset is stored in files organized per directory for user the 'user' directory contains one file per user named user/user_xxx.txt, with xxx the id of the user [15],[16] Each user file contains the following information (one information per line) the login of the user, the name of the user, the gender of the user, age of the user

Login and name are chosen by the user during the first session. gender and age are filled during the account creation.

Common passphrases:

The 'passphrases' directory contains the inputs when the users typed the imposes login and password. There is a sub – dataset similar to all the public benchmarks: all the users type the same login and password. Samples of each user are stored in a directory name 'passphrases \user.xxx' where 'xxx' is the user id. The samples folder name is based on the timestamp of the sample. The list of the sample is presented in the text file named 'passphrases\user.xxx\captures.txt.\'. each line is the folder name of one sample. the index file is ordered by chronological order. unique password.

The password directory contains the inputs of the sub-dataset where each user possesses his own login and password. The genuine and imposter samples of user xxx are stores in the folder password and are indexed by password\user.xxx\genuine\capture.txt. the genuine samples folder nemesis based on the timestamp of the sample. Folder password\user.xxx\imposter contains the list of imposter samples (other users trying to impersonate xxx). the samples are indexed in passwords\user.xxx\imposter\captures.txt. the imposter samples folder name is based on the id of the imposter and the timestamp of the samples. thus, passwords\user_001\imposter \imposter_002_2010-10-18711:39:14 if the sample of an imposter wanting to impersonate user 001.sample representation. Each sample is stored in a folder containing meta-data, raw data (in order to let researchers to compute their own extracted features), extracted features commonly used in the literature.

Here is the display each file

UserAgent.txt: the user agent string of the web browser used to type (can be used to analyses the browser habits of the user)

Userid.txt: the id of the user who have typed the text

Data.txt: the acquisition date of the samples

Genuine .txt: A file containing 1for a samples typed by the user and 0 for a sample typed by an imposter

Login.txt: The string of the login

Password.txt: the string of the password

1_raw_press.txt: The press events of the login. one event per line with: the code of the key, the timestamp of event.

1_raw_release.txt: the release events of the login .one event per line with: the code of the key, the timestamp of the event.

P_raw_press.txt: The press events of the password. one event per line with: the code of the key, the timestamp of the event.

P_raw_release.txt: the release events of the password. One event per line with: the code of the key, the timestamp of the event.

1_pp.txt: the extracted press to press time of the login.

1_pr.txt: the extracted press to release time of the login.

1_rp.txt: the extracted release to press tie of the login

1_rr.txt: the extracted release to release tie of the login

1_release_codes.txt: the list of codes of key released.

1_total.txt: the total typing time of the login

P_pp.txt: the extracted press to press time of the password

P_rp.txt: the extracted release to press time of the password

P_rr.txt: the extracted release to release time of the password

P_release_codes.txt: list of codes of key release

P_total.txt: the total typing time of the password

Table .2: Dataset Description

NB of users:	118
NB of genuine sample:	9 087
NB of impostor samples:	10 043
NB of imposed samples:	9346

Table .3: Repartition of samples

User	118 Users
Gender	86 males 17 females
Age Category **(between 16 and 35 years old)**	≥ 20 years old (81men, 16 women); ≤ 20 years old (5 men, 1 women)

For the creation of the biometric database, some experimentation tools are required such as a laptop; two external keyboards (French keyboard for users in France and Norwegian keyboard for users in Norway) i.e. AZERTY and QWERTY, respectively; and an application to collect the keystroke dynamics data. The location and position of the hardware are in a fixed position and immoveable throughout the session for the authenticity of the outcomes. According to experts, the best password is a sentence [3]. Hence, for the purpose of this study for keystroke dynamics, we present 5 passphrases as shown in Table 2, which are between 17 and 24 characters (including spaces) long, chosen from some of the well-known or popular names or artists (known both in France and Norway), denoted P_1 to P_5. We asked all of the participants to type these 5 different passphrases 20 times. We use the GREYC Keystroke software [5] to capture biometric data. A screenshot of this software is shown in Figure 1. We define two classes of the way of typing; gender category; age category denoted as C_1 and C_2, respectively as follows:

Gender: C_1 = Male; C_2 = Female.

Age: C_1 = ≥20 years old; C_2 = ≤ 20years old.

The data that we had obtained from the 5 passphrases as listed in Table 2 are keystroke dynamics data, as mentioned earlier in the article. Keystroke dynamics data consist of information containing a field of four timing values namely: the timing pressure of when the two buttons are pressed (*ppTime*); the timing release of when the two buttons are released (*rrTime*); the timing of when one button is released and the other is pressed (*rpTime*) that is the latencies between keystrokes; and the timing of when one button is pressed and the other is released (*prTime*) that is the time durations of keystrokes [5,6]. These data however, do not match exactly to the durations and latencies of keys because their ordering is based on time and not key code [5]. We use the keystroke template *vector*, which is the concatenation of the four mentioned timing values to perform our data analysis by classifying two classes for each category

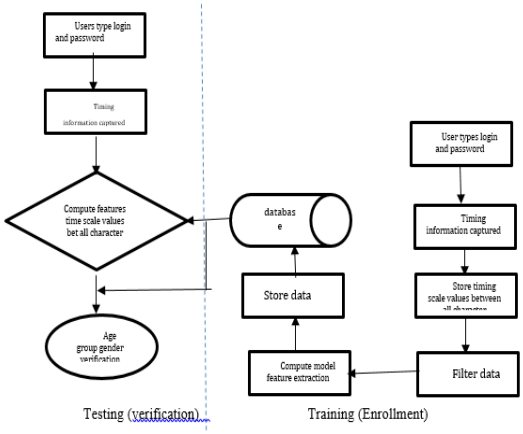

Fig.4: workflow diagram of age and gender prediction

B. Performance calculation:

The execution of a biometric framework is by and large described by the receiver operating characteristic (ROC) It can be condensed by the equal error rate (EER), the point on the bend where the false acceptance rate (FAR)and false rejection rate (FRR) are equivalents. Other framework assessment criteria incorporate productivity, flexibility, convenience, and comfort. Performance measures the execution of a biometric framework as far as procurement and recognizing error.

The end goal to assess the execution of a biometric framework, we by and large need a test benchmark and execution measurements. As per the International Organization for Standardization ISO/IEC 19795-1, the execution measurements are partitioned into three sets: Acquisition execution measurements, for example, the Failure-To-Enroll rate (FTE). Check framework execution measurements, for example, the Equal Error Rate (EER). Identification framework execution measurements, for example, the False-Negative and the False-Positive Identification Rates (FNIR and FPIR, separately).

Effectiveness: Effectiveness shows the capacity of a technique to accurately separate genuine and imposter. Execution pointers utilized by the inquires about are compressed as take after.

False Rejection Rate (FRR) refers to the rate proportion between erroneously denied honest to genuine clients against the aggregate number of authentic clients getting to the system. Once in a while known as False Nonmatching Rate (FNMR) or sort 1 error. A lower FRR infers less rejection rate and less access by genuine users. False Acceptance Rate (FAR) is characterized as the rate proportion between dishonestly acknowledged unapproved clients against the aggregate number of intruders getting to the framework. Terms, for example, False Match Rate (FMR) or sort 2 blunder alludes to a similar significance. A littler FAR shows an imposter accepted Equal Error Rate (EER) is utilized to decide the general exact accuracy and in addition a similar estimation against different frameworks. It might be here and there referred for as Crossover Error Rate (CER). Result examination depicted in the following segment will basically be express with FAR, FRR, and EER

$$FRR = \frac{Number\ of\ refused\ genuines}{Total\ no\ of\ genuines}$$

$$FAR = \frac{Number\ of\ Accepted\ imposter}{Total\ no\ of\ imposter}$$

Where P represents positive rate and N represents Negative rate, to predict accuracy =(tp+tn)/Sensitivity =tp_rate; specificity = tn_rate precision =tp/(tp+p); if f measure calculates = 2*(precision*recall)/(precision).

Table.4: performance calculation

Classification	True positive rate	False positive rate	recall	F-measure	Accuracy
male above 20	86.1	13.8	91.1	88.5	87.23
Male below 20	86.6	13.3	86.6	86.6	86.53
Female above 20	87.5	12.5	87.5	87.5	87.45
Female below 20	82.3	17.6	93.3	87.5	87.45

Classifiers Results:

We had performed several simulations with BPNN for computations on three different aspects of the data. The first results deal with the averaged (over 100 iterations) recognition rates for the four soft categories for different percentage of training data, from 1% to 90%. Then these results are completed by confidence intervals computation, based on a re-sampling and shuffling of the data.

Gender Recognition

The results of the recognition rates on different learning ratios with males (C_1) and females (C_2) for passphrases P_1 to P_3. The recognition rate, depending on the considered passphrase, is between 85to 95% for a ratio over or equal to 50%.

Age Category Recognition

The results of the recognition rates on different learning ratios age category for passphrases P_1 to P_3. The obtained recognition rate tends to vary more than for other soft categories, but stays between 85% and 90%, which are nevertheless quite good results.

IV. Conclusions and future work:

In this paper, we propose a new soft biometric approach for keystroke dynamics. It consists of predicting the user's way of typing by defining the gender, the age category whereby the 92% results were obtained. Another part of this work is the creation of a substantial database, with 118users, from France and Norway, with 100 samples per user. The obtained results could be used as a reference model to assist the biometric system to better recognize a user by a way he/she types on a keyboard. Hence, it would strengthen the authentication process by hindering an impostor trying to enter into the system. Having made a face image capture during the data collection session, we also plan to exploit the facial image capture to further enhance the performances by using a fusion method as our future work. Another work in progress consists in studying the fusion of several soft categories, to enhance the recognition.

V. REFERENCES

[1] Giot, R., El-Abed, M., Rosenberger, C." Greyc keystroke: a benchmark for keystroke dynamics biometric systems" IEEE Computer Society (2009)

[2] Giot, R., El-Abed, M., Rosenberger, C. "Keystroke dynamics overview" In Yang, D.J.,

ed.: Biometrics /Book 1. Volume 1. InTech 157–182, (July 2011)

[3] Junhong Kim, Haedong Kim, Pilsung Kang "Keystroke dynamics-based user authentication using freely typed text based on user-adaptive feature extraction and novelty detection" Applied soft computing, Elsevier, School of Industrial Management Engineering, Korea University, Seoul, South Korea, (2017)

[4] R. Joyce, G. Gupta, "Identity authentication based on keystroke latencies", Commun. ACM 33 ,Pg. No, 168–176. (1990)

[5] P. Kang, S. Park, S. Hwang, H.j Lee, S. Cho, "Improvement of Keystroke Data Quality Through Artificial Rhythms and Cues", Computers & Security, 27, pp. 3–11., (2008)

[6] Jain, A., Dass, S., Nandakumar, K.: "Soft biometric traits for personal recognition systems. In: Proceedings of International Conference on Biometric Authentication", (2004)

[7] Epp, C., Lippold, M., Mandryk, R." Identifying emotional states using keystroke dynamics. "In: Proceedings of the 2011 annual conference on human factors in computing systems., pg. No-715–724., (2011)

[8] Giot, R., El-Abed, M., Rosenberger, C.: Keystroke dynamics overview. In Yang, D.J., ed.: Biometrics / Book 1. Volume 1. InTech., pg.no 157–182, (July 2011)

[9] Syed-Idrus, S.Z., Cherrier, E., Rosenberger, C., Bours, P." A preliminary study of a new soft biometric: finger recognition for keystroke dynamics". In: 9th Summer School for Advanced Studies on Biometrics for Secure Authentication: Understanding Man Machine Interactions in Forensics and Security Applications. June 11-15 (2012)

[10] Nikos D. Zervas, Giorgos P. "Evaluation of Design Alternatives for the 2-D-Discrete Wavelet Transform" IEEE Transactions of circuit and systems and video Technology" volume 11, no.,12, December 2001

[11] M. Vishwanath, R. M. Owens, M. J. Irwin, "VLSI architectures for the discrete wavelet transform," IEEE Trans. Circuits Syst. II, vol. 42, pp. 305–316, May 1995.

[12] J. T. Kim et al., "Scalable VLSI architectures for lattice structure-based discrete wavelet transform," IEEE Trans. Circuits Syst. II, vol. 46, pp. 1031–1043, Aug. 1998.

[13] C. Chakrabarti, M. Vishwanath, and R. M. Owens, "Architectures for wavelet transform: A survey," J. VLSI Signal Processing, vol. 4, pp.171–192, 1996.

[14] P. Wen-Shiaw and L. Chen-Yi, "An efficient VLSI architecture for separable 2-D discrete wavelet transform," in Proc. 1999 Int. Conf. Image Processing (ICIP99), vol. 2, pp. 754–758, Oct. 1999

[15] Syed zulkarnain, syed Idrus , Christophe Rosenberger " soft biometrics Database :A Benchmark for keystroke dynamics biometric system" conference paper "researchgate.net/publication/261040398., January 2013

[16] Romain Giot, Mohamad EL-Abed and Christophe Rosenberger, "Web-Based Benchmark for Keystroke Dynamics Biometric Systems:" A statistical Analysis", by published in the proceedings of the IIHMSP, Conferences 2012

Themed Section : Engineering and Technology
© 2018 IJSRSET | Volume 5 | Issue 3 | Print ISSN: 2395-1990 | Online ISSN : 2394-4099

Eliminating Grid Side Converter and Using Solid State Transformer In Wind Energy Conversion System

V. Devi Priya[1], Dr. Nishat Kanvel[2]

[1]Applied Electronics, Department Of Electronics And Communication Engineering, Thanthai Periyar Government Institute of Technology Vellore , Tamilnadu, India

[2]Associate Professor, Department Of Electronics And Communication Engineering, Thanthai Periyar Government Institute of Technology, Vellore Tamilnadu, India

ABSTRACT

In wind energy conversion systems, the fundamental frequency step-up transformer acts as a key interface between the wind turbine and the grid which creates the power losses in the system. Recently, there have been efforts to replace this transformer by an advanced power electronics based solid-state transformer (SST). This paper proposes a configuration that combines the doubly fed induction generator (DFIG) based wind turbine and SST operation. The main objective of the proposed configuration is to interface the turbine with the grid while providing enhanced operation and performance. In this work, SST controls the active power to/from the rotor side converter (RSC), thus, eliminating the grid side converter (GSC). The proposed system meets the recent grid code requirements of wind turbine operation under fault conditions. Additionally, it has the ability to supply reactive power to the grid when the wind generation is not up to its rated value. A detailed simulation study is conducted to validate the performance of the proposed configuration.

Keywords : Solid State Transformer ,doubly fed induction generator ,power electronic transformer ,fault ride through.

I. INTRODUCTION

Over the last decade, the penetration of renewable energy sources has been increasing steadily in the power system. In particular, wind energy installations have grown rapidly with global installed capacity increasing from 47.6 GW in 2004 to 369.6 GW[2]. Amongst the many technologies that exist for wind energy conversion systems (WECS), doubly fed induction generators (DFIG) have been prevalent due to variable speed operation[1], high power density and lower cost. DFIG based WECS consist of an induction generator whose stator is directly connected to the grid while its rotor is connected via back to back converters known as the rotor side converter (RSC) and grid side converter (GSC), respectively.

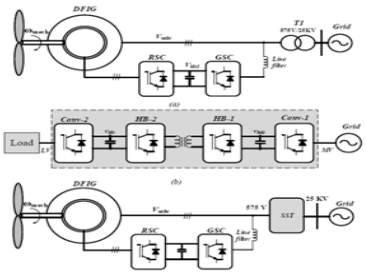

FIG:DFIG with RSC and GSC

The generator is normally operated at a range of 500 V- 700 V and is connected to the transmission network (11-33 kV) through a transformer that acts as an integral part of the WECS to interface the wind turbine and the grid.[5] Recently, there has been much interest in developing an alternative to the

traditional fundamental frequency transformer using solid-state devices. The solid-state transformer (SST) achieves voltage conversion through a series of power electronics devices while offering multiple advantages, such as, smaller size, improved power quality and fault tolerant features.

A power distribution system based on SST advanced in solid state technology have made SST more liable today leading to increased research in feasibility and physical realization.

A promising 10 KVA prototype has been developed and presented further the use of high voltage silicon carbide power devices for SST has been explored and presented.SST can act as a interface between the grid and generation sources. However research showing the detailed configuration for integrating existing technologies is limited[7]. Here work is reported on using SST in a micro grid based on renewable resources.SST is used to interface a wind park based on squirrel cage induction generator (SCIG) with the grid. However a detailed analysis on fault ride through requirement and reactive power support has not been conducted.

A new configuration is proposed that combines the operation of DFIG based WECS and SST[1]. This configuration acts as a interface between and grid while eliminating the GSC of DFIG. Moreover, it is essential to have fault ride through (FRT) incorporated in DFIG system to meet the grid code requirements. In the proposed work, the developed configuration allows DFIG to ride through faults seamlessly, which is the aspect (FRT) has not been addressed in the earlier work on SST interfaced WECS.

The SST technology has enhanced the power quality as compared to the normal step- up transformer. The SST acts as a key interface between the wind turbine and the grid. The main objective is to provide the regulated voltage in the power system and enhance the power quality[9] .The control techniques is proposed in the system. The RSC control technique explained in the system defines the two way injection and ejection of real and reactive power to the system .

The DFIG is used for the variable speed operation ,high power density and lower cost. The stator of DFIG is directly connected to grid while the rotor is connected to back- to- back converter known as Rotor side converter(RSC) AND Grid side converter(GSC).The SST performs the operation of voltage conversion through the power electronics devices for compensation purpose[6]s. It implements smaller size ,improved power quality and fault tolerance features. Reactive power is not supported in (SCIG) squirrel cage induction generator. so we go for DFIG. The DFIG based wind turbine system is the lightest among the current wind system. DFIG along with SST provides further reduction in volume and weight.[7]

Thus the system utilizes the SST along with the DFIG promotes the high power quality and voltage regulation. This will be achieved through the matlab simulation which proposes the wind turbine model and the simulation mode[8]l. Moreover , it is essential to have fault ride through(FRT) incorporated in DFIG system to meet the grid code requirements.

II. PROPOSED SYSTEM DESCRIPTION

The widely used DFIG based WECS configuration is shown in. The stator terminals of the machine are connected directly to the grid while the rotor terminals are connected via back to back converters. The RSC allows for variable speed operation of the machine by injecting or drawing active power from the rotor. The GSC maintains the DC link by transferring the active power from the rotor to the grid or vice versa. The step up transformer T1, is the interface between the DFIG system and grid.

Three stage SST configuration is shown in where it connects the grid to a distribution load. Conv-1 is a fully controlled three-phase converter connected to the high voltage grid (11-33 kV). It draws real power from the grid and maintains the high voltage DC bus. This high voltage DC is converted to high frequency AC voltage by a half bridge converter (HB-1) which is

then stepped down using a smaller sized high frequency transformer. This transformer provides the galvanic isolation between the grid and load. A second half bridge converter (HB-2) converts the low voltage AC to low voltage DC voltage . This DC bus supports conv-2 which maintains the three-phase/single phase supply voltage to the load by producing a controlled three phase voltage. The configuration thus performs the function of a regular transformer allowing for bi-directional power flow using a series of power electronics devices [5-10].

This paper presents the configuration, that the fundamental frequency transformer is replaced by the SST. The proper control of SST converter that is close to the stator of DFIG, addressed as machine interfacing converter (MIC), can aid the machine in its operation[2]. Thus, it is proposed to eliminate the GSC in the DFIG system configuration by incorporating its role in SST.

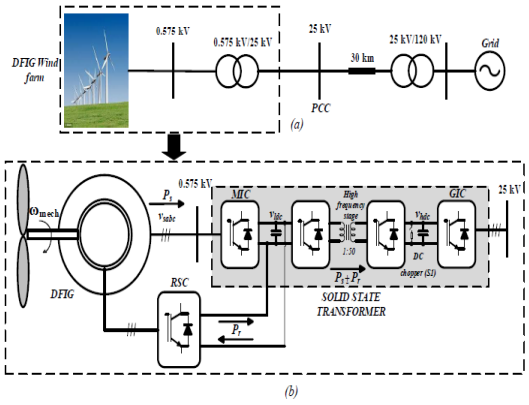

(a) Regular DFIG configuration and (b) Proposed SST based DFIG configuration.

. A. Solid State Transformer(SST)

The solid-state transformer (SST) achieves voltage conversion through a series of power electronics devices while offering multiple advantages, such as, smaller size, improved power quality and fault tolerant feature where it connects the grid to a distribution load. Conv-1 is a fully controlled three-phase converter connected to the high voltage grid (11-33 kV). It draws real power from the grid and maintains the high voltage DC bus. This high voltage DC is converted to high frequency AC voltage by a half bridge converter (HB-1) which is then stepped down using a smaller sized high frequency transformer. This transformer provides the galvanic isolation between the grid and load. A second half bridge converter (HB-2) converts the low voltage AC to low voltage DC voltage (Vldc) . This DC bus supports conv-2 which maintains the three-phase/single phase supply voltage to the load by producing a controlled three phase voltage. The configuration thus performs the function of a regular transformer allowing for bi-directional power flow using a series of power electronics devices. SST was used in an SCIG based WECS replacing the step-up transformer between the turbine and grid. It was shown that SST can improve the voltage profile at the terminals of the SCIG.In [21], it has been reported that a DFIG based wind turbine is the lightest amongst the current wind systems which also explains its wide commercial use. Moreover, in the proposed configuration, the GSC present in traditional DFIG systems is removed making the machine setup further lighter. On the other hand, SST being used in an AC/AC system is expected to be 25% smaller in volume than traditional low frequency transformer . Thus, the use of SST to interface a DFIG based wind system can be expected to provide further reduction in weight and volume when compared to other wind systems with the fundamental frequency transformer.

B. RSC and GSC

The widely used DFIG based WECS, The stator terminals of the machine are connected directly to the grid while the rotor terminals are connected via back to back converters. The RSC allows for variable speed operation of the machine by injecting or drawing active power from the rotor. The GSC maintains the DC link by transferring the active power from the rotor to the grid or vice versa. The step up transformer T1, is the interface between the DFIG system and grid.

Three stage SST configuration is shown in Fig. 2 (b), where it connects the grid to a distribution load. Conv-1 is a fully controlled three-phase converter connected to the high voltage grid (11-33 kV). It draws real power from the grid and maintains the

high voltage DC bus (. This high voltage DC is converted to high frequency AC voltage by a half bridge converter (HB-1) which is then stepped down using a smaller sized high frequency transformer. This transformer provides the galvanic isolation between the grid and load. A second half bridge converter (HB-2) converts the low voltage AC to low voltage DC voltage (. This DC bus supports conv-2 which maintains the three-phase/single phase supply voltage to the load by producing a controlled three phase voltage. The configuration thus performs the function of a regular transformer allowing for bi-directional power flow using a series of power electronics devices [5-10].

As mentioned earlier, the use of SST in WECS has been explored by Xu et al. in [10]. SST was used in an SCIG based WECS replacing the step-up transformer between the turbine and grid. It was shown that SST can improve the voltage profile at the terminals of the SCIG. While the focus of [10] was on SCIG, possible configuration for DFIG systems was also showcased that is represented in Fig. 2 (c). The step-up transformer T1 in Fig. 2 (a) is directly replaced by the SS

III. CONTROL TECHNIQUES

A. RSC control

The rotor side control ensures the variable speed operation of DFIG by enabling the generator to work in super synchronous or sub synchronous modes. In super synchronous mode, the total power generated is partially evacuated through the RSC. Under sub synchronous modes, the RSC injects active power into the rotor. The RSC in the proposed converter is controlled using a decoupled synchronous frame reference. The -axis of the reference frame is aligned with the machine stator voltage. On doing this, as per (3), the torque produced by the machine can be directly controlled by controlling the -axis rotor current . Moreover, the reactive power produced at the stator terminal can also be controlled by controlling the -axis rotor current

B. MIC control

The MIC is the first stage of the SST connecting the low voltage machine output to the high frequency stage. This converter is controlled to maintain 1 p.u. voltage (0.575 kV) at 50 Hz at the stator terminals of the machine.

The control is achieved by generating a reference voltage and comparing the -axis component of the reference with the voltage at the output of the converter ( ). The power generated at the stator terminals of the machine is thus absorbed by the low voltage DC bus connected to MIC operating at 1.15 kV.

C. GIC control

While the control of other converters remains the same in fault and normal conditions, GIC is controlled differently during fault conditions. The control and operation of GIC is discussed in two modes. Fault detection switches are used that are triggered when a fault is detected. Firstly, the operation of the proposed configuration is shown under normal grid conditions. In this scenario , the wind turbine is operated at a speed of 13 $m\ s$ thus not producing peak power. The wind turbines produce a total of 4.2 MW active power. Like general DFIG, the system delivers this wind generated active power to the grid through the SST.

That is, there is no reactive power support from the GIC. The grid voltages and currents at the output of the GIC. The stator terminal voltages and machine currents at 0.575 kV

D. High frequency stage control

The high frequency stage transforms the low voltage DC bus voltage (1.15 kV) into high voltage DC (50 kV). The DC voltages are converted into high frequency AC voltages by the two half bridge converters. Power is transferred by introducing a phase shift between the AC voltages of the two converters linked together by a high frequency transformer.

The control objective of high frequency stage, in the proposed configuration, is to maintain the low voltage DC bus voltage at a constant level. In order to achieve this, the reference voltage ∗ is compared with the measured value and the resulting error is processed by a PI controller which produces the required phase shift ϕ that transfers the active power from the low voltage DC bus to the high voltage DC bus.

TABLE I
SYSTEM PARAMETERS

Parameter	Value
System Data	
Rated power	5 MVA
No. of wind turbines	3
Wind Turbine data	
Rated power	1.5 MW
Rated wind speed	15m/s
Generator Data	
Rated apparent power	1.66 MVA
Rated voltage	0.575 kV
No of poles	6
Rated frequency	50 Hz
Stator to rotor turns ratio	575/1975
Stator resistance, Inductance	0.0023 p.u.,0.18 p.u.
Rotor resistance, inductance	0.0016 p.u.,0.16 p.u.
Inertia constant	0.685 s
SST Data	
Low voltage DC bus (v_{ldc})	1.15 kV
operating frequency	3 kHz
HF transformer turns ratio	1:50
HF transformer inductance	5.95 µH
High voltage DC bus (v_{hdc})	50 kV

IV. SIMULATION AND EXPERIMENTAL RESULTS

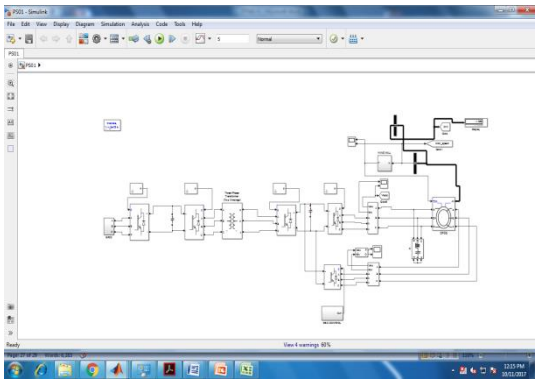

The simulation diagram is implemented in the above model which involves wind turbine, DFIG and RSC control.The variable speed operation is executed in the DFIG.The scope in every module is used to get the simulation result.

A. Wind Turbine Model

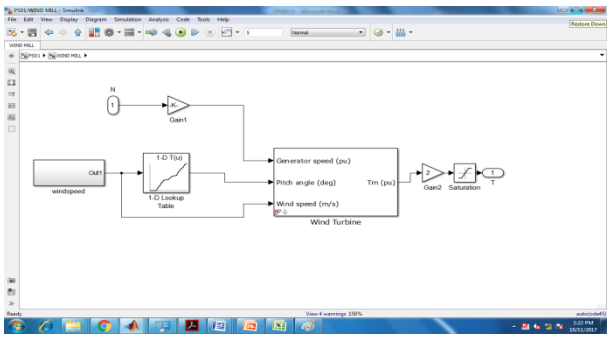

This is the wind turbine model in which the generator speed, pith angle, wind speed is calculated.

B. Simulink Output

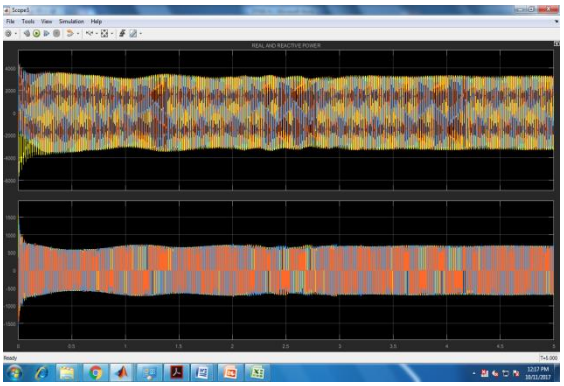

Both the real and reactive power waveforms is implemented in simulation.

C. Windmill Waveform

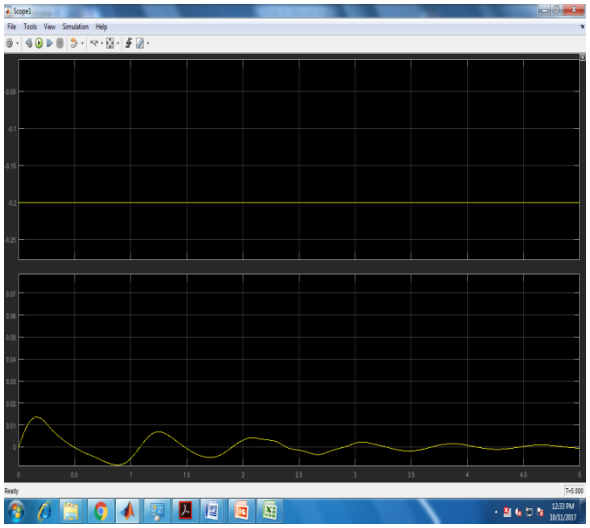

The power produced by the wind turbine is implemented with the current and voltage waveforms. These are the output waveforms which experimentally obtained using MATLAB/SIMULINK.

V. CONCLUSION

In this , a new system configuration that combines DFIG and SST operation has been proposed. This configuration replaces the regular fundamental frequency transformer with advanced power electronics based SST. The key features of the proposed configuration are outlined below:

- Replacement of regular fundamental frequency transformer with SST leading to smaller footprint.
- Direct interface with SST to inject active power.
- Elimination of GSC in a standard DFIG system as the active power to/from RSC is regulated by MIC.
- Simplified DFIG control as machine supports only active power. The reactive power is supported by GIC during both normal and fault conditions.
- Seamless fault ride through operation during both symmetrical and unsymmetrical faults as per the latest grid codes.

VI. REFERENCES

[1]. "Global Wind Report, Annual market update, 2014", Global Wind Energy Council.

[2]. S. Muller, M. Deicke, R. W. De Doncker, "Doubly fed induction generator systems for wind turbines," IEEE Ind. App. Mag., vol. 8, no. 3, pp.26-33, May/Jun. 2002.

[3]. R. Pena, J. Clare, and G. Asher, "Doubly fed induction generator using back-to-back converters and its application to variable-speed wind energy generation," in Proc. Inst. Electr. Eng.—Elect. Power Appl., vol.1 43, no. 3, pp. 231–241, May 1996.

[4]. X. She, A. Q. Huang and R. Burgos, "Review of Solid-State Transformer Technologies and Their Application in Power Distribution Systems," IEEE J. Emerg. Sel. Topics Power Electronics, vol. 1, no. 3, pp. 186-198, Sept. 2013.

[5]. J. L. Brooks, "Solid State Transformer Concept Development," Naval Material Command, Civil Engineering Laboratory, Naval Construction Battalion Ctr., Port Hueneme, CA, 1980.

[6]. X. She, X. Yu, F. Wang and A. Q. Huang, "Design and Demonstration of a 3.6-kV–120-V/10-kVA Solid-State Transformer for Smart Grid Application," IEEE Trans. Power Electron., vol. 29, no. 8, pp. 3982-3996, Aug. 2014.

[7]. S. Madhusoodhanan, A. Tripathi, D. Patel, K. Mainali, A. Kadavelugu,S. Hazra, S. Bhattacharya, K. Hatua, "Solid-State Transformer andMV Grid Tie Applications Enabled by 15 kV SiC IGBTs and 10 kVSiC MOSFETs Based Multilevel Converters," in IEEE Trans, Ind.

App., vol. 51, no. 4, pp. 3343-3360, July-Aug. 2015.[8]. Fei Wang, Gangyao Wang, A. Huang, Wensong Yu, Xijun Ni ,"Design and operation of A 3.6kV high performance solid state transformer based on 13kV SiC MOSFET and JBS diode," in Proc. IEEE Energy Conversion Congress and Exposition (ECCE), Sept.2014.

[9]. Y. Jie, Z. Wu and S. Bhattacharya, "Power dispatch strategy in micro grid integrated with solid state transformer," in Proc. IEEE Power Eng. Soc. Gen. Meeting, 2013, pp. 1-5.

[10]. X. She, A. Q. Huang, F. Wang and R. Burgos, "Wind Energy System With Integrated Functions of Active Power Transfer, Reactive Power Compensation, an Voltage Conversion," IEEE Trans. Ind. Electron. ,vol. 60, no. 10, pp. 4512-4524, Oct. 2013

Themed Section : Engineering and Technology
© 2018 IJSRSET | Volume 5 | Issue 3 | Print ISSN: 2395-1990 | Online ISSN : 2394-4099

A Survey on Detection of Keratoconus

R. Kanimozhi[1], Dr. R. Gayathri[2]
[1]Research Scholar, [2]Assistant Professor
Department of Electronics & Communication Engineering, Annamalai University, Chidambaram, Tamilnadu, India

ABSTRACT

Keratoconus is a progressive corneal disease characterized by central thinning and steepening of the corneal curvature. The progressive nature of this disease leads to increased myopia and irregular corneal astigmatism, which decrease visual acuity and visual quality. Corneal topography is the primary diagnostic tool for keratoconus detection, and pachymetry data and corneal aberrations are also commonly used. Recently, tomographic measurements using optical coherence tomography and corneal biomechanical indices have been used. In incipient and subclinical keratoconus, the use of a single parameter as a diagnostic factor is not sufficiently accurate. In these cases, the use of algorithms and predictive models is necessary. In this paper we discuss new approaches for the early detection of keratoconus.

Keywords: Keratoconus detection, tomographic measurements, corneal, primary diagnostic tool

I. INTRODUCTION

The eye comprises of three concentric layers: an outer fibrous tunic and nurturing that includes the sclera and the cornea; a layer in the middle, vascular and pigmented, which includes the choroid, ciliary body and the iris, and an inner layer of nerve elements; the retina. The interior of the eyeball contains fluid under pressure and is divided into the anterior and posterior compartments, which contain aqueous humor and vitreous body respectively, together with the lens and inserts [1].

The Keratoconus (QC), is the most common corneal ectasia. There is great variability in the incidence of QC, due to suspicious stage it is difficult to establish a diagnosis. The QC also known as keratoconus anterior (QCA), is a corneal alteration that takes the form of a cone which normally is located in central or apical area of the cornea. The prevalence rate is 1 per 2000 inhabitants in the general population [2].

The correlation between the anterior and posterior corneal shape in keratoconus has been also investigated [3,4] and its potential diagnostic value have been also even evaluated. A comprehensive analysis of this relationship can be performed by means of geometric modeling enabling the characterization of the human cornea. We previously validated the use of some new indices based on an innovative morphogeometric modeling of the corneal structure for the detection of keratoconus. The current study is a continuation of this research by confirming the diagnostic ability of the morphogeometric indices developed but in a larger sample of patients as well as by creating a new predictive model of detection of incipient keratoconus based on the combination of such indices.

II. Related works

Naoyuki Maeda et.al [5] presented the detection of keratoconus patterns on video keratography which is important for screening candidates for refractive surgery and for studying the genetic basis of keratoconus. Three quantitative approaches to identifying keratoconus from video keratographic information to examine the limitations and

capabilities of each test and to determine their suitability for use in the clinical setting

P. Perissutti et.al [6] discussed the utilization of neural networks for the automatic identification of keratoconus from corneal maps, using 9 previously selected objective parameters, were compared. The keratoconus is an asymmetrical pathology, sometimes mono lateral, while the maps of normal eyes and of congenital astigmatism are more often symmetrical. So they compared two methods, the first (monocular) in which each eye is considered alone and the second (binocular) in which information from both eyes of the same subject are the input of the neural network. The binocular information could in fact improve the ability of the neural network to identify the keratoconus corneo topographic patterns.

YARON S. RABINOWITZ et.al [7] presented the differential diagnosis of keratoconus includes keratoglobus, pellucid marginal degeneration and Terrine s marginal degeneration. Contact lenses are the most common treatment modality. When contact lenses fail, corneal transplant is the best and most successful surgical option. Despite intensive clinical and laboratory investigation, the etiology of keratoconus remains unclear. Clinical studies provide strong indications of a major role for genes in its etiology. Video keratography is playing an increasing role in defining the genetics of keratoconus, since early forms of the disease can be more accurately detected and potentially quantified in a reproducible manner. Laboratory studies suggest a role for degradative enzymes and proteinase inhibitors and a possible role for the interleukin-1 system in its pathogenesis, but these roles need to be more clearly defined.

Filippo Castiglione et.al[8], discussed the keratoconus index (KI) which is a new biometric parameter to make diagnosis and to follow the development of the keratoconus in human eyes. Using images from an ultrasound biomicroscope, we show a semi-automatic method to speed up the computation of the KI.

Jack T. Holladay et.al [9] discussed the ability to detect and diagnose suspicious to advanced keratoconus will enable the exclusion of patients at risk for corneal ectasia after corneal refractive surgery. Earlier detection of forme fruste keratoconus may lead to earlier intervention. The specificity and sensitivity of the various automated keratoconus screening software are still not adequate for broad clinical use.3,4 Most of these automated detection programs cannot accurately classify suspicious topographies with an adequate degree of reliability.3,4 It is precisely these suspicious cases that cause clinicians the most difficulty. To date, a thorough clinical and topographic examination by the ophthalmologist is still requisite for keratoconus detection. This article presents the use of the OPD Scan II (Optical Path Difference Scanning System II; NIDEK Co Ltd, Gamagori, Japan) combined with clinical features to screen for keratoconus

Fatemeh Toutounchian et.al[10] presented Artificial intelligence algorithm to find Keratoconus by employing features of topographical map of eye. These features are obtained by Pentacam and extracted by topographical images of eye via image processing techniques. We provide a dataset of the topographical images of eye by Pentacam in about six months and experts provide labels explaining if the images show sign of Keratoconus or they are suspect to keratoconus. This paper employs 82 topography maps of eye from dataset and classifies them into two categories: Normal (n=47) and Keratoconus (n=35). We use 12 features of each map as the input of a classifier. These classifiers are artificial Neural Network.

George Asimellis et.al [11] surveyed the standard keratoconus grading scale (Pentacam®-derived Amsler Krumeich stages) compared to corneal irregularity indices and best spectacle-corrected distance visual acuity (CDVA). Patients and methods Two-hundred and twelve keratoconus cases were evaluated for keratoconus grading, anterior surface irregularity indices (measured by Pentacam imaging), and subjective refraction (measured by CDVA). The correlations between CDVA, keratometry, and the Scheimpflug keratoconus grading and the seven anterior surface Pentacam-derived topometric indices index of surface variance, index of vertical

asymmetry, keratoconus index, central keratoconus index, index of height asymmetry, index of height decentration, and index of minimum radius of curvature were analyzed using paired two-tailed t-tests, coefficient of determination (r2), and trendline linearity.

Murat Ucar et.al [12] defined a new classification method for detecting keratoconus based on statistical analysis and to realize the prediction of these classified data with intelligent systems. 301 eyes of 159 patients and 394 eyes of 265 refractive surgery candidates as the control group have been used for this study. Factor analysis, one of the multivariate statistical techniques, has been mainly used to find more meaningful, easy to understand, and independent factors amongst the others.

Valter Wellington Ramos Junior et.al[13] a modified GAADT algorithm approach is presented for blind inversion of channels. The use of this technique is justified here because of the small number of samples. In this situation, gradient-like algorithm fails because it is very difficult to obtain a good estimation of statistics (score function, pdf, etc,). Optimization using GAADT in all situations of classification analysis gives a good performance.

M. A. Valdes-Mas et.al [14] proposed a new approach based on Machine Learning to predict astigmatism in patients with keratoconus (KC) after ring implantation. KC is a non-inflammatory, progressive thinning disorder of the cornea, resulting in a protrusion, myopia and irregular astigmatism. The intracorneal ring implantation surgery has become a suitable technique to deal with keratoconus without the need of a corneal transplant. Two machine learning (ML) classifiers based on artificial neural network and a decision tree were used in this work.

Manmohan Singh et.al [15] presented the mechanical properties of tissues can provide valuable information about tissue integrity and health and can assist in detecting and monitoring the progression of diseases such as keratoconus. Optical coherence elastography (OCE) is a rapidly emerging technique, which can assess localized mechanical contrast in tissues with micrometer spatial resolution. In this work they presented a noncontact method of optical coherence elastography to evaluate the changes in the mechanical properties of the cornea after UV-induced collagen cross-linking. A focused air-pulse induced a low amplitude (μm scale) elastic wave, which then propagated radially and was imaged in three dimensions by a phase-stabilized swept source optical coherence tomography system.

K.Vijay Chandra et.al [16] presented with the corneal diseases using NI VISION Assistant in LabVIEW. NI Vision for LabVIEW is a part of the NI VDM is a Library of LabVIEW used to develop machine vision and scientific imaging applications. The diseases and disorders affecting the cornea are many but only few of them are discussed in this paper. They are: Corneal Infections, Dry Eye, Keratoconus, and Allergies.

Sarah Ali Hasan et.al[17] presented to differentiate the Astigmatism from Keratoconus using Axial Topographic images. In the proposed algorithm, shape recognition is used for classification.

Riccardo Vinciguerra et.al [18] presented to evaluate the ability of a new combined biomechanical index called the Corvis Biomechanical Index (CBI) based on corneal thickness profile and deformation parameters to separate normal from keratoconic patients. Methods: Six hundred fifty-eight patients (329 eyes in each database) were included in this multicenter retrospective study. Patients from two clinics located on different continents were selected to test the capability of the CBI to separate healthy and keratoconic eyes in more than one ethnic group using the Corvis ST (Oculus Optikgeräte GmbH, Wetzlar, Germany). Logistic regression was employed to determine, based on Database 1 as the development dataset, the optimal combination of parameters to accurately separate normal from keratoconic eyes.

R. Mercatelli et.al [19], presents to investigate this anomaly by means of Second Harmonic Generation (SHG) microscopy, using an optical scheme relevant for clinical applications. In particular, we propose a method based on 3D correlation of SHG image stacks, able to appreciate statistical differences in the orientation distribution of sutural lamellae between healthy and keratoconic corneas. The proposed

method offers the potential for diagnosing keratoconus in an early stage.

Irene Ruiz Hidalgo et.al [20] presents to evaluate the performance of a support vector machine algorithm that automatically and objectively identifies corneal patterns based on a combination of 22 parameters obtained from Pentacam measurements and to compare this method with other known keratoconus (KC) classification methods.

Eduardo Pinos-Vélez et.al [21] presents work the simulation and modeling of the human eye in order to determine the degree of involvement of keratoconus, as a tool for early diagnosis Presumptive diagnosis tool for the specialist, in such a way that they can take the necessary actions to control this disease. The information of images of the human eye, are used for the analysis in the various stages of keratoconus, through digital processing developed in free software.

Francisco Cavas-Martı´nez et.al[22] presents to characterize corneal structural changes in keratoconus using a new morphogeometric approach and to evaluate its potential diagnostic ability.

AntonioMartínez-Abad et.al [23] discussef laser refractive surgery has increased markedly in recent years, making the detection of corneal abnormalities extremely relevant. For this reason, an accurate diagnosis of clinical or subclinical keratoconus is critical. Corneal topography is the primary diagnostic tool for keratoconus detection, and pachymetry data and corneal aberrations are also commonly used. Recently, tomographic measurements using optical coherence tomography and corneal biomechanical indices have been used. In incipient and subclinical keratoconus, the use of a single parameter as a diagnostic factor is not sufficiently accurate. In these cases, the use of algorithms and predictive models is necessary.

Francisco Cavas-Martínez et.al[24] presented numerous tomographic indices for the detection of keratoconus risk. When the indexes based on corneal volume are analyzed, two problems are presented: on the one hand, they are not very sensitive to the detection of incipient cases of keratoconus because they are not locally defined in the primary developmental region of the structural abnormalities; and on the other hand, they do not register the geometric decomposition driven by the asymmetry present during the disease progression. This work performed a morphogeometric modeling of the cornea by the aid of CAD tools and using raw topographic data (Sirius system, CSO, Firenze). For this method, four singular points present on the corneal surfaces were located.

III. Conclusion

In this paper, we survey some papers related to detection of keratoconus. Through this paper, we got an overview of the current researches related to various techniques and methods of keratoconus detection. Although this paper study does not conclude the best method, but the results of experiments that have been conducted by previous researchers explained briefly. And also useful for future researchers who want to know the current researches related to detection of keratoconus.

IV. REFERENCES

[1] N F. D. &. S. R. Palastanga, "Anatomía y movimiento del ojo humano. Estructura y funcionamiento," Paidotribo, 2007.

[2] R YS., "Keratoconus," Surv Ophthalmol, vol. 42, pp. 291-319, 1998.

[3] Pinero DP, Alio JL, Aleson A, Escaf Vergara M, Miranda M. Corneal volume, pachymetry, and correlation of anterior and posterior corneal shape in subclinical and different stages of clinical keratoconus. Journal of cataract and refractive surgery. 2010;36(5):814?25. Epub 2010/05/12. doi: 10.1016/j.jcrs.2009.11.012 . [PubMed]

[4] Montalban R, Alio JL, Javaloy J, Pinero DP. Correlation of anterior and posterior corneal shape in keratoconus. Cornea. 2013;32(7):916?21. Epub 2013/05/15. doi: 10.1097/ICO.0b013e3182904950 .[PubMed]

[5] Naoyuki Maeda, Stephen D. Klyce, Naoyuki Maeda, Stephen D. Klyce, Michael K. Smolek, ?Comparison of Methods for Detecting Keratoconus Using Videokeratography?, Arch Ophthalmol. 1995;113(7):870-874. doi:10.1001/archopht.1995.01100070044023.

[6] P Perissutti*, A.P. Accardo**, S. Pensiero", M.L. Salvetat,? AUTOMATIC KERATOCONUS DETECTION BY MEANS OF A NEURAL NETWORK: COMPARISON BETWEEN A MONOCULAR AND A BINOCULAR APPROACH.?, Proceedings of the 20th Annual International Conference of the ZEEE Engineering in Medicine and Biology Society, Vol. 20, No 3,1998.

[7] YARON S. RABINOWITZ, MD,? Keratoconus?, © 1998 by Elsevier Science Inc.

[8] Filippo Castiglione* and Francesco Castiglione,? Estimating the Keratoconus Index from Ultrasound Images of the Human Cornea? IEEE TRANSACTIONS ON MEDICAL IMAGING, VOL. 19, NO. 12, DECEMBER 2000.

[9] Jack T. Holladay, MD, MSEE, FACS? Keratoconus Detection Using Corneal Topography?, Journal of Refractive Surgery Volume 25 October (Suppl) 2009.

[10] Fatemeh Toutounchian, Jamshid Shanbehzadeh, Mehdi Khanlari,? Detection of Keratoconus and Suspect Keratoconus by Machine Vision?,proceedings of the international multi conference of engineers and computer scientists 2012 volume I,IMECS 2012,MARCH 14-16 2012,hong kong.

[11] George Asimellis, Anastasios John Kanellopoulos,? Revisiting keratoconus diagnosis and progression classification based on evaluation of corneal asymmetry indices, derived from Scheimpflug imaging in keratoconic and suspect cases", in Clinical ophthalmology (Auckland, N.Z.)7(default):1539-1548 • July 2013.

[12] Murat Ucar1 , Baha Sen2 , Hasan Basri Cakmak, A Novel Classification and Estimation Approach for Detecting Keratoconus Disease with Intelligent Systems?. ©2013 IEEE

[13] Valter Wellington Ramos Junior,Roberta Vilhena Vieira Lopes, Joao Marcelo Lyra, Guilherme Ribeiro, Antonio Fernando de S. Bezerra, Luis Claudius Coradine,? An Application of Algorithm Based on Abstract Data Types to the Keratoconus Diagnosis?.

[14] M. A. Valdes-Mas, Jos ´ e D. Mart ´, Mar´ia J. Ruperez, Cristina Peris and Carlos Monserrat," Machine Learning for Predicting Astigmatism in Patients with Keratoconus after Intracorneal Ring Implantation", 978-1-4799-2131-7/14/$31.00 ©2014 IEEE.

[15] Manmohan Singh* , Jiasong Li* , Srilatha Vantipalli, Shang Wang, Zhaolong Han, Achuth Nair, Salavat R. Aglyamov, Michael D. Twa, and Kirill V. Larin,? Noncontact Elastic Wave Imaging Optical Coherence Elastography (EWI-OCE) for Evaluating Changes in Corneal Elasticity due to Cross-Linking?, 1077-260X (c) 2015 IEEE.

[16] K.Vijay Chandra, K.Rashmi,? DETECTION OF CORNEAL DISEASES USING NI VISION ASSISTANT IN Lab VIEW?, 978-1-4673-9825-1/15/$3l.00 ©2015 IEEE.

[17] Sarah Ali Hasan, Dr. Mandeep Singh,? An Algorithm to differentiate Astigmatism from Keratoconus in Axial Topgraphic Tmages?, 20i5international Conference on industrial Instrumentation and Control (IClC) Col/ege o/Engineering Pune, India. May 28-30, 2015.

[18] Riccardo Vinciguerra, Renato Ambrósio Jr, Ahmed Elsheikh, Paolo Vinciguerra,? Detection of Keratoconus With a New Biomechanical Index?, in Journal of refractive surgery (Thorofare, N.J.: 1995)32(12):803-810 • December 2016.

[19] R. Mercatelli1*, F. Ratto2, F. Rossi2, F. Tatini2, L. Menabuoni3, Riccardo Nicoletti5, Roberto Pini2, F.S. Pavone4,1,6, and R. Cicchi1," Morphological Characterizazion of Human Keratoconic Corneas by SHG Microscopy?.

[20] Irene Ruiz Hidalgo, MSc,*? Pablo Rodriguez, MSc, PhD,? Jos J. Rozema, MSc, PhD,*? Sorcha Ní Dhubhghaill, MBBS, PhD,*? Nadia Zakaria, MBBS, PhD,*? Marie-José Tassignon, MD, PhD,*? and Carina Koppen,? Evaluation of a Machine-Learning Classifier for Keratoconus Detection Based on Scheimpflug Tomography?, Cornea Volume 35, Number 6, June 2016.

[21] Eduardo Pinos-Vélez, Marco Baculima-Pintado, Mónica Cruz-Cabrera and Luis Serpa-Andrade," Modeling of the human eye as a tool to determine the degree of involvement of keratoconus using the image processing", 978-1-5386-3403-5/17/$31.00 ©2017 IEEE.

[22] Francisco Cavas-Marti´nez1 *, Laurent Bataille1,2,3, Daniel G. Ferna´ndez-Pacheco1 , Francisco J. F. Cañavate1 , Jorge L. Alio," A new approach to keratoconus detection based on corneal morphogeometric analysis", PLOS ONE | September 8, 2017.

[23] Antonio Martínez-Abad,David P.Piñero,? New perspectives on the detection and progression of keratoconus?, Journal of Cataract & Refractive Surgery,Volume 43, Issue 9, September 2017, Pages 1213-1227.

[24] Francisco Cavas-Martínez, Laurent Bataille, Daniel G. Fernández-Pacheco, Francisco J. F. Cañavate& Jorge L. Alio,? Keratoconus Detection Based on a New Corneal Volumetric Analysis?, Scientific Reportsvolume 7, Article number: 15837(2017).

Themed Section : Engineering and Technology
© 2018 IJSRSET | Volume 5 | Issue 3 | Print ISSN: 2395-1990 | Online ISSN : 2394-4099

Survey on Gain and Bandwidth Enhanced Metamaterial based Microstrip Patch Antenna

K. Mahendran[1], Dr. R. Gayathri[2]

[1]Research scholar, Department of Electronics and Communication Engineering, Chidambaram, Tamil Nadu, India

[2]Assistant Professor, Department of Electronics and Communication Engineering, Chidambaram, Tamil Nadu, India

ABSTRACT

Microstrip antennas are widely employed in communication system and seekers. Printed antennas provided attractive features such as low profile, low weight and low production cost. These small printed antennas suffers due to narrow bandwidth and low gain. To overcome the drawback, metamaterial technology comes into picture. Metamaterial is used to design a small printed antenna with high gain and wider bandwidth. A survey of various techniques used in Metamaterial based print antennas are presented in this paper.

Keywords : Split Ring Resonators, Metamaterials (MTM), Negative Index Materials (NIM)

I. INTRODUCTION

Metamaterials are artificial materials which exhibits unique properties which cannot be achieved by conventional material. Simply Metamaterials are man-made twisted and composite structures with the assemblies of multiple (metal- Plastic) elements. The properties of the material is not from the base material, it depends on the designed structure. The shape, geometry, size and orientation of the metamaterial will manipulate the Electromagnetic waves.[1]

1.1 Basics of Metamaterial

Recently, there has been growing interest in the study of metamaterials both theoretically and experimentally. Metamaterials (MTM) are artificial materials engineered to have properties that may not be found in nature. The invention of metamaterial was started in 1960s. In 1967, Victor Georgievich Veselago [2] studied the electrodynamics of substances with simultaneously negative values of dielectric permittivity (ε) and magnetic permeability (μ). Positive permeability and permittivity are the basic properties of conventional materials available in nature called as Double Positive (DPS) materials. Metamaterials are termed as Double Negative (DNG) materials due to the property of negative dielectric permittivity (ε) and magnetic permeability (μ). Metamaterials consist of two concentric metallic rings with a split on each ring .this structure represent a LC resonator, which exhibits magnetic resonance. G. Veselago found that the Poynting vector of the plane wave (group velocity) is antiparallel to the direction of the phase velocity, which is contrary to the conventional case of plane wave propagation in natural media. So he mention the term "left-handed substance," that this term is equivalent to "substance with negative group velocity". Although metamaterial does not present in nature, interesting properties were theoretically predicted for these substances, such as the reversal of the Snell Law, Doppler Effects,

and Cherenkov radiation etc. Metamaterials are sometimes referred to as Negative Index Materials (NIM) as they exhibit negative index of refraction. .

Metamaterial structure consists of Split Ring Resonators (SRRs) to produce negative permeability and thin wire elements to generate negative permittivity. SRR is a novel design consisting of two concentric rings with a split on each ring. The structure is called resonator since it exhibits a certain magnetic resonance at a certain frequency. Split ring resonators can result in an effective negative permeability over a particular frequency region. The SRR structure is formed by two concentric metallic rings with a split on opposite sides. This behaves as an LC resonator with distributed inductance and capacitance that can be excited by a time-varying external magnetic field component of normal direction

II. Structure of Metamaterial

There are mainly 4 types of metamaterial structures as antenna substrate:

- 1-D Split Ring structure
- Symmetrical Ring structure
- Omega structure
- S structure

All the metamaterial antennas are designed based on any one of these substrate structures. 1-D structures are easier to fabricate and construct. Symmetrical Ring structure tends to yield clean retrieval response as there is less ringing effect from time-domain simulation. Also there is less coupling between the *E* field and the *H* field. Omega-shaped structure is a new metamaterial structure. But the increased complexity in the structure. There are no rings or rod parts are present in S structure and hence the results are relatively better. In comparison with other three structures, the Symmetrical-Ring structure provides a better directional beam and is easier to tune its permeability because of its rings are symmetrical.[3]

III. Properties of Metamaterial

Consider the Maxwell's first order differential equations,

$$\nabla \times E = -j\omega\mu H \qquad (1)$$

$$\nabla \times H = j\omega\epsilon E \qquad (2)$$

Where ω is an angular frequency.

For a plane-wave electric & magnetic fields like

$$E = E_0 e(-jk\ .r + j\omega t) \qquad (3)$$

$$H = H_0 e(-jk\ .r + j\omega t) \qquad (4)$$

where k is a wave vector, the equations (1) and (2) will become

$$k \times E = \omega\mu H \qquad (5)$$

$$k \times H = -\omega\epsilon E \qquad (6)$$

For simultaneous positive values of ε and μ, the vectors E, H and **k** make a right handed orthogonal system and wave will propagate in forward direction. For simultaneous negative values of ε and μ, equations (5) and (6) can be rewritten as

$$k \times E = \omega|\mu|H \qquad (7)$$

$$k \times H = \omega|\epsilon|E \qquad (8)$$

Energy flow is determined by the real part of the Poynting Vector

S = ½ (E x H*)

For simultaneous change of sign of permittivity and permeability, the direction of energy flow is not affected, therefore, the group velocity will be positive for both left-handed and right-handed system.

Refractive index is given as

$$n = \pm\sqrt{\epsilon\mu}$$

And phase velocity is given as $$v_p = \frac{c}{n}$$

where c is the velocity of light in vacuum.

For right handed system, n is positive, thus the phase velocity will be positive. Therefore, energy and wave will travel in same direction resulting in forward wave propagation.

For left-handed system, n is negative, thus the phase velocity is negative. Hence the direction of energy flow and the wave will be opposite resulting in backward wave propagation. Backward waves may commonly appear in non-uniform waveguides. [4],[5],[6].

IV. Metamaterials in Patch Antenna

There are various issues while we design a patch antenna such as - compactness in size, high gain, directivity enhancement, increased bandwidth, and suppressed sidelobes. Metamaterials are being used for improving the performance of patch antennas.

4.1 Directivity and Gain Enhancement

Effective permittivity can be expressed as

$$\epsilon_{eff} = 1 - \omega_p / \omega^2$$

where ω_p and ω are the plasma frequency and the frequency of the electromagnetic wave.

When resonant frequency is equal to plasma frequency, the effective permittivity will be zero.

$$If\ \omega = \omega_p \quad then \quad \epsilon_{eff} = 0$$
$$n = \sqrt{\epsilon_{eff}\ \mu_{eff}} = 0$$

Thus when operating at the plasma frequency, there will be zero index of refraction. Directivity and gain can be increased by using metamaterial as antenna substrate.

If a source is embedded in a substrate with zero index of refraction, then according to Snell's law, the exiting ray from substrate will be close normal to the surface. Then, all the refracted rays will be in almost the same direction around the normal. Therefore, if the operating frequency is closer to the plasma frequency, directivity can be improved.

a) A metamaterial for directive emission

Enoch *et al.,* had used metamaterial as substrate [7]. The layers of copper grids separated by foam were used as metamaterial. This metamaterial possessed the plasma frequency at about 14.5 GHz. Monopole antenna fed by a coaxial cable was used as a source of excitation and the emitting part of the monopole was approximately centered at the center of the metamaterial substrate. And also a ground plane was added to substrate. It had the best directivity at 14.65 GHz. Since the metamaterial has a plasma frequency at about 14.5 GHz, the index of refraction is close to zero at this frequency. According to Snell's law, the refracted ray from the metamaterial will be very close to the normal of it. Hence he obtained the best directivity at 14.65 GHz.

I.Wu. *et al.,* used the same technique for obtaining high directivity [8] as used in [7]. He used the dipole antenna as source of emission instead of monopole antenna. The dipole antenna was embedded in metamaterial substrates. The periodic structures of rods, or of both rods and rings were used as metamaterial. Ground planes were not used there. He used the different methodology and the process of analysis. He placed method for farfield radiation was used.

b) ***Emitting antenna fabricated by anisotropic metamaterial***

Y. G. Ma *et al.,* represented that the directivity of an EM emission could be more improved by embedding the source in an anisotropic metamaterial with either effective permittivity or effective permeability nearly zero [9].

The difference between this [7] and the technique of Enoch *et al.,* The first one lies in the problem of impedance mismatch between the ε-near-zero (ENZ) matrix and surrounding air. The metamaterial used was anisotropic with effective permittivity near zero, allowing it to match the surrounding media at the proper polarizations. By using the anisotropic slab, the emitted wave received in surrounding air exhibits the characteristics of plane wave same as the straight wavefront parallel to the interface shows when it is propagating along ± x axis [10]. It was shown that the high directivity can be supported by this anisotropic matrix.

C) Improvement of Characteristics of Microstrip Antenna Using of two Metamaterial Superstrate

R. Khajeh Mohammad Lou *et al.,* used two types of metamaterial superstrates [11] to increase directivity, gain and bandwidth. Directivity enhancement was based on zero index refraction phenomenon. The radiation energy of patch antenna is concentrated

near zero index refraction. The S coupled and Double split rings were used as metamaterial superstrates.

Using 5×7 array of the coupled S-shaped structures, the near zero refractive index was observed in the frequency range of 13.5-17.5 GHz. Hence the radiated energy will be concentrated in this frequency range and directivity will be maximum. A 6×7 array of Double split ring structures near zero refractive index was also used.

The metamaterial superstrate layer was placed about one third of the operating wavelength, *i.e.,* λ/3 above ground plane to increase the gain.

D) Microstrip Patch Antenna with Pentagonal Rings

Bimal Garg, *et al.,* presented a "Pentagonal Rings" shaped metamaterial cover [12] to enhance the gain and directivity of microstrip patch antenna. The designed metamaterial has negative values for both effective permittivity and permeability. The metamaterial cover was placed at a height of 3.2 mm from the ground plane. As left handed metamaterial has the property of focusing radiations of antenna [14], the directivity had been increased about 2.019 dB and the gain had improved.

E) Gain Enhancement using Patterned Structures

Le-Wei Li, *et al.,* used the completely different approach [18] to enhance the bandwidth and gain of a conventional patch antenna. He applied the planer metamaterial patterned structures directly on the upper patch and bottom ground of the substrate. Periodically distributed isolated micro triangles gaps were designed on the upper patch and the periodically distributed cross strip gaps were designed on the bottom ground plane. A capacitive-inductive equivalent circuit was formed by the coupling of upper patch and bottom ground plane. Thus, a backward wave was induced which travelled along the plane of patch. Therefore, the radiation along the patch direction was enhanced which in turn increased the bandwidth and gain.

F) Left-handed Metamaterial Structure in Antenna Cover

Zhongqing Wang, *et al.,* designed a left-handed metamaterial cover [20] to enhance the gain and directivity of antenna. This left handed metamaterial cover was designed with a microstrip line, two symmetrical triangular split ring resonators printed on the substrate. There were also two gaps cut on the metal ground plane which made it DGS. This left handed metamaterial cover has negative permittivity and permeability in various frequency bands. When the left-handed metamaterial cover was placed above the antenna, the gain and directivity of antenna was increased and resonant frequencies were shifted towards lower side.

V. Bandwidth Enhancement

a) Broadband Dual-Mode Monopole Antenna

Marco A. Antoniades, *et al.,* presented a printed monopole antenna loaded with metamaterial to achieve broadband dual mode operation [21]. The metamaterial used was negative refractive index transmission line. The metamaterial loading was adjusted to support even mode current at 5.5 GHz which transforms the antenna into short folded monopole. At 3.55 GHz, the ground plane radiates due to in phase current along its top edges. The ground plane radiates a dipole mode orthogonal to folded monopole mode, thus resulting a wideband of 4.06 GHz.

b) Broadband Microstrip Antenna with Left-Handed Metamaterials

Merih Palandoken, *et al.,* presented a compact broadband microstrip antenna [22] loaded with left-handed metamaterial and dipole. The proposed antenna consists of six unit cells of negative refractive index metamaterials fashioned in 2×3 antenna array, and a dipole. The impedance of antenna was matched with a stepped impedance transformer. It was also matched with rectangular slot cut in the truncated ground plane. The phase compensation and the coupled LH resonance properties resulted into its broad bandwidth (63 %) over the band 1.3-2.5 GHz.

C) ***Series-Fed Metamaterial Microstrip Antenna Array***

Lang Wang, *et al.,* presented a series fed array of rectangular microstrip metamaterial patches [23]. This series fed array of metamaterial patches enhanced the bandwidth and gain of the antenna. The feedline connecting the metamaterial patches was off-centered. The shunt fed array was also used for providing bandwidth but it has large dimensions.

d) *Broadband and High gain Metamaterial Microstrip Antenna*

Lang Wang, *et al.,* Presented that by applying the planar metamaterial patterned structures directly on the upper patch and bottom ground of the dielectric substrate, so the patch antenna can have an excellent performance.[24] Normally in conventional microstrip antenna, patch is mounted on a substrate and backed by a conducting ground plane. The paper proposed that a planar LHM pattern on the rectangular patch antenna mounted on the substrate is designed to enhance its horizontal radiation as well as to broaden its working bandwidth via its coupling with the conducting ground backed to the substrate and patterned in a different way. On the upper patch, the periodic gaps are designed in the form of isolated micro triangles while on the bottom ground plane. Periodically distributed cross strip-line gaps are designed. To maintain the transmission consistency of input energy, the metal in and around the feed-line area is, however, not etched.

The proposed antenna is designed to have the 0.4 mm gap at the bottom, and the 10 dB bandwidth which is standardly defined for engineering applications falls within 5.3 and 8.5 GHz which is 3.2 GHz in bandwidth and is 16 times wider than the conventional antenna. He also analyzed that When the gap at the bottom becomes 0.3 mm, the 10 dB bandwidth turns within 5.7 and 8.6 GHz which is 2.9 GHz in bandwidth, and is 14.5 times wider than the conventional antenna.

e) Bandwidth enhanced printed dipole antenna

M.A. W. Noordin *et al.,* presented that the dipole is built on top a ceramic based substrate. In order for matching the ground plane was truncated and made partial.[27] By loading the end of the dipole, means for uniform current distribution. The metamaterial elements were loaded on the shape of triangle, which provides capacitive loading. This metamaterial loading was placed on top of the dipole antenna. The designed antenna works on 1.3 to 2.2 GHz. The antenna has a total bandwidth of 56 % at the lowest resonant frequency.

VI. CONCLUSION

With the rapid development of wireless communication Microstrip patch antennas are crucial. But these microstrip antennas have some limitations amongst its numerous advantages. Several investigations are going on to improve the gain and bandwidth of patch antenna. The studies have come up with a concept of metamaterial substrates. This survey various Metamaterials techniques were summarized to enhance the gain and bandwidth of printed antennas.

VII. REFERENCES

[1] J. B. Pendry, A. J. Holden, D. J. Robbins and W. J. Stewart, ‘‘Magnetism from Conductors and Enhanced Non- Linear Phenomena”, IEEE Trans. Microwave Theory Tech., vol. 47, **(1969)**, pp. 207584.

[2] V. G. Veselago, “The Electrodynamics of substances with simultaneously negative value of epsilon and mu”, Soviet Phys. Usp., vol. 10, no. 4, **(1968)**, pp. 509-514.

[3] W Wang, B.-I. Wu, J. Pacheco, X. Chen, T. Grzegorczyk and J. A. Kong, “A study of using metamaterials as antenna substrate to enhance gain”, PIER 51 **(2005),** pp. 295–328.

[4] C. Caloz, H. Okabe, H. Iwai and T. Itoh, “Transmission line approach of left-handed metamaterials”, Proc. USNC/URSI Nat. Radio Sci. Meeting, **(2002)**, pp. 39, San Antonio, TX.

[5] P. A. Belov, R. Marque´s, S. I. Maslowski, I. S. Nefedov, M. Silveirinha, C. R. Simovski and S. A. Tretyakov, “Strong spatial dispersion in wire media in the very large wavelength limit”, Phys. Rev. Lett., vol. 67, paper 113103, **(2003)**.

[6] L. D. Landau, E. M. Lifshitz and L. P. Pitaevskii, "Electrodynamics of Continuous Media Pergamon", New York, **(1984)**.

[7] S. Enoch, G. Tayeb, P. Sabouroux, N. Guerin and P. Vincent, "An metamaterial for directive emission", Phys. Rev. Lett., vol. 89, no. 21, no. 213902, **(2002)**.

[8] I. Wu, W. Wang, J. Pacheco, X. Chen, T. Grzegorczyk and J. A. Kong, "An study of using metamaterials as antenna substrate to enhance gain", Progress In Electromagnetics Research, PIER, vol. 51, **(2005)**, pp. 295-328.

[9] Y. G. Ma, P. Wang, X. Chen and C. K. Ong, "Near-field plane-wave-like beam emitting antenna fabricated by anisotropic metamaterial", Applied Phys. Lett., vol. 94, no. 044107, **(2009)**.

[10] J. B. Pendry, D. Schurig and D. R. Smith, "Controlling Electromagnetic Fields", Science, vol. 312, no. 1780, **(2006)**.

[11] R. K. M. Lou, T. Aribi and C. Ghobadi, "Improvement of Characteristics of Microstrip Antenna Using of Metamaterial Superstrate", International Conference on Communication Engineering, **(2010)**, pp. 126129.

[12] B. Garg, N. Agrawal, V. Sharma, A. Tomar and P. Dubey, "Rectangular Microstrip Patch Antenna with ''Pentagonal Rings'' Shaped Metamaterial Cover", International Conference on Communication System and Network Technologies IEEE, **(2012)**, pp. 40-44.

[13] D. R. Smith, W. J. Padilla, D. C. Vier, *et al.,* "Composite medium with simultaneously negative permeability and permittivity", Phys. Rev. Lett., vol. 84, **(2000)**, pp. 4184-4187.

[14] N. Engheta and R. W. Ziolkowski, "Metamaterial Physics & Engineering Explorations", **(2006)**.

[15] H. Attia, O. Siddiqui and O. M. Ramahi, "Artificial Magneto-superstrates for Gain and Efficiency Improvement of Microstrip Antenna Arrays", PIERS Online, vol. 6, **(2010)**.

[16] H. Attia and O. M. Ramahi, "EBG superstrate for gain and bandwidth enhancement of microstrip array antennas", Proceeding of IEEE Antennas and Propag. Society International Symposium, **(2008)**, pp. 1-4.

[17] Y. J. Lee, J. Yeo, R. Mittra and W. S. Park, "Application of electromagnetic bandgap (EBG) superstrates with controllable defects for a class of patch antennas as spatial angular filters", IEEE Trans. Antennas Propagation, vol. 53, no. 1, **(2005)**, pp. 224-235.

[18] L.-W. Li, Y.-N. Li, T. S. Yeo, J. R. Mosig and O. J. F. Martin, "An broadband and high-gain metamaterial microstrip antenna", Applied Phys. Lett., vol. 96, no. 164101, **(2010)**.

[19] O. M. Haraz and A.-R. Sebak, "Gain enhancement in Ultra-Wideband Antennas backed by a suspended ground or covered with metamaterial superstrates", IEEE Conference, **(2012)**.

[20] Z. Wang, B. Li and L. Peng, "Application of Novel Left-handed Metamaterial Structure in Antenna Cover", iWEM Proceedings, IEEE, **(2012)**.

[21] M. A. Antoniades and G. V. Eleftheriades, "An Broadband Dual-Mode Moopole Antenna using NRI-TL Metamaterial Loading", Antennas and Wireless Propagation Letters, IEEE, vol. 8, **(2009)**, pp. 258-261.

[22] M. Palandoken, A. Grede and H. Henke, "Broadband Microstrip Antenna with Left-Handed Metamaterials", IEEE Transactions on Antennas and Propagation, vol. 57, no. 2, **(2009)**, pp. 331-338.

[23] L. Wang, L. Wang and J. L.-W. Li, "An Series-Fed Metamaterial Microstrip Antenna Array of Broadband and High-Gain", iWEM Proceedings, IEEE, **(2012)**.

[24] L.-W. Li, Y.-N. Li, T.-S. Yeo, J. R. Mosig and O. J. F. Martin, "Addendum: 'A Broadband and High gain Metamaterial Microstrip Antenna' [Appl. Phys. Lett. 96, 164101,2010]", Appl. Phys. Lett., vol. 99, **(2011)**,

[25] L.-W. Li, Y.-N. Li and J. R. Mosig, "Design of a Novel Rectangular Patch Antenna with Planar

Metamaterial Patterned Substrate", (Invited Paper), Proc. of 2008 Int'l Workshop on Antennas Technology, Chiba, Japan, **(2008)**, pp. 123-126.

[26] L.-W. Li and K. Xiao, "Braodband and High-Gain Metamaterial Microstrip Arrays", (Invited Paper), Proc. of 2010 European Conference on Antennas and Propagation (EuCAP201O), Barcelona, **(2010)**.

[27] M.A. W. Nordin and M.T. Islam, "A Bandwidth enhanced printed dipole antenna with metamaterial – inspired loading", IEEE International conference, Malaysia **(2013).**

Organised by

National Conference Emerging Trends in RF and Engineering Sciences (ETRES'18) , Department of Electronics & Communication Engineering Annamalai University, Chidambaram, Tamil Nadu, India

Publisher

Technoscience Academy

Website : www.technoscienceacademy.com
Email: info@technoscienceacademy.com